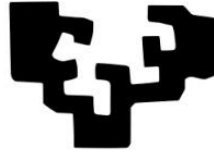


eman ta zabal zazu



Universidad
del País Vasco

Euskal Herriko
Unibertsitatea

PhD Thesis

Biophysical properties of sphingolipid-deficient cell membranes

Biofisika Institute (UPV/EHU, CSIC)

Department of Biochemistry and Molecular Biology

Faculty of Science and Technology

University of the Basque Country (UPV/EHU)

Bingen Gutiérrez Monasterio

**Supervisors: Dr. F. M. Goñi
Dr. X. Contreras**

Leioa 2021

EDUKIAK

LABURDURAK	XIX
1. KAPITULUA: SARRERA ETA HELBURUAK	3
1.1. Zelula Mintzak	3
1.2. Mintz Lipidoak	6
1.2.1. Mintz lipidoen sailkapena	7
1.2.2. Lipidoen banaketa	10
1.2.3. Lipidoen polimorfismoa eta geometria	11
1.2.4. Mintz lipidoen albo banaketak	15
1.3. Proteina-Lipido Elkarrekintzak	19
1.4. Esfingolipidoak	20
1.4.1. SMaren sintesia eta SPT entzima	23
1.4.2. SPTa eta gaixotasun genetiko bat	27
1.5. Helburuak	28
2. KAPITULUA: TEKNIKA ESPERIMENTALAK	31
2.1. Lipido Ereduen Sistemak	31
2.1.1. Geruza anitzeko besikulak (MLV)	33
2.1.2. Lamela bakarreko besikulak	34
2.2. Zelula Mintzak	40
2.2.1. Mintz plasmatikozko besikula erraldoiak (GPMV)	42
2.2.2. PMzko partxeen formakuntza	44
2.2.3. Zelulen lipido erauzketa	45
2.3. Fosfolipidoen Zehaztapena (Fiske entsegua)	46
2.4. Argi Barreiatze Dinamikoa (DLS)	47
2.5. Mikroskopia Konfokal Fluoreszentea	48
2.6. Mintzaren Ordena Molekularra (Laurdan Entsegua)	50
2.7. Proteina Kontzentrazioaren Neurketa	53
2.8. Proteina Adierazpena eta Purifikazioa	54
2.8.1. Transformazioa	55
2.8.2. Adierazpena	55
2.8.3. <i>E.coli</i> tik erauzitako DNA plasmidikoa	56
2.8.4. Purifikazioa	56
2.9. Proteina Elektroforesia	57

2.10. Western Blottinga.....	57
2.11. Ugaztun Zelulen Hazkuntza	57
2.11.1. Zelula hazkuntzen hasiera eta mantenua	58
2.11.2. Zelula mintzaren lipido konposizioaren aldaketak.....	59
2.11.3. Zelula kultiboen ikuskapena.....	62
2.12. Indar Atomikodun Mikroskopia (AFM).....	63
2.13. Fluxu Zitometria.....	67
2.14. Masa Espektrometria.....	68
3. KAPITULUA: PARTXEAK ETA BABAK: CHO ZELULEN MINTZ PLASMATIKOAREN BI PRESTAKINEN KONPOSIZIO ETA PROPIETATE BIOFISIKOEN ARTEKO KONPARAKETA	77
3.1. Sarrera	77
3.2. Materialak eta Teknika Esperimentalak	79
3.2.1. Materialak.....	79
3.2.2. Zelula hazkuntza	79
3.2.3. Laginen prestaketa.....	79
3.2.4. Laurdan bidezko Polarizazio Orokorra (GP).....	82
3.2.5. Irudiak hartzea.....	83
3.2.6. Data eta irudien analisia	83
3.2.7. Fluoreszentzia espektrometrikoren analisia.....	84
3.2.8. AFMa	84
3.2.9. Masa espektroskopia (MS) analisia.....	85
3.3. Emaitzak eta Eztabaida	88
3.3.1. PMaren purifikazioa.....	88
3.3.2. Laurdan fluoreszentzia bidezko GPa.....	89
3.3.3. AFM mikroskopia eta indar espektroskopia	93
3.3.4. Lipido ikerketa	95
3.4. Ondorioak.....	98
3.5. Material Gehigarria	99
CHAPTER 4: CHO/LY-B CELL GROWTH UNDER LIMITING SPHINGOLIPID SUPPLY: CORRELATION BETWEEN LIPID COMPOSITION AND BIOPHYSICAL PROPERTIES OF SPHINGOLIPID-RESTRICTED CELL MEMBRANES.....	107
4.1. Introduction	107
4.2. Materials and Methods	109
4.2.1. Materials.....	109
4.2.2. Cell growth.....	109

4.2.3. Growth rate and viability tests	110
4.2.4. Sample preparation.....	111
4.2.5. SM quantification with lysenin	113
4.2.6. Laurdan General Polarization.....	114
4.2.7. AFM	116
4.2.8. Mass spectroscopic analysis.....	117
4.2.9. Quantitation of lipids per cell.....	119
4.3. Results	120
4.3.1. CHO-derived mutant cells can grow and survive with extremely low sphingolipid concentrations in the culture medium	120
4.3.2. Membrane lipid order decreases with sphingolipid restriction	124
4.3.3. Breakthrough forces of plasma membranes decrease with sphingolipid restriction	128
4.3.4. Sphingolipid composition changes after a 250-fold reduction in sphingolipid supply, with smaller effects on glycerophospholipids.	132
4.4. Discussion	137
4.4.1. CHO and LY-B cells grown in standard medium	137
4.4.2. CHO and LY-B cells grown in SL-deficient medium.....	139
4.4.3. Homeostatic adaptations	140
4.5. Conclusions.....	141
4.6. Supplementary material.....	143
CHAPTER 5: PLASMA MEMBRANE EFFECTS OF SPHINGOLIPID-SYNTHESIS INHIBITION BY MYRIOCIN IN CHO CELLS: A BIOPHYSICAL AND LIPIDOMIC STUDY	155
5.1. Introduction.....	155
5.2. Materials and Methods.....	157
5.2.1. Materials.....	157
5.2.2. Cell growth.....	157
5.2.3. Growth rate and viability tests	158
5.2.4. Sample preparation.....	159
5.2.5. SM quantification with lysenin	159
5.2.6. Laurdan General Polarization (GP).....	160
5.2.7. Atomic Force Microscopy.....	161
5.2.8. Mass spectroscopic analysis.....	162
5.3. Results	164
5.3.1. Growth and viability.....	164
5.3.2. Lysenin-staining	166

5.3.3. Membrane lipid order decreases with sphingolipid restriction	169
5.3.4. Breakthrough force of myriocin-treated CHO cells plasma membranes is decreased	171
5.3.5. Lipidomic analysis of myriocin-treated vs. non-treated CHO cells	172
5.4. Discussion	175
5.4.1. Myriocin effects on cell growth and composition	175
5.4.2. Lipid composition and physical properties	177
5.4.3. Chemical vs. genetic suppression of SPT activity	178
5.5. Supplementary Material	180
CHAPTER 6: PLASMA MEMBRANE SPHINGOMYELIN DEPLETION BY CYCLODEXTRINS: PHYSICAL AND COMPOSITIONAL CONSEQUENCES	187
6.1. Introduction	187
6.2. Materials and Methods	189
6.2.1. Cell growth	189
6.2.2. Lipid-loaded or non-loaded CD treatment	189
6.2.3. Viability test	190
6.2.4. Lysenin-mediated SM quantification	190
6.2.5. Filipin staining	191
6.2.6. Laurdan General Polarization	191
6.2.7. AFM	192
6.2.8. Mass spectroscopic analysis	193
6.2.9. RBC CD treatment	195
6.3. Results and Discussion	195
6.3.1. An overview of M α CD and M β CD properties	195
6.3.2. Cell viability	196
6.3.3. CD treatment for SM depletion in PM	199
6.3.4. Plasma membrane GP after CD treatment	202
6.3.5. Breakthrough forces after CD treatment	204
6.3.6. RBC experiments	205
6.3.7. Mass spectroscopic measurements	206
6.4. Concluding Remarks	209
6.5. Supplementary Material	211
CHAPTER 7: SPHINGOLIPID RESTRICTION IN HAP1 CELLS THAT CONSTITUTIVELY CONTAIN LOW AMOUNTS OF SPHINGOLIPIDS	225
7.1. Introduction	225
7.2. Materials and Methods	227

7.2.1. Cell growth.....	227
7.2.2. Cell growth and viability tests.....	228
7.2.3. Sample preparation.....	228
7.2.4. SM quantification with lysenin	230
7.2.5. Mass spectroscopic analysis.....	231
7.2.6. Gas chromatography–mass spectrometry for cholesterol assay	232
7.2.7. Quantitation of lipids per cell.....	233
7.2.8. Laurdan General Polarization.....	233
7.2.9. AFM	235
7.3. Results.....	236
7.3.1. Cell growth.....	236
7.3.2. Viability.....	239
7.3.3. Lysenin-staining	239
7.3.4. Mass-spectrometric measurements.....	241
7.3.5. Membrane lipid order measurements.....	245
7.3.6. Breakthrough force measurements	248
7.4. Discussion	251
7.5. Supplementary Material	255
8. KAPITULUA: ESFINGOLIPIDOAK ETA KOLESTEROLA, EGITURA LIPIDOAK BAINO GEHIAGO	265
8.1. Sarrera	265
8.2. Zeramida Testuinguruan: Esfingolipidoen Seinalizazioa.....	266
8.3. Zeramida: Hilkortasun-Etengailua Ulertzeko Saiakera.....	267
8.4. Lipido-Domeinuak: Kolesterola eta Lipido-Urmaelaren Hipotesiaren Gaur Egungo Egoera	270
8.5. Zeramidetan Aberastutako Domeinuak: Ikuspuntu Zelularrak eta Garrantzia Terapeutikoa	273
8.6. Ondorioak.....	276
CHAPTER 9: OVERVIEW AND CONCLUSIONS	279
9.1. Patches and Blebs: Two Plasma Membrane Preparations From CHO Cells	279
9.2. LY-B: A CHO Cell Line with Genetically Induced SL-Restricted Cell Membranes	280
9.3. SL Synthesis Inhibition by Myriocin in CHO Cells: A Biophysical and Lipidomic Study	281
9.4. SM Depletion in Plasma Membrane by CD: Physical and Compositional Consequences	281
9.5. SL Restriction in HAP1 Cells that Constitutively Contain Low Amounts of SL	282

9.6. Sphingolipids and Cholesterol “sociability”	283
9.7. Advances Related to the Role of SL in Cell Function	284
9.8 Conclusions	286
9. KAPITULUA: LABURPENA ETA ONDORIOAK	289
9.1. Partxeak eta Babak: CHO Zelulen Mintz Plasmaticoaren Prestakinak Lortzeko Bi Aukera Ezberdin	289
9.2. LY-Ba: SPT Funtzioa Ez Duen Genetikoki Eraldatutako CHO Zelula Lerroa.....	290
9.3. Miriozina Bidezko CHO Zelulen SL Sintesiaren Inhibizioa: Ikerketa Biofisiko eta Lipidomikoa	291
9.4. CD Bidez Mintz Plasmatikoko S ^M a Murriztea: Eraginak Konposizio eta Ezaugarri Fisikoetan	292
9.5. Jatorriz SL Kantitate Txikia Duten HAP1 Zelulen SL Errestrikzioa	293
9.6. Esfingolipido eta Kolesterolaren “soziabilitatea”	294
9.7. S ^L ek Zelulen Funtzioan Duten Eginkizunarekin Erlazionatutako Aurrerapenak	295
9.8. Ondorioak.....	297
BIBLIOGRAFIA	301
ARGITARATZEAK	337
Tesi Honekin Lotura Dutenak	337
Beste Argitaratze Batzuk.....	337
ESKER ONAK	341

LABURDURAK

λ_{ex}	Excitation wavelength <i>Kitzikatze uhin luzera</i>	D	Diffusion coefficient <i>Difusio koefizientea</i>
λ_{em}	Emission wavelength <i>Igortze uhin luzera</i>	DB	Double bond <i>Lotura bikoitza</i>
η	Viscosity of the medium <i>Medioaren likatasuna</i>	Di-4-ANEPPS	4-(2-(6-(Dibutylamino)-2-naphthalenyl)ethenyl)-1-(3-sulfopropyl)pyridinium hydroxide inner salt, 4-(2-(6-(Dibutylamino)-2-naftalenil)etenil)-1-(3-sulfopropil)piridinio gatz hidroxidoa
A_0	Area of the molecule at the lipid-water interface <i>Lipido-ur fase arteko molekularen azalera</i>	DiIC₁₈	(5)-DS (1,1'-Dioctadecyl-3,3',3'-tetramethylindodicarbocyanine-5,5'-disulfonic acid <i>Azido (5)-DS (1,1'-dioktadezil-3,3',3',3'-tetrametilindodikarbozianina-5,5'disulfonikoa</i>
A_H	Cross-sectional area in the hydrophobic tail <i>Isats hidrofobikoaren zeharkako sekzioaren azalera</i>	DLS	Dynamic light scattering <i>Argi barreiatze dinamikoa</i>
AFM	Atomic force microscopy <i>Indar atomikozko mikroskopioa</i>	DLPC	Dilauroyl-phosphocholine <i>Dilauroil-fosfokolina</i>
AOS	α -oxoamine synthase <i>α-oxoamina sintasa</i>	DOPC	1,2-dioleoyl-sn-glycero-3-phosphocholine <i>1,2-dioleoil-sn-glizero-3-fosfokolina</i>
BCA	Bis-cinchoninic acid <i>Azido bis-zinkonikoa</i>	DMEM: F12	Dulbecco's Modified Eagle Medium: Nutrient Mixture F-12, <i>Dulbeccoren eraldatutako eagle medioa: F-12 nutriente nahastea</i>
C	Crystalline phase <i>Fase kristalinoa</i>	DMSO	Dimethyl sulfoxide <i>Dimetil sulfoxidoa</i>
CD	Cyclodextrin <i>Ziklodextrina</i>	DPPC	Dipalmitoylphosphatidylcholine <i>Dipalmitoilfosfatidilkolina</i>
Cer	Ceramide <i>Zeramida</i>	DSC	Differential scanning calorimetry <i>Ekortze kalorimetria diferentziala</i>
CHO	Chinese hamster ovarian <i>Hamster txinatarraren obarioa</i>	DTT	Dithiothreitol <i>Ditiotreitola</i>
Chol	Cholesterol <i>Kolesterola</i>	ER	Endoplasmic reticulum <i>Erretikulu endoplasmatikoa</i>
CL	Cardiolipin <i>Kardiolipina</i>	ESI	Electrospray ionization <i>Elektroesprai ionizazioa</i>
CML	Chronic myeloid leukemia <i>Leuzemia mieloide kronikoa</i>		
CoA	Coenzyme A <i>A koentzima</i>		
CRISPR	Clustered regularly interspaced short palindromic repeats <i>Errepikapen palindromiko labur elkartuak eta erregulariki tartekatuak</i>		

EtOH	Etanol <i>Etanola</i>	HPLC	High performance liquid chromatography <i>Errendimendu altuko kromatografia likidoa</i>
FA	Fatty acid <i>Gantz azidoa</i>	HSN1	Hereditary sensory neuropathy type I <i>I motako zentzumen neuropatia heredatua</i>
FACS	Fluorescence - activated cell sorting cytometry <i>Fluoreszentzia bidez aktibatutako zelulen sailkatzea</i>	I	Emission intensity <i>Igortze intentsitatea</i>
FBS	Fetal bovine serum <i>Behi fetuko seruma</i>	I_B	Intensity collected by NDD 1 <i>NDD1ek batutako intentsitatea</i>
FITC	Fluorescein isothiocyanate <i>Fluoreszeina isotiozianatoa</i>	I_R	Intensity collected by NDD 2 <i>NDD2k batutako intentsitatea</i>
FLIM	Fluorescence lifetime imaging microscopy <i>Fluoreszentzia biziraupenaren mikroskopia</i>	IMEM	Iscoves' s modified eagle medium <i>Aldatutako Iscove eagle medioa</i>
FWHM	Full width at half maximum <i>Zabalera altuera maximoaren erdian</i>	IPTG	Isopropyl β -D-thiogalactoside, <i>Isopropil β-D-tiogalaktosidoa</i>
G	Correction factor <i>Zuzentze faktorea</i>	Kan	Kanamycin <i>Kanamizina</i>
GC	Gas chromatography <i>Gas kromatografia</i>	kB	Boltzmann constant <i>Boltzmannen konstantea</i>
GC-MS	Gas- chromatography-mass spectrometry <i>Gas kromatografia-masa espektrometria</i>	L	Lamellar phase <i>Fase lamelarra</i>
GeoMean	Geometrical mean <i>Batez beste geometrikoa</i>	Lα	Disordered or fluid phase <i>Fase desordenatua edo jariakorra</i>
GP	General Polarization <i>Polarizazio Orokorra</i>	Lβ	Gel phase <i>Gel fasea</i>
GPL	Glyrecophospholipid <i>Glizerofosfolipidoa</i>	Lβ'	Ripple phase <i>Fase uhinduna</i>
GPMV	Giant plasma membrane vesicles <i>Mintz plasmatikoaren besikula erraldoiak</i>	LB	Lysogenyc broth <i>Salda lisogenikoa</i>
GUV	Giant unilamellar vesicles <i>Lamela bakarreko geruza erraldoiak</i>	Lc	Liquid crystalline phase <i>Fase likido kristalinoa</i>
H	Hexagonal phase <i>Fase hexagonala</i>	LC-MS	Liquid chromatography-mass spectrometry <i>Kromatografia likidoa-masa espektrometria</i>
HexCer	Hexosylceramide <i>Hexosilzeramida</i>	Lo	Liquid ordered phase <i>Fase likido antolatua</i>
HOPG	Hydrophobic graphite <i>Grafito hidrofobikoa</i>	LUV	Large unilamellar vesicles <i>Lamela bakarreko besikula handiak</i>
		MαCD	Methyl- α -cyclodextrin <i>Metil-α-ziklodextrina</i>

MβCD	Methyl- β -cyclodextrin <i>Metil-β-ziklodextrina</i>	PE	Phosphatidylethanolamine <i>Fosfatidiletanolamina</i>
M	Micellar phase <i>Mizela fasea</i>	PFA	Paraformaldehyde <i>Paraformaldehidoa</i>
MLV	Multilamellar vesicles <i>Lamela anitzeko besikulak</i>	PG	Phosphatidylglycerol <i>Fosfatidilglizerola</i>
MRM	Multiple reaction monitoring <i>Erreakzio anitzen monitorizazioa</i>	PI	Phosphatidylinositol <i>Fosfatidilinositola</i>
MS	Mass-spectrometry/Mass spec <i>Masa-espektrometria</i>	PLL	Polylysine <i>Polilisina</i>
MTBE	Methyl tert-butyl ether <i>Metil tert-butil eterra</i>	PLP	Pyridoxal 5-phosphate <i>Piridoxal 5-fosfatoa</i>
NBD-PE	N-(7-Nitrobenz-2-Oxa-1,3-Diazol-4-yl)-1,2-Dihexadecanoyl-sn Glycero-3-Phosphoethanolamine, Triethylammonium Salt <i>N-(7-Nitrobenz-2-Oxa-1,3-Diazol-4-il)-1,2-Dihexadecanoil-sn Glizero-3-fosfoetanolamina, Trietilamonio gatza</i>	PM	Plasma membrane <i>Mintz plasmatikoa</i>
NDD	Non-descanned detector <i>Deskaneatu gabeko detektorea</i>	PS	Phosphatidylserine <i>Fosfatidilserina</i>
NIST	National institute of standards and technology <i>Estandare eta teknologiaren nazioarteko institutua</i>	Q	Cubic phase <i>Fase kubikoa</i>
NI-NTA	Nickel-nitrilotriacetic acid <i>Azido nikel-nitrilotriazetikoa</i>	RBC	Red blood cells <i>Globulu gorriak</i>
NSOM	Near-field scanning optical microscopy <i>Eremu hurbileko eskaneatze mikroskopio optikoa</i>	Rh	The hydrodynamic radius of spherical particles <i>Partikula esferikoen erradio hidrodinamikoa</i>
NT	Non toxic <i>Ez toxikoa</i>	SDS-PAGE	Sodium dodecyl sulfate polyacrylamide gel electrophoresis <i>Sodio dodezil sulfatozko poliakrilamida gel elektroforesia</i>
OD	Optical density <i>Dentsitate optikoa</i>	SL	Sphingolipid <i>Esfingolipidoak</i>
ORM	Orosomuroid <i>Orosomukoidea</i>	SM	Sphingomyelin <i>Esfingomielina</i>
P	Oblique phase <i>Fase zeharra</i>	Sph	Sphingosine <i>Esfingosina</i>
PA	Phosphatidic acid <i>Azido fosfatidikoa</i>	SPIONS	Coated superparamagnetic iron oxide nanoparticles <i>Gaineztatutako burdin oxido nanopartikula superparamagnetikoak</i>
PC	Phosphatidylcholyne <i>Fofatidilkolina</i>	SPT	Serine palmitoyl transferase <i>Serina palmitoil transferasa</i>
PDI	Polydispersity index <i>Polidispertsitate indizea</i>	SPTLC1/2/3	Serine palmitoyltransferase long chain base subunit 1/2/3 <i>Serina palmitoiltransferasaren kate luzeko basearen 1/2/3 azpiunitatea</i>

STED	Stimulated emission depletion microscopy <i>Estimulatutako igortze jeitsiera mikroskopia</i>
SLB	Supported lipid bilayers <i>Sostengatutako lipido geruza bikoitzak</i>
SLD	Soft laser desorption <i>Laser desortzio ahula</i>
SPB	Supported planar bilayers <i>Sostengatutako geruza bikoitz lauak</i>
STM	Scanning tunneling microscope <i>Tunel eskaneatze mikroskopia</i>
SUV	Small unilamellar vesicles <i>Lamela bakarreko besikula txikiak</i>
T	Temperature <i>Tenperatura</i>
TBS	Tris buffer saline <i>Gatzdun tris tanpoia</i>
T_m	Mild-point transition temperature <i>Fusiorako trantsizio tenperatura</i>
Tx-100	Triton X-100 <i>Triton X-100a</i>
UV	Ultraviolet <i>Ultramoreia</i>

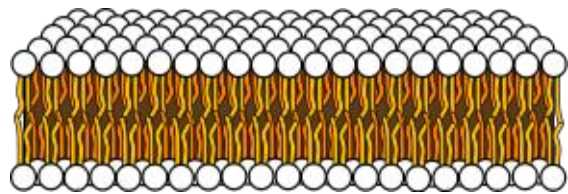
1. KAPITULUA:
SARRERA ETA HELBURUAK

1. KAPITULUA: SARRERA ETA HELBURUAK

1.1. Zelula Mintzak

Mintz biologikoek zelulen hesi gisa jardutearen oinarriko funtzioa betetzen dute. Zitoplasma kanpoaldeko ingurutik banatu eta zelularen forma mantentzen duen mintzari mintz plasmatikoa (PM, ingelesezko plasma membrane) deritzo. Zelula osoaz gain, zelula barneko organuluak ere mintz batek mugatzen ditu.

Mintzak erdiiragazkorak diren eta zelulako gune ezberdinak banatzearen oinarriko eginkizuna duten lipido geruza bikoitzak dira. Hau da, molekula ez-polar gehienentzako era ez-hautakorrean jarduten duten hesi iragazkorak dira. Mintzen bidez, zelula kanpoko eta barneko guneen, eta zelula konpartimentu ezberdinen artean, polarrak diren eta/edo karga elektrikoa duten substantzien elkartruke hautakorra arautzen da. Mintzek, inguratzen duten guneko egoera ioniko espezifiko eta funtsezko pH maila mantentzearen ardura daukate, honela, organuluen funtzio egoki bat bermatuz. Zelularen eta organuluen muga hesitzeaz eta zelula barneko molekulen zirkulazioa arautzeaz gain, mintzek beste hainbat eginkizun betetzen dituzte: zenbait entzimen aktibitatearen erregulazioa ahalbidetzen dute, seinalizazio prozesu ugaritan bigarren mezularien iturri gisa jarduten dute, zelula konpartimentuen arteko gradiente kimiko eta karga elektrikoak mantentzen dituzte eta zelularen diferentziazioan, atxikiduran eta heriotzan ere parte hartzen dute. Hitz gutxitan, zelula mintzak hesi pasibo soilak izatek oso urrun dauden egiturak dira. Zelulek, lipido espezifikoak sintetizatze eta lipido hauek organulu jakinetako mintz zehatzetara eramateko mekanismoak garatu dituzte. Lipido mintzen erregulazio eta metabolismoak, zelularen “horma” funtzioetik haratako doan erregulazio bioaktiboaren rola daukala esan daiteke (errebisio gaurkotuetarako ikusi Luckey, 2008a; Yeagle, 2016; Stillwell, 2016).

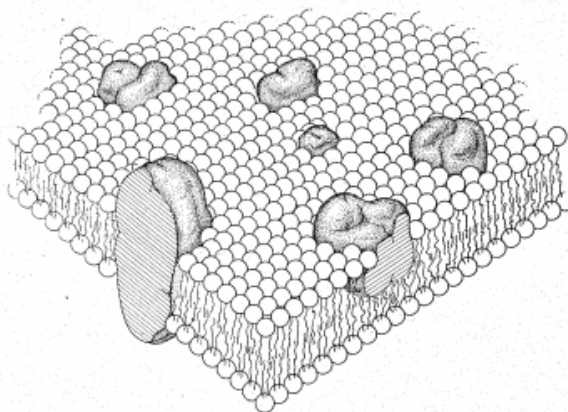


1.1 irudia. Lipido geruza bikoitzaren egitura.

Mintzaren egitura, taldeburu polarra eta hidrokarbonozko kate ez-polarra daukaten lipido anfipatikoz osatutako geruza bikoitz bat da. Lipido anfipatikoak ezin dira uretan disolbatu eta ingurune urtsuan dispersatzen direnean, maiz, bata bestearen

aurka kokatuta dauden bi geruzetan antolatzen dira. Non itsas hidrofobikoak geruza bikoitzaren erdigunerantz eta buru polarrak inguru urtsuarekin kontaktuan kokatzen diren (1.1 irudia). Era honetako bat-bateko agregazioak, “efektu-hidrofobiko” deritzen fenomenoaren ondorioz gertatzen dira (Tanford, 1974).

Beharbada, mintzen ikerketaren jatorria 1895 urtean egon daiteke, orduan behatu baitzuen lehen aldiz Ernest Overtonek zeluletan zehar gertatzen zen substantzia ez-polarren difusioa. Overtonek (1895) antzekotasun bat antzeman zuen mintzean zehar barreiatzen ziren substantzien, eta substantzia horiek oliba olioan zeukaten disolbagarritasunaren artean. Aurkikuntza honek zelula mugatzen duen egitura lipidoz osatuta egon zitekeela pentsatzera eraman zuen. Hogeita hamar urte beranduago, Gorter eta Grendelek (1925), eritrozitoen lipido erauzketak uretan okupatzen zuen azalera zelularen gainazalarentzat kalkulatuak diren bikoitza zela frogatu zuten. Honen bidez, mintzen oinarritzko egitura lipido geruza bikoitz bat zela ondorioztatu zuten. 1935ean, Danielli eta Davsonek zelula mintzen eredu bat proposatu zuten, zeinetan β konformazioan zeuden proteinek lipidozko geruza bikoitza sandwich eran gaineztatzen zuten (Danielli & Davson, 1935). Mikroskopia elektroniko bidez lortutako zenbait ebidentzia (Robertson, 1959), eta iragazkortasunaren inguruko ikerketa kimiko eta fisiko eguneratuago batzuen konbinazioak (Maddy & Malcolm, 1965; Lenard & Singer, 1966; Zahler *et al.*, 1966), mintzean aurkitzen diren proteina eta lipido molekula indibidualen mugikortasuna barneratzen zuen eredu baten sorrera ekarri zuen. Izan ere, 1972an, ordura arteko jakinduria konbinatuz, Singer eta Nicolsonek “mosaiko jariakorraren” eredu bat proposatu zuten (Singer & Nicolson, 1972). Gaur egun hau da hain zuzen ere mintz biologikoen egituraren oinarritzko eredu gisa onartuena den modeloa (1.2 irudia).



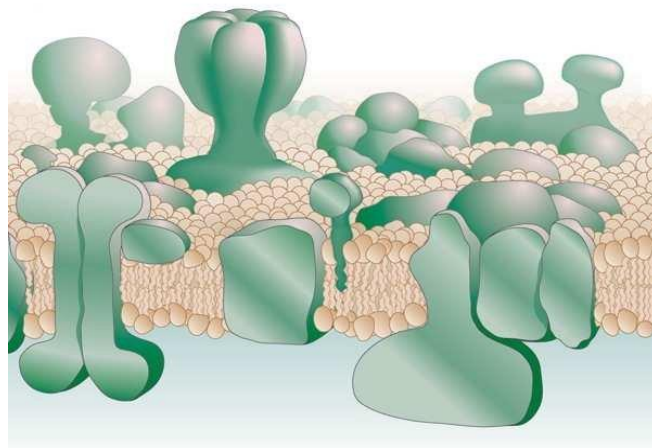
1.2 irudia. Singer eta Nicolsonek proposaturiko mintz eredu bat (Singer & Nicolson, 1972).

“Mosaiko jariakorra” ereduaren arabera, mintza lipido geruza bikoitz bat da, zeinak zenbait proteina (anfifiliko) bere baitan txertatuak (proteina *integralak* / barne-proteinak), eta beste batzuk elkarrekintza elektrostatiko bidez mintzaren gainazalera lotuak (proteina *periferikoak* / kanpo-proteinak) dauzkan. “Jariakor” hitzak lipido eta

proteinak mintzaren planoan albotz barreiatu daitezkeela esan nahi du, horrela, beraien arteko elkarrekintzak gertatzea erraztuz. Bestalde, eredu honetan, geruza bikoitzaren geruza batetik besterako mugimendua; hau da, translokazioa, nabarmenki mugatua dago. Zelula mintzen asimetria kontzeptua, jadanik Singer – Nicolson ereduaren eredu aipatua izan zen: lipido molekula, lipido geruza bikoitzaren bi geruzen artean era heterogeneo batean banatuta daude; hau da, geruza bikoitzeko geruzetako bakoitza lipido jakinetan aberastuago dago. Barne eta kanpo geruzen arteko proteina banaketa hertsiki asimetrikoa da. Gainera, karbohidratoak soilik mintzeko barne proteinetara eta geruza bikoitzaren kanpo geruzan kokatutako lipidoetara elkartuta daude.

Simons eta Ikonenek (1997) Singer – Nicolson ereduaren aldaera bat proposatu zuten. Bertan, esfingolipido (SL) eta kolesterol (Chol)-ean aberastuta dauden lipidozko nanoegituren kontzeptua deskribatuz. Beraien esanetan, mota honetako egiturek seinaleen transdukzio prozesuetan zeresana daukaten proteinak erakartzeko gaitasuna daukate. Egitura hipotetiko hauek “raft” (urrael) gisa izendatu zituzten. Raft hipotesiak zelula mintz eta mintz ereduaren albotz heterogeneotasunean interesa piztu bazuen ere, eskala nano batean une-laburreko egiturak ikusteko dauden zailtasun teknikoak direla eta, beraien existentziaren inguruko eztabaida izugarria da (Goñi, 2019). Beste hitz

batzuetan, aztoratu gabeko zelula bizien gainazalaren irudi zuzenetan inork nanodomeinak (10-200 nm) ikusi ez izanagatik, beraien inguruko eszeptizismoa oso handia da (Edidin, 2003; Munro, 2003; Rosetti *et al.*, 2017). Gaur egungo ikuspuntuaren arabera, raftak zelula mintzetako nanodomeinu mota bat izan daitezke, zeintzuen ezaugarriak,



1.3 irudia. Engelmanek proposaturiko Singer-Nicolson mintz eredu gaurkotua (Engelman, 2005).

teknika egokien gabeziaren ondorioz, ondo definitu gabe dauden (Goñi, 2014, 2019; Goñi *et al.*, 2020).

Hamarkadetako ikerketen ostean lortutako zenbait kontzeptu berrik mosaiko jariakorraren eredu osatu eta hedatu dute (Engelman, 2005; Feigenson, 2007; Goñi, 2014) (1.3 irudia). Gaur egun, mintzak aztorapen handia eragiten duten proteinez

gainezka daudela onartzen da. Gainera, lipido geruza bikoitza ez da lehen pentsatzen egitura ordenatu eta homogeneo gisa ikusten. Mintzaren okerdura parametroak, lipido geruza bikoitzaren geruza batetik besterako lipido molekulen mugimenduak, lipido faseak, eta lamelarrak ez diren egiturak deskribatu dira. Hauetaz gain, alboz banatutako mintz domeinuen ikerketek, lipido geruza bikoitzaren ikuspuntu dinamikoago batera bultzatu gaituzte (Engelman, 2005; Feigenson, 2007; Goñi, 2014; Goñi *et al.*, 2020).

1.2. Mintz Lipidoak

Lipidoek mintzaren zurruntasuna osatzen dute (zelula mintzen masaren %50 inguru lipidoek osatzen dute). Mintz lipido natural gehienak anfipatikoak dira eta disoluzio urtsuetan dispertsatzen direnean, normalean, beraien artean geruza bikoitzeko agregazioak sortzen dituzte. Aurretik esan den bezala, egitura funtzioaz gain, lipidoek beste hainbat funtzio biologiko garrantzitsu betetzen dituzte: Seinaleen transdukzioan eta molekulen errekonozimendu prozesuan jardun dezakete, transkripzio osteko proteina-lipido eraldaketetan substratu izan daitezke, edota lipido tantatxo gisa energia gordailu gisa joka dezakete (Mouritsen, 2005; van Meer *et al.*, 2008; Ridgway & McLeod, 2016; Gurr *et al.*, 2016; Harayama & Riezman, 2018).

Mintz lipido gehienek, beraien osagai hidrofobiko gisa, gantz azidoak dauzkate. Gantz azido bat azido monokarboxiliko bat da, zeina aseba edo asegabea izan daitekeen. Gantz azidoek, normalean, 4-24 karbono (C) atomoz osatutako kateak izan ohi dituzte. Hauek, kate-labur (4-6 C), kate-ertain (8-10 C), kate-luze (12-18 C), eta kate-oso-luze (20 C edo gehiago) gisa sailkatzen dira. Egiturari dagokionez, lipido gehienak antzekoak badira ere, beraien kate hidrofobikoko C kopuruaren arabera edo asegabete mailaren aldaera txikien bidez, beraien ezaugarriak asko alda daitezke. Azken aipatutako bi hauek esaterako, mintzen

1.1 taula. Lipido mintzetan aurkitzen diren gantz azido ohikoenak

Izena	Egitura
Laurikoa	12:0
Miristikoa	14:0
Palmitikoa	16:0
Estearikoa	18:0
Linoleikoa ($\Delta_{9,12}$)	18:2
Linolenikoa ($\Delta_{9,12,15}$)	18:3
Arakidikoa	20:0
Lignozerikoa	24:0
Palmitoleikoa (Δ_9)	16:1
Oleikoa (Δ_9)	18:1
Arakidonikoa ($\Delta_{5,8,11,14}$)	20:4
Nerbonikoa (Δ_9)	24:1

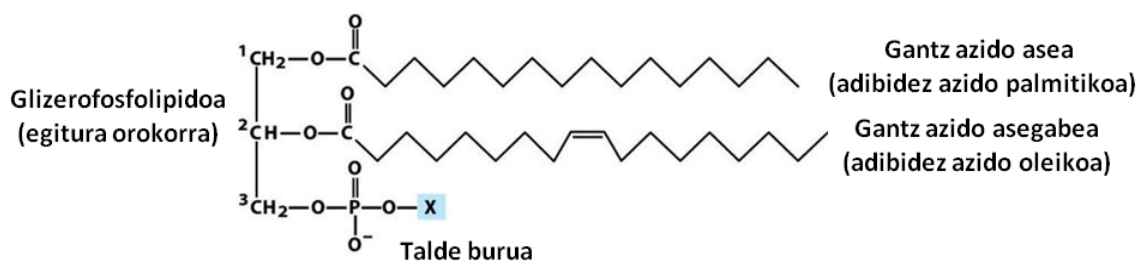
jariakortasuna baldintzatzen dute; baxuagoa da gantz azidoak guztiz aseak dauzkaten kate aziliko luzeko lipidoz osatutakoentzat (Chapman, 1975; Kates & Kuksis, 1980; Cullis *et al.*, 1983). Lipido mintzetan aurkitzen diren gantz azido ohikoenak 1.1 taulan laburbiltzen dira.

1.2.1. Mintz lipidoen sailkapena

Lipidoen egitura kimikoa beraien ezaugarri fisikokimikoekin guztiz lotua dago. Beraz, lipidoek zelula mintzetan nola jokatzen duten ulertzeko, ezinbestekoa da beraien aniztasun kimikoan erreparatzea. Animalien zelula mintzetan gailentzen diren lipidoak glizerolipidoak, esfingolipidoak (SL) eta esterolak dira.

1.2.1.1 Glizerolipidoak

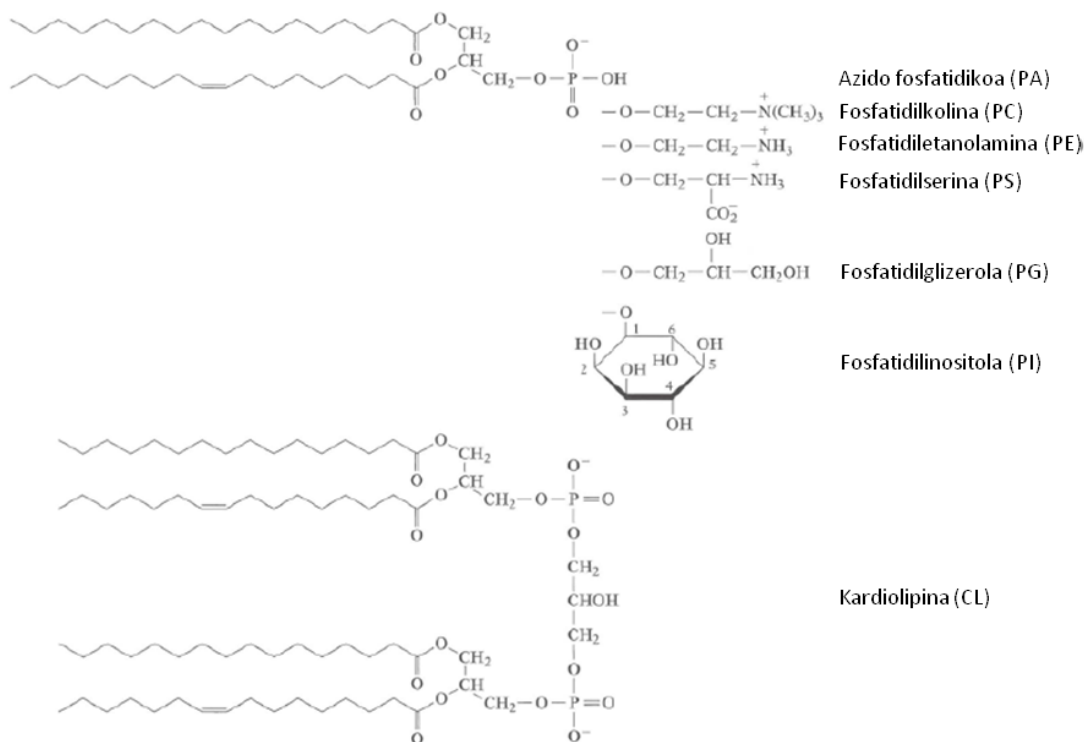
Glizerolipidoak eukariotoen zelula mintzetako lipido ugariak dira. Beraien artean glizerofosfolipidoak (animalien mintzetan ugariak) eta glizeroglikolipidoak (landare berde eta algetan ugariak) ezberdintzen dira. Glizerofosfolipidoen egitura (1.4 irudia) glizerol molekula batean oinarritzen da, zeinari bi gantz azido (normalean bata asea eta bestea asegabea) *sn*-1 eta *sn*-2 kokapeneko C atomoetara batzen zaizkion. Bestalde, glizerolaren *sn*-3 kokapeneko C-ra fosfato talde bat lotua daukate. Naturan aurkitzen diren mintzetan, fosfato taldera esterifikatua dagoen alkohol taldearen arabera, hainbat glizerofosfolipido mota aurki ditzakegu. Glizerofosfolipido arruntenak 1.5 irudian agertzen dira. Animalietan fosfatidilkolina (PC) da ugariena (1.5 irudia).



1.4 irudia. Glizerofosfolipidoen egitura (Nelson & Cox, 2008).

Glizeroglikolipidoak kantitate ugarian ageri dira landareen eta zenbait bakterioen mintzetan. Hauek, glizerolaren *sn*-3 C-ra fosfato taldea lotua izatearen ordez, lotura glikosidiko bidez mono- (edo oligo-)sakarido talde bat itsatsita dute. Naturan

aurkitzen den lipido polar ugariena tilakoideen mintzetan ageri den monogalaktosilglicerola da (Gounaris & Barber, 1983).



1.5 irudia. Glizerofosfolipido ohikoenen egitura kimikoak (Luckey, 2008).

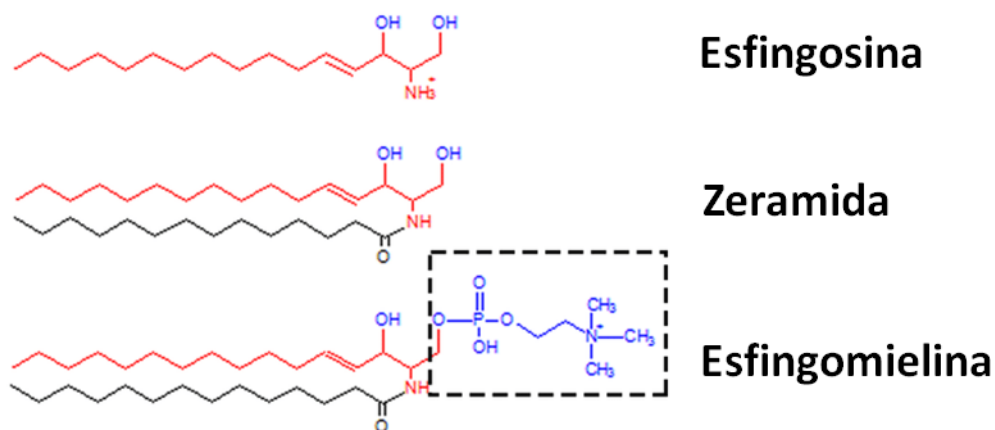
1.2.1.2 Esfingolipidoak

SL eta glizerolipidoen arteko ezberdintasuna ondorengoa da: SLeK, beraien kate nagusi gisa glizerola izatearen ordez, kate luzedun molekula bat dute. Molekula hau normalean esfingosina (Sph) izeneko aminooktadezil alkohol kate luze asegabe bat izan ohi da (1.6 irudia). Talde burutzat, C1ean kokatutako talde hidrofílico bat, fosforilkolina hondar bat edo azukre bat (zerebrozidoak), edo batzuk (gangliozidoak), izan ohi dute. SLeK, egitura funtzioaz gain, beste hainbat funtzio espezifiko betetzen dituzte; adibidez, seinalizazio prozesuetan bigarren mezulari gisa jardun dezakete (Hannun *et al.*, 1986; Kolesnick, 1987; Hannun & Obeid, 2008; Kolesnick *et al.*, 2000).

Sphak, Sph-1-fosfatoak (S1P), zeramidak (Cer) eta Cer-1-fosfatoak (C1P), SL simple gisa ezagutzen den taldea osatzen dute (Goñi & Alonso, 2006). Amida lotura baten bidez Spharen C2ko amino taldera gantz aziliko bat (normalean ase) lotzen denean Cera sortzen da. Cera prozesu apoptosikoetan eginkizun garrantzitsuak dituen

seinalizazio lipidoa da (Hannun *et al.*, 1986; Kolesnick, 1987). Cerari fosforilkolina molekula bat lotzen zaionean, esfingomielina (SM) sortzen da (1.6 irudia).

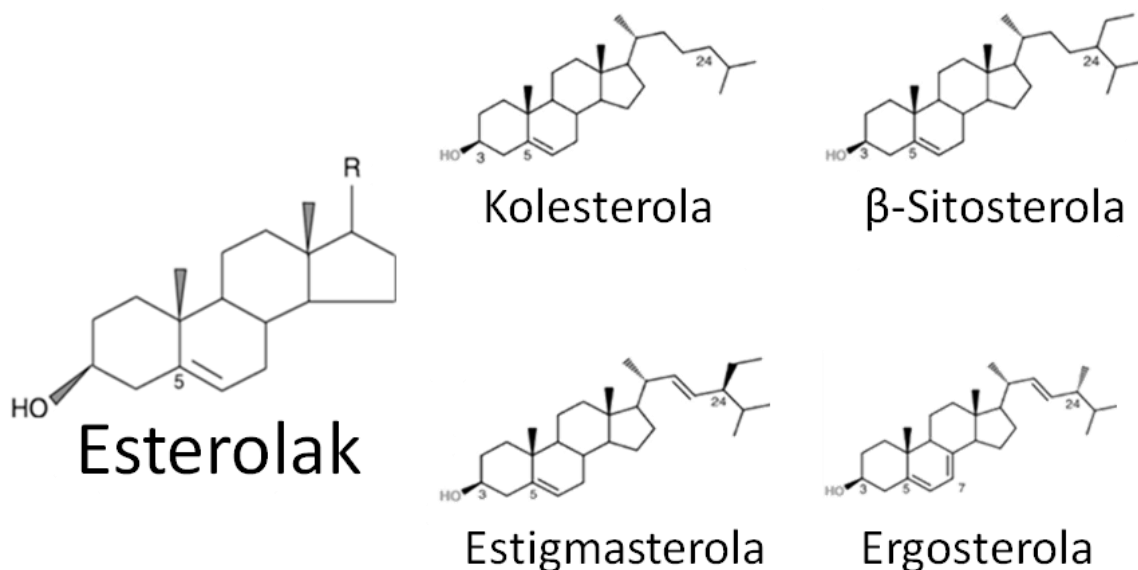
Cerari lotura glikosidiko bidez buru polar gisa azukre hondarrak lotzen zaizkionean glikoesfingolipidoak sortzen dira. Azukre molekula hauek kopuru eta mota ezberdinekoak izan daitezke. Honen arabera, glikoesfingolipidoak bi taldetan sailkatzen dira: zerebrozidoak (azukre sinple batez edo biz osatuak, adibidez glukosa edo galaktosa), eta gangliosidoak (zenbait azukre molekulez osatuak, gutxienez horietako bat azido sialikoa).



1.6 irudia. Spharen, Ceraren eta SMaren egitura kimikoak (Lakshini, 2016).

1.2.1.3. Esterolak

Oso hidrofobikoak diren molekula hauek zelula mintzetako lipido ez-polar ugariak dira. Esterolen sintesia, normalean, isoprenoideen metabolismoko mebalonatoaren bidezidorean oinarritzen da. Esterolak hidrokarbonozko isats bati lotutako lau eraztunezko egitura batez (beste lipido batzuekin nahastean geruza bikoitzean txertatzen dena) eta hidroxilo talde aske batez (faseen artean kokatzen den talde polarra) osatuta daude. Organismoaren arabera, mintzetan aurkitzen den esterol mota ugariena ezberdina izan ohi da: legamien esterol nagusia ergosterola da, landareena estigmasterola eta β sitosterola eta animaliena berriz Chola (1.7 irudia). PMan, Chol molekulak kantitate handian aurkitzen dira; zenbait zelula motetan, adibidez odoleko globulu gorrietan (RBC, ingelesezko red blood cells), lipido guztien %30a izatera hel daiteke.



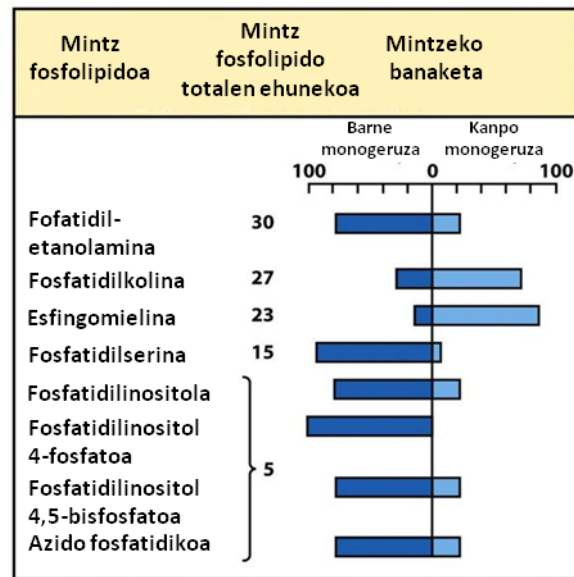
1.7 irudia. Esterol molekula ugarienen egitura. [Scolaro *et al.* (2020)etik birmarraztua].

1.2.2. Lipidoen banaketa

Lipidoen inguruan egindako ikerketek, taldeburu eta kate aziliko ezberdindun 1000 lipido motatik gorako existentzia frogatu dute. Dibertsitate honetaz gain, lipido espezieak organuluetan zehar era heterogeneo batean banatuta daude. Banaketa heterogeneo hau, organuluen guneko-lipido-metabolismoarekin lotuta dago. Zenbait lipido sintetizatuak izan diren lekutik kanpo garraiatuak izaten dira azken helmugara iritsi arte, non beraien funtzioa gauzaten duten.

Erretikulu endoplasmatikoa, Golgi aparatua eta mitokondriak bezalako organuluek lipido sintesirako sistema autonomoa dute. Hau da, beraien lipido egitura osatzen duten lipido moten artetik gutxienez bat, edo batzuk, sintetizatzeke gai dira. Bestalde, zenbait organulu, adibidez PMA, beste gune konkritu batzuetatik garraiatutako lipidoz osatuta daude. Sistema hauek zelulen heterogeneotasunaren adibide garbiak dira. Izan ere, Golgi aparatua SLen sintesian espezializatuta badago ere, ia sintetizatutako molekula guzti horien jomuga PMA da. Bestalde, kardiolipina sintetizatzen duten organulu bakarrak mitokondriak dira. Erretikulu endoplasmatikoak berriz, triazilglicerol eta kolesteril esterrak, eta Cer molekulak, sintetizatzen ditu (van Meer *et al.*, 2008).

Mintz barneko heterogeneotasuna ere existitzen da. Hau da, lipido geruza bikoitza osatzen duten geruzetako bakoitzean lipido molekulak era asimetriko batean banatuta daude. Kontzeptu hau 1972an mosaiko jariakorraren ereduan proposatua (Singer & Nicolson, 1972), eta geroago van Deenen eta taldekideengatik frogatua (Verkleij *et al.*, 1973), izan zen. Lipido asimetria, monogeruza konkretu batean kokatutako lipidoen sintesi aktibo bidez sortzen da eta lipidoen noranzko bakarreko translokazioa kontrolatzen duten lipido



1.8 irudia. RBCen PMko fosfolipidoen banaketa (Nelson & Cox, 2008).

garraiatzaile jakinen bidez mantentzen da. Honen adibide argia, PMan eta Golgi aparatuan gertatzen dena da hain zuzen ere: PCa eta SMA, batez ere, kanpo monogeruzetan kokatuta dauden bitartean, fosfatidiletanolamina eta fosfatidilserina barne geruzetan aurkitzen dira (1.8 irudia). Erretikulu endoplasmaticoaren asimetria mantentzeko, bertan berriki sintetizatzen diren lipido molekulen erdia kanpo geruzara garraiatu behar da. Dena den, geruza bikoitzeko geruza batetik besterako lipido molekulen mugimendua mugatua dago. Izan ere, buru polar bat erdigune hidrofobiko batean zehar mugitzeko gainditu behar den energia hesia oso handia izateaz gain, lipido berrien txertatzearen kausaz, mugimendua zailtzen duten albo tentsioak ugaritzen dira. Dena den, zenbait proteinek (flipasak eta flopasak) mintzaren alde batetik besterako garraioan laguntzen dute. Horrela, mugimendua gertatzeko beharrezkoa den energia jaitsiz (Contreras *et al.*, 2010).

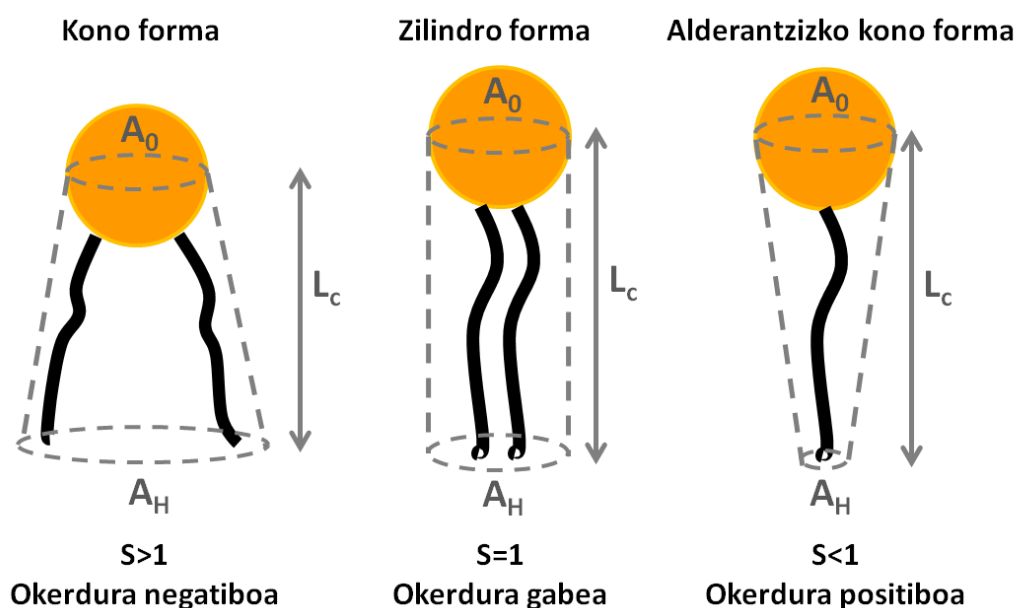
1.2.3. Lipidoen polimorfismoa eta geometria

Geruza bikoitzaren lodiera, jariakortasuna, faseen arteko polaritatea, okerdura, edo karga elektrikoa, mintzetan kontuan eduki behar diren garrantzia handiko alderdiak dira. Izan ere, ezaugarri hauek berebiziko garrantzia izan dezakete mintzaren funtzio jakinak arautzerako orduan. Lipido molekula gehienak uretan dispersatzean lamela formako mintzetan antolatu ohi dira. Dena den, lamela egitura ez daukaten beste egitura

batzuk ere existitzen dira. Hauek, mintzen fusio eta fisioan, ugalketan, besikula bidezko garraioan eta birusen infekzioak bezalako zenbait prozesu biologikotan, garrantzia esanguratsua izan dezakete (Larsson, 1989; Chernomordik, 1996; Epan, 1998; Burger, 2000; Basañez, 2002).

1980an, Jacob Israelachvili, lipido molekulek dauzkaten berezko geometriek, lamela diren eta ez diren egituren formakuntzak baldintzatzen dituztela proposatu zuen. Hau da, lipidoaren buru polarraren eta bere isats hidrofobikoaren zeharkako-ebakiduraren azaleraren arteko erlazioak, mintza sortzerakoan lipidoak antolatzen diren era zehazten duela hain zuzen ere (Israelachvili *et al.*, 1980).

Lipidoen geometria edo forma orokorra 3 motatan sailka daiteke: kono forma, zilindro forma eta alderantzizko-kono forma (1.9 irudia).



1.9 irudia. Lipidoen geometria.

Geometria hauek errazago ezberdindu daitezke ondorengo formula erabiliz:

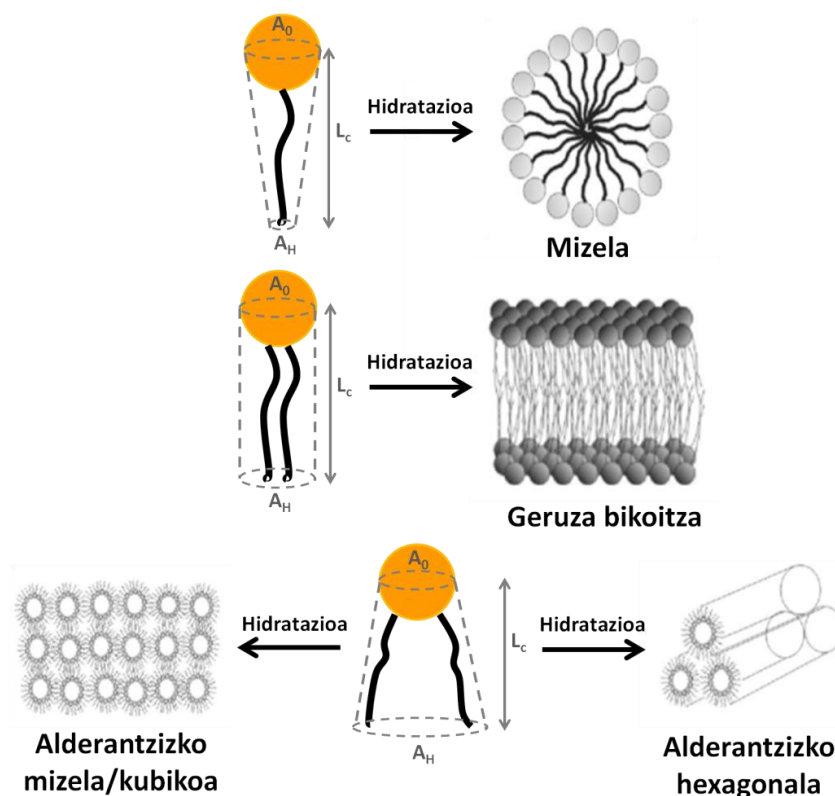
$$S = \frac{V}{A_0 \cdot L_c}$$

Non, V lipido molekularen bolumena, A_0 lipido-ur fase artean molekulak daukan azalera eta L_c kate aziliko luzatuaren luzera diren. S parametroa, A_0 eta isats

hidrofobikoaren zeharkako-ebakiduraren azaleraren (A_H) erlazioaren arabera ere izan daiteke.

A_0/A_H erlazioa ondorengo eran interpreta daiteke:

- $A_0 = A_H$ ($S = 1$): Molekulak zilindro forma dauka, beraz zero okerdura. Mintzak sortzerakoan geruza bikoitz leun bezala antolatzen diren PCa eta SMA bezalako molekulen kasua da (1.10 irudia).
- $A_0 < A_H$ ($S > 1$): Molekulak kono forma dauka, beraz mintzek okerdura negatiboa izango dute. Fosfatidiletanolamina, diazilglicerola edo esterol lipidoz osatutako mintzen kasua da. “Hexagono” formak (tutu forma) sortzeko joera daukate (1.10 irudia).
- $A_0 > A_H$ ($S < 1$): Molekulak alderantziko-kono forma dauka, beraz mintzek okerdura positiboa izango dute. Lisofosfolipidoak bezalako lipidoak mizeletan antolatzen dira (1.10 irudia).



1.10 irudia. Lipido geometria eta agregazio egiturak. [Hafez & Cullise (2001)etik birmarraztua].

Luzzatik (1968), X-izpietako ebidentzietan oinarrituz, sailkapen bat proposatu zuen. Saretzearen arabera, dimentsio bakarreko mizela (M) edo lamela (L) fasea, dimentsio biko hexagono (H) edo zeharra (P) den fasea, eta hiru dimentsioko fase kubikoa (Q) edo kristalinoa (C) ezberdindu zituen.

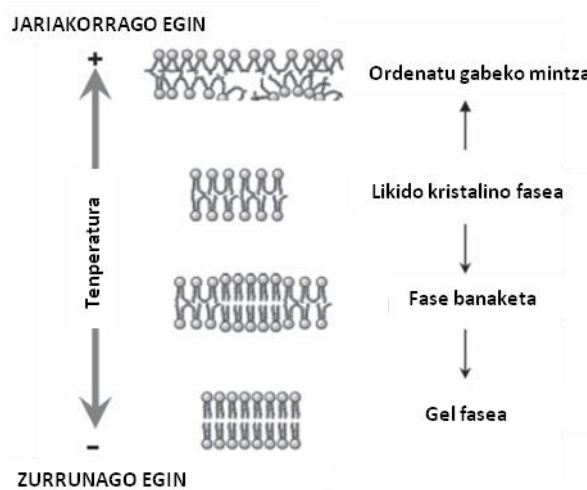
Fusio prozesuetan ematen den poro formakuntza eta fisio aurretik sortzen den lepo egitura, fase hexagonala bezalako lamela ez diren egituren formakuntzen bidez gobernatuak egon daitezke (Cheng *et al.*, 1986; Hong *et al.*, 1988; Nieva *et al.*, 1995; Gilbert, 2016). Fase hau morfologikoki hexagono formako paketatzea daukaten zilindro paralelo gisa deskribatu daiteke. Hexagono faseak 2 motatakoak izan daitezke: a) lipidoaren kate azilikoak zilindroen erdialderantz begira daude, edo b) kate azilikoak beste zilindroen isats hidrofobikoekin kontaktuan eta buru polarrak zilindroen erdialdean daude.

Kate azilikoaren paketatze mailaren arabera, fase desordenatu edo jariakorra ($L\alpha$), kate azilikoak mintzaren planoarekiko era perpendikularrean dauden fase ordenatua edo gel fasea ($L\beta$), fase jariakor eta gelaren tarteko ezaugarriak dituen fase jariakor-antolatua (L_o), gantz aziliko kateak mintzaren planoarekiko inklinatuak dituen fase uhinduna ($L\beta'$) eta kristal fasea (L_c) ezberdintzen dira.

Gel fasean, lipidoak era dentsuago (zurrunago) batean paketatuak daude; hau da, paketatze maila baxuagoa duen fase jariakorrean baino antolatuagoak daude. $L\alpha$ fasea, gutxienez asegabetze bat duen kate azilikoazko lipidoz osatutako mintzei dagokio. Hauek albo edo errotazio difusio ahalmena dute eta beraz, beraien kate azilikoak oso egoera desordenatuan daude. Bestalde, $L\beta$ faseak, albo eta errotazio mugimendua mugatua daukaten lipido aseaz osatuak egon ohi dira. Hau da, giro tenperaturan kate azilikoak oso antolatuta dituen lipidoz.

Temperaturak eragin handia dauka mintzen fasean (1.11 irudia). Gel fasean dagoen geruza bikoitz bat berotzen bada, C-C *gauche* konformazioaren proportzioa igo egiten da, ondorioz, fase desordenatuago bat sortuz. Fase aldaketa gertatzen den tenperatura, urte tenperatura (T_m) bezala ezagutzen da, eta beste metodo batzuen artean, ekortze kalorimetria diferentziala (DSC, ingelesezko differential scanning calorimetry) erabiliz iker daiteke. Geletik fase jariakorrerako trantsizioa, maiz, fase trantsizio nagusi gisa ezagutzen da. 37°Ctik gorako T_m a izateak, tenperatura

fisiologikoan lipido horiek gel fasean existitu daitezkeela esan nahi du. Lipido gehienek temperatura fisiologikoan mintz jariakorrak sortzen dituzte. Beraien T_m altua dela kausa, soilik lipido jakin batzuk daukate giro temperaturan gel domeinuak sortzeko ahalmena; batez ere SL aseak.



1.11 irudia. Temperaturak mintzaren jariakortasunean duen eragina. [Los & Murata (2004)tik birmarraztua].

Temperaturaz gain, ur kantitatea, indar ionikoa, pHa, katioi dibalente kopurua eta mintzean dauden proteinen

ezaugarri espezifikoak bezalako beste faktore batzuk ere lipidoen azalera eta bolumenean eragina dute. Gainera, hainbat lipidoz sortutako mintzetan, aldi berean existitzen diren fase ezberdineko domeinuak sor daitezke. Gertaera hau lipido bakoitzak elkarrekintzak gauzatzeko duen joera eta trantsizio temperatura ezberdinak direla medio gertatzen da. Izan ere, beraien nahasturek trantsizio konplexuak sor ditzakete.

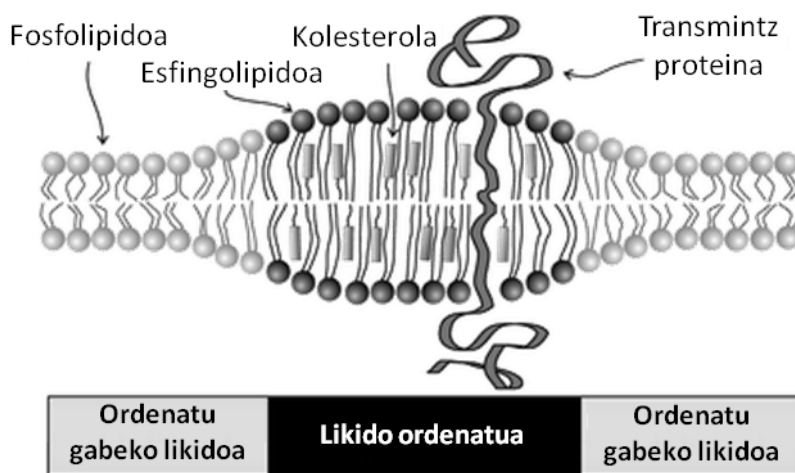
1.2.4. Mintz lipidoen albo banaketak

Lipidoak mintzetan era heterogeneo batean banatuta daude. Heterogeneotasuna mintzen artean existitzeaz gain, mintz beraren barnean ere existitzen da. Nanometro gutxi batzuetatik mikroietara bitarteko tamaina izan dezaketen albo heterogeneotasunak, lipido eta proteina zehatzetan aberastuak eta inplikazio biologiko garrantzitsudunak (adibidez seinalizazio plataformak) izan litezke (Simons & Ikonen, 1997; Kolesnick *et al.*, 2000; Grassme *et al.*, 2001). Lipido bakoitzak izan ditzakeen elkarrekintza molekularrak, bere ezaugarri fisikoek eta daukan geometria konketuak baldintzatzen ditu, eta elkarrekintza hauen izaeraren arabera, albo banaketak sor litezke.

Phillips *et al.*ek (1970), egoera jakin batzuetan lipidoak alboz banatu, eta egitura aldetik ezaugarri berezidun (lipido faseak) lipido domeinuak sor daitezkeenaren lehen zantzuak plazaratu zituen. Berak, DSCa erabiliz, PC espezie ezberdinen des-nahastea balioztatu zuen. Dena den, ideia honek ez zuen arreta lar jaso (batez ere biologoengandik) Simons eta Ikonenek “raft” (urmaelaren) hipotesia postulatu zuten arte (Simons & Ikonen, 1997). Hasiera batean, raftak, SL eta Cholelan aberastutako

mikrodomeinu iragankor bezala deskribatu ziren, zeintzuk zelula barneko lipidoen trafiko eta zelularen seinalizazioarekin erlazioa daukaten proteina espezifikoekin lotu daitezkeen (Simons & Ikonen, 1997).

Raften definizio gaurkotuago bat ondorengo hau izan daiteke: esterol eta SLetan aberastutako proteina espezifikodun nanoeskala dinamikoko egitura ordenatuak, non atsedendiko egoera metaegonkorra aktibatua izan daitekeen lipido-lipido, proteina-lipido eta protein-proteina elkarrekintza espezifikoak gertatzeko (Simons & Sampaio, 2011). Deskribapen honetan, hasiera bateko “mikro” eskala kontzeptua, “nano” eskalagatik ordezkatu eta 1997ko definizioa natura “iragankorraren” ordezkari, beraien karaktere “dinamikoak” adierazten da (1.12 irudia). Mugimendu mugatua daukaten proteinen presentziak ere, domeinu hauen existentzian eragin garrantzitsua izango luke (Tomishige *et al.*, 1998). Mintzeko proteina integralen zitoesketoko proteinekiko ainguraketak adibidez, translaziozko difusioa (baina ez errotaziozkoa) mugatzen du. Gainera, proteina hauek lotzeaz gain, lipidoak aktinara ere itsats daitezke, zeinak beraien albo banaketa kontrolatuko lukeen (Edidin, 2006).



1.12 irudia. SL eta Chol nahastez sortutako lipid domeinu baten ilustrazioa (Semrau & Schmidt, 2009).

PMak daukan inguru konplexu eta heterogeneoa kontuan hartuta, lipidoek PMan izan lezaketen albo banaketak ikertzeko mintz ereduen sistemak erabili ohi dira. Lipidoen alboz banatzeko gaitasuna, batez ere beraien egiturarekin lotuta dago. Nahiz eta lipidoak zelula mintzetan aurkitzen diren osagai guztien artean soilik bakarra izan, normalean, lipido konkretuak baino ez dira aukeratzen mintz ereduak sortu eta PMan egon litezkeen albo banaketak erreplikatzeko (Feigenson, 2007).

Alde batetik, kate aziliko luze eta asedun lipidoak era dentso batean paketatuta, edo oso antolatuta dauden faseetan banatuta agertu ohi dira. Gainera, normalean, beraien C-C loturak guztiz *trans* konformazioan aurkitzen dira, honela, egitura lineal bat mantenduz. Gertaera honek fase paketatuta eta ordenatuen formazioa errazten du. Beste aldetik, kate azilikoetako lotura bikoitzen presentziak paketatze defektuen eta fase desordenatu eta jariakorren formakuntzan laguntzen du. Temperatura igotzean, *gauche* konformazioak ugartu eta fase desordenatuen sorrera errazten da (Luckey, 2008). Kate azilikoan asegabeteen presentziaz gain, buru polarrek dauzkaten intrintseko ezaugarriek, edota hidrogeno loturak sortzeko gaitasuna bezalako beste faktore batzuek ere, albo banaketan funtsa diren lipido-lipido elkarrekintzetan berebiziko garrantzia dute (Tamm & McConnell, 1985; Edidin, 2003; Veatch & Keller, 2005; Goni *et al.*, 2008).

Tm altuko eta kate aziliko asedun SLak Cholarekin eta fosfatidilkolinarekin nahastean, lipido domeinuak sortzen dira (Goni *et al.*, 2008). Zenbait ikerketen bidez ikusi izan denez, kate azilikoaren ordena molekular berean, Cholak SMarekiko daukan afinitatea, PCak SMarekiko daukan afinitatea baino altuagoa da (Lönnfors *et al.*, 2011). Izan ere, SMaren fase arteko guneak, amida bat, hidroxilo libre bat eta amida karbonil talde bat dauzka. Honek, SMari hidrogeno lotura emaile eta hartzaile gisa jarduteko aukera ematen diolarik (Pascher, 1976; Kolesnick *et al.*, 2000; Slotte, 2016). Bestalde, PCak hidrogeno lotura hartzaile gisa soilik joka dezaketen bi ester karbonil dauzka. Ondorioz, Cholaren eta SMaren arteko elkarrekintzak, PCaren eta SMaren artekoak baino indartsuagoak dira.

Cerak ere, lipido jakin batzuekin nahastean, albo banaketak sortzeko ahalmena dauka (Goñi & Alonso, 2009). Mintz ereduetan ikusi izan denez, SMA eta Cera nahasten direnean, oso ordenatuak diren gel-motako domeinuak sortzen dira (Sot *et al.*, 2006; Busto *et al.*, 2009; Catapano *et al.*, 2011). PMan gertatzen den esfingomielinasa bidezko SMaren degradazioak Cer domeinuak sor ditzake. Hauek, bidezidor apoptosikoen seinalizazioan inplikatuak egon litezke (Kolesnick *et al.*, 2000; Mullen & Obeid, 2012; Henry *et al.*, 2013).

Mintz ereduetan egindako SM, Chol eta Cer nahaste hirukoizdun ikerketetan ikusi izan denez, Chol eta Cerak SMarekin elkar ekitearren lehiatzen dira. Megha eta Londonek (2004), Chol, Cer eta SMdun mintzetan, Cerak Chola raft-motako egituretatik baztertzeko ahalmena duela ikusi zuten (Megha & London, 2004; Chiantia

et al., 2006; Nyholm *et al.*, 2010). Beste ikerketa batzuek ere, SMak Cerarekiko daukan afinitate handiagoa baieztatu dute, ziur aski SMaren hidrogeno lotura ahalmen handiagoa dela eta (Chiantia *et al.*, 2006; Sot *et al.*, 2008). Gainera, SMaren taldeburuaren tamainak garrantzia gutxiago dauka SM eta Ceraren arteko elkarrekintzetan, SM eta Cholaren artean gauzatzen direnetan baino (Artetxe *et al.*, 2013).

Nahiz eta nanodomeinuen existentzia argitaratu zenetik gaiaren inguruko hamaika ikerketa plazaratu diren, ugaztun zeluletan daukaten tamaina txiki, bizi-iragankor eta konposizio molekular konplexuek, egitura hauen ikuskatze zuzena asko mugatu izan dute (Goñi *et al.*, 2020). Legamietan mikroietako tamainadun domeinuak ikusi izan badira ere, kasu hauetan, mintz-zitoeskeleto elkarrekintzak ez du lipidoen eta proteinen difusioa ugaztun mintzetan bezain beste mugatzen (Valdez-Taubas & Pelham, 2003; Rayermann *et al.*, 2017). Mintz ereduetan egin diren ikerketa gehienak, proteinen gabezia eta konposizio jakinetan egin izan badira ere, kontuan eduki behar da zelula bizi baten barnean baldintzak etengabe aldatzen direla. Gainera, gune konkretu bakoitzean, iraupen ezberdina duten eta sortu berri diren ezaugarriak ageri ohi dira (Rosetti *et al.*, 2017).

Atsedenean dauden ugaztun zeluletan, raften tamaina nanometro mailan (10-200 nm) dagoela onartzen da (Jacobson *et al.*, 2007; Simons & Sampaio, 2011; Goñi *et al.*, 2020; Kusumi *et al.*, 2020). Lipido bat normalean 1 $\mu\text{m/s}$ ko abiaduran barreiatzen da, honek zera esan nahi du: lipidoa gutxienez segundo batez egonkorra bada, raftak lipidoaren mugimendua mikroietako distantzian eragin lezakeela. Dena den, raftak ez dira zertan orekan dauden egiturak izan behar (Sezgin *et al.*, 2015). Izan ere, prozesu biologiko motaren arabera, denbora eskala ezberdinetan existitzen direla suposatzen da (maiz milisegundotan).

Aspektu dinamikoei erreparatuz, zelula batean ematen diren inguruaren pH aldaketak, eta zelulara helarazitako seinale kimikoak, normalean, aldi berean ematen diren gertaerak dira. Bestalde, mintz ereduetan soilik aldaketa txiki batzuk hartzen dira aintzat. Aipatzekoa den beste puntu bat albo difusio indizea izango litzateke: zelula kanpo matrizea edo/eta kanpo proteinen presentzia dela eta, ugaztun zelulen mintzek GUV gehienetan aurkitzen den ingurua baino inguru likatsuago bat izan ohi dute (Sahoo & Schwille, 2013).

Lipido geruza bikoitzeko geruzetako batek bestearengan duen eragina ere kontuan hartu beharko litzateke. Mintz eredu gehienek ikerketetan, geruza batean aurkitzen den domeinua beste geruzako domeinuarekin batera kokatzen dela ikusi da (Perlmutter & Sachs, 2011). Dena den, PMA eta Golgi aparatua bezalako mintzak asimetrikoak dira (Verkleij *et al.*, 1973; Devaux, 1991; Lorent *et al.*, 2020). Eremu-hurbileko eskaneatze mikroskopia optikoa (NSOM, ingelesezko near-field scanning optical microscopy), estimulatutako emisio murrizketaren mikroskopia (STED, ingelesezko stimulated emission depletion microscopy) eta egiturazko argidun mikroskopia (SIM, ingelesezko structured-illumination microscopy) bezalako super-erresoluziozko teknikek, perturbatu gabeko zelula bizietako lipido nanodomeinuen existentziaren inguruan argia isurtzen lagun lezakete. Mintz ereduetan domeinuak existitzen direla argi badago ere, benetazko zelulen mintzetan duten existentzia eztabaida handiko gaia da (Munro, 2003; Pike, 2006; Burns *et al.*, 2017; Sezgin *et al.*, 2017; Goñi, 2019). Eztabaida honetako gaur egungo ikuspuntu ezberdinak berriki argitaratutako zenbait berrikuspenetan azaltzen dira (Bieberich, 2018; Goñi, 2019; Goñi *et al.*, 2020; Levental *et al.*, 2020).

1.3. Proteina-Lipido Elkarrekintzak

Lipido geruza bikoitzetan aurkitzen diren proteinek, mintz biologikoetan gertatzen den aktibitatearen gehiengoa gauzatzen dute. Adibidez, karga gabeko molekula txikiak mintzean zehar libreki barreiatu daitezkeen arren, proteinak dira molekula handiagoen difusioa kontrolatzen duten egiturak. Proteina hauetako batzuk zenbait substantzien garraio aktiboa gauzatzen dute; beste batzuk berriz, poroak edo kanalak sortuz, difusioa posible egiten dute. Askok, aktibitate entzimatikoa ere badaukate (Yeagle, 2012). Mintz proteinak normalean kanpo- edo barne-proteina gisa sailkatzen dira. Dena den, horietako askok ez dute beraien bizitza guztia mintzari lotua igarotzen. Proteina batzuk mintzekin elkarrekintza itzulgarriak gauzatzen dituzten bitartean, beste batzuk iraupen-luzeko elkarrekintzak edo elkarrekintza ez-itzulgarriak izaten dituzte (Goñi, 2002). Proteina prenilatuak, gantz azilatutako proteinak eta glikosilfosfatidilinositolari lotutako proteinak (GPI, ingelesezko glycosylphosphatidylinositol-linked proteins) lipido jakinei era sendo batean lotutako proteina integralak dira (Voet *et al.*, 2013). Lipido-proteina elkarrekintza sinpleena, erretikulu sarkoplasmatikoko Ca^{2+} -ATPasa gisa aurkeztu ohi da, egoera jariakorrean dauden fosfolipidoekin ausaz nahasten den proteina hain zuzen ere (Gómez-Fernández

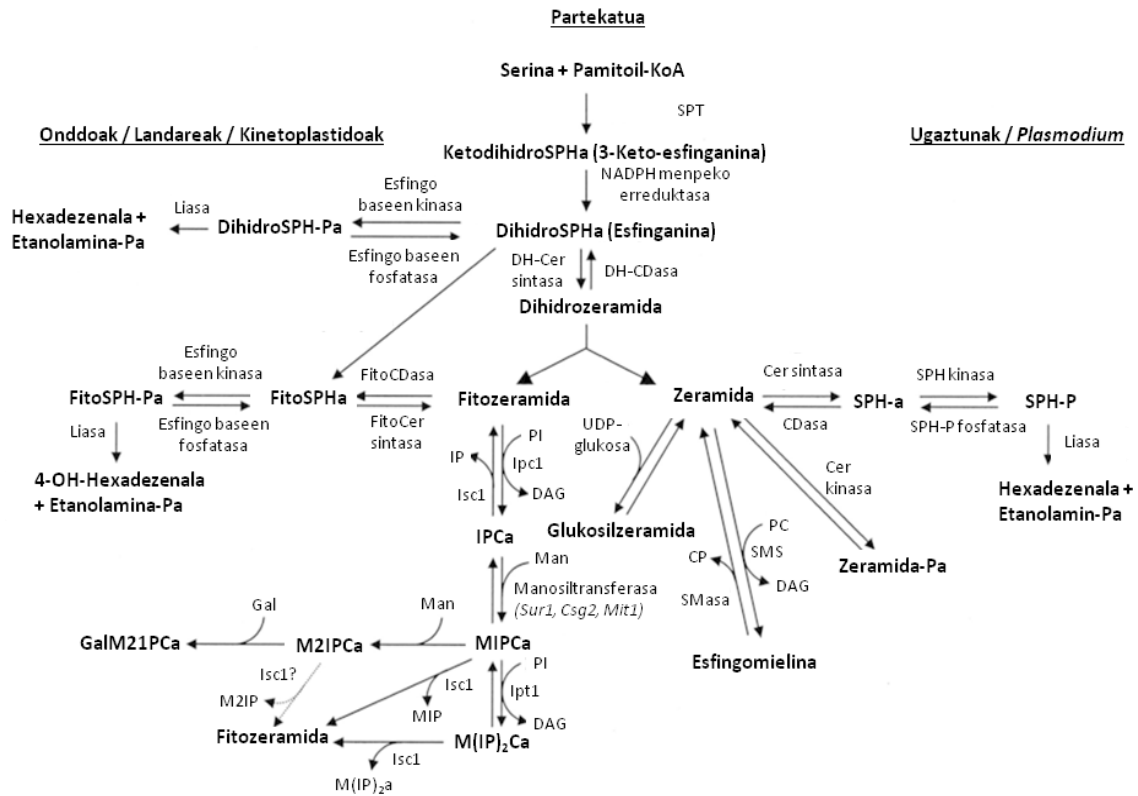
et al., 1979). Proteina domeinu jakin batzuk, fosfolipidoekin mintzaren gainazalean lotzen dira. Beste batzuk berriz, mintzaren okerdura bezalako ezaugarri fisikoak ezagutzen dituzte (Antonny, 2011). Proteina-mintz asoziazioak, mintzaren berezitasun jakin batzuen ezagupena gauzaten duten proteina domeinu espezifikoetan oinarrituak egon daitezke (Hurley, 2006; Lemmon, 2008; Moravcevic *et al.*, 2010).

1.4. Esfingolipidoak

SLak, J.L.W. Thudichumek (1884) aurkitu zituen Sphingx mitologiko gisa izendatuz. Hiru esfingolipido base nagusi existitzen dira: Spha edo (2S, 3R, 4E)-2-amino-4-oktadezeno-1, 3-diola (ugariena), dihidroesfingosina (ugaztun zeluletan), eta fitoesfingosina (4-hidroxi-dihidroesfingosina) (landare eta onddoetan) (Karlsson, 1970). Urte askoz, SLak egitura lipido inertetzat hartuak izan badira ere, SLen seinalizazio bidezidorraren aurkikuntzaren ostean (Hannun *et al.*, 1986; Kolesnick, 1987), hainbat zientzialarik beraienengan arreta jarri zuten. Orduetik, SLak seinalizazio bidezidor ezberdinetan bigarren mezulari gisa jardun dezaketen molekula bioaktibo gisa onartuak izan dira (Kolesnick *et al.*, 2000; Hannun & Obeid, 2008; Bartke & Hannun, 2009; Goñi *et al.*, 2014; Carreira *et al.*, 2015). Izan ere, lipido plataformak sortzeko daukaten gaitasuna, funtzio biologiko ezberdinekin lotu da (Futerman & Hannun, 2004; Goñi & Alonso, 2006; Staneva *et al.*, 2009; Stancevic & Kolesnick, 2010; Castro *et al.*, 2014).

Sph sinpleenetik glikoesfingolipido konplexuagoetara doan SL naturalen aukera zabal bat existitzen da. Seinalizazioan nabarmenenak diren bost SLak, SMA, Spha, Cera, SIPa eta Cer1Pa dira (Goñi *et al.*, 2014; Gomez-Munoz *et al.*, 2016). Beraien biosintesia, batez ere erretikulu endoplasmatikokoan eta Golgi aparatuan gertatzen da: Sintesiaren lehen pausua erretikulu endoplasmatikokoan gertatzen da; hemen, serina palmitoiltransferasa (SPT, ingelesezko serine palmitoyltransferase) entzimak, L-serina eta azil-koenzimaA kondentsatzen ditu 3-ketoesfinganina sortzeko. Badirudi entzima honek SLen biosintesiko mugatze pausua katalizatzen duela, beraz SLen erregulazio homeostasikoaren entzima kritikotzat hartzen da. Hurrengo urratsean, NADPH menpeko erreduktasa baten bidez, 3-ketoesfinganina, dihidroesfingosinara erreduzitzen da. Gero, dihidrozeramida sintasa bidez dihidrozeramidara azilatu, eta ostean, dihidrozeramida desaturaza bidez, Cera sortzeko desaturatzen da (1.13 irudia). Cera zelularen lipido homeostasian funtsezko molekula dela pentsatzen da. Izan ere, SL arrunten eta dihidroesfingolipidoen oreka arau lezake (Fabrias *et al.*, 2012). Orain arte

dihidroesfingolipidoak gehien bat lipido inertetzat hartuak izan direnez, ez dira sakonki ikertu. Dena den, zenbait ikerketek biologikoki aktiboak izan daitezkeela iradokitzen dute (Siddique *et al.*, 2015).



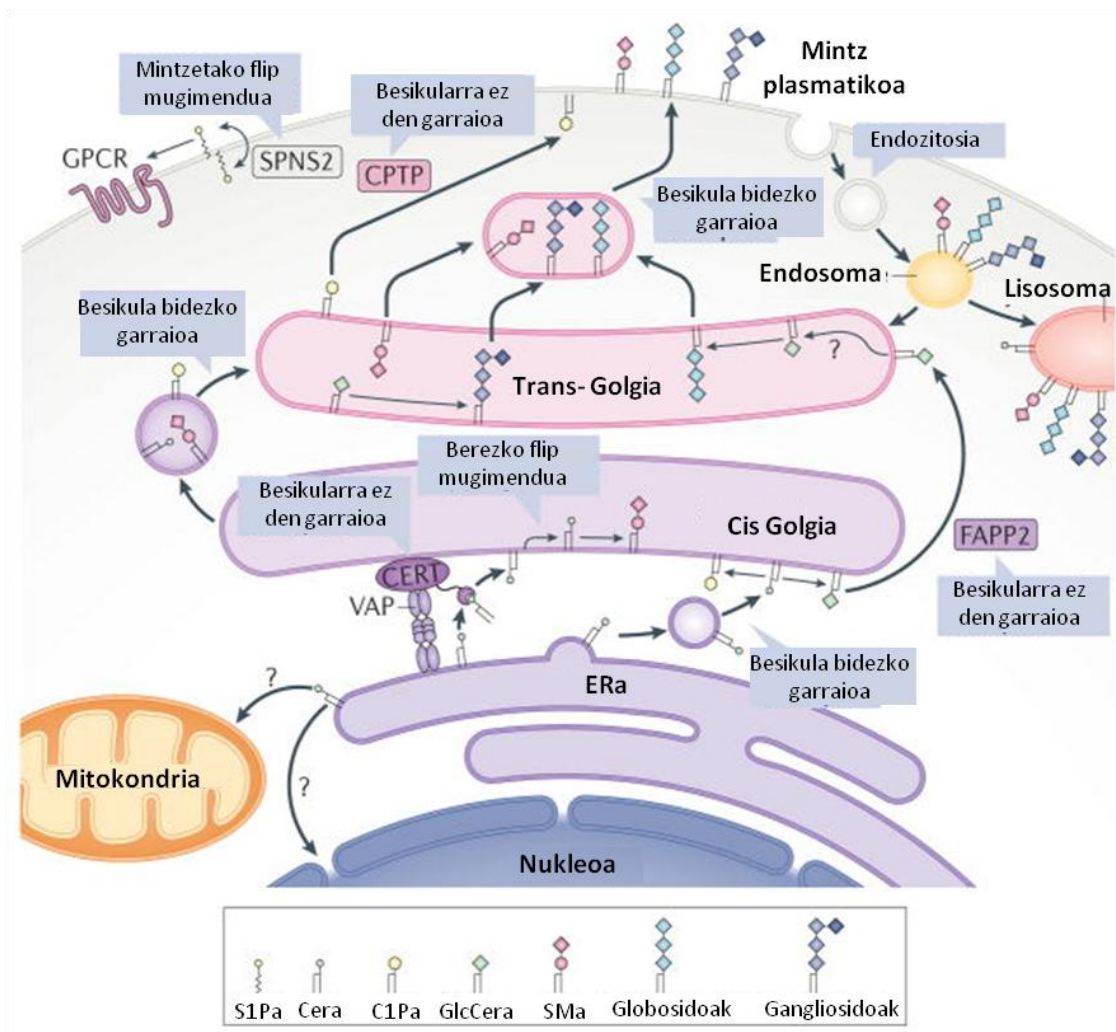
1.13 irudia. SLen sintetirako bidebidorra (Heung *et al.*, 2006).

Ceraren biosintesiko entzima guztiak erretikulu endoplasmaticoaren mintzaren zitosoleko orrian daude (Tidhar & Futerman, 2013). Dena den, SMaren biosintesiaren azken pausua Golgi aparatuko lumen aldeko mintzean gertatzen da (Huwiler *et al.*, 2000). Cera, proteina espezifikoaren bidez Golgi aparatua garraiatu eta bertan SMa eta glikoesfingolipido konplexuak sintetizatzen dira. Hauek, besikula bidezko garraioz PMra eramaten dira (1.14 irudia).

Zelula lerro eta funtzioaren arabera, SL sintesiaren bidebidorra ezberdina izan daiteke. Ondorengo eran sailkatzen da (Sadeghlar *et al.*, 2000):

- *De novo* sintesia. SPT entzimak gauzatutako L-serina eta palmitoil-KoAren kondentsazio bidez hasten da. 3-ketodihidroesfingosina sortzen da, zeina, aurretik azaldu den bezala, hainbat SLtara eraldatua izango den (Gault *et al.*, 2010).

- Lisosometako hidrolisi bidezko birziklapenaren bidezidorra. Lisosometako SLaren hidrolisiaren bidez Spha eta esfinganina sortzen dira. Molekula hauek (dihidro)zeramida sortzeko birazilatu eta ondoren Golgira garraiatu daitezke, non metabolizatuagoak izan daitezkeen (Gillard *et al.*, 1998).
- Golgi aparatu bidezko SL natibo edo partzialki hidrolizatuak dauden SLen birziklapena. Beharrezko du glikoesfingolipido natibo, edo partzialki hidrolizatuak dauden glikoesfingolipidoak endosometatik Golgi aparatura garraiatzea, non azukre kateak luzatuak izan daitezkeen (Robinson *et al.*, 1992).
- PMan gertatzen den sintesia. SMA PMan kokatua dagoen SM sintasa bidez sintetiza daiteke. Dena den, bidezidor honek ziur aski eragin txikia du. Izan ere, Golgi aparatuan gertatzen den sintesiarekin alderatua oso urria da (Futerman *et al.*, 1990; Van Helvoort *et al.*, 1994).



1.14 irudia. SL metabolismoaren konpartimentalizazioa (Hannun & Obeid, 2008).

SLen metabolismoaren modulazioaren ikerketa, Niemann-Picka, Alzheimerra, Parkinsona, esklerosi anizkoitza edo Huntingtona bezalako hainbat gaixotasunen aurka jarduteko estrategia baliagarria izan daiteke (Barth *et al.*, 2011; Morad & Cabot, 2012; Dai *et al.*, 2014; Giussani *et al.*, 2014; Hannun & Obeid, 2018; Matanes *et al.*, 2019).

1.4.1. SMaren sintesia eta SPT entzima

SL mota guztien artean, ugaztun zeluletan SMA (kolina fosfozeramida) da ugariena, fosfolipido guztien %5-10a osatzen duelarik. Maila baxuagoko zenbait animalia zelulek, SMA izan ordez, etanolamina fosfozeramida dute (Hori & Sugita, 1993). Onddo eta landare zelulek berriz, fosfoinositoldun SLak sortzen dituzte (Dickson, 1998).

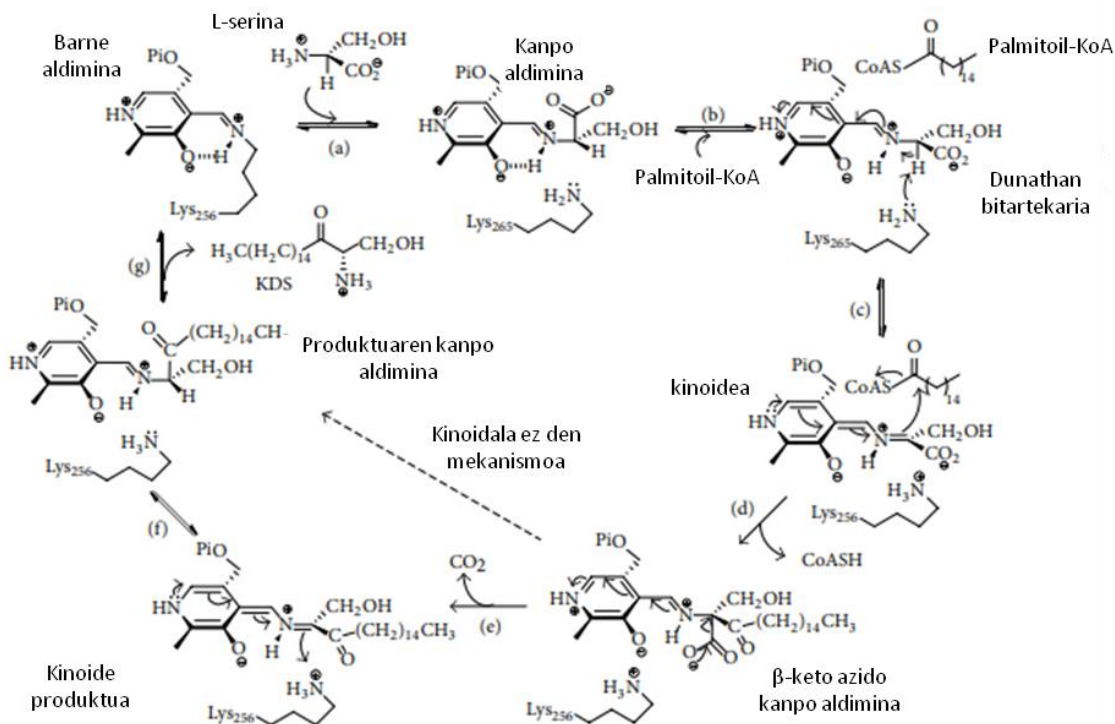
SM sintesiaren bidezidorra eta hau gertatzen den zelula barneko kokapen zehatza oraindik eztabaidatuak diren arren, pausu nagusiak Golgi aparatuan eta PMan gertatzen direla uste da. Zenbait ikerketetan, SMaren sintesia trans-Golgian (TG) gertatzen dela iradoki da (Griswold, 1998; Sadeghlar *et al.*, 2000). Gainera, SMaren gehiengo *de novo* bidezidorraren bidez sortzen dela pentsatzen da, zeinaren azken pausuan fosforilkolina talde bat Cerera transferitzen den. Bidezidorreko entzima nagusia SPT entzima da. SPTak serina eta palmitoil KoAren arteko kondentsazioa gauzatzuz 3-ketodihidroesfingosina sortzen du. Bere erregulazioak SLaren bitartekari metabolikoen, esfingo baseen eta Ceraren pilaketa ekiditen du. Izan ere, molekula hauek, kantitate handian zelularentzako kaltegarriak izan daitezke.

SPTaren aktibitatea Lcb1 eta Lcb2 (LCB1 eta LCB2 geneak) izeneko 2 azpiunitaterekin lotuta dago (Pinto *et al.*, 1992). Ugaztunen cDNA homologoei eta bere produktuei dagokienez ere, LCB1 eta LCB2 nomenklatura erabiltzen da, nahiz eta SPTLC1 eta SPTLC2 erabiltzea egokiagoa izango litzateke. 1997an, ugaztunen cDNA homologoak diren LCB1 eta LCB2 sagu, gizaki eta Txinako Hamsterraren Obarioko (CHO, ingelesezko Chinese Hamster Ovarian) zeluletatik isolatuak izan ziren (Hanada *et al.*, 1997). CHO zeluletan purifikatutako entzima honetan LCB1 eta LCB2 azpiunitateak 1:1 erlazioan zeudela ikusi zen (Hanada *et al.*, 2000).

SPTa AOS (ingelesezko α -oxoamine synthase) familiako PLP (ingelesezko pyridoxal-5-phosphate)-menpeko entzima da. Deskarbozilaziozko Klaseina-motako kondentsazio erreakzio baten bidez 3 ketodihidroesfingosina sortzen du. Eukariotoen

SPT entzimak mintzari lotutako hainbat azpiunitateko entzimak diren bitartean, bakterioen entzimak homodimero zitoplasmatikoak dira.

Bakterioen SPTetan oinarrituz, 3 dimentsioko egiturak proposatu izan dira. *S. paucimobilis* izeneko bakterio Gram-negatibo baten SPTaren isolaketak, entzima honen egituraren ikerketa gauzatzea ahalbidetu zuen (Ikushiro *et al.*, 2001). SPTak katalizatzen duen erreakzio entzimatikoa ondorengo eran laburbil daiteke (1.15 irudia): (a) L-serina bidezko barne aldiminaren transaminazioa, kanpo aldimina PLP-L-serina bitartekaria sortuz; (b) palmotoil-KoAren loturak konformazio aldaketa eta Lys265 bidezko kanpo aldimina baten deprotonazioa eragiten du, horrela kinoide / karbanioi bitartekari bat sortuz; (c) kinoide / karbanioiak tioesterra erasotzen du, (d) β keto azidoaren kanpo aldiminaren sorrera eta KoASHaren kanporaketa; (e) CO_2 aren kanporaketa ketodihidroesfingosina produktu kinoidea sortzeko; (f) ketodihidroesfingosinaren birprotonazioa; (g) ketodihidroesfingosina kanporatzeko transaminazioa eta Lys 265ri lotutako PLP bidezko barne aldiminaren konponketa.



1.15 irudia. SPTaren erreakzio mekanismoaren proposaketa (Beattie *et al.*, 2013).

Legamien eta ugaztunen aminoazido mailan %40ko antzekotasuna existitzen da, ugaztun ezberdinen artean berriz %95ekoa (Hanada *et al.*, 1997). Giza LCB1 (SPTLC1) genea, 15 exoiz osatua dago (85kbp inguru, 9q21-q22 kromosoman kokatuta). LCB2

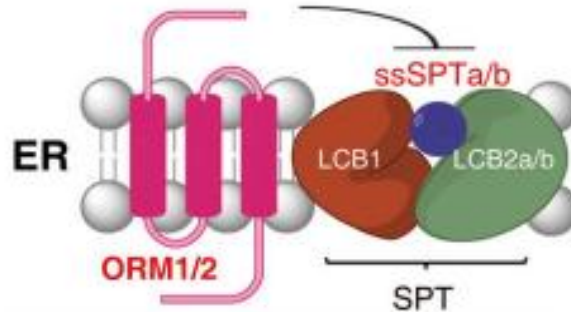
(SPTLC2) geneak berriz 12 exoi dauzka (110 kbp, 14q24.3–q31 kromosoman kokatuta).

Ugaztunetan LCB1 eta LCB2 azpiunitateek %20ko antzekotasuna partekatzen dute (53- eta 63-KDa hurrenez hurren) (Hanada *et al.*, 1997). Bakoitzak oso hidrofobikoa den mintz-arteko domeinu bakarra dauka (Weiss & Stoffel, 1997). Ikerketek iradokitzen dutenaren arabera, LCB1 eta LCB2a erretikulu endoplasmatikoko I motako mintzeko barne-proteinak dira, non LCB1aren N eta C amaierak lumen eta zitosolerantz begira dauden hurrenez hurren (Yasuda *et al.*, 2003). Gune katalitikoa zitosolera begira dagoela proposatua izan da (Mandon *et al.*, 1992).

Hornemann *et al.*ek (2006) LCB2aren beste isoforma bat (SPTLC3 geneak kodetutako LCB3a) identifikatu zutenetik, eukariotoen SPT konplexuaren azpiunitate eta arautzaile gehigarrien existentzia iradoki da. Bi isoforma hauek ugaztunetan funtzio ezberdina izan lezakete (nahiz eta landareetan funtzionalki erredundanteak diren) (Dietrich *et al.*, 2008). *Drosophila* eta antzekoek soilik isoforma bat daukaten bitartean, badirudi goi mailako eukariotoek LCB2-motako bi isoformak dauzkatela. Izan ere, Gable *et al.*ek (2000) heterodimeroarekin elkartutako, eta legamien SPTaren aktibitate optimorako beharrezkoa den, Tsc3 izeneko azpiunitate txiki gehigarri bat aurkitu zuten. Gainera, ugaztunetan, LCB1–LCB2 (*SPTLC1/SPTLC2* edo *SPTLC1/SPTLC3*) dimerora lotzean, SPTaren aktibitatea 10 aldiz handitzeko ahalmena daukaten beste azpiunitate txiki bi (ssSPTa eta ssSPTb) identifikatu dira. Breslow *et al.* (2010) eta Han *et al.*ek (2010), legamien orosomukoide (ORM, ingelesezko orosomucoide) proteinek SPTaren aktibitatea negatiboki arautzen dutela ikusi zuten. Badirudi SPT konplexuak lau LCB1-LCB2 heterodimerodun konplexu oktamerikoa sor lezakeela, eta ziur aski, ssSPT, ORM eta Sac1 azpiunitateekin harremana daukala (Bourquin *et al.*, 2011) (1.16 irudia).

SPT aktibitate ez-egokidun ugaztun zelula lerroei dagokienez, 1990ean, SL biosintesisirako tenperaturarekiko sentikorra zen SPT termolabildun CHO zelularen mutante bat isolatu zen, SPB-1 izeneko (Hanada *et al.*, 1990). Zelula honek ezin zuen 40°Ctan SLrik *de novo* sintetizatu. Beraz, tenperatura honetan zelulen hazkuntza egoki bat izateko, zelulek kanpotik gehitutako SL iturri bat behar zuten. SPB-1 zelula lerroan oinarrituz, ez soilik 40°Ctan, baizik eta edozein tenperatura fisiologikotan, bere hazkuntza egoki baterako SL gehikuntza bat behar zuen CHO zelula mutante bat

sintetizatu zuten, LY-B zelula lerroa hain zuzen ere (Hanada *et al.*, 1998). Ebidentzia hauekin, SPTa, eukariotoen SLen *de novo* sintesirako hasierako urratsaren arduraduna zela frogatu zen.



1.16 irudia. SPT konplexuarentzako proposaturiko eredua. [Li *et al.* (2016)etik birmarraztua].

SPT aktibitate gabeko giza zelula lerroak ere sintetizatuak izan dira. Honen adibide da HAP1 SPTLC1(-) zelula lerro ia haploidea (ingelesezko near haploid). Organismo eukarioto gehienek guraso bakoitzetik genoma kopia bat heredatzen dute (diploideak izanik), ondorioz, kopia baten delezio mutazioak, normalean, beste kopiaren bidez konpentsatuak izan ohi dira. Beste hitz batzuetan, alelo bat aldatzen denean, fenotipo mailako ondorioak beste aleloarekin estaltzen dira. Konpentsazio hau ekiditeko, ondo ezagutzen den estrategia bat zelula lerro ia haploideak erabiltzean datza. Gizakietan, leuzemia (Oshimura *et al.*, 1977; Andersson *et al.*, 1995) eta kondrosarkomak (Bovée *et al.*, 1999) bezalako tumore batzuk ia haploideak diren zelula somatikoak dauzkate. Honela ba, leuzemia mieloide kronikodun gaixo batetik abiatuz, KBM-7 giza zelula lerro ia haploide bat isolatzea eta era egonkor batean kultibatzea lortu zen (Kotecki *et al.*, 1999). Zelula lerro honek kromosoma guztien kopia bakarra dauka, 8. Kromosoma osoa, eta 15. kromosomaren zati bat izan ezik.

Ama zelula pluripotenteak sortzeko, KBM-7 zelulak birprogramatu (Takahashi & Yamanaka, 2006; Carette *et al.*, 2010) eta fibroblasto morfologiadun HAP1 zelula lerro ia haploidea sortu zen (Carette *et al.*, 2011). HAP1 zelulak, itsatsita hazten diren, eta 8. kromosomaren bigarren kopia ez daukaten, baina 15. kromosomaren zati baten bi kopia (bat 19. kromosomara fusionatua) mantentzen dituzten zelulak dira (SPTLC1 genea 9q21–q22 kromosoman kokatuta dago). HAP1 zelulak CRISPR/Cas bidez editatuz, beraien SPTLC1 genearen 4. exoiean 11 bpko delezio bat eragin eta SPT defektibodun HAP1 SPTLC1(-) (edo HAP-SPT) giza zelula lerro bat sortu zen.

Tesi honetan, zelulen mintzetatik SMA eta beste SL batzuk kentzean hauek jasaten dituzten eragin biofisikoak ikertzearen helburuz, CHO eta HAP1 basatiak eta SPT aktibitate gabeko LY-B eta HAP1-SPT zelula lerro mutatuak erabili dira.

1.4.2. SPTa eta gaixotasun genetiko bat

Nerbio sistema zentrolean lipido mota anitz aurki daitezke, garun garapen arrunt eta neuronen funtzionamendu egoki baterako denak beharrezkoak direlarik (Eoin, 2005; Chianese *et al.*, 2017). Lesio mekaniko edota patologiarene batek lipidoen bidezidorrean eragindako neuronen edozein anormaltasunen ondorioz, hainbat motako gaixotasun neurodegeneratibo, desoreka mental, edo apoplexia sor daitezke (Shamim *et al.*, 2018). Ikusi izan denez, Alzheimerra, Parkinsona, Esklerosi Anizkoitza, Huntingtona, eskizofrenia eta desoreka bipolarrak bezalako hainbat gaixotasun neurodegeneratibo, lipido homeostasiaren erregulazio ez egoki batekin lotuak egon daitezke (Zarrouk *et al.*, 2018; Hallett *et al.*, 2019).

Behe gorputz adarren eta neurona autonomoen degenerazioa eragiten duen I motako herentziazko zentzumen neuropatia (HSN1, ingelesezko hereditary sensory neuropathy type I) izenekoa ere, lipidoen erregulazio ez egoki batekin lotutako gaixotasuna da (Dyck, 1993). HSN1a, 9q22 kromosomako akats batekin lotu da. Akats honek, giza LCB1ean (SPTLC1) mutazio bat eragiten duen Cys133 edo Val144 aminoazido hondarretan du eragina. Bejaoui *et al.*ek (2002) erakutsi zutenaren arabera, nahiz eta HSN1 gaixoen orekako LCB1 eta LCB2 azpiunitate kantitateak normalak izan, HSN1 linfoblastoek SPT aktibitatea, eta beraz SLen *de novo* sintesia, murriztua dute. Ikusi izan denez, mutaturako LCB1 proteinek LCB2 azpiunitatearekin lotuz konplexua sortzeko ahalmena mantentzen badute ere, SPT ez aktibo bat sortzen dute. Jakina da, LCB1eko aminoazido sekuentziako Cys133 eta Val144 ingurua legamietatik ugaztunetara oso kontserbatua dagoela, eta biak, LCB2aren PLP-lotura gunetik hurbil kokatuak daudela iradoki da (Gable *et al.*, 2002). Hori dela eta, aminoazido sekuentzia hau gune katalitikoaren formakuntzan inplikaturik dagoela uste da.

1.5. Helburuak

Tesi honetan, SLEk zelula hazkuntzan eta mintzen konposizio eta ezaugarri fisikoetan duten eginkizuna ikertu nahi da.

Tesi honetako helburu zehatzak ondorengoak dira:

- CHO eta HAP1 zeluletan SMA eta beste SL batzuk gutxituak direnean, PMaren, eta zelula barneko mintzen jariakortasunaren aldaketak definitzea (laurdan fluoroforoz neurtutako “polarizazio orokor” bidez).
- CHO eta HAP1 zeluletan SMA eta beste SL batzuk gutxituak direnean, PMaren, eta zelula barneko mintzen, apurtze indarrek jasaten dituzten aldaketak Indar Atomikozko Mikroskopioz bereizgarritzea.
- CHO eta HAP1 zeluletan SMA eta beste SL batzuk murriztuak direnean, masa espektroskopia (lipidomika) erabiliz, PMak eta zelula barneko mintzek eragiten duten lipidoen erantzun homeostasikoaren inguruko informazioa lortzea.
- SLen inguruan dagoen informazio zelular eta molekularra oinarritzat hartuz, gure aurkikuntzak SLEk zelulan duten funtzioaren deskripzio bateratu bat definitzea.

2. KAPITULUA

TEKNIKA ESPERIMENTALAK

2. KAPITULUA: TEKNIKA ESPERIMENTALAK

2.1. Lipido Ereduen Sistemak

Zelula mintzak, lipidoez gain, proteinaz eta azukrez osatuta daude. Mintzek, zelula eta organulu motaren arabera aldakorra den konposizio oso konplexua daukate. Konplexutasun eta aldakortasun horiek dira hain zuzen ere, eredu sistemak benetako mintzak modu definitu eta sinplifikatuago batean imitatzeko erabiltzearen arrazoi nagusia. Mintz ereduaren artean erabilienak, geruza bakarrak, geruza bikoitz leunak eta liposomak dira. Mintz ereduak, lipido puruzko konposizio sinplez edo konplexuagoak diren benetako zelulen mintzen erauzkinez osatuak egon daitezke. Lipido nahastura horietan proteinak gehituz, errealistagoak diren mintz biologikoak garatu daitezke. Lipido eredu sistemak oso erreminta erabilgarriak dira mintzen osagaien, ezaugarri biofisikoen, eta bertan gertatzen diren elkarrekintzen ikerketetan.

Gaur egun arte, mintzen ezaugarri biofisikoen gehiengoa, mintz ereduaren bitartez ikertua izan da. Lehen mintz eredu sistema esperimentalak, gaur egun “Langmuir monogeruza” gisa ezagutzen dena izan zen. Sistema hau, aire-ur fase-arte batean zabalduko fosfolipido geruza batean oinarritzen da (Langmuir, 1917). Urteen poderioz, Langmuir monogeruzak eta bere eraldaketak, mintzen eta filmen ikerketa biofisiko asko gauzatzeko erabili izan dira.

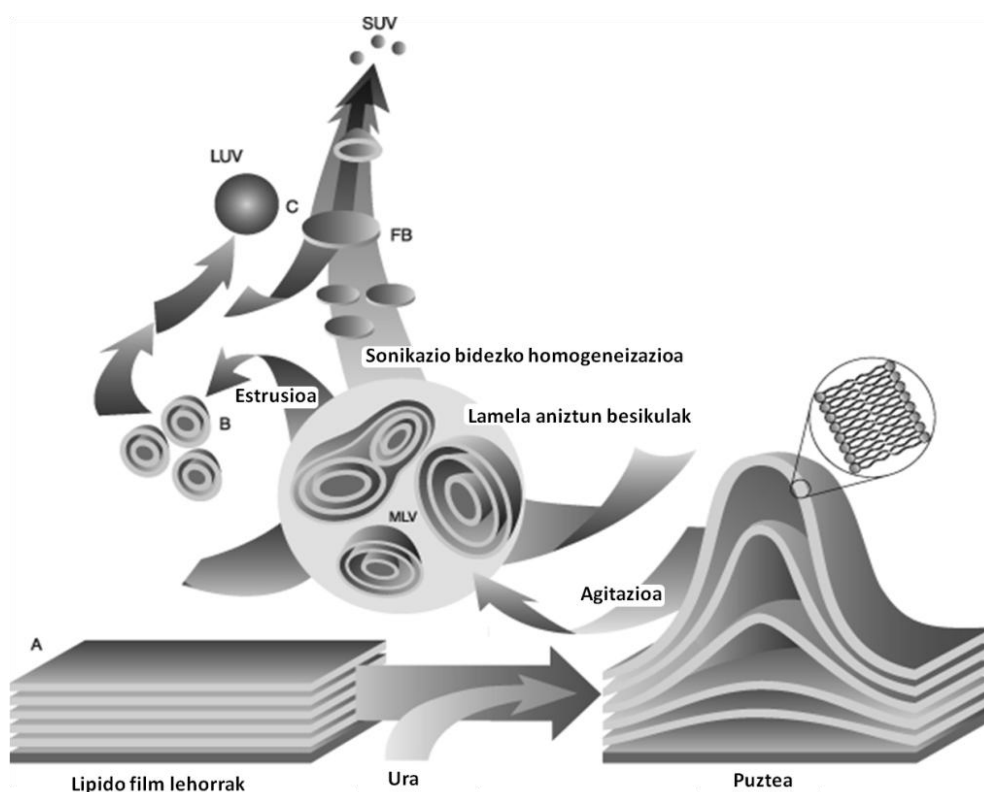
Mueller eta Rudinek (1962), lipido mintz beltz (BLM, ingelesezko black lipid membrane) gisa ezagutzen den sistema eredu erabilgarri bat deskribatu zuten. BLM bat, zulo txikidun (mm 1 baino txikiagoa) plastikozko orri sendo batek bitan banatutako ml gutxiko edukieradun ganbera bat erabiliz sortzen da. Intereseko fosfolipidoz (disolbatzaile organikoan disolbatua) bustitako pintzel bat erabiliz, zulo honetan zehar lipido geruza bikoitza sortzen da. BLMa, ioi kanal, edota mintzean txertatzeko gaitasuna duten proteinak ikertzeko erabil daiteke. Muntaiaren bidez konduktantzia bezalako ezaugarriak era zuzen batean neur baitaitezke.

Bi hamarkada geroago, Tamm eta McCannellek (1985), sostengatutako lipido geruza bikoitzak (SLB, ingelesezko supported lipid bilayers) izeneko mintz eredu sistema erabilgarri bat deskribatu zuten. SLBak, normalean, intereseko konposiziodun

fosfolipido besikulak gainazal jakin baten gainean gehitu eta berezko era batean fusionatu ostean gainazalean zehar zabalduz sortzen dira. SLB eredu sistema, indar atomikozko mikroskopia (AFM, ingelesezko atomic force microscopy) bidezko ikerketak gauzatzeko erreminta egokia da (Singh & Keller, 1991).

Mintz eredu sistema guztien artean erabiliena, fosfolipido besikulak edo liposomak dira. Hauek, Alec D. Bangham (1964) hematologo Britaniarrak, “mesofase esmetiko” gisa deskribatu zituen.

Lipido molekula disoluzio urtsu batean dispersatzean, berez, disoluzio urtsu hori beraien baitan barneratzen duten lipido geruza bikoiztun egiturak sortzen dira (Bangham & Horne, 1964) (2.1 irudia). Egituraketa hau, lipidoen natura anfipatikoaren ondorioz gertatzen da; buru polarrak disoluzio urtsuarekin kontaktuan eta azil kate hidrofobikoak bertatik urrun kokatzen direlarik.

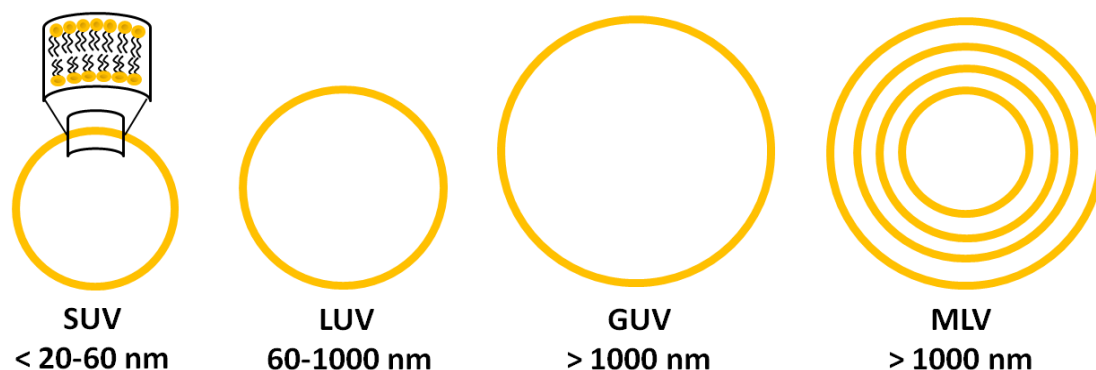


2.1 irudia. Liposomen formakuntza eskema. <http://avantilipids.com-etik> hartua.

Nahiz eta liposometatik lortutako emaitzak ezin daitezkeen era zuzen batean zelula mintzetan gertatzen denarekin lotu, mintz osagaien elkarrekintzak ebaluatzeko erabil daitezke. Liposomak, mintz fusioa, fisioa, jarioa, disolbagarritasuna, flip-flop

mugimendua eta lipido-proteina elkarrekintzak bezalako hainbat fenomeno biofisiko neurtzeko erabiltzen dira. Gainera, industria farmazeutiko, kosmetiko eta janari eta nutrizio industrietan, kapsulatutako molekulen garraiatzaile izateko ere balio dute (Yingchoncharoen *et al.*, 2016). Beraien erabilera medikoen artean esanguratsuena, minbizien aurkako terapietan droga garraiatzaile gisa jardutearena da (Fenske & Cullis, 2008; Tan *et al.*, 2010).

Liposomak, beraien artean, daukaten geruza edo lamela kopuru eta diametroaren arabera ezberdintzen dira. Lamela kopurua kontuan hartuz, lamela bakarreko eta lamela aniztun liposomak ezberdin ditzakegu. Lamela bakarrekoei dagokienez, geruza bikoitz bakar batez osatuak daude eta tamainaren arabera, geruza bakarreko besikula txikiak (SUV, ingelesezko small unilamellar vesicles) (20-60 nmko diametroa), geruza bakarreko besikula handiak (LUV, ingelesezko large unilamellar vesicles) (100-1000 nmko diametroa), edo geruza bakarreko besikula erraldoiak (GUV, ingelesezko giant unilamellar vesicles) (μm 1 baino gehiagoko diametroa) izan daitezke. Lamela bat baino gehiago dauzkatenak, lamela anitzeko besikula (MLV, ingelesezko multilamellar vesicles) gisa ezagutzen dira (2.2 irudia).



2.2 irudia. Tamaina ezberdineko liposomen errepresentazioa eta fosfolipido egituraketa.

(Irudia ez dago eskalan marraztua).

2.1.1. Geruza anitzeko besikulak (MLV)

MLVen formakuntza liposoma guztien artetik sinpleena eta azkarrena da. Bangham (1964) konturatu zen, lipidoak uretan dispertsatzean, zenbait lamela zentrokidedun “esferulozito” batzuk sortzen zirela. Deskribatu zituen egiturak, gaur egun MLV gisa ezagutzen diren lamela anitez osatutako lipido besikulak ziren. Liposoma hauek era erraz batean lor daitezke aurretik hutsean lehortutako lipido film

baten gainean ur disoluzio bat gehitu eta lagina nahasiz. MLVek, normalean 7–10 geruza bikoitz zentrokide izan ohi dituzte, eta tamainan heterogeneoak (mikroi bat eta zenbait mikroien artean) dira. DSCaren, NRMaren edo X-izpiaren bidez, MLVak lipido faseen karakterizaziorako erabil daitezke.

1. Protokoloa. Geruza anitzeko besikulak (MLV)

1. Intereseko lipido kontzentrazioak kloroformo/metanol (2:1/v/v)ean disolbatuz, lipido stockak prestatzen dira.
2. Stocketik abiatuz, beirazko test tutuetara behar den lipido kantitatea gehitzen da.
3. Nitrogeno gas fluxu bat erabiliz disolbatzaile organikoa lurruntzen da.
4. Disolbatzaile organikoaren edozein traza guztiz baztertzeko eta lipido film lehor bat lortzeko, lagina huts handiko lehorgailu batean jartzen da (gutxienez 2 orduz).
5. Lipidoa hidratatzeko filmaren gainean disoluzio urtsu bat gehitu (lipidoaren trantsizio fase nagusiko tenperaturaren gainetik) eta suspentsioa bortex bidez nahasten da.
6. Puntu honetan MLVak dagoeneko sortuak badaude ere, laginak 10 minutuz bainu sonikazioz sonikatuz lagin homogeneoagoak lortzen dira (hidratazio tenperatura berean).
7. Fiske entseguaren bidez azken lipido kontzentrazioa txekiatzen da (ikusi 2.3 atala).

2.1.2. Lamela bakarrekoko besikulak

Lamela anitzeko besikulak prestatzea erraza eta azkarra bada ere, zenbait fenomeno biofisikoren ikerketa gauzatzeko lamela bakarrekoko egiturak behar dira. MLVen tipula itxurako egitura oztopo garrantzitsua izan daitekeen kasuetan lamela bakarrekoko besikulak erabili ohi dira.

2.1.2.1. Lamela bakarrekko besikula handiak (LUV)

LUVak prestatzeko, polikarbonatozko mintz porotsuetan zehar MLVen estrusio mekanikoa gauzatzen da (Mayer, 1986).

2. Protokoloa. Lamela bakarrekko besikula handiak (LUV)

1. MLVak sortzen dira (1. protokoloa).
2. MLVei 10 izozte/urtze ziklo burutzen zaizkie.
 - a. Nitrogeno likidoa (min 1), laginak izozteko.
 - b. Ur bainua (3 min), laginak urtzeko (lipidoaren trantsizio fase nagusiko tenperaturaren gaineratik).
3. Laginak intereseko diametroko porodun polikarbonatozko mintzean zehar (0.1-0.4 μm) 10 aldiz estruitzen dira. Prozesuan zehar, tenperatura, lipidoen trantsizio fase nagusiko tenperaturaren gaineratik egon behar da.
4. Metodologian zehar izandako lipido galeraren ondorioz, Fiske entseguaren bidez laginek duten fosfato (P) kontzentrazioa txekiatzen da (ikusi 2.3 atala).
5. Argi barreiatze dinamikoa (DLS, ingelesezko dynamic light scattering) erabiliz besikulen tamaina txekiatzen da (ikusi 2.4 atala).

2.1.2.2. Geruza bakarrekko besikula txikiak (SUV)

SUVak besikula diren mintz eredu sistema txikiak dira. Tamaina txiki honek (60 nm inguru) okerdura estres handia ematen die, horrela, mintz fusio eta fisio prozesuak ikertzeko modelo egokian bihurtuz (Nieva *et al.*, 1989). Beraien kanpo monogeruzako lipido kontzentrazioa barnekoa baino altuagoa da (Szoka & Papahadjopoulos, 1980).

SUVak lortzeko, MLVak bainu sonikazioz edo punta bidezko sonikazioz sonikatzen dira.

3. Protokoloa. Lamela bakarreko besikula txikiak (SUV)

1. MLVak sortzen dira (1. protokoloa).
2. SUVak sortzeko MLVak bi modutan sonika daitezke:
 - a. Ordu batez FB-15049 (Fisher Scientific Inc., Waltham, MA) bainu sonikatzailaren (hidratazio tenperatura berberean) bidez.
 - b. Soniprep 150 (MSE, Londres, EB) punta sonikatzaila bidez. 10 s *on*, 10 s *off*, 40 min eta 11.5 Hz-ko frekuentzian. Sonikazioan erabilitako titaniozko puntaren hondarrak hauspeatzeko asmoz, laginak zentrifugatu egiten dira.
3. Metodologia honek eragin lezakeen lipido galeraren ondorioz, Fiske entseguaren bidez azken lipido P kontzentrazioa txekiatzen da (ikusi 2.3 atala).
4. DLS bidez besikulen tamaina balioztatzen da (ikusi 2.4 atala).

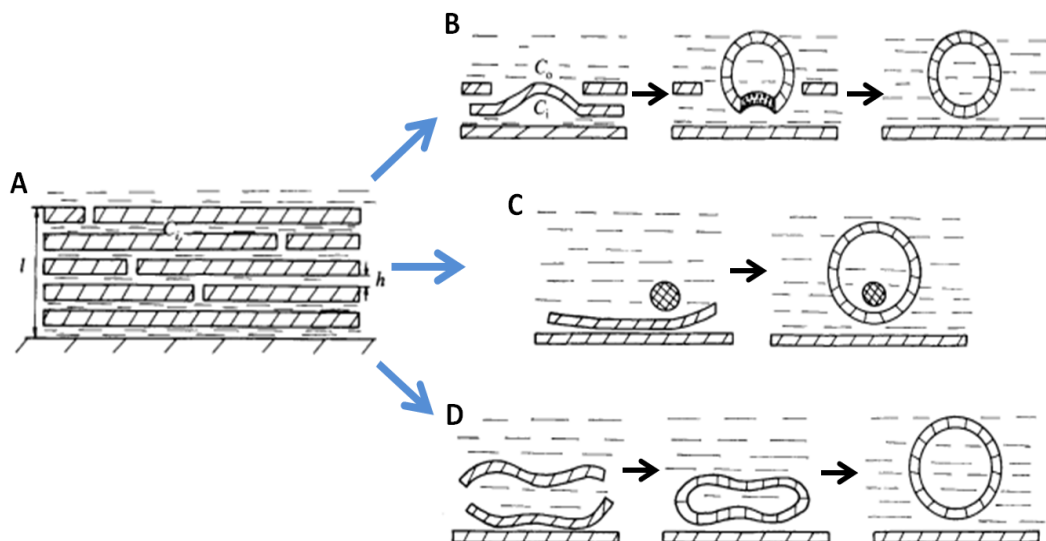
Lan honetan, SUVak **a)** AFM neurketetarako beharrezko diren zelulen lipido erauzketaz egindako sostengatutako geruza bikoitz lauak (SPB, ingelesezko supported planar bilayers) sortzeko; **b)** zelulen erauzketa lipidikoen laurdan bidezko polarizazio orokorraren (GP, ingelesezko general polarization) neurketetarako eta **c)** zelulak esfingolipido (SL, sphingolipids) gehigarri elikatzeke, erabili dira.

2.1.2.3. Lamela bakarreko besikula erraldoiak (GUV)

Mintzak ikuskatzeko SUVak eta LUVak baino handiagoak diren mintz ereduak behar dira; mikroietako tamainadun diametroa (zelula baten tamaina) daukaten GUVak hain zuzen ere.

GUVak, Reeves eta Dowbenek (1969) deskribatu zituzten. GUVak sortzeko, lipido film lehorrak 24 orduz lipidoen trantsizio fase nagusiko tenperaturaren gainetik zegoen disoluzio urtsuen eraginpean jarri zituzten. Urteen poderioz jatorrizko teknika

hobetua izan da, eta gaur egun existitzen den GUVen formakuntzarako metodo erabiliena Angelova *et al.*ek deskribatu zutena da. Metodo hau, lipido film lehorrak korrante elektrikoaren eraginpean dauden disoluzio urtsuekin kontaktuan jartzean oinarritzen da (Angelova & Dimitrov, 1986; Angelova *et al.*, 1992; Montes *et al.*, 2007).



2.3 irudia. Angelova eta Dimitrovek proposatutako liposoma erraldoien formakuntza mekanismo posiblea. A, Planoarekiko paraleloa den lipido geruzaren eredua. B-D, Liposoma formakuntzaren mekanismo posibleak. [Angelova & Dimitrovetik (1986) birmarraztua].

Tesi honetan, mintzak mikroskopia bidez ikuskatzeko, platinozko kable batera itsatsitako GUVak sortu dira. Honetarako, Luis A. Bagatolli (University of Southern Denmark, Odense, Danimarka) irakasleak diseinatutako ganbera berezi bat erabili da.



2.4 irudia. GUVen elektroformazioan erabilitako politetrafluoroetilenozko (PFTE) ganbera eta unitate zilindrikoak.

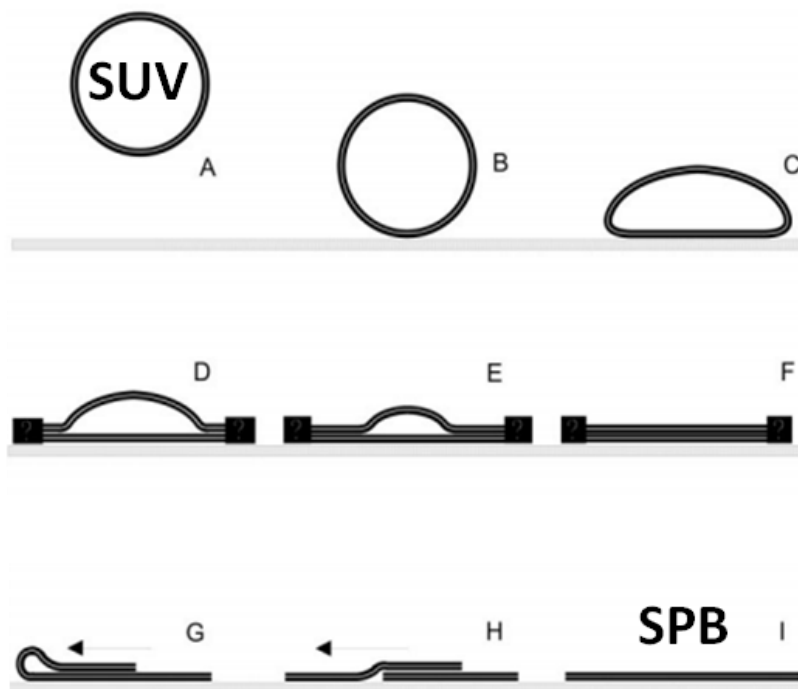
4. Protokoloa. Lamela bakarreko besikula erraldoiak (GUV)

1. Intereseko zunda fluoreszentea eta lipidoa (0.2 mMeko kontzentrazioan) kloroformoa:metanol (2:1 v/v)ean disolbatzen dira.
2. PTFEz eginiko unitate zilindrikoetara lotuak dauden platinozko elektrodoen gainazalera stock disoluzioaren 2 edo 3 μ l gehitzen dira (2.4 irudia).
3. Disolbatzaile organikoaren hondarrak guztiz kentzeko, platinozko elektrododun unitate zilindrikoak huts handian mantentzen dira (gutxienez 90 minutuz).
4. Ostean, unitateak bereziki diseinatutako ganberaren putzutxoetan sartzen dira (2.4 irudia). Platinozko kableak beirarekin kontaktu hurbilean egongo dira. Izan ere, aurretiaz ganberari beirazko estalki bat itsasten zaio.
5. Ur bainu bat erabiliz, ganbera trantsizio fase nagusiko tenperaturaren gainetik dagoen tenperaturan orekatzen da (gutxienez 15 minutuz).
6. Intereseko tanpoia ganberaren tenperatura berean orekatu ostean, platinozko kableak tanpoiz estaltzen dira.
7. Platinozko elektrodoak sorgailu batera konektatu eta 2 orduz intereseko korrante elektrikoa aplikatzen da. Pausu honetan platinozko kableetara itsatsitako besikulak sortzen dira.
8. Korrante elektrikoa eta ur bainua itzali eta 30 minutuz ganbera orekatzen uzten da.
9. Azkenik, GUVak ikuskatzeko, ganbera alderantzikako mikroskopio konfokal batean jartzen da.

2.1.2.4. Sostengatutako geruza bikoitz lauak (SPB)

SPBak, jatorrian, sostengatutako lipido geruza bikoitz gisa izendatu ziren (Singh & Keller, 1991). Jass eta kolaboratzaileek (2000), SPBak lehen aldiz AFMan erabiltzeko metodo bat garatu zuten.

SPBen formakuntzan, SUVak, berriki esfoliatutako mika gainazal batean adsorbatzen dira. Adsortzio hau mikaren natura hidrofobikoa dela medio gertatzen da: SUVak mikarekin kontaktatzean, besikulak mika gainazalean zehar zabaltzen dira. Dena den, SUVen zabaltze mekanismoa azkarra ez izateaz gain, ez dago guztiz argi prozesua nola gertatzen den. Jass eta kolaboratzaileek mekanismo honen eredu bat proposatu zuten. Eredu honetan azaltzen denaren arabera, SUVak mikaren gainean jartzen direnean, besikulak deformazio handi bat jasan eta beraien aurkako poloetako guneetako geruza bikoitzen gainjartze bat gertatzen da. Izan ere, okerdura estresak sortutako tentsioak, besikulak beraien ertzetan haustea eta geruza bikoitzak gainjartzea eragingo luke. Azken pausuan, gainean dagoen geruza bikoitzak beheko geruza bikoitzean zehar irrist egingo luke, gainazal solidoan geruza bikoitz homogenero bakar bat sortu arte (2.5 irudia).



2.5 irudia. Jass *et al.*ek proposatutako SPBen formazio mekanismoa [Jass *et al.*etik (2000) birmarratua]

Mg^{2+} edo Ca^{2+} bezalakoa katioi dibalenteen gehikuntzak (Attwood *et al.*, 2013), eta trantsizio tenperatura altuenaren gainetiko laginaren beroketak (Alessandrini *et al.*, 2012), prozesuan laguntzen dute.

5. Protokoloa. Sostengatutako geruza bikoitz lauak (SPB)

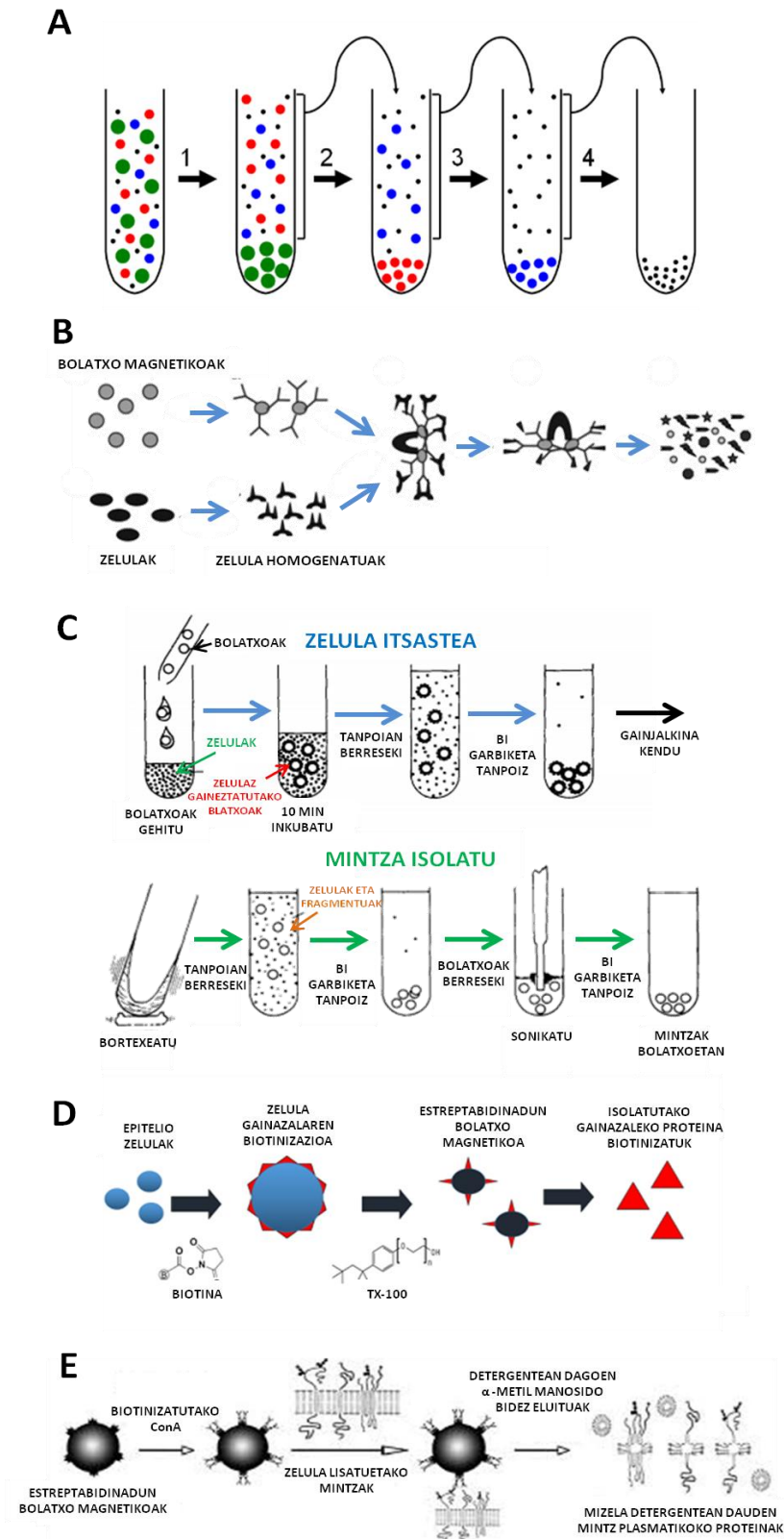
1. SUVak FB-15049 bainu sonikatzailan (Fisher Scientific Inc., Waltham, MA) sortzen dira (3. protokoloa).
2. Mika orri bat esfoliatu eta "BioCell" tenperatura kontrolatzailean (JPK Instruments, Berlin, Alemania) kokatzen da.
3. Mika gainean Ca^{2+} dun tanpoia gehitzen da.
4. Ca^{2+} dun tanpoiaren gainera SUVen suspentsioa gehitzen da.
5. Lagina $1^{\circ}C/min$ berotzen da trantsizio tenperaturara iritsi arte.
6. Laginak tenperatura honetan 30 minutuz mantenduz, SUVak zabaldu eta SPBak sortzen dira. Lagina, momentu oro, kaltzio gabeko tanpoiz eta miliQ H_2O_z hidratatuta egon behar da.
7. SPBak geldoki hozten dira (giro tenperaturan).
8. Tenperatura kontrolatzailea intereseko tenperaturan jarri eta SPBak entsegu tanpoiarekin garbitzen dira.
9. SPBak AFM punta bidez eskaneatzen dira.

Lan honetan, CHO, LY-B, HAP1 eta HAP1-SPT zelula erauzkinen bidez sortutako SPBak erabili dira.

2.2. Zelula Mintzak

Mintz ereduak ez daukate naturan aurkitzen diren proteina-lipido elkarrekintza konplexurik (Sezgin & Schwille, 2012). Arrazoi honengatik, mintzen biokimika eta biofisika ikerketak gauzatzeko benetako zelulen mintz frakzioak erabili ohi dira. Nahiz eta mintz plasmatikoa (PM, ingelesezko plasma membrane) biologo molekular eta zelular askorentzat arreta berezia pizten duen egitura izan, eskuragarri dauden PM

prestakin metodo gehienak (2.6 irudia) denbora luzekoak eta etekin baxukoak izateaz gain, maiz, prestakinak zelularen beste mintz frakzio batzuekin kutsatuak egon ohi dira.



2.6 irudia. Existitzen diren PM isolatze metodo batzuk. [Boone *et al.*etik (1969); Cohen *et al.*etik (1977); Lawson *et al.*etik (2006) eta Lee *et al.*etik (2009) birmarrastua]

Gaur egungo PM isolatze metodo gehienak zentrifugazio diferentzialeko pausuen segidetan (Boone *et al.*, 1969), edota mintz proteina espezifikoaren aurkakoak diren antigorputz monoklonaldun bola magnetikoen erabileran (Lawson *et al.*, 2006) oinarritzen dira. Ikusi izan denez, amiloideez estaliriko burdin oxidozko nanopartikula paramagnetikoak (SPIONS, ingelesezko aminolipid-coated superparamagnetic iron oxide nanoparticles) adibidez, PMra itsats daitezke. Horrela, bere purifikazio magnetikoa ahalbidetuz (Tharkeshwar *et al.*, 2017). Zelula gainazala biotinizatu ostean, PMa isolatzeko, biotina eluzio lehiakor baten estrategia ere erabil daiteke (Das *et al.*, 2013). Beste metodo batzuk, zelulak lisatu ostean, PMra itsasten diren polilisilaz (PLL) gaineztatutako akrilamida bolatxoak erabiltzean oinarritzen dira (Cohen *et al.*, 1977). PM isolatze teknika gehigarri bat, lektina-afinitate kromatografia da (Bhattacharyyas *et al.*, 1987). Teknika honetan, mintzeko proteina glukozilatuak batzeko gehien erabiltzen den molekula konkanabalina A da (Bhattacharyyas *et al.*, 1987; Lee *et al.*, 2009).

Tesi honetan, PM prestakinak lortzeko bi teknika ezberdin erabili izan dira: mintz plasmatikozko besikula erraldoiak (GPMV, ingelesezko giant plasma membrane vesicles) eta PMzko partxeak.

2.2.1. Mintz plasmatikozko besikula erraldoiak (GPMV)

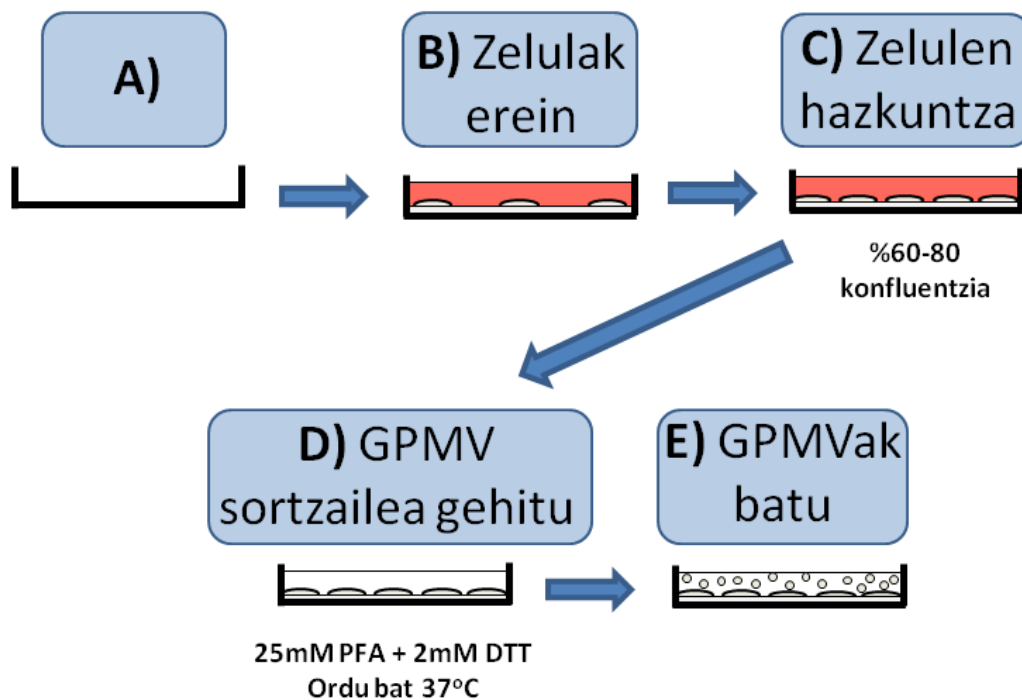
Hoguek (1919), gatz hipotonikodun disoluzioek zeluletan duten eragina aztertu zuen. Zelula kultiboetan gehitutako ur destilatuak, zelulen gainazalean besikula antzeko egitura batzuk sortzen zituela behatu zuen. Hauei “zelula gainazaleko baba” deitu zien. Zenbait urte beranduago, Scottek (1976), aurkikuntza horiek hedatu eta babak zelula gainazaletik askatuz, suspentzioan geratzeko prozesu bat garatu zuen.

PMzko besikulen mediorako askatzea eragiteko, aldehido eta disulfuroen agente blokeatzaile diren konposatu ugari erabil daitezke. Gaur egun, babak GPMV gisa ere ezagutzen dira, eta jakina da, zelulen gainean %1–5 (bol/bol) etanol, azetona, formaldehido edo dimetil sulfoxido (DMSO) gehituz ere lor daitezkeela (Baumgart *et al.*, 2007). Baba hauek, mikroskopia optiko bat erabiliz era egoki batean ikuska daitezke.

Tesi honetan, paraformaldehido (PFA) eta ditiotreitol (DTT) bidezko gehikuntzaz sortutako GPMVak erabili dira (2.7 irudia).

6. Protokoloa. Mintz plasmatikozko besikula erraldoiak (GPMV)

1. Zelulak, T25 flaskoetan %60-80 konfluentzia arte hazten dira.
2. Zelulak, GPMV tanpoiz (2 mM CaCl₂, 10 mM HEPES, 150 mM NaCl, pH 7.4) bi aldiz garbitzen dira.
3. Zelulak, GPMVen formazio errektiborekin (berriki prestatutako 2 mM DTT eta 25 mM PFA, GPMV tanpoian disolbatuta) 37°Ctan ordu batez inkubatzen dira.
4. Inkubazioaren ostean, GPMVdun GPMV errektiboa flaskoetatik batu eta 5 minutuz 1100 rpm-tan zentrifugatzen da (zelula osoak hauspeatzeko).
5. Gainjalkina batu ostean, GPMVak hauspeatzeko, laginak 20 minutuz 14.000 xg-tan zentrifugatzen da.
6. Azkenik, gainjalkina baztertu eta GPMVak 500 µl GPMV tanpoian berreskitzen dira.



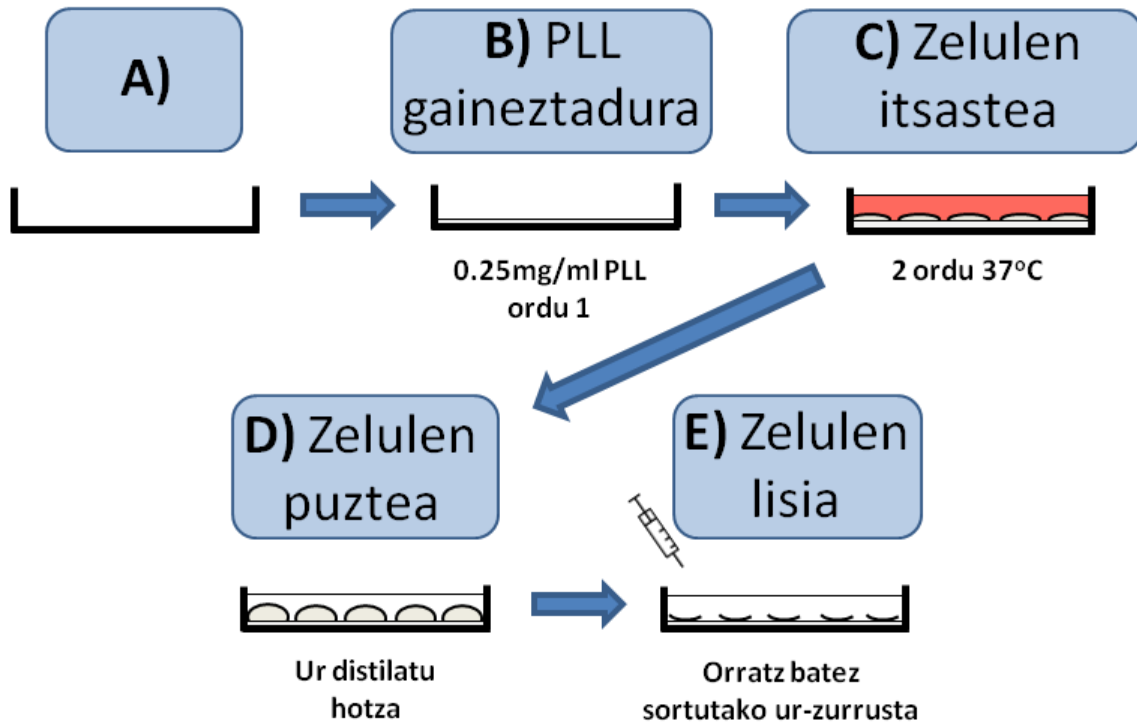
2.7 irudia. GPMVen formazio prozesua.

2.2.2. PMzko partxeen formakuntza

Isolatze teknika hau Bezrukov *et al.*ek (2009) garatu zuten itsatsitako zeluletatik era zuzenean eskuragarriak diren PM kantitate handiak lortzeko asmoz. Teknika honetan, zelulak polilisinaz gaineztatutako gainazal batean itsatsi ostean, izotz-hotz ur destilatu bidezko lisi hipotonikoa gauzatzen da. Azkenik, garbiketa pausu batzuen ostean, kanporatutako zelula barneko osagaiak kentzea lortzen da (2.8 irudia).

7. Protokoloa. PMzko partxeen isolatzea

1. Beirazko oinarridun plakatxoak edota mika orriak PLLz gaineztatu eta fluxu laminardun kanpian 30 minutuz, giro tenperaturan eta UV erradiazio pean uzten dira.
2. Gehiegizko PLLa kendu eta plakatxoak edo mika orriak bi aldiz PBSz garbitzen dira. Zelulak %50eko konfluentziaz erein eta 2 orduz inkubatzen dira gainazalera itsats daitezen.
3. Inkubazioaren ostean itsatsi gabeko zelulak kentzeko, Tris tanpoi (150 mM NaCl, 25 mM Tris, 2 mM KCl) hotzez bi garbiketa burutzen dira.
4. Zelulei ur destilatu hotza gehitu (2 minutu) hauen puztea eragiteko.
5. 20 mlko xiringari lotuta dagoen 19X1-1/2(TW)A orratzez sortutako ur-zurrusta presio baten bidez, zelulen apurtze mekanikoa eragiten da. Honetarako, plakak ur-zurrustarekiko 60 gradutan orientatu eta apurka-apurka biratzen dira. Emaidza gisa, itsatsitako PMzko partxeak eta kanporatutako zelula barneko osagaiak lortzen dira.
6. Kanporatutako zelula barneko osagaiak kentzeko, PBSz bi garbiketa pausu burutzen dira.
7. Purifikazioaren kalitatea txeketzeko, zelula osoak eta purifikatutako PMzko partxeak Di-4-ANEPPS ($\lambda_{ex} = 465 \text{ nm}$, $\lambda_{em} = 635 \text{ nm}$) mintz markatzaile orokorraz eta organulu konkretuekiko espezifikoak diren fluoroforoz markatzen dira.



2.8 irudia. PMzko partxe formazio prozesua.

2.2.3. Zelulen lipido erauzketa

Proteinak, mekanikoki, inklusio zurrun gisa ulertzen dira. Gainera, eredu teoriko gehienetan, inklusio hauek mintz batean txertatzean, mintzak zurrundu egiten direla ikusi da (Agrawal *et al.*, 2016). Biomintzak proteinez gainezka daudela kontuan edukiz, Ahyayauch *et al.*ek (2018) erabilitako metodoa jarraituz, zelula osoen eta PM partxeen lipido erauzketak gauzatu dira.

8. Protokoloa. Lipido erauzketa

1. Laginak hauspeatu eta azido perklorikoz (60% v/v) disgregatzen dira.
2. 20.000 xg-tan zentrifugatu ostean, gainjalkina baztertu, hauspeakinak erauzketa tutuetara mugitu eta 2.5 ml kloroformo:metanol (2:1)ean berreskitzen dira.
3. Laginak 15 minutuz nahasten dira.

4. Laginetara hotz dagoen 0.1 mM HCl disoluzioaren 5 ml gehitzen dira. Denboraren poderioz desagertzen den emultsio baten sorreraren ondorioz, laginak momentu batez esnetsu bilakatzen dira. Laginak homogenizatu ostean, 20 minutuz 1700 xg-tan zentrifugatu dira.
5. Gainjalkinak baztertu eta behe partean dagoen lipidodun fase organikoak kontu handiz beste ontzi batera pasatzen da.
6. Fiske entsegu bidez, fosfolipido kontzentrazioa neurtzen da (ikusi 2.3 atala).

2.3. Fosfolipidoen Zehaztapena (Fiske entsegua)

Normalean, liposomen kontzentrazioa lipido P gisa zehazten da. Prozesu hau Fiske eta Subbarowek (1925) fosforo inorganikoaren entsegu gisa garatu zuten. Lipido Pa kuantifikatzeko asmoz, Bartlettek (1958) eta Böttcher eta Priesek (1961), jatorrizko entsegua eraldatu zuten. Laburki, hasteko fosfolipidoak hidrolizatu eta beraien fosfato taldeak askatzen dira. Ostean, askatutako fosfato taldeek disoluzioa kontzentrazioaren menpeko era batean koloreztatuko duen errektibo espezifikoekin erreakzionatuko dute.

9. Protokoloa. Fosfolipidoen zehaztapena (Fiske entsegua)

1. Kalibrazio kurba: 1 mM NaH_2PO_4 disoluzio estandar batetik abiatuz, 0, 25, 50, 75, eta 100 nmol P test tutuetara gehitzen dira (bi erreplika). Laginaren lipido kontzentrazioa tutu hauekin egindako kalibrazio kurbaren bidez zehazten da.
2. Lagina (hiru erreplika) tutu ezberdinetan gehitzen da (gutxi gora behera 50 nmol lipido P, kalibrazio kurbaren erdian geratzeko).
3. Tutu bakoitzera 500 μl %60 azido perkloriko (HClO_4) gehitu, bortexeatu eta tutuak 205°Ctan dagoen bloke berogailu batera sartzen dira (gutxienez 45 minutuz). Prozesu honetan fosfolipidoak hidrolizatu eta fosfato inorganikoak askatzen dira.

4. Fosfolipidoen hidrolisiaren ostean, tutuak giro tenperaturan hoztu eta 4 ml 1 X amonio heptamolibdato (22 g $[(\text{NH}_4)_6\text{Mo}_7\text{O}_{24}\cdot 4\text{H}_2\text{O}]$, 143 ml H_2SO_4 , 857 ml H_2O) eta 500 μl %10 azido askorbiko gehitzen da.
5. Tutuak bortxeatzen dira. Lehendabizi fosfato inorganikoak molibdatoarekin, eta gero azido askorbikoarekin erreakzionatuz, hori koloreko disoluzioa sortzen da.
6. Tutuak, irakiten dagoen uraren barnean sartzen dira (7 minutuz). Prozesu honetan, disoluzioak fosfato kantitatearen arabera kolore urdina hartuko du.
7. Azkenik, tutuak hoztu eta Ultrospec 500 pro espektrofotometroa erabiliz [Amersham Biosciences (Piscataway, NJ, USA)], laginek 812 nmtan daukaten absortzio neurtzen da.

2.4. Argi Barreiatze Dinamikoa (DLS)

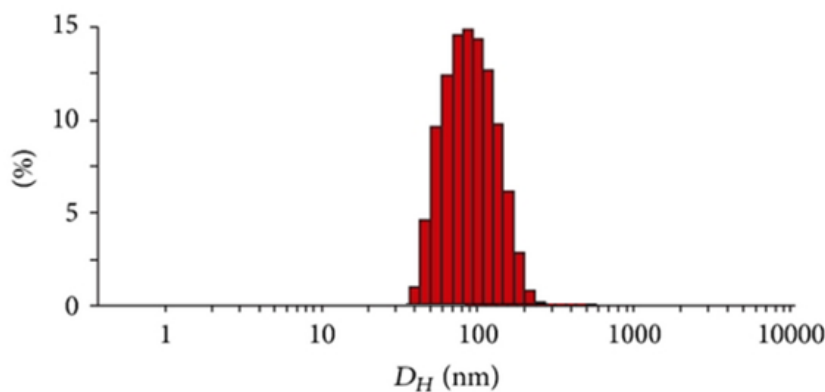
Liposomen formakuntzaren ostean, hauek izan behar duten tamaina daukatela ziurtatu behar da. Horretarako, argi barreiatze dinamiko (DLS, ingelesezko dynamic light scattering) gailuaren bidez, partikulek laginean duten browndar higidura neurtzen da. Abiadura hau Stokes-Einsten ekuazioan txertatuz, partikulen neurria zehazten da:

$$D = \frac{K_B T}{6 \pi \eta R_h}$$

Non, D difusio koefizientea, K_B Boltzmannen konstantea, T tenperatura, η medioaren likatasuna, eta R_h partikula esferikoen erradio hidrodinamikoa diren.

DLSaren funtsa ondorengoa da: laser izpi baten bidez lagina argiztatu eta besikulen mugimenduaren ondorioz ekoiztu den barreiatutako argiaren fluktuazio intentsitatea neurtzen da. Zenbait algoritmo erabiliz, besikulen tamainaren, eta neurriaren homogeneousazio banaketa (polisakabanatze indizea, PDI, ingelesezko polydispersity index) lor daitezke. PDIa, 0tik (disoluzio monodispersoak, homogeneousoak) 1era (disoluzio polidispersoak, heterogeneoak) bitartekoa izan daiteke.

Tesi honetan, besikulen tamainak neurtzeko, 0.6 nmtik 6 μ m-tara bitarteko detekzio esparrua eta 5 mW ($\lambda = 633$ nm)ko He-Ne laser izpia duen Malvern Zeta-Sizer Nano ZS (Malvern Instruments, Malvern, Erresuma Batua) bat erabili da. Giro tenperaturan dauden laginak akril-kubetetan gehitu eta barreiatutako argia, izpiarekiko 173°tan kokaturiko fotobiderkatzaile baten bidez detektatzen da. Emaitzak instrumentuaren software komertzialaren bidez analizatzen dira.



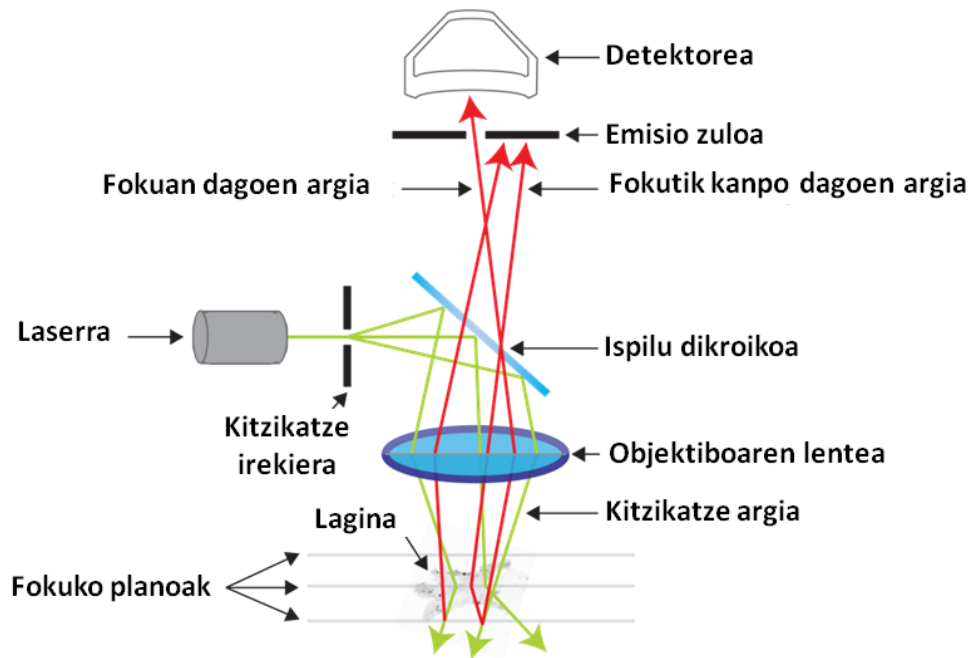
2.9 irudia. DLSz neurtutako 100 nmko diametro-dun PC LUV prestakin baten neurri banaketa.

2.5. Mikroskopia Konfokal Fluoreszentea

Mikroskopia konfokala, Marvin Minskyk 1955ean garatu zuen. Laginaren geruza fin batetik iristen den fluoreszentiaren detekzioa ahalbidetzen duen mikroskopia fluoreszente aurreratu bat da. Mikroskopia honen bidez, langar gutxiagoko eta kontraste hobedun erresoluzio altuko irudiak atera daitezke. Gainera, hiru dimentsioko (3D) irudiak ere lor daitezke. Bere garapenak, mikroskopia optikoko aurrerakuntza garrantzitsuenetariko bat suposatu zuen.

Mikroskopia epifluoreszente eta konfokalaren artean dagoen ezberdintasuna detektorera iristen den fluoreszentzia datza. Mikroskopia konfokalaren mekanismoa ondorengoa da: hasteko, lagina ispilu dikroiko batera zuzendua dagoen laser izpi batez kitzikatzen da. Ostean, ispiluak objektiboan zehar lagineko puntu txiki batera zuzendua den argia aukeratuko du. Gero, igorria den fluoreszentzia, ispilu dikroiko beretik zulo txiki batera zuzentzen da. Azkenik, zulo txikiak enfokatu den planoko fluoreszentzia detektorera pasatzen utziko du, enfokatu gabea berriz, blokeatu egingo du.

Aurretik esan bezala, mikroskopia konfokal batek 3D irudiak eraikitzeke aukera ematen du, x-y planoaren z mugimenduak kontrolatuz, 3D irudiak sortzeke konbina daitezkeen irudi serieak atera baitaitezke.



2.10 irudia. Mikroskopia konfokal fluoreszente baten osagaiak.

<https://imb.uq.edu.au/facilities/microscopy/hardware-software/confocal-microscopes-tik> hartua.

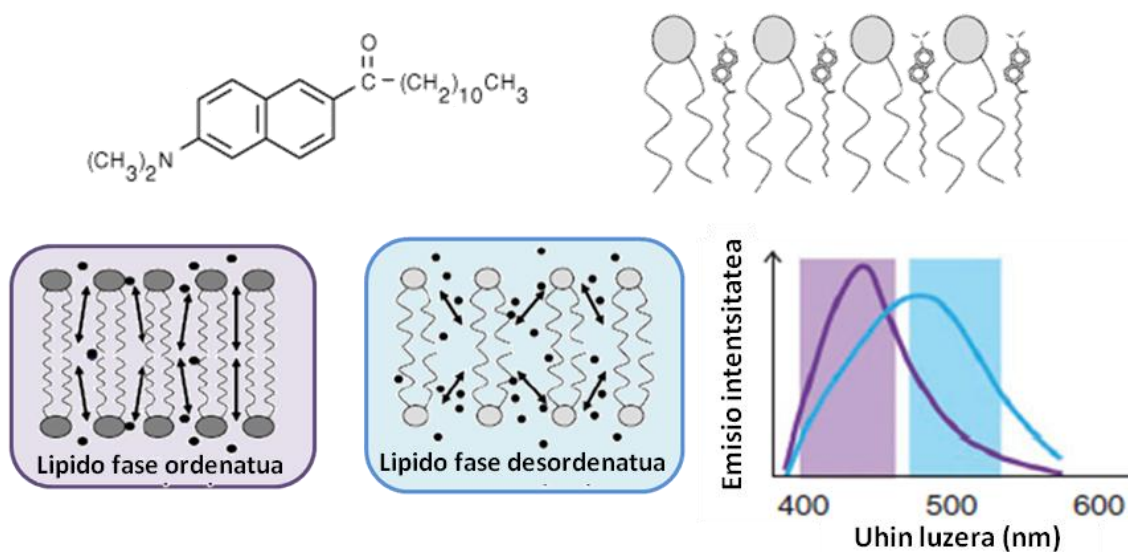
Mikroskopia konfokala, maiz, GUVen mintzetako albo banaketen karakterizazioan erabiltzen da (Bagatolli, 2006). Domeinuekiko afinitate ezberdina daukaten zunda fluoreszenteak erabiliz, liposoma erraldoietan sortzen diren lipido domeinuak ikus daitezke. Zunda horien artean aurkitzen dira domeinu ordenatuagoetara doan Rhodamina PEa, edo domeinu desordenatuagoetara doazen DiI edo naptopireno zunda hidrofobikoak (Juhasz *et al.*, 2010; Baumgart *et al.*; Klymchenko & Kreder, 2014). Beste markatzaile batzuk, adibidez NBD-zeramida, domeinu jariakor eta gel domeinuetan era homogeneo batean banatzen dira (Sot *et al.*, 2006). Zunda fluoreszenteak, normalean, Ceran aberastutako domeinu oso zurrunetan sartzeko zailtasunak izan ohi dituzte.

Fotoi aniztun kitzikatzearen garapenarekin, ohiko mikroskopia fluoreszenteen aurrerapen garrantzitsu bat plazaratu zen. Bere erroak duela 90 urte Maria Göppert Mayerrek (1931) idatzitako funtsezko lan batean egon daitezke. Teknika honen gaur egungo bertsioan, bi-fotoizko absortzio bidez fluoroforoak kitzikatzeko,

femtosegunduetako zabalera duen taupadadun laserra erabiltzen da, fotoien uhin luzera fluoroforoaren absortzio bandaren bikoitza delarik. Bi fotoien absortzio prozesua laser izpiaren fokuko puntuan soilik gertatzen da. Beraz, enfokatu gabeko fluoreszentzia ekidin dezakeen mikroskopia konfokalaren aldaera bat dela esan genezake. Fotoi aniztun kitzikatzearen abantaila nagusia, kitzikatzeko infragorria erabiltzean datza, horrela, UV argiaren erabilera ekidinez. Gainera, soilik fokuko puntua kitzikatzen denez, fluoroforoaren fotozuriketa murrizten da (Diaspro *et al.*, 2006).

2.6. Mintzaren Ordena Molekularra (Laurdan Entsegua)

Laurdan (6-lauroil-1,2-dimetilaminonaftalenoa), Gregorio Weberrek (1979) sintetizatutako eta naftalenoan oinarritutako fluoroforo bat da (2.11 irudia). Laurdan fluoroforoak, hurrenez hurren 2 eta 6 posizioan kokatzen diren, eta disolbatzaile polarretan daukan karga partzialaren banaketaren ondorioz, dipolo momentu bat ematen dioten elektroi emaile (alkil amino taldea) eta hartzaile bana (azil talde ordezkoaren karbonil taldea) dauzka. Laurdan fluoroforoak, kitzikatzen denean, bere dipolo momentua ugaritzearen eraginez inguruko disolbatzailearen dipoloaren birorientazioa eragin dezake. Birorientazio honek, bere kitzikatzeko egoeraren energia murriztea eta bere emisio espektroan desplazamendu bat ikustea eragiten du. Desplazamendu hau, Parasassi *et al.*ek (1990) proposatutako polarizazio orokorraren (GP, ingelesezko general polarization) funtzioa erabiliz ikertzen da.



2.11 irudia. Laurdan fluoroforoa. [Sanchez *et al.*etik (2010) birmarratua].

GPa, mintzen lipido ordena ikertzeko edo lipidoen trantsizio fase nagusia antzemateko erabil daiteke. Maiz, mintzaren jariakortasun/zurruntasun indikatzaile gisa erabiltzen da. Lipido mintz baten laurdan fluoroforoaren emisio maximoa 440 nmra desplazatua dagoenean, mintz hori gel fasean dagoela esan ohi da. Bestalde, likido kristalino fasean, espektroa alde gorriantz mugitzen da, gutxi gora behera 490 nmrantz (Krasnowska *et al.*, 1998) (2.11 irudia).

Ekuazioa:

$$GP = \frac{I_{440} - I_{490}}{I_{440} + I_{490}}$$

Non:

I_{440} = Emisio intentsitatea 440 nmtan.

I_{490} = Emisio intentsitatea 490 nmtan.

GP funtzioaren balioa -1.0etik +1.0era doa.

Tesi honetan, zelula oso, GPMV, PMzko partxe edo zelula erauzkinez sortutako mintz ereduen (SUVak edo GUVak) laurdan bidezko GP neurketak burutu dira. Alde batetik kubeta espektroskopikoetan eta beste aldetik mikroskopioan.

10. Protokoloa. Mintz polarizazioa kubetan

1. Zelula osoak, GPMVak (6. protokoloa), PMzko partxeak (7. protokoloa) edo SUVak (3. protokoloa) prestatzen dira. 82.5 μM lipido eta 0.75 μM laurdan kontzentrazioan.
1. Quanta Master 40 espektrofluorometro (Photon Technology International) bat erabiliz espektro fluoreszentea neurtzen da. λ_{ex} 360 nm eta λ_{em} 400 nmtik 600 nmra.
2. Azkenik, neurtutako espektrotik GP balioa kalkulatu da.

11. Protokoloa. Mintz polarizazioa bi-fotoizko mikroskopioan

1. Zelula osoak, GPMVak (6. protokoloa), PMzko partxeak (7. protokoloa), edo GUVak (4. protokoloa) prestatu eta %1 (%mol) laurdanekin nahasten dira.
2. Laginak Leica TCS SP5 II mikroskopio batean (Leica Microsystems GmbH, Wetzlar, Alemania) kokatu eta 63x ur-murgiltzeko objektibo bat (irekiera numerikoa, NA, ingelesezko numerical aperture = 1.2) erabiliz eta 400 Hztan, eskaneatutako lerroko 512×512 pixeldun irudiak hartzen dira (fotoaukeraketa ekiditeko laginak plano ekuatorialean irudikatzen dira).
3. Entsegu ezberdinen arteko konparaketa ahalbidetuko duen G zuzenketa faktorea kalkulatu da. Honetarako, laginen markaketan erabilitako fluoroforoaren kontzentrazioak (DMSO puruan disolbatua) duen GP balioa kalkulatu da (Owen *et al.*, 2012).
4. Lurdanez markatutako laginen bi-fotoizko irudiak ateratzeko, 780 nmtan finkatutako titanio zafirozko taupadadun laser bat (Mai-Tai Deepsee, Spectra-Physics) erabiltzen da.
 - a. Des eskaneatu gabeko (NDD, ingelesezko non-descanned) detektore hibridoak erabiliz emisio fluoreszentea batzen da. Des eskaneatutako fotobiderkatzailearekin alderatuz sentsibilitate altuagoa erakusten baitute.
 - b. NDD1 bidez (435 ± 20 nmtan) emisio espektroaren alde urdina batzen da. Alde gorria berriz NDD2 bidez (500 ± 10 nmtan).
 - c. Bi-fotoizko kitzikapenerako, laginaren planoko irradiazioa $\approx 500 \text{ GW} \cdot \text{cm}^{-2}$ koa da (Parasassi & Gratton, 1997).

5. MATLABean (MathWorks, Natick, MA) oinarritutako *software* bat erabiliz irudiak prozesatu eta GP balioak kalkulatu dira.

- a. Irudiaren kanal bakoitza, inguruko 2-pixelen batez besteko intentsitatez leundu eta GP balioa kalkulatu da:

$$GP = \frac{I_B - G \times I_R}{I_B + G \times I_R}$$

Non, I_B NDD1ek batutako intentsitatea, I_R NDD2k batutako intentsitatea, eta G zuzenketa faktorea diren.

- b. Zelula osoko irudietan, intereseko gunea (PMA) eskuz hautatu da zelulen gainerako osagaietatik bereizteko.

2.7. Proteina Kontzentrazioaren Neurketa

Proteina kontzentrazioa, azido bis-zinkoninikoaren (BCA, ingelesezko bis-cinchoninic acid) proteina entsegua erabiliz kuantifikatu da (Thermo Fisher Scientific, Waltham, MA). BCA kolore formakuntza, proteinak daukan zisteina edo zistina, tirosina eta triptofano aminoazido hondarren arabera da. Proteinen konposizio aldaeren ondorioz sortutako ezberdintasunak katearen bidez murrizten dira, egitura honek ere kolorearen formakuntzan eragina baitu.

12. Protokoloa. Azido bis-zinkoninikoaren (BCA) entsegua

1. Behi serum albumina (BSA) estandarren diluzioak prestatu dira.
2. A (BCA/karbonato tanpoi alkalino tartrato) eta B errektiboa (%4 $\text{CuSO}_4 \cdot 5\text{H}_2\text{O}$) hurrenez hurren 50:1 erlazioan nahasiz, BCA errektiboa prestatu da.
3. Estanda eta lagin bakoitzaren 25 μl , 96 putzuxoko plakan gehitu da (3 erreplika).

NT-liseninatik abiatuz sortua izan zen (Mizuno *et al.*, 2011). Horretarako KpnI (*Klebsiella pneumoniae* lortua) eta HindIII (*Haemophilus influenzae* lortua) errestrikzio entzimak erabiliz, Dronpa sekuentzia mCherryren sekuentziagatik aldatu zen.

2.8.1. Transformazioa

Zelulak ligazio produktuarekin transformatzeko, *E. coli* bakterio kompetentea izotzetan urtu eta *E. coli* BL21 (DE3) zeluletara DNA plasmidikoaren μl 1 gehitzen da. Lehenengo, bakterioak 30 minutuz izotzean inkubatzen dira. Ostean, 45 segundoz 42°C tako bero-txoke bat ematen zaie. Jarraian, zelulen errekupeazioa bermatzeko, lagina izotz ontzi batera mugitu eta 3 minutuz inkubatzen da. Zelulen errekupeazioa lortzeko, zelulak 200 μl lisogenia salda (LB, ingelesezko lysogeny broth) medioan gehitu eta 37°C tan dagoen irabiazio inkubatzailean ordu batez uzten dira. Kultiboaren 50 μl , kanamizidun (Kan) agar plaka batean zabaldu eta 37°C tan gau osoko inkubazioa gauzatzen da. Soilik interesekoa den bektorearen kopia batez edo hainbatez transformatutako bakterioak haziko dira kolonietan.

2.8.2. Adierazpena

Plasmidoa *Escherichia coli* BL21 (DE3)n hedatu eta proteina errekonbinantea LB medioan adierazten da. Plakatik *E. coli* BL21 (DE3)aren kolonia bat heldu, 70 ml LBdun flasko batera gehitu eta gau guztiko inkubazioa gauzatzen da (37°C tan dagoen inkubatzaile orbital batean).

Hurrengo egunean, gaueko kultiboaren 25 ml, 500 ml LB-Kandun (10 $\mu\text{g}/\text{mL}$) flasko batera gehituz eta 0.6 – 0.8ko dentsitate optikoa (OD, ingelesezko optical density) izatera iristen den arte (650 nmtan) haziz, handitzen da. Kultiboa 37°C tan inkubatzen da (200 rpm-ko agitazioz). Gero, 0.4 mM isopropil β -D-tiogalaktosido (IPTG) gehitu eta laginak 16°C tan dagoen agitazio orbitalezko inkubatzaile batean 72 orduz inkubatzen dira. Azkenik, JLA-9.100 errotoredun (Beckman Coulter, Brea, CA, AEB) Beckman Coulter zentrifuga bat erabiliz, laginak zentrifugatu (15 minutuz, 6000 rpm-tan, 4°C tan) eta osteko purifikazioak gauzatzeko asmoz, bakterio hauspeakinak -80°C tan gordetzen dira.

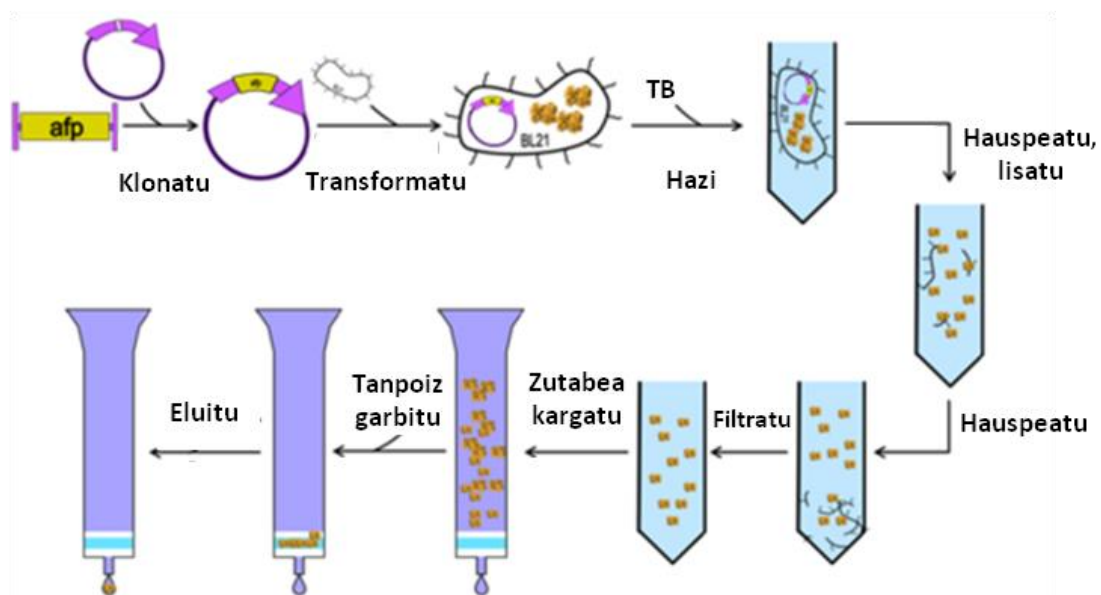
2.8.3. *E.coli*tik erauzitako DNA plasmidikoa

*E. coli*tik DNA plasmidikoa (1 µg/mL) erauzteko, eskala txikiko QIAprep Spin Miniprep kit (Qiagen, Hilden, Alemania) purifikazio teknika erabiltzen da. Manufakturaizailearen jarraibideen arabera, gau osoko bakterio kultiboari lisi alkalinoa, eta osteko DNA purifikazioa gauzatzen zaio. Azkenik, DNA kontzentrazioa zehaztu eta DNA plasmidikoa -20°C-tan gordetzen da.

2.8.4. Purifikazioa

Proteina errekonbinantea NI-NTA *superflow* kartutxo (Qiagen, Hilden, Alemania) bat erabiliz purifikatu eta imidazol bidez eluitzen da (Veiga-da-cunha *et al.*, 2012).

Hasteko, ml 1eko HisTrap HP (Ni²⁺) zutabea, urez eta A tanpoiz (Tris 50 mM, NaCl 300 mM, imidazola 20 mM, antipain 10mg/ml eta leupeptin 10 mg/mL) garbitzen da. Gero, laginaren 75 ml (25 ml x 3tan banatua) A tanpoiz bi aldiz diluitu, 20 mM imidazolera doitu eta 5 ml/minko fluxuz zutabean kargatzen da. Proteina eluziorako, B tanpoiaren (Tris 50 mM, NaCl 300 mM imidazola 500 mM, antipain 10mg/ml eta leupeptin 10 mg/ml) gradiente bat erabiltzen da (1 mlko frakzioak batzen dira). Azkenik, laginak NAP-5 zutabe batean desgazitzen dira.



2.13 irudia. Proteinaren adierazpen eta purifikazio eskema.

<https://2009.igem.org/Team:Washington/Project-etik hartua>.

2.9. Proteina Elektroforesia

%12,5 edo 15 (w/v)eko akrilamida gelak erabiliz, SDS-PAGE bidezko proteinen banaketa lortzen da. Laginak β -merkaptotanol gehigarridun Laemmli kargatze tanpoiz (6x) nahastu, eta 5 minutuz 90°Ctan berotzen dira. Pisu molekularren markatzaile gisa, esparru zabaleko estandar zehatzak (Bio-Rad) erabiltzen dira. Elektroforesia, *running* tanpoian (25 mM Tris, 190 mM glizina, 3.5 mM SDS) eta 150 Van gauzatzen da. Gela, %40 (v/v) metanol eta %10 (v/v) azido azetiko disoluzioan, 0.1% (v/v) Coomassie Brilliant Blue R-250a duen tanpoiz gutxienez 10 minutuz inkubatuz markatzen da. Azkenik, %10 (v/v) azido azetiko disoluzioa erabiliz, *backgrounda* kendu eta proteinen ikuskapen azkar baterako, Gel Doc™ EZ Imager (Bio-Rad) batez gelaren irudiak hartzen dira.

SDS-PAGEaren bidez NT-lisenina errekonbinanteak esperotako tamaina (45 KDa) daukala baieztatu ostean, alikuotak -80°Ctan gordetzen dira (%5 glizeroldun, 20 mM NaCl, 25 mM HEPES, pH 7.2 tanpoian). 280 nmtako absorbantziaren bidez proteinen kontzentrazioa zehazten da.

2.10. Western Blottinga

Trans-Blot® (Bio-Rad) ekipamendu baten bidez, proteinak SDS-PAGE geletatik nitrozelulosazko mintzetara transferitzen dira. Trans-blot filtro paperez eta nitrozelulosazko mintzez gel sandwich bat prestatu eta transferentzia tanpoiz [48 mM Tris, 30 mM glizina, 1.3 mM SDS, MetOH:H₂O (1:5), pH 8] hidratatzen da. Proteina transferentzia, 22 Vtan, 30 minutuz eta giro tenperaturan gauzatzen da. Proteina transferentziaren ostean, mintzak %5 esne gaingabetudun fosfato tanpoiz (PBS; 137 mM NaCl, 3 mM KCl, 80 mM Na₂HPO₄, 7 mM KH₂PO₄) blokeatu eta antigorputz primario eta sekundario espezifikoz inkubatzen dira. Mintzaren garbiketaren ostean, SuperSignal™ West Pico substratu kimilumineszentedun Curix 60 prozesatzaile (Thermo Fisher Scientific, Waltham, MA) batekin proteinaren detekzioa gauzatzen da.

2.11. Ugaztun Zelulen Hazkuntza

Tesi honetan, hamster jatorriko *wild type* CHO-K1 (ATCC, Manassas, Virginia, AEB) eta akastun serina palmitoiltransferasa (SPT) duen LY-B (Hanada *et al.*, 1998) (RIKEN BioResource Research Center Koyadai, Japonia) zelula lerroak, eta giza

jatorriko HAP1 (katalogo zenbakia C631, Horizon, Waterbeach, AEB) eta akastun SPTa duen HAP1 SPTLC1(-) (katalogo zenbakia HZGHC003579c012, Horizon, Waterbeach, EB) zelula lerroak (HAP-SPT gisa ere deitua) erabili dira.

2.1 taula. CHO-K1 eta HAP-1 zelula lerroen informazio orokorra.

	CHO-K1	HAP-1
Organismoa	<i>Cricetulus griseus</i> , hamster, txinatarra	<i>Homo sapiens</i> , gizakia
Ehuna	Obarioa	Tumorea
Morfologia	Epitelio motakoa	Epitelio motakoa
Kultibo ezaugarriak	Itsatsiak	Itsatsiak
Biosegurtasun maila	1	1
Generoa	Emea	-
Akastun SPT lerroa	LY-B	HAP1-SPT

2.11.1. Zelula hazkuntzen hasiera eta mantenua

Pase kopuru baxuan dauden zelula lerroak, sarri, %10 DMSO eta %40 fetuko behi seruma (FBS, ingelesezko fetal bovine serum) duen hazkuntza medion izoztu eta N₂ likidoan gordetzen dira. Izoztean 1°C/minutuko abiaduran gauzatzen da, horretarako isopropanoldun kutxak erabiltzen dira. Azkenik, zelulak bere baitan dauzkaten kriotutuak -80°Cko tenperaturara heltzean, N₂ likidodun *racketara* mugitzen dira.

Zelulak errekuperatzeko, kriotutuak 37°Ctan azkar urtu eta ohiko hazkuntza medioan 10 aldiz diluitu ostean, zelulak gau osoan zehar bertan eduki behar dira. Hurrengo egunean, DMSO trazaraz kentzeko, medioa aldatzen da.

Zelulak %70-80 konfluentzian daudenean, zelula hazkuntza 15 - 20 aldiz diluitzen da. Zelula lerro baten hazkuntza maila, maiz, “zelula pase” gisa ezagutzen da.

Zelulak, 37°Ctan eta %5eko CO₂ko atmosfera hezean hazten dira. Aurkakorik esaten ez bada, CHO/LY-B zelulak DMEM:F12 (Dulbecco's Modified Eagle Medium: Nutrient Mixture F-12) medioan, eta HAP1/HAP1-SPT zelulak IMEM (Iscoves' Modified Eagle Medium) medioan hazten dira. Biak, %10 FBS, 100 U/ml penizilina, 100 U/ml streptomizina, eta 6 mM glutamina gehigarriak.

2.11.2. Zelula mintzaren lipido konposizioaren aldaketak

Tesi honetan, zelula mintzaren konposizioa aldatzeko, hiru metodo erabili dira: **a)** SPT entziman akastunak diren zelula mutanteen erabilera; **b)** miriozina bidezko SPTaren inhibizioa; **c)** lipidoz kargatutako edo kargatu gabeko ziklodextrina (CD) bidezko zelulen tratamendua.

2.11.2.1. Zelulen moldatzea: medio normala vs. FBS gabeziadun medioa

Nahiz eta akastun SPTa duten zelulek ezin ditzaketen SLak *de novo* sintetizatu, SLak hazkuntza mediotik hartu eta asimilatzeke gaitasuna mantentzen dute (Hanada *et al.*, 1998). Horregatik, beraien mintzek SL kontzentrazio baxua izatea lortzeko, zelulak FBS gabeziadun (FBS kantitate baxuak) medioan hazteke moldatu behar izan dira.

13. Protokoloa. Medio urrirako zelulen moldatzea

1. Zelulak, %10 FBSdun medioan (medio normala/estandarra edo 10 gisa deitua, bere FBS ehunekoari erreferentzia eginez) ereiten dira.
2. 24 orduren ostean, %15-25 konfluentzia lortzen denean, medio estandarra kendu, zelulak PBS bidez garbitu eta FBS portzentai baxudun (medio urri gisa deitua) medioa gehitzen da (%0.04 CHO/LY-B zelulentzat edo %0.4 HAP1/HAP1-SPT zelulentzat).
3. Edozein entsegu burutu aurretik, zelulak medio honetan, 24, 48, 72 edo 96 orduz hazten dira.

2.11.2.2. Miriozina tratamendua

Hainbat dira existitzen diren SLen bidezidorreke entzima espezifikoek inhibitzailak. SL guztien murrizpenaren efektua neurtzeko estrategia bat, SLen bidezidorraren lehen erreakzioa katalizatzen duen entzima inhibitzean datza. Entzima honen inhibitzaila ez-natural selektiboen artean, β -kloroalanina (Babita *et al.*, 2002) eta L-zikloserina (Hinkovska-Galcheva *et al.*, 2003) aurkitzen dira. Gainera, SPTa, onddo-aurkako B esfingofungina estereoisomeroaren (Zweerink *et al.*, 1992) eta *Myriococcum albomycesetik* (Kluepfel *et al.*, 1972) isolatutako onddo-aurkako miriozina antibiotiko

(Chalfant *et al.*, 2001; Solomon *et al.*, 2003; Li *et al.*, 2014) naturalen bidez ere inhibi daiteke.

Lan honetan, CHO zelulen SPT entzimaren aktibitatea blokeatzeko eta ondorioz, zelulen mintzean gertatzen diren aldaketa biofisikoak neurtzeko, miriozina erabili da. Aldaketa hauek, SPTLC1 azpiunitateko mutazio kausaz SPT entzima aktibitatea galdu duen zelula lerro baten, LY-B zelula lerroaren, ezaugarriekin (Hanada *et al.*, 1998; Monasterio *et al.*, 2021a) alderatu dira.

14. Protokoloa. Miriozina tratamendua

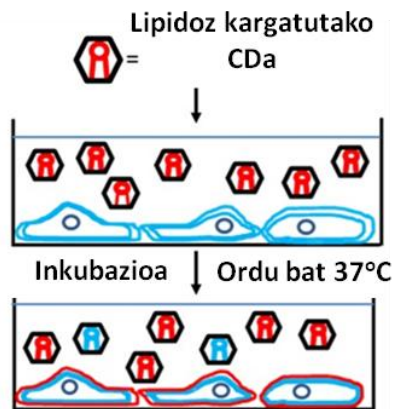
1. CHO eta LY-B zelulak DMEM:F12 medio estandarrean ereiten dira.
2. 24 ordu igaro ostean, medio estandarra medio urriarengatik ordezkatu eta DMSOan disolbatutako 2.5 μ M miriozina (Sigma-Aldrich, St. Luis, MO, AEB) gehitzen da.
3. Edozein esperimentu gauzatu aurretik, zelulak 24, 48 edo 72 orduz medio honetan hazten dira.

2.11.2.3. Ziklodextrina (CD) bidezko lipido erauzketa edo elkartrukea

CDa Villiersek (1891) aurkitu zuen. Ziur aski, almidoia digeritzeko *Bacillus amylobacteren* hazkuntza ez puruak erabili zituelako. Villiersek, entsegu batean material kristalino baten kantitate txikia lortu zuen, baliteke bere hazkuntzan *Bacillus macerans* bakterioa aurkitzen zelako. Produktu kristalino hau zelulolisina gisa izendatu zuen. 12 urte beranduago, Schardingerek (1903) bi produktu kristalino isolatu eta kristalizatutako dextrina α eta dextrina β gisa izendatu zituen. Ordutik, hainbat eraldatutako CD sintetizatu izan dira (Szejtli, 2004).

Freudenberg, Cramer, French eta Rundlen bidez, 1938-1952 bitartean, MaCD, M β CD eta MyCDen egitura kimikoak aurkitu ziren (Freudenberg & Meyer-Delius, 1938; French & Rundle, 1942; Cramer, 1954). CDek uretan disolbagarri egiten duten kanpo atal hidrofilikoko bat, eta hainbat ostalari hidrofobikorekin inklusio konplexuak sortzeko ahalmena ematen dioten barrunbe ez polar bat daukate. MaCD, M β CD eta

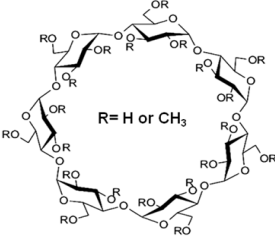

$M\gamma$ CD, α -(1,4)- lotura glukosiliko bidez elkar lotutako sei, zazpi, eta zortzi azukrez osatuak daude hurrenez hurren (Szejtli, 2004).



2. 14 irudia. CD bidezko zelulen tratamendua. [Li *et al.*etik (2016) birmarrastua].

Jakina da, zelula mintzen geruza bikoitzetako bakoitzak lipidoen banaketa asimetriko bat duela. Alor honetan zeresana izan dezakete CDek. Izan ere, CDen barrunbe ez polarrek mintzekin kontaktatzean, lipido jakin batzuk harrapatzeko daukaten gaitasuna dela eta, CDak mintz asimetrikoak ikertzeko erabilgarri izan daitezke, lipido erauzketa soilik geruza bikoitzaren kanpo geruzatik gauzatzen baitute. CDak lipido zehatzez kargatzen badira, noranzko bakarreko erauzketa burutu beharrean, lipido elkartrukea gauzatzeko erabili daitezke (Li *et al.*, 2016) (2.14 irudia).

2.2 taula. $M\alpha$ CDaren eta $M\beta$ CDaren arteko konparaketa.

	Metil- β -Ziklodextrina (M β CD)	Metil- α -Ziklodextrina (M α CD)
		
Formula molekularra	$C_{42}H_{70-n}O_{35} \cdot (CH_3)_n$	$C_{36}H_{60-n}O_{30} \cdot (CH_3)_n$
Glukopiranosita unitate kopurua	7	6
Disolbagarritasuna [25°C, ura (% w/v)]	1.85	14.5
Kanpo diametroa (Å)	15.4	14.6
Barrunbearen diametroa (Å)	6.0–6.5	4.7–5.3
Batez besteko pisu molekularra	1310	1127
Fosfolipido erauzketa	$\alpha > \beta$ (Ohtani <i>et al.</i> 1989)	
Kolesterol erauzketa	$\beta > \alpha$ (Ohtani <i>et al.</i> 1989)	
Proteina erauzketa	$\beta > \alpha$ (Ohtani <i>et al.</i> 1989)	

Tesi honetan, M α - eta M β -CDeK, *wild type* CHO eta akastun SPTa duen LY-B zelula lerroen PMan duten eraginaren ikerketa konparatiboa burutu da. Kontrol lagin bezala, giza RBCak ere erabili izan dira.

15. Protokoloa. Lipidoz kargatutako edo kargatu gabeko CD bidezko zelulen tratamendua

1. Intereseko konposiziodun MLV besikulak [PC, PC:Chol (1:1), PC:SM (1:1) edo PC:SM(1:3)] sortzen dira (1. protokoloa), kasu honetan DMEM:F12 medioan.
2. CD puruen laginak edo MLV + CD nahasteak (lipidoz kargatutako CDak), 30 minutuz 37°Ctan inkubaten dira (Li *et al.*, 2019).
3. Lipidoz kargatutako edo kargatu gabeko CD laginak zelula gainean gehitu eta ordu batez 37°Ctan inkubaten dira. Inkubazio honetan lipido elkartrukea edo erauzketa gertatuko da.
4. Edozein entsegu burutu aurretik PBS tanpoi bidezko garbiketa 2 burutzen dira.

2.11.3. Zelula kultiboen ikuskapena

Zelulak, tinkotu gabe, hau da irudikapen bizian, edota tinkotuta ikuska daitezke. Zelulak tinkotzeko, metanola bezalako disolbatzaile organikoak edo paraformaldehidoa (PFA) bezalako erretikulazio erreaktiboak erabili daitezke. Disolbatzaile organikoek zelula deshidratatu eta beraien lipidoak erauzten dituzten arren, antigenizitatea mantentzen dute. Beraz, zitoskeletoaren eta mintzetara lotutako antigenoen ikerketetarako egokiak dira. Erretikulazio erreaktiboek zelulen arkitektura hobeto mantentzen duten arren, antigenizitatea murrizten dute. Izan ere, zenbait aminoazidoen albo taldeen artean metileno zubiak eraikiz jarduten dute.

Tesi honetan, zelulen arkitektura mantentzea ezinbestekoa denez, zelulen tinkotzea, hauek 15 minutuz giro tenperaturan dagoen %4 PFA-dun (Sigma-Aldrich) tanpoian (PBSan disolbatua) utziz burutu da. Zelulak ikuskatu aurretik, gehiegizko PFA kentzeko PBS bidezko garbiketa pausu bat burutu eta zelulak PBS tanpoian uzten dira.

Zelula bizien ikuskapenerako, zelulak 35 mmko beirazko oinarridun plakatoetan [MatTek Corp. (Ashland, MA, AEB) edo IBIDI, (Gräfelfing, Alemania)] erin eta irudikapenaren unean %50 – 70 konfluentzia izan arte hazten dira.

2.12. Indar Atomikodun Mikroskopia (AFM)

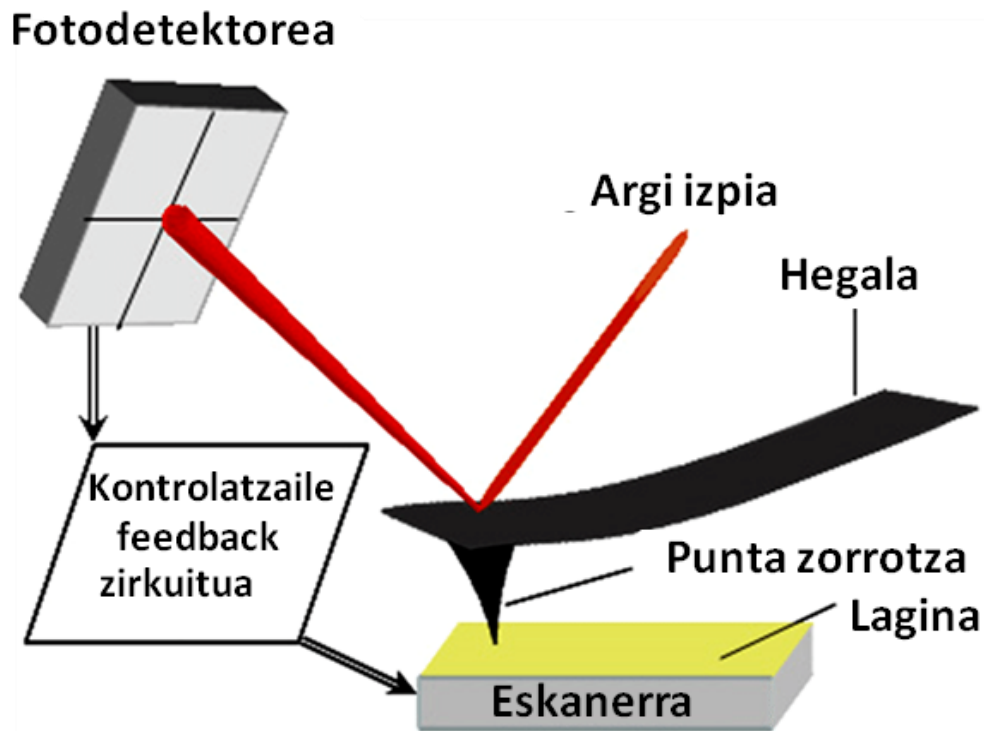
AFMa, mintz biologikoen informazio topografikoa erresoluzio altuan (1 nm baino gutxiago x ardatzean eta 0.1-0.2 nm y ardatzen) lortzeko teknika sendoenetarikoa bat da. AFMa, erresoluzio atomikodun gainazalak eskaneatze bidezko eskaneatze mikroskopio (STM, ingelesezko scanning tunneling microscope) mota bat da. Beraien jatorrian, STMek konduktantzia daukaten gainazalak soilik eskaneatzea ahalbidetzen bazuten ere, Nobel saria jaso zuen Binning eta Rohrerren (1986) asmakuntzak edozein motatako gainazalak (biologikoak barne) ikertzea posible egin zuen. AFMak, lagin baten neurketa topografikoa egiteaz gain, bere analisi mekanikoa, kimikoa eta funtzionala ere posible egiten ditu.

AFM bidez hainbat lagin biologiko mota eskaneatze daitezke: mintz biologikoak, zelula biziak edo ehunak. Lipido domeinuen (Chiantia *et al.*, 2006), eta proteina, DNA edo RNA bezalako molekula txikien ikerketarako ere oso teknika interesgarria da.

AFMaren oinarria ondorengoa da: Hegal malgu baten ertzean itsatsita dagoen punta txiki baten bidez gainazala eskaneatu eta hegalak daukan mugimenduaren arabera, laginaren informazio topografikoa lortzen da. Ispilu bat erabiliz, laser izpia hegalaren punta amaieran enfokaturik dagoen, eta posizioarekiko sentikorra den, lau-kuadrantedun fotodetektore batera islatzen da. Laginaren x-y planuarean eskaneatze prozesuan puntak altuera ezberdineko egituraren bat aurkitzen duenean, fotodetektoreak laser izpiaren mugimendua detektatu eta mikroskopioak z ardatzean gertatzen den hegalaren deflekzio bat antzematen du. Fotodetektorearen seinalea feedback zirkuitu batean zehar pasa eta z-planoan zehar izandako mugimendua laginaren topografiarekin erlazionatzen da. Modu honetan, laserraren lau kuadranteen arteko mugimendua potentzial diferentzia bidez kontrolatu, eta nm azpiko erresoluziodun irudi topografikoak eskuratzen dira (2.15 irudia).

Eskaneatutako materialaren ezaugarrien arabera, AFMaren erresoluzioa aldatu egin daiteke. Beraz, ezinbestekoa da kasu bakoitzean punta egokia aukeratzea: Puntaren

forma, gaineztadura, momentu konstantea eta erresonantzia frekuentzia espezifikoak izan behar dira.

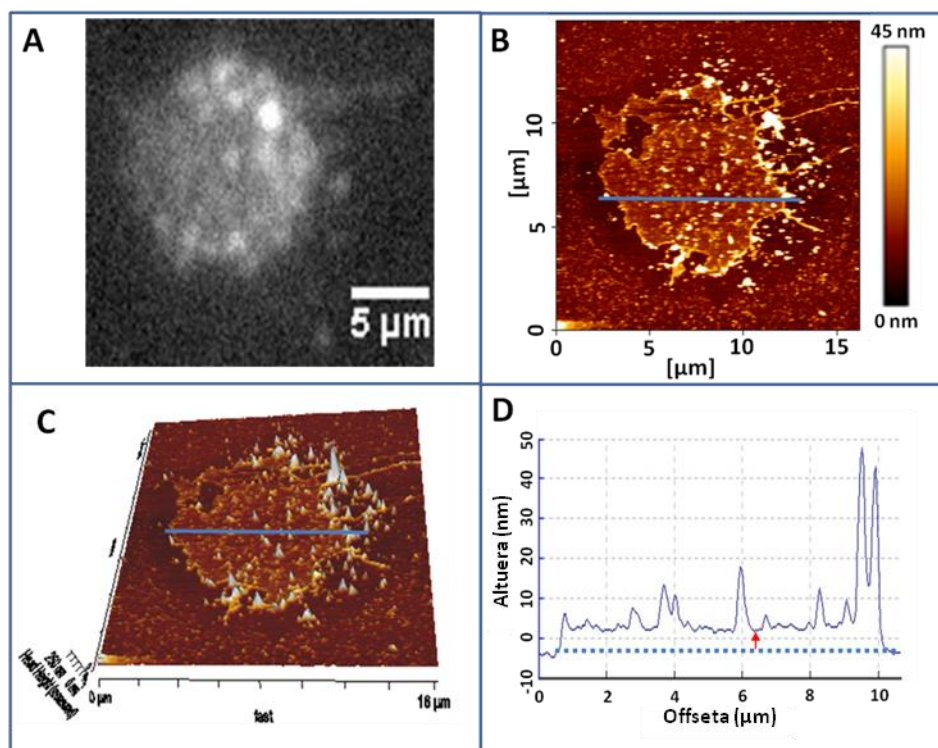


2.15 irudia. AFM osagaien irudikapen eskematikoa. [Pletikapic & DeNardisetik (2017) birmarraztua].

Normalean, siliziozko (aire neurketetan) edo silizio nitrikozko (inguru urtsuetarako neurketetan) puntak erabili ohi dira. Puntak lauki edo hiruki formakoak izan daitezke eta gehienetan, metalezko gaineztadura batez hauen islagarritasun gaitasuna ugartzen da. Puntak, proteina-proteina edo zelula-zelula elkarrekintzen ikerketetarako molekula espezifikoak funtzionalizatu daitezke. Silizio nitrikozko puntekin, 0.01 N/mtik 100 N/mrako momentu konstantedun hegala erabili ohi dira. Dena den, lagin biologikoen biguntasunaren ondorioz, hauek eskaneatzean momentu konstantea 1 N/m azpitik egotea (normalean 0.01-0.5 N/m artean) komeni da.

Lagina kokatzen deneko gainazala ere elementu garrantzitsua da: batzuetan grafito hidrofobikozko (HOPG, ingelesezko hydrophobic graphite) eta beirazko gainazalak erabiltzen badira ere, hauek ez daukate mikak daukan atomikoki leuna den gainazalik. Tesi honetan, nanometro gutxi batzuetako egiturak (lipido geruza bikoitzak edo PMzko partxeak) neurtu behar direla kontuan izanda, negatiboki kargaturiko mika

orri hidrofiliiko moskovitak erabili dira. Beraien erabilileraren aurretik, behar beharrezkoa da mikaren goi orria momentuan bertan esfoliatzea.



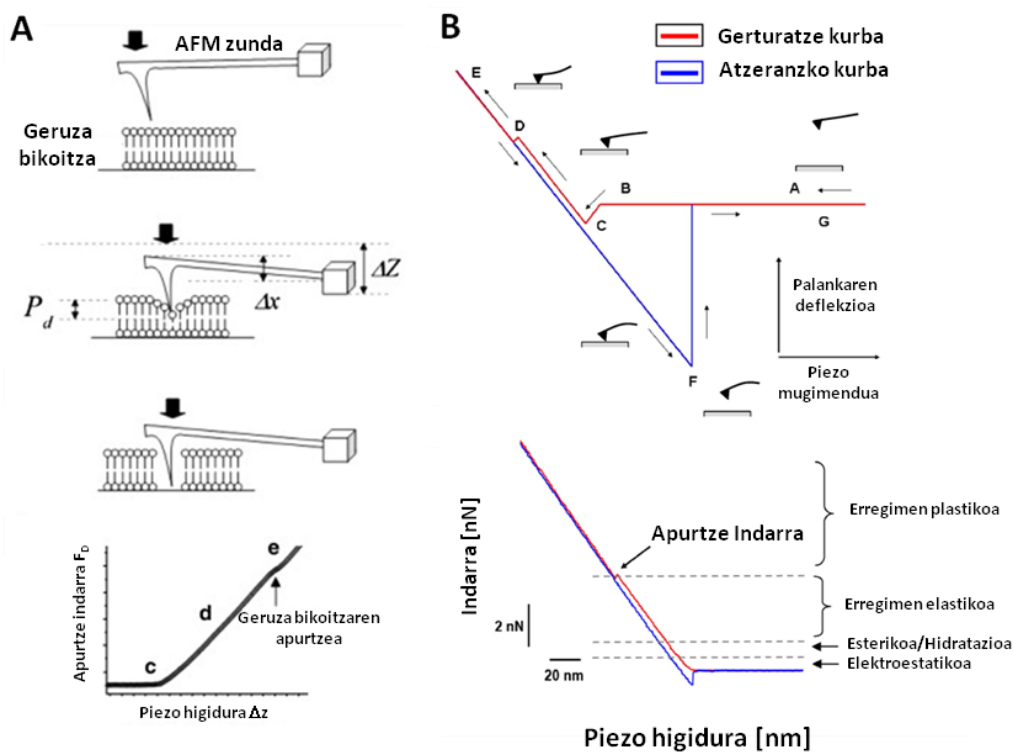
2.16 irudia.PMzko partxe baten irudi topografikoa.

Indar ionikoaren aldaerek SPBen erresistentzia mekanikoa alda dezakete (Garcia-Manyes & Sanz, 2010). Neurketa egoki bat burutzeko pHa eta indar ionikoa optimoak izan behar dira. Beraz, erabiltzen den tanpoia kontu handiz hautatu behar da. Gainera, eskaneatze abiadura, eskaneatze angelua eta/edo puntaren bidez aplikaturiko indarra ere, era egoki batean kontrolatu behar dira. Alessandrini eta Faccik, teknikaren inguruko berrikuspen zehaztu bat argitaratu zuten (Alessandrini & Facci, 2005).

AFM neurketak bi modu ezberdinetan burutu daitezke; **a)** kontaktu eran, non punta fisikoki laginarekin kontaktuan dagoen, edo **b)** aldikako (tapping) eran, non punta ez dagoen une oro laginarekin kontaktuan. Kontaktuan eran laginaren eta puntaren arteko indarra beti aurkakoa da. Eskaneatze prozesuan zehar aplikaturiko indarra konstante mantentzen da, hori lortzeko gertatzen diren mugimendu piezo bertikalak grabatzen direlarik. Nahiz eta era honekin erresoluzio maila altuena lortzen den, aplikatzen den indarraren ondorioz, geruza bikoitzak bezalako laginak hondatu egin daitezke. Albo deflekzioa eta seinalearen errorea neurtuz, punta eta laginaren arteko marruskaduraren

informazioa biltzen da. Beraz, konposizio kimiko ezberdineko guneak ezberdinu daitezke.

Aldikako eran, punta ez dago une oro laginarekin kontaktuan; hegalaren oszilazioak zeresan nabarmena dauka bere erresonantziaren frekuentzian. Bai elkarretaratze, baita urrutze indarrak existitzen dira, beraz, teknika hau laginarentzako ez da hain erasokorra. Bere garapenak lagin bigunen analisia eta hegal zurrunagoen erabilera ahalbidetu zuen. Lan honetan, kontaktu era erabiliz, laginen 512 x 512 pixeleko irudiak hartu dira.



2.17 irudia. Apurtze prozesua eta softwarearen bidez sortutako indar kurba. [Garcia-Manyes & Sanzetic (2010) birmarraztua].

AFMa indar espektroskopia eran ere erabil daiteke (Rief *et al.*, 1997). Modu honetan, geruza bikoitza zulatuz mintzaren karakterizazio mekanikoa ahalbidetzen duen apurtze indarra neurtzen da. Honela ba, mintz prestakin ezberdinen erresistentzia mekanikoak neurtuz, lipido sistemak egoera konkretu jakinetan nola jokutzen duten identifika daiteke.

Prozesua ondorengo eran laburbildu daiteke; **a)** puntak mintzaren gainean, berau zulatu arteko presioa egiten du. Ondorioz, indar kurban, piku batean eraldatzen den

laserraren deflekzio bat detektatuko da; **b)** puntak mika sakatzen du indar maximoa aplikatzen den arte; **c)** atzeranzko prozesua hasten da. 2.17 irudian apurtze prozesua eta software bidezko indar kurbaren sorrera azaltzen da.

Tesi honetan, PMzko partxeen eta zelulen lipido erauzketez eginiko SPBen, irudi topografikoak eta indar espektroskopikodun analisia, eta GPMVen indar espektroskopikodun analisia gauzatu da.

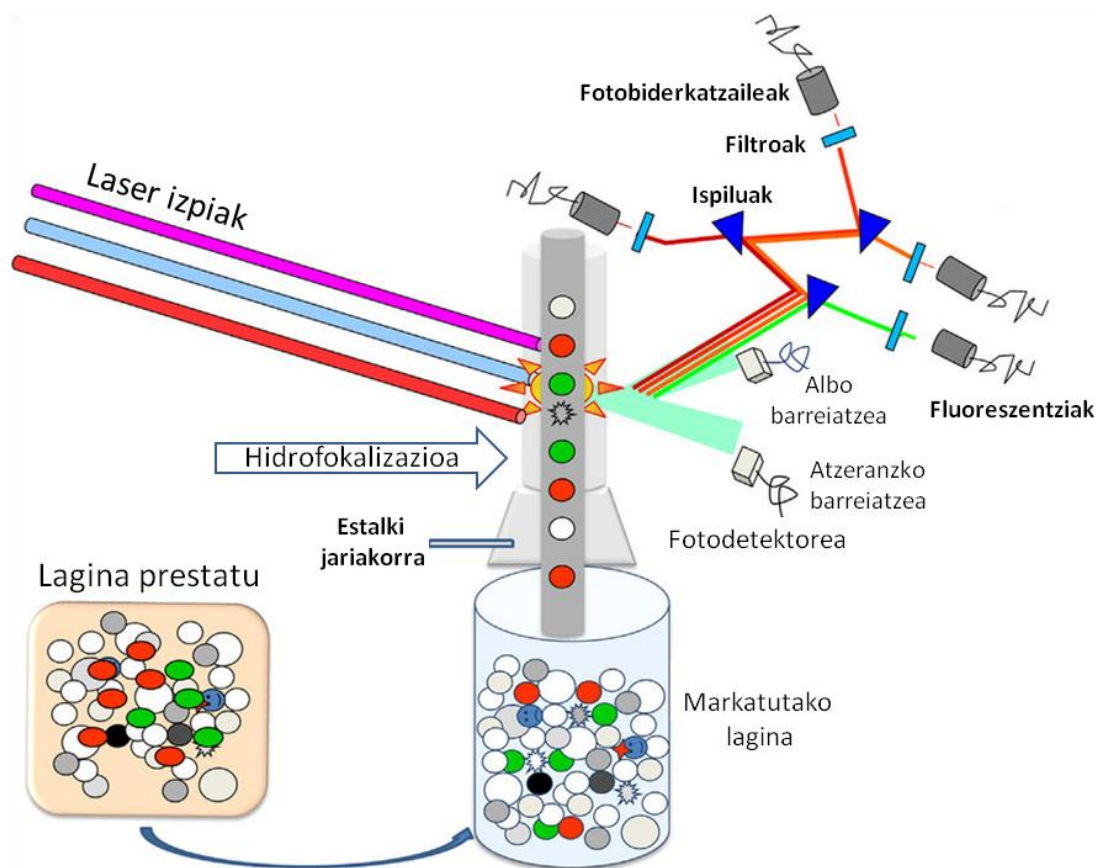
2.13. Fluxu Zitometria

Fluxu zitometria, 1960ko hamarkadan Mack Fulwylerrek (1965) garatutako eta nahaste jariakor eta heterogeneo batean zelulak zenbatu eta profilatzeko argia erabiltzen duen biologia zelularreko teknika analitiko bat da. Zelulak dauzkan nahaste jariakor heterogeneo batean oinarrituz, hainbat parametroekin lotutako informazioa lortzeko modu azkar, zehatz eta sinple bat da.

Bere funtsa ondorengoa da: zelulak kanal estu batetik zehar banan-banan pasatzen diren bitartean argi batez argizatzen dira. Sentsoreek, zelulek errefraktatzen edo igortzen duten argi mota detektatu eta informazio guztia bateratu ostean, laginaren irudi ulergarri bat gauzatzen da (2.18 irudia).

Tesi honetan, fluoreszentzia bidez aktibatutako zelulen sailkatzedun (FACS, ingelesezko Fluorescence-Activated Cell Sorting cytometry) Calibur (Becton-Dickinson, Franklin Lakes, NJ, AEB) gailu bat erabili da zelulen bizitasuna eta lipido espezifikoaren kuantifikazioa gauzatzeko.

Bizitasun entseguetarako, zelula apoptosikoen markaketa Anexina-V-Fluoreszeina isotiozianatoz (FITC), eta zelula nekrotikoen markaketa ioduro propidioz, burutu da. Betiere, anexina V-FITC detekzio kitaren manufakturatzaileak adierazitako moduan. Anexina V-FITC fluoreszentzia intentsitatea FL-1 kanal fluoreszentean neurtu zen, $\lambda_{ex} = 488$ nm eta $\lambda_{em} = 530$ nmtan. Ioduro propidioa berriz, FL3 kanalean, $\lambda_{ex} = 532$ nm eta $\lambda_{em} = 561$ nmtan. SMA, lipido honekiko espezifikoa den liseninari itsatsitako mCherryaren intentsitatea neurtuz kuantifikatu zen, FL-3 kanala erabiliz, $\lambda_{ex} = 532$ nm eta $\lambda_{em} = 561$ nmtan.



2.18 irudia. Fluxu zitometriaren oinarriak. [Depince-Berger *et al.*etik (2016) birmarrastua].

2.14. Masa Espektrometria

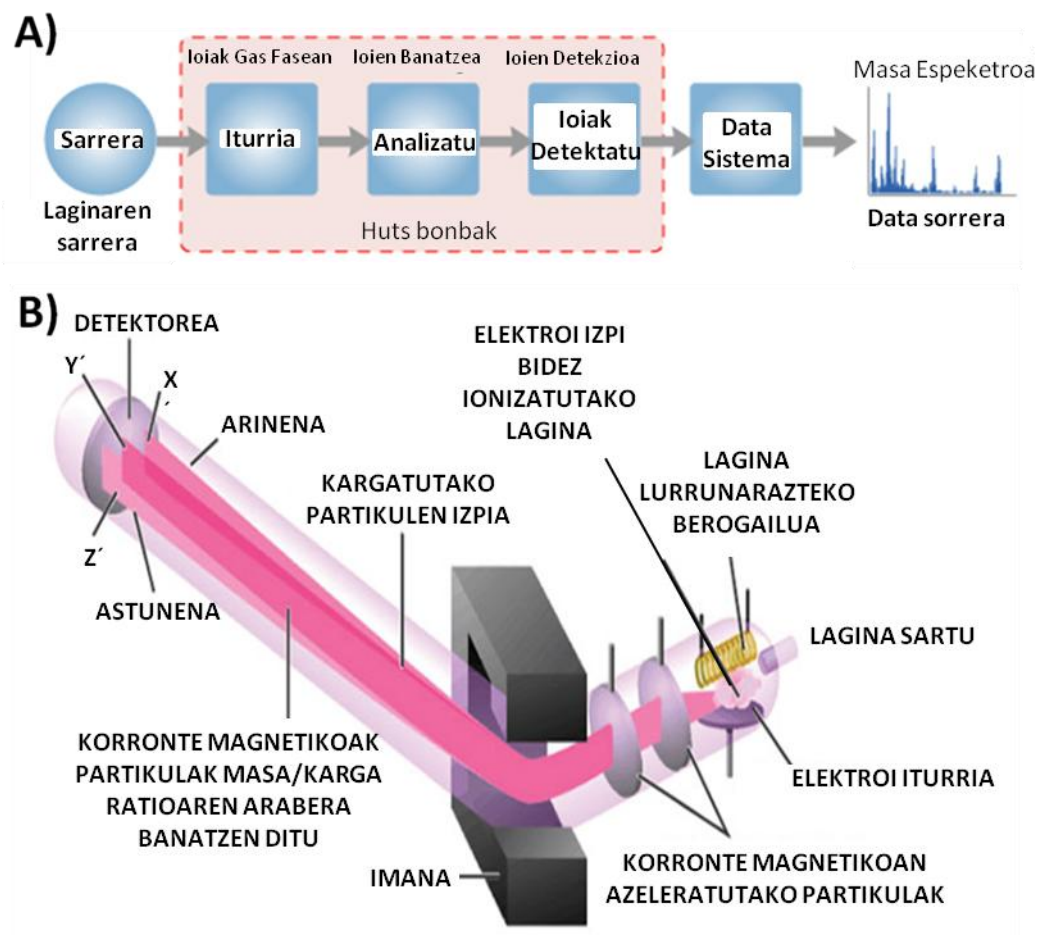
Masa espektrometria (MS edo mass-spec), ezezagunak diren osagaiak identifikatzeko, ezagunak diren osagaiak kuantifikatzeko edo molekula ezberdinen ezaugarri kimiko eta egitura ezaugarriak karakterizatzeko erabiltzen den teknika bat da.

Wilhelm Wien (1898) izan zen MS aren erroak garatu zituen. Wienek, izpi positiboak beraien karga-masa ratioaren arabera banatzen zituen korrante elektriko eta magnetiko perpendikular dun gailu bat eraiki zuen. Wien, ratio hori tutuan sartutako gasaren naturaren arabera zela ohartarazi zen.

1907 eta 1913 bitartean, Wiene lanean oinarrituz, J.J. Thomsonek (1913) MSaren teknikan zenbait aurrerapen egin zituen. Thomsonen tutuan ioiak angelu txikietan eta bi norabide perpendikularretan zehar deflektatzen ziren, eta ioi hauek, beraien bideetan jarritako plater fotografikoetan kurba paraboliko batzuen serieak sortzen zituzten. Parabola bakoitza masa-karga ratio zehatzeko eta kokapen jakineko ioi

espezifikoki zegoen hain zuzen ere. Beranduago, Thomsonek hasierako plater fotografiko hura arrakala paraboliko bat zeukan erretilu metaliko batengatik ordezkatu zuen. Laburki, positiboki kargatutako ioi izpi bat, korrante elektriko eta magnetiko konbinatu batekin zehar pasatzen zuten, honela, masa espektrografoa sortuz (ioien masa karga ratioa neurtzen zuten lehen espektrometria gailuak masa espektrografo gisa deitu ziren).

A. Jeffreyk 1918an, eta F.W. Astonek 1919an, MS modernoek teknika garatu zituzten. Espektrografo eta masa espektrometroen arteko ezberdintasuna ondorengoa da: lehenak masa balioren espektroak plater fotografiko batean grabatzen dituen bitartean, masa espektrometro batek ioi izpiak fosforozko pantaila batera zuzentzen ditu.



2.19 irudia. MSaren oinarria eta espektrometroaren funtsezko osagaiak.

[<https://microbenotes.com/mass-spectrometry-ms-principle-working-instrumentation-steps-applications/-etik-birmarraztua>].

Azken urteetan MSarekin lotutako hainbat Nobel sari eman dira: 1989an Hans Dehmelt eta Wolfgang Paulik jaso zuten harrapatutako ioien teknika garatzearen. 2002an, John Bennett Fennek eta Koichi Tanakarik: Lehenak elektroesprai ionizazioaren (ESI, ingelesezko electrospray ionization) garapenagatik eta bigarrenak laser bigunaren desortzioaren (SLD, ingelesezko soft laser desorption) garapenagatik, eta teknika honek makromolekula biologikoen ionizazioan dauzkan aplikazio anitzengatik.

Laburbilduz, MSak, laginak ionizatu eta beraien masa karka (m/z) ratioaren arabera banatzen ditu. Ostean ioi mota bakoitzaren kopuru erlatiboa neurtuz, molekula aitzindariaren gaineko natura eta egituraren informazioa emateko.

Masa espektrometroa 3 osagai nagusitan oinarritzen da. **a)** ikertzen ari garen substantziatik gas ioiak sortzeko balioko duen ioizko gainazal bat; **b)** ioiak beraien masa karga ratioaren arabera dagokien masadun osagaiekin lotuko dituen analizatzailea; **c)** detektatutako eta ebatzitako ioi espezie bakoitzaren kopuru erlatiboa grabatuko duen detektore sistema. Gainera, huts handia mantentzen duen laginen sarrerarako sistema bat, eta informazioa lortzeko eta analitzeko ordenagailu bat ere beharrezkoak dira.

Lipidoen toki eta denbora zehatzeko egitura eta funtzio analisisa, lipidomika gisa ezagutzen da. Lipidomika metodologia ezagunenak, ESI iturria eta lau-polo hirukoizdun analizatzaileak behar dituzte. Tesi honetan, MS bidez zelula osoen eta PM prestakinen lipidoak kuantifikatu dira.

16. Protokoloa. MS neurketarako lipido erauzketa

(Guri *et al.*, 2017)

1. Lagin suspentsioa 2 mlko tutuetara pasatzen da.
2. 360 μ l metanol gehitu eta laginak nahasten dira.
3. Laginetara lipido estandarren nahaste bat (ikusi 2.3 taula) gehitu eta laginak Cell Disruptor Genie (Scientific Industries, Inc) bat erabiliz 10 minutuz 4°Ctan irabiatzen dira.
4. 1.2 ml metil-*tert*-butil eter (MTBE) gehitu eta laginak ordu batez giro tenperaturan inkubatzen dira (750 rpm-tan irabiatuz).

5. Laginetara 200 µl H₂O gehitzen dira.
5. Giro temperaturan egiten den 10 minutuko inkubazioaren ostean, laginak 10 minutuz 1.000 xg-tan zentrifugatzen dira. Horrela, faseen banaketa lortuz. Goi fasea (organikoa) 13 mmko erroka tapadun beirazko tutuetara pasatzen da.
6. Behe fasera “goi fase artifizialaren” [MTBE/metanola/ura (10:3:1.5, v/v/v)] 400 µl gehitu eta lagina 10 minutuz inkubatzen da.
7. Inkubazioaren ostean, lagina 10 minutuz 1.000 xg-tan zentrifugatu eta goi fasea (organikoa) aurreko goi fasearekin bateratzen da.
8. Lipido erauzketaren kopuru totala 3 alikuota berdinetan banatzen da (bat fosfolipidoentzat, beste bat esterolentzat eta beste bat SLentzat).
9. Laginak nitrogenoko fluxu batean edo 50°Ctan dagoen zentribap batean lehortzen dira.

SL analisiaren aurretik laginetatik fosfolipidoak kentzeko, alikuotak metilaminazko tratamenduz desazetilatzen dira (Clarke metodoa).

17. Protokoloa. SL analisirako metilamina tratamendua

1. Lipido lehorraren gainean 0.5 ml monometilamina errektibo [Metanola/H₂O/*n*-butanola/metilamina disoluzioa (4:3:1:5 v/v)] gehitu eta laginak 5 minutuz sonikatzen dira.
2. Laginak nahasi eta ordu batez 53°Ctan inkubatzen dira. Jarraian laginak lehortu egiten dira.
3. Monometilaminaz trataturiko lipidoak *n*-butanol erauzketaren bidez desgazitzen dira:
 - a. Lipido erauzi lehorrak 300 µl urez asetutako butanolean berreskitzen dira.
 - b. Laginak bortexeatu eta 5 minutuz sonikatzen dira.

- c. 150 µl H₂O (LC-MS gradua) gehitu, laginak bortexeatu eta 10 minutuz 3.200 xg-tan zentrifugatzen dira.
 - d. Goi fasea (butanolaren fasea) 2 mlko beirazko anbar tutuetara mugitzen da.
 - e. H₂Oz asetutako 300 µl butanol gehitu, laginak bortexeatu eta 10 minutuz 3.200 xg-tan zentrifugatzen dira.
 - f. Bi goi faseak bateratzen dira.
 - g. Butanola N₂ gas fluxu batean edo zentribapean lehortzen da.
4. Laginak lehortu, tutuak N₂z bete eta -80°Ctan gordetzen dira.

18. Protokoloa. Laupolo hirukoizdun masa espektrometro baten bidezko glizerofosfolipido eta SLen detekzioa

1. Fosfolipido eta SL alikuotak 250 µl kloroformo/metanol (1:1 v/v)ean berreseki eta 5 minutuz sonikatzen dira.
2. Fosfolipidoak, modu negatiboko disolbatzailean [kloroformoa/metanola (1:2) + 5 mM amonio azetatoa] 4 aldiz eta modu positibokoan [kloroformoa/metanola/ura (2:7:1 v/v) + 5 mM amonio azetatoa] 10 aldiz diluitzen dira. SLak modu positiboko disolbatzailean 10 aldiz diluitzen dira.
3. SLen molekula espezieen identifikaziorako, laupolo hirukoizdun TSQ Vantage (Thermo Fisher Scientific, Waltham, MA) MS batean, tandem MSa gauzatzen da (lipido mota bakoitzarentzako detekzio baldintzak 2.3 taulan). Zeramida espezieak, ur galeraz, lehen laupoloan kuantifikatzen dira.
4. Lipido kontzentrazioa barne estandarren arabera kalkulatu eta lipido erauzketa bakoitzerako lipido kopuru osoaren arabera normalizatzen da (% mola).

2.3 taula. Lipido mota ezberdinentzako MS detekzio baldintzak.

Lipido mota	Estandarra	Polaritatea	Modua	Ioien m/z	Kolisio energia
Fosfatidilkolina [M+H] ⁺	DLPC	+	Ioi produktua	184.07	30
Fosfatidiletanolamina [M+H] ⁺	PE31:1	+	Ioi neutroaren galera	141.02	20
Fosfatidilinositola [M-H] ⁻	PI31:1	-	Ioi produktua	241.01	44
Fosfatidilserina [M-H] ⁻	PS31:1	-	Ioi neutroaren galera	87.03	23
Kardiopina [M-2H] ²⁻	CL56:0	-	Ioi produktua	Kate aziliko	32
Zeramida [M+H] ⁺	C17Cer	+	Ioi produktua	264.34	25
Dihidrozeramida [M+H] ⁺	C17Cer	+	Ioi produktua	266.40	25
Hexosilzeramida [M+H] ⁺	C8GC	+	Ioi produktua	264.34	30
Hexosildihidrozeramida [M+H] ⁺	C8GC	+	Ioi produktua	266.40	30
Esfingomielina [M+H] ⁺	C12SM	+	Ioi produktua	184.07	26

19. Protokoloa. Chol neurketarako gas kromatografiazko MSa (Guan *et al.*, 2010)

1. Laginak VF-5 ms 15 m × 0.32 mm i.d. DF = 0.10 dun FactorFour kapilaritate zutabe batekin ekipatutako VARIAN CP-3800 gas kromatografo batean xiringatu, eta -70 eVko energian eta 250°Ctan dagoen laupolo hirukoizdun Varian 320 MS batean analizatzen dira.
2. Laginak 45°Ctan dagoen zutabe labean sartu eta bertan 4 minutuz mantentzen dira. Ostean, tenperatura 195°Cra (20°C/min) igotzen da.
3. Esterolak 195°Ctik 230°Cra (4°C/min) doan gradiente lineal batez eluitu ostean, 320°Cra (10°C/min) berotzen dira.
4. Kolesterola bere erretentzio denboraren arabera identifikatzen da (ergosterol estandar batekin konparatuz) eta fragmentazio patroiak Estandar eta Teknologiaren Nazioa Institutuaren (NIST) datu basearekin konparatzen dira.

3. KAPITULUA

PARTXEAK ETA BABAK:

CHO ZELULEN MINTZ

PLASMATIKOAREN BI

PRESTAKINEN KONPOSIZIO

ETA PROPIETATE

BIOFISIKOEN ARTEKO

KONPARAKETA

3. KAPITULUA: PARTXEAK ETA BABAK: CHOZELULEN MINTZ PLASMATIKOAREN BI PRESTAKINEN KONPOSIZIO ETA PROPIETATE BIOFISIKOEN ARTEKO KONPARAKETA

3.1. Sarrera

Mintz ereduak luzaroan erabili izan dira mintzen arteko ikerketa biofisikoak burutzeko. Hauek, lipido mintz sintetikoetan heterogeneotasunak ikustea ahalbidetu dute (Bangham *et al.*, 1964; Duzgunes, 2009; Morigaki & Tanimoto, 2018). Dena den, mintz ereduak molekula edota zelula sistemak berreraikitze edota beraien hainbat propietate imitatze erabilgarriak diren arren, zelula natiboaren mintz antolakuntzak guztiz argitu gabe dirau. Izan ere, mintz ereduak ez dituzte ez konposizioaren konplexutasunik ezta proteinen sintesi edota naturan aurkitzen diren proteina-lipido elkarrekintzarik mantentzen, gainera, ez daukate zitoeskeletorik (Sezgin & Schwille, 2012). Hau kontuan izanda, gaur egun, ikerketa biokimikoak eta biofisikoak gauzatzeko, mintz prestakin azpizelularrak gero eta beharragoak izaten ari dira. Horien artean, mintz plasmaticoak (PM) daukan zelula eta inguruaren arteko banatze eginkizun berezia dela eta, biologo molekular eta zelularren artean arreta berezia piztu du.

PM prestakinak lortzeko teknika gehienak denbora luzeko metodoetan oinarritzeaz gain, sarritan, lortzen diren laginak errendimendu gutxikoak eta beste organulu batzuekin kutsatuak egon ohi dira. PMaren isolamendu metodo gaurkotuenak zentrifugazio diferentzialetako pausuetan oinarritzen dira (Boone *et al.*, 1969). PMaren errendimendu hobek lortzeko teknikak, PMarekiko espezifikoak diren antigorputz monoklonalak atxikita dauzkaten bolatxo magnetikoak erabiltzean datzate (Lawson *et al.*, 2006). Gainera, era ezberdinean gaineztatutako burdin oxidodun nanopartikula superparamagnetikoak (SPIONS) ere, zelularen konpartimentu espezifikoetara itsasteko gaitasuna daukate. Aminolipidoz estaliriko SPIONSak adibidez, PMari lot dakizkioke, horrela, bere purifikazio magnetikoa ahalbidetuz (Tharkeshwar *et al.*, 2017). Beste estrategia erabilgarri bat gainazalaren biotinizazioarena da. Zelularen gainazala biotinizatu ostean, PMaren isolamendurako biotina eluzioa lehiakor bat erabil daiteke

(Das *et al.*, 2013). Beste metodo batzuk, polilisinaz estaliriko akrilamida bolatxoan erabileran oinarritzen dira, zeintzuk, zelula lisatuetan PMra itsatsiko diren (Cohen *et al.*, 1977). PMaren beste isolamendu teknika bat lektinarekiko afinitate kromatografian oinarritzen da (Bhattacharyyas *et al.*, 1987). Metodo hau mintz mota bakoitzean dauden azukre espezifikoetaz baliatzen da. Izan ere, lektinak, azukreei itsasteko espezifikotasun ezberdina duten azukre-lotze proteina talde bat dira. PMan azukre molekuluak beti kanpoaldeko orrian dauden bitartean, mintz intrazelularretan organuluaren barne aldera begira daude. Glikozilaturiko mintz proteinetara lotzeko erabiltzen den lektina erabilgarriena konkanabalinaA izeneko da (Bhattacharyyas *et al.*, 1987; Lee *et al.*, 2009).

Ikerketa hau, CHO zelulen PMaren konposizio eta propietate fisikoak deskribatzera bideratua dago. Gure aurkikuntzen balioa indartzeko, beraien artean oso ezberdinak diren PM prestakinak lortzeko bi metodo erabili dira. Horietako bat Bezrukov *et al.*ek (2009) garatu zuten gainazal batera itsatsitako zeluletatik abiatuz era zuzen batean PM kantitate handiak lortzeko. Metodo hau polilisinaz estaliriko gainazal batera itsatsitako zeluletan oinarritzen da. Gero, zelulak 4°C azpitik dagoen ur destilatuarekin kontaktuan jarritz, beraien lisi hipotoniko bat eragiten da. Azkenik, askaturiko zelula barneko edukia mediotik kentzeko zenbait garbiketa burutzen dira. Eraitza gisa PM prestakin oso onak diren “partxeak” lortzen dira. Bigarren metodoa PMzko besikula erraldoien (GPMV; Giant Plasma Membrane Vesicles) prestakinean oinarritu zen, zeintzuk PM isolatuaren lagin gisa hartuak diren (Scott, 1976; Baumgart *et al.*, 2007). GPMV hauek, zelula kultibora %1–5 (vol/vol) etanol, azetona, formaldehido edo DMSO gehituz lor daitezke (Baumgart *et al.*, 2007). Besikulazioa gatz ezberdinez eragiteaz gain, tanpoi hipertonikoak erabiliz ere lor daitezke (Piccolo *et al.*, 2012). “Baba” hauek mikroskopia optikoen bidez era egoki batean ikusi daitezke.

“Baba” eta “partxe” prestakinak konparatu eta karakterizatzeko mikroskopia bidezko ikuskapenak, Laurdan fluoreszentsia bidezko polarizazio orokorra (GP, General Polarization), indar atomikodun mikroskopia (AFM, Atomic Force Microscopy) eta masa espektrometria (MS) analisia erabili ziren. Laurdan bidez neurturiko GPa eta AFM bidezko indar espektroskopikoa aukeratzearen arrazoia, oso fundamentu fisiko ezberdinak izanik, biek, elkarri lotutako parametroak ematen dituztela da. Batak mintzaren ordena eta besteak mikro-zunda baten bidez zeharkatua izateko erresistentzia mekanikoa, hain zuzen ere.

MSak parametro kimiko baten informazioa ematen du: mintzaren lipido konposizioa, zeinak ikusitako ezaugarri fisikoen zergatia ulertzen laguntzen duen.

3.2. Materialak eta Teknika Esperimentalak

3.2.1. Materialak

CHO-K1 zelula lerroa ATCCn (Manassas, VA) erosi zen. Zelulen hazkuntzan erabilitako produktuak; DMEM:F12 (Dulbecco's Modified Eagle Medium: Nutrient Mixture F-12) FBSa (Fetal Bovine Serum, fetuko behi seruma), penizilina, estreptomizina eta GlutaMax gehigarria Thermofisherren (Waltham, MA) lortu ziren. Produktu organikoak Thermofisherrekoak (Waltham, MA) izan ziren. Fluoroforo denak; Di-4-ANEPP, Hoechst 33342, BODYPY FL C5-ceramide eta Mitotracker Green, Thermofisherren (Waltham, MA) eskuratu ziren. Tanpoien prestaketarako erabilitako gatzak; Tris, NaCl, Tris, KCl, NaCl, CaCl₂, HEPES Sigma-Aldrichen (San Luis, Misuri, Estatu Batuak) erosi ziren. Erreaktibo guztiak (gatz eta disolbatzaile organikoak) gradu anatilikokoak izan ziren.

3.2.2. Zelula hazkuntza

Ikerketa hau egiteko CHO-K1 (ATCC, Manassas, VA) zelula lerroa erabili zen. Zelulak DMEM:F12 (Dulbecco's Modified Eagle Medium: Nutrient Mixture F-12) medioan hazi ziren, zeinak %10 FBS, 100 U/ml penizilina, 100 U/ml estreptomizina, eta 6 mM glutamina (GlutaMax bidez gehitua) zituen. Zelulak 37°Ctan eta %5eko CO₂ atmosfera hezean kultibatu ziren. Zelula kultiborako produktu guztiak Thermofisherren (Waltham, MA) erosi ziren.

3.2.3. Laginen prestaketa

Neurketak egiteko, zelula osoak, zelula osoen lipido erauzketak, GPMVak (bapak), gainazalera itsatsitako partxeak eta lamela bakarreko besikula erraldoiak (GUV; Giant Unilamellar Vesicles) erabili ziren.

3.2.3.1. Zelulen lipido erauzketa

Lipido erauzketa Ahyayauch *et al.*en (2018) bezala gauzatu zen. Laburki, hasteko zelula *pelletak* 60% (v/v) azido perklorikotan berreseki ziren. Gero, laginak

Partxeak eta babak: CHO zelulen mintz plasmaticoaren bi prestakinen konposizio eta propietate biofisikoen arteko konparaketa

14000 xg-tan 15 minutuz zentrifugatu eta gainjalkina kendu zen. *Pelletak* erauzketa tutuetara mugitu eta bertan 2.5 ml kloroformo:metanolean (2:1) (v/v) berreseki eta 15 minutuz nahastu ziren. Ostean, 5 ml 0.1 mM HCl gehitu, laginak homogeneousatu eta 1700 xg-tan 20 minutuz zentrifugatu ziren. Gainjalkinak kendu ziren lipidodun fase organikoak beheko aldean zirauen bitartean. Azkenik fosfato analisi bidez fosfolipidoen kontzentrazioa neurtu zen.

3.2.3.2. GPMVen eraketa.

CHO zelulen babatzea eragin zen (3.S1 irudia). Zelulak T25 *flasketan* konfluentzia lortu arte hazi eta bi aldiz GPMV tanpoiz (2 mM CaCl₂, 10 mM HEPES, 150 mM NaCl, pH 7.4) garbitu ziren. Gero, zelulak GPMV formazio erreaktiboz (momentuan prestatu 2 mM ditiotritol eta 25 mM paraformaldehidodun GPMV tanpoia) ordu batez eta 37°Ctan inkubatu ziren.

Inkubazioaren ostean, GPMVdun GPMV erreaktiboa *flasketatik* batu eta 14000 xg-tan 20 minutuz zentrifugatu zen. Ostean, gainjalkina kendu eta ditiotritol eta paraformaldehido hondarrak guztiz kentzeko bi zentrifugazio pausu burutu ziren. Azkenik, GPMVak 500 µl GPMV tanpoian berreseki ziren (Manni *et al.*, 2015).

3.2.3.3. PM partxeen isolamendua.

Zelulen PMak Bezrukov *et al.*ek (2009) deskribatu bezala isolatu ziren. Hitz gutxitan, kristalezko oinarridun plakak (edo mika orriak) polilisinaz gaineztatu eta 30 minutuz giro tenperaturan eta UV erradiaziopean fluxu laminarreko kanpian utzi ziren. Gehiegizko polilisina kendu eta plaka edota mika orriak bi aldiz PBSz garbitu ziren. Zelulak %50eko konfluentzian erein eta gainazalera itsasteko helburuz 2 orduz inkubatu ziren. Inkubazio ostean itsatsi gabeko zelulak kentzeko, Tris tanpoia erabiliz (150 mM NaCl, 25 mM Tris, 2 mM KCl) bi garbiketa burutu ziren. Gero, zelulak 2 minutuz ur destilatu hotzean mantenduz beraien putzea eragin zen. Ostean, 20 mL-ko xiringa bati lotutako 19X1-1/2(TW)A orratz batekin sortutako presio fluxu baten bidez zelulen apurketa mekanikoa lortu zen. Honetarako plakak fluxuarekiko 60 gradutan jarri eta prozesuan zehar xumeki biratuak izan ziren. Emaizta gisa, zelularen barne edukia kanporatua izan zen, PMak gainazalera itsatsiak jarraitzen zuten bitartean. Azkenik, hiru garbiketa pausu burutu ziren kanporatutako zelula barneko edukia kentzeko.

Purifikazioaren kalitatea txekatzeko, zelula osoak eta isolatutako PM partxeak fluoroforoz markatu ziren. Alde batetik, fluoreszentzia orokor gisa Di-4-ANEPPDHQ ($\lambda_{\text{ex}} = 465 \text{ nm}$, $\lambda_{\text{em}} = 635 \text{ nm}$) eta bestetik, organulu bakoitzerako espezifikoak diren fluoroforoz tindatu ziren. Nukleoa, $2.8 \mu\text{M}$ Hoechst 33342an ($\lambda_{\text{ex}} = 361 \text{ nm}$, $\lambda_{\text{em}} = 497 \text{ nm}$) 10 minutuz 37°C tan edukiz tindatu zen, Golgi aparatua $10 \mu\text{M}$ BODYPY FL C5-ceramide ($\lambda_{\text{ex}} = 500 \text{ nm}$, $\lambda_{\text{em}} = 510 \text{ nm}$) 30 minutuz 37°C tan izanez eta mitokondrien tindaketa $0.75 \mu\text{M}$ Mitotracker Greenan ($\lambda_{\text{ex}} = 488 \text{ nm}$, $\lambda_{\text{em}} = 510 \text{ nm}$) 30 minutuz 37°C tan edukiz. Fluoroforo guztiak Thermofisherren (Waltham, MA) erosi ziren.

Irudiak Leica TCS SP5 II mikroskopio konfokal bat (Leica Microsystems GmbH, Wetzlar, Alemania) erabiliz hartu ziren. Fluoreszentzia intentsitatea neurtzeko ImageJ *softwarea* erabili zen: Fluoroforo bakoitzaren fluoreszentzia intentsitatea neurtu eta organulu espezifiko bakoitzaren kontaminazioa kuantifikatu zen. Emaitzak 3.S2 irudian ageri dira.

3.S2A eta 3.S2D irudietan zelula osoak eta PM partxeak Di-4 ANEPPDHQ fluoroforo orokorrez, eta nukleoarekiko espezifikoa den Hoechst 33342z markatuak ikus daitezke; PM laginak nukleo seinalearen %1.4a bakarrik dauka. 3.S2B irudian Mitotracker Green bidezko mitokondrien markaketa antzeman daiteke. PMaren purifikazio ostean, mitokondrioekiko espezifikoa den Mitotracker seinalea, %4.7ra jaitsi zen (3.S2B eta 3.S2E irudiak). 3.S2C irudian Bodipy FL C5-Cer fluoroforo bidez markatutako Golgia begietsi daiteke. 3.S2F irudiak, txoke osmotiko bidezko PM formakuntza ostean Golgi mintzen %6.8ak laginean dirauela erakusten du. Balio numerikoen bitartez, daukagun purutasun maila neurtu eta Bezrukov *et al.*ek (2009) lortu zutenarekin alderatu dugu, bi balio serieak oso antzekoak direlarik.

3.2.3.4. GUV formakuntza

GUVak Angelova eta Dimitrovek (1988) garatutako elektroformazio metodoaren modifikazio baten bidez eta Industrias Técnicas ITCK (Bilbo, Espainia) emandako PRETGUV 4 ganbera bat erabiliz sortu ziren.

3.2.3.5. SUV formakuntza

Hasteko, disolbatzailearen edozein hondar kentzearen, laginak 2 orduz hutsean eduki ziren. Gero, lipidoak PBS tanpoiean berreseki eta zunda bidezko Soniprep 150 sonikatzaile (MSK, Londres, Erresuma Batua) batez sonikatuz SUVak sortu ziren.

3.2.4. Laurdan bidezko Polarizazio Orokorra (GP)

Laurdan fluoreszentzia bidezko GPa maiz erabiltzen da mintzen jariakortasun/zurruntasun adierazle gisa. Lipido bat gel fasean dagoenenean, Laurdan emisioak bere maximoa 440 nmko uhin luzeran izan ohi du. Likido kristalino fasean berriz, espektroa 490 nmko uhin luzerantz mugitzen da (Krasnowska *et al.*, 1998). GP neurketak zelula osoetan, GPMVetan, PM partxeetan edota lipido erauzkinekin sortutako mintz ereduetan (SUV edo GUVak) burutu ziren.

3.2.4.1. Zelula osoak

Kristal oinarriko plaketan hazitako zelulak, 5 minutuz 5 μ M (amaierako kontzentrazioa) Laurdan (Molecular Probes, Eugene, OR) fluoroforoz markatu, eta PBS bidezko zenbait garbiketa burutu ostean, zelulak ikuskatu ziren.

3.2.4.2. Babak (GPMVak)

5 μ M Laurdanekin nahastutako babak polilisinaz gaineztatutako kristal oinarridun plakatxoetara (MatTek, Ashland, OR) gehitu ziren. Babak ikuskatu aurretik 3 ordu itxaron ziren GPMVak hauspeatu zitezen.

3.2.4.3. Partxeak

Partxeak sortzeko polilisinaz gaineztatutako kristal oinarridun plakak eabili ziren. Partxeak 5 minutuz, 5 μ M (amaierako kontzentrazioa) Laurdan bidez markatu ziren. Azkenik, beraien ikuskapena burutu aurretik PBS bidezko bi garbiketa burutu ziren.

3.2.4.4. GUVak

Aurretik erauzitako eta kloroformo:metanol (2:1)ean disolbatutako 0.2 mM lipido, 0.01 mM Laurdanekin nahastu zen. Lipido *stock* honetako 3 μ l Pt elektrodoen

gainean jarri eta 2 orduz laginak hutsean mantenduz, disolbatzaile organikoaren trazuak kendu ziren. Gero, 400 μ l 300 mM sakarosa tanpoi bidez Pt elektrodoak estali eta uhin elektrikoaren sorgailu (TG330 function generator, Thurlby Thandar Instruments, Huntington, Erresuma Batua) batera konektatu ziren. Sorgailuak txandakako korrante baldintzetan zirauen (10 Hz, 2.5 VRMS 120 minutuz). GUVak ikuskatzeko, beraien formakuntzaren ostean, ganbera mikroskopia konfokal fluoreszente batean kokatu zen.

3.2.5. Irudiak hartzea

Irudiak Leica TCS SP5 II (Leica Microsystems GmbH, Wetzlar, Alemania) mikroskopia bat erabiliz eta ur-murgiltzeko 63x objektibo baten (irekiera numerikoa, NA, numerical aperture=1.2) bidez eskuratu ziren. Eskaneatutako lerroko 512×512 pixeldun argazkiak 400 Hz-tan atera ziren. Fotoaukeraketa ekiditeko, imajinak plano ekuatorialean jaso ziren. Laurdan bidez markatutako laginen bi-fotoizko irudiak hartzeko, 780 nmtan jarritako taupadazko titanio-zafirozko (Mai-Tai Deepsee, Spectra-Physics) laser bat erabili zen. Fluoreszentsia emisioa eskaneatu gabeko (NDD; non-descanned) detektore hibridoak erabiliz batu zen. Izan ere, eskaneatutako fotobiderkatzaileekin alderatuz sentikortasun altuagoa erakusten dute.

Alde batetik, emisio espektroaren alde urdina, NDD 1 bidez 435 ± 20 nmtan, eta bestetik, alde gorria, NDD 2 bidez, 500 ± 10 nmtan batu ziren. Bi-fotoizko kitzikapenerako laginaren planoaren irradiatzea $\approx 500 \text{ GW} \cdot \text{cm}^{-2}$ -koa izan zen (Parasassi & Gratton, 1997).

3.2.6. Data eta irudien analisisia

Zelulen, baben, PM partxeen eta GUV irudien GPa kalkulatzeko MATLABen (MathWorks, Natick, MA) oinarritutako *softwarea* erabili zen (Carravilla *et al.*, 2015). Gutxienez lagin bakoitzeko 150 argazki analizatu ziren. Kanal bakoitzeko irudiak inguruko 2-pixelen batez bestearekin leunduak izan ziren eta GP balioa hurrengo ekuazioa erabiliz kalkulatu zen:

$$GP = \frac{I_B - G \times I_R}{I_B + G \times I_R}$$

Non I_B , NDD1ek batutako intentsitatea, I_R , NDD2k batutako intentsitatea eta G, zuzentze faktorea diren. G zuzentze faktorea, erabilitako fluoroforo kontzentrazio

beraren GPa neurtuz kalkulatu zen, kasu honetan DMSO puruan disolbatua (Owen *et al.*, 2012).

Zelula osoetan, intereseko gunea, hau da PMA, eskuz hautatu zen zelulen gainerako osagaietatik banatzeko asmoz.

3.2.7. Fluoreszentzia espektrometrikoaren analisisa

Zelula osoak, erauzitako lipidoz sortutako SUVak, GPMVak edota PM partxeak Laurdan bidez tindatu ziren. Zelula osoen, GPMVen eta PM partxeen 82.5 μM lipido, zuzenean, 0.75 μM Laurdan kontzentrazioz (amaierako kontzentrazioa) markatu ziren. Kloroformo:metanol (2:1)ean disolbatutako lipido erauziak Laurdan fluorforoarekin nahastu eta disolbatzaile organikoa guztiz lehortu arte, N_2 fluxu baten bidez lurrundu zen. Gero, disolbatzailearen edozein hondar kentzeko, laginak 2 orduz hutsean eduki eta lipidoak tanpoi egokian (NaCl 150 mM, Hepes 25 mM, pH 7.4) berreseki ziren (82.5 μM lipido eta 0.75 μM Laurdan, bukaerako kontzentrazioak). Sonikaturiko SUVak zunda bidezko Soniprep 150 sonikatzaille (MSK, Londres, Erresuma Batua) batez sonikatuz sortu ziren. Fluoreszentzia neurketak QuantaMaster 40 espektrofluorometro (Photon Technology International, Lawrenceville, NJ) bat erabiliz egin ziren (Santis *et al.*, 2018).

3.2.8. AFMa

GPMVen, PM partxeen eta zelulen lipido erauzketez sortutako bigeruzak leunak (SPB, supported planar bilayers) AFM bidez eskaneatu ziren. Kalitate altuko V-2 urradura gabeko mikak (Asheville-Schoonmaker Mica Co., Newport News, VA) erabili ziren. Hasteko, BioCell (JPK Instruments, Berlin, Alemania) batean kokaturiko 1.2 cm^2 -ko mika orri batean 3 mM CaCl_2 tanpoidun 180 μL gehitu ziren. Gero, CHO zelulen lipido erauzketaz sorturiko 0.4 mM kontzentraziodun 80 μL SUV jarri ziren. BioCell-aren tenperatura mailaz maila igo zen (5°C 5 minuturo) 80°C ra iritsi arte. Besikulak mikaren gainazalean zabal zitezen, tenperatura horretan 30 minutuz mantendu ziren. Ostean, laginak 30 minutu gehiagoz giro tenperaturan utzi ziren hauek orekara iritsi zitezen. Azkenik, zabaldu gabeko besikulak eta Ca^{2+} katioiak kentzeko, kaltzio gabeko tanpoia erabiliz 5 garbiketa egin ziren (Monasterio *et al.*, 2017).

3.2.8.1. Babak.

Mika orrian GPMVen kokapen zehatza zein zen jakiteko, lehendabizi, babak Di-4-ANEPPDHQ fluoroforoa erabiliz markatu ziren. Gero, 3 ordu itxaron ziren laginak polilisinaz gaineztatutako mika orriaren gainean sedimentatu zitezten.

3.2.8.2. PM partxeak

Isolaturiko PM partxeak aurretik azaldu den bezala prestatu ziren; kasu honetan, kristal oinarritzko plakak erabili orde, polilisinaz estaliriko mika orriak erabiliz.

3.2.8.3. Neurketa topografikoak

Laginen neurketa topografikoak kontaktu eskaneatze bidez egin ziren. Honetarako NanoWizard II AFM (JPK Instruments, Berlin, Alemania) bat erabili zen. Neurketa egoki bat burutzeko, AFMa Leica mikroskopio bati erantsia eta bibrazioak ekiditeko Halcyonics Micro 40 mahai batean (Halcyonics, Inc., Menlo Park, CA) kokatua zegoen. Aldi berean esparru akustiko (JPK Instrument) baten barnean aurkitzen zen. Irudiak ateratzeko, 0.1 edo 0.5 N/m-ko konstante malgudun V formako MLCT Si_3N_4 *cantileverra* (Bruker, Billerica, MA) erabili zen. Laginen lodiera “zeharkatutako lerroaren” altuera analisi bidez onetsi zen. GPMVak miken gainazalean zabaltzen ez zirenez, beraien irudi topografikoak ezin izan ziren gauzatu.

3.2.8.4. Indar espektroskopikozko neurketak

V formadun MLCT Si_3N_4 *cantileverrak* (Bruker, Billerica, MA), lipido gabeko tanpoiean murgildutako mika orriak erabiliz, 0.1 edo 0.5 N/m-ko konstante malguan kalibratu ziren. Horretarako metodo termikoa erabili zen. Indar espektroskopikoa 1 $\mu\text{m/s}$ -ko abiaduran gauzatu zen. Indar koskak, kurba bakoitzerako trazu hedatuko jauzi moduan zehaztu ziren. Gutxienez lagin mota bakoitzeko 3 lagin eskaneatu ziren eta hauetako bakoitzean 50-100 kurba gauzatu ziren.

3.2.9. Masa espektroskopia (MS) analisia

3.2.9.1. Lipido erauzketa

Lipido erauzketa eraldatutako metil-tert-butil-eter (MTBE) protokoloa erabiliz gauzatu zen (Guri *et al.*, 2017a). Laburki, plakak izotz gainean kokatuak zeuden

Partxeak eta babak: CHO zelulen mintz plasmaticoaren bi prestakinen konposizio eta propietate biofisikoen arteko konparaketa

bitartean, zelulak PBS hotzez garbitu eta 500 µl PBS hotz erabiliz arraspatu ziren. Zelula suspentsioa 2 ml-ko tutuetara pasatu eta 3200 rpm-tan 5 minutuz eta 4°Ctan zentrifugatu ziren. Gainjalkina kendu ostean, laginak -20°Ctan gorde edota zuzenean beraien erauzketa egiteko erabili ziren. GPMV eta PM partxeak aurretik azaldu den moduan prestatu ziren. Ostean, laginetara 360 µl metanol gehitu eta hauek bortexeatu ziren. Lipido estandarrez osatutako nahaste bat (ikus 3.1 taula) gehitu eta laginak Cell Disruptor Genie (Scientific Industries, Inc) bat erabiliz 10 minutuz 4°Ctan bortexeatu ziren. Gero, MTBEa (1.2 mL) gehitu eta laginak ordu batez giro tenperaturan irabiatu ziren (750 rpm). Faseen banaketa 200µl H₂O gehituz eragin zen; laginak 10 minutuz giro tenperaturan inkubatu ostean 1000 xg-tan 10 minutuz zentrifugatu ziren. Goiko fasea (organikoa) 12 mm-ko erroka tapadun kristalezko tutuetara pasatu eta beheko fasea, 400 µl goi fase artifizial [MTBE/metanola/ura (10:3:1.5, v/v/v)] erabiliz, berriz erauzi zen. Bi goi-faseak konbinatu, kopuru osoa 3 alikuotetan banatu (fosfolipidoentzat, esterolentzat eta esfingolipidoentzat) eta Zentribapa (50°Ctan) edota nitrogeno fluxu bat erabiliz, laginak lehortu ziren. SL alikuotak metilamina tratamenduz (Clarke metodoa) deazilatu ziren (fosfolipidoak kentzeko). Horretarako 0.5 mL monometilamina erreaktibo [MeOH/H₂O/n-butanola/metilamina soluzioa (4:3:1:5 v/v)] lipido lehorren gainean gehitu eta laginak sonikatu ziren (5 minutuz). Ostean, laginak ordu batez 53°Ctan inkubatu ziren irabiatzen zeuden bitartean. Azkenik, lehortu egin ziren. Monometilaminaz trataturiko lipidoak n-butanol erauzketa bidez desgazitu ziren. Horretarako H₂Oz asetutako n-butanolaren 300 µl lipido lehorren gainean gehitu zen. Laginak bortexeatu, 5 minutuz sonikatu eta hauen gainean MS-graduko 150 µl ur gehitu zen. Nahasketa bortexeatu eta 3200 xg-tan 10 minutuz zentrifugatu ziren. Goiko fasea 2 mL-ko ambar ontzitzoetara pasatu zen. Beheko fasea, H₂O-z asetutako 300 µl n-butanol erabiliz, bi aldiz gehiagotan erauzi zen. Goi fase guztiak konbinatuak eta aurrean azaldu den bezala lehortuak izan ziren.

3.2.9.2. Glizerofosfolipido eta esfingolipidoen detekzioa kuadrupolo hirukoizdun masa espektrometroan

Fosfolipidoen eta esfingolipidoen alikuotak 250 µl kloroformo/metanol (1:1 v/v)ean [kromatografia-likido (LC, Liquid Chromatography)-MS/ erresoluzio altuko kromatografia likido (HPLC, High Performance Liquid Chromatography) gradukoa] berreseki eta 5 minutuz sonikatu ziren. Laginak 96 putzutzoko plateran pipeteatu ziren (azken bolumena = 100 µl). Lipido guztidun (TL, Total Lipids) laginak modu

negatiboko disolbatzailean [kloroformoa/metanola (1:2) + 5 mM amonio azetatoa] 4 aldiz diluitu ziren. Modu positibodun disolbatzailean berriz (kloroformoa/metanola/ura (2:7:1 v/v) + 5 mM amonio azetatoa) 10 aldiz. Esfingolipidoak 10 aldiz diluitu ziren, betiere modu positiboko disolbatzailean. Ostean, plaka masa espektrometroan jarri zen. Esfingolipidoen espezie molekularren identifikazioa eta kuantifikazioa gauzatzeko tandem masa espektroskopia gauzatu zen. Horretarako, ioi iturri nanofluxu robotikoarekin [Nanomate HD (Advion Biosciences, Ithaca, York Berria)] ekipatutako TSQ Vantage Triple Stage Quadrupole masa espektrometroa (Thermo Fisher Scientific, Waltham, MA) erabiliz, monitorizaturiko erreakzio multiplea burutu zen. Lipido mota bakoitzarentzako talka energia optimizatu zen.

3.1 Taula. Lipido mota bakoitzarentzako MS detekzio baldintzak.

Lipido mota	Estandarra	Polaritatea	Modua	Ioien m/z	Kolisio energia
Fosfatidilkolina [M+H] ⁺	DLPC	+	Ioi produktua	184.07	30
Fosfatidiletanolamina [M+H] ⁺	PE31:1	+	Ioi neutroaren galera	141.02	20
Fosfatidilinositola [M-H] ⁻	PI31:1	-	Ioi produktua	241.01	44
Fosfatidilserina [M-H] ⁻	PS31:1	-	Ioi neutroaren galera	87.03	23
Kardiopina [M-2H] ²⁻	CL56:0	-	Ioi produktua	Kate azilikoa	32
Zeramida [M+H] ⁺	C17Cer	+	Ioi produktua	264.34	25
Dihidrozeramida [M+H] ⁺	C17Cer	+	Ioi produktua	266.40	25
Hexosilzeramida [M+H] ⁺	C8GC	+	Ioi produktua	264.34	30
Hexosildihidrozeramida [M+H] ⁺	C8GC	+	Ioi produktua	266.40	30
Esfingomielina [M+H] ⁺	C12SM	+	Ioi produktua	184.07	26

Lipido bakoitzarentzako detekzio baldintzak 3.1 taulan ageri dira. Zeramida espezieak lehen kuadrupoloan gauzatutako ur galeraz kuantifikatu ziren. Erreplika biologiko bakoitza 2 erreplika teknikotan neurtu zen eta erreplika hauetako bakoitza 3 neurketetan. Lipido kontzentrazioa barne estandarren arabera kalkulatu zen, ostean lipido erauzketa bakoitzeko lipido totalarekiko normalizatu zen (% mol).

3.2.10.3. Kolesterola neurtzeko gas kromatografiako (GC) masa espektrometria

Lipido erauzketak gas kromatografia (GC, Gas Chromatography)-MS bidez analizatu ziren (Guan *et al.*, 2010). Laburki, laginak 15 m × 0.32 mm i.d. DF = 0.10eko FactorFour VF-5ms zutabe kapilar batez ekipatutako VARIAN CP-3800 GC an xiringatu eta kuadrupolo hirukoizdun GCaren elektroien energia -70 eV-an finkatu eta laginak 250°Ctan analizatu ziren. Hasteko, laginak 45°Ctan zegoen labe zutabeen jarri

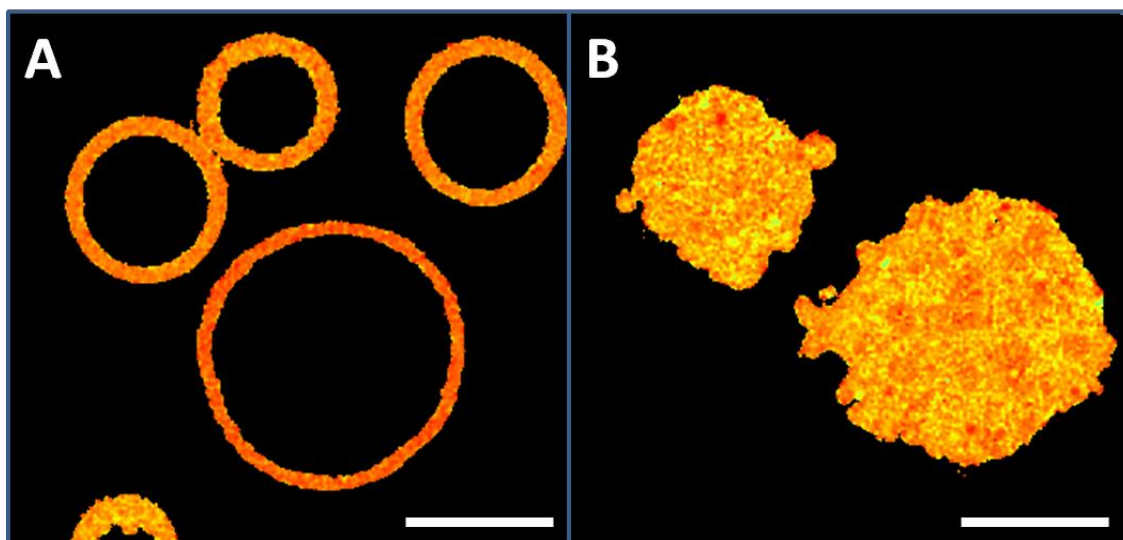
Partxeak eta babak: CHO zelulen mintz plasmaticoaren bi prestakinen konposizio eta propietate biofisikoen arteko konparaketa

ziren eta bertan 4 minutuz utzi ostean, 195°Ctara (20°C/min) berotu ziren. Esterolak gradiente lineal batez 195°Ctik 230°Cra (4°C/min), eluituak izan ziren. Gero, 320°Cra berotuak. Kolesterol bere erretentzio denboraren bidez (ergosterol estandar batekin konparatuz) eta NIST datu baseko zatiketa patroiekin alderatuz, identifikatu zen.

3.3. Emaitzak eta Eztatbaida

3.3.1. PMaren purifikazioa

Fluoreszenteki markatutako CHO zelula osoak, PM partxeak eta babak mikroskopio konfokal baten bidez ikuskatu ziren. 3.1A irudiak Laurdan bidez markatutako zenbait GPMV erakusten ditu. GPMVek forma esferikoa dute. Barne egiturarik ez dutenez, beraien plano ekuatorialeko irudiek eraztun morfologia hartzen dute. Bestalde, PM partxeak gainazal batera itsatsiak daudenez, egitura laua dute, hortaz, gainazal guztian zehar markatuta ageri dira (3.1B irudia). Beraien tamainei dagokienez, GPMVen diametroak 3-20 μm bitartekoak dira [altuera maximoaren erdian duten zabalera (FWHM, Full Width at Half Maximum): 12.3 ± 3.3 , batez besteko balioa \pm SD], bestalde PM partxeek 8-25 μm bitarteko diametroak dituzte (FWHM: 16.6 ± 4.4 , batez besteko balioa \pm SD).

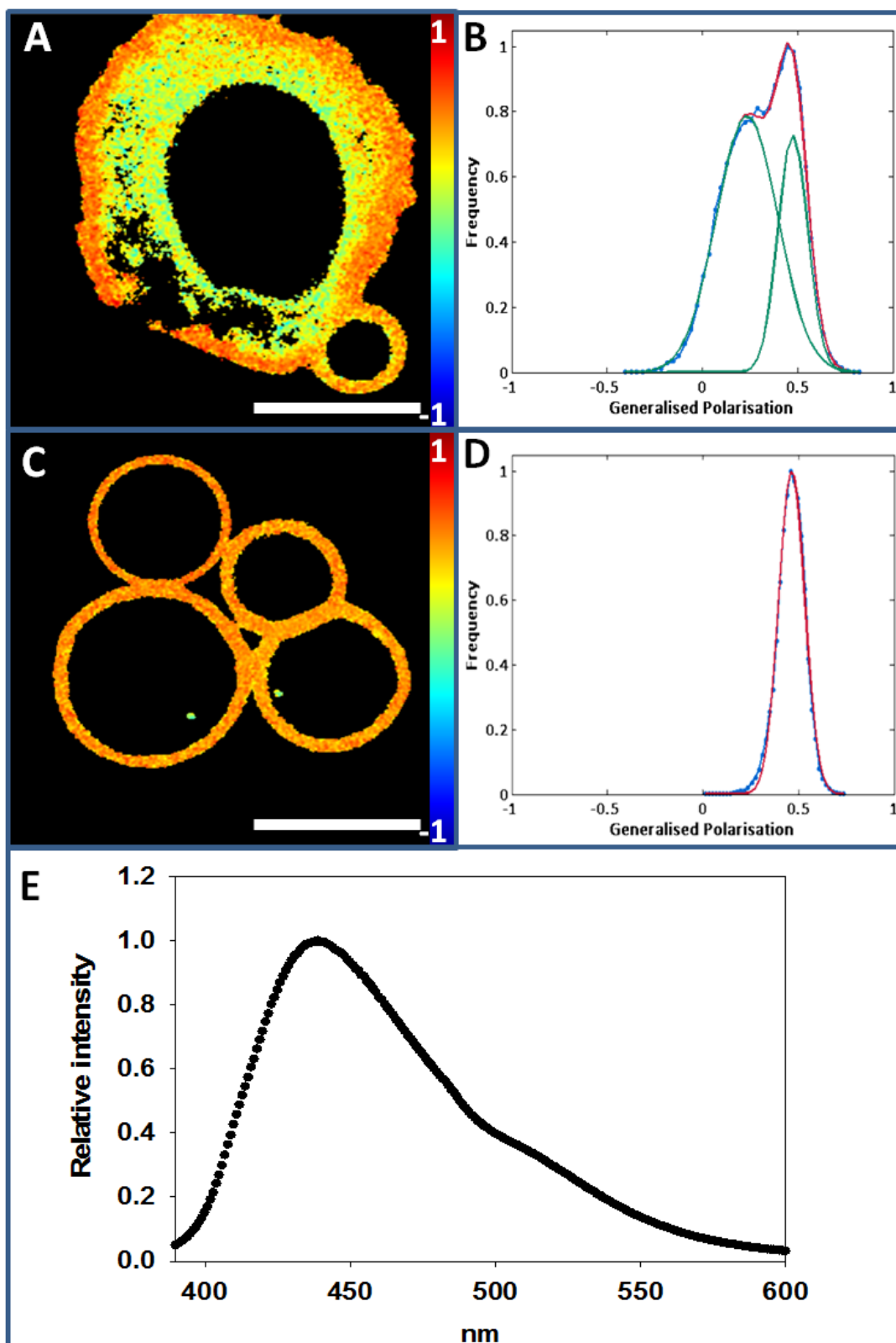


3.1 irudia. CHO zelularen PMaren prestakinak. A, GPMV edo babak. B, PM partxeak. Barra = 10 μm .

3.3.2. Laurdan fluoreszentzia bidezko GPa

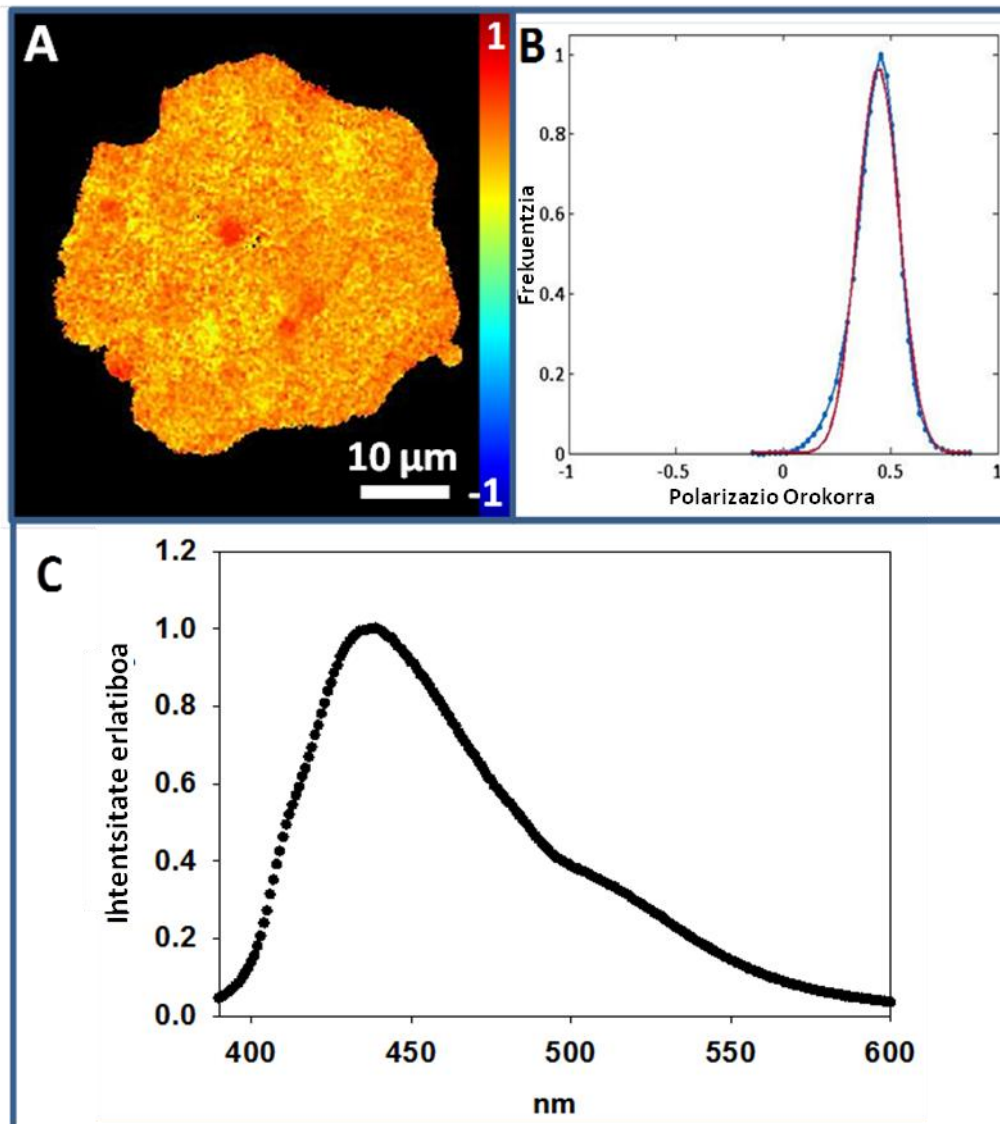
3.S1 irudian paraformaldehido eta ditiotreitol bidez, CHO zelula baten GPMV sorreraren pauso ezberdinak ikus daitezke. Laurdan bidez markaturiko baba-formazio irudian (3.2A) bi gune ezberdinak daitezke: zurrunago bat (laranja-gorria), zeina PM ari dagokion, eta jariakorra den beste bat (hori-berdea), gune intrazelularrari dagokiona. GP analisiak erakusten duenez, -1etik +1era doan eskalan, PMak 0.52 ± 0.04 -ko GP balioa du (20°Ctan). Gune intrazelularrak berriz, 0.20 ± 0.08 -koa (20°Ctan) (3.2B irudia). Datu hauek indartzeko hainbat kontrol esperimentu burutu ziren.

GPMVen formakuntzaren ostean, Laurdan fluoroforo markaturiko GPMV bakanduen irudiak atera ziren (3.2C irudia). Kolore intentsitatearen analisiak 0.47 ± 0.06 -ko (20°Ctan) populazioa homogeneo baten existentzia frogatu zuen (3.2D irudia). 3.2E irudiak isolaturiko GPMVen emisio espektroa erakusten du. Bertan, 20°Cko tenperatua konstantean gauzatutako analisi espektrometrikotan, 440 nmko uhin luzera inguruan maximo bat duela ikusi zen. Eraitza honek adierazten duenez, baldintza hauetan, GPMVaren gainazalak, batez beste fase ordenatu baten ezaugarriak ditu. Nahiz eta jariakorra (eta/edo zurrunagoak) diren nanodomeinuen koexistentzia ezin dezakegu baztertu.



3.2 irudia. 20°Ctan burututako GPMVen formakuntza eta GP neurketa. **A**, CHO zelula baten GPMV formakuntza (batez besteko GP balioa 0.44). **B**, A irudiaren polarizazio orokorraren grafikoa. **C**, CHO zeluletatik sorturiko GPMVen Laurdan markaketa. **D**, A irudiaren polarizazio orokorraren grafikoa. **E**, CHO zelula baten Laurdan emisio espektroa. Barra 10 μm .

PM purifikazio prozesuak partxeak gainzalean zehar hedatzea suposatzen du. Honek, partxeek morfologia irregular bat izatea eragiten du. 3.3A irudian Laurdan bidez markatutako CHO zelula baten PM partxe bakandu bat ikus daiteke. GP analisiarekin lotutako kolore intentsitatearen grafikoak tontor maximo bakarra detektatzen du, 0.44 ± 0.05 -ean (20°C tan) hain zuzen ere (3.3B irudia).

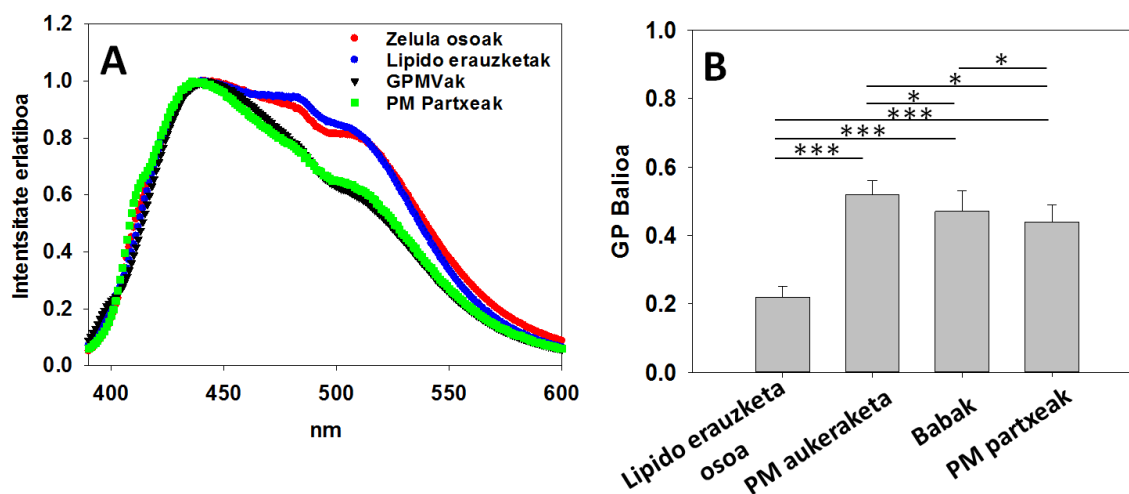


3.3 irudia. PM partxeen Laurdan markaketa (20°C tan). A, CHO zelula baten PM partxearen markaketa. B, A irudiaren polarizazio orokorraren banaketa grafikoa. C, CHO zelulen PM partxeen emisio espektroa.

3.3C irudiak espektrofluorimetro baten bidez neurtutako PM partxeen Laurdan emisio espektroa erakusten du. Partxeak itsatsita dauzkan gainazala arraspatu ostean, suspentsioa, Laurdan bidez markatu eta lagina espektrofluorometroan analizatu zen (20°C tako tenperatura konstantean). Emisio maximodun tontorra 440 nm inguruan

neurtu zen. Honek, baldintza hauetan, PM partxeko kate aziliko gehienak egoera ordenatu batean daudela esan nahi du. GPMVetan gauza bera ikusi zen. Aurretik esan bezala, honek ez du ordena molekular ezberdineko bestelako nanodomeinuen existentzia baztertzen.

3.4 irudian, hainbat laginek 40°Ctan daukaten Laurdan GP espektroa konpara daiteke. Zelula osoek eta zelula osoen lipido erauzkinekin egindako SUVek antzeko portaera daukate (3.4A irudia). Gainera, GPMV eta PM partxeek gainjartzen diren espektroak daukate. Azken aipaturako hauek, uhin luzera laburragoetara bideratuak daude. Emaitza honek, PM laginek, zelula oso edota zelula osoko lipido erauzkinekin egindako mintzek baino egitura ordenatuagoa dutela esan nahi du (3.4A irudia). Emaitza hauek aurretik argitaratutako zenbait ikerketekin bat datoz (Owen *et al.*, 2012; Aron *et al.*, 2017; Sezgin *et al.*, 2017). Gertakizun honen baieztapen sakonago baterako, Laurdan emisio espektroak 20 eta 30°Ctan ere neurtu ziren. Kasu hauetan ere antzeko ondorioetara iritsi zen (3S3 irudia).



3.4 irudia. Laurdan GP neurketak. **A**, Laurdan fluoreszentzia bidezko mintz fosfolipidikoen emisio espektroa. Gorria, CHO zelula osoak; urdina, CHO zelulen lipido erauzkinekin sortutako SUVak; beltza, CHO zelulen babak; berdea, CHO zelulen PM partxeak. Espektroak 40°Ctan neurtuak. **B**, Mikroskopioko irudietatik lortutako Laurdan GP balioak (20°Ctan, n = 150, balioa = batez bestekoa ± SD). Estatistikoki adierazgarriak diren ezberdintasunak ANOVA eta Student t test bidez neurtu ziren. Adierazgarritasuna: (*) p<0.05; (**) p<0.01; (***) p<0.001.

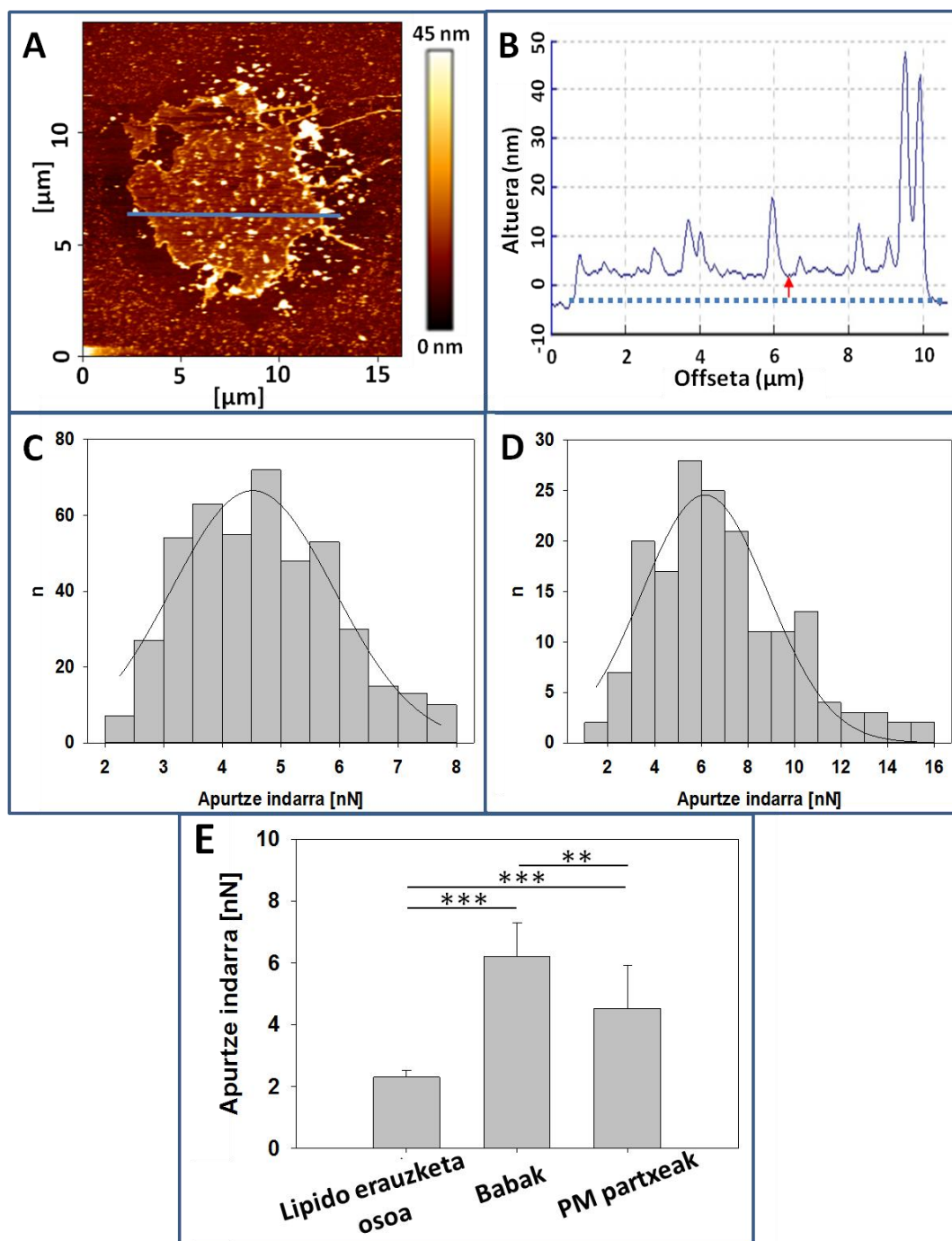
3.4B irudiak PM prestakin eta zelula osoen lipido erauzkinekin artean existitzen diren ezberdintasunak erakusten ditu. Datuak mikroskopioko irudietatik lortu ziren (20°Ctan). Estatistikoki (ANOVA eta Student t testa) ezberdintasun oso adierazgarriak existitzen dira zelula osoen lipido erauzkinekin eta PMen (zelula osoen irudietatik

hautatutako PMak, babak eta PM partxeak) neurketen artean. Zelula osoen lipido erauzketen bidez egindako mintzen GP balioa, PMen lagin ezberdinen neurketa guztien balioa baino baxuagoa izan zen. Honek, zelula osoko lipido erauzketen bidez egindako mintzek PMa baino ordena baxuagoa dutela adierazten du. Emaitzak iradokitzen duenez, zelula batean dauden lipido mintzen ordena kontuan hartuz, bi populazio ezberdin existitzen dira: alde batetik, PMak eta bestetik, mintz intrazelularrak. Jakina da PMak mintz intrazelularrak baino ordena molekular altuagoko mintzak direla (Owen *et al.*, 2012). Zelula osoen lipido erauzien bidez egindako mintzen laginean, zeluka barneko mintzek, PMak baino askoz masa erlatibo altuagoa dute, eta beraz, azken honen GP balioak, GP balio orokorrean eragin baxua du. Ondorioz, zelula osoen lipido erauzkinekin egindako mintzen GP balioa, mintz intrazelularren GP balioaren oso antzekoa da, zehatz mehatz 0.22 ± 0.03 -koa (20°C tan).

PM prestakin ezberdinen artean ere ezberdintasunak existitzen dira (3.4B irudia). PM hautatuaren GP balioa 0.52 ± 0.04 da, GPMVena 0.47 ± 0.06 -koa eta PM partxeena 0.44 ± 0.05 -koa (20°C tan). ANOVA eta Student t testaren arabera ezberdintasunak estatistikoki oso adierazgarriak dira.

3.3.3. AFM mikroskopia eta indar espektroskopia

3.5A irudiak CHO zelula baten PM partxearen irudi topografikoa erakusten du. Partxe honek ertz irregularrak dauzka eta batez besteko $10 \mu\text{m}$ -dun diametroa du. 3.5B irudian, 3.5A irudian ageri den lerro urdinaren zeharkako lerroaren profil topografikoa ikus daiteke. Gezi gorriak PM partxearen batez besteko lodiera adierazten du ($\approx 4 \text{ nm}$). Lodiera hau bat dator lipido geruza bikoitz jariakorretan sarritan neurtutako lodierarekin. Mintzaren zenbait gune zehatzetan askoz lodiagoak diren egiturak ere neur daitezke. Agian, proteina, azukre edota PM partxearen sorreran sortutako tolesdurak direla eta. 3.5C irudiak PM partxe baten apurketa indarraren banaketa grafikoa erakusten du, zeinak $4.5 \pm 1.4 \text{ nN}$ -ko batez besteko balioa duen. Bestalde, 3.5D irudian, CHO zelulen GPMVen apurketa indarren banaketa grafikoa erakusten da; batez besteko balioa $6.2 \pm 1.1 \text{ nN}$. GPMVen mintzen zabaltze egoki bat gauzatzeko zailtasunak zirela eta, ezin izan zen beraien irudi topografikorik atera.



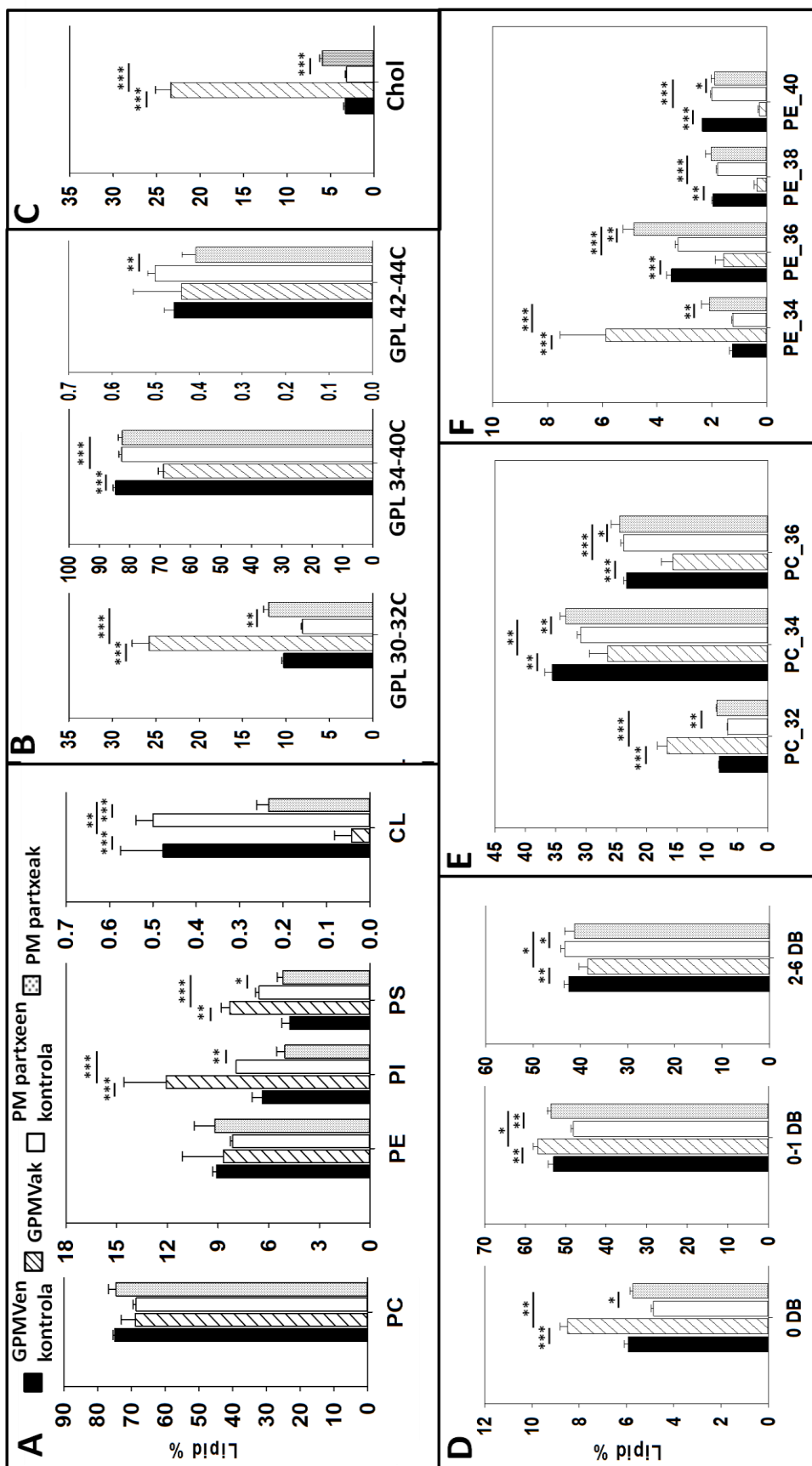
3.5 irudia. AFM neurketak. **A**, Polilisina gaineztatutako mika orriaren gainean dagoen CHO zelularen PM partxearen irudi topografikoa. **B**, 3.5A irudian adierazitako lerro urdinaren zeharkako lerroaren topografia grafikoa. **C**, PM partxearen apurtze indarraren distribuzio grafikoa. **D**, GPMVen apurtze indarraren distribuzio grafikoa. **E**, Prestakin ezberdinen apurtze indarren batez besteko balioen arteko konparaketa. Zelula osoen erauzketaen apurtze indarren balioa CHO zelulen lipido erauzkinekin egindako SPBetatik lortu zen. (n= gutxienez 160, balioa = batez bestekoa ± SD) Estatistikoki adierazgarriak diren ezberdintasunak ANOVA eta Student t test bidez kalkulatu ziren. Adierazgarritasuna: (*) p<0.05; (**) p<0.01; (***) p<0.001.

CHO zelulen lipido erauzketen bidez sortutako SPBen apurtze indarrari dagokionez, batez beste 2.3 ± 0.22 nN-takoa izan zen (3.5E irudia). GP balioekin gertatzen den bezala, zelula osoen lipido erauzketekin sortutako mintzen apurtze indarra, PM prestakinena baino baxuagoa da (ikus Laurdan GP balio eta AFM bidezko apurtze indarraren arteko korrelazioa 3.S2 irudian).

GPMV eta PM partxeen artean existitzen diren ezberdintasunak ez dira azaltzeko batere errazak. GPMVen formakuntzan zehar, paraformaldehidoak mintzen ezaugarrietan eragina izan lezake. Izan ere, errektibo hau zelula eta ehunen tinkotze protokoloetan erabili ohi da.

3.3.4. Lipido ikerketa

Ikertzen ari garen mintz prestakinen lipido moten datu guztiak material gehigarrian ageri dira (3.S1 taula eta 3.S5 irudia). CHO zelula osoen eta PM prestakinen lipido banaketaren laburpen bat 3.6 irudian ageri da. 3.6A irudian fosfolipidoen banaketa erakusten da. Neurtutako lagin guztietan, fosfatidilkolina, fosfolipido guztien %70 inguru da. Kolesterolarekin batera mintzaren jariatortasun homeostasia mantentzeaz eta glizerofosfolipidoen (GPL) saturazio maila kontrolatzeaz arduratzen den fosfatidiletanolaminari dagokionez ($\approx 10\%$) (Antwerpen & Govaerts, 2016), zelula oso eta PM prestakinen artean ez dago estatistikoki adierazgarria den ezberdintasunik (3.6A irudia). PE/PC erlazioa mintzaren jariatortasunean eragina duen parametro gisa proposatua izan da (Antwerpen & Govaerts, 2016). Lipido datuetan ikus daitekeenez PE/PC erlazioa ia berdin-berdina da, bai GPMV eta bere kontrolaren artean (0.126 eta 0.121 hurrenez hurren), baita zelula oso eta PM partxeen (0.134 and 0.136 hurrenez hurren) artean ere. Fosfatidilinositolari eta fosfatidilserinari dagokienez, zelula osoen eta PM prestakinen artean, estatistikoki adierazgarriak diren ezberdintasunak existitzen dira. Fosfolipido hauek kantitate urriagoan ageri dira PM partxeetan (baina ez GPMVetan) zelula osoetan baino. Kalvodova *et al.*ek (2009) *baby hamster kidney* (BHK) zelulekin eta Lorizate *et al.*ek (2013) HeLa eta MT4 zelulekin ikusitako portaera bera daukatela dirudi. Bestalde, neurtutako laginetan, mintz mitokondrialetan %10 inguru den kardiolipina lipidoa (van Meer *et al.*, 2008) ez da fosfolipido guztien %0.5 baino gehiago izatera iristen (3.6A irudia).



3.6 irudia. Masa espektroskopia bidezko zelula oso eta PM prestakinen lipido analisisa. A, Fosfolipido guztiak; B, Glizerofosfolipido labur, luze eta oso luzeak; C, Kolesterolia; D, Fosfolipidoen asetze maila (DB = lotura bikoitzak; Doble Bond); E, Kate azilikoaren luzeraren arabera fosfatidilkolinen banatzea; F, Kate azilikoaren luzeraren arabera fosfatidiletanolaminaren banatzea. Barrak: beltz zurruna, GPMV prestakinetarako trataturiko zelula osoak; marratua, GPMVak (babak); hutsa, MP prestakinetarako trataturiko zelula osoak; puntuduna, MP partxeak; adierazgarritasuna: (*) p<0.05; (**) p<0.01; (***) p<0.001

CHO zelula osoen glizerofosfolipidoen kate azilikoaren luzeraren banaketa Sampaio *et al.*ek (2011) eta Gerl *et al.*ek (2012) *Madin-Darby canine kidney* (MDCK) zelulekin ikusitakoaren antzekoa da (3.6B irudia). PM prestakinei dagokienez (3.6B irudia) kate-laburdun (30-32C) glizerofosfolipidoak, bai GPMV, baita PM partxeetan, zelula osoko erauzkintan baino ugariagoak dira. PM prestakinetan, kate laburdun glizerofosfolipido hauen kopuruaren igoera, kate luzedun glizerofosfolipidoen kopuruaren jaitsiera batekin orekatzen da. ANOVA eta Student t testak ezberdintasunak estatistikoki adierazgarriak direla erakusten du. PM laginen artean, GPMVek, PM partxeek baino kate labur gehiagoko, eta luze (34-40C) gutxiagoko, glizerofosfolipidoak daukate. Oso luzeak (42-44C) diren glizerofosfolipidoek dagokienez, proportzio baxuan existitzeaz gain, prestakin ezberdinen artean ezberdintasun txikiak daukate.

Lipidoen asegarritasun mailaren datuak 3.6D irudian ageri dira. CHO zelula osoen lipidoen asegarritasun balioak aurreko ikerketetan neurtutakoen antzekoak dira (van Meer *et al.*, 2008). Zelula osoen lipido erauzketak eta PM prestakinak beraien artean konparatzen baditugu, estatistikoki adierazgarriak diren ezberdintasunak existitzen dira. Azken aipatutakoek, fosfolipido poliasegabe gutxiago eta guztiz asetutako gehiago daukate.

CHO zelulen fosfatidilkolina espezieak beraien gantz azido katearen luzeraren (gantz aziliko bien luzeraren batuketa) arabera konparatzen baditugu (3.6E irudia), 32C espeziea; hau da, bi kate aziliko gehikuntzaz 32C atomo dauzkaten PCak, PM prestakinetan ugariagoak dira. Gauza bera gertatzen da 34C eta 36Cko PCekin PM partxeetan, baina ez GPMVetan (3.6E irudia). Emaidza bat dator Lorizate *et al.*ek (2013) ikusitakoarekin, zeintzuek HeLa eta MT4 zelulen PMan 32Cdun PCak ugariagoak direla ikusi zuten. Fosfatidiletanolaminaren gantz azido konposizioari dagokionez, adierazgarriena, 40Cdun fosfatidiletanolaminak, edozein PM prestakinetan zelula osoan baino urriagoak direla da (3.6F irudia). Gainera, Lorizate *et al.*ek (2013) HeLa zeluletan ikusi zuten bezala, 34Cko PEak, bai PM partxeetan baita GPMVetan ere, zelula osoetan baino ugariagoak dira. 36 eta 38Cko PEak kontutan hartuz, GPMV eta PM partxeen artean estatistikoki adierazgarriak diren ezberdintasunak existitzen dira, ziur aski beraien prestakuntza metodo ezberdinaren ondorioz.

Zelula osoen erauzketak, PM prestakinak baino kolesterol kantitate gutxiago dauka. PMA kolesterolean aberastua dagoela erakusten duen emaitza hau, bat dator

aurretik beste ikerketa talde batzuk argitaratutako lanekin (Lorizate *et al.*, 2013; Kalvodova *et al.*, 2009; Harayama & Riezman, 2018). Sezgin *et al.*ek (2015) M β CD bidezko kolesterol kopuruaren murrizketaz, PMaren GPa jaitsi egiten dela ikusi zuten. Honek aditzera ematen du, kolesterolak, GPL aseekin batera, PMari organulu intrazelularren mintzei baino zurruntasun handiagoa ematen diola. Zelula osoen lipido erauzkintan, lipido guztien %3.3 \pm 0.2a baino ez da kolesterola. Bestalde, balio hau %5.9 \pm 0.3ra igotzen da PM partxeetan eta % 23.4 \pm 1.77ra GPMVetan (3.6C irudia). PMan dagoen kolesterol kontzentrazio altuagoa, gantz azido poliasegabeen proportzio baxuagoarekin batera (3.6D irudia), bat datoz Laurdan (3.4 irudia) eta AFM (3.5 irudia) bidez lortutako emaitzekin. PMa zelula osoen lipido erauzkinekin sortutako mintzak baino ordenatuago eta paketatuago dagoela erakutsiz. Ez dago guztiz argi GPMV eta partxeen arteko kolesterol kopuruaren arteko ezberdintasunaren zergatiaren azalpena. Antzeko kolesterol kopuru altuak, beste PM prestakin batzuetan, hala nola GPMV edota silika bolatxo metodoetan, aurkitu izan dira (Lorizate *et al.*, 2013). Dena den, Keller *et al.*ek (2009) frogatutakoarekin lotua egon daiteke, zeintzuk GPMVen formakuntza prozesuan zehar, PMan lipidoen arteko albo-banaketa gertatzen dela ikusi zuen.

3.4. Ondorioak

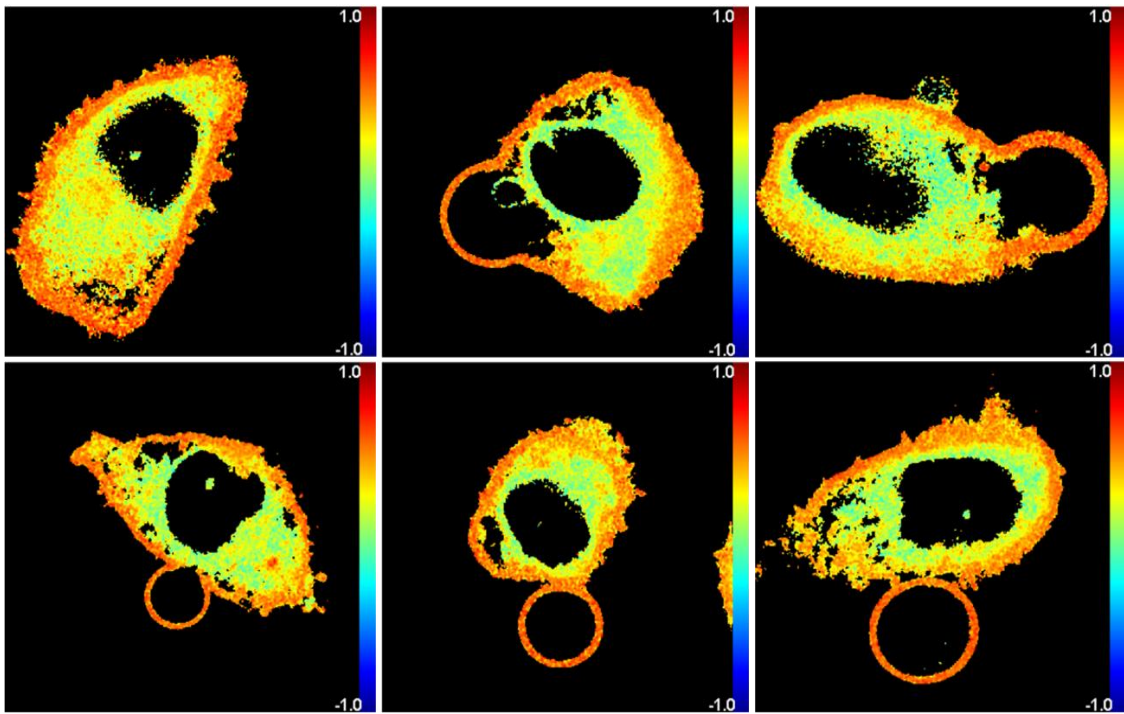
Laburbilduz, erakutsitako emaitzek, CHO zelulen PMaren egitura, biofisika eta biokimika ikertzeko erabilgarri izan daitekeen PM prestakinak kopuru egokian isolatzeko bi metodo ezberdin deskribatu dira. Lipidoen ordena molekularra eta erresistentzia nanomekanikoa antzekoa da GPMV (baba) eta PM partxeen artean, eta ezberdina (altuagoa), zelula osoen lipido erauzkinekin egindako mintzekin alderatuz. PMak lipido konposizioan ere berezitasunak erakusten ditu: aberatsa da kolesterolean eta erlatiboki urria gantz azido poliasegabeetan. PM prestakin eta zelula osoko mintzen arteko ezberdintasun hauek ez dute ezkutatu behar baba eta partxeen artean aldaerak (txikiagoak, baina adierazgarriak) existitzen direla. Ziur aski metodo bakoitzean erabilitako berezitasunen ondorioz. Ikerketa honek CHO zelulen PMaren, eta agian zitoeskeletoaren, egitura eta funtzio ikerketa sakonagoak egiteko atea irekitzen du.

3.5. Material Gehigarria

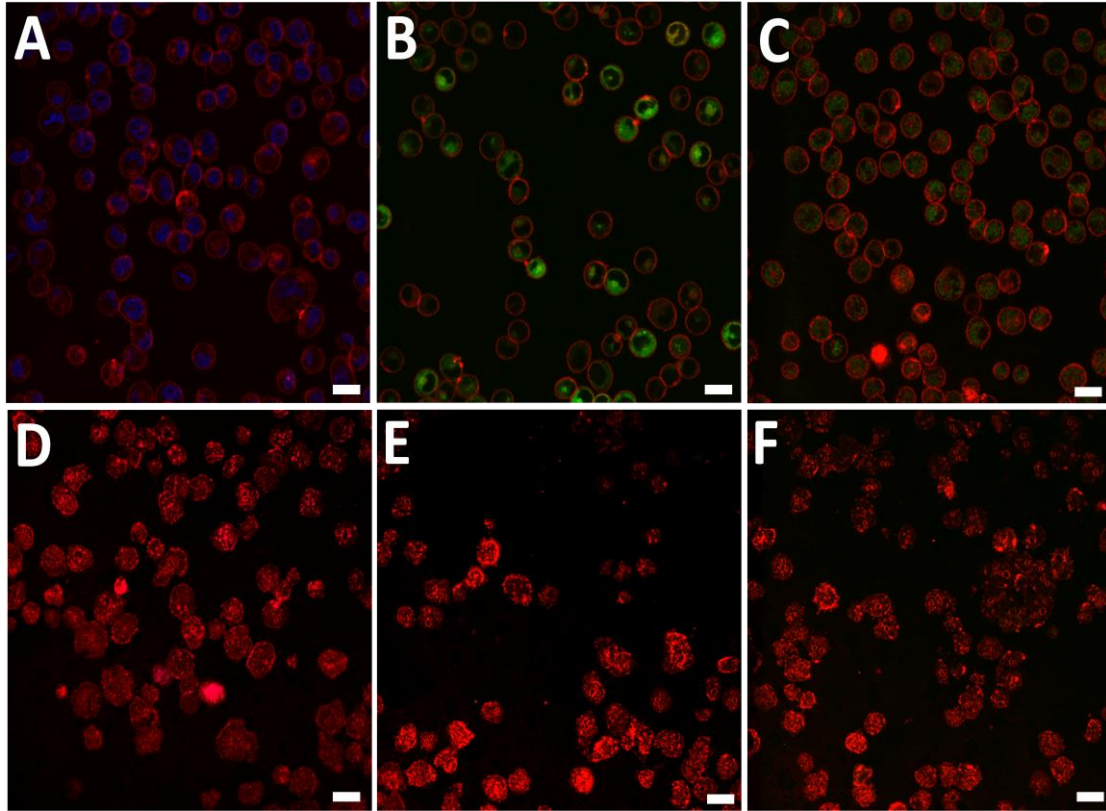
3.S1 Taula. CHO zelula oso eta mintz plasmatico prestakinen [babak (edo GPMVak) eta partxeak] informazio lipidomikoaren laburpena.

<https://drive.google.com/file/d/14Cep3h8bYxGxkStf-dJwHWycGnsXRe5X/view?usp=sharing>

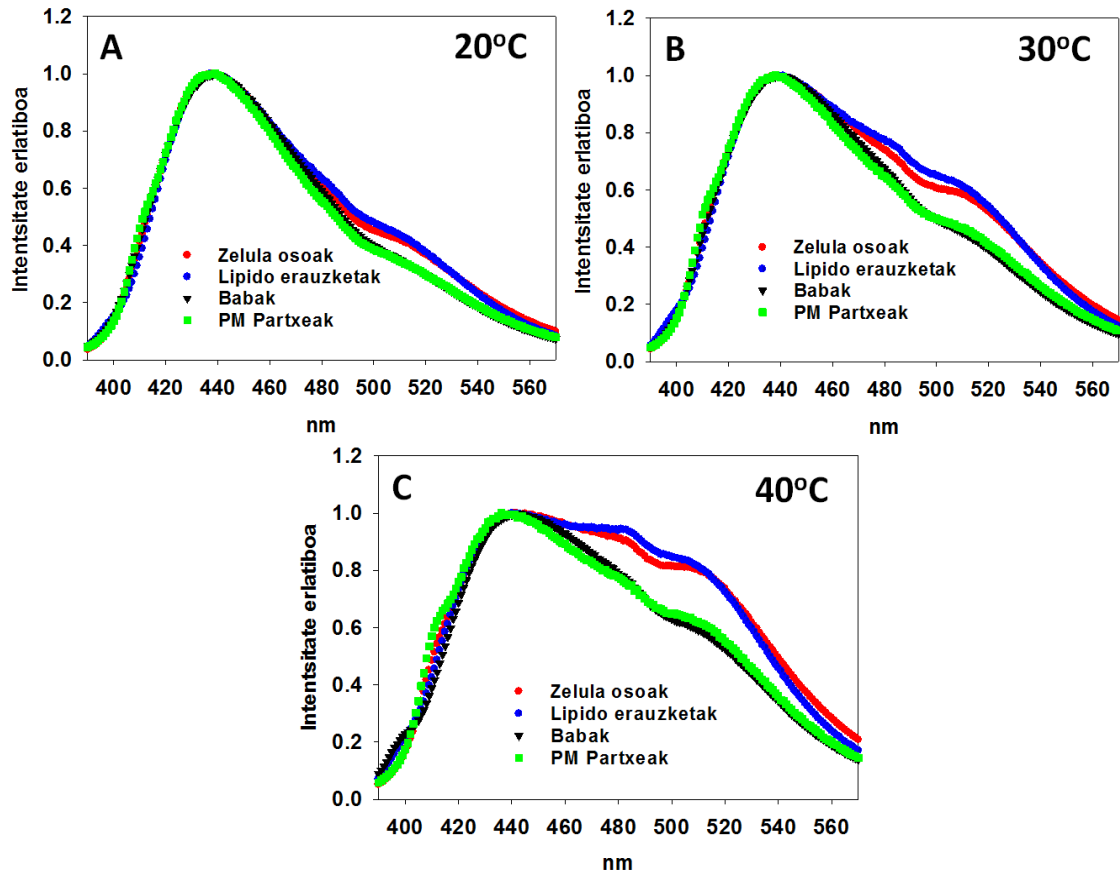
Partxeak eta babak: CHO zelulen mintz plasmaticoaren bi prestakinen konposizio eta propietate biofisikoen arteko konparaketa



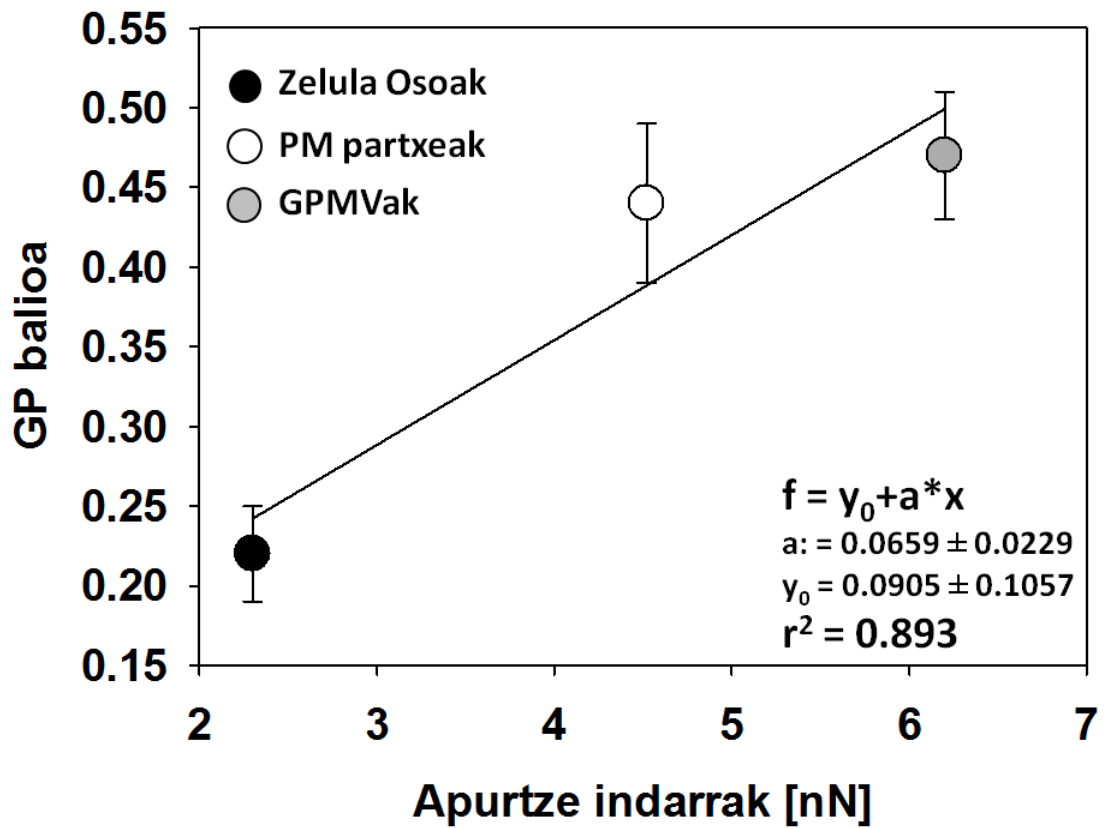
3.S1 irudia. GPMVen formakuntza pauso ezberdinak.



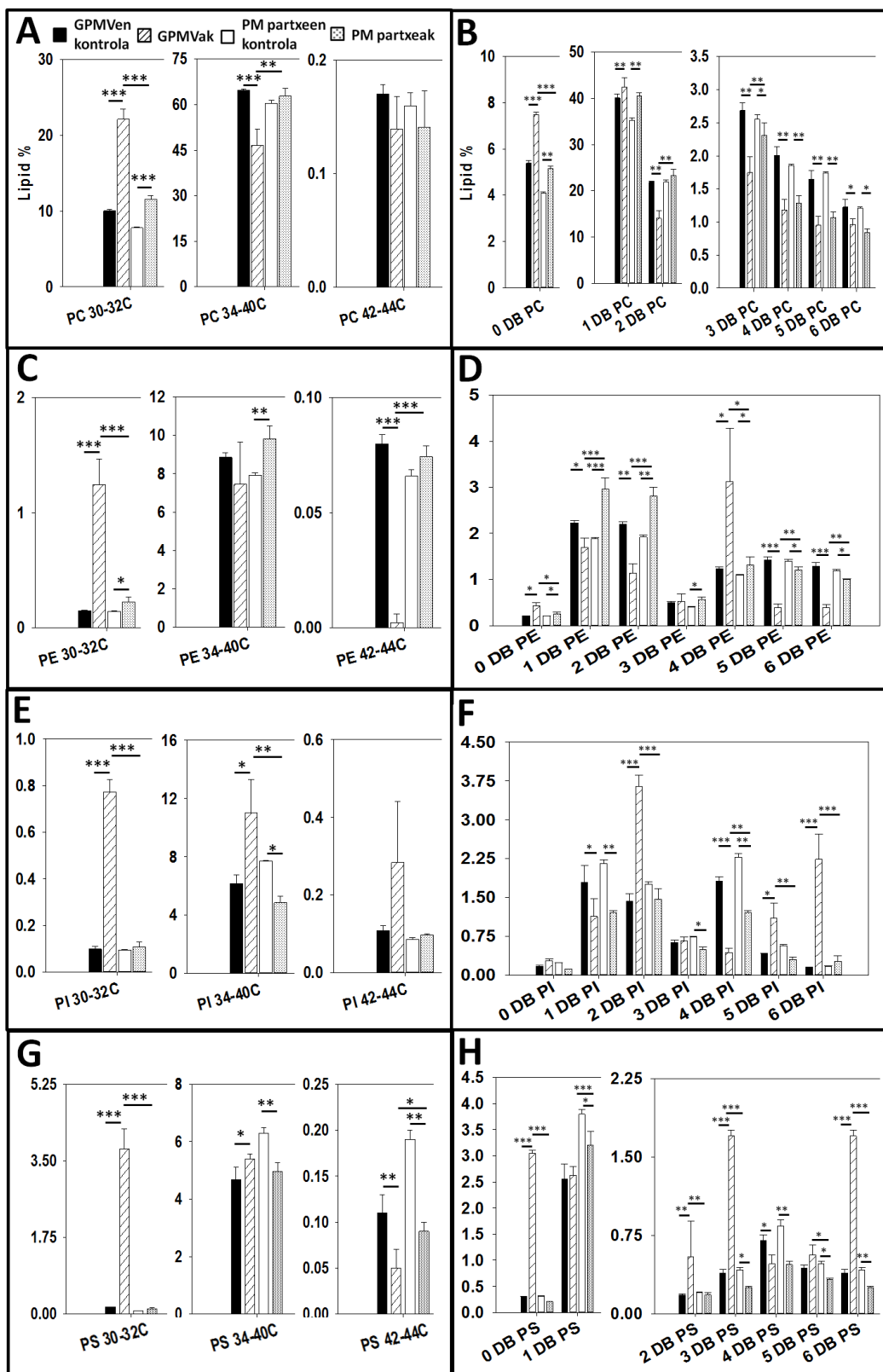
3.S2 irudia. PM partxeen purifikazioa. (A-C), zelula osoak; (D-F), PM partxeak. Lagin guztiak Di-4 ANEPPDHQ zunda fluoreszentez markatu dira mintz guztien markatzaile orokor gisa. Gainera, organulueko espezifikoak diren ondorengoko fluoroforoak erabili dira: Hoechst 33342 nukleorako (A eta D), Mitotracker Green mitokondrioetarako (B eta E), Bodipy-FL-C5-Cer Golgi aparaturoko (C eta F). Barra = 20 μm .



3.S3 irudia. Laurdan bidezko GP neurketak. Laurdan floresentzia bidez fosfolipido mintzetan adierazitako fase fluktuazioak (A) 20°C, (B) 30°Ctan eta (C) 40°Ctan. Gorria, CHO zelula osoak; urdina, CHO zelulen lipido erauzketatik sortutako SUVak; beltza, CHO zelulen babak; berdea, CHO zelulen PM partxeak.



3.S4 irudia. AFM – Laurdan fluoreszentzia korrelazioa. Laurdan GP balioa eta geruza bikoitzen apurtze idarraren arteko korrelazioa erregresio lerro gisa erakusten da ($r^2 = 0.893$). Puntu esperimentalak zelula osoei (beltza), PM partxeei (zuria), eta GPMVei (zirkulu grisa) dagozkie. Batez besteko balioa \pm S.D.



3.S5 irudia. Kate luzera eta asetze mailaren (DB = lotura bikoitz, ingelesezko double bond) araberako lipido banaketa. **A** eta **B**, PCa; **C** eta **D**, PEa; **E** eta **F**, PIa, **G** eta **H**, PSa. Barrak: beltza, GPMVak prestatzeko trataturiko zelulak; marratua, GPMVak (babak); hutsa, PM partxeak prestatzeko trataturiko zelulak; grisa PM partxeak. Adierazgarritasuna: (*) $p < 0.05$; (**) $p < 0.01$; (***) $p < 0.001$.

CHAPTER 4:

CHO/LY-B CELL GROWTH

UNDER LIMITING

SPHINGOLIPID SUPPLY:

CORRELATION BETWEEN

LIPID COMPOSITION AND

BIOPHYSICAL PROPERTIES

OF SPHINGOLIPID-

RESTRICTED CELL

MEMBRANES

CHAPTER 4: CHO/LY-B CELL GROWTH UNDER LIMITING SPHINGOLIPID SUPPLY: CORRELATION BETWEEN LIPID COMPOSITION AND BIOPHYSICAL PROPERTIES OF SPHINGOLIPID-RESTRICTED CELL MEMBRANES

4.1. Introduction

Sphingolipids (SL) are characterized by a sphingoid structural backbone, sphingosine being the most abundant base in mammals (Merrill *et al.*, 1997). *In vivo* studies of the SL roles are hampered, among other reasons, by the fact that they can be either synthesized *de novo* or taken up from the diet. A plausible approach would be to investigate mutant cells containing the smallest possible amounts of SL, or even none at all, but this is not a straightforward procedure because SL appear to be essential for cell growth and survival (Nieto *et al.*, 2008; Adachi-Yamada *et al.*, 2015; Li *et al.*, 2018). In particular, SL are considered as instrumental in the architecture of eukaryotic cell membranes. Apart from stabilizing the lamellar structure and helping to maintain its asymmetry, the tendency of certain SL to undergo lateral phase separation to form micro or nanodomains has been characterized (Chiantia & London, 2013; Goñi & Alonso, 2009; Simons & Ikonen, 1997; Goñi, 2019). Lipids and proteins co-localize with these domains, in which sphingomyelin (SM) is the most abundant SL (Yasuda *et al.*, 2016), and cholesterol (Chol) is often present (Simons & Ikonen, 1997; Goñi, 2019). The sphingoid base provides SL with hydrogen-bonding acceptors and donors (amide and free hydroxyl groups, respectively) that are rare in glycerophospholipids, leading to a dense intermolecular hydrogen-bonding network (Boggs, 1987; Schmidt *et al.*, 1977). Hydrogen bonding allows SM to interact preferentially with Chol (Estep *et al.*, 1979; Keyvanloo *et al.*, 2018) and with ceramide (Cer) (Goñi & Alonso, 2009), and recent studies have found that sphingomyelin (SM), Cer and Chol are able to coexist in a single ternary gel phase (at a 54:23:23 mol ratio) with intermediate properties between

SM-Cer enriched gel domains and Chol-driven liquid-ordered phases (Busto *et al.*, 2014). The above data have been obtained mostly from model membrane studies. Investigations at the cellular level have allowed to assign a wide variety of functions to SL, including apoptosis, cell growth, cell membrane function, tumor formation, drug resistance, degranulation, and phagocytosis, among others (Albi & Magni, 2008; Kolesnick, 2002; Spiegel & Milstien, 2003; Luberto *et al.*, 2002a). Alterations in the normal activities of SM-cycle enzymes have been linked to many central nervous system-related pathologies such as Alzheimer's, Parkinson's, ischemia/hypoxia, depression, schizophrenia or Niemann-Pick diseases (Kamil *et al.*, 2016). Specific SL functions have often been characterized in cells with decreased amounts of SL, using either SL-degrading enzymes (e.g. sphingomyelinases or ceramidases) (Ziesemer *et al.*, 2019), or specific enzyme inhibitors (Albi & Magni, 2008; Holleran *et al.*, 1991; Feingold, 1991; Dougherty *et al.*, 2006), of which the SPT inhibitor myriocin is a good example (Fujita *et al.*, 1994; Huang *et al.*, 2019; Mikłosz *et al.*, 2013; Li *et al.*, 2014).

Procedures to decrease the SL contents of cells constitute good tools to determine their potential functions *in vivo*. *De novo* SL biosynthesis is initiated by the condensation of L-serine with palmitoyl CoA. This reaction is catalyzed by SPT to generate 3-ketodihydrosphingosine. 3-Ketodihydrosphingosine is then converted to dihydrosphingosine, which is N-acylated and (most of it) dehydrogenated at the endoplasmic reticulum to form Cer. After moving to the Golgi apparatus, Cer is converted to SM or glycosphingolipids (Goñi & Alonso, 2009; Gault *et al.*, 2010). Finally, these complex SL are translocated to the PM (Merrill *et al.*, 2007; Ziulkoski *et al.*, 2001). Thus, SPT is a key enzyme for the regulation of cellular SL content (Yasuda *et al.*, 2016; Merrill *et al.*, 2007). Using a genetic selection method in CHO cells (Hanada *et al.*, 1998), the Hanada lab isolated the defective LY-B cell line, which had a loss of function of serine palmitoyltransferase (SPT) enzyme activity through a defective SPTLC1 subunit. The mutant cells maintained the ability to take up and metabolize exogenous sphingoid bases from the culture medium (Hanada *et al.*, 1998). Mutant LY-B and wild type CHO cells could be comparatively studied to determine the effect of SL depletion on the biophysical properties of cell membranes. LY-B cells have been used in multiple studies exploring SL effects, and their interaction with glycerophospholipid metabolism (Bejaoui *et al.*, 2002; Nakamura *et al.*, 2015; Mise *et al.*, 2005; Han *et al.*, 2009) SM synthases, which use Cer and phosphatidylcholine as

substrates to produce SM and diacylglyceride, are used in the *de novo* synthesis pathway, sometimes also involved in reutilization of ceramide (Ziulkoski *et al.*, 2001; Chakraborty & Jiang, 2013) from exogenous or endogenous sources. In a previous work (Monasterio *et al.*, 2020) plasma membrane (PM) preparations from CHO cells and model membranes prepared from their lipid extracts had been characterized. In the present study we have applied those methods to the study of SL-synthesis deficient LY-B cells to determine the role of SL on cell growth, membrane physical properties and composition.

4.2. Materials and Methods

4.2.1. Materials

Wild type CHO (ATCC, Manassas, Virginia, U.S.) and a serine-SPT deficient CHO cell line, known as LY-B (Hanada *et al.*, 1998) (RIKEN BioResource Research Center, Koyadai, Japan), were used in this study. Cell culture products; DMEM:F12 (Dulbecco's Modified Eagle Medium: Nutrient Mixture F-12) FBS (Fetal Bovine Serum), penicillin, streptomycin, and GlutaMax supplement were purchased from Thermofisher (Waltham, MA). Organic solvents were from Thermofisher (Waltham, MA). All fluorophores; Di-4-ANEPP, Hoechst 33342, BODYPY FL C5-ceramide, Mitotracker Green were purchased from Thermofisher (Waltham, MA). Salts for buffer preparation, Tris, NaCl, Tris, KCl, NaCl, CaCl₂, HEPES (Sigma-Aldrich, St Louis, MO, US). All reagents (salts and organic solvents) were of analytical grade.

4.2.2. Cell growth

Wild type CHO (ATCC, Manassas, Virginia, U.S.) and a serine-SPT deficient CHO cell line, known as LY-B (Hanada *et al.*, 1998) (RIKEN BioResource Research Center, Koyadai, Japan), were used in this study. Unless otherwise mentioned, cells were grown on DMEM:F12 (Dulbecco's Modified Eagle Medium: Nutrient Mixture F-12) medium containing 10% FBS (Fetal Bovine Serum), 100 U/ml penicillin, 100 U/ml streptomycin, and 6 mM glutamine (GlutaMax supplemented) at 37°C and 5% CO₂ humidified atmosphere. All cell culture products were purchased from Thermofisher (Waltham, MA).

4.2.2.1. Cell adaptation: Standard vs. deficient (low-FBS) medium

CHO and LY-B cells were adapted to growth in deficient (low-FBS) medium. For this purpose, cells were first seeded in DMEM:F12 medium containing 10% FBS, 100 U/ml penicillin and 100 U/ml streptomycin, and 6 mM glutamine (this medium will be referred to as 'standard medium'). After 24-h cell growth, when a 15-25% confluence was reached, the standard medium was discarded, cells were washed with PBS buffer (137 mM NaCl, 3 mM KCl, 80 mM Na₂HPO₄, 7 mM KH₂PO₄), and DMEM:F12 medium containing 0.04% FBS, 100 U/ml penicillin, 100 U/ml streptomycin and 6 mM glutamine was added (this medium will be named 'FBS-deficient' or 'SL-deficient medium'). Cells were grown in the appropriate medium for 24, 48, 72 or 96 h. Other low-FBS media (5%, 2.5% or 1.25%) were also used in some specific cases.

4.2.3. Growth rate and viability tests

4.2.3.1. Cell growth

2.65×10^5 cells were seeded in 25 cm² flasks in standard medium and grown for 24 h until 15 – 25% confluence. Then, the standard medium was discarded, cells were washed twice with PBS, and the appropriate medium (standard or deficient) was added. Cells were grown for 24, 48, 72 or 96 h. Quantification was performed by cell counting with a hemocytometer (BioRad TC20 Automated Cell Counter, Hercules, CA). Protein was assayed with the colorimetric Pierce BCA Protein Assay Kit (ThermoFisher, Waltham, MA). SM (0.2 mg/5 ml; $\approx 80 \mu\text{M}$ SM), sphinganine (0.0125 mg/5ml $\approx 8 \mu\text{M}$), cerebroside (at 0.2 mg/5 ml, $\approx 55 \mu\text{M}$) or sphingosine (0.02 mg/5 ml, $\approx 13 \mu\text{M}$) were used for this purpose.

4.2.3.2. Viability test.

Flow cytometry was performed to evaluate how the decreased FBS concentration in the medium affected cell viability (Galisteo-González *et al.*, 2020). Cells were stained with Annexin-V-FITC and propidium iodide as indicated in the manual of the annexin V-FITC detection kit (CalbioChem, Darmstadt, Germany), and fluorescence was measured using a FACS Calibur flow cytometer (Becton-Dickinson, Franklin Lakes, NJ) as in Ahyayauch *et al.* (2018). Annexin V-FITC fluorescence

intensity was measured in fluorescence channel FL-1 with $\lambda_{\text{ex}} = 488$ nm and $\lambda_{\text{em}} = 530$ nm, while FL-3 was used for propidium iodide detection, with $\lambda_{\text{ex}} = 532$ nm and $\lambda_{\text{em}} = 561$ nm. All measurements were performed in triplicate. Data analysis was performed using Flowing Software 2.

4.2.4. Sample preparation

Intact cells (whole cells), two different PM preparations (giant plasma membrane vesicles, known as GPMV or blebs, and PM patches) and SUV or GUV formed with whole-cell or PM lipid extracts were used.

4.2.4.1. PM preparations

PM preparations were obtained as described in Monasterio *et al.* (2020). Briefly, GPMV formation was induced adding the GPMV formation reagent [freshly prepared 2 mM dithiothreitol, 25 mM paraformaldehyde in GPMV buffer (2 mM CaCl_2 , 10 mM HEPES, 150 mM NaCl, pH 7.4)] to T25 flasks with cells at confluence. Cells were incubated for 1 h at 37°C. After incubation, the GPMV-containing GPMV reagent was collected from the flasks and centrifuged at 14,000 $\times g$ for 20 min. The supernatant was discarded, the pellet was resuspended in GPMV buffer, and the sample was centrifuged at 14,000 $\times g$ for 20 min. The procedure was repeated twice to remove traces of dithiothreitol and paraformaldehyde. Finally, the GPMV were resuspended in 500 μl GPMV buffer (Manni *et al.*, 2015).

PM patches were isolated by a modification (Monasterio *et al.*, 2020) of the protocol described by Bezrukov *et al.* (2009). In summary, cells were seeded at approximately 50% confluence and incubated for 2 h so that they adhered to the support. After incubation, 2 washing steps were performed using cold TBS (Tris Buffer Saline: 150 mM NaCl, 25 mM Tris-HCl, 2 mM KCl) to discard non-attached cells. Then, cold distilled water was added for 2 min to induce cell swelling. Mechanical cell disruption was achieved using a pressure stream from a 20-ml syringe coupled to a 19X1-1/2(TW)A needle. In the process, intracellular contents were released, while PM stayed attached to the support. Several washing steps were performed to discard the released intracellular contents. Purification quality was checked using Di-4-ANEPPDHQ ($\lambda_{\text{ex}} = 465$ nm, $\lambda_{\text{em}} = 635$ nm) as a general fluorescent staining, together with organelle-specific fluorophores as described in Monasterio *et al.* (2020). Images

were taken in a Leica TCS SP5 II microscope (Leica Microsystems GmbH, Wetzlar, Germany) at room temperature with ImageJ software. The fluorescence intensities of the various markers were comparatively measured in PM patches and intact cells, so that specific organelle contamination could be estimated.

4.2.4.2. Whole cell lipid extract

Lipid extraction was performed following the method used in Ahyayauch *et al.* (2018). Briefly, cell pellets were first dispersed in aqueous perchloric acid (60% v/v), then centrifuged at 14,000 xg for 15 min, and the supernatant was discarded. Pellets were resuspended in 2.5 ml chloroform:methanol (2:1, v/v) and samples were mixed for 15 min. Then, 5 ml cold 0.1 mM HCl was added to the mixture. After homogenizing, samples were centrifuged at 1,700 xg for 20 min. Supernatants were discarded while the lipid-containing organic phase remained in the bottom layer. Phospholipid concentration was assayed as inorganic phosphorus after acid digestion.

4.2.4.3. PM patch lipid extraction

PM patches were formed following the above mentioned protocol (Bezrukov *et al.*, 2009; Monasterio *et al.*, 2020). Chloroform:methanol (2:1) organic solvent was used to recover the lipid fraction of the attached PM patches.

4.2.4.4. GUV formation

GUV were formed in a PRETGUV 4 chamber supplied by Industrias Técnicas ITC (Bilbao, Spain) using the modified electroformation method (Montes *et al.*, 2010) first developed by Angelova and Dimitrov(1986).

4.2.4.5. SUV formation

The sample was kept under vacuum for 2 h to remove solvent traces and the lipids were swollen in PBS buffer. SUV were obtained by sonication of the swollen lipid suspensions with a probe-type Soniprep 150 sonicator (MSK, London, U.K.) for 10 min, in 10-s on, 10-s off intervals.

4.2.5. SM quantification with lysenin

4.2.5.1. Lysin-mCherry expression and purification

The non-toxic monomeric C-terminal domain of the SM-specific toxin, NT-lysenin, was expressed and purified as described by Carquin *et al.* (2014). Briefly, the expression plasmid pET28/lysenin encoded NT-lysenin as a fusion protein with an N-terminal 6xHis-tag followed by the monomeric red fluorescent protein mCherry. The plasmid was expanded in *Escherichia coli* BL21 (DE3) and the recombinant protein was expressed in lysogeny broth (LB) medium at 16°C for 72 h in the presence of 0.4 mM isopropyl β -D-thiogalactoside. Bacterial extracts were prepared as described (Maliekal *et al.*, 2006) and the recombinant protein was purified using an Ni-NTA Superflow cartridge (Qiagen, Hilden, Germany) and eluted with imidazol (Veiga-da-cunha *et al.*, 2012). Fraction analysis by SDS-PAGE revealed recombinant NT-lysenin with the expected size (45 kDa). The most enriched fractions were pooled, concentrated, and desalted. The aliquots were stored in 20 mM NaCl and 25 mM Hepes pH 7.2 and 5% glycerol at -80°C. Protein concentration was calculated by measuring absorbance at 280 nm.

4.2.5.2. SM staining and quantification with lysenin-mCherry.

Whole cells and PM patches were stained with lysenin-mCherry (for SM) and NBD - PE [(N - (7 - Nitrobenz - 2 - Oxa - 1,3 - Diazol - 4 - yl) - 1,2 - Dihexadecanoyl - sn - Glycero - 3 - Phosphoethanolamine, Triethylammonium Salt] fluorophore (the latter a general membrane stain) and samples were visualized using a confocal microscopy Nikon D-ECLIPSE C1 (Nikon, Melville, NY). In whole cells the mCherry signal was also quantified using a FL-3 FACS Calibur flow cytometer (Becton-Dickinson, Franklin Lakes, NJ) with $\lambda_{\text{ex}} = 532$ nm and $\lambda_{\text{em}} = 561$ nm.

For sample visualization, cells were seeded in glass-bottom dishes and grown as above. Cells were first stained with 100 μ M NBD-PE as a control for general membrane staining. A washing step was performed with PBS, and lysenin-mCherry was added at 100 μ M. For flow cytometry analysis, cells were stained in suspension at a final concentration of 100 μ M lysenin-mCherry.

4.2.6. Laurdan General Polarization

Laurdan is a fluorescence polarity probe whose emission undergoes a spectral shift due to the reorientation of water molecules in the glycerol backbone region of the membrane, and this shift can be correlated to the lipid phase (Krasnowska *et al.*, 1998). In the gel phase, when little water is present, laurdan maximum emission is around 440 nm, whereas in the liquid crystalline phase the spectrum is red shifted to around 490 nm. Intact cells, PM preparations and model membranes formed with lipid extracts have been used to compare the laurdan fluorescence of CHO and LY-B cells grown in standard and deficient media. Both fluorescence microscopy imaging and spectrofluorometric analysis have been performed for laurdan fluorescence characterization.

4.2.6.1. Confocal microscopy

Intact cells grown in glass-bottom dishes were stained with laurdan (Molecular Probes, Eugene, OR) as follows: First, cell culture medium was discarded and two PBS washing steps were performed. Then, for laurdan staining, laurdan dissolved in DMSO was added to a final concentration of 5 μ M and cells were incubated at 37°C for 5 min. Finally, a washing step with PBS was conducted prior to cell visualization. Similarly, PM patches formed as described above were stained with 5 μ M laurdan.

GPMV were stained with laurdan by adding 5 μ M (final concentration) of the fluorophore dissolved in DMSO. GPMV were transferred to polylysine-coated glass-bottom dishes (MatTek, Ashland, OR) and vesicles were left to sediment for 3 h before visualization (Manni *et al.*, 2015). For GUV, 0.2 mM lipid extracts in chloroform:methanol (2:1, v/v) were mixed with 0.01 mM laurdan. 3 μ l of the lipid stocks were added onto the surface of Pt electrodes and solvent traces were removed under high vacuum for at least 2 h. The Pt electrodes were then covered with 400 μ l of 300 mM sucrose buffer and the Pt wires were connected to an electric wave generator (TG330 function generator, Thurlby Thandar Instruments, Huntington, United Kingdom) under alternating current field conditions (10 Hz, 2.5 VRMS for 2 h) at 37°C. After GUV formation, the chamber was placed on an inverted confocal fluorescence microscope for GUV visualization.

4.2.6.2. Image acquisition and analysis

A Leica TCS SP5 II microscope (Leica Microsystems GmbH, Wetzlar, Germany) was used for image acquisition. A 63x water-immersion objective (numerical aperture NA = 1.2) was used and samples were imaged at 512 x 512 pixel and 400 Hz per scanning line. Equatorial planes were imaged to avoid photoselection effects. A pulsed titanium-sapphire (Mai-Tai Deepsee, Spectra-Physics) laser tuned at 780 nm was used for two-photon imaging of laurdan-labeled samples. Fluorescence emission was collected by non-descanned (NDD) hybrid detectors, as they offer higher sensitivity compared to descanned photomultipliers. The blue edge of the emission spectrum was collected by NDD 1 at 435 ± 20 nm and the red edge by NDD 2 at 500 ± 10 nm. Irradiance at the sample plane was ≈ 500 GW·cm⁻² for two-photon excitation (Parasassi & Gratton, 1997).

Generalized polarization (GP) value of samples was calculated using a MATLAB (MathWorks, Natick, MA) based software. Images were smooth in each channel with 2 pixel averaging, and the GP value was calculated using the following equation (Carravilla *et al.*, 2015):

$$GP = \frac{I_B - G \cdot I_R}{I_B + G \cdot I_R}$$

where I_B is the intensity collected by NDD 1, I_R is the intensity collected by NDD 2, and G is the correction factor. The G factor is calculated measuring the GP value of the same fluorophore concentration used in sample staining, dissolved in this case in pure DMSO (Owen *et al.*, 2012). In whole cell images, the region of interest, i.e. the PM, was selected when required.

4.2.6.3. Fluorescence spectroscopic analysis

PM preparations, and SUV formed with whole cell or PM lipid extracts were measured in a spectrofluorometer. Samples (82.5 μ M lipid concentration) were labeled with 0.75 μ M laurdan. For this purpose lipid extracts in chloroform:methanol (2:1) were mixed with laurdan and the solvent was evaporated to dryness under a stream of N₂. Then, the sample was kept under vacuum for 2 h to remove solvent traces and the lipids were swollen in buffer (NaCl 150 mM, Hepes 25 mM, pH 7.4). Sonicated SUV were obtained as described above and fluorescence measurements were performed using a

QuantaMaster 40 spectrofluorometer (Photon Technology International, Lawrenceville, NJ) (Santis *et al.*, 2018).

4.2.7. AFM

Contact mode AFM imaging has been used to study bilayer topography, looking at possible lateral segregation effects through bilayer thickness analysis. A NanoWizard II AFM (JPK Instruments, Berlin, Germany) was used to perform topographic measurements under contact mode scanning (constant vertical deflection). For measurements, the AFM was coupled to a Leica microscope and mounted onto a Halcyonics Micro 40 antivibration table (Halcyonics, Inc., Menlo Park, CA) and inside an acoustic enclosure (JPK Instruments, Berlin, Germany) (Monasterio *et al.*, 2017). V-shaped MLCT Si₃N₄ cantilevers (Bruker, Billerica, MA) with nominal spring constants of 0.1 or 0.5 N/m were used. The sample thickness was estimated by cross-section height analysis (García-Arribas *et al.*, 2015).

4.2.7.1. Force Spectroscopy

V-shaped MLCT Si₃N₄ cantilevers (Bruker, Billerica, MA) with nominal spring constants of 0.1 or 0.5 N/m were individually calibrated in a lipid-free mica substrate in assay buffer using the thermal noise method. After proper bilayer area localization by means of AFM topography and direct epifluorescence microscopy, force spectroscopy was performed at a speed of 1 μm/s. Force steps were determined for each of the indentation curves as reproducible jumps within the extended traces. At least three independent sample preparations were scanned for each case and 50-100 curves were measured in each sample.

Topographic images and force spectroscopy analysis of PM patches and supported planar bilayers (SPB) formed from lipid extracts, and force spectroscopy analysis of GPMV were performed. GPMV topographic observations could not be performed for experimental reasons, these structures would not flatten on the mica for AFM examination.

SPB were prepared on high V-2 quality scratch-free mica substrates (Asheville-Schoonmaker Mica Co., Newport News, VA). 180 μL assay buffer containing 3 mM CaCl₂ was added onto a 1.2 cm² freshly cleaved mica substrate mounted onto a BioCell

(JPK Instruments, Berlin, Germany). Then, 80 μ L sonicated 0.4 mM SUV formed with CHO or LY-B lipid extract was added on top of the mica. BioCell temperature was gradually increased (5°C every 5 min) up to 80°C. Vesicles were let to adsorb and extend for 30 min keeping the sample temperature at 80°C. Samples were left to equilibrate for 30 min at room temperature before performing five washing steps with CaCl₂-free buffer in order to discard non-adsorbed vesicles and remove the remaining Ca²⁺ cations (Monasterio *et al.*, 2017). Isolated PM patches for force spectroscopy were prepared as previously described (Bezrukov *et al.*, 2009; Monasterio *et al.*, 2020), this time using polylysine-coated mica slips instead of glass-bottom dishes. GPMV were first stained using Di-4-ANEPPQHD to allow detection on the mica slip. Then, samples were left for 3 h to sediment over the polylysine-coated mica slip before measurements were performed.

4.2.8. Mass spectroscopic analysis

Mass spectroscopic analysis was performed essentially as described in Monasterio *et al.* (2020). A methodological summary follows.

4.2.8.1. Sample treatment

Lipid extraction was performed using a modified methyl *tert*-butyl ether (MTBE) protocol (Guri *et al.*, 2017a). Briefly, cells were washed with cold PBS and scraped off in 500 μ L cold PBS on ice. The suspension was transferred to a 2 ml tube in which it was spun down at 3200 rpm for 5 min at 4°C. After removing the PBS, samples were stored at -20°C or directly used for further extraction. GPMV and PM patch samples were prepared as previously mentioned. Then, 360 μ L methanol was added and vortexed. A mixture of lipid standards (Table 4.1) was included and samples were vortexed for 10 min at 4 °C using a Cell Disruptor Genie (Scientific Industries, Inc., Bohemia, NY). MTBE (1.2 mL) was then added and the samples were incubated for 1 h at room temperature with shaking (750 rpm). Phase separation was induced by adding 200 μ L H₂O. After 10 min incubation at room temperature, the sample was centrifuged at 1,000 xg for 10 min. The upper (organic) phase was transferred to a 13-mm screw-cap glass tube and the lower phase was extracted with 400 μ L artificial upper phase [MTBE/methanol/water (10:3:1.5, v/v/v)]. The two upper phases were combined and the total lipid extract was divided in 3 equal aliquots [one for phospholipids (TL), one

for sterols (S) in 2-mL amber vials, and one for sphingolipid (SL) detection in a 13-mm glass tube] and dried in a Centrivap at 50°C or under a nitrogen flow. The SL aliquot was deacylated by methylamine treatment (Clarke method) to remove glycerophospholipids. 0.5 mL monomethylamine reagent [MeOH/H₂O/n-butanol/methylamine solution (4:3:1:5 v/v)] was added to the dried lipid, followed by sonication (5 min). Samples were then mixed and incubated for 1 h at 53°C and dried (as above). The monomethylamine-treated lipids were desalted by n-butanol extraction. 300 µl H₂O-saturated n-butanol was added to the dried lipids. The sample was vortexed, sonicated for 5 min and 150 µl MS-grade water was added. The mixture was vortexed thoroughly and centrifuged at 3200 xg for 10 min. The upper phase was transferred to a 2-mL amber vial. The lower phase was extracted twice more with 300 µl H₂O-saturated n-butanol and the upper phases were combined and dried (as above).

4.2.8.2. Glycerophospholipid and sphingolipid detection in a Triple Quadrupole Mass Spectrometer

TL and SL aliquots were resuspended in 250 µl chloroform/methanol (1:1 v/v) (LC-MS/HPLC grade) and sonicated for 5 min. The samples were pipetted in a 96-well plate (final volume = 100 µl). The TL were diluted 1:4 in negative-mode solvent (chloroform/methanol (1:2) + 5 mM ammonium acetate) and 1:10 in positive-mode solvent (chloroform/methanol/water (2:7:1 v/v) + 5 mM ammonium acetate). The SL were diluted 1:10 in positive-mode solvent and infused onto the mass spectrometer. Tandem mass spectrometry for the identification and quantification of sphingolipid molecular species was performed using Multiple Reaction Monitoring (MRM) with a TSQ Vantage Triple Stage Quadrupole Mass Spectrometer (ThermoFisher Scientific, Waltham, MA) equipped with a robotic nanoflow ion source, Nanomate HD (Advion Biosciences, Ithaca, NY). The collision energy was optimized for each lipid class. The detection conditions for each lipid class are listed in table 4.1. Cer species were also quantified with a loss of water in the first quadrupole. Each biological replica was read in 2 technical replicas (TR). Each TR comprised 3 measurements for each transition. Lipid concentrations were calculated relative to the relevant internal standards and then normalized to the total lipid content of each lipid extract (mol %).

4.2.7.3. Gas chromatography–mass spectrometry for cholesterol assay

Lipid extracts were analyzed by GC-MS as described previously (Guan *et al.*, 2010). Briefly, samples were injected into a VARIAN CP-3800 gas chromatograph equipped with a FactorFour Capillary Column VF-5ms 15 m × 0.32 mm i.d. DF = 0.10, and analyzed in a Varian 320 MS triple quadrupole with electron energy set to -70 eV at 250°C. Samples were applied to the column oven at 45°C, held for 4 min, then temperature was raised to 195°C (20°C/min). Sterols were eluted with a linear gradient from 195°C to 230°C (4°C/min), followed by rising to 320°C (10°C/min). Cholesterol was identified by its retention time (compared with an ergosterol standard) and fragmentation patterns, which were compared with the NIST library.

Table 4.1. MS detection conditions for the different lipid classes.

Lipid Class	Standard	Polarity	Mode	m/z ion	Collision Energy
Phosphatidylcholine [M+H] ⁺	DLPC	+	Product ion	184.07	30
Phosphatidylethanolamine [M+H] ⁺	PE31:1	+	Neutral ion loss	141.02	20
Phosphatidylinositol [M-H] ⁻	PI31:1	-	Product ion	241.01	44
Phosphatidylserine [M-H] ⁻	PS31:1	-	Neutral ion loss	87.03	23
Cardiolipin [M-2H] ²⁻	CL56:0	-	Product ion	acyl chain	32
Ceramide [M+H] ⁺	C17Cer	+	Product ion	264.34	25
Dihydroceramide [M+H] ⁺	C17Cer	+	Product ion	266.40	25
Hexosylceramide [M+H] ⁺	C8GC	+	Product ion	264.34	30
Hexosyldihydroceramide [M+H] ⁺	C8GC	+	Product ion	266.40	30
Sphingomyelin [M+H] ⁺	C12SM	+	Product ion	184.07	26

4.2.9. Quantitation of lipids per cell

An estimate of the amounts of lipids per cell, or per weight protein, was obtained as follows. Szeliiova *et al.* (2020) measured the average dry weight of CHO cells as 264 pg/cell. Alberts *et al.* (1994) indicated that the mammalian cell contained 10 dry wt% phospholipids and 7 dry wt% other lipids. Moreover, the average amount of protein per cell was measured experimentally with the BCA protein assay. Cell numbers were counted with a hemocytometer. From the above data, and knowing from MS analysis the concentration of a given lipid in a sample, the amount of such lipid per cell and per wt protein could be estimated.

4.3. Results

4.3.1. CHO-derived mutant cells can grow and survive with extremely low sphingolipid concentrations in the culture medium

4.3.1.2. Growth and viability

The extent to which CHO (wild type) and LY-B (SPT-defective) cell adaptation to a SL-deficient medium affected cell division ratio and integrity was assessed. FBS was the only external source of SL for cell growth, thus FBS in the growth medium was the only SL source for LY-B cells. SL-deficient growth media were prepared containing 0.04% FBS, i.e. a 250-fold decrease with respect to the standard conditions (10% FBS). Cell count measurements were performed using a BioRad TC20 hemocytometer. Figure 4.1A shows a comparison between cell growth in standard (containing 10% FBS) or SL-deficient (containing 0.04% FBS) medium. Both cell lines (CHO and LY-B) grew steadily for at least 96 h in full medium (10% FBS), and both divided, even if slowly, for the first 72 h in a low-SL medium. After 72 h in the SL-limited medium cell quantity decreased. The difference between CHO and LY-B cell-growth ratios was not statistically significant when they were grown in standard medium. Nevertheless, in SL-deficient medium CHO and LY-B cells behaved differently. After 72 h, CHO cell number was 47% of control (complete medium), while LY-B growth was only 18%. Growth rates of cells treated with the SPT inhibitor myriocin (2.5 μ M) (Capasso *et al.*, 2017) and grown in deficient medium were also measured as an additional control. CHO cell growth ratio was decreased to the level of LY-B cells grown in deficient medium. Moreover, myriocin treatment did not affect the growth of LY-B cells (data not shown). The results concur in suggesting that the different behaviour of CHO and LY-B cells in our study is due to the lack of an active SPT in the latter strain.

Ancillary experiments were performed in which cell growth after 72 h in media with different degrees of SL-limitation was measured (Fig. 4.S1A and 4.S1B). Cell counts were performed as in figure 4.1 (Fig. 4.S1A) and total cell protein was quantified with a BCA protein assay (Fig. 4.S1B). After 72 h, differences in growth were already significant between CHO and LY-B cells when medium contained 5% FBS. No LY-B cell growth could be reliably measured with FBS concentrations below 0.04%. In a

different series of experiments, cell growth was intended on delipidated FBS-containing medium, but no cell division could be observed.

To ascertain that the difference between CHO and LY-B cell division ratio at low FBS concentrations was indeed due to a lack of SL, we tested whether LY-B cells were able to reach the full growth rates when the SL-deficient medium was supplemented with SL. For this purpose, equimolar mixtures of egg PC and the sphingolipid under study were sonicated in buffer and added to the culture flasks in various amounts. The best recoveries were achieved with sphingomyelin (SM) or sphinganine (Fig. 4.S1E). Figure 4.1B shows that LY-B cells grown in SL-deficient medium for 72 h reached $\approx 80\%$ of the control growth when 0.2 mg SM was added per T25 culture flask (5 ml; 80 μM SM), while there was no difference in the case of CHO cells. With 0.0125 mg sphinganine/flask (8 μM), cells grown in SL-deficient medium under the same conditions recovered 81% of the high-FBS control value (Fig. 4.S1C). Supplementation with pure PC vesicles did not have any effect when compared to the growth of LY-B cells in the non-supplemented, FBS-deficient medium (Fig. 4.S1E). Cerebroside (16% recovery at 0.2 mg/flask, 55 μM) and sphingosine (33% recovery at 0.02 mg/flask, 13 μM) supplementations were also tested (Fig. 4.S1E). It was concluded that it is the lack of SPT activity what makes the main difference between CHO and LY-B cell division ratios in SL-deficient medium.

As a further control to ascertain that the main effects of lowering FBS concentration were due to the low supply of SL, the time-course of cell growth in SL-deficient medium supplemented with SM and treated with sphingomyelinase inhibitors was measured (Fig. 4.1C). When cells were treated with 5 μM acid sphingomyelinase inhibitor fluphenazine dihydrochloride or 20 μM neutral sphingomyelinase inhibitor GW4869, the effect that SM addition had on cell growth recovery was suppressed. There was no statistically significant difference between the growth of cells treated with sphingomyelinase inhibitor grown in SM supplemented deficient medium and the non-treated LY-B cells grown in deficient medium (Fig. 4.1C).

CHO/LY-B cell growth under limiting sphingolipid supply: correlation between lipid composition and biophysical properties of sphingolipid-restricted cell membranes

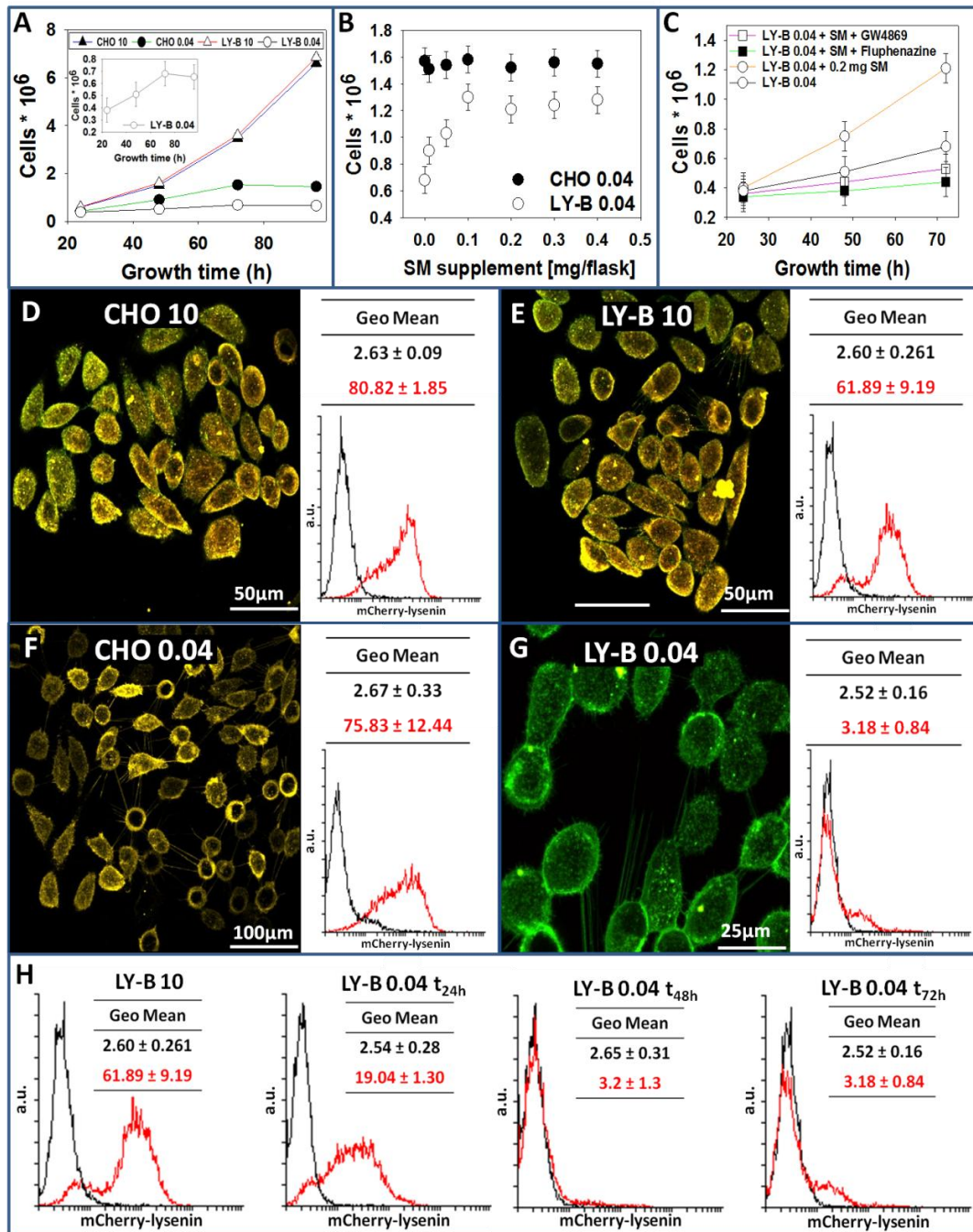


Figure 4.1. LY-B cells can grow on very small amounts of sphingolipids. (A) LY-B (empty symbols) and CHO (filled symbols) cell growth as a function of time in standard (10% FBS) (triangles) and sphingolipid-deficient (0.04% FBS) (circles) medium. Inset: LY-B cell growth in sphingolipid-deficient medium, Y-axis expanded (B) LY-B and CHO cell growth after 72 h in sphingolipid-deficient medium supplemented with SM [seeded cells: 0.25×10^6 ; medium volume = 5 ml]. (C) LY-B cell growth as a function of time in sphingolipid-deficient (0.04% FBS) medium supplemented with SM (0.2 mg \approx 80 μ M) (circles) and treated with sphingomyelinase inhibitors, flufenazine or GW4869 (squares) (seeded cells: 0.25×10^6). In A-C, data correspond to average values \pm S.D. ($n = 3$). In A, error bars are smaller than the symbols. **Fluorescence images and flow cytometry-mediated mCherry-lysenin (red) quantification.** CHO (D) and LY-B (E) cells grown in standard medium. CHO (F) and LY-B (G) cells grown in SL-deficient medium. NBD-PE (green) was used in fluorescence images for general membrane staining. Measurements are shown after 72-h growth. Geometric mean \pm S.D. ($n = 3$). (H) Flow cytometry: time-dependent mCherry-lysenin quantification in LY-B cells grown (from left to right) in standard medium, or deficient medium for 24 h, 48 h, and 72 h. Histograms in black correspond to control cells (without mCherry-lysenin staining) and those in red, to the sample of interest (mCherry-lysenin signal). Geometric mean \pm S.D. ($n = 3$).

The possible effect of low cell growth/ SL-deficient medium on cell viability was then tested using flow cytometry analysis with Annexin-V-FITC and propidium iodide. Flow cytometry analyses demonstrated that, despite the low growth rate, 86% of LY-B cells grown in SL-deficient medium for 72 h remained viable (Fig. 4.S2E). Ethanol-treated CHO cells (Fig. 4.S2A) were used as a positive control for non-viable cells. 95% CHO cells (Fig. 4.S2B) and 95% LY-B cells (Fig. 4.S2D) grown in standard medium were viable. With respect to cells grown in SL-deficient medium, 92% CHO (Fig. 4.S2C) and 86% LY-B (Fig. 4.S2E), as well as 89% LY-B grown in SM-supplemented medium (Fig. 4.S2F) were viable. These plots are representative data used to quantify results shown in figures 4.1A and 4.S1. Considering that even LY-B cells grown in 0.04 FBS retained a fair viability, these cells were considered as a good tool to obtain reliable information on the putative effects of a defective SPT activity on their biophysical properties.

4.3.1.3. Lysenin-staining

Cells were stained with SM-specific NT-lysenin-mCherry and visualized with confocal microscopy. LY-B cells grown in standard medium were stained with the general membrane stain NBD-PE (green) and also with lysenin fused to mCherry (red) (Fig. 4.1E). LY-B cells grown in SL-deficient medium appeared thoroughly stained with NBD-PE, but only little dots of mCherry were seen (Fig. 4.1G), indicating a remarkable decrease of SM in this sample.

MCherry-lysenin staining shows that CHO (Fig. 4.1D) and LY-B (Fig. 4.1E) grown in standard medium were both stained with lysenin and NBD-PE, but flow cytometry analysis revealed that mCherry intensity was lower in LY-B cells (Fig. 4.1E) than in CHO ones (Fig. 4.1D). Moreover, when CHO cells were grown in SL-deficient medium, staining remained almost unchanged during the experiment (Fig. 4.1F). However, with LY-B cells grown in deficient medium (Fig. 4.1G and 4.1H), lysenin fluorescence was largely decreased in the first 24 h of growth, and 48 h were enough to achieve a full lysenin-mCherry signal depletion (Fig. 4.1G and 4.1H). In parallel with these observations, the same behavior was detected in PM patches, prepared as described previously (Bezrukov *et al.*, 2009; Monasterio *et al.*, 2020) (Fig. 4.S3). PM patches from LY-B cells grown in deficient medium for 72 h (Fig. 4.S3D) exhibited very little lysenin-mCherry signal as compared with other PM patches (Figs. 4.S3A-C).

In summary, both CHO and LY-B cell lines grew to a similar extent in standard medium. In SL-deficient medium LY-B cells growth was lower than that of CHO cells, but they were still viable. Normal growth was recovered when the SL-deficient medium was supplemented with SM. Lysenin fluorescence was largely decreased in LY-B in the first 24 h of growth in deficient medium, and 48 h were enough to achieve a full lysenin-mCherry signal depletion, while, under the same conditions, CHO cells showed only a slight decrease in lysenin-reacting SM.

4.3.2. Membrane lipid order decreases with sphingolipid restriction

Laurdan generalized polarization (GP) experiments were performed to evaluate how the SPT activity suppression affected the rigidity/fluidity of cell membranes. GP provides an estimation of membrane lipid molecular order. GP values of whole cell lipid extracts, PM patches, GPMV and PM lipid extracts were measured using both two-photon microscopy and spectrofluorometry. In our previous work we performed laurdan GP experiments of CHO cell derived samples (Monasterio *et al.*, 2020). Now we have also measured GP values of SPT-suppressed LY-B cells. Figure 4.2A depicts a laurdan-stained whole CHO cell grown in standard medium and its selected PM pixels, accompanied by their GP distribution plots. In a scale from -1 to 1, a red color and a value close to 1 indicated a more rigid/ordered region, while blue color and a value close to -1 indicated a more fluid region. In the whole cell images, two different regions could be distinguished, the more ordered PM and the more disordered/fluid intracellular membranes. These two populations were clearly detected in the pixel intensity distribution graphs, where two maxima were seen (blue line), respectively around 0.2 and around 0.5 for CHO cells grown in standard medium as in Monasterio *et al.* (2020). The PM was less fluid than the intracellular membranes, perhaps due to its barrier role (Owen *et al.*, 2012). The red lines indicate an average of the two peak intensities. In general, PM pixels were selected from the corresponding whole cell image in order to discard intracellular GP signal. PM signal was selected in laurdan images from CHO cells grown in standard (Fig. 4.2A) and SL-deficient (Fig. 4.2C) medium and LY-B cells grown in standard (Fig. 4.2B) and SL-deficient medium (Fig. 4.2D) for 72 h.

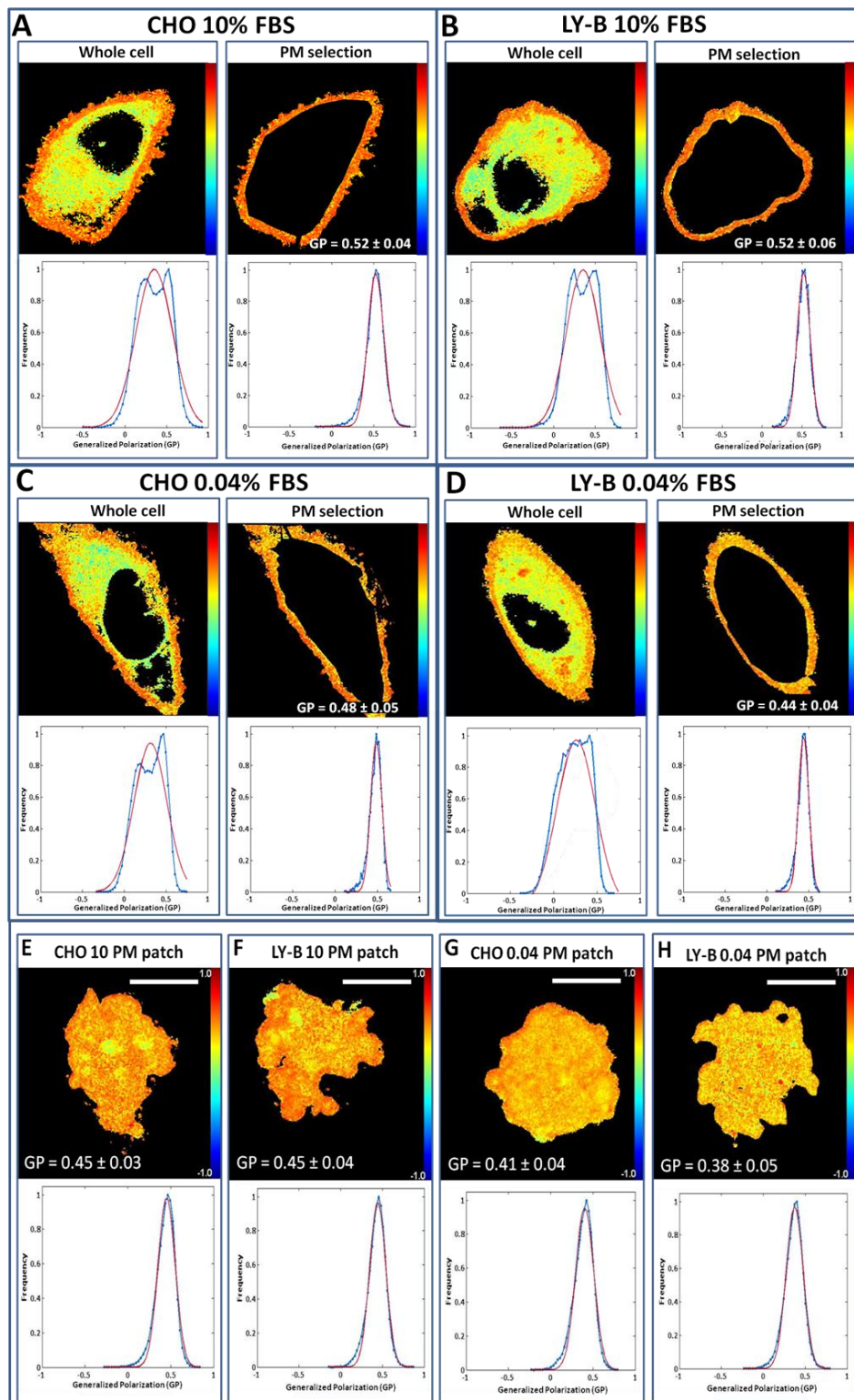


Figure 4.2. Laurdan staining and GP processing of cells and patches. Representative whole-cell, PM selection and the corresponding Laurdan generalized polarization plots of CHO cells grown in (A) standard and (C) deficient medium, and LY-B cells grown in (B) standard and (D) deficient medium. PM patches and the corresponding Laurdan generalized polarization plots of CHO cells grown in (E) standard and (G) deficient medium, and LY-B cells grown in (F) standard and (H) deficient medium. Blue lines indicate pixel intensity distribution; red lines indicate average pixel intensities. Note in whole-cell images that we can distinguish two different regions (blue lines): the more rigid PM and the more fluid intracellular membranes. GP are given as average values \pm S.D. ($n = 150$).

As seen in table 4.2, GP values of the selected PM region decreased when FBS in the medium was lowered to 0.04%; LY-B cell PM GP went from 0.52 down to 0.43, while CHO cell GP value decreased more moderately, from 0.52 to 0.47. Student's t test revealed that the difference between cells grown in standard and SL-deficient medium was statistically significant, both for CHO and LY-B cells. GP images of PM appeared to be homogenous, but the presence of nanodomains could not be ruled out because of the spatial and temporal resolution limit of conventional two photon microscopy (Frisz *et al.*, 2013b, 2013a; Nicovich *et al.*, 2018).

GP values of isolated PM preparations were also measured. GP of PM patches derived from LY-B cells, decreased on average from 0.45, (Fig. 4.2F), to 0.38 (Fig. 4.2H), when changing standard for deficient medium. Meanwhile CHO-cell PM patches underwent a smaller decrease, from 0.45 (Fig. 4.2E) to 0.41 (Fig. 4.2G). Figure 4.S4 summarizes all CHO and LY-B cell-derived samples that were imaged with laurdan. The corresponding GP values and the statistically significant differences according to Student's t test are shown in table 4.2. In short, two different PM preparations (PM patches and GPMV) were measured. In GPMV (Figs. 4.S4A and 4.S4B) or PM patches (Figs. 4.S4E and 4.S4F) no significant differences between CHO and LY-B cells grown in standard medium were found. However, when cells were grown in SL-deficient medium, the GP value decreased in both cell lines. This was observed for all samples, but it was particularly noticeable for LY-B cells and their derived PM preparations. This is an indication that LY-B cells grown in SL-deficient medium possess more fluid/less ordered membranes than when grown in standard medium. GP values of PM patches from LY-B cells grown in deficient medium and supplemented with SM (Fig. 4.5A) or sphinganine (Fig. 4.5B) were also measured (see Fig. 4.S1C, D.). No significant differences were found with the GP values of PM patches from CHO cells grown in deficient medium (Fig. 4.2G).

Mechanically, proteins are usually regarded as rigid inclusions in the lipid bilayer. Many theoretical studies have proposed that a membrane will become stiffer due to the presence of these rigid bodies (Agrawal *et al.*, 2016). Taking into account that the membrane bilayer is crowded with proteins, which may affect the rigidity/fluidity index, GUVs were formed with whole cell and PM lipid extracts as in Monasterio *et al.* (2020) and their GP values were also measured (Fig. 4.S4 and Table 4.2). The data in Figure 4.S4 show that, according to GP values, the bilayers formed

with the PM lipid extract of LY-B cells grown in SL-deficient medium (Fig. 4.S4L) were significantly more fluid than those formed with the corresponding CHO PM lipids (Fig. 4.S4K) (Table 4.2). GUVs formed with whole cell lipid extract were also studied. Again, statistically significant differences existed (Table 4.2) between LY-B grown in deficient medium and those grown in standard medium (Figs. 4.S4N and 4.S4P).

Table 4. 2. Laurdan GP values obtained from two-photon microscopy images.

Statistically significant differences were calculated with ANOVA and Student's t test with similar results. n=150. Significance of differences between CHO 10 and CHO 0.04: (#) $p < 0.05$; (##) $p < 0.01$. Differences between LY-B 10 and LY-B 0.04 (***) $p < 0.001$.

	CHO 10	CHO 0.04		LY-B 10	LY-B 0.04	
PM selection of 2-photon microscopy images	0.52 ± 0.04	0.47 ± 0.05	##	0.52 ± 0.06	0.44 ± 0.04	***
GPMV	0.44 ± 0.04	0.40 ± 0.03	##	0.45 ± 0.04	0.36 ± 0.04	***
PM patches	0.45 ± 0.03	0.41 ± 0.04	#	0.45 ± 0.04	0.38 ± 0.05	***
GUVs of PM patches lipid extract	0.40 ± 0.05	0.36 ± 0.05	#	0.38 ± 0.03	0.31 ± 0.04	***
GUVs of whole cell lipid extract	0.22 ± 0.03	0.13 ± 0.04	##	0.18 ± 0.04	0.06 ± 0.03	***

GP values in whole cell lipid extracts (cells grown in standard medium) were lower than the corresponding values in whole membranes, probably because of the rigidifying effect of proteins (Agrawal *et al.*, 2016; Shchelokovskyy *et al.*, 2011; Bouvrais *et al.*, 2008; Tristram-nagle *et al.*, 2010), and a statistically significant difference existed between GP values of CHO and LY-B GP lipid extracts. To confirm this point, SUV formed from whole cell lipid extracts were used to measure the emission spectrum of laurdan at different temperatures as in Monasterio *et al.* (2020). The spectrum at 20°C showed only slight differences between the 4 samples (Fig. 4.S5A). All samples had their emission maxima around 440 nm, indicating the rigid behavior of the membrane at this temperature. Still, the GP values derived from these emission spectra showed statistically significant differences between CHO and LY-B cells grown in standard medium, GP = 0.20 and 0.16 respectively (Fig. 4.S5D). This difference increased when cells were grown in SL-deficient medium, with GP = 0.14 and 0.04 respectively (Fig. 4.S5D).

At 30°C (Fig. 4.S5B), the emission maxima of samples grown in deficient medium exhibited a spectral component centered at ≈ 490 nm. This was particularly clear in the spectrum of SUV formed from whole cell lipid extract of LY-B grown in SL-deficient medium, indicating a more fluid behavior. These effects were even more marked when the temperature was increased to 40°C. GP values derived from these emission spectra are summarized in figure 4.S5D. Laurdan emission spectra of PM preparations at 40°C were also recorded (Fig. 4.S6). In most cases the spectra were red shifted (towards higher disorder) when the SL source was made scarce, however GPMV samples appeared to keep their degree of high order irrespective of the SL source.

Thus, when CHO and LY-B cells were grown in standard medium, PM preparations of both cell lines exhibited similar GP values (around 0.45). This parameter suffered a larger decrease in LY-B (to around 0.37) than in CHO (to around 0.40) when cells were grown in SL-deficient medium. However, LY-B lipid extract GP values were lower than the corresponding CHO samples when cells were grown in either SL-deficient medium or in standard medium.

4.3.3. Breakthrough forces of plasma membranes decrease with sphingolipid restriction

Whole cell lipid extracts, PM patches and GPMV were studied with an atomic force microscope (AFM), mainly in the force spectroscopy mode, to detect putative differences in breakthrough forces between the various samples. In our previous work we performed comparative AFM experiments of exclusively CHO-cell derived samples (Monasterio *et al.*, 2020). In this work we extend those findings, measuring also SL-depleted cells. Figure 4.3 shows the topology of PM patches from LY-B cells grown in standard (Fig. 4.3A) or SL-deficient (Fig. 4.3B) medium. The corresponding images of PM patches from CHO and LY-B cells are shown in parallel in figures 4.4A-D. According to topographic images, a minimum thickness of 5 nm was regularly observed in all samples (red arrow), corresponding to the thickness of a lipid bilayer (Umagai *et al.*, 2006). Other membrane components, perhaps (glyco)proteins or protein aggregates, gave rise to the higher elements in the AFM pictures. No significant differences were seen between PM patch thicknesses of the various samples.

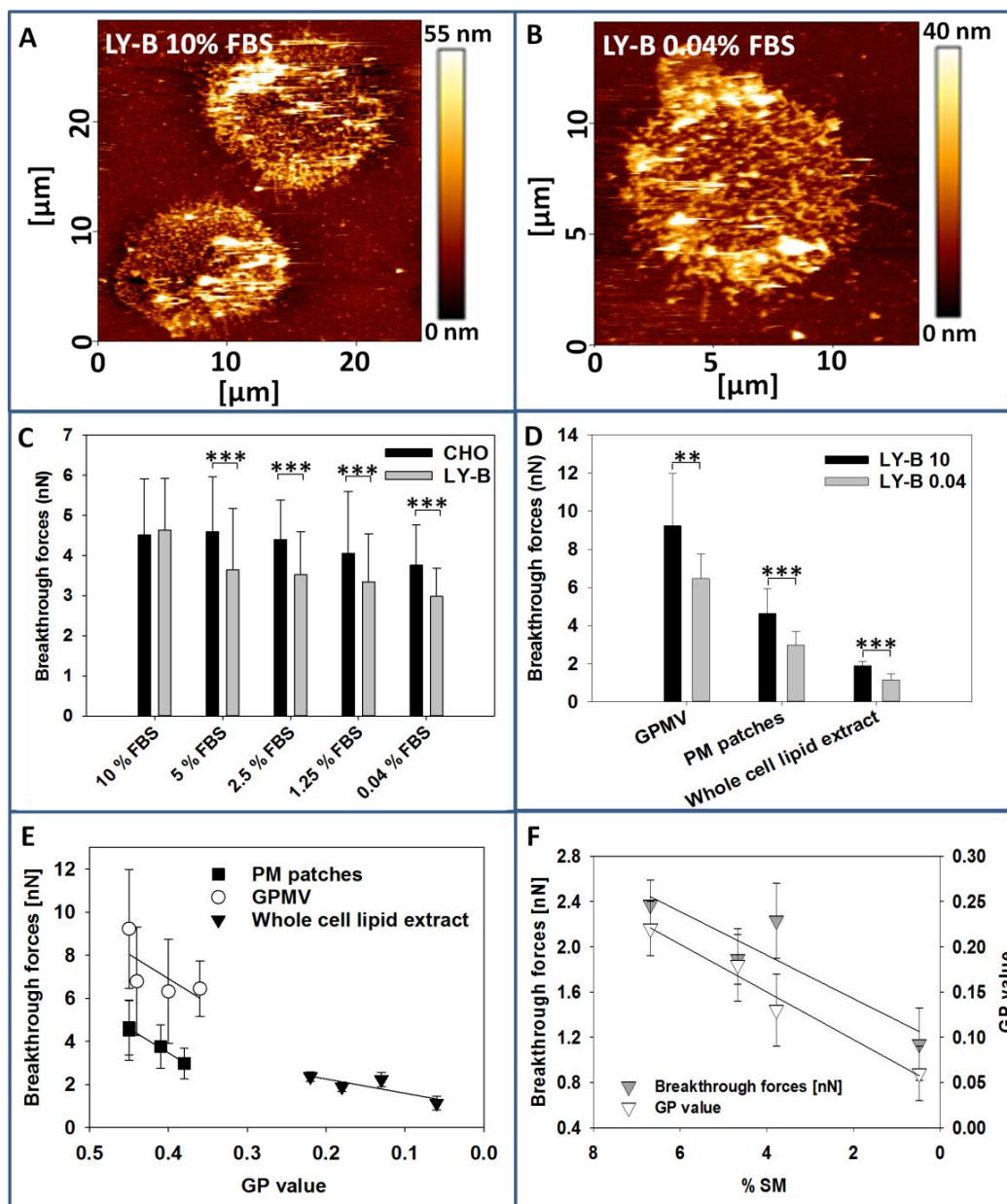


Figure 4.3. AFM measurements and correlation with laurdan GP and composition data. Topographic image of PM patches from LY-B cells grown in (A) standard or (B) sphingolipid-deficient (0.04% FBS) medium. **Force spectroscopy:** (C) Breakthrough forces for PM patches from CHO (black bars) and LY-B (gray bars) cells grown in media containing different FBS concentrations. (D) Breakthrough forces for GPMV, PM patches and whole cell lipid extracts from LY-B cells grown in standard (black bars) or sphingolipid-deficient (0.04% FBS) (gray bars) medium. Average values \pm S.D. ($n = 150-170$). Statistical significance was calculated with ANOVA or Student's t-test, with similar results: (*) $p < 0.05$; (**) $p < 0.01$; (***) $p < 0.001$. (E) **AFM - laurdan fluorescence correlation.** The correlations between laurdan GP and bilayer breakthrough forces are shown as regression lines ($y = y_0 + ax$). The experimental points correspond to PM patches (full squares, $y_0 = -5.54 \pm 0.59$; $a = 22.51 \pm 1.39$; $r^2 = 0.992$), GPMV (empty circles, $y_0 = -2.17 \pm 7.13$; $a = 22.70 \pm 17.22$; $r^2 = 0.465$) and whole cells (full triangles, $y_0 = 0.93 \pm 0.50$; $a = 6.62 \pm 3.14$; $r^2 = 0.689$). Average values \pm S.D. ($n = 150-170$). (F) **Correlation between [SM] and physical properties.** The correlations between SM concentration in bilayers (whole cell lipid extracts), and laurdan GP and bilayer breakthrough forces, are shown as regression lines. Breakthrough forces: (grey triangles, $y_0 = 1.16 \pm 0.29$; $a = 0.19 \pm 0.06$; $r^2 = 0.82$) or GP values: (empty triangles, $y_0 = 0.045 \pm 0.013$; $a = 0.026 \pm 0.000$; $r^2 = 0.97$). Average values \pm S.D. ($n = 150-170$).

The breakthrough force distributions showed no significant differences between the PM patches from CHO (4.52 nN) and LY-B (4.64 nN) cells grown in 10% FBS standard medium (Fig. 4.3C). Nevertheless, when the FBS contents in the medium was 5% or lower, the breakthrough forces decreased gradually for both samples, but particularly in PM patches from LY-B cells (Fig. 4.3C). Significant differences existed between PM patches of both cell lines when FBS in the medium was 5% or lower (Fig. 4.3C). With the minimum FBS concentration in the growth medium (0.04%), the breakthrough forces decreased from 4.52 (standard medium) to 3.76 nN (SL-deficient medium) for CHO cells, while LY-B cell PM patches underwent a larger decrease from 4.64 nN (standard medium) to 2.98 nN (deficient medium). Breakthrough force distribution values of PM patches from LY-B cells grown in deficient medium and supplemented with SM (Fig. 4.5C) or sphinganine (Fig. 4.5D) were also measured. No difference existed between them and the values obtained from PM patches of CHO cells grown in deficient medium (Fig. 4.4B).

GPMV breakthrough forces were also measured. In GPMV derived from LY-B cells they decreased significantly when cells were grown in SL-deficient medium (9.23 in standard vs. 6.45 in deficient medium). Breakthrough forces of GPMV derived from CHO cells grown in standard and deficient media were also assessed (Fig. 4.S7), but no significant differences were found in this case. For lipid-supported planar bilayers (SPB) Figure 4.3D shows that the breakthrough force required for piercing the SPB from LY-B lipid extract decreased significantly when cells were grown in deficient medium (1.89 in standard medium vs. 1.14 in SL-deficient medium).

Topographic images of SPB from whole CHO and LY-B cell lipid extracts grown in standard medium were also scanned (Figs. 4.4E-H). The images did not exhibit statistically significant differences; thickness was around 5 nm in all cases and lipid domains could not be distinguished. Breakthrough forces of SPB formed with the CHO cell lipid extract were also measured (Fig. 4.S7). In agreement with the results obtained from lipid extract GP measurements (Table 4.2), the breakthrough forces were significantly different between CHO (Fig. 4.4E) and LY-B (Fig. 4.4F) cells grown in standard medium (Fig. 4.S7). This difference became larger when CHO (Fig. 4.S4G) and LY-B (Fig. 4.4H) cells were grown in deficient medium (Fig. 4.S7).

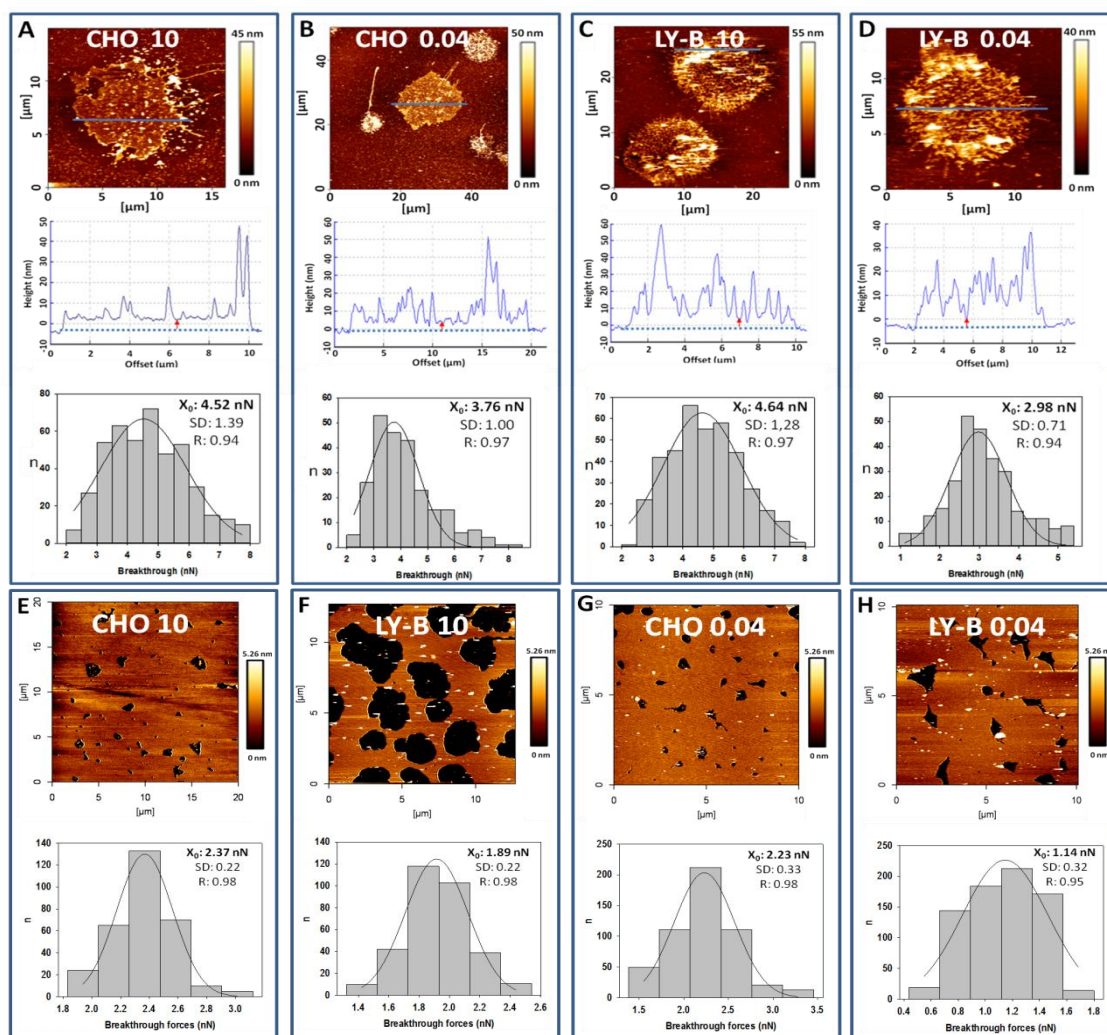


Figure 4.4. Topographic images and breakthrough force distributions of supported planar bilayers. (A-D) From top to bottom, topographic image, topographic profile (along the blue line) and breakthrough distributions of PM patches from CHO cells grown in standard (A) or SL-deficient medium (B), and from LY-B cells grown in standard (C) or SL-deficient (D) medium. The small red arrow below the topographic profiles corresponds to 5 nm, the average thickness of a bare lipid bilayer. (E-H) Bilayers formed from whole cell lipid extracts. CHO (E) and LY-B (F), cells grown in standard medium. CHO (G) and LY-B (H) cells grown in SL-deficient medium. For breakthrough distributions, $n = 150-170$.

Breakthrough force measurements were in good agreement with laurdan GP values. Whole cell lipid extracts and PM patches exhibited the expected behavior, the LY-B cells grown in deficient medium showing the lowest values in both techniques (Figs. 4.3E, F). A linear correlation was observed between changes in SM levels and changes in GP and breakthrough forces (Figs. 4.3E, F).

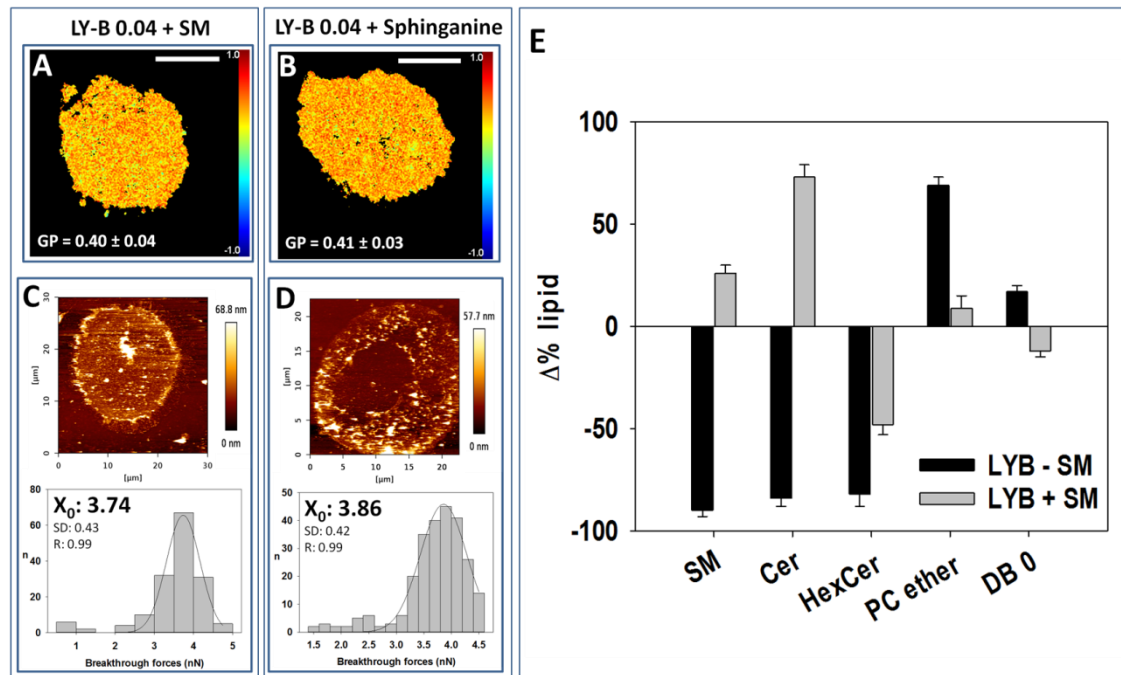


Figure 4.5. Effect of SL supplementation on the biophysical properties and lipid redistribution of LY-B cells grown in deficient medium. (A, B) Laurdan-stained PM patches derived from LY-B cells grown in (A) SM-, or (B) Sph-supplemented deficient medium. (C, D) Topographic image and breakthrough force distribution of PM patches derived from LY-B cells grown in (C) SM- or (D) Sph-supplemented deficient medium. (E) Redistribution of selected lipids in LY-B cells grown in SM-supplemented (+SM) or non-supplemented (-SM) deficient medium as compared with CHO cells. Results are shown as percentage increase or decrease with respect to CHO cells grown in deficient-medium. DB0 = no double bond, i.e. saturated chain lipids.

To summarize, CHO and LY-B PM patch breakthrough forces had similar values (around 4.5 nN) when the cells were grown in standard medium. In deficient medium this value decreased more markedly for LY-B (2.98 nN) than for CHO (3.76 nN). As to breakthrough forces in GPMV, those in vesicles derived from LY-B were also decreased (from 9.23 nN to 6.45 nN), but not those obtained from CHO. Finally, lipid extract GP value differences were also detectable when cells were grown in standard medium (1.89 nN for LY-B and 2.37 nN for CHO). The latter values decrease in LY-B (to 1.14 nN), but not in CHO (2.23 nN), when growing in SL-deficient medium.

4.3.4. Sphingolipid composition changes after a 250-fold reduction in sphingolipid supply, with smaller effects on glycerophospholipids.

Analyzing the lipid redistribution undergone by cells with suppressed SPT activity is crucial for a proper understanding of the existing membrane order/disorder differences between CHO and LY-B cells in high- and low-SL media, and their capacity

of homeostatic regulation. In order to clarify the changes in the cell lipid pathways, a lipidomic study of whole cell and PM preparations of CHO and LY-B cells grown in standard and deficient media was performed. For GPMV formation, but not for PM patch preparations, cells had been in contact with dithiothreitol and paraformaldehyde, thus different controls were used for each case as in Monasterio *et al.* (2020).

Figures 4.6A-C shows the amounts of different SL (SM, Cer and HexCer) when CHO and LY-B cells were grown in medium containing different FBS concentrations. These three specific SL were selected among the lipidomic data respectively because SM is the most abundant SL, Cer is particularly important in cell signaling, and HexCer is at the origin of the biosynthetic pathway leading to the complex glycosphingolipids. Significant differences were seen between SM amounts in CHO and LY-B cells (Fig. 4.6A). When cells were grown in standard medium, the SPT-deficient LY-B cells contained 43% less SM than CHO cells.

When the amount of FBS in the medium was decreased, total SM was also lower in both wild type and mutant cells. Nevertheless, the decrease was greater in LY-B than in CHO cells, 90% vs 25% with the lowest FBS concentration (0.04%) (Fig. 4.6A). In cells grown in standard medium, LY-B contained 70% less Cer than CHO cells. When FBS concentration was decreased, the total Cer amount was also diminished in both cell lines. As with SM, the reduction was larger in LY-B than in CHO cells, 66% vs. 38% (in 0.04% FBS-containing medium). Figure 4.6C shows the corresponding values for HexCer. LY-B grown in 10%-FBS medium contained 70% less HexCer than CHO, in agreement with the Cer data (Fig. 4.6B). When FBS in the medium was decreased, HexCer also decreased by 50% in LY-B cells grown in 0.04% FBS-containing medium, but it increased by 85% in CHO (Fig. 4.6C). Considering the PM patches, SM, Cer and HexCer were all lower in LY-B 0.04 PM patches than in LY-B 10 ones. In summary, in LY-B cells the three SL under study exhibited a similar decrease (55-70%) with the reduction of FBS, at variance with CHO cells, suggesting that, in the latter, an active *de novo* SL synthesis could occur. The situation with GPMV was, however, different, mainly in that Cer and HexCer increased when the cells (either CHO or LY-B) were grown in 0.04 FBS medium (Figs. 4.7B, C).

CHO/LY-B cell growth under limiting sphingolipid supply: correlation between lipid composition and biophysical properties of sphingolipid-restricted cell membranes

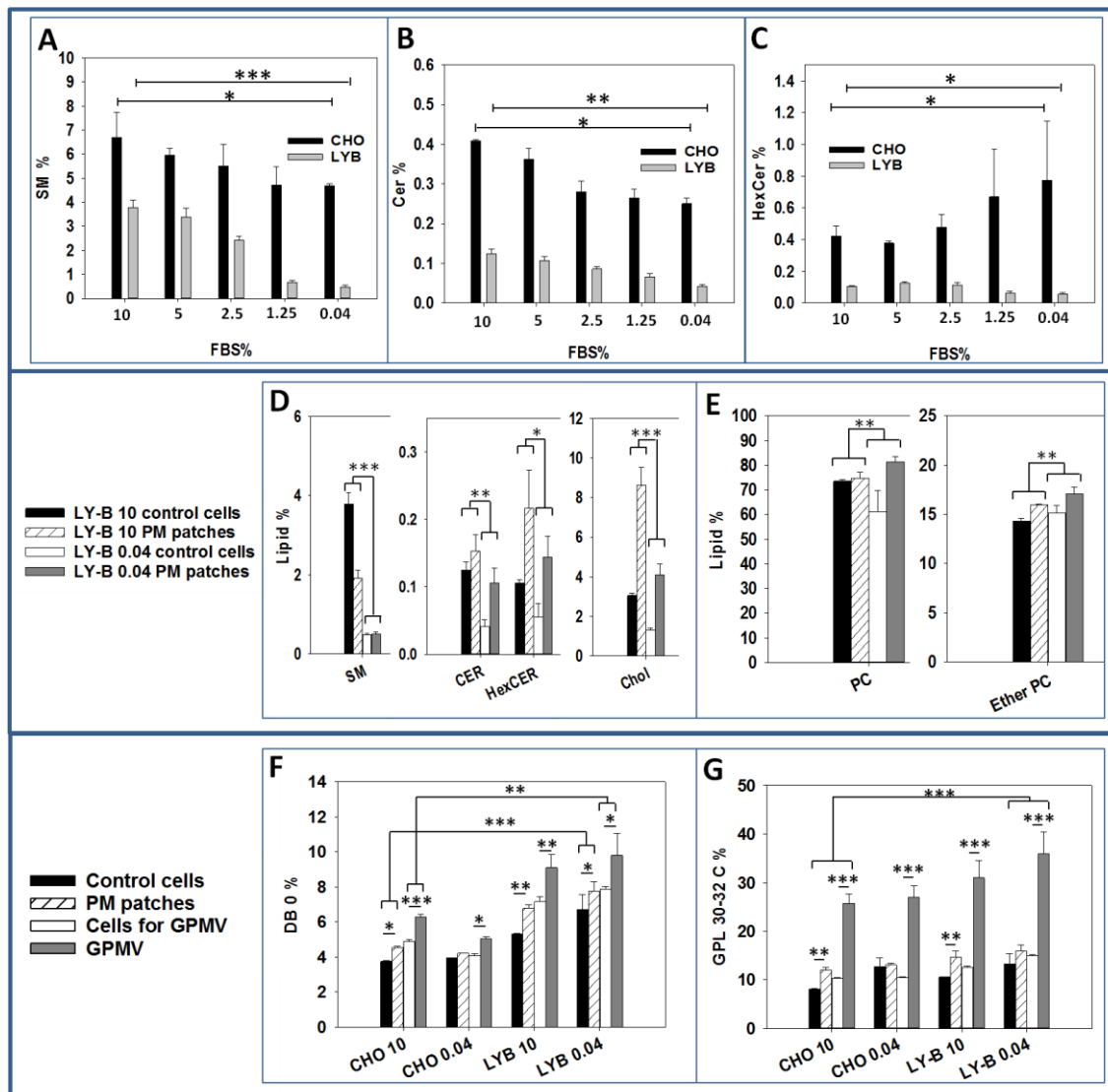


Figure 4.6. Lipidomic analysis of CHO and LY-B cells. Total SM (A), Cer (B) and HexCer (C) from CHO (black bars) or LY-B (gray bars) whole cells grown in media containing various concentrations of FBS. (D, E) A comparison of lipid compositions of whole cell and PM patches of LY-B cells grown in standard or sphingolipid-deficient (0.04% FBS) media. Only selected lipids are included in the figure. A comprehensive description of the various lipid compositions can be seen in the Supplementary Material Table 4.S1 and Figure 4.7. (F) Fully saturated (DB0 = no double bonds) and (G) short-chain (30-32C) GPL of whole cells treated for GPMV preparation, GPMV, cells treated for PM patch preparation, and PM patches. n=3. Statistical significance was calculated with ANOVA or Student's t-test, with similar results. Significance: (*) p<0.05; (**) p<0.01; (***) p<0.001. Lipid percentages were computed over the total lipid amount measured with the mass spectrometer.

With low-FBS medium, Chol levels were decreased in both cell lines (Fig. 4.7D). Since FBS is a major source of lipids and proteins for cell growth under our conditions, the drastic reduction from 10% to 0.04% in the SL-deficient medium induces partial cell starvation. Chol synthesis is known to decrease in fasting conditions (Smith *et al.*, 2017; Kovanen *et al.*, 1975; Désert *et al.*, 2008). Moreover, LY-B PM preparations had larger amounts of Chol than the whole cell average, for cells grown in

high- and low-FBS (Fig. 4.6D). This had been observed by Monasterio *et al.* (2020) for the case of CHO cells.

Glycerophospholipid (GPL) acyl chain also changed along with SL deprivation. In figure 4.6E we can see that ether PC was increased in LY-B 0.04 cells. GPL acyl chain saturation and length also play an important role in the physical properties of the membrane bilayer, specifically on its disorder/fluidity. Specifically, unsaturated and shorter acyl-chain- containing GPL increase membrane fluidity (van Meer *et al.*, 2008). In figure 4.6F the distribution of fully saturated GPL of control and two PM preparations (patches and GPMV) is shown. PM preparations had more fully saturated and less polyunsaturated (2-6 double bounds) GPL (Fig. 4.7J-L) than their respective controls in all measured samples (Monasterio *et al.*, 2020). The differences were larger in the case of GPMV. Comparing CHO and LY-B grown in standard medium, LY-B had more fully saturated GPL in all cases. In addition, when FBS in the medium was decreased, the saturated GPL increased in LY-B, while in CHO cells they remained almost constant (Fig. 4.6F).

As to the GPL chain length distribution, PM preparations were richer in 30-32 C chains than whole cells, the difference being larger for the GPMV (Fig. 4.6G) (Monasterio *et al.*, 2020). GPL of LY-B grown in standard medium contained more 30-32 C acyl chains than CHO 10 in all measured samples. This difference was increased when LY-B were grown in 0.04% FBS medium. Conversely, CHO 0.04 chain-length values remained constant (Fig. 4.6G). In summary LY-B cells synthesized shorter and more saturated GPL in their homeostatic response to SM depletion. A comprehensive description of the various lipid compositions can be seen in the table 4.S1 and figure 4.7.

The homeostatic response undergone by LY-B cells grown in deficient medium and supplemented with SM (Fig. 4.5E) was also observed. Data are shown as percent increase or decrease when compared to the amounts found in CHO cells grown in deficient medium. SM and Cer levels were totally recovered, becoming even higher than the control values. However, for reasons that remain unexplained, the HexCer CHO amounts were not reached. PC ethers increased when LY-B cells were grown in deficient medium; this increase was suppressed with SM supplementation. Fully saturated GPL levels were slightly decreased with SM supplementation (Fig. 4.5E).

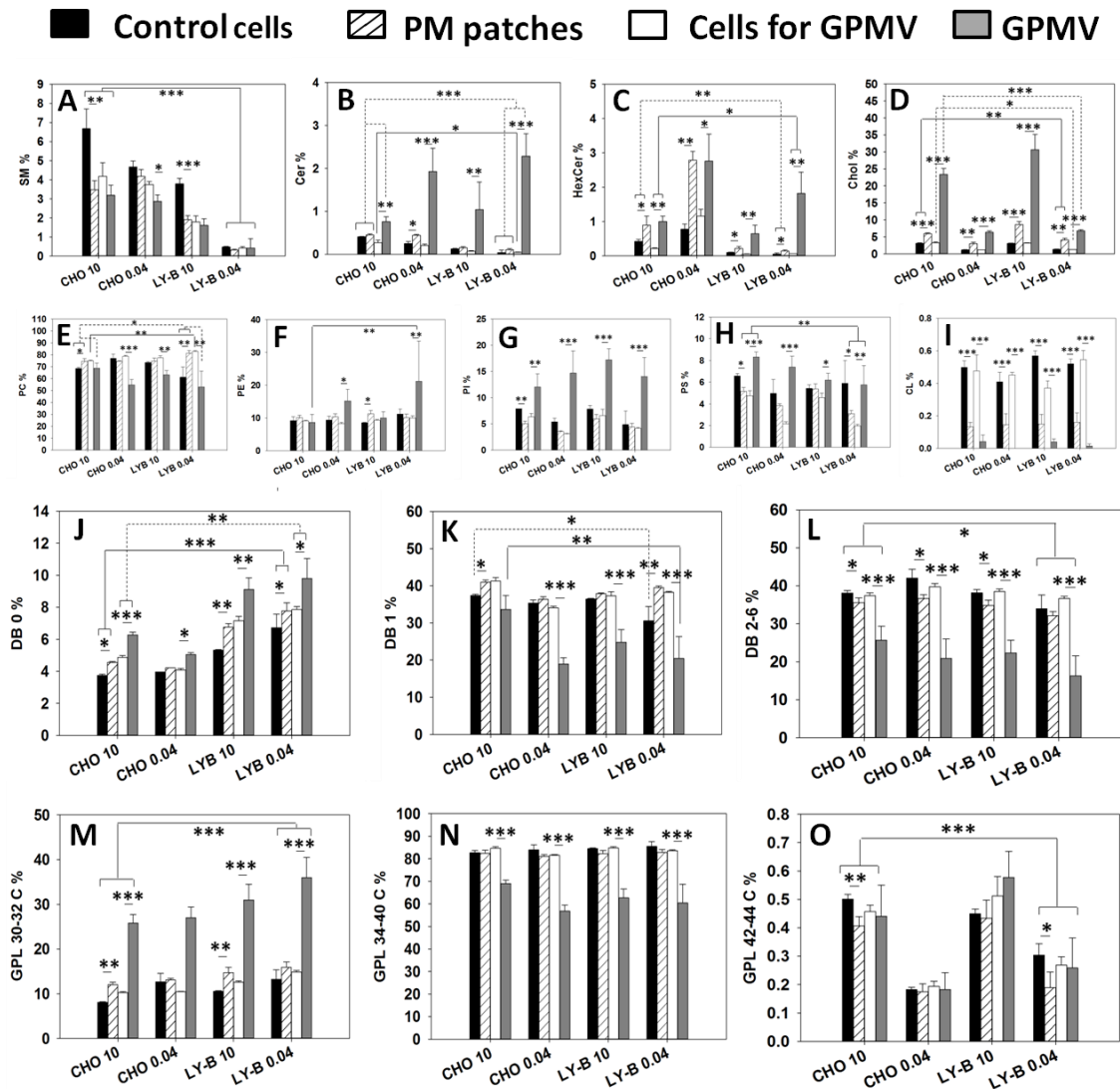


Figure 4.7. Lipidomic analysis of whole cells and plasma membrane preparations. SM (A), Cer (B), Hex Cer (C), Chol (D), PC (E), PE (F), PI (G), PS (H), CL (I). **J-L:** GPL saturation distribution (number of double bonds per GPL molecule). No double bonds (DB 0) (J), one double bond per molecule (DB 1) (K), two – six double bonds per molecule (DB 2-6) (L). **M-O:** GPL length distribution (number of C atoms in the two acyl chains). 30-32 C (M), 34-40 C (N), 42-44 C (O). Mean values \pm S.D. (n = 3). Statistical significance was calculated with ANOVA and Student's t-test: (*) p<0.05; (**) p<0.01; (***) p<0.001. Lipid percentages were computed over the total lipid amount measured with the mass spectrometer.

A quantitative estimate of the amount of SM and Chol, two representative lipids in this context, was carried out as described under Methods. The results can be seen in figure 4.S8. With respect to Chol, the concentration in CHO cells grown in SL-medium was 33% of those grown in standard medium (data in pg Chol/cell), and the corresponding figure for LY-B was 45% (Fig. 4.S8B). As for SM data, CHO cells grown on medium with 0.04% FBS contained 68% of the SM found in cells grown on 10% FBS (data in pg SM/cell) (Fig. 4.S8B), or 53% (in pg SM/ng protein) (Fig. 4.S8A).

For the SPT-defective LY-B cells, the corresponding figures are 15% (Fig. 4.S8B), and 16% (Fig. 4.S8A). Thus, a 250-fold reduction in sphingolipid supply to LY-B cells leads to a 6-fold decrease in membrane sphingolipids.

As a summary of the lipidomic results, SM, Cer and HexCer concentrations were lower in LY-B PM patches than in CHO ones when grown in standard medium. All three SL were similarly decreased (55-70%) with the reduction in FBS. LY-B cells contained larger amounts of Chol than CHO ones in both standard and SL-deficient media. With respect to the GPL fatty acyl distribution, LY-B had more saturated and shorter GPL fatty acids than CHO cells. These groups of fatty acids, together with PC ethers, were increased in LY-B and maintained in CHO when FBS concentration was decreased. For LY-B in SL-deficient medium SM decreased both in GPMV and in PM patches but Cer and HexCer were increased with lower FBS concentrations (Figs. 4.7A-C).

4.4. Discussion

LY-B cells grown in SL-deficient medium were used to understand the effects that a defective SPT activity might have on the biophysical properties of the cell. SPT-defective cells grown with very low SL concentrations were viable (Fig. 4.S2E) and they were able to recover the control growth rates when the SL-deficient medium was supplemented with SM (Fig. 4.1B) or sphinganine (Fig. 4.S1C).

4.4.1. CHO and LY-B cells grown in standard medium

4.4.1.1. Whole cells

Comparing SL levels in CHO and LY-B cells grown in standard medium, they happened to be markedly lower in the mutant cells. Considering the three most abundant SL, SM was 43% lower in LY-B cells (Fig. 4.6A), Cer was 66% lower (Fig. 4.6B), and HexCer was 70% lower (Fig. 4.6C). This indicated that the *de novo* pathway could be a major SL synthesis source. This result is in agreement with the one published by Ziulkoski *et al.* (2001) where they used fumonisin B1 and β -chloroalanine to determine the contribution of the different pathways to the synthesis of SM in Sertoli cells. They found that 40% of 16:0 and 61% of 18:0, 18:1 and 18:3 SM was synthesized by the *de novo* pathway. They also observed that these values could be increased when

the requirement for cell membranes was greater, as in rapidly dividing cells (Ziulkoski *et al.*, 2001). In contrast with the SL results, Chol concentrations were similar in CHO and LY-B cells grown in standard medium (Fig. 4.7D). In addition, comparison of both kinds of cells in standard medium showed small changes in GPL, LY-B contained more fully saturated, and less monounsaturated GPL than CHO, chain length distributions in GPL being virtually the same (Figs. 4.6F, G).

4.4.1.2. PM preparations

Important differences were found between the whole cell and PM lipid compositions, as anticipated from the studies in CHO by Monasterio *et al.* (2020) Both for CHO and LY-B preparations, PM patches contained less SM (about one half), more HexCer and more Chol than the whole cells. GPMV had also less SM but contained higher amounts of HexCer, and particularly of Cer and Chol. Changes in GPL were moderate or low, except for cardiolipin, that was almost absent in the PM preparations (Figs. 4.7A-D, I). The higher amounts of Chol in PM patches (Fig. 4.7D) could be a major factor responsible for compensating PM molecular order even with lower SM levels. Neither laurdan GP of GPMV nor laurdan GP or breakthrough forces of PM patches showed any statistically significant difference between CHO and LY-B grown in 10% FBS (Table 4.2, Fig. 4.3C).

GPMV constitute a frequently used PM preparation (Monasterio *et al.*, 2020; Manni *et al.*, 2015; Sezgin *et al.*, 2012; Skinkle *et al.*, 2020). However, the lipidomic data showed that their lipid composition departed from those of the whole cells and from other PM preparations (patches). In particular, GPMV were enriched in Cer (Fig. 4.7B) and HexCer (Fig. 4.7C), and they also exhibited an unusual enrichment in PI (Fig. 4.7G). Furthermore, their GPL were enriched in saturated fatty acids (Fig. 4.7J), and contained correspondingly less unsaturated chains, specifically with 2-6 double bonds per GPL molecule (Fig. 4.7L). Also, the proportion of medium-length fatty acids (C30-32 per GPL molecule) increased at the expense of the longer ones (C34-40) (Figs. 4.7 M, N). All these are peculiarities of GPMV, in which they differed from all other cell and membrane preparations, with either 10% or 0.04% FBS. The fact that these changes were not modified by SL depletion, and that some of them affected mainly GPL, makes GPMV a less useful membrane preparation in the context of our study. GPMV penetration required consistently higher breakthrough forces than PM patches (Fig.

4.S7). This could be related to the enrichment in Cer and HexCer found in GPMV with respect to whole cells (Fig. 4.7B, C). Both Cer and HexCer are known to increase membrane lipid order (Alonso & Goñi, 2018; González-Ramírez *et al.*, 2019; Varela *et al.*, 2017) GPMV have been shown to be permeable to hydrophilic macromolecules (Skinkle *et al.*, 2020), and this could again be related to the increased Cer, and partly HexCer, since these SL happen to increase membrane permeability (González-Ramírez *et al.*, 2019; Alonso & Goñi, 2018). The observed increases in GP and breakthrough forces could be secondary to the use of dithiothreitol in GPMV formation. As seen in Epstein *et al.* (2012), dithiothreitol can be responsible for increasing Cer concentrations even in SPT-suppressed cell lines, without altering SM values. Those authors concluded that dithiothreitol could induce the ‘unfolded protein response’ and this would lead to an over-expression of the SPT LCB1 subunit mRNA, partially recovering its activity. Dithiothreitol was also shown to affect lipid–lipid and lipid–protein interactions and to integrate directly into lipid membranes (Gerstle, R., Desai, R. & Veatch, 2017).

4.4.2. CHO and LY-B cells grown in SL-deficient medium

When LY-B cells were grown in SL-deficient medium, SM and Chol percent levels were markedly decreased, respectively by about 5-fold and 2-fold, with no comparable changes in Cer or HexCer, and the derived PM patches followed parallel trends (Figs. 4.6A, D and Figs. 4.7A, D). In CHO cells the decrease in SM concentration was less clear, and HexCer levels actually increased somewhat, other SL varying as in LY-B (Fig. 4.6A, C), with the corresponding PM patches showing similar trends (Figs. 4.7A-D). Growth in SL-deficient medium did not cause any remarkable changes in GPL, nor in their associated fatty acids (Fig. 4.7E-N), with the exception that the very long fatty acids (C42-44 per GPL molecule) whose concentration was in any case very low, were further decreased with the low FBS medium. Note that the largest decrease in SM, the most abundant SL, occurred in LY-B cells deprived of SL in the growth medium, thus the two factors appear to be required, lack of SL in the nutrients and lack of capacity to synthesize the sphingosine precursor, to obtain low-SL cells.

With respect to the PM preparation, laurdan GP indicated a decreased lipid order (increased bilayer fluidity) in all samples under study (Table 4.2) and breakthrough forces decreased accordingly, more in LY-B than in CHO cells and membranes (Figs. 4.3B, C). As a result, PM patches from LY-B cells were less ordered and more easily

penetrable (Table 4.2, Fig. 4.3C). The close correlation between decrease in SM concentration in cell membranes, as a result of SL deprivation in the nutrients, decrease in GP values and decrease in breakthrough forces can be seen in figures. 4.3C, D. (Only data from whole cell lipid extracts are included in figure 4.3D, for simplicity).

4.4.3. Homeostatic adaptations

At least some of the observed changes in membrane lipid composition as a result of gene suppression or of changes in nutrient media could be explained in terms of homeostatic responses to the novel situations. Perhaps the main observation in terms of adaptation is the remarkable resilience of LY-B cells that, when grown under extremely low SL concentrations (250-fold below standard conditions), are still able to divide while keeping SL concentrations just 6-fold lower than the standard value, and membrane physical properties not far away from the wild-type cells. Examining the data in more detail, and specifically comparing CHO and LY-B cells grown in 10% FBS medium, hints on adaptation to lack of *de novo* SL synthesis could be retrieved. In particular, as described above, the only notable change between the lipidomes of those two cell lines, grown under standard conditions, is the clear decrease in SL as percent total lipids (one-half on average) in the LY-B cells (Fig. 4.7), while Chol levels did not vary. The percent concentration of SM, the most abundant sphingolipid, went from 6.7% to 3.8% (Fig. 4.7A). Parallel changes were recorded in PM patches derived from those cells. This was not accompanied by any changes in the measured physical properties of the membranes, laurdan GP (Table 4.2) or AFM breakthrough forces (Fig. 4.3C). Perhaps the observed variation in SL concentration was not enough to cause any observable physical changes, and a very minor, or no adaptation was required.

The situation was different when cells were grown in SL-deficient medium. In LY-B cells SM concentration dropped by one order of magnitude when cells were grown in 0.04% instead of 10% FBS. Other SL, as well as Chol, were decreased in parallel. PM patches underwent similar changes as the whole cell lipids. Perhaps as a consequence of these changes, the membranes became more easily penetrable, and lipids became less ordered (Table 4.2 and Fig. 4.3) when FBS concentration was lowered. Simultaneously, fatty acyl unsaturation was decreased (Figs. 4.7J-L), a phenomenon that could have the effect of increasing lipid order, thus tending to compensate the decrease in bilayer-ordering SM. Our results regarding the increase in

ether lipids in sphingolipid-depleted cells fit previous observations (Jiménez-Rojo *et al.*, 2020) and confirm the co-regulation between these two lipid classes.

When CHO cells were grown in SL-deficient medium the proportion of HexCer was considerably increased, by about 2-fold. This increased HexCer synthesis (that could not occur in LY-B cells because of their low sphingosine availability, due to the lack of SPT activity), may be one of the homeostatic responses that wild-type cells carry out under starvation. HexCer is at the origin of the complex glycosphingolipid biosynthetic pathway (Merrill *et al.*, 1997). Glycosphingolipids are required for cellular differentiation and there are human diseases resulting from defects in their synthesis (Van Meer *et al.*, 2003). This may be one of the reasons for the different dividing ratios of CHO and LY-B in SL-deficient medium (Fig. 4.1A). CHO, but not LY-B cells, may over-express the HexCer synthesis to continue cell division in order to buffer the nutrient depletion condition. As discussed above, Chol levels in CHO and LY-B grown in standard medium remained invariant, and this could help in maintaining membrane rigidity under conditions of low SM (Fig. 4.7D, J). Nevertheless, as Chol synthesis decreases under cell starvation conditions, rigidity cannot be maintained in this manner under SL-deficient conditions. When FBS in the medium was decreased, saturated GPL were increased in LY-B (Fig. 4.6F), while in CHO cells they remained almost constant.

4.5. Conclusions

The present study has demonstrated that in cells lacking the SPT activity, SM, Cer and HexCer are markedly decreased in all measured samples (controls and PM preparations).

Fully saturated GPL are increased and polyunsaturated ones are decreased. Synthesizing more saturated GPL can be the way that LY-B cells have to compensate the low SM. Cholesterol may also have some influence in that response but its effect is minimized when its levels are decreased because of starvation. The SM-depleted cells try to maintain membrane order undergoing a homeostatic response, although they achieve it only partially as their PM are more fragile when grown in SL-deficient medium.

These changes in lipid order and membrane rigidity caused by low SL could be linked to a variety of phenomena in cell physiology and pathology. Alterations in the

normal activities of the SM-cycle enzymes have been associated to many central nervous system and neurodegenerative diseases (Kamil *et al.*, 2016). Specific SM species have been found to bind membrane proteins thereby modifying their functions (Contreras *et al.*, 2012). The capacity shown by certain cells in this paper to grow under extremely demanding low concentrations of SL opens the way to a variety of functional studies on the role of SL in membranes.

4.6. Supplementary material

Table 4.S1. A summary of the various lipid compositions of CHO and LY-B cells.

https://drive.google.com/file/d/1zAdo-hq1sodXNL3QwALzXwlmW8m_Anir/view?usp=sharing

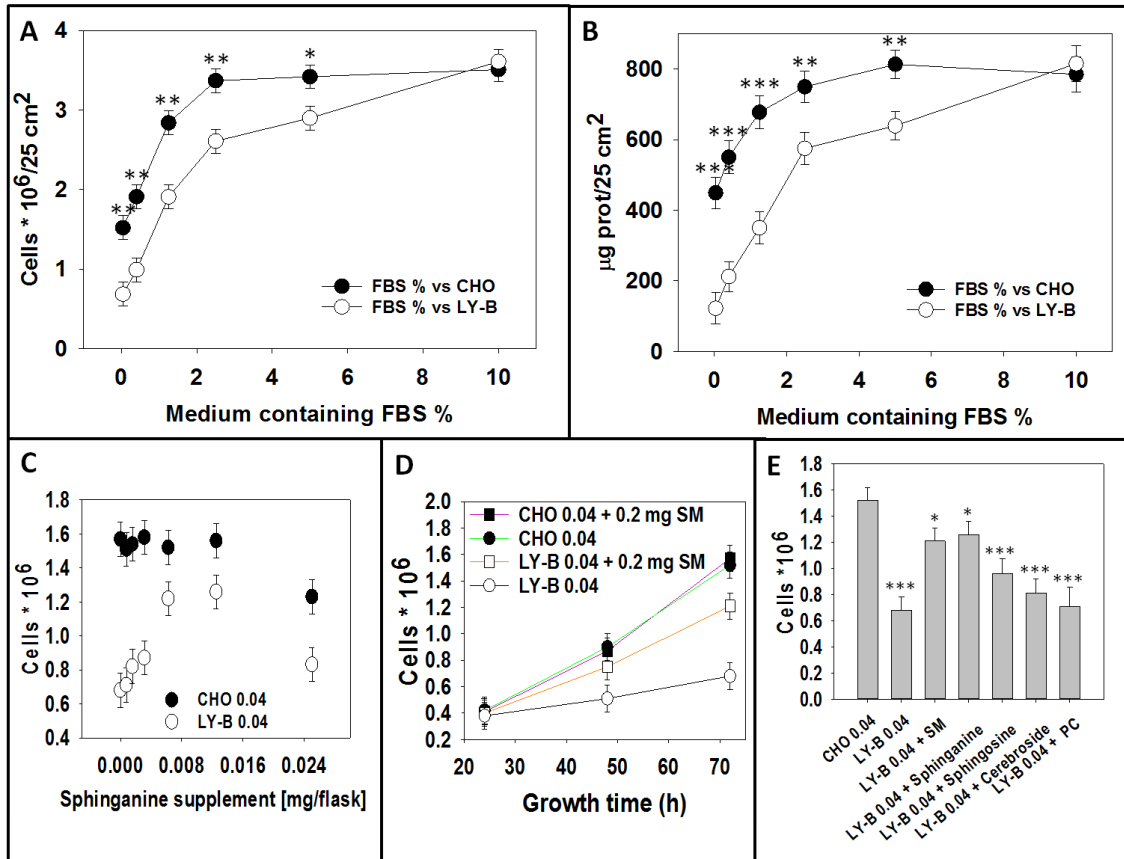


Figure 4.S1. CHO and LY-B cell growth measurements. (A) Cell counts, and (B) protein contents, per 25 cm²-flask, as a function of %FBS in the medium (growth time: 72 h). (C) LY-B (empty symbols) and CHO (filled symbols) 72 h cell growth in deficient medium as a function of sphinganine supplementation (seeded cells: 0.25 * 10⁶). (D) Cell counts of LY-B (empty symbols) and CHO (filled symbols) as a function of time in sphingolipid-deficient medium (circles) and sphingolipid-deficient medium supplemented with (0.2 mg/5ml = 80 µM) (squares). (E) LY-B and CHO cell growth after 72 h in non-supplemented or supplemented sphingolipid-deficient medium (seeded cells: 0.25 * 10⁶). Means ± S.D. (n = 3). In A, B, E, statistical significance was calculated with ANOVA and Student's t-test. Significance: (*) p<0.05; (**) p<0.01; (***) p<0.001.

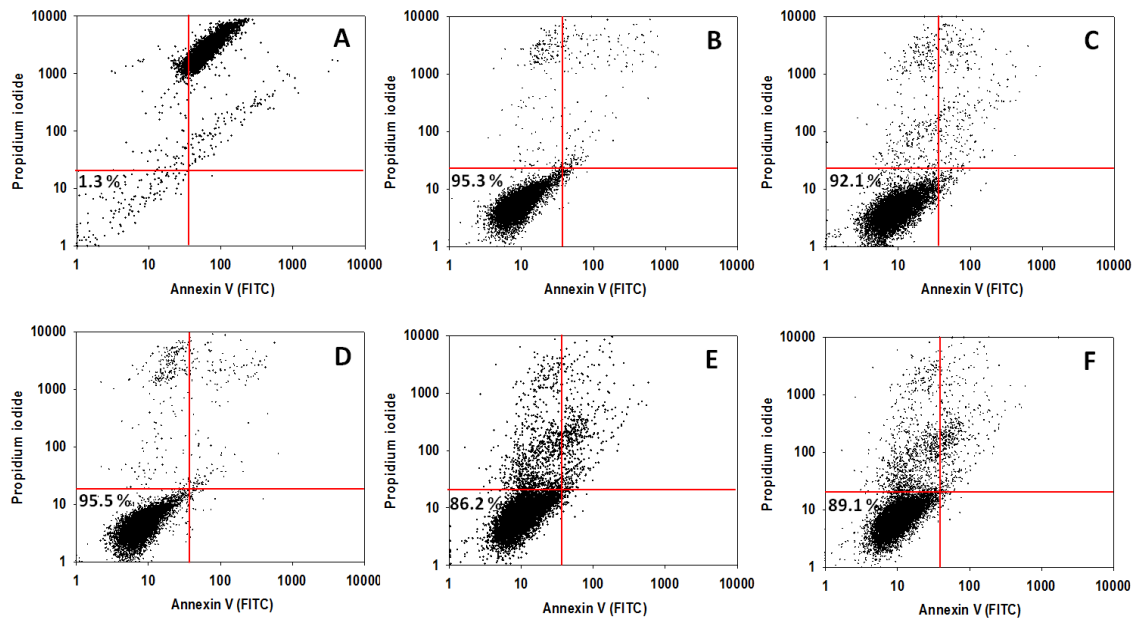


Figure 4.S2. CHO and LY-B cell viability after 72 h in standard and SL-deficient medium. (A) Control, CHO cells treated with 50% (v/v) EtOH. **(B)** CHO grown in 10% FBS- or **(C)** in 0.04% FBS-containing medium. **(D)** LY-B grown in 10% FBS- or **(E)** in 0.04% FBS- containing medium. **(F)** LY-B grown in 0.04% FBS- + 0.2 mg SM-containing medium.

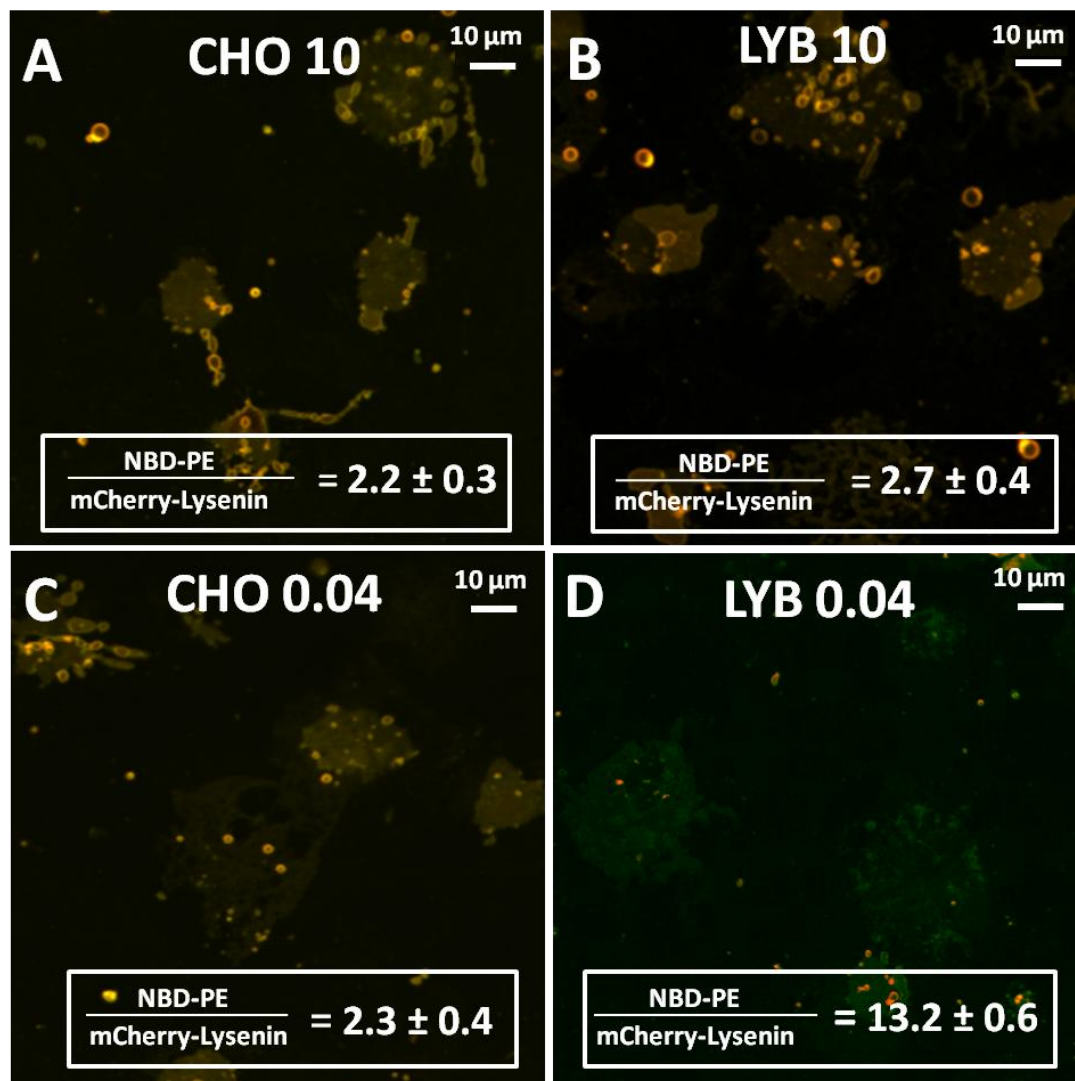


Figure 4.S3. Fluorescence images of PM patches stained with mCherry-lysenin (red). CHO (A) and LY-B (B) cells grown in standard medium; CHO (C) and LY-B (D) cells grown in deficient medium. NBD-PE (green) was used in fluorescence images as membrane staining control. NBD-PE/mCherry-lysenin intensity ratios are given for each case. Mean value ± S.D. (n = 20).

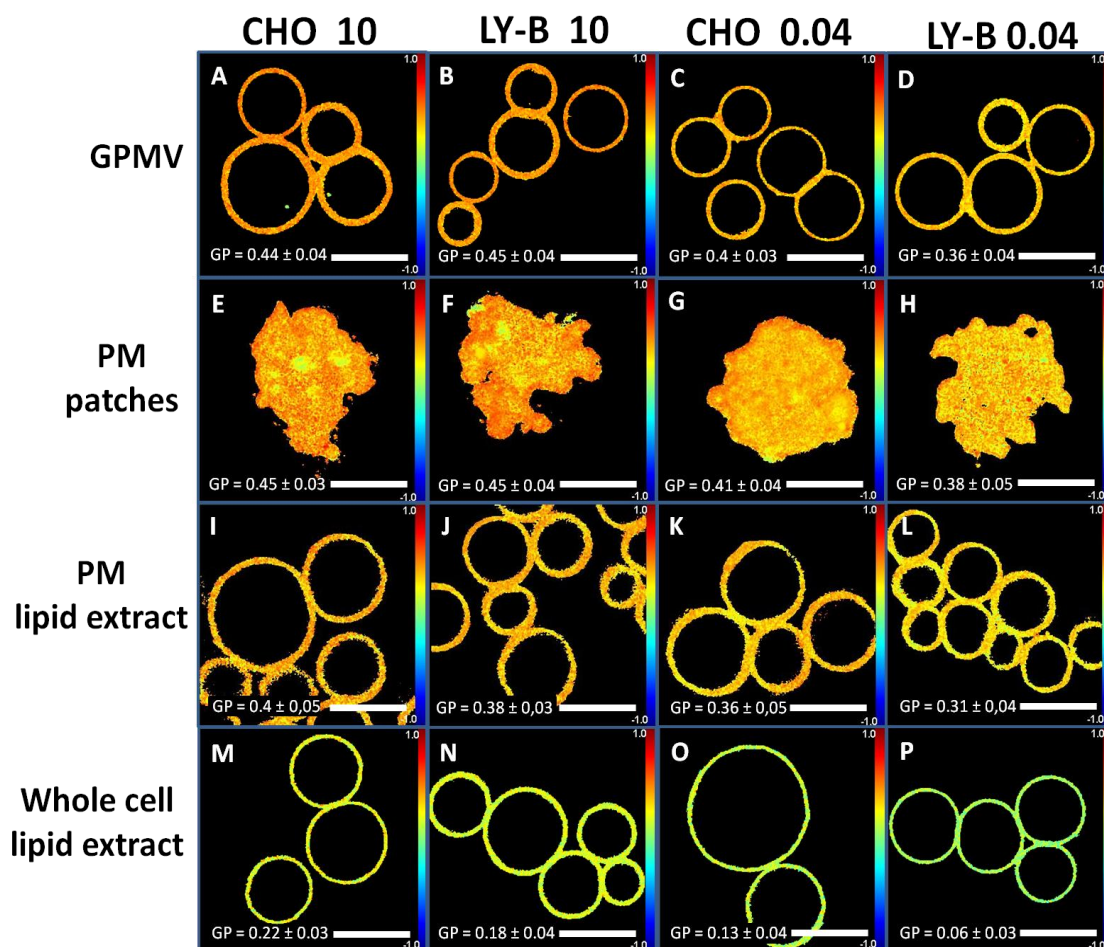


Figure 4.S4. Two-photon microscopy images of samples stained with laurdan and the corresponding GP measurements. A-D GPMV of: CHO cells grown in standard medium (**A**), LY-B cells grown in standard medium (**B**), CHO cells grown in deficient medium (**C**) and LY-B cells grown in deficient medium (**D**). Bar = 10 μ m. **E-H** PM patches of: CHO cells grown in standard medium (**E**), LY-B cells grown in standard medium (**F**), CHO cells grown in deficient medium (**G**) and LY-B cells grown in deficient medium (**H**). Bar = 30 μ m. **I-L** GUV formed from PM lipid extract of: CHO cells grown in standard medium (**I**), LY-B cells grown in standard medium (**J**), CHO cells grown in deficient medium (**K**) and LY-B cells grown in deficient medium. Bar = 10 μ m. **M-P**. GUV formed from whole cell lipid extracts of: CHO cells grown in standard medium (**M**), LY-B cells grown in standard medium (**N**), CHO cells grown in deficient medium (**O**) and LY-B cells grown in deficient medium (**P**). Bar = 10 μ m. GP values are given as averages \pm S.D. (n = 3).

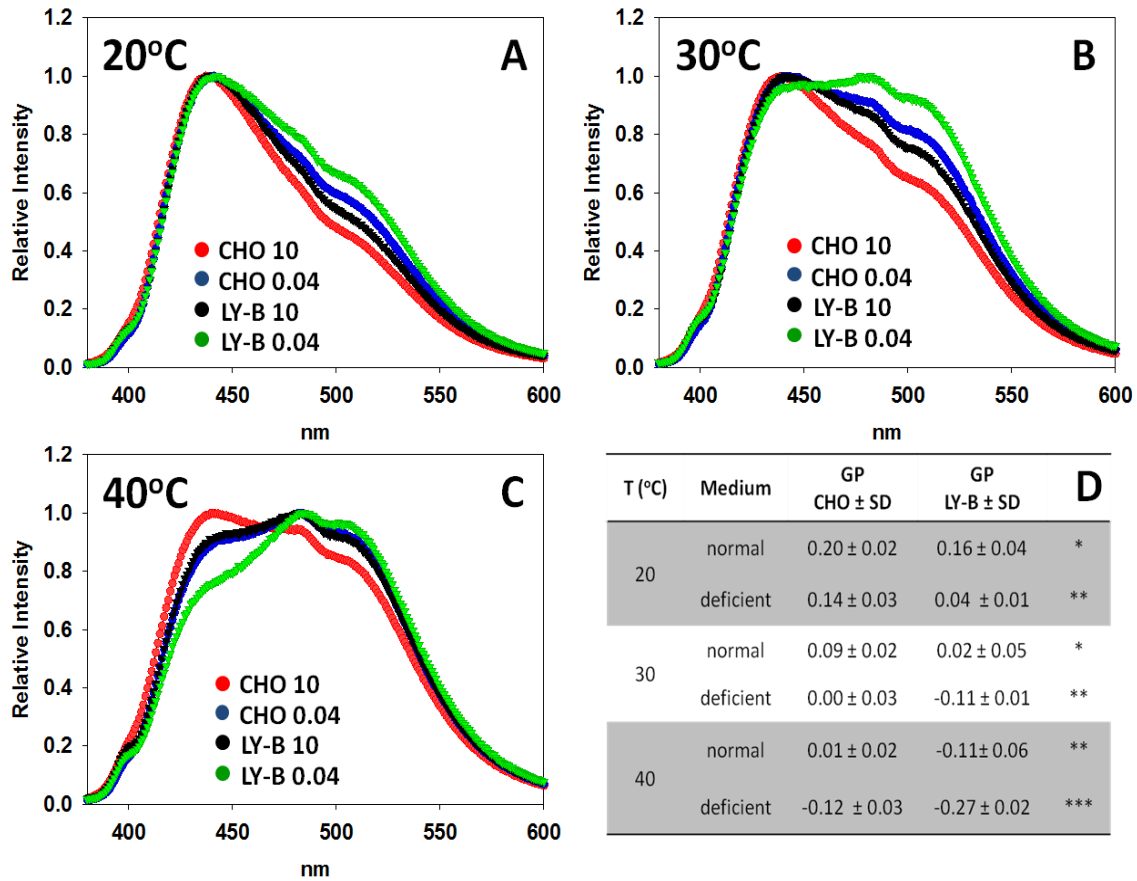


Figure 4.S5. Laurdan emission spectra of SUV formed from whole cell lipid extracts. Spectra at 20°C (A), 30°C (B) and 40°C (C). GP values (table) (D). Red spectra: SUV formed from CHO (10% FBS) lipid extracts. Blue spectra: SUV formed from CHO (0.04% FBS) lipid extracts. Black spectra: SUV formed from LY-B (10% FBS) lipid extract. Green spectra: SUV formed from LY-B (0.04% FBS) lipid extract. Values in the table are averages ± S.D. (n = 3). Statistical significance was calculated with Student's t-test: (*) p<0.05; (**) p<0.01; (***) p<0.001.

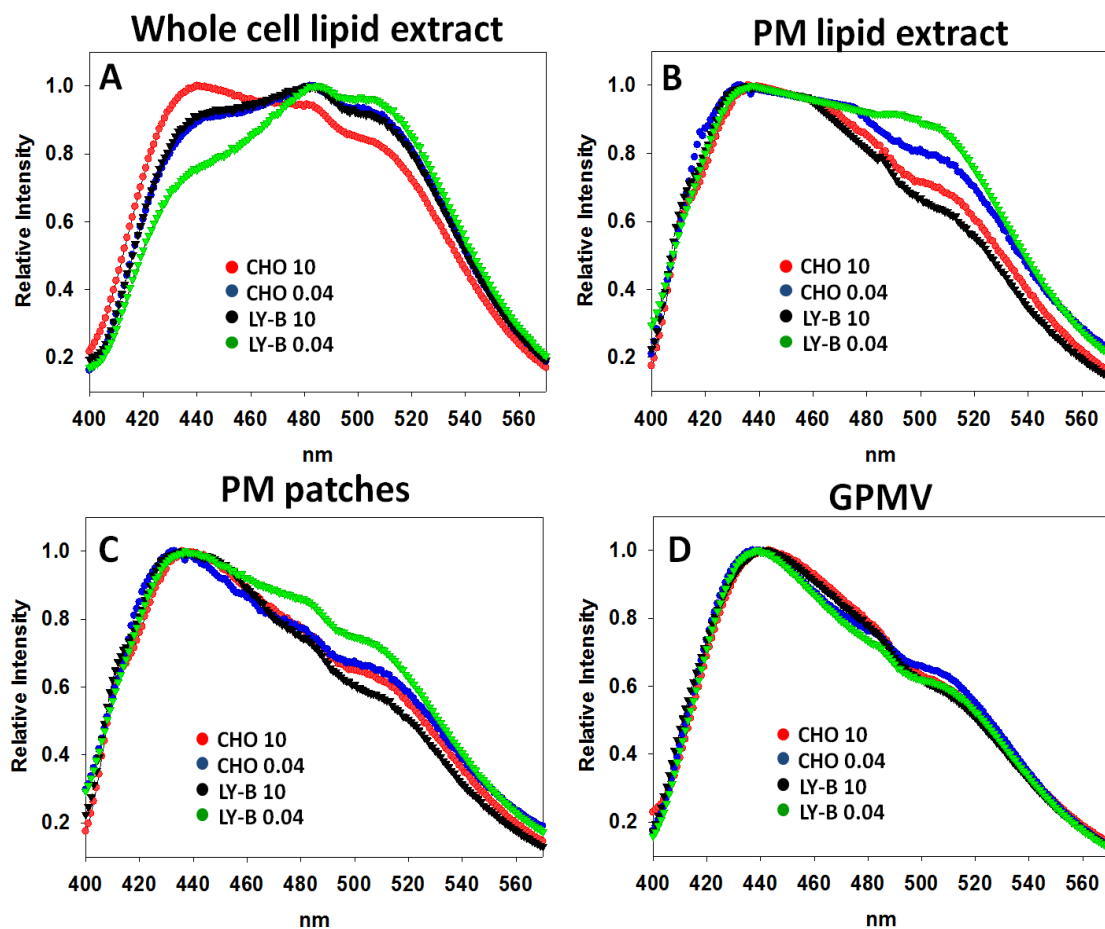


Figure 4.S6. Laurdan emission spectra at 40°C. LUV formed from: whole cell lipid extract (A), PM lipid extract (B), PM patches (C) and GPMV (D). Red spectra: SUV formed from CHO (10% FBS) lipid extracts. Blue spectra: SUV formed from CHO (0.04% FBS) lipid extracts. Black spectra: SUV formed from LY-B (10% FBS) lipid extract. Green spectra: SUV formed from LY-B (0.04% FBS) lipid extract.

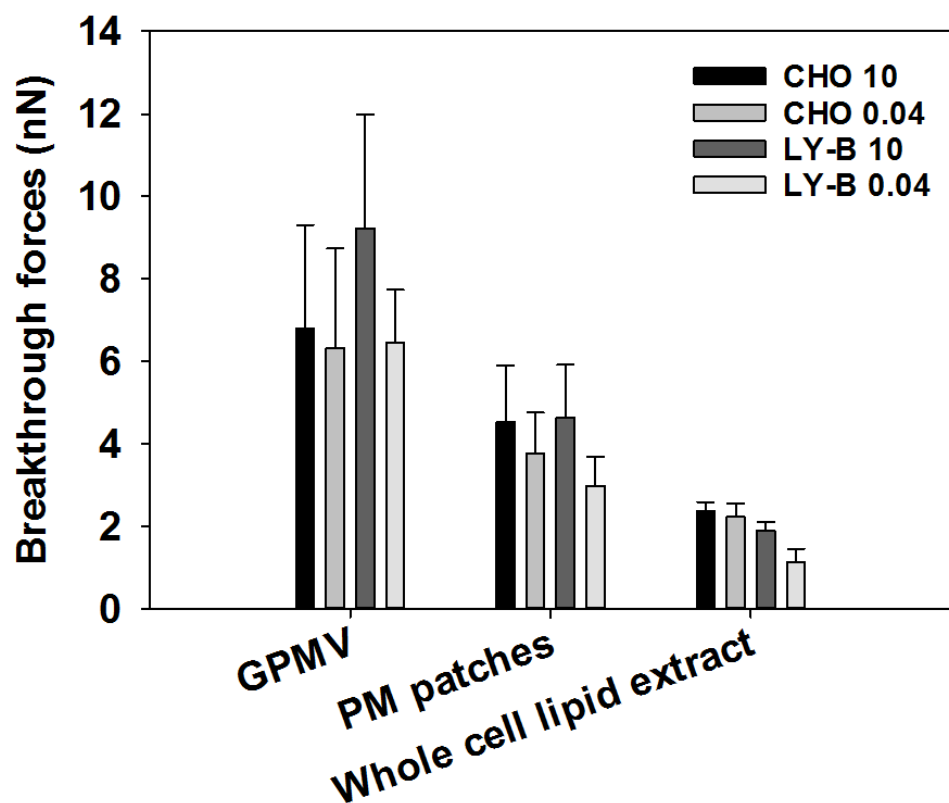


Figure 4.S7. Force spectroscopy: breakthrough values of GPMV, PM patches and whole cell lipid extracts of CHO and LY-B cells grown in normal and deficient medium. Mean values \pm S.D. (n = 3). Statistical significance was calculated with Student's t-test: (*) $p < 0.05$; (**) $p < 0.01$; (***) $p < 0.001$.

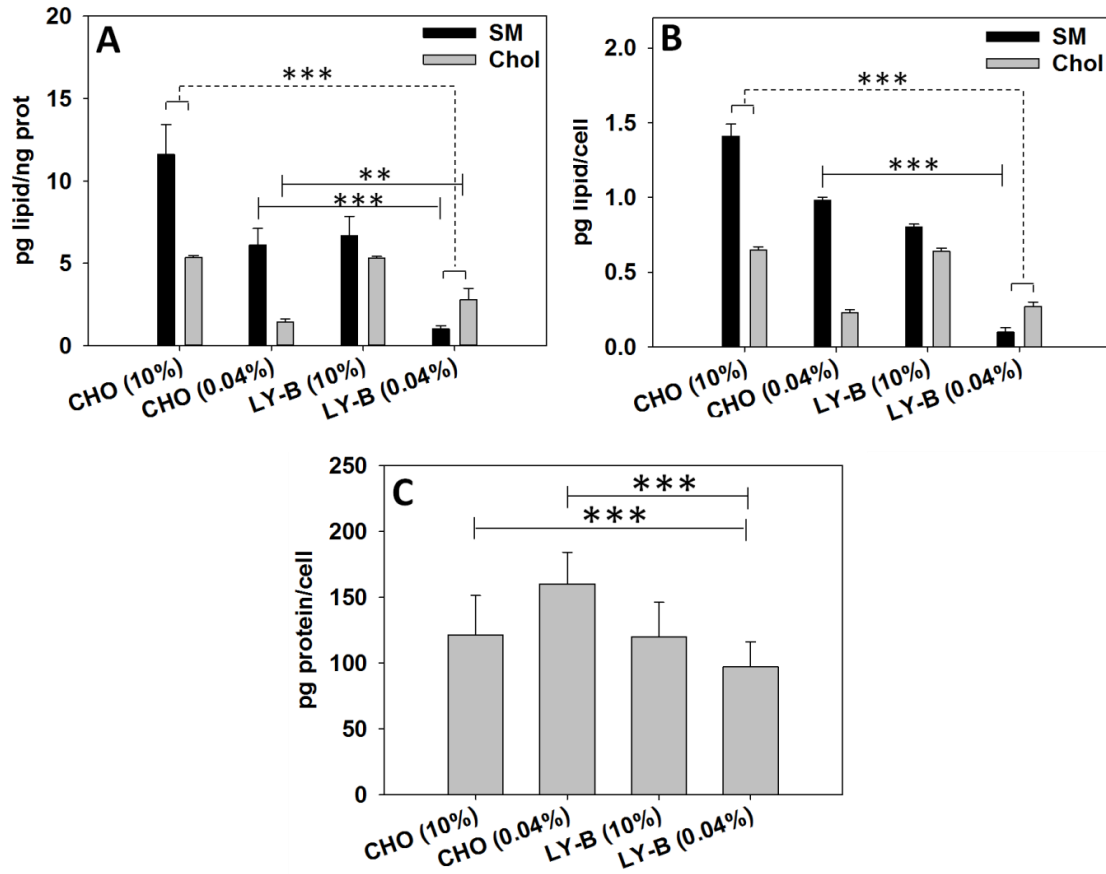


Figure 4.S8. SM and Chol contents per cell and per ng protein in the various preparations. SM and Chol pg/ng protein (A). SM and Chol pg/cell (B). pg protein/cell (C). Average values \pm S.D. ($n = 3$). Statistical significance was calculated with ANOVA and Student's t-test: (**) $p < 0.01$; (***) $p < 0.001$.

CHAPTER 5:

PLASMA MEMBRANE

EFFECTS OF SPHINGOLIPID-

SYNTHESIS INHIBITION BY

MYRIOCIN IN CHO CELLS: A

BIOPHYSICAL AND

LIPIDOMIC STUDY

CHAPTER 5: PLASMA MEMBRANE EFFECTS OF SPHINGOLIPID-SYNTHESIS INHIBITION BY MYRIOCIN IN CHO CELLS: A BIOPHYSICAL AND LIPIDOMIC STUDY

5.1. Introduction

Sphingolipids (SL) are considered as fundamental structural components of biological membranes. They are involved in many important and different biological roles, such as cell proliferation, differentiation, apoptosis, and ageing, as well as embryogenesis (Iessi *et al.*, 2020). Most SL metabolic reactions are bidirectional, thus metabolites are interconvertible and it is often the specific species ratio what determines the cell fate (Spiegel & Milstien, 2003). In addition, SL metabolic effects vary depending on the cell type, subcellular compartment, cell cycle phase, or extracellular stimulus (Tomassini & Testi, 2002; Luberto *et al.*, 2002b). An example of the complex effects of SL metabolites is given by sphingosine-1-phosphate and ceramide (Cer), the former is a second messenger for cell survival and proliferation, while the latter can induce cell death (Kolesnick, 2002; Sharma *et al.*, 2004).

Many aspects of SL function in cells remain to be understood. One testable improve our understanding of SL roles consists of examining the effects of SL restriction in cells. Lowering SL concentrations in the growth medium has little effect by itself, since mammalian cells can usually synthesize their own SL. Thus, researchers in this field have focused their attention on the first, pacemaker enzyme in the SL synthetic pathway, serine palmitoyl transferase (SPT). This enzyme catalyzes the reaction between palmitoyl-CoA and L-serine to synthesize 3-dehydro-D-sphinganine (Pinto *et al.*, 1992). Combining SL restriction in the growth medium (usually lowering the concentration of fetal bovine serum, FBS) with annulling SPT activity could lead to a very severe dearth of SL in the cells. SPT activity could be removed following one of at least two strategies, either genetic mutation or chemical inhibition.

As an example of the former approach, using a genetic selection method in CHO (Hanada *et al.*, 1998), the Hanada lab isolated the defective LY-B cell line, which had a loss of function of SPT enzyme through a defective SPTLC1 subunit. The mutant cells maintained the ability to take up and metabolize exogenous sphingoid bases from the culture medium (Hanada *et al.*, 1998). LY-B cells have been used in multiple studies exploring the effects of SL, and of their interaction with glycerophospholipid metabolism (Bejaoui *et al.*, 2002b; Mise *et al.*, 2005; Han *et al.*, 2009; Nakamura *et al.*, 2015). Mutant LY-B and wild type CHO cells could be comparatively studied to determine the effect of SL depletion on the biophysical properties of cell membranes. In our previous study (Monasterio *et al.*, 2020b) a significant decrease in the rigidity of LY-B cell membranes was observed using laurdan fluorescence, as well as a decrease in membrane breakthrough forces (membrane nanomechanical resistance) assessed by atomic force microscopy (AFM) (Monasterio *et al.*, 2020b). Concomitantly, SL concentration in membranes was drastically reduced, with partially compensating changes in glycerophospholipids (Monasterio *et al.*, 2020b).

An alternative strategy to detect the effects of an overall SL decrease would be the specific inhibition of the SPT enzyme. Among the non-natural selective inhibitors of this enzyme are β -chloroalanine (Gupta & Tiwary, 2002) and L-cycloserine (Hinkovska-Galcheva *et al.*, 2003). In addition, SPT can be inhibited with natural products such as stereoisomers of the antifungal sphingofungin B (Zweerink *et al.*, 1992) and the antifungal antibiotic myriocin (Chalfant *et al.*, 2001; Solomon *et al.*, 2003; Li *et al.*, 2014), isolated from *Myriococcum albomyces* (Kluepfel *et al.*, 1972). The antifungal myriocin has been applied to a variety of studies. In Jurkat acute leukemia cells, myriocin blocks the ceramide de novo synthesis (Gupta *et al.*, 2004). In particular it inhibits formation of long-chain Cer species which stimulate proteasomal activation with subsequent activation of caspases (Kroesen *et al.*, 2003). Myriocin has also been used for identifying several SPT inhibition effects in membrane structure and functions. For example, the role of skin sphingosine in the permeation of levodopa (a hydrophilic drug) across rat skin (Gupta & Tiwary, 2002), the paradoxical effects on barrier permeability homeostasis (Holleran *et al.*, 1991) and the delays of mammalian epidermal barrier recovery after acute perturbation (Feingold, 1991) have been studied.

In the present study we explore the effects of myriocin-induced SPT inactivation in CHO cells. In particular, the consequences on cell growth, lipid composition, and membrane physical properties have been considered. A novel plasma membrane (PM) preparation ('PM patches') has been used (Bezrukov *et al.*, 2009; Monasterio *et al.*, 2020a). The study has been performed following the steps of the previous publication with genetically modified CHO cells (LY-B cells) (Monasterio *et al.*, 2020b), so that the respective results can be compared. The LY-B study design was such that the effects of FBS removal, namely loss of sphingolipids and loss of other components in the serum, could not be properly differentiated. Myriocin allows the specific inhibition of SPT even in the presence of a full complement of FBS. Conversely our study might unveil myriocin effects other than SPT inhibition.

5.2. Materials and Methods

5.2.1. Materials

Wild type CHO (ATCC, Manassas, Virginia, U.S.) and a serine-SPT deficient CHO cell line, known as LY-B (Hanada *et al.*, 1998) (RIKEN BioResource Research Center, Koyadai, Japan), were used. Cell culture products; DMEM:F12 (Dulbecco's Modified Eagle Medium: Nutrient Mixture F-12) FBS (Fetal Bovine Serum), penicillin, streptomycin, and GlutaMax supplement were purchased from Thermofisher (Waltham, MA). Organic solvents were from Thermofisher (Waltham, MA). All fluorophores; were purchased from Thermofisher (Waltham, MA). Salts for buffer preparation (KCl, NaCl, CaCl₂, HEPES), myriocin, L- α -phosphatidylcholine from chicken egg (PC), sphingomyelin from chicken egg (SM) and D-erythro-sphinganine (sphinganine) were purchased from Sigma-Aldrich (St. Louis, MO, U. S.). All other reagents (salts and organic solvents) were of analytical grade.

5.2.2. Cell growth

CHO and LY-B (Hanada *et al.*, 1998) were used in this study. Cells were grown on DMEM:F12 (Dulbecco's Modified Eagle Medium: Nutrient Mixture F-12) medium containing 10% FBS (Fetal Bovine Serum), 100 U/ml penicillin, 100 U/ml streptomycin, and 6 mM glutamine (GlutaMax supplemented) at 37°C and 5% CO₂ humidified atmosphere. All cell culture products were purchased from Thermofisher (Waltham, MA, US).

5.2.2.1. Myriocin treatment

CHO and LY-B cells were first seeded in DMEM:F12 medium containing 10% FBS, 100 U/ml penicillin and 100 U/ml streptomycin, and 6 mM glutamine (this medium will be referred as ‘standard medium’). After 24-h the standard medium was changed by DMEM:F12 medium containing either 10% or 0.04% FBS, 100 U/ml penicillin and 100 U/ml streptomycin and 6 mM Glutamine (the medium containing 0.04% FBS will be named ‘FBS-deficient’ or ‘SL-deficient medium’). Then myriocin (Sigma-Aldrich, St. Louis, MO, US) dissolved in DMSO was added to a final concentration of 2.5 μ M (Capasso *et al.*, 2017) and cells were cultured for 24, 48 or 72 h before any experiment was performed.

5.2.3. Growth rate and viability tests

5.2.3.1. Cell growth

2.65×10^5 cells were seeded in 25 cm² flasks in standard medium and grown for 24 h until 15 – 25% confluence. Then, the standard medium was discarded, cells were washed twice with PBS, and the appropriate medium (standard or deficient, with or without 2.5 μ M myriocin) was added. Cells were grown for 24, 48 or 72 h. Quantification was performed by cell counting with a hemocytometer (BioRad TC20 Automated Cell Counter, Hercules, CA).

5.2.3.2. Viability test

Flow cytometry experiment was performed to evaluate how the myriocin treatment affected cell viability (Galisteo-González *et al.*, 2020). Cells were stained with Annexin-V-FITC and propidium iodide as indicated in the manual of the annexin V-FITC detection kit (CalbioChem, Darmstadt, Germany) and fluorescence was measured using a FACS Calibur flow cytometer (Becton-Dickinson, Franklin Lakes, NJ) as in Ahyayauch *et al.* (2018). Annexin V-FITC fluorescence intensity was measured in fluorescence channel FL-1 with $\lambda_{\text{ex}} = 488$ nm and $\lambda_{\text{em}} = 530$ nm, while FL-3 was used for propidium iodide detection, with $\lambda_{\text{ex}} = 532$ nm and $\lambda_{\text{em}} = 561$ nm. All measurements were performed in triplicate. Data analysis was performed using Flowing Software 2.

5.2.4. Sample preparation

Intact cells (whole cells) and PM patches have been used. Intact cells were grown as explained above. PM patches were isolated by a modification (Monasterio *et al.*, 2020a) of the protocol described by Bezrukov *et al.* (2009). In summary, cells were seeded at approximately 50% confluence and incubated for 2 h so that they adhered to the support. After incubation, two washing steps were performed using cold TBS (Tris Buffer Saline: 150 mM NaCl, 25 mM Tris-HCl, 2 mM KCl) to discard non-attached cells. Then, cold distilled water was added for 2 min to induce cell swelling. Mechanical cell disruption was achieved using a pressure stream from a 20-ml syringe coupled to a 19X1-1/2(TW)A needle. In the process, intracellular content was released, while PM stayed attached to the support. Several washing steps were performed to discard the released intracellular content. Purification quality was checked using Di-4-ANEPPDHQ ($\lambda_{\text{ex}} = 465 \text{ nm}$, $\lambda_{\text{em}} = 635 \text{ nm}$) as a general fluorescent staining, together with organelle-specific fluorophores as described in Monasterio *et al.* (2020a). Nuclei were stained using 2.8 μM Hoechst 33342 ($\lambda_{\text{ex}} = 361 \text{ nm}$, $\lambda_{\text{em}} = 497 \text{ nm}$) for 10 min at 37°C, Golgi apparatus was stained using 10 μM BODYPY FL C5-ceramide ($\lambda_{\text{ex}} = 500 \text{ nm}$, $\lambda_{\text{em}} = 510 \text{ nm}$) for 30 min at 37°C, and mitochondrial staining was performed with 0.75 μM Mitotracker Green ($\lambda_{\text{ex}} = 488 \text{ nm}$, $\lambda_{\text{em}} = 510 \text{ nm}$) for 30 min at 37°C. All fluorophores were purchased from Thermofisher (Waltham, MA). Images were taken with a Leica TCS SP5 II microscope (Leica Microsystems GmbH, Wetzlar, Germany) at room temperature with ImageJ software. The fluorescence intensities of the various markers were comparatively measured in PM patches and intact cells, so that specific organelle contamination could be estimated.

5.2.5. SM quantification with lysenin

5.2.5.1. Lysin-mCherry expression and purification

The non-toxic monomeric C-terminal domain of the SM-specific toxin, non-toxic- (NT) lysenin, was expressed and purified as described by Carquin *et al.* (2014). Briefly, the expression plasmid pET28/lysenin encoded NT-lysenin as a fusion protein with an N-terminal 6xHis-tag followed by the monomeric red fluorescent protein mCherry. The plasmid was expanded in *Escherichia coli* BL21 (DE3) and the recombinant protein was expressed in lysogeny broth (LB) medium at 16°C for 72 h in

the presence of 0.4 mM isopropyl β -D-thiogalactoside. Bacterial extracts were prepared as described (Maliekal *et al.*, 2006) and the recombinant protein was purified using an Ni-NTA Superflow cartridge (Qiagen, Hilden, Germany) and eluted with imidazol (Veiga-da-cunha *et al.*, 2012). Fraction analysis by SDS-PAGE revealed recombinant NT-lysenin with the expected size (45 kDa). The most enriched fractions were pooled, concentrated, and desalted. The aliquots were stored in 20 mM NaCl and 25 mM Hepes pH 7.2 and 5% glycerol at -80°C . Protein concentration was calculated by measuring absorbance at 280 nm.

5.2.5.2. SM staining and quantification with lysenin-mCherry

SM in whole cells and PM patches was stained with lysenin-mCherry and samples were visualized using a confocal microscopy Nikon D-ECLIPSE C1 (Nikon, Melville, NY). Samples were stained with lysenin-mCherry at 100 μM prior to visualization. PM patches, but not whole cells, were first stained with 100 μM NBD-PE as a control for all-lipid staining. A washing step was performed with PBS, and lysenin-mCherry was added at 100 μM final concentration. Whole-cell mCherry signal was also quantified using a FL-3 FACS Calibur flow cytometer (Becton-Dickinson, Franklin Lakes, NJ) with $\lambda_{\text{ex}} = 532$ nm and $\lambda_{\text{em}} = 561$ nm.

5.2.6. Laurdan General Polarization (GP)

Laurdan is a fluorescence polarity probe whose emission undergoes a spectral shift due to the reorientation of water molecules in the glycerol backbone region of the membrane, and this shift can be correlated to the lipid phase (Krasnowska *et al.*, 1998). In the gel phase, when little water is present, laurdan maximum emission is around 440 nm, whereas in the liquid crystalline phase the spectrum is red shifted to around 490 nm. Intact cells and PM patches have been used to compare the laurdan fluorescence of myriocin treated or non-treated CHO and LY-B cells. Samples were stained with 5 μM laurdan (Molecular Probes, Eugene, OR) for 5 min and two PBS washing steps were performed prior to cell visualization.

5.2.6.1. Image acquisition and analysis

Images were acquired and analysed as described in Monasterio *et al.* (2020b). In summary, a Leica TCS SP5 II microscope (Leica Microsystems GmbH, Wetzlar,

Germany) with a 63x water-immersion objective (numerical aperture NA = 1.2) was used and samples were imaged at 512 x 512 pixel and 400 Hz per scanning line. Equatorial planes were imaged to avoid photoselection effects. A pulsed titanium-sapphire (Mai-Tai Deepsee, Spectra-Physics) laser tuned at 780 nm was used for two-photon imaging of laurdan-labeled samples. Fluorescence emission was collected by non-descanned (NDD) hybrid detectors, as they offer higher sensitivity compared to descanned photomultipliers. The blue edge of the emission spectrum was collected by NDD 1 at 435 ± 20 nm and the red edge by NDD 2 at 500 ± 10 nm. Irradiance at the sample plane was $\approx 500 \text{ GW}\cdot\text{cm}^{-2}$ for two-photon excitation (Parasassi & Gratton, 1997). Three independent experiments were performed, taking 50 PM patches images in each time.

GP value of samples was calculated using a MATLAB (MathWorks, Natick, MA) based software. Images were smooth in each channel with 2 pixel averaging, and the GP value was calculated using the following equation (Carravilla *et al.*, 2015):

$$\text{GP} = \frac{I_B - G \cdot I_R}{I_B + G \cdot I_R}$$

where I_B is the intensity collected by NDD 1, I_R is the intensity collected by NDD 2, and G is the correction factor. The G factor is calculated measuring the GP value of the same fluorophore concentration used in sample staining, dissolved in this case in pure DMSO (Owen *et al.*, 2012). The region of interest, i.e. the PM, was selected.

5.2.7. Atomic Force Microscopy

Topographic images and force spectroscopy analysis of PM patches were performed. PM patches were prepared as previously described (Bezrukov *et al.*, 2009; Monasterio *et al.*, 2020a), using this time polylysine-coated mica slips instead of glass-bottom dishes. PM patches were first stained using Di-4-ANEPPQHD to allow detection on the mica slip.

Samples were measured as described in Monasterio *et al.* (2020b). In summary, contact mode AFM imaging has been used to study bilayer topography, looking at possible lateral segregation effects through bilayer thickness analysis. A NanoWizard II AFM (JPK Instruments, Berlin, Germany) was used to perform topographic

measurements under contact mode scanning (constant vertical deflection). For measurements, the AFM was coupled to a Leica microscope and mounted onto a Halcyonics Micro 40 antivibration table (Halcyonics, Inc., Menlo Park, CA) and inside an acoustic enclosure (JPK Instruments, Berlin, Germany) (Monasterio *et al.*, 2017). V-shaped MLCT Si₃N₄ cantilevers (Bruker, Billerica, MA) with nominal spring constants of 0.1 or 0.5 N/m. The sample thickness was estimated by cross-section height analysis (García-Arribas *et al.*, 2015).

For Force Spectroscopy, V-shaped MLCT Si₃N₄ cantilevers (Bruker, Billerica, MA) with nominal spring constants of 0.1 or 0.5 N/m were individually calibrated in a lipid-free mica substrate in assay buffer using the thermal noise method. After proper bilayer area localization by means of AFM topography and direct epifluorescence microscopy, force spectroscopy was performed at a speed of 1 μm/s. Force steps were determined for each of the indentation curves as reproducible jumps within the extended traces. At least three independent sample preparations were scanned for each case and 50-100 curves were measured in each sample.

5.2.8. Mass spectroscopic analysis

Mass spectroscopic analysis was performed essentially as described in Monasterio *et al.* (2020a). A methodological summary follows.

5.2.8.1. Sample treatment.

Lipid extraction was performed using a modified methyl *tert*-butyl ether (MTBE) protocol (Guri *et al.*, 2017a). Briefly, cells or PM patches were washed with cold PBS and scraped off in 500 μl cold PBS on ice. The suspensions were transferred to a 2 ml tube and spun down at 3200 rpm for 5 min at 4°C. After removing the PBS, samples were stored at -20°C or directly used for further extraction. Then, 360 μl methanol was added and vortexed. A mixture of lipid standards (Table 5.1) was added and samples were vortexed for 10 min at 4°C using a Cell Disruptor Genie (Scientific Industries, Inc., Bohemia, NY). MTBE (1.2 ml) was then added and the samples were incubated for 1 h at room temperature with shaking (750 rpm). Phase separation was induced by adding 200 μl H₂O. After 10 min incubation at room temperature, the samples were centrifuged at 1,000 xg for 10 min. The upper (organic) phase was transferred to a 13-mm screw-cap glass tube and the lower phase was extracted with 400

μl artificial upper phase [MTBE/methanol/water (10:3:1.5, v/v/v)]. The two upper phases were combined and the total lipid extract was divided in 3 equal aliquots (one for phospholipids (TL), one for sterols (S) in 2-ml amber vials, and one for SL detection in a 13-mm glass tube) and dried in a Centrivap at 50°C or under a nitrogen flow. The SL aliquot was deacylated by methylamine treatment (Clarke method) to remove glycerophospholipids. 0.5 ml monomethylamine reagent [MeOH/H₂O/n-butanol/methylamine solution (4:3:1:5 v/v)] was added to the dried lipid, followed by sonication (5 min). Samples were then mixed and incubated for 1 h at 53°C and dried (as above). The monomethylamine-treated lipids were desalted by n-butanol extraction. 300 μl H₂O-saturated n-butanol was added to the dried lipids. The sample was vortexed, sonicated for 5 min and 150 μl MS-grade water was added. The mixture was vortexed thoroughly and centrifuged at 3200 $\times g$ for 10 min. The upper phase was transferred to a 2-ml amber vial. The lower phase was extracted twice more with 300 μl H₂O-saturated n-butanol and the upper phases were combined and dried (as above).

5.2.8.2. Glycerophospholipid and sphingolipid detection on a Triple Quadrupole Mass Spectrometer.

TL and SL aliquots were resuspended in 250 μl chloroform/methanol (1:1 v/v) (LC-MS/HPLC grade) and sonicated for 5 min. The samples were pipetted in a 96-well plate (final volume = 100 μl). The TL were diluted 1:4 in negative-mode solvent (chloroform/methanol (1:2) + 5 mM ammonium acetate) and 1:10 in positive-mode solvent (chloroform/methanol/water (2:7:1 v/v) + 5 mM ammonium acetate). The SL were diluted 1:10 in positive-mode solvent and infused onto the mass spectrometer. Tandem mass spectrometry for the identification and quantification of SL molecular species was performed using Multiple Reaction Monitoring (MRM) with a TSQ Vantage Triple Stage Quadrupole Mass Spectrometer (ThermoFisher Scientific, Waltham, MA) equipped with a robotic nanoflow ion source, Nanomate HD (Advion Biosciences, Ithaca, NY). The collision energy was optimized for each lipid class. The detection conditions for each lipid class are listed below (table 5.1). Cer species were also quantified with a loss of water in the first quadrupole. Each biological replica was read in 2 technical replicas (TR). Each TR comprised 3 measurements for each transition. Lipid concentrations were calculated relative to the relevant internal standards and then normalized to the total lipid content of each lipid extract (mol %).

5.2.8.3. Gas chromatography–mass spectrometry for cholesterol assay

Lipid extracts were analyzed by GC-MS as described previously (Guan *et al.*, 2010). Briefly, samples were injected into a VARIAN CP-3800 gas chromatograph equipped with a FactorFour Capillary Column VF-5ms 15 m × 0.32 mm i.d. DF = 0.10, and analyzed in a Varian 320 MS triple quadrupole with electron energy set to –70 eV at 250°C. Samples were applied to the column oven at 45°C, held for 4 min, then raised to 195°C (20°C/min). Sterols were eluted with a linear gradient from 195°C to 230°C (4°C/min), followed by rising to 320°C (10°C/min). Cholesterol was identified by its retention time (compared with an ergosterol standard) and fragmentation patterns, which were compared with the NIST library.

Table 5.1. MS detection conditions for the different lipid classes.

Lipid Class	Standard	Polarity	Mode	m/z ion	Collision Energy
Phosphatidylcholine [M+H] ⁺	DLPC	+	Product ion	184.07	30
Phosphatidylethanolamine [M+H] ⁺	PE31:1	+	Neutral ion loss	141.02	20
Phosphatidylinositol [M-H] ⁻	PI31:1	-	Product ion	241.01	44
Phosphatidylserine [M-H] ⁻	PS31:1	-	Neutral ion loss	87.03	23
Cardiolipin [M-2H] ²⁻	CL56:0	-	Product ion	acyl chain	32
Ceramide [M+H] ⁺	C17Cer	+	Product ion	264.34	25
Dihydroceramide [M+H] ⁺	C17Cer	+	Product ion	266.40	25
Hexosylceramide [M+H] ⁺	C8GC	+	Product ion	264.34	30
Hexosyldihydroceramide [M+H] ⁺	C8GC	+	Product ion	266.40	30
Sphingomyelin [M+H] ⁺	C12SM	+	Product ion	184.07	26

5.3. Results

5.3.1. Growth and viability

This Chapter is devoted to the effects of myriocin on SL synthesis and membrane properties in CHO or LY-B cells. Results are occasionally shown of cells grown in SL-deficient medium. The latter are only for comparative purposes, they have been shown in chapter 4. Cell count measurements were performed using a BioRad TC20 hemocytometer to assess the effect of myriocin treatment on CHO (wild type) and LY-B (SPT-defective) cell division rate and integrity. Figure 5.1A shows a comparison between myriocin-treated and non-treated cell growth rate in SL-deficient (containing 0.04% FBS) medium. Student's t-test revealed that there was a statistically significant

difference between myriocin-treated and non-treated CHO cell division ratio; myriocin treatment made CHO cell growth much slower (Fig. 5.1A). The LY-B cell division rate was equally low in the presence or absence of myriocin. In addition, there was no statistically significant difference between treated CHO cells and non-treated/treated LY-B cells grown in SL-deficient medium. Comparison between cell division ratios in standard and deficient medium is shown in figures 5.S1A and 5.S1B; myriocin treatment had no effect on the cell division rate when CHO or LY-B cells were grown in standard medium, but some inhibition took place in CHO cells grown on deficient medium (Figs. 5.S1A and 5.S1B).

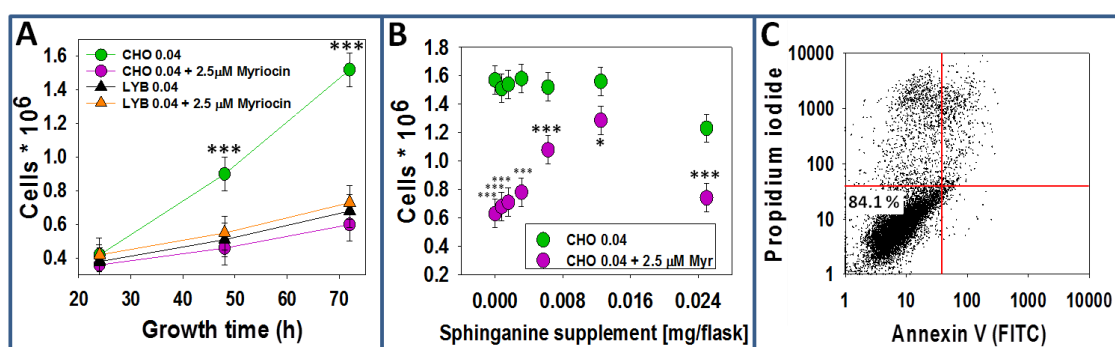


Figure 5.1. Myriocin-treated CHO and LY-B cell growth. (A) LY-B and CHO cell growth as a function of time in sphingolipid-deficient (0.04% FBS) medium, plus/minus 2.5 μM myriocin. Statistical symbols correspond to differences between green circles (CHO 0.04) and the other three samples. (B) Myriocin-treated and non-treated CHO cell growth after 72 h in sphingolipid-deficient medium supplemented with sphinganine (seeded cells: 0.25 * 10⁶). Values are given as average values ± S.D. (n = 3) (C) A representative FACS assessment of cell viability of CHO cells after 72 h in sphingolipid-deficient medium plus 2.5 μM myriocin. Three independent experiments were performed counting 10000 cells in each case. Significance: (*) p<0.05; (***) p<0.001.

To ascertain that the poor cell growth at low FBS concentrations was indeed due to the lack of SL, and not to the absence of other nutrients putatively present in FBS, it was tested whether myriocin-treated CHO cells were able to reach the full growth rates when the SL-deficient medium was supplemented with SL. For this purpose, equimolar mixtures of egg PC and SM or sphinganine were sonicated in DMEM:F12 medium and added to the culture flasks in various amounts. A good recovery was achieved with sphinganine (Figs. 5.1B and 5.S1E) or SM (Fig. 5.S1C) supplementation.

Figure 5.1B shows that myriocin-treated CHO cells grown on SL-deficient medium for 72 h reached ≈78% of the control growth when 0.0125 mg sphinganine was added per T25 culture flask (8 μM final concentration), while larger concentrations

appeared to have a toxic effect. In the case of SM, 0.1 mg/flask or higher (40 μ M or higher) supplementation made myriocin-treated CHO cells reach 75% of the control growth (Fig. 5.S1C), as seen in Monasterio *et al.* (2020b). It was concluded that myriocin-mediated lack of SPT activity could be masked when appropriate SL supplementation was added in the deficient-medium. The toxic effect of sphinganine might be due its membrane-permeabilizing effects (Contreras *et al.*, 2006), that is not observed with SM.

Cell viability was tested performing flow-citometry analysis of cells stained with Annexin-V-FITC and propidium iodide (Fig. 5.1C). Flow-citometry analyses demonstrated that 84% of CHO cells grown in SL-deficient medium for 72 h and treated with 2.5 μ M myriocin remained viable (Fig. 5.1C), similar to the 86% value obtained with non-treated LY-B cells grown in SL-deficient medium (Monasterio *et al.*, 2020b).

5.3.2. Lysenin-staining

Cells were stained with SM-specific NT-lysenin-mCherry and visualized with confocal microscopy (Fig. 5.2). Non-myriocin treated CHO cells grown in standard (Fig. 5.2A) or SL-deficient medium (Fig. 5.2C), as well as treated CHO cells grown in standard medium (Fig. 5.2B), appeared thoroughly stained with mCherry. However, only little dots of mCherry were seen in myriocin-treated CHO cells grown in SL-deficient medium (Fig. 5.1D), indicating a remarkable SM decrease in this sample. In LY-B cells (Figs. 5.2E-H), the lysenin signal decrease observed in figure 5.2G and 2H was most probably due to their mutated SPT enzyme (Monasterio *et al.*, 2020b) and not because of the myriocin treatment, as differences are not seen between non-treated (Fig. 5.2G) and treated (Fig. 5.2H) LY-B cells grown in deficient medium.

For lysenin-mCherry quantification, flow-citometry was performed (Fig. 5.3). In the first 24 h, CHO cells grown in a deficient medium and treated with 2.5 μ M myriocin, underwent a two-fold lysenin signal decrease as compared with the CHO cells grown in a standard medium (Fig. 5.3A). On the contrary, there was no statistically significant difference between CHO cells grown in standard medium and non-treated CHO cells grown in deficient medium (Fig. 5.3A) as seen in Monasterio *et al.* (2020b). 72 h were needed to achieve a total SM depletion in myriocin-treated CHO cells grown in deficient medium (Fig. 5.3B). In the case of LY-B cells, myriocin

treatment did not affect the mCherry-lysenin values (Figs. 5.3C and 5.3D), as there was no statistically significant difference between treated and non-treated LY-B cells grown in deficient medium, neither after 24 h (Fig. 5.3C), nor after 72 h (Fig. 5.3D).

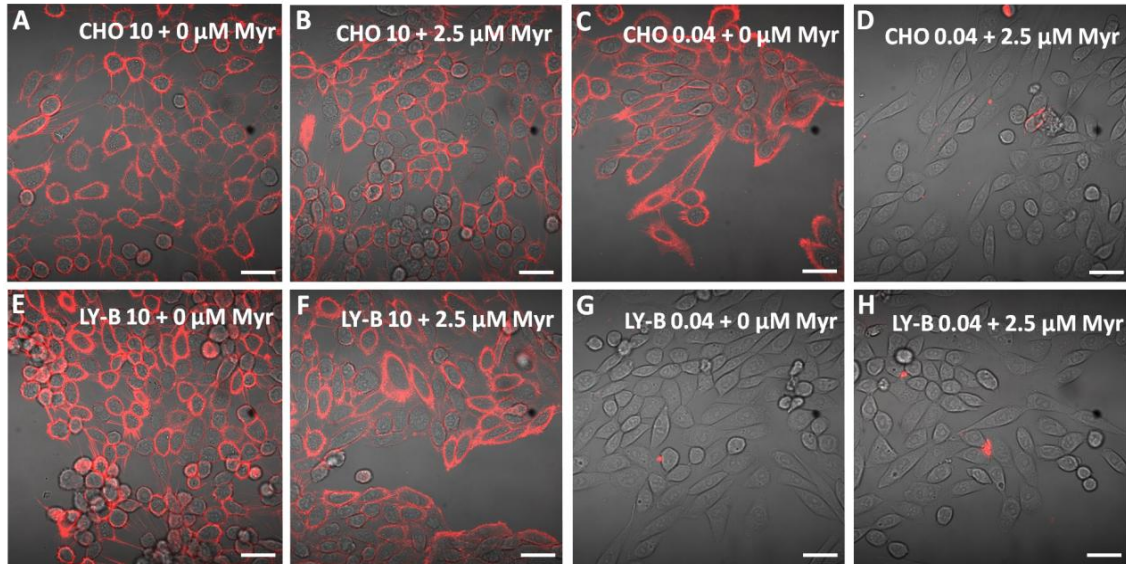


Figure 5.2. mCherry-Lysenin-stained myriocin-treated or non-treated cells after 72 h growth. Non-treated (A) and myriocin-treated (B) CHO cells in standard medium. Non-treated (C) and myriocin-treated (D) CHO cells in deficient medium. Non-treated (E) and myriocin-treated (F) LY-B cells in standard medium. Non-treated (G) and myriocin-treated (H) LY-B cells in deficient medium. Bar = 75 μ m.

For an easier comparison between genetically mutated LY-B and myriocin-treated CHO cells, figure 5.3E shows a comparative table of CHO/LYB signal ratios. The most significant conclusion is that after 24 h myriocin treatment, CHO cells had twice the signal intensity of LY-B, and that this difference was suppressed after 72 h. No statistically significant difference was found between LY-B and myriocin-treated CHO cells at this stage. Results indicate that a faster SM depletion was obtained in mutated, SPT-defective LY-B than in myriocin-treated CHO cells.

In parallel, PM patches of myriocin-treated and non-treated CHO cells were also visualized with lysenin-mCherry. PM patches of CHO cells treated with 2.5 μ M myriocin and grown in deficient medium for 72 h (Fig. 5.S2B) exhibited little lysenin-mCherry signal dots (indicated with white arrows), while the non-treated CHO cell PM patches grown in the same medium were extensively stained (Fig. 5.S2A).

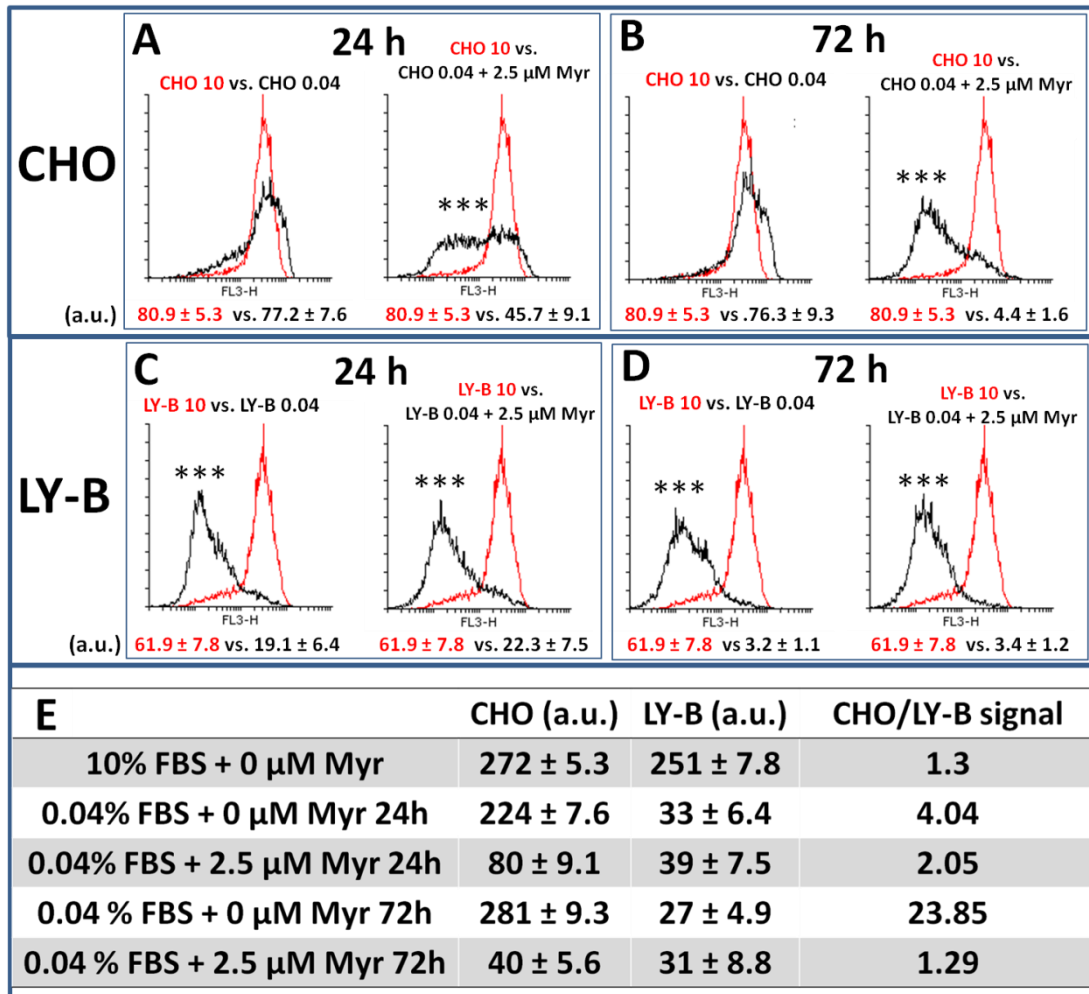


Figure 5.3. FACS-mediated, quantification of cell staining with SM specific mCherry-lysenin as a function of time. CHO cells grown in standard medium vs. myriocin-treated or non-treated CHO cells grown in deficient medium for 24 h (A) or 72 h (B). LY-B cells grown in standard medium vs. treated or non-treated LY-B cells grown in deficient medium for 24 h (C) or 72 h (D). Total CHO and LY-B lysenin-mCherry signals and CHO/LY-B lysenin-mCherry signal ratios (E). Histograms in red correspond to control cells (CHO or LY-B grown in standard-medium); histograms in black correspond to the samples of interest, as indicated in each case. Geometric mean ± S.D. (n = 3). Representative histograms are shown; three independent experiments were performed counting 10000 cells in each case. Statistical significance was calculated with ANOVA or Student’s t-test, with similar results. Significance: (***) p<0.001.

In summary, both non-treated CHO and LY-B cell lines grew to a similar extent in standard medium (Fig. 5.1A). Myriocin was effective in reducing cell growth rates only for CHO cells grown under limiting SL conditions. When using SL-deficient medium, myriocin-treated CHO cells growth was similar to that of LY-B and lower than that of non-treated CHO cells (Fig. 5.1A). Control growth of myriocin-treated cells in SL-deficient medium was recovered when the culture broth was supplemented with a

proper SL (Fig. 5.1B). Lysenin fluorescence was largely decreased in myriocin-treated (but not in non-treated) CHO cells in the first 24 h of growth in deficient medium. Nevertheless, they contained higher SM amounts than non-treated LY-B cells (grown in deficient medium) and 72 h were needed to achieve a full lysenin-mCherry signal depletion comparable to the one observed in LY-B cells (Figs. 5.2, 5.3 and 5.S2).

5.3.3. Membrane lipid order decreases with sphingolipid restriction

Laurdan generalized polarization (GP) provides an estimation of membrane lipid molecular order (Krasnowska *et al.*, 1998). To evaluate how SPT activity suppression affected the rigidity/fluidity of cell membranes, laurdan GP experiments were performed. GP values of myriocin-treated and non-treated CHO cells PM patches were measured using two-photon microscopy.

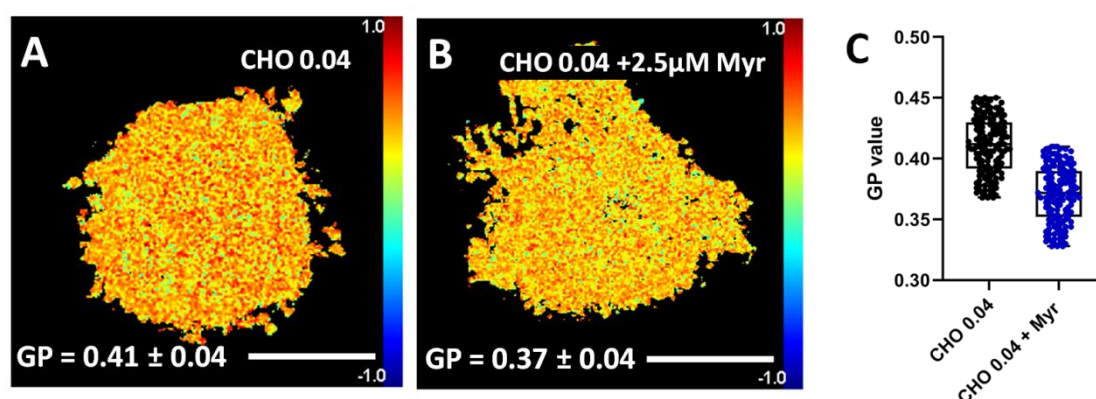


Figure 5.4: Two-photon microscopy images of PM patches stained with laurdan for GP measurements. PM patches of non-treated (A) and myriocin-treated (B) CHO cells grown in deficient medium. (C) Box plot graph of GP values of non-treated (black) and myriocin-treated (blue) CHO cell PM patches. GP are given as average values \pm S.D. Three independent experiments were performed; $n = 150$ (50 PM patches \times 3 replicates). Statistical significance was calculated with ANOVA or Student's t-test, with similar results: $p=0.03$. Bar = 30 μ m.

Figure 5.4A depicts a PM patch from a CHO cell grown in deficient medium and stained with laurdan. In the -1 to +1 color scale at the right hand of the picture, the red color and a value close to +1 indicated a more rigid/ordered region, while blue color and a value close to -1 indicated a more fluid region. The GP value of PM patches derived from CHO cells treated with 2.5 μ M myriocin and grown in deficient medium for 72 h (Fig. 5.4B) decreased on average from 0.41 to 0.37 compared with the non-treated CHO cells (Fig. 5.4A) grown in the same medium. Figure 4C shows a box plot graph of individual GP values of non-treated (black) and myriocin-treated (blue) CHO cell PM

patches. The Student's t test showed that a statistically significant difference existed between myriocin-treated and non-treated CHO-cell PM patches.

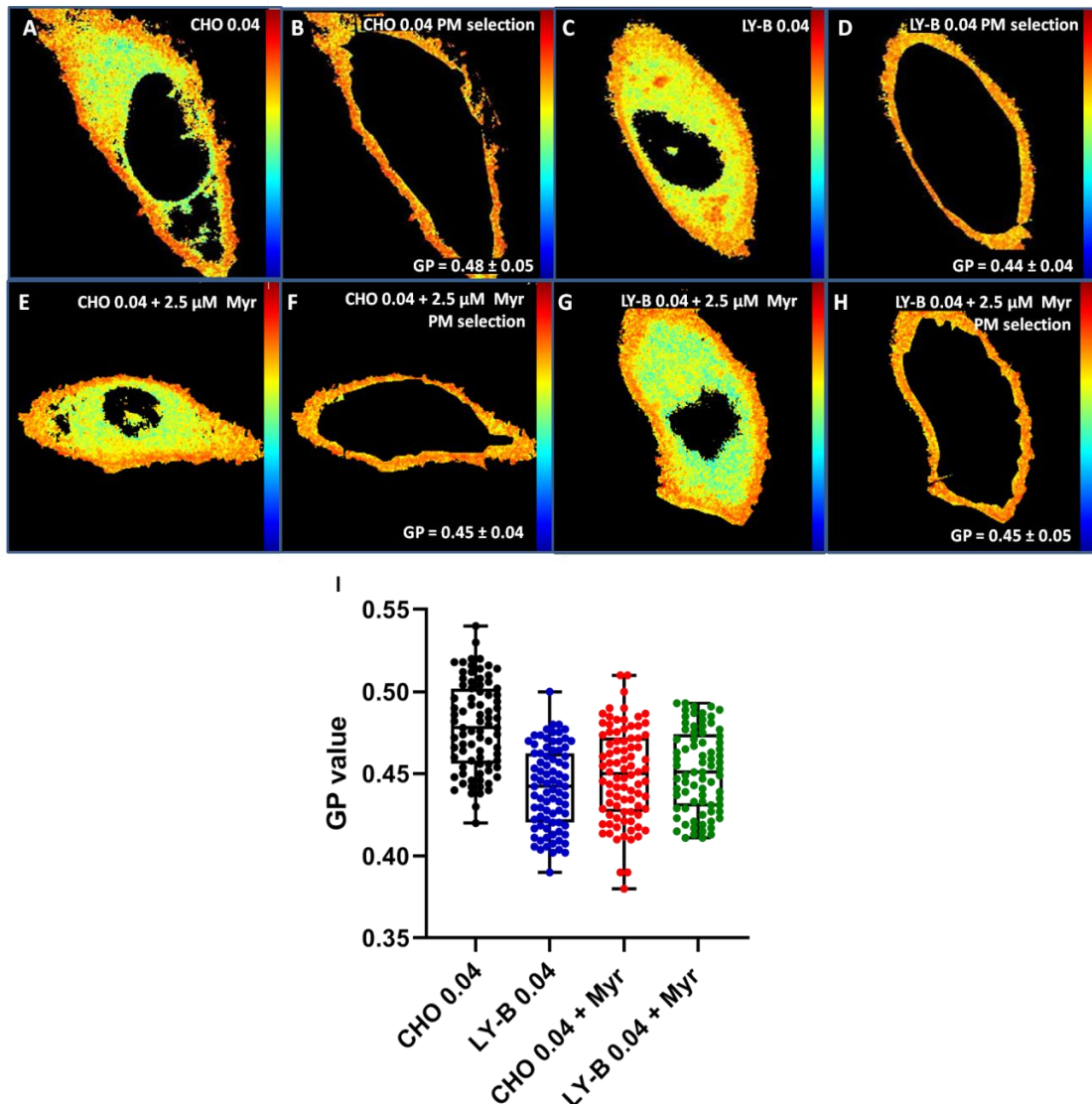


Figure 5.5. Laurdan staining and GP processing. A representative CHO cell grown in deficient medium (A), and the PM selection of the cell in panel A (B). A representative LY-B cell grown in deficient medium (C), and the PM selection of the cell in panel C (D). A representative 2.5 μM myriocin-treated CHO cell grown in deficient medium (E), and the PM selection of the cell in panel E (F). A representative 2.5 μM myriocin-treated LY-B cell grown in deficient medium (G), and the PM selection of the cell in panel E (H). Box plot graph of GP values of non-treated and myriocin-treated CHO (black and blue dots) and LY-B (red and green dots) PM selection values are given as average values ± S.D. Three independent experiments were performed; n = 75 (25 Pm selection x 3 replicates). Treated vs non-treated CHO cell p = 0.027. Statistical significance was calculated with ANOVA or Student's t-test.

In figure 5.5 whole cells stained with laurdan and the corresponding optically selected PM are shown. In whole cell images (Figs. 5.5A, 5.5C, 5.5E and 5.5G) two

different regions could be distinguished, the more ordered PM and the more disordered/fluid intracellular membranes. In a previous work we showed that the two GP values were around 0.5 for PM and 0.2 for intracellular membranes (Monasterio *et al.*, 2020a), indicating that the PM was less fluid than the intracellular membranes, perhaps due to its barrier role (Owen *et al.*, 2012).

PM pixels of treated and non-treated CHO and LY-B cells grown in SL-deficient medium for 72 h were measured for GP (Figs. 5.5B, 5.5D, 5.5F and 5.5H). The GP value of the PM region of myriocin-treated CHO cells decreased from 0.48 (Fig. 5.5B) down to 0.45 (Fig. 5.5F), while treated (Fig. 5.5H) and non-treated (Fig. 5.5D) LY-B cell PM GP value was constant at around 0.45. Figure 5I shows a box plot graph of GP values of non-treated and myriocin-treated CHO (black and blue dots) and LY-B (red and green dots) PM selection. Student's t test revealed that the difference between myriocin-treated CHO cells grown in SL-deficient medium was significantly lower. On the contrary, there was no statistically significant difference between treated and non-treated LY-B cell PM.

5.3.4. Breakthrough force of myriocin-treated CHO cells plasma membranes is decreased

Figure 5.6 shows the topology and breakthrough force distribution of PM patches derived from non-treated (Fig. 5.6A) and myriocin-treated (Fig. 5.6B) CHO cells grown in deficient medium for 72 h. According to topographic images, even if membrane components other than the bilayer, perhaps (glyco)proteins or protein aggregates, gave rise to protruding elements, a minimum thickness of 4-5 nm that corresponds to the thickness of a lipid bilayer was measured (Umagai *et al.*, 2006); no statistically significant difference in thickness was observed between treated and non-treated CHO cells.

The breakthrough force distributions showed a significant difference between the PM patches derived from non-treated (3.76 nN; Fig. 5.6A) and treated (2.77 nN; Fig. 5.6B) CHO cells grown in deficient medium. This result is similar to the one obtained in Monasterio *et al.* (2020b) when LY-B cell PM patches exhibited a large decrease, from 4.64 nN to 2.98 nN, when grown in normal or deficient medium (Monasterio *et al.*, 2020b).

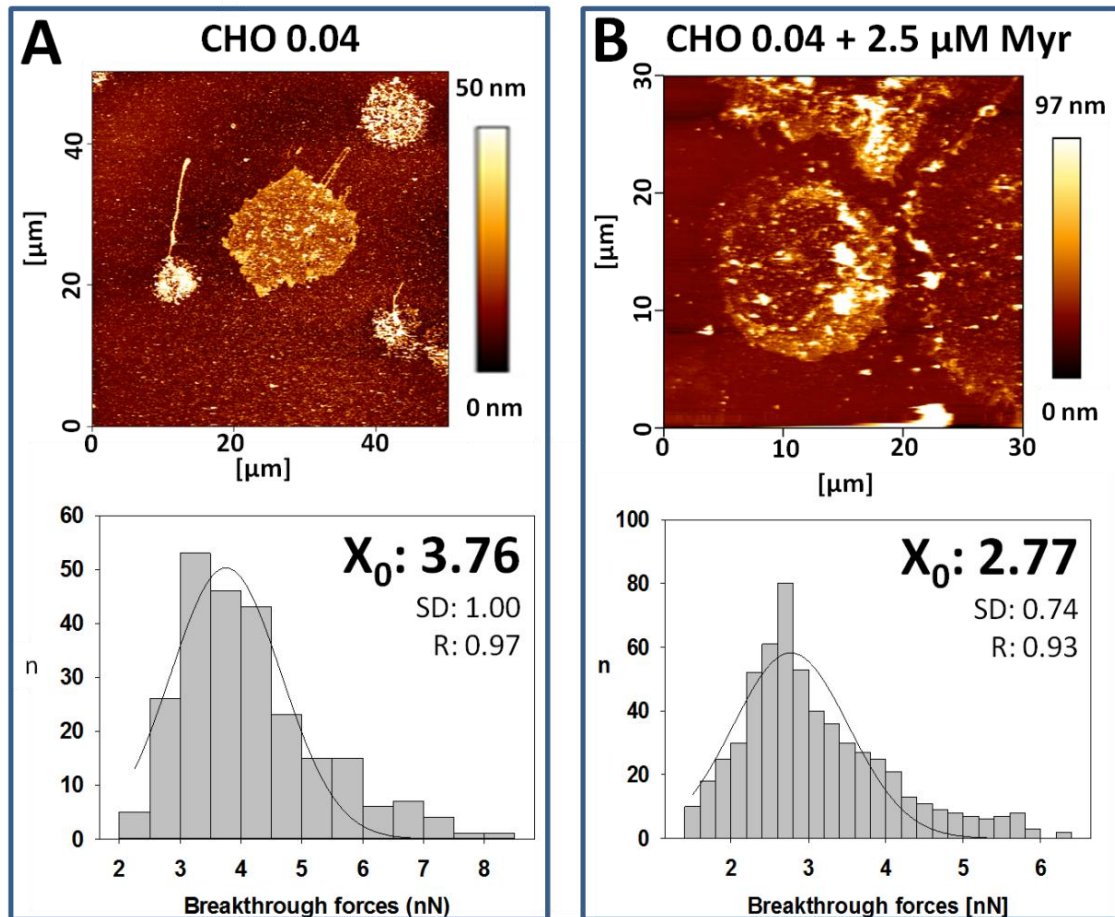


Figure 5.6. Topographic image and breakthrough force distributions of PM patches. PM patches from non-treated (A) and myriocin-treated (B) CHO cells grown in deficient medium. Three independent experiments were performed; $n = 150-170$ (50-60 breakthrough forces \times 3 replicates). Statistical significance was calculated with ANOVA or Student's t-test, with similar results: $p=0.0008$.

Breakthrough force measurements were in good agreement with laurdan GP values (Fig. 5.4). PM patches exhibited the expected behavior, the myriocin-treated CHO cells grown in deficient medium showing lower values in both parameters (Figs. 5.4 and 5.6) when compared with non-treated cells.

5.3.5. Lipidomic analysis of myriocin-treated vs. non-treated CHO cells

To understand the existing membrane order/disorder differences between myriocin-treated and non-treated CHO cells and their capacity of homeostatic regulation, a lipidomic study of PM patches (Fig. 5.7) and whole cells (Fig. 5.S3) was performed. A comprehensive description of the various lipid compositions can be seen

in the supplementary material table 5.S1. The data are given in mole% of the lipid extract.

5.3.5.1. Plasma membrane patches.

Some specific lipidomic results can be highlighted. Among the various SL classes, SM (by far the most abundant SL), Cer (an important SL in cell signaling) and HexCer (precursor of the complex glycosphingolipids) were selected (Figs. 5.7A-C). All three (SM, Fig. 5.7A; Cer, Fig. 5.7B and HexCer, Fig. 5.7C) significantly decreased in CHO cell PM patches (0.04% FBS) when treated with 2.5 μ M myriocin (73% decrease for SM, 37% for Cer, and 85% for HexCer). However, the corresponding SL values of LY-B patches remained unchanged, or even increased slightly (Figs. 5.7 A-C), perhaps because of their low values in non-treated cells: even if SM (Fig. 5.7A), Cer (Fig. 5.7B) and HexCer (Fig. 5.7C) amounts were largely decreased in myriocin-treated CHO cell PM patches, they were still twice (or larger) those of the non-treated LY-B cells (0.04% FBS). The latter observation is in agreement with the lysenin staining images in figures 5.2, 5.3 and 5.S2.

Glycerophospholipid (GPL) acyl chain saturation and length also play an important role in the physical properties of the membrane bilayer, specifically on its disorder/fluidity, unsaturated and shorter acyl-chain GPL increasing membrane fluidity (van Meer *et al.*, 2008). In figure 5.7D and 5.7E the distribution of GPL saturation degree is shown. While in myriocin-treated LY-B cells GPL saturation degree in PM patches remained unchanged, in myriocin-treated CHO cells the fraction of fully saturated GPL increased (Fig. 5.7D) and that of polyunsaturated GPL (2-6 double bounds) decreased (Fig. 5.7E). In addition, PM patches from non-treated LY-B cells grown in deficient medium had a similar GPL saturation distribution as those from treated CHO cells grown in the same medium (Fig. 5.7D and 5.7E).

Considering GPL chain-length distribution, when myriocin-treated CHO cells were grown in deficient medium, their 30-32 C acyl-chain GPL remained unchanged (Fig. 5.7F), while a slight but statistically significant increase in very long (42-44C) acyl-chain GPL was observed (Fig. 5.7H).

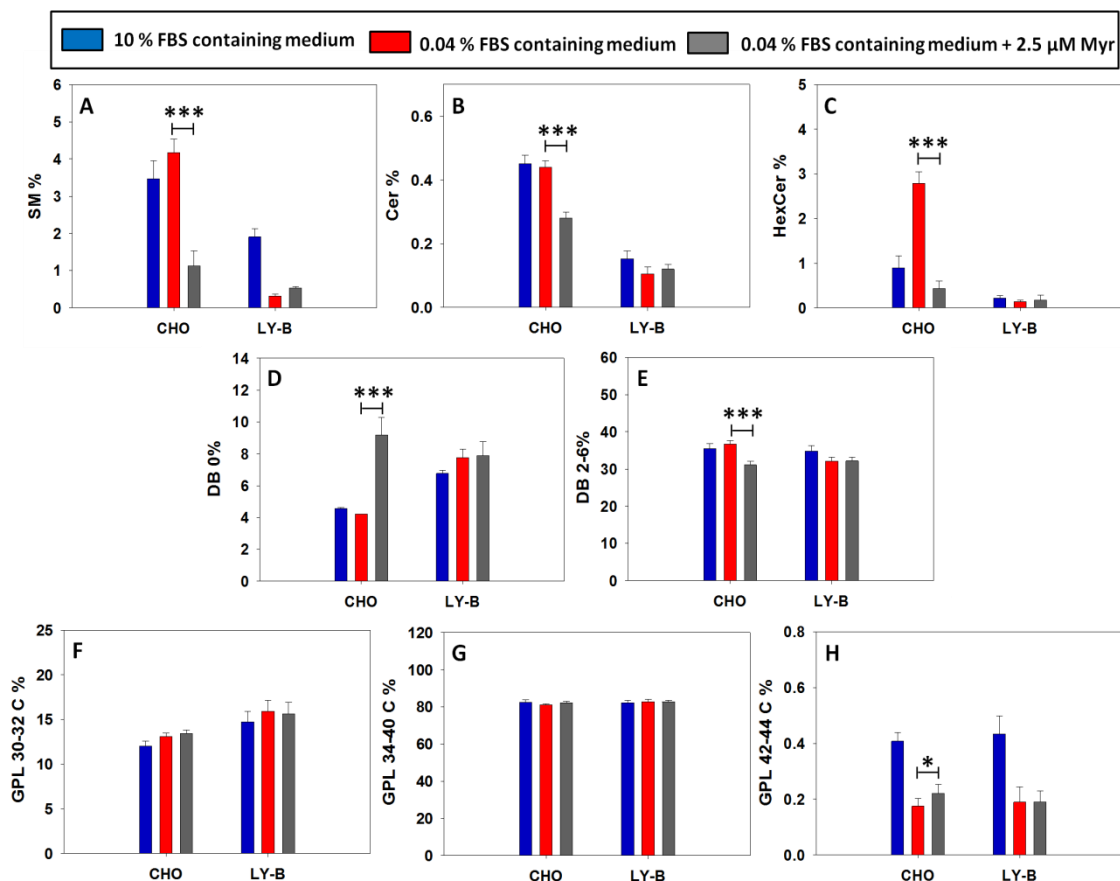


Figure 5.7. Myriocin treatment effects on the lipid composition of CHO and LY-B plasma membrane patches. Total SM (A), Cer (B) and HexCer (C). Fully saturated (DB = double bond) (D) and polyunsaturated (E) GPL. Short-chain (30-32C) (F), long-chain (34-40C) (G) and very-long chain (42-44C) GPL (H). Only selected lipids are included in the figure, a comprehensive description of the various lipid compositions can be seen in the Supplementary Material table 5.S1. n=3. Statistical significance was calculated with ANOVA or Student's t-test, with similar results. Significance: (*) p < 0.05; (***) p < 0.001.

5.3.5.2. Whole cell extracts

The lipidomic distribution of treated and non-treated whole CHO and LY-B cells grown in deficient media is shown in figure 5.S3. The results are remarkably similar to those found with the corresponding plasma membrane preparations, perhaps suggesting an active intracellular traffic.

5.3.5.3. Cholesterol

Cholesterol was determined by mass spectrometry separately from the fatty acid-containing lipids, as indicated under Methods. The results are given in table 5.2. Decreasing FBS concentration in the growth medium from 10% to 0.04% decreased

cholesterol concentrations in the cell membranes by about one-half. However, myriocin failed to have any significant effect on the amount of cholesterol in cells grown under limiting SL concentrations.

Table 5.2. Myriocin effect on cholesterol concentration in whole cell extracts from CHO or LY-B cells grown under limiting SL concentration. Results are given as mole percent of total lipid extract. Average \pm S.D. (n = 3).

Cell type	[FBS]	Myriocin	Mole % Whole cells	Mole % PM patches
CHO	10%	-	3.12 \pm 0.17*	5.91 \pm 0.29*
CHO	0.04%	-	1.56 \pm 0.19	3.12 \pm 0.20
CHO	0.04%	2.5 μ M	1.36 \pm 0.07	3.43 \pm 0.42
LY-B	10%	-	3.05 \pm 0.13*	8.65 \pm 0.90*
LY-B	0.04%	-	1.22 \pm 0.01	3.85 \pm 0.51
LY-B	0.04%	2.5 μ M	1.26 \pm 0.03	3.65 \pm 0.10

5.3.5.4. In summary

Myriocin effects on lipid composition were almost exclusively detected under conditions when myriocin hampered cell growth, i.e. CHO cells grown under limiting SL conditions. SM (Fig. 5.7A), Cer (Fig. 5.7B) and HexCer (Fig. 5.7C) concentrations in the PM were markedly lower in myriocin-treated than in non-treated CHO cells. Even if treated cells exhibited a large SL decrease, their levels were still larger than those of non-treated LY-B cell PM patches. According to GPL acyl chain length and saturation, myriocin-treated CHO cells synthesized longer (Fig. 5.7H) and more saturated (Fig. 5.7D) GPL, perhaps in a homeostatic response to myriocin-mediated SM depletion. The correlation between CHO cell PM changes in lipid composition and in biophysical properties is graphically expressed in figure 5.8.

5.4. Discussion

5.4.1. Myriocin effects on cell growth and composition

Most natural compounds with potent SPT-inhibitory properties, such as myriocin, are structural analogues of Sph (Miyake *et al.*, 1995), a bioactive molecule modulating a variety of cell functions (Hannun & Linardic, 1993; Cartier & Hla, 2019). The polyfunctionality of Sph might suggest that myriocin would have additional biological activities apart from the inhibitory effect of the *de novo* synthesis of SL. When an inhibitory compound is highly specific, the cellular effect that this compound

produces should be the same as the one caused by the genetic inactivation of the target, the SPT enzyme in our case. On the contrary, if the cellular response to a drug is different from the one achieved by genetic inactivation of the target enzyme, the drug might have additional effects. In a previous investigation we used a genetically modified CHO cell line defective in SPT (the LY-B cell line) to perform biophysical measurements and check their homeostatic response to SL deprivation (Monasterio *et al.*, 2020b). In the current study we have used myriocin to specifically inhibit SPT and compare the chemical inhibition results with the ones obtained after genetic modification (LY-B results) (Monasterio *et al.*, 2020b), thus addressing myriocin specificity against the SPT enzyme activity.

When cell growth of myriocin-treated CHO and of non-treated LY-B cells were compared, slight, only slight differences were found. Myriocin-treated CHO cells were able to recover to a large extent the control (non-treated CHO cell) growth rates when the SL-deficient medium was supplemented with sphinganine (Figs. 5.1B and 5.S1F). When externally supplied to the culture medium, sphinganine is utilized for formation of Cer and complex SL in CHO cells, thereby bypassing the SPT reaction inhibition. A similar behavior was observed with SM supplementation (Fig. 5.S1C). Nevertheless, control (non-treated CHO grown in deficient medium) values were not reached (Fig. 5.1B). This failure to recover full growth by addition of exogenous SL molecules in the presence of the SPT inhibitors could occur because some sphingosine-like compounds, as it is the case for myriocin, are known to inhibit sphingosine kinase (Yatomi *et al.*, 1996). This inhibition would lead to the decrease of sphingosine-1-phosphate cell levels. Sphingosine-1-phosphate has been described as a second messenger favoring cell proliferation and survival (Spiegel *et al.*, 1998; Lidgerwood *et al.*, 2018; Yoshino *et al.*, 2019). According to other studies, growth rate recovery is not achieved either when the used SPT inhibitor is L-Cycloserine or β -chloro-L-alanine (Hanada *et al.*, 2000b) instead of myriocin.

Alternatively, the different growth rates of myriocin-treated and non-treated CHO cells (Fig. 5.1A) may be related to the over-expression of HexCer observed in non-treated CHO, but not in myriocin-treated CHO cell patches upon lowering FBS concentration in the medium (Fig. 5.7C). HexCer is at the origin of the complex glycosphingolipid biosynthetic pathway (Merrill *et al.*, 1997). Glycosphingolipids are

essential cell components involved, among other effects, in cell growth and differentiation (Van Meer *et al.*, 2003). However, in general, the external addition of Sph is not expected to mimic completely the de novo synthesis: the “initial” location of Sph is different and the intracellular traffic and distribution are also expected to be different as well as the biophysical changes at the PM and in the membrane of different organelles, probably affecting cellular signaling and homeostasis in different ways, in addition to the already mentioned toxic effects. These more general effects should also be considered.

Comparing the SL levels in PM patches derived from myriocin-treated and non-treated CHO cells grown in deficient medium, it can be concluded that the former exhibit significantly lower SL values. Three representative SL, SM (Fig. 5.7A), Cer (Fig. 5.7B) and HexCer (Fig. 5.7C), were largely decreased, by 73%, 37% and 85% respectively. These results are in good agreement with the ones published by Ziulkoski *et al.* (2001), who achieved a 40%-61% of SM decrease using fumonisin B1 and β -chloroalanine. An important myriocin effect is that a more rapid SM depletion is obtained in mutated defective- SPT containing LY-B than in the myriocin-treated CHO cells (Figs. 5.2, 5.3 and 5.S2). In addition, SM, Cer and HexCer levels, even if their amounts are markedly decreased by myriocin treatment, they are still larger in treated CHO cells than in non-treated LY-B cells (0.04% FBS).

5.4.2. Lipid composition and physical properties

SL depletion is probably what makes PM patches derived from myriocin-treated CHO cells to show a decreased laurdan GP (indicating a decreased lipid order, or increased bilayer fluidity) (Figs. 5.4 and 5.5) and a lowered breakthrough force distribution (increased membrane penetrability) (Fig. 5.6). GP images from PM patches derived from myriocin-treated CHO cells appeared to be homogenous, but the presence of nanodomains could not be ruled out because of the spatial and temporal resolution limit of conventional two photon microscopy (Frisz *et al.*, 2013b, 2013a; Nicovich *et al.*, 2018).

In addition, comparison of myriocin-treated and non-treated CHO cells showed changes in their GPL distribution. Myriocin-treated cells contained more fully saturated (Fig. 5.7D) and less polyunsaturated (Fig. 5.7E) GPL than non-treated ones. This could

help in partially maintaining membrane rigidity under conditions of low SM. This is also in accordance with the results obtained from the LY-B cells containing a mutated, non-functional SPT (Monasterio *et al.*, 2020b). According to chain length distribution, LY-B cells grown in deficient medium contain more short fatty acids (C30-32C per GPL molecule) than myriocin-treated CHO cells (Monasterio *et al.*, 2020b). The correlation between changes in lipid composition and in physical properties of CHO cell PM is graphically expressed in figure 5.8.

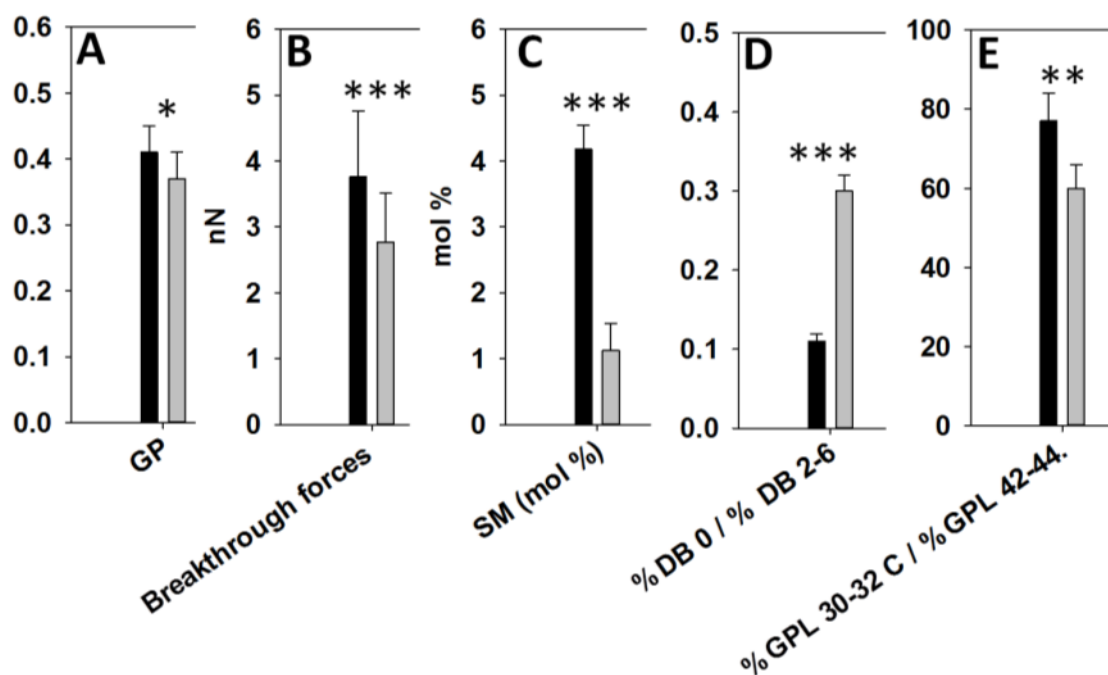


Figure 5.8. A correlative presentation of myriocin effects on the plasma membranes of CHO cells grown on SL-deficient medium. Black bars: control, non-myriocin treated cells; grey bars: myriocin-treated cells. (A) Laurdan general polarization in PM patches (data from Fig. 4). (B) Bilayer breakthrough forces obtained by AFM in the force-spectroscopy mode (data from Fig. 6). (C) Mole percent SM contents in PM patches (data from Table 5.S1 and Fig. 5.7A). (D) Saturated/unsaturated fatty-acyl mole ratio (data from Table 5.S1 and Fig. 5.7D, E). (E) Short-chain/very-long-chain fatty-acyl mole ratio (data from Table 5.S1 and Fig. 5.7 F, H). Significance: (*) $p < 0.05$; (**) $p < 0.01$ (***) $p < 0.001$.

5.4.3. Chemical vs. genetic suppression of SPT activity

The present study presents a phenotypic comparison between mutant cells (LY-B) specifically defective in a cellular function (*de novo* SL synthesis), and wild-type CHO cells exposed to a chemical inhibitor of the SPT activity function (myriocin) as a rational approach for evaluating how specific an inhibitor compound can be. The main difference between the two approaches is that LY-B cells lack a functional SPT

complex because they cannot synthesize the LCB1 subunit, while the myriocin-mediated inhibition only blocks the SPT function, but the protein is still present. This may have important implications, for example the drug-inhibited protein may lack a certain activity but may still interact with some binding partners, as many proteins have multiple activities and/or functions and may participate in multiple disparate pathways, processes, and/or multiprotein complexes and structures.

Considering the above data, very similar results were achieved with both the pharmacological and genetic tools. Myriocin-treated SM-depleted CHO cells reacted to maintain membrane order undergoing a homeostatic response, although they achieved it only partially, as their PM were more fragile when grown in SL-deficient medium. The same occurred with non-treated LYB cells (Monasterio *et al.*, 2020b).

The capacity shown by certain cells, e. g. myriocin-treated CHO cells or genetically modified LY-B cells, to grow under extremely demanding low concentrations of SL opens the way to a variety of functional studies on the role of SL in membranes. Nevertheless, natural compound as myriocin or fumonisin may display toxicity in humans, hence the chemical inhibition process may be less suitable for human studies (Stockman-Juvala, H. Savolainen, 2008). The LCB1 protein is specifically involved in the formation of the SPT complex, thus a therapy that includes modifying SPT activity might show good results in the treatment of cardiovascular diseases, such as atherosclerosis (Hojjati *et al.*, 2005; Park *et al.*, 2008). Other studies provided evidence that inhibition of *de novo* Cer synthesis improves glucose homeostasis and enhances whole-body insulin responsiveness in rodent models of type-2 diabetes (Holland *et al.*, 2007). Moreover, it has been shown that it also reduces body weight, ameliorates glucose homeostasis, and reverses hepatic steatosis in diet-induced nonalcoholic fatty liver disease (Kurek *et al.*, 2013). In addition, it has been seen that the blockage of *de novo* synthesis of Cer and HexCer significantly suppresses neurodegenerative phenotypes associated with α -synuclein overexpression (Lin *et al.*, 2018).

5.5. Supplementary Material

Table 5.S1. A summary of the various lipid compositions of CHO and LY-B cells after and before Myriocin treatment.

<https://drive.google.com/file/d/1UZw6fgvZiRRLduLq51mpRHdsOS8XHKPT/view?usp=sharing>

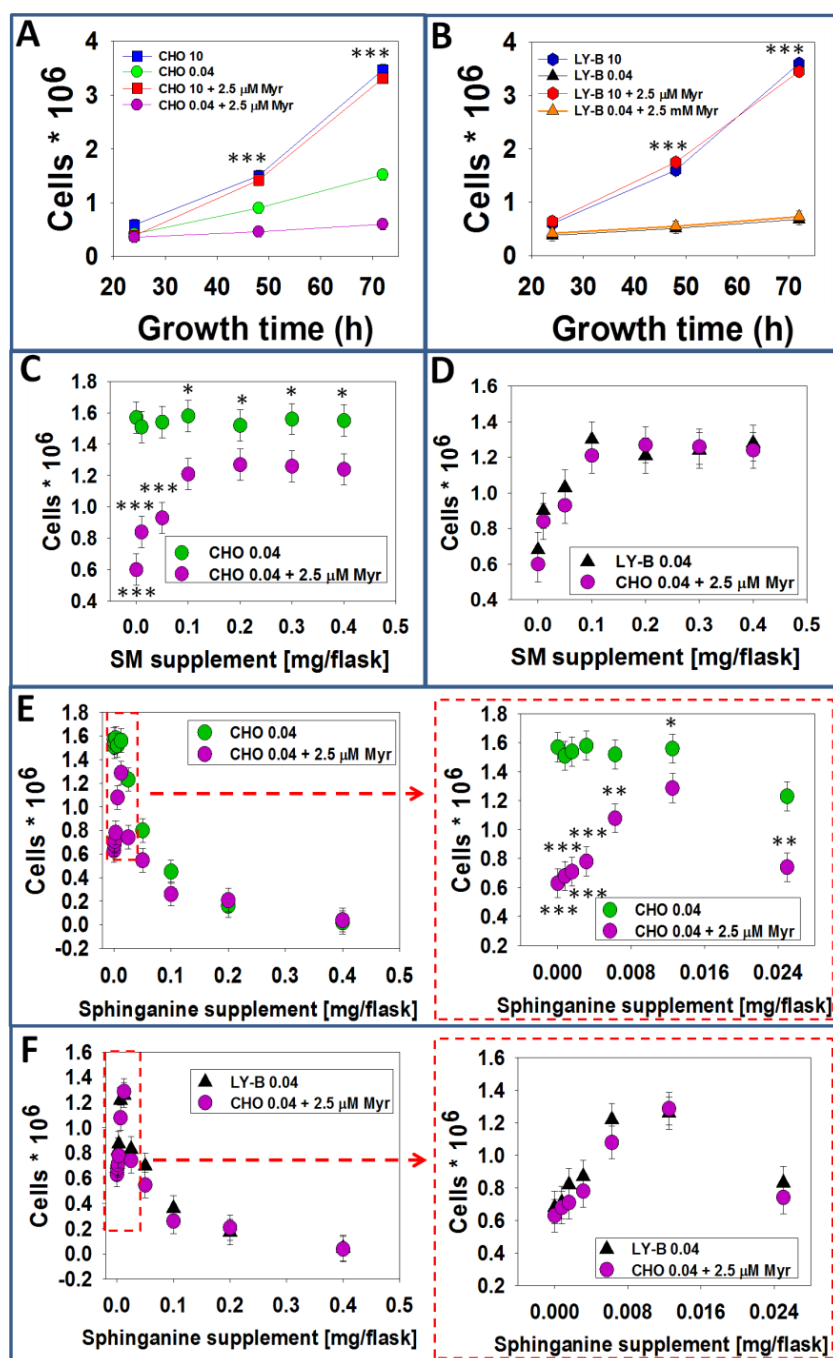


Figure 5.S1. Growth of myriocin-treated and non-treated CHO and LY-B cells. CHO (A) or LY-B (B) cell growth as a function of time in 0 or 2.5 μ M myriocin-containing, standard (10% FBS) or spingolipid-deficient (0.04% FBS) medium (seeded cells: 0.25×10^6). Statistical symbols correspond to differences between purple circles (CHO 0.04 + 2.5 μ M Myr) and the other three samples in panel A and between triangles (LY-B 0.04 + 0 or 2.5 μ M Myr) and circles (LY-B 10 + 0 or 2.5 μ M Myr). (C) Myriocin-treated vs. non-treated CHO cell growth after 72 h in spingolipid-deficient medium supplemented with SM (seeded cells: 0.25×10^6). (D) Myriocin-treated CHO vs. non-treated LY-B cells growth after 72 h in spingolipid-deficient medium supplemented with SM (seeded cells: 0.25×10^6). Myriocin-treated vs. non-treated CHO (E) and LY-B (F) cell growth after 72 h in spingolipid-deficient medium supplemented with sphinganine (seeded cells: 0.25×10^6). Significance: (*) $p < 0.05$; (**) $p < 0.01$ (***) $p < 0.001$.

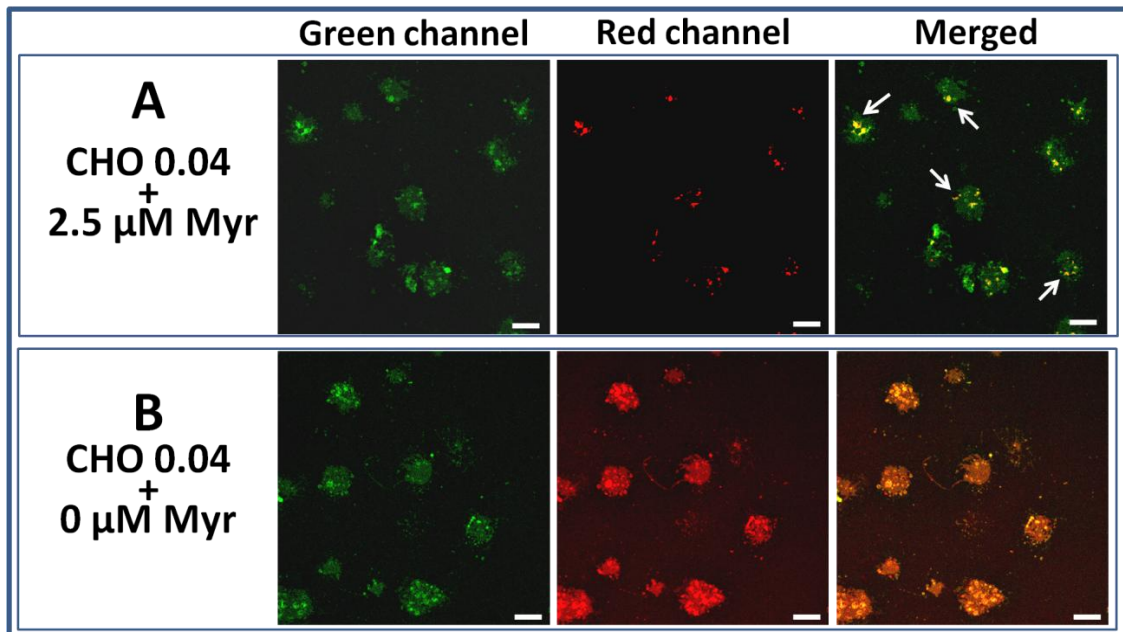


Figure 5.S2. Fluorescence images of PM patches stained with mCherry-lysenin (red). Myriocin treated (A) and non-treated CHO cells (B) grown in deficient medium. Bar = 50 μ m. NBD-PE (green) was used in fluorescence images as a general membrane staining control.

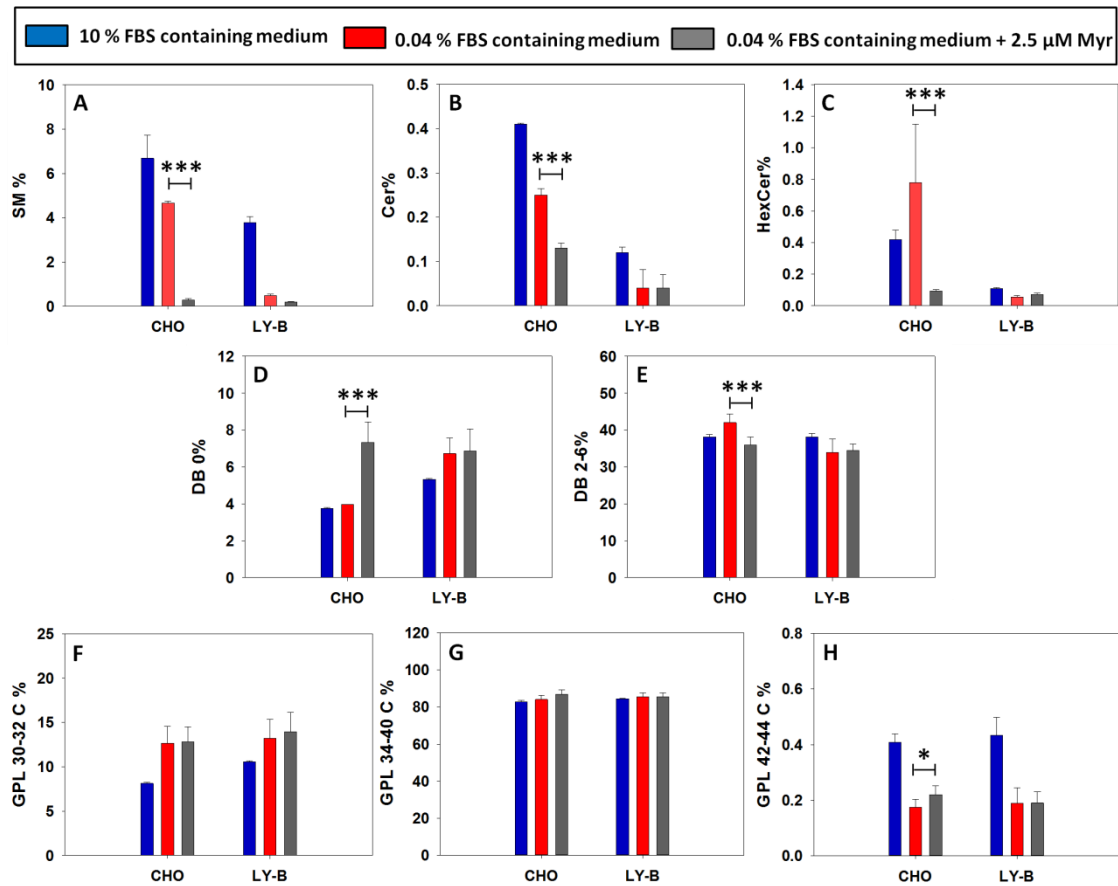


Figure 5.S3. Myriocin treatment effects on the lipid composition of CHO and LY-B whole cell lipid extracts. Total SM (A), Cer (B) and HexCer (C). Fully saturated (DB = double bond) (D) and polyunsaturated (E) GPL. Short-chain (30-32C) (F), long-chain (34-40C) (G) and very-long chain (42-44C) GPL (H). Only selected lipids are included in the figure, a comprehensive description of the various lipid compositions can be seen in the Supplementary Material table 5.S1. $n=3$. Statistical significance was calculated with ANOVA or Student's t-test, with similar results. Significance: (*) $p<0.05$; (***) $p<0.001$.

**CHAPTER 6: PLASMA
MEMBRANE SPHINGOMYELIN
DEPLETION BY
CYCLODEXTRINS: PHYSICAL
AND COMPOSITIONAL
CONSEQUENCES**

CHAPTER 6: PLASMA MEMBRANE SPHINGOMYELIN DEPLETION BY CYCLODEXTRINS: PHYSICAL AND COMPOSITIONAL CONSEQUENCES

6.1. Introduction

Cyclodextrins (CD) are the subject of extensive research as well as of inventions (over 1000 patents or patent applications in the past 5 years) (Martin Del Valle, 2004). CD were first discovered by M.A. Villiers (1891), using probably impure cultures of *Bacillus amylobacter* to digest starch. He obtained only a small amount of crystalline material because *Bacillus macerans* might also have been present in his culture (Schmid, 1989). Villiers named the crystalline product cellulodin. In 1903, Schardinger isolated two crystalline products, named crystallized dextrans α and β (Eastburn & Tao, 1994). Finally, it was in 1935 when γ -dextrin was isolated (Stella & Rajewski, 1997). Since then, several modified CD have also been produced (Szejtli, 2004).

In 1942 the structures of methyl- α -cyclodextrin (M α CD) and methyl- β -cyclodextrin (M β CD), and in 1948 that of methyl- γ -cyclodextrin (γ CD), were determined by X-ray crystallography (Buschmann & Schollmeyer, 2002). It was concluded that CD's possess a hydrophilic surface that makes them soluble in water, while being capable of forming inclusion complexes with a wide variety of hydrophobic guest molecules because of their inner non-polar cavity (Szejtli, 1989). M α CD, M β CD and γ CD are composed of six, seven and eight α -(1,4)-linked glycosyl units, respectively (Dass & Jessup, 2000). Among them, M β CD is the most frequently used, partly for its low price (Szejtli, 2004). Cell membranes exhibit an asymmetric distribution of lipids across the bilayer; the exoplasmic leaflet of the plasma membrane (PM) of eukaryotic cells often contains large amounts of phosphatidylcholine (PC) and sphingolipids (SL) such as sphingomyelin (SM), whereas the cytoplasmic leaflet is enriched in phosphatidylethanolamine and phosphatidylserine (Kiessling *et al.*, 2009). As their non-polar cavity provides CD with the ability to entrap specific lipids when

interacting with membranes, these dextrins have been used in the study of membrane asymmetry because they can only extract lipids from the outer leaflet. This technique has been commonly used with model membranes (Almeida, 2009). For example, Chiantia *et al.* developed a method to produce stable small (Cheng *et al.*, 2009) and giant (Chiantia *et al.*, 2011) asymmetric unilamellar vesicles with a wide variety of lipid compositions based on M β CD-mediated lipid exchange. Human red blood cells (RBC) have also been treated and studied with different CD. Othani *et al.* found that, depending on the CD, the potencies for solubilizing various components of erythrocytes varied in the order: M α > M β > M γ for phospholipids, M β > M γ > M α for cholesterol (Chol) and M β > M γ > M α for proteins. They concluded that CD could increase membrane fluidity through removal of Chol into the aqueous phase (Ohtani *et al.*, 1989).

More recently, CD has been used on cultured cells. Kainu *et al.* (2010) proved that M β CD can extract Chol and other lipids from cell PM, greatly perturbing cell growth and decreasing cell viability. CD could also be loaded with lipids to perform lipid exchange, instead of a unidirectional extraction. When efficient incorporation of natural species with similar hydrophobicities was performed, cells could survive without significantly compromising growth or viability (Kainu *et al.*, 2010). Li *et al.* (2016) concluded that M α CD catalyzed lipid exchange replacing SL and phospholipids in the outer leaflet of the PM of living mammalian cells. The exchanged exogenous lipids could include unnatural lipids, but not Chol. This happens because M α CD have a smaller hydrophobic cavity than M β CD, that prevents their interaction with sterols, M α CD being as a result much less perturbing for the cell (Martin Del Valle, 2004). They concluded that 70–80% of the cell SM resided in the PM outer leaflet. Recently, Li *et al.* (2019) have used M α CD to optimize lipid/CD ratio in order to avoid cell damage, and have also analyzed the physical changes that occur in the PM after CD treatment. Moreover, Straková *et al.* applied mechanosensitive flipper probes to report on global membrane tension changes in fluorescence lifetime imaging microscopy (FLIM) images of living COS-7 cells. In cells treated with myriocin, the flipper 3 probe exhibited a clearly reduced lifetime (3.84 ns), suggesting that the lipid order indeed decreased (Straková *et al.*, 2020).

Previous work from this laboratory has dealt with the biophysical properties that SL confer to cell membranes (Goñi & Alonso, 2009; Alonso & Goñi, 2018; González-

Ramírez *et al.*, 2019; Goñi *et al.*, 2020). In Monasterio *et al.* (2021a), a CHO-derived cell line with a defective sphingosine palmitoyl transferase (SPT) was used (LY-B cell line). Under conditions such that SM contents of whole cells was decreased by 65%, their PM fluidity, assessed by laurdan generalized polarization (GP), and nanomechanical breakthrough forces were also decreased, by 15% and 35% respectively. Mass-spectrometry measurements concluded that LY-B were able to respond by synthesizing shorter and more saturated glycerophospholipids, but even so the native membrane properties were only partially recovered (Monasterio *et al.*, 2021a). Similar results were found with native CHO cells in which SPT had been specifically inhibited with myriocin (Monasterio *et al.*, 2021b).

As a continuation to our previous studies, comparative analyses of M α CD and M β CD effects on the PM of wild type CHO and SPT-deficient LY-B cell lines were carried out. Laurdan generalized polarization and AFM-mediated force spectroscopy of PM samples were measured in combination with mass-spectroscopic analysis of membrane lipid contents.

6.2. Materials and Methods

6.2.1. Cell growth

Wild type CHO (ATCC, Manassas, VA, US) and SPT-deficient CHO cell line, known as LY-B (Hanada *et al.*, 1998) (RIKEN BioResource Research Center Koyadai, Japan), were used in this study. SPT is the key enzyme in SL biosynthesis.

Cells were grown on Dulbecco's Modified Eagle Medium: Nutrient Mixture F-12 (DMEM:F12), containing 10% fetal bovine serum (FBS), 100 U/ml penicillin and streptomycin, and 6 mM glutamine (GlutaMax-supplemented) at 37°C and 5% CO₂ humidified atmosphere. All cell culture products were purchased from Thermofisher (Waltham, MA, US).

6.2.2. Lipid-loaded or non-loaded CD treatment

Incubation of MLV vesicles with CD was performed for lipid-loaded CD treatment. First, pure egg phosphatidylcholine (PC), PC:Cholesterol (Chol) (1:1), PC:Sphingomyelin (SM) (1:1), or PC:SM (1:3) MLV were formed. For this purpose, lipid

samples were kept under vacuum for 2 h to remove solvent traces. Then, lipids were swollen in DMEM:F12 medium buffer. For CD lipid loading, 7.5 mM (unless otherwise stated) M α CD (Cyclodextrin-Shop, AraChem, Tilburg, Netherlands) or M β CD (Sigma-Aldrich, St. Louis, MO, U. S.) and 3 mM MLV (unless otherwise stated) were mixed at the desired ratios and incubated at 37°C for 30 min as described by Li *et al.* (2019) (1 and 2 mM MLV concentration have also been used in specific cases). Then, lipid loaded- or non-loaded CD samples (together with MLV in the case of loaded CD) were added to cultured cells and incubated for 1 h at 37°C for lipid exchange or extraction. 3 PBS washing steps were performed before the measurements.

6.2.3. Viability test

Flow cytometry analysis was performed to evaluate whether CD treatment affected cell viability. A FACS Calibur (Becton-Dickinson, Franklin Lakes, NJ, US) cytometer was used to detect apoptotic or necrotic cells after staining with Annexin-V-FITC and with propidium iodide as indicated in the manual of the annexin V-FITC detection kit (CalbioChem, Darmstadt, Germany). Annexin V-FITC fluorescence intensity was measured in fluorescence channel FL-1 with $\lambda_{\text{ex}} = 488$ nm and $\lambda_{\text{em}} = 530$ nm, while propidium iodide was detected in FL-3, with $\lambda_{\text{ex}} = 532$ nm and $\lambda_{\text{em}} = 561$ nm. All measurements were performed in triplicate. Data analysis was performed using the flowing software 2 program.

6.2.4. Lysenin-mediated SM quantification

Lysenin is a SM-specific toxin. For SM visualization and quantification, the nontoxic (NT) monomeric C-terminal domain, NT-lysenin, was used. Lysenin was expressed and purified as described by Carquin *et al.* (2014). Briefly, NT-lysenin with an N-terminal 6xHis-tag followed by the monomeric red fluorescent protein mCherry ($\lambda_{\text{ex}}=587$ nm and $\lambda_{\text{em}}= 610$ nm) was encoded by the expression plasmid pET28/lysenin* as a fusion protein. *Escherichia coli* BL21 (DE3) was used for plasmid expansion and the recombinant protein was expressed in lysogeny broth (LB) medium at 16°C for 72 h in the presence of 0.4 mM isopropyl β -D-thiogalactoside. Bacterial extracts were prepared as previously described (Maliekal *et al.*, 2006) and a NI-NTA Superflow cartridge (Qiagen, Hilden, Germany) was used for the recombinant protein purification, and imidazol for its elution (Veiga-da-cunha *et al.*, 2012). Fraction analysis by SDS-

PAGE revealed recombinant NT-lysenin at the expected size (45 KDa). Most enriched fractions were pooled, concentrated, and desalted. The aliquots were stored in 20 mM NaCl and 25 mM Hepes, pH 7.2 and 5% glycerol at -80°C. Protein concentration was calculated by measuring the absorbance at 280 nm.

Cells were stained at a final concentration of 100 μ M lysenin and images were acquired with a Nikon D-ECLIPSE C1 confocal microscope (Nikon, Melville, NY, US) Lysenin-mCherry signal was quantified with a FACS Calibur cytometer (Becton-Dickinson, Franklin Lakes, NJ, US) using the FL-3 channel with $\lambda_{\text{ex}} = 532$ nm and $\lambda_{\text{em}} = 561$ nm.

6.2.5. Filipin staining

To confirm or discard cholesterol extraction, cells were treated with CD and stained with cholesterol-specific filipin III from *Streptomyces filipinensis* (Sigma-Aldrich, St. Louis, MO, US) prior to confocal microscopy image acquisition. For filipin staining, treated or non-treated cells were rinsed 3 times with PBS before cell fixation [3% paraformaldehyde (PFA) for 1 h at room temperature]. After incubation, PFA was discarded and 1.5 mg glycine/ml in PBS was added for 10 min at room temperature to quench the PFA. Then, cells were stained with 0.05 mg/ml filipin III in PBS with 10% FBS for 2 h at room temperature. Finally, cells were rinsed 3 times with PBS prior to cell visualization.

A Leica TCS SP5 II microscope (Leica Microsystems GmbH, Wetzlar, Germany) was used for image acquisition. A 63x water-immersion objective (numerical aperture, NA = 1.2), was used and samples were imaged at 512 x 512 pixels and 400 Hz per scanning. Filipin III was excited at 360 nm and its emission was collected at 460 nm.

6.2.6. Laurdan General Polarization

Laurdan is a probe that can be correlated to the lipid phase of membranes. When it is excited, its emission undergoes a spectral shift due to the reorientation of water molecules present in the glycerol backbone region of the membrane (Krasnowska *et al.*, 1998). In the gel phase, C-laurdan maximum emission peak is around 440 nm, whereas

in the liquid crystalline phase the spectrum peaks around 490 nm. This shift can be quantified using the generalized polarization (GP):

$$GP = \frac{I_B - G \cdot I_R}{I_B + G \cdot I_R}$$

where I_B is the intensity collected by detector NDD 1, I_R is the intensity collected by detector NDD 2, and G is the correction factor. The GP value of the same laurdan concentration dissolved in pure DMSO was measured for the G factor calculation (Owen *et al.*, 2012).

Cells grown in glass-bottom dishes were stained with a final concentration of 5 μ M Laurdan (Molecular Probes, Eugene, OR) for 5 min. Several washes were performed with PBS prior to cell visualization. A Leica TCS SP5 II microscope (Leica Microsystems GmbH, Wetzlar, Germany) was used for image acquisition. A 63x water-immersion objective (numerical aperture, NA = 1.2) was used and samples were imaged at 512 x 512 pixels and 400 Hz per scanning line. A pulsed titanium-sapphire (Mai-Tai Deepsee, Spectra-Physics, Milpitas, CA, US) laser tuned at 780 nm was used for two-photon imaging of samples. Fluorescence emission was collected by non-descanned (NDD) hybrid detectors. The blue edge of the emission spectrum was collected by NDD 1 at 435 ± 20 nm and the red edge by NDD 2 at 500 ± 10 nm. Irradiance at the sample plane was $\approx 500 \text{ GW} \cdot \text{cm}^{-2}$ for two-photon excitation (Parasassi & Gratton, 1997).

GP value of samples was calculated using a MATLAB (MathWorks, Natick, MA, US) based software. Images were smoothed in each channel with 2-pixel averaging, the PM was selected and the GP value was calculated using the above equation (Carravilla *et al.*, 2015).

6.2.7. AFM

Force spectroscopy analysis of PM patches was performed as follows. First, cells were cultured on mica slices and CD treatment was performed. Then, isolated PM patches were prepared as previously described (Bezrukov *et al.*, 2009; Monasterio *et al.*, 2020).

PM patches were imaged using a NanoWizard II AFM (JPK Instruments, Berlin, Germany) under contact mode scanning (constant vertical deflection). For sample identification, the AFM was coupled to a Leica microscope and mounted onto a Halcyonics Micro 40 antivibration table (Halcyonics, Inc., Menlo Park, CA, US) and inside an acoustic enclosure (JPK Instruments, Berlin, Germany). V-shaped MLCT Si₃N₄ cantilevers (Bruker, Billerica, MA, US) with nominal spring constants of 0.1 or 0.5 N/m (García-Arribas *et al.*, 2015) were used. These cantilevers were individually calibrated with a lipid-free mica substrate in assay buffer using the thermal noise method. After a proper PM patch was localized, force spectroscopy was performed at a speed of 1 μm/sec. Force steps were determined for each of the indentation curves as reproducible jumps within the extended traces. At least three independent sample preparations, with 50-100 measurements in each of them, were studied.

6.2.8. Mass spectroscopic analysis

Mass spectroscopic analysis of PM patches was performed as described in Monasterio *et al.* (2020). Lipid extraction was performed prior to lipid analysis, as detailed below.

6.2.8.1. Lipid extraction

Lipid extraction was carried out using a modified methyl-*tert*-butyl ether (MTBE) protocol (Guri *et al.*, 2017). PM patch samples were prepared as previously mentioned (Monasterio *et al.*, 2020). Then, 360 μl methanol was added and vortexed. A mixture of lipid standards (Table 6.S1) was added and samples were vortexed for 10 min at 4°C using a Cell Disruptor Genie (Scientific Industries, Inc., Bohemia, NY, US). MTBE (1.2 mL) was then added, and the samples were incubated for 1 h at room temperature with shaking (750 rpm). Phase separation was induced by adding 200 μl H₂O. After 10 min incubation at room temperature, the sample was centrifuged at 1,000 xg for 10 min. The upper (organic) phase was transferred to a 13 mm screw-cap glass tube and the lower phase was extracted with 400 μl artificial upper phase [MTBE/methanol/water (10:3:1.5, v/v/v)]. The two upper phases were combined, and the total lipid extract was divided into 3 equal aliquots [one for phospholipids (TL), one for sterols (S) in 2-ml amber vials, and one for SL detection in a 13-mm glass tube] and dried in a Centrivap at 50°C or under a nitrogen flow. The SL aliquot was deacylated by

methylamine treatment (Clarke method) to remove phospholipids. 0.5 ml monomethylamine reagent [MeOH/H₂O/*n*-butanol/methylamine solution (4:3:1:5 v/v)] was added to the dried lipid, followed by sonication (5 min). Samples were then mixed and incubated for 1 h at 53°C and dried (as above). The monomethylamine-treated lipids were desalted by *n*-butanol extraction. 300 µl H₂O-saturated *n*-butanol was added to the dried lipids. The sample was vortexed, sonicated for 5 min and 150 µl MS-grade water was added. The mixture was vortexed thoroughly and centrifuged at 3200 xg for 10 min. The upper phase was transferred to a 2-ml amber vial. The lower phase was extracted twice more with 300 µl H₂O-saturated *n*-butanol and the upper phases were combined and dried (as above).

6.2.8.2. Glycerophospholipid and SL detection on a Triple Quadrupole Mass Spectrometer

TL and SL aliquots were resuspended in 250 µl chloroform/methanol (1:1 v/v) (LC-MS/HPLC grade) and sonicated for 5 min. The samples were pipetted in a 96-well plate (final volume = 100 µl). The TL were diluted 1:4 in negative-mode solvent (chloroform/methanol (1:2) + 5 mM ammonium acetate) and 1:10 in positive-mode solvent (chloroform/methanol/water (2:7:1 v/v) + 5 mM ammonium acetate). The SL were diluted 1:10 in positive-mode solvent and infused onto the mass spectrometer. Tandem mass spectrometry for the identification and quantification of SL molecular species was performed using Multiple Reaction Monitoring (MRM) with a TSQ Vantage Triple Stage Quadrupole Mass Spectrometer (Thermo Fisher Scientific, Waltham, MA, US) equipped with a robotic nanoflow ion source, Nanomate HD (Advion Biosciences, Ithaca, NY, US). The collision energy was optimized for each lipid class. The detection conditions for each lipid class are listed in table 6.S1. Cer species were also quantified with a loss of water in the first quadrupole. Each biological replica was read in 2 technical replicas. Each technical replica comprised 3 measurements for each condition. Lipid concentrations were calculated relative to the relevant internal standards and then normalized to the total lipid content of each lipid extract (mol %).

6.2.8.3. Gas chromatography–mass spectrometry for cholesterol assay

Sterol-containing lipid extracts were analyzed by GC-MS as described previously (Guan *et al.*, 2010). Briefly, samples were injected into a VARIAN CP-3800 gas chromatograph equipped with a FactorFour Capillary Column VF-5ms 15 m × 0.32 mm i.d., DF = 0.10, and analyzed in a Varian 320 MS triple quadrupole with electron energy set to -70 eV at 250°C (Varian, Palo Alto, CA, US). Samples were applied to the column oven at 45°C , held for 4 min, then raised to 195°C ($20^{\circ}\text{C}/\text{min}$). Sterols were eluted with a linear gradient from 195 to 230°C ($4^{\circ}\text{C}/\text{min}$), followed by rising to 320°C ($10^{\circ}\text{C}/\text{min}$). Chol was identified by its retention time (compared with an ergosterol standard) and fragmentation patterns, which were compared with the NIST library.

6.2.9. RBC CD treatment

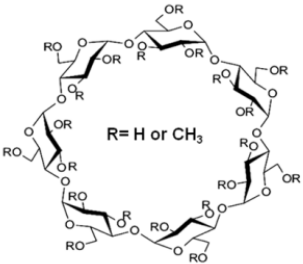
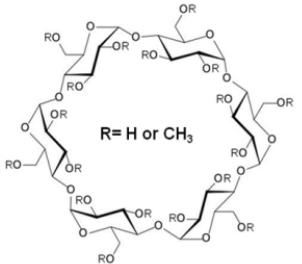
For a proper $\text{M}\alpha\text{CD}$ and $\text{M}\beta\text{CD}$ comparison, human RBC were also used in this study. RBC lack intracellular organelles and their PM contains large cholesterol amounts. Non-loaded CD treatment of RBC was performed, and cells were stained with m-Cherry-lysenin prior to confocal microscopy visualization. Hemolysis quantification (Cortajarena *et al.*, 2001) and laurdan GP measurements (Monasterio *et al.*, 2020) were also performed.

6.3. Results and Discussion

6.3.1. An overview of $\text{M}\alpha\text{CD}$ and $\text{M}\beta\text{CD}$ properties

Table 6.1 summarizes the major structural and functional differences between $\text{M}\alpha\text{CD}$ and $\text{M}\beta\text{CD}$. The main difference is the number of glucopyranose units they contain; $\text{M}\alpha\text{CD}$ is composed of 6 units, while $\text{M}\beta\text{CD}$ contains 7. Thus, $\text{M}\alpha\text{CD}$ molecules have a smaller cavity ($4.7\text{--}5.3$ Å) as compared with $\text{M}\beta\text{CD}$ ($6.0\text{--}6.5$ Å) (Martin Del Valle, 2004). The absence or the presence of this extra glucopyranose unit leads to a different capability of lipid extraction from the membranes. It is usually accepted that $\text{M}\alpha\text{CD}$ is potentially more efficient in phospholipid extraction, while $\text{M}\beta\text{CD}$ has an improved ability to extract Chol and proteins (Ohtani *et al.*, 1989).

Table 6.1. Comparison between M α CD and M β CD

	Methyl- β -Cyclodextrin (M β CD)	Methyl- α -Cyclodextrin (M α CD)
		
Molecular Formula	$C_{42}H_{70-n}O_{35} \cdot (CH_3)_n$	$C_{36}H_{60-n}O_{30} \cdot (CH_3)_n$
Number of glucopyranose units (Martin del Valle <i>et al.</i> 2004)	7	6
Solubility in water at 25°C (% w/v) (Martin del Valle <i>et al.</i> 2004)	1.85	14.5
Outer diameter (Å) (Martin del Valle <i>et al.</i> 2004)	15.4	14.6
Cavity diameter (Å) (Martin del Valle <i>et al.</i> 2004)	6.0–6.5	4.7–5.3
Average Molecular Weight (Martin del Valle <i>et al.</i> 2004)	1310	1127
Phospholipids extraction	$\alpha > \beta$ (Ohtani <i>et al.</i> 1989)	
Cholesterol extraction	$\beta > \alpha$ (Ohtani <i>et al.</i> 1989)	
Protein extraction	$\beta > \alpha$ (Ohtani <i>et al.</i> 1989)	

6.3.2. Cell viability

CHO and LY-B cells were treated with different concentrations of loaded or non-loaded M α CD or M β CD, and stained with annexin and propidium iodide in order to perform viability measurements. Figure 6.1 summarizes the percent viable cells as obtained from flow cytometry analysis. Comparing CHO and LY-B cells, no statistically significant difference between controls (0.0 mM CD) for both cell lines was found; they had similar viabilities around 95-98% (Figs. 6.1A and 6.1B). 100% corresponds to the number of CHO or of LY-B cells, as appropriate, prior to CD treatment.

Cell viability remained unchanged when cells were treated with loaded or non-loaded 2.5 mM or 5 mM M α CD (Fig. 6.1A). However, when cells were treated with 7.5 mM or 10 mM non-loaded M α CD, the viability of LY-B, but not of CHO, decreased significantly. Nevertheless, when the same concentration of M α CD concentration had been loaded with PC, LY-B cells remained as viable as the controls (Fig. 6.1A).

When cells were treated with non-loaded 2.5 mM M β CD, cell viability did not differ from control (Fig. 6.1B). Some CHO cells started dying when treating them with non-loaded 7.5 mM (or higher) M β CD, while LY-B did so with 5 mM (or higher) of the same reagent. Focusing on the lipid-loaded M β CD, viability differed greatly depending on whether it was loaded with pure PC or with a PC:Chol (1:1) mixture (Fig. 6.1B). Treatment with PC-loaded 5 mM (or higher) M β CD on LY-B cells (7.5 mM or higher for CHO cells), caused extensive cell death. However, when loading was performed with a PC:Chol (1:1) mixture, the viabilities were greatly increased in both cell lines. Note the difference in the particular case of 7.5 mM M β CD treatment: viability was around 30% (in both cell lines) after PC-loaded M β CD treatment, while PC:Chol (1:1) loading of M β CD made cells as viable as controls (95-98%). To further support the idea that M β CD had to be loaded with PC:Chol (1:1) in order to maintain the viability levels of control cells after treatment, differently treated cells were stained with SM-specific lysenin and imaged in a confocal microscope to analyze their morphological differences (Fig. 6.S1). When CHO (Fig. 6.S1B) or LY-B (Fig. 6.S1E) cells were treated with 5 mM PC:Chol (1:1)-loaded M β CD, the morphology of most cells did not vary from their respective controls (Fig. 6.S1A for CHO and Fig. 6.S1D for LY-B), they remained attached and maintained the typical epithelial cell morphology, suggesting that they were viable, as confirmed by the flow cytometry measurements (Fig. 6.1B). On the contrary, when cells were treated with 5 mM PC-loaded M β CD (Fig. 6.S1C for CHO and Fig. 6.S1F for LY-B), most cells were detached from the surface and exhibited a rounded shape, indicating their lack of viability, also confirmed by flow cytometry measurements (Fig. 6.1B). When the M β CD concentration used for cell treatment was equal or higher than 10 mM, even if it was loaded with PC:Chol (1:1), cell viability was largely decreased (Fig. 6.1B). mCherry-lysenin signal differences are shown in figure 6.S1, and will be later discussed in detail in the section 6.3.3.

The existing differences in cell viabilities after M α CD or M β CD treatment could be related to the unequal capacities of the CD's for Chol extraction. As shown in figure 6.S2, filipin signal was greatly decreased from the CHO-cell PM after cells were subjected to M β CD treatment (Fig. 6.S2D), while PM filipin signal from M α CD-treated cells remained unchanged (Fig. 6.S2B). The different Chol extraction capacity was in accordance with the results by Ohtani *et al.* (1989). In summary, it seemed that an extensive Chol extraction from the PM could lead to cell death, a death that can be

overcome when half of the M β CD is loaded with Chol molecules (Fig. 6.1B), thus enabling lipid exchange to recover the original PM Chol levels previously described by other groups (Klein *et al.*, 1995; Kainu *et al.*, 2010).

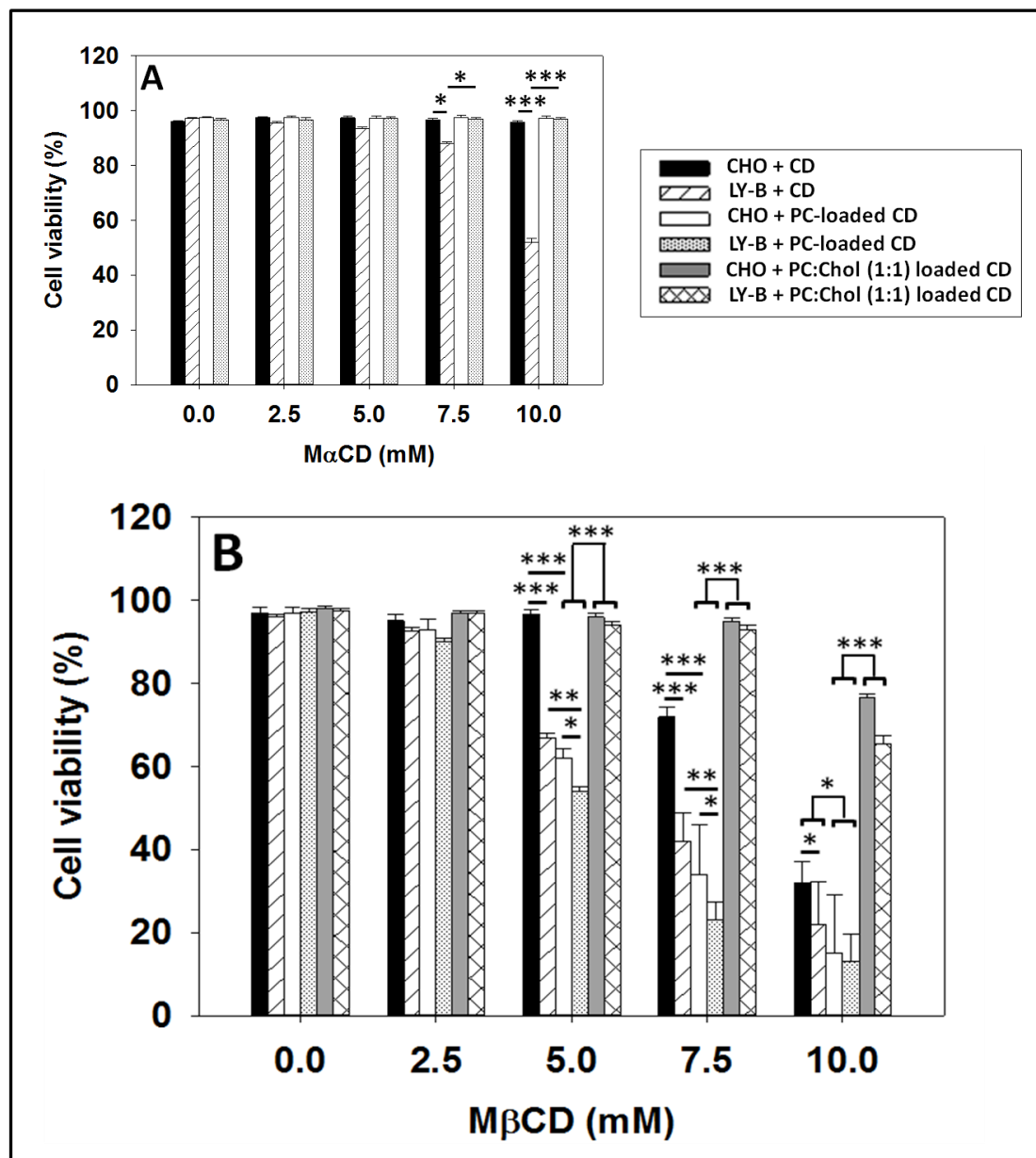


Figure 6.1. M α CD and M β CD treatment effects on CHO and LY-B cell viability. CHO and LY-B cell viability after treatment with lipid-loaded or non-loaded M α CD (A) and M β CD (B). Bars: solid black, CHO cells treated with non-loaded CD; striped, LY-B cells treated with non-loaded CD; empty, CHO cells treated with PC-loaded CD; dotted, LY-B cells treated with PC-loaded CD; gray, CHO cells treated with PC:Chol (1:1)-loaded CD; double-striped, LY-B cells treated with PC:Chol (1:1)-loaded CD. 100% corresponds to the number of CHO or LY-B cells, as appropriate, prior to CD treatment. Statistical significance was calculated with ANOVA or Student's t-test, with similar results: (*) p<0.05; (**) p<0.01; (***) p<0.001.

After CD treatment, LY-B cells had always an equal or lower viability than CHO cells (Figs. 6.1A and 6.1B). Probably, both cell lines lost similar amounts of lipids, but originally LY-B cells had lower SM quantities than CHO cells (Monasterio *et al.*, 2021a). Thus, when performing CD-mediated PM lipid extraction, LY-B cells reached more easily the critical minimum SM quantity required for a proper PM stabilization and this greatly affected their survival.

In short, M β CD had a more drastic effect on cell viability than M α CD. Cell death could be greatly buffered when a proper CD loading was used. In further experiments, prior to the biophysical measurements, M β CD were loaded with a PC:Chol (1:1) mixture in order to combine SL extraction with a reliable cell viability.

6.3.3. CD treatment for SM depletion in PM

CHO and LY-B cells were treated with different concentrations of loaded or non-loaded M α CD or M β CD, stained with SM-specific mCherry-lysenin, visualized in a confocal microscope, and their SM quantified by flow-cytometry in a FACS Calibur cytometer. Figure 6.2 shows how, when cells were treated with 5 mM PC:Chol (1:1)-loaded M β CD, the lysenin signal markedly decreased in LY-B cells (Fig. 6.2F), while CHO-cell signal suffered just a small decrease (Fig. 6.2B), as compared with their respective controls (Fig. 6.2A for CHO and Fig. 6.2E for LY-B). When 7.5 mM CD was used, not only LY-B (Fig. 6.2G), but also CHO (Fig. 6.2C) cells suffered a considerable signal decrease. With higher concentrations, the lysenin signal was no longer present, and the cells took a round shape, indicating that they were detaching from the surface, thus, dying (Fig. 6.2D for CHO and Fig. 6.2E for LY-B), as confirmed by flow cytometry measurements (Fig. 6.1B).

When PC-loaded M α CD treatment was performed, an extensive lysenin signal decrease occurred in both cell lines when they were treated with 5 mM (Fig. 6.3B for CHO and Fig. 6.3F for LY-B), or higher CD concentrations (Fig. 6.3C, 6.3D, 6.3G and 6.3H). In addition, and contrary to what happened with 10 mM PC:Chol (1:1)-loaded M β CD (Fig. 6.2D and Fig. 6.2H), the same concentration of M α CD did not lead to cell detachment, neither with CHO (Fig. 6.3D), nor with LY-B (Fig. 6.3H), indicating that cells remained viable as seen in figure 6.1A.

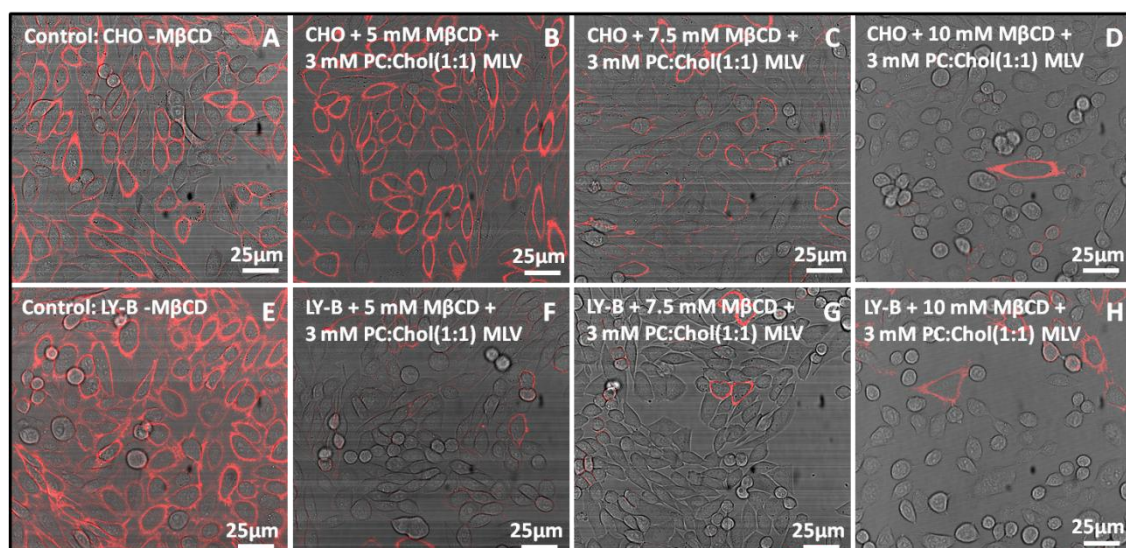


Figure 6.2. CHO and LY-B cells treated with PC:Chol (1:1)-loaded M β CD and stained with lysenin-mCherry. Control CHO cells (A), CHO cells treated with pre-loaded 5 mM (B), 7.5 mM (C) and 10 mM M β CD (D). Control LY-B cells (E), LY-B cells treated with pre-loaded 5 mM (F), 7.5 mM (G) and 10 mM M β CD (H).

Microscopy images help in understanding CD-induced SM depletion, however flow cytometry measurements were also performed for a more precise lysenin quantification. Figure 6.4 shows that, when cells were treated with either loaded or non-loaded 2.5 mM M α CD or M β CD, lysenin depletion was more evident in LY-B (Fig. 6.4B) than in CHO (Fig. 6.4A) cells. When 5 mM or higher concentrations of non-loaded M α CD were used, lysenin signal depletion was similar in both cell lines. Nevertheless, in the case of non-loaded M β CD, differences between both cell lines existed in all measured CD concentrations, depletion of the lysenin signal being more marked in the LY-B cells.

Comparing both CD's, it can be concluded that M α CD achieves a larger SM depletion, i.e. its potency for SM extraction is higher: with 7.5 mM CD, PC-loaded M α CD caused a 90% depletion of the lysenin signal in both cell lines (Fig. 6.4A for CHO and Fig. 6.4B for LY-B cells). With the same concentration of PC:Chol (1:1)-loaded M β CD treatment, a signal decrease of only 40% in CHO cells (Fig. 6.4A), and 60% in LY-B cells (Fig. 6.4B) was measured. This is probably due to the fact that, as previously mentioned, wild type CHO cells contain more SM than LY-B ones (Monasterio *et al.*, 2021a).

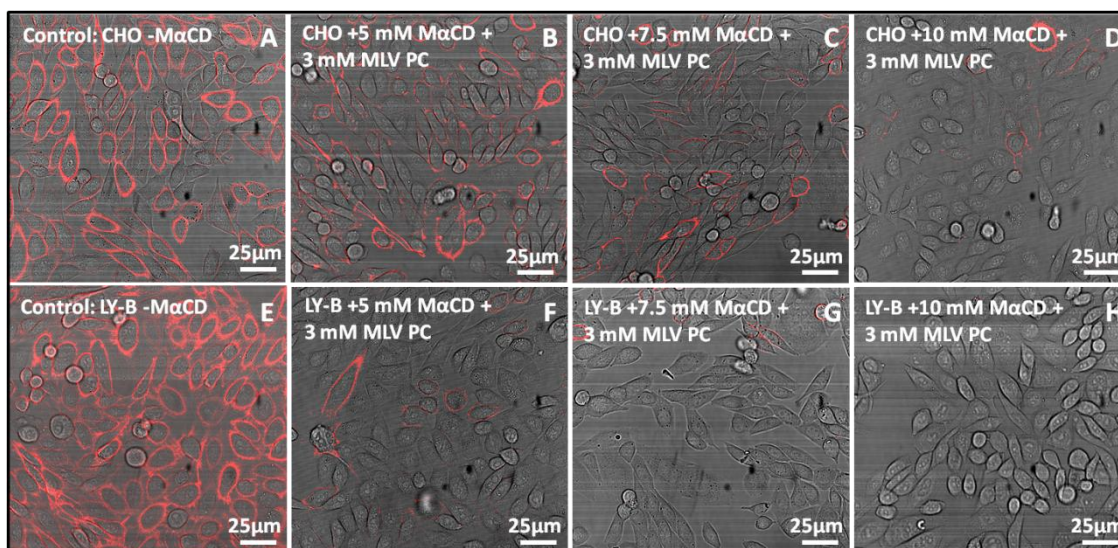


Figure 6.3. CHO and LY-B cells treated with PC-loaded M α CD and stained with lysenin-mCherry. Control CHO cells (A) and CHO cells treated with pre-loaded 5 mM (B), 7.5 mM (C) and 10 mM M α CD (D). Control LY-B cells (E) and LY-B cells treated with pre-loaded 5 mM (F), 7.5 mM (G) and 10 mM M α CD (H).

Additional differences existed when comparing values from cells treated with loaded vs. non-loaded CD (Fig. 6.4). The loading of M α CD caused the decrease of the lysenin signal to be more pronounced. In the case of M β CD treatment, a more extensive lysenin signal decrease was also achieved with loaded vs. non-loaded CD, however the differences were smaller than in the previous case. This indicated that the lipid exchange between PM and loaded CD occurred more readily than the non-loaded CD-mediated unidirectional extraction of the PM lipids.

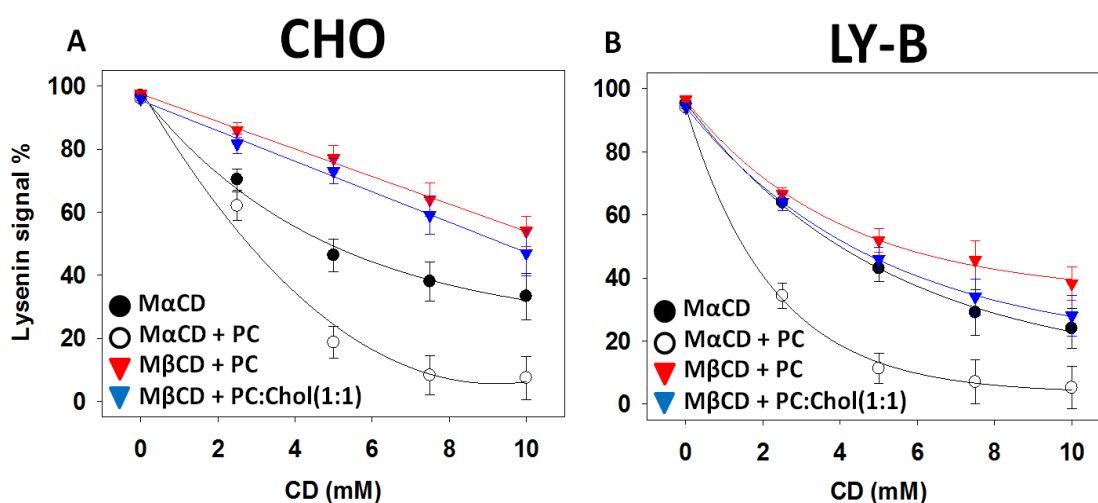


Figure 6.4. Flow cytometry mCherry-lysenin quantification after treating cells with loaded and non-loaded CD. CHO (A) and LY-B cells (B).

PC:SM (1:1)- (Fig. 6.S3) or PC:SM (1:3)- (Fig. 6.S4) loaded M α CD were also used to prove that SM exchange could take place affecting the total SM amount. Figure 6.S3 shows that when 7.5 mM PC:SM (1:1)-loaded M α CD was used, CHO (Fig. 6.S3B) and LY-B (Fig. 6.S3B) cells retained a constant lysenin signal, and that they remained attached to the surface. Nevertheless, when cells were treated with 7.5 mM M α CD pre-loaded with 1 mM (Fig. 6.S4A), 2 mM (Fig. 6.S4B) or 3 mM PC:SM (1:3) (Fig. 6.S4C), cells were detached from the surface, indicating a toxic effect of large SM quantities (Malinsky & Opekarová, 2016). Apart from obtaining cells with a PM depleted in SM, the possibility of performing the insertion of particular SM species makes this technique of interest for studying the properties of SM with defined lipid compositions, as suggested by Li *et al.* (2019).

6.3.4. Plasma membrane GP after CD treatment

The effect of CD on the molecular order of CHO and LY-B cell PM was computed by measuring the GP value of the laurdan fluorophore. For this purpose, CD-treated and non-treated cells were labeled with laurdan and imaged in a two-photon confocal microscopy, prior to image processing with a MATLAB-based software (MathWorks, Natick, MA). Treated LY-B cells had in all cases lower GP values (corresponding to a lower molecular order) than treated CHO cells (Fig. 6.5). Figure 6.5B shows that when cells were treated with PC-loaded M α CD, the occurring changes were similar in CHO and LY-B PM GP values; in both cases PM GP value decreased linearly from 0.52 to 0.44 between 0 and 7.5 mM CD concentrations (PM GP did not decrease further with 10 mM PC-loaded M α CD treatment). Even if the global decrease was similar, statistically significant differences existed between the PM GP values of both cell lines when they were treated with 2.5 mM and 5 mM PC-loaded M α CD, CHO membranes being slightly more disordered than those of LY-B.

2.5 mM or 5 mM PC:Chol (1:1)-loaded M β CD treatments were not enough to produce a decrease in CHO-cell PM GP (Fig. 6.5A), but they did so in LY-B ones (from 0.52 to 0.49 at 2.5 mM and to 0.48 at 5 mM). Nevertheless, when 7.5 mM CD was used, CHO-cell PM GP was also decreased (from 0.52 to 0.48), and from 0.52 to 0.46 in LY-B cells. When cells treated with 10 mM PC-loaded M β CD were laurdan-stained and their fluorescence measured, their GP was markedly decreased to 0.42. Nevertheless, results at this CD concentration may not be fully reliable as cells suffered a large

decrease in viability (Fig. 6.1B). Table 6.S2 summarizes the average PM GP values shown in figure 6.5.

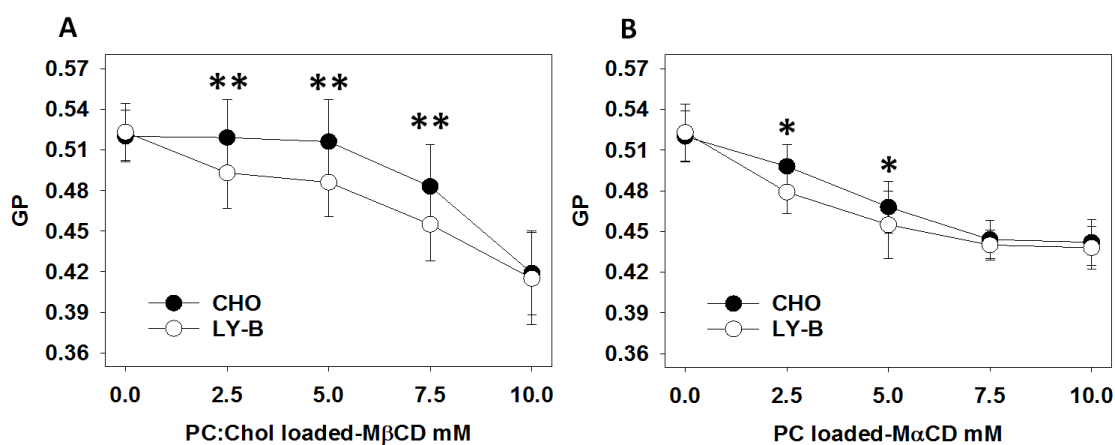


Figure 6.5. Laurdan GP of isolated plasma membrane patches of CD-treated CHO and LY-B cells. GP values after treatment with increasing concentrations of PC:Chol (1:1)-loaded MβCD (A) and PC-loaded MαCD (B). Statistical significance was calculated with ANOVA or Student's t-test, with similar results: (*) $p < 0.05$; (**) $p < 0.01$.

In all previous cases, a concentration of 3 mM MLV was used for CD loading. Incubation with varying MLV concentrations at a constant MαCD concentration of 7.5 mM was also performed in order to estimate the MαCD saturation level (Table 6.S3). Significant differences were not observed when cells were treated with CD pre-incubated with either 1 mM, 2 mM or 3 mM PC MLV. Thus 1 mM MLV appears to be enough for achieving saturation of 7.5 mM MαCD.

Incubation with MαCD loaded with 1, 2, or 3 mM PC:SM (1:1), or PC:SM (1:3), followed by cell treatment and PM GP measurements was also performed. As shown in table 6.S3, there was no significant difference between PM GP values of the non-treated cells (Control MαCD) and those treated with 1, 2, or 3 mM PC:SM (1:1)-loaded MαCD. This suggested that, when a correct SM exchange was performed, membrane packing could be kept constant. Again, as in the case of PC-loaded MαCD, there was no significant difference when using MαCD pre-loaded with either 1, 2 or 3 mM PC:SM (1:1) (Table 6.S3).

Cells were also treated with MαCD pre-loaded with 1, 2 or 3 mM PC:SM (1:3), and PM GP values were larger than the controls (Table 6.S3). Nevertheless, these values are not very meaningful, as cells appeared rounded in microscopy images (Fig. 6.S4), indicating that they were not viable.

6.3.5. Breakthrough forces after CD treatment

AFM-mediated breakthrough forces were measured in PM patches derived from CD-treated cells. Figure 6.6 shows the distribution of the non-treated (control) and treated CHO and LY-B PM patch breakthrough forces. No significant difference was detected between PM breakthrough forces of non-treated CHO (Fig. 6.6A) and LY-B (Fig. 6.6C) cells. Cell treatments with lipid-loaded CD made PM patches more fragile in all measured cases. Average breakthrough forces of PM patches derived from PC-loaded α CD-treated CHO cells was 38% lower than the controls, respectively 6.76 nN (Fig. 6.6A) and 4.22 nN (Fig. 6.6B), while in the case of LY-B the decrease was of 50%, from 7.06 nN (Fig. 6.6D) to 3.51 (Fig. 6.6E). Focusing on cells treated with PC:Chol (1:1)-loaded β CD, the breakthrough force of CHO PM patches was lowered by 25%, from 6.76 nN (Fig. 6.6A) to 5.07 nN (Fig. 6.6C), while the corresponding LY-B values decreased by 43% from 7.06 nN (Fig. 6.6D) to 4.03 nN (Fig. 6.6F).

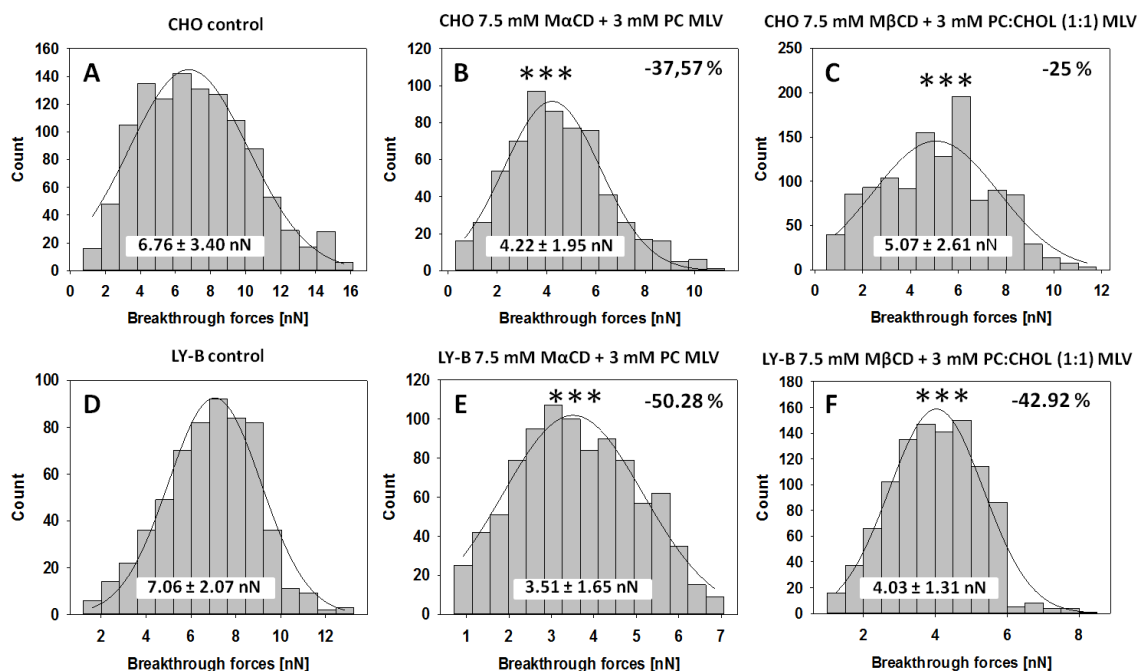


Figure 6.6. Breakthrough forces of PM patches, measured by AFM in the force-spectroscopy mode. Control CHO cells (A). CHO cells treated with 7.5 mM PC-loaded α CD (B). CHO cells treated with 7.5 mM PC:Chol (1:1)-loaded β CD (C). Control LY-B cells (D). LY-B cells treated with 7.5 mM PC-loaded α CD (E). LY-B cells treated with 7.5 mM PC:Chol (1:1)-loaded β CD. Statistical significance was calculated with ANOVA or Student's t-test, with similar results: (***) $p < 0.001$.

In summary, (i) when comparing treated CHO and treated LY-B cells, the PM patch breakthrough forces are lower in the latter case. (ii) PM patches from PC-loaded M α CD-treated cells were more fragile than patches from PC;Chol (1:1)-loaded, M β CD-treated cells. Figure 6.S5 shows overlaying histograms of PM patch breakthrough forces for a proper comparison of the different treatments.

Results of GP and breakthrough forces values are in good agreement. When GP was lowered, indicating membrane lipid disordering (Fig. 6.5), breakthrough forces were correspondingly decreased (Fig. 6.6).

6.3.6. RBC experiments

It is known that human RBC contain a large proportion of Chol in the PM (≈ 45 mol% of total membrane lipid) (Ahyayauch *et al.*, 2018). Taking into account that M α CD and M β CD differ in their affinity for Chol (among other molecules), RBC were treated with non-loaded CD, and their mCherry-lysenin images (Fig. 6.S6), their degree of hemolysis (Fig. 6.S7) and their PM GP values (Fig. 6.S7) were measured. Figure 6.S6 shows that when RBC were treated with 2.5 mM non-loaded M α CD (Fig. 6.S6B), mCherry-lysenin fluorescence emission was greatly decreased. In contrast, RBC treated with an equivalent M β CD concentration (Fig. 6.S6F) showed only a small signal decrease. A minimum of 5 mM M β CD (Fig. 6.S6G) was needed to achieve RBC mCherry-lysenin signal depletion. This confirms that M α CD has a larger capacity for SM extraction than its β counterpart, as seen above for CHO and LY-B cells (Fig. 6.4). It should also be noted that samples treated with 5 mM (or higher) M β CD (Fig. 6.S6G and Fig. 6.S6H) contained after treatment less RBC than samples treated with the same M α CD concentrations (Fig. 6.S6C and 6.S6D), indicating that many cells had been disrupted in the former case.

For more precise measurements, the degree of hemolysis was also measured in combination with the GP value (Fig. 6.S7). There was no significant difference between the degree of hemolysis of non-treated cells, and that of cells treated with 0.5 mM M α - (Fig. 6.S7A) or M β - (Fig. 6.S7B) CD. Nevertheless, a decrease of the GP value from 0.46 to 0.41 in the case of M α CD (Fig. 6.S7A) and from 0.46 to 0.40 (Fig. 6.S7B) in the case of M β CD was measured. With 2.5 mM CD treatment, 16% hemolysis was observed for M β CD (Fig. 6.S7B), while only 4% of the RBC were disrupted with an

equivalent M α CD concentration (Fig. 6.S7A). Treating RBC with larger M α CD concentrations GP was kept constant around 0.38, while hemolysis increased, reaching 70% cell disruption at 10 mM M α CD concentration (Fig. 6.S7A). With M β CD, GP decreased to values around 0.2 with 5 mM M β CD, and remained constant with larger CD concentrations, while hemolysis increased up to 85% with 10 mM M β CD treatment (Fig. 6.S7B). Figure 6.S7C includes a comprehensive data collection of all measured RBC GP and hemolysis values.

6.3.7. Mass spectroscopic measurements

Figure 6.7 shows selected data from the lipidomic analysis of PM patches derived from CD-treated CHO and LY-B cells. The full data are collected in table 6.S4. As a continuation to our previous studies on SL deprivation in CHO and LY-B cells (Monasterio *et al.*, 2021a, 2021b) the CD effects on SM, Cer, and HexCer concentrations have been considered in detail.

The SM fraction was largely decreased when cells were treated with either M α CD or M β CD (Fig. 6.7A). The decrease was higher with M α CD than with M β CD treatment (Fig. 6.7A). In addition, when CD was loaded with lipids other than SM, the decrease was even higher (for both CD types), indicating that lipid exchange was more easily performed than the unidirectional extraction (Fig. 6.7A). This decrease is in accordance with the flow cytometry lysenin-mCherry measurements (Fig. 6.4): in CHO cells, lysenin signal (flow cytometry) and percent SM (mass spectrometry) decreased respectively by 62% and 64% when treated with non-loaded M α CD (71% and 75% for LY-B cells), and by 82% and 80% when treated with PC-loaded M α CD (93% and 90% for LY-B cells). With non-loaded M β CD the corresponding decreases were 36% and 48% in CHO cells (54% and 53% for LY-B cells). The comparable figures for CHO cells treated with PC:Chol (1:1)-loaded M β CD were 59% and 56% (66% and 69% for LY-B cells). These data are summarized in figure 6.S8A.

Ceramide (Cer) is a metabolic product of SM, and an important molecule in stress signaling (Kolesnick *et al.*, 2000; Goñi & Alonso, 2009). According to the data in figures 6.7A and 6.S8A, when cells were treated with M α CD, Cer was decreased in PM patches from both cell lines, but more clearly so in LY-B than in CHO. In addition, when M α CD was loaded with PC, a larger decrease was observed. With the M β CD

treatment, the effect was opposite, Cer was increased in both cell lines (more in LY-B cells). When M β CD was loaded with a PC:Chol (1:1) mixture, the Cer proportion in CHO cell PM was similar to the untreated cells, while it increased in LY-B cells. Cer increases can be related with pre-apoptotic signals. As shown by the viability plots (Fig. 6.1), the LY-B cells started dying when treated with non-loaded M β CD (Fig. 6.1B), indicating that they are more sensitive to CD than the CHO cells. Nevertheless, this viability was partly recovered when the M β CD was loaded with a PC:Chol (1:1) mixture (Fig. 6.1B). Figure 6.S8A shows Cer percentage increases or decreases with respect to non-treated CHO or LY-B cells.

HexCer, a SL at the origin of the biosynthetic pathways for the complex glycosphingolipids, also increased treating cells with both, non-loaded M α CD and M β CD, but more so with M β CD, and especially in LY-B cell PM patches (Fig. 6.7A). After treating cells with loaded CD, HexCer values were in all cases lower than when treating them with non-loaded CD. Again, as mentioned for Cer, this could be related to the generation of pre-apoptotic signals. Since LY-B cells contain a defective SPT enzyme, a homeostatic response is activated, intended to buffer the effects that SM depletion may cause (Monasterio *et al.*, 2021a). Thus, LY-B may be more sensitive to an additional lipid alteration, as is the case of the CD-catalyzed lipid extraction or exchange. In turn, the homeostatic response machinery of LY-B cells may not be as efficient or ready as the CHO one, CHO having a full set of SL-related genes, thus helping them to respond to the CD-induced rapid lipid modulations. Figure 6.S8A shows HexCer percentage increases or decreases with respect to non-treated CHO or LY-B cells.

Taking into account the available CD literature, an overall phospholipid decrease could be expected after treating cells with non-loaded CD, and the decrease should be reverted when the CD were loaded with specific lipid molecules (Ohtani *et al.*, 1989). Nevertheless, statistically significant differences did not exist between the phosphatidylcholine proportions of CD treated and non-treated cell PM patches (Fig. 6.7B). In addition, the existing differences for phosphatidylethanolamine and phosphatidylinositol were not conclusive as they did not follow a clear pattern in both cell lines. Phosphatidylserine however was clearly lowered after cell treatment. Figure 6.S8B shows phospholipid increases or decreases with respect to non-treated CHO or LY-B cells.

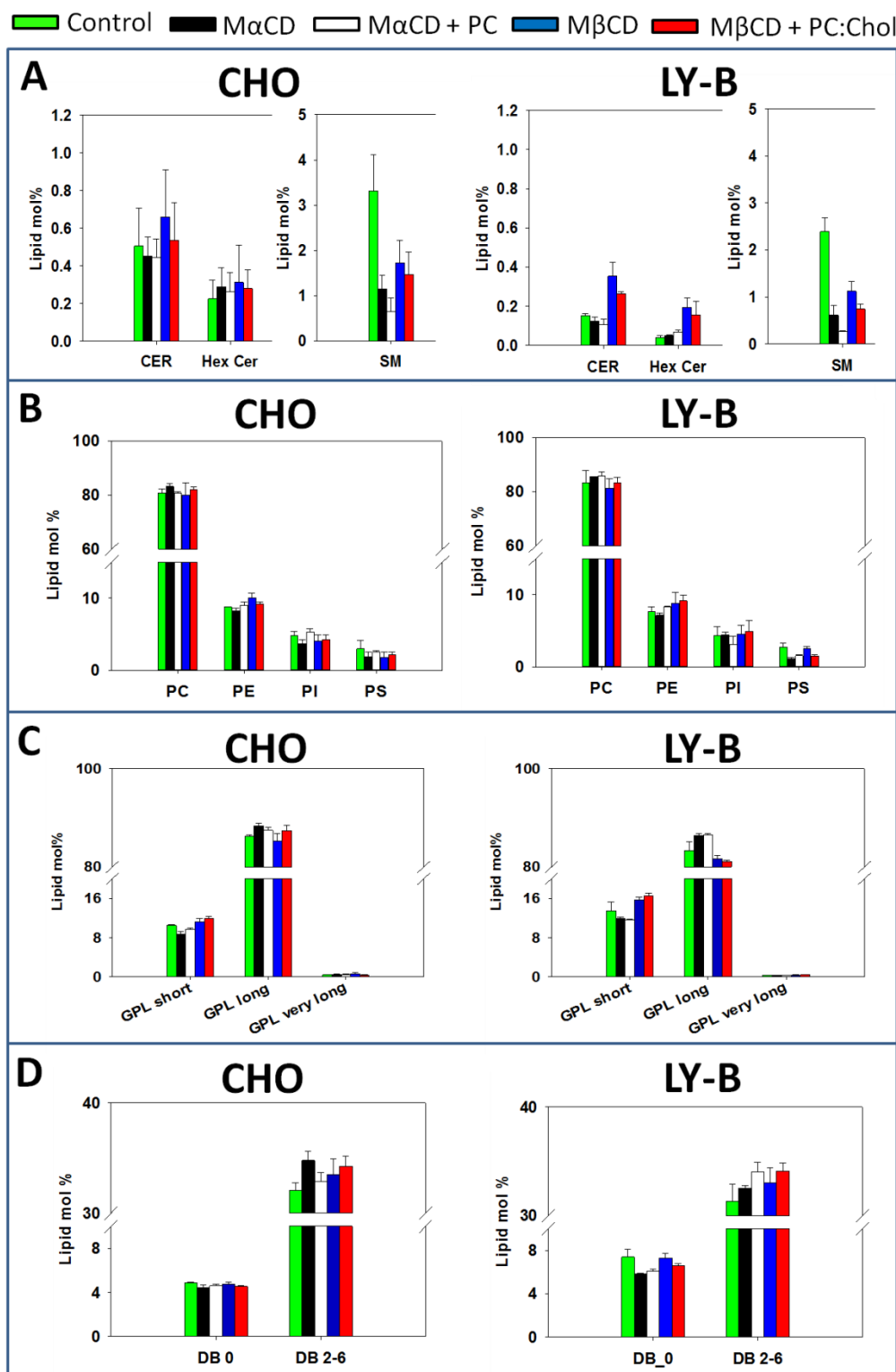


Figure 6.7. Lipidomic analysis of PM patches derived from CD-treated CHO and LY-B cells. Cer, HexCer and SM (A). PC, PE, PI and PS (B). GPL length distribution; short GPL: 30-32 C, long GPL: 34-40 C, very long GPL:42-44 C (C). GPL saturation distribution; no double bonds (DB 0), two – six double bonds per molecule (DB 2-6) (D). Green boxes, control cells; black boxes, cells treated with 7.5 mM non-loaded M α CD; white boxes, cells treated with 7.5 mM PC-loaded M α CD; blue boxes, cells treated with 7.5 mM non-loaded M β CD; red boxes, cells treated with 7.5 mM PC:Chol (1:1)-loaded M β CD. Data in mole% of total lipid extract.

Focusing on glycerophospholipid (GPL) chain-length distribution (Fig. 6.7C), the most relevant fact is that M α CD treatment caused a decrease of short-chain (30-32C) GPL, while the opposite happened with M β CD: short-chain GPL were increased. This may be related to the cavity size of each CD type. M α CD contains a smaller cavity than M β CD (4.7 – 5.3 Å vs. 6.0 – 6.5 Å respectively). M α CD may be less efficient in accommodating large (long-chain) GPL. Conversely, as M β CD has a larger cavity, this may explain the lack of preference for short-chain GPL. Nevertheless, the reason why short-chain GPL were increased after M β CD treatment remains unclear. Figure 6.S8C shows GPL length distribution percentage changes with respect to non-treated CHO or LY-B cells.

Fully saturated GPL were decreased and polyunsaturated ones increased when treating cells with either loaded or non-loaded M β CD and M α CD (Fig. 6.S8D). The opposite occurred with LY-B cells when growing in a SL-deficient medium for 72 h, in which case fully saturated GPL were increased (Monasterio *et al.*, 2021a).

6.4. Concluding Remarks

M α CD and M β CD are remarkably efficient tools for modulating PM lipid composition, in particular for SM depletion. They constitute a significant alternative to more complex methods, such as engineering of lipid metabolic pathways (Dowhan, 2009), or to slower and less specific procedures such as the use of biochemical inhibitors (Adada *et al.*, 2016; Delgado *et al.*, 2006). Cholesterol-specific filipin signal was greatly decreased from CHO cell PM after treatment with non-loaded M β CD. However, PM filipin signal in M α CD-treated cells remained unchanged under those conditions, indicating a clear difference between the respective cholesterol-extraction powers of M α CD and M β CD. In addition, when M β CD was loaded with a PC:Chol mixture, the PM filipin signal was recovered. Among both CD, the β form had a more drastic effect on cell viability as compared to M α CD. Nevertheless, its toxic effect could be greatly buffered when a proper CD loading is used: PC for M α CD and PC:Chol(1:1) for M β CD. According to our biophysical results, values of GP and breakthrough forces were in good agreement. In both cases, values were lowered after treating cells with CD, indicating a more fluid, less stiff membrane. This decrease was larger for cells treated with PC-loaded M α CD than for those treated with PC:Chol (1:1)-loaded M β CD. Flow cytometry and mass spectrometric measurements were also in agreement, both

detecting a loss of SM. In short, M α CD led to a larger SM depletion than M β CD, and CD loading increased the loss of the lysenin signal. Lysenin (flow cytometry) and SM (mass spectrometry) were decreased by respectively 62% and 64% after treatment with non-loaded M α CD (71% and 75% for LY-B cells), and by 82% and 80% when treated with PC-loaded M α CD (93% and 90% for LY-B cells). Decreases of 36% and 48% were measured when CHO cells were treated with non-loaded M β CD (54% and 53% for LY-B cells), and decreases of 59% and 56% were respectively measured when treating CHO cells with PC:Chol (1:1)-loaded M β CD (66% and 69% for LY-B cells).

M α - and M β -CD treatment of RBC helped in understanding the existing differences between the properties of both CD. A similar decrease in laurdan GP values (from 0.46 to 0.40-0.41) and no hemolysis was measured when treating RBC with 0.5 mM M α - or M β -CD. Higher M α CD concentrations did not further decrease GP, but they increased hemolysis. However, treatment with M β CD concentrations >0.5 mM caused a large GP signal decrease, accompanied with a higher hemolysis than the one measured with similar concentrations of M α CD. These differences were probably due to the high Chol extraction caused by M β CD, but not by M α CD. The RBC membrane can act as a simplified model of the plasma membranes of the more complex mammalian nucleated cells, and reflect the CD effects on these structures.

Taking into account the existing differences between the non-loaded and loaded CD, it appears that lipid exchange is more easily performed than the unidirectional lipid extraction. In addition, apart from obtaining cells with SM-depleted PM, the exchange method would also make possible the introduction of particular SM species of interest in the PM, in order to observe their biophysical properties.

6.5. Supplementary Material

Table 6.S1. MS detection conditions for the different lipid classes.

Lipid Class	Standard	Polarity	Mode	m/z ion	Collision Energy
Phosphatidylcholine [M+H] ⁺	DLPC	+	Product ion	184.07	30
Phosphatidylethanolamine [M+H] ⁺	PE31:1	+	Neutral ion loss	141.02	20
Phosphatidylinositol [M-H] ⁻	PI31:1	-	Product ion	241.01	44
Phosphatidylserine [M-H] ⁻	PS31:1	-	Neutral ion loss	87.03	23
Cardiolipin [M-2H] ²⁻	C12SM	-	Product ion	acyl chain	32
Ceramide [M+H] ⁺	C17Cer	+	Product ion	264.34	25
Dihydroceramide [M+H] ⁺	C17Cer	+	Product ion	266.40	25
Hexacylceramide [M+H] ⁺	C8GC	+	Product ion	264.34	30
Hexacyldihydroceramide [M+H] ⁺	C8GC	+	Product ion	266.40	30
Sphingomyelin [M+H] ⁺	C12SM	+	Product ion	184.07	26

Table 6.S2. Laurdan GP values of CHO and LY-B PM after treatment with 3 mM PC:Chol (1:1)-loaded M β CD or PC-loaded M α CD. Data in red correspond to samples in which a severe decrease in cell viability was observed (see Fig. 6.1).

	Control -CD - MLV	Control + PC MLV	Control + PC:Chol(1:1)	+ 2.5 M α CD + PC	+ 2.5 M β CD + PC:Chol(1:1)	+ 5 M α CD + PC
CHO	0.520 \pm 0.019	0.517 \pm 0.013	0.523 \pm 0.016	0.498 \pm 0.016	0.519 \pm 0.028	0.468 \pm 0.019
LY-B	0.523 \pm 0.021	0.515 \pm 0.024	0.516 \pm 0.031	0.479 \pm 0.016	0.493 \pm 0.026	0.455 \pm 0.025
	+ 5 M β CD + PC:Chol(1:1)	+ 7.5 M α CD + PC	+ 7.5 M β CD + PC:Chol(1:1)	+ 10 M α CD + PC	+ 10 M β CD + PC:Chol(1:1)	
CHO	0.516 \pm 0.031	0.444 \pm 0.014	0.483 \pm 0.031	0.442 \pm 0.017	0.419 \pm 0.031	
LY-B	0.486 \pm 0.025	0.440 \pm 0.011	0.455 \pm 0.027	0.438 \pm 0.016	0.415 \pm 0.034	

Table 6.S3. Laurdan GP values of CHO and LY-B PM after treatment with PC- or PC:SM-loaded M α CD. Data in red correspond to samples in which a severe decrease in cell viability was observed (see Fig. 6.1).

Cells and lipids	Control (-M α CD)	7.5 mM M α CD, no lipid	7.5 mM M α CD, 1 mM lipid	7.5 mM M α CD, 2 mM lipid	7.5 mM M α CD, 3 mM lipid
CHO PC	0.520 \pm 0.019	0.491 \pm 0.020	0.454 \pm 0.014	0.451 \pm 0.014	0.444 \pm 0.014
LYB PC	0.523 \pm 0.021	0.487 \pm 0.023	0.452 \pm 0.017	0.442 \pm 0.032	0.440 \pm 0.011
CHO PC:SM (1:1)	0.520 \pm 0.019	0.491 \pm 0.020	0.523 \pm 0.019	0.534 \pm 0.021	0.533 \pm 0.014
LY-B PC:SM (1:1)	0.523 \pm 0.021	0.487 \pm 0.023	0.515 \pm 0.023	0.526 \pm 0.016	0.522 \pm 0.014
CHO PC:SM(1:3)	0.520 \pm 0.019	0.491 \pm 0.020	0.543 \pm 0.015	0.556 \pm 0.032	0.575 \pm 0.008
LY-B PC:SM(1:3)	0.523 \pm 0.021	0.487 \pm 0.023	0.514 \pm 0.032	0.535 \pm 0.024	0.556 \pm 0.017

Table 6.S4. A summary of the various lipid compositions of CHO and LY-B PM after and before loaded or non-loaded $M\alpha$ or $M\beta$ treatment.

<https://drive.google.com/file/d/1SvdF0IFo8-mZYg8CRRfnTL7tZHtB6hMn/view?usp=sharing>

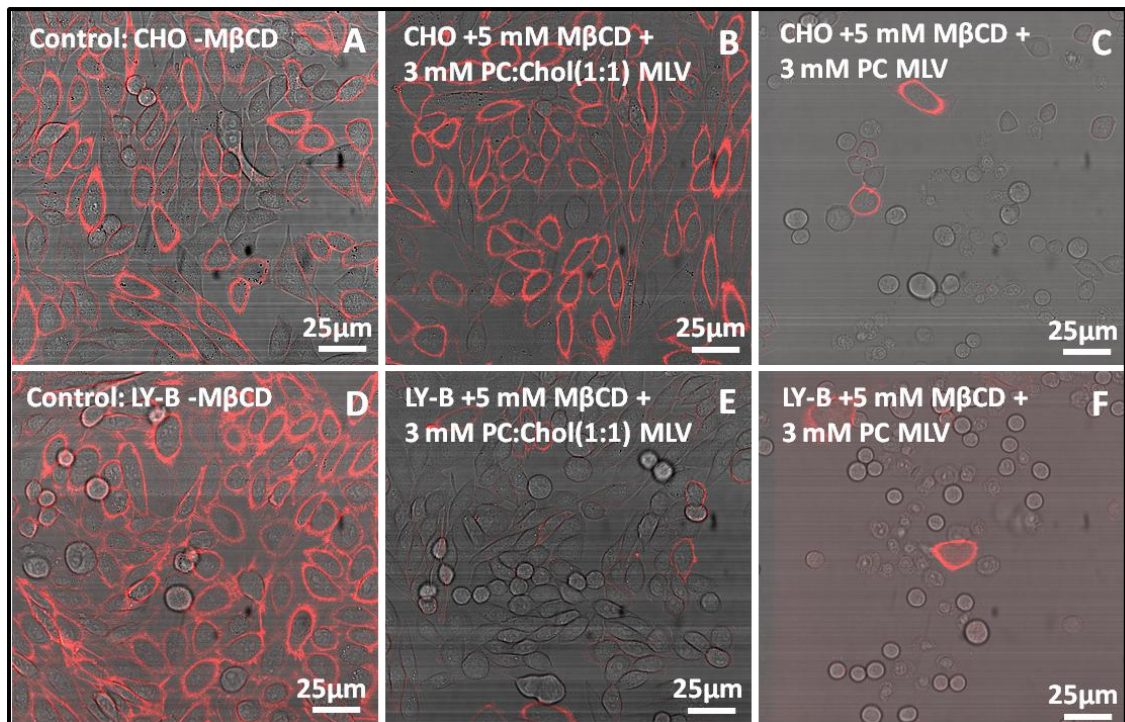


Figure 6.S1. MβCD-treated and lysenin-mCherry-stained CHO and LY-B cell morphology according to PC or PC:Chol(1:1) premixing. CHO control, untreated cells (A), and CHO cells treated with 5 mM MβCD premixed with PC:Chol (1:1) (B) or PC (C) MLV. LY-B control, untreated cells (D), and LY-B cells treated with 5 mM MβCD premixed with PC:Chol (1:1) (E) or PC (F) MLV.

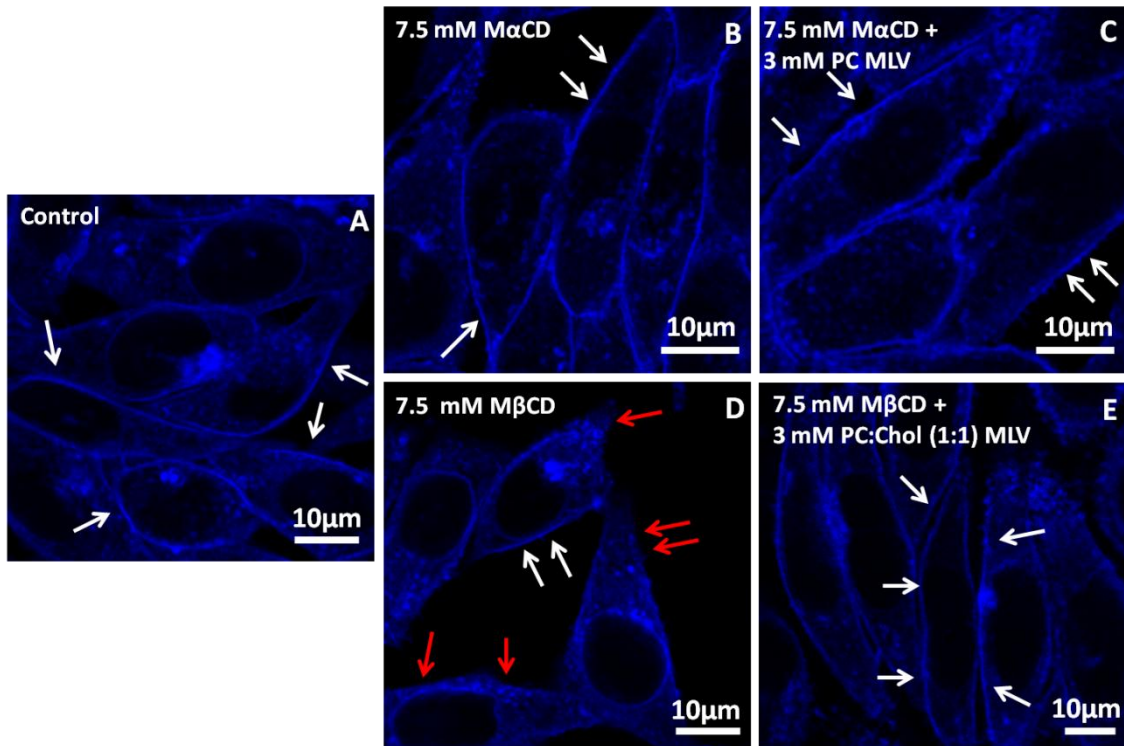


Figure 6.S2. Fluorescence images of CHO cells stained with cholesterol-specific filipin. Control, untreated cells (A). Cells treated with 7.5 mM MαCD (B). Cells treated with 7.5 mM MαCD premixed with PC MLV (C). Cells treated with 7.5 mM MβCD (D). Cells treated with 7.5 mM MβCD premixed with PC:Chol(1:1) MLV (E). White arrows indicate PM with filipin signal, red arrows indicate plasma membrane with only a faint or no filipin signal.

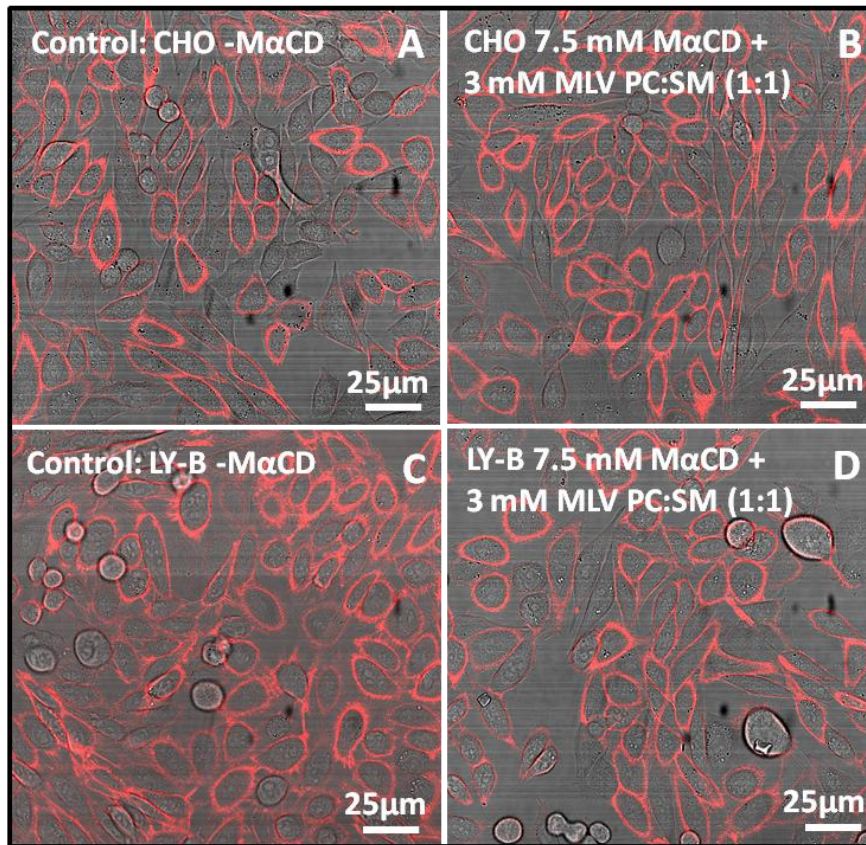


Figure 6.S3. CHO or LY-B cells treated with MαCD preloaded with PC:SM (1:1) and stained with lysenin-mCherry. CHO cells, control (A). CHO cells treated with 7.5 mM preloaded MαCD (B). LY-B cells, control (C). LY-B cells treated with 7.5 mM preloaded MαCD (D)

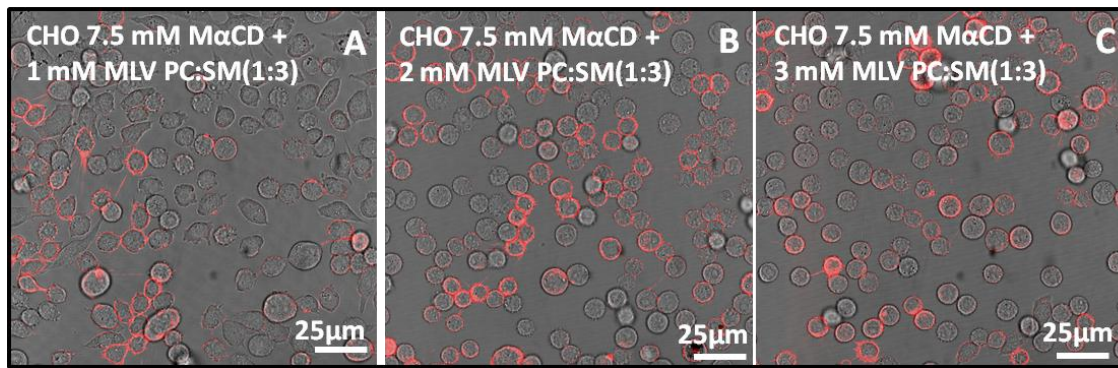


Figure 6.S4. CHO cells treated with 7.5 mM PC:SM (1:3)-loaded α CD and stained with lysenin-mCherry. 1 mM PC:SM (1:3) (A), 2 mM PC:SM (1:3) (B), 3 mM PC:SM (1:3) (C).

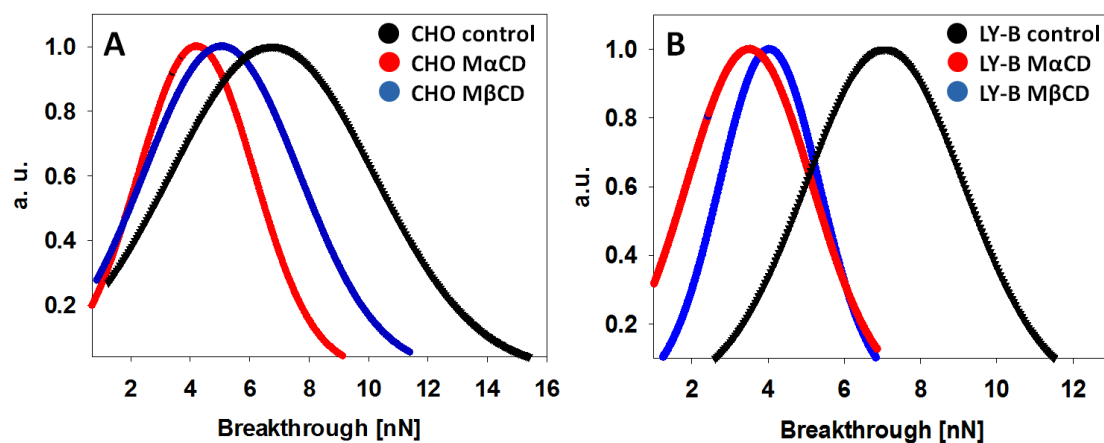


Figure 6.S5. AFM force spectroscopy. Breakthrough force histograms for PM patches of CHO and LY-B cells, treated with loaded or non-loaded CD. CHO cells (A), LY-B cells (B). Black lines, control. Red lines, cells treated with α CD preloaded with PC. Blue line, cells treated with β CD preloaded with PC:Chol.

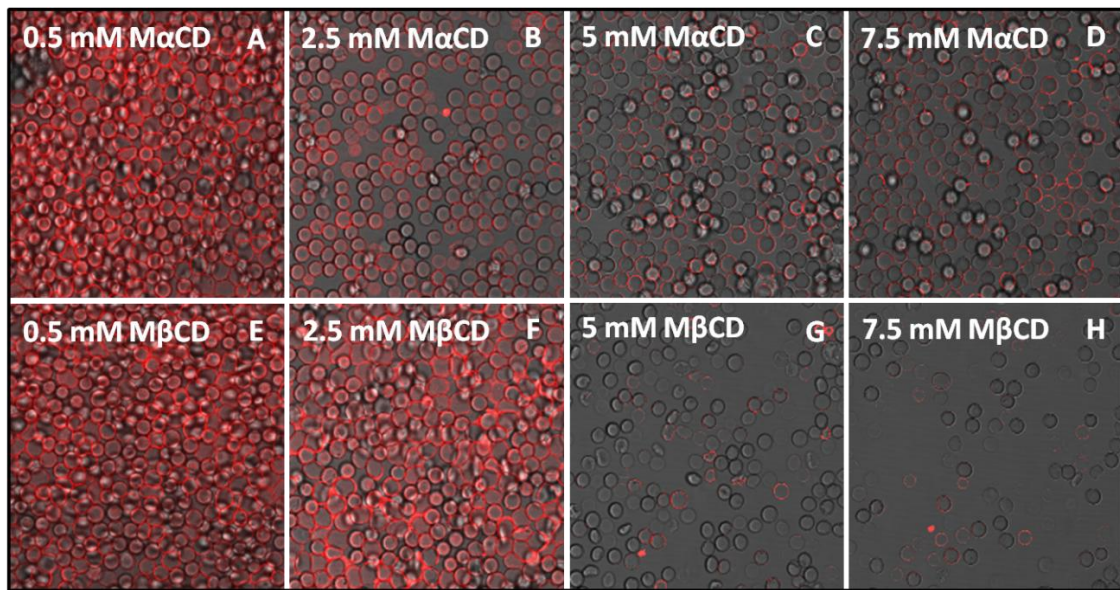


Figure 6.S6. mCherry-lysenin staining of RBC after treating with increasing CD concentrations. 0.5 (A); 2.5 (B); 5 (C) and 7.5 mM (D) MαCD; or 0.5 mM (E); 2.5 mM (F); 5 mM (G) and 7.5 mM (H) MβCD.

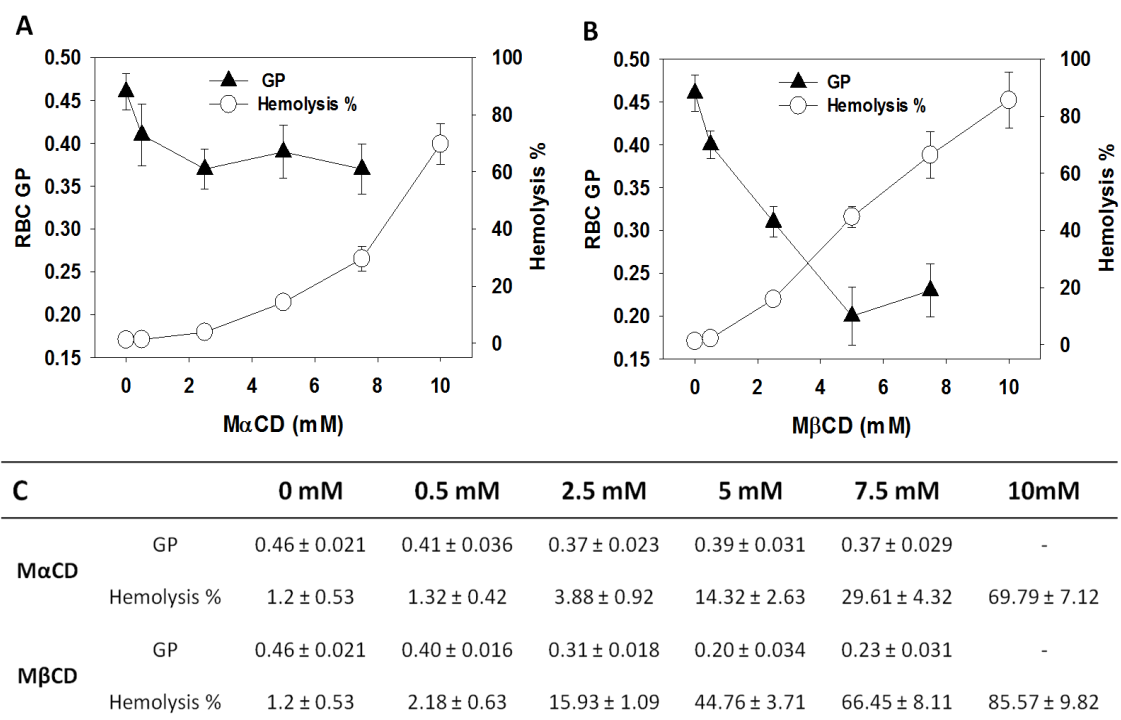


Figure 6.S7. RBC hemolysis and laurdan GP changes after MαCD (A) or MβCD (B) treatment. Values (average ± SD, N = 150) of RBC GP measurements (C).

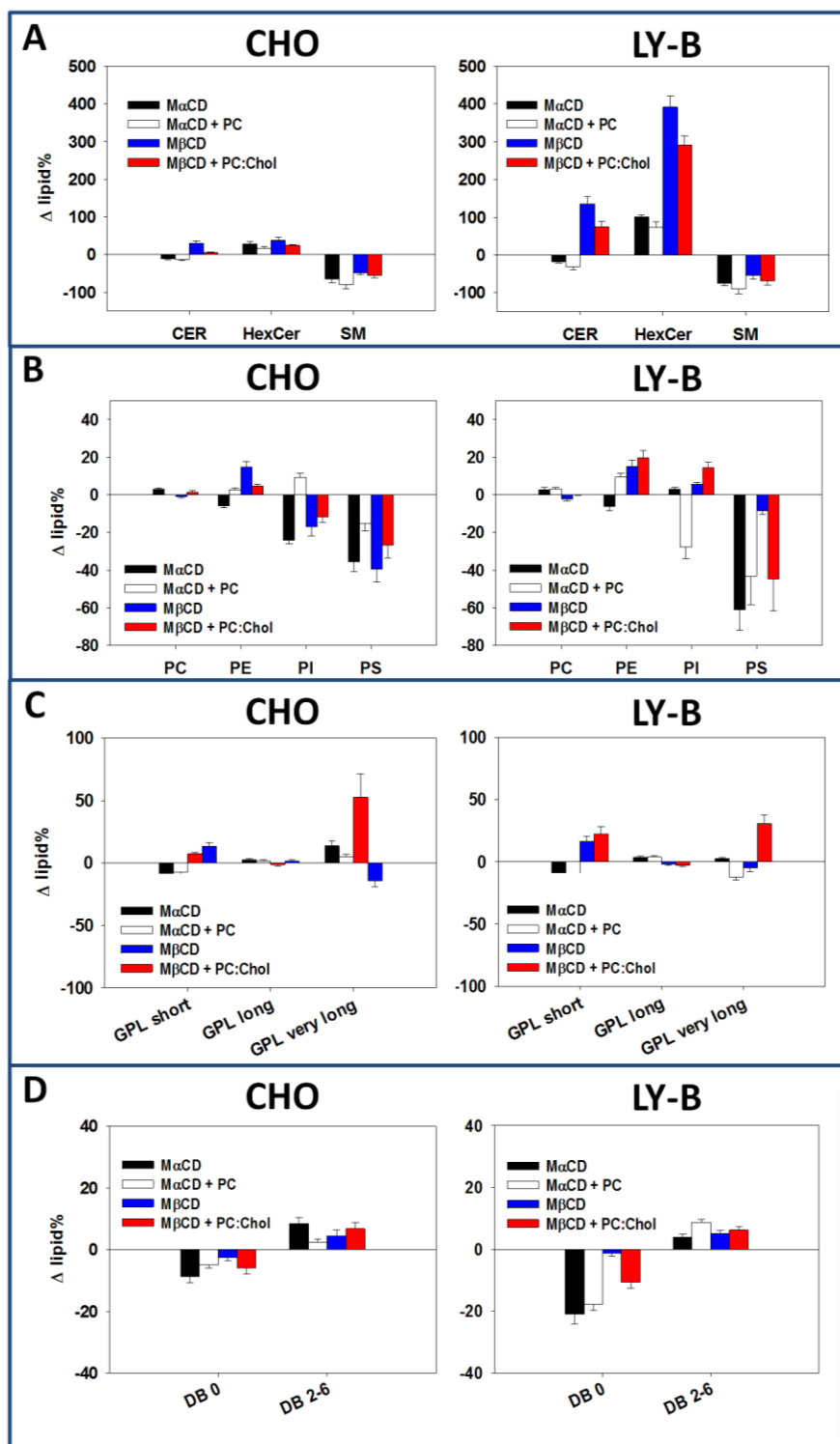


Figure 6.S8. Lipidomic analysis of PM patches derived from CD-treated CHO and LY-B cells. Values correspond to percentage increases or decreases with respect to non-treated CHO or LY-B cells. Cer, HexCer and SM (A), PC, PE, PI and PS (B). GPL length distribution, short GPL: 30-32 C, long GPL: 34-40 C, very long GPL: 42-44 C (C). GPL saturation distribution, zero double bonds (DB 0), two – six double bonds per molecule (DB 2-6) (D). Black boxes, cells treated with 7.5 mM non-loaded MαCD; white boxes, cells treated with 7.5 mM MαCD loaded with PC; blue boxes, cells treated with 7.5 mM non-loaded MβCD; red boxes, cells treated with 7.5 mM MβCD loaded with PC and Chol.

**CHAPTER 7: SPHINGOLIPID
RESTRICTION IN HAP1 CELLS
THAT CONSTITUTIVELY
CONTAIN LOW AMOUNTS OF
SPHINGOLIPIDS**

CHAPTER 7: SPHINGOLIPID RESTRICTION IN HAP1 CELLS THAT CONSTITUTIVELY CONTAIN LOW AMOUNTS OF SPHINGOLIPIDS

7.1. Introduction

For over a half century sphingolipids (SL) have been thought to be important for the stability of cell membranes (Thudichum, 1884; Stoffel, 1971) and much has been learned about the biophysical properties of “simple” SL (Goñi *et al.*, 2014) and “more complex” glycoSL (Maggio *et al.*, 2006). Their biophysical properties vary with the SL class, for instance water solubility decreases from the relatively water-soluble sphingosine-1-phosphate, to ceramides (Cer), the latter being perhaps the least polar/most hydrophobic lipids in biological membranes (Goñi *et al.*, 2014). Certain SL in lipid bilayers undergo lateral phase separation to form microdomains (Chiantia & London, 2013; Goñi *et al.*, 2014). Additional lipids and proteins co-localize with these microdomains where cholesterol (Chol) is often present. Indeed, a special relationship exists between some SL, e.g. ceramides, and Chol because of the mutual displacement observed in liquid-ordered domains (Megha & London, 2004; Garcia-Arribas *et al.*, 2016; Alonso & Goñi, 2018). Moreover, SL affect the accessibility of cholesterol to enzymes (Ibarguren *et al.*, 2010) and cellular efflux (Gulshan *et al.*, 2013), and recent studies have found that sphingomyelin (SM), Cer and Chol are able to coexist in a single ternary gel phase (54:23:23 mol ratio) with intermediate properties between SM/Cer-enriched domains and Chol-driven liquid-ordered phases (García-Arribas *et al.*, 2015). These observations were mostly obtained using model membranes, and they justify the interest of performing parallel biophysical studies on the role of SL in cell membranes. One approach in this direction would be the analysis of membrane properties of cells containing minimal amounts of SL.

Serine palmitoyltransferase (SPT) is the enzyme that catalyzes the key first reaction in the *de novo* SL synthesis pathway. It is composed of at least three different subunits: SPTLC1, SPTLC2, and SPTLC3. SPTLC1 differs clearly from the other two, sharing 21% identity with either SPTLC2 or SPTLC3, while SPTLC2 and SPTLC3 are

≈70% identical among them (Hornemann *et al.*, 2006). Even the precise role of each individual SPT subunit is unknown; cells containing a deficient SPTLC1 lack the enzyme activity (Monasterio *et al.*, 2021a), but SPTLC2 and SPTLC3 appear to be partly redundant (Lone *et al.*, 2020). In previous studies several techniques have been used to obtain SL-restricted cell membranes and study their biophysical properties. A hamster cell line with a defective SPT enzyme [LY-B (Hanada *et al.*, 1998)], derived from the well-known CHO, was used, and cells were grown under limiting conditions of exogenous SL. It was concluded that LY-B cells with depleted SL levels reacted to maintain the native membrane lipid-packing level undergoing a homeostatic response, increasing the proportion of fully saturated glycerophospholipids (GPL) and decreasing the polyunsaturated ones (Monasterio *et al.*, 2021a). Adaptation was only partial as their plasma membrane (PM) was still fragile as compared with the native cells (Monasterio *et al.*, 2021a). In a different line of studies, the SPT inhibitor myriocin was used to block *de novo* SL synthesis in wild-type CHO cells (Monasterio *et al.*, 2021b). Similar results were obtained as with the LY-B cells grown in low-SL medium (Monasterio *et al.*, 2021b). Further, a fast-acting cyclodextrin-mediated CHO and LY-B cell treatment concluded that M α - and M β - cyclodextrins were efficient tools to modulate PM lipid composition, in particular for SM depletion. Data obtained with laurdan fluorescence microscopy and atomic force microscopy were consistent with more fluid, less stiff membranes in partially SM-depleted cells.

In the present study a human SPT-defective cell line, the near-haploid HAP1 SPTLC1(-) strain was used to measure the biophysical properties of its membranes, in comparison with the previous results. The reason for using a near-haploid cell line is that most eukaryotic organisms inherit one genome copy from each parent, thus being diploid. In consequence, deleterious mutations of one of the copies are normally compensated by the other one. In other words, when one allele is altered, the phenotypic consequences are normally buffered by the other allele. To avoid this compensation, a well-known strategy is to use near-haploid cell lines, as found in some human tumors e.g. leukemias (Oshimura *et al.*, 1977; Andersson *et al.*, 1995) or chondrosarcomas (Bovéé *et al.*, 1999). The SPT-defective HAP1-SPT(-) cell line was created as follows: A near-haploid human KBM-7 cell line was isolated and stably grown from a chronic myeloid leukemia patient (Kotecki *et al.*, 1999). This cell line has one copy of every chromosome, except chromosome 8 and a portion of chromosome 15. KBM-7 cells

were reprogrammed to induce pluripotent stem cells (Takahashi & Yamanaka, 2006; Carette *et al.*, 2010) and give rise to a near-haploid fibroblast-like morphology cell line, the HAP1 cell line (Carette *et al.*, 2011). HAP1 cells are adherent and lack the second copy of chromosome 8, but they still have two copies of a fragment of chromosome 15, one of which is fused to chromosome 19 (SPTLC1 gene is located in chromosome 9q21–q22). This HAP1 cells were edited by CRISPR/Cas to contain an 11 bp deletion in exon 4 of the SPTLC1 gene and create a SPT-defective human cell line. In this study, a comparison of membrane biophysical properties between wild type HAP1 and mutated HAP1 SPTLC1(-) cell lines has been performed.

7.2. Materials and Methods

7.2.1. Cell growth

Wild type HAP1 (catalog ID C631, Horizon, Waterbeach, UK) and a SPT-deficient HAP1 cell line, known as HAP1-SPTLC1(-) (catalog ID HZGHC003579c012, Horizon, Waterbeach, UK), were used in this study. HAP1-SPTLC1(-) cell line will be referred to as HAP1-SPT for simplicity. Cells were grown on IMDM (Iscove's Modified Dulbecco's Medium) containing 10% FBS (Fetal Bovine Serum), 100 U/ml penicillin, 100 U/ml streptomycin, and 6 mM glutamine (GlutaMax supplemented) at 37°C and 5% CO₂ humidified atmosphere. All cell culture products were purchased from Thermofisher (Waltham, MA, US).

7.2.1.1. Cell adaptation: Standard vs. SL-deficient (low-FBS) medium

HAP1 and HAP1-SPT cells were adapted to grow in SL-deficient (low-FBS) medium. For this purpose, cells were first seeded in IMDM containing 10% FBS, 100 U/ml penicillin and 100 U/ml streptomycin, and 6 mM glutamine (this medium will be referred to as 'standard medium'). After 24-h cell growth, when a 15-25% confluence was reached, the standard medium was discarded, cells were washed with PBS buffer (137 mM NaCl, 3 mM KCl, 80 mM Na₂HPO₄, 7 mM KH₂PO₄), and IMDM medium containing 0.4% FBS, 100 U/ml penicillin and 100 U/ml streptomycin and 6 mM glutamine was added (this medium will be named 'FBS-deficient' or 'SL-deficient medium'). Cells were grown in the appropriate medium for 24, 48 or 72 h.

7.2.2. Cell growth and viability tests

7.2.2.1. Cell growth

2.65×10^5 cells were seeded in 25 cm² flasks in standard medium and grown for 24 h. Then, the standard medium was discarded, cells were washed twice with PBS, and the appropriate medium (standard or deficient) was added. Cells were grown for 24, 48 or 72 h and quantification was performed by cell counting with a hemocytometer (BioRad TC20 Automated Cell Counter, Hercules, CA).

7.2.2.2. Viability test

Flow cytometry was used to evaluate how the decreased FBS concentration in the medium affected cell viability (Galisteo-González *et al.*, 2020). Cells were stained with Annexin-V-FITC and propidium iodide as indicated in the instructions manual of the annexin V-FITC detection kit (CalbioChem, Darmstadt, Germany) and fluorescence was measured using a FACS Calibur flow cytometer (Becton-Dickinson, Franklin Lakes, NJ) as in Ahyayauch *et al.* (2018). Annexin V-FITC fluorescence intensity was measured in fluorescence channel FL-1 with $\lambda_{\text{ex}} = 488$ nm and $\lambda_{\text{em}} = 530$ nm, while FL-3 was used for propidium iodide detection, with $\lambda_{\text{ex}} = 532$ nm and $\lambda_{\text{em}} = 561$ nm. All measurements were performed in triplicate. Data analysis was performed using Flowing Software 2.

7.2.3. Sample preparation

Intact cells (whole cells), two different PM preparations (giant plasma membrane vesicles, known as GPMV or blebs, and PM patches) and SUV or GUV formed with whole-cell lipid extracts were used.

7.2.3.1. PM preparations

PM preparations were obtained as described in Monasterio *et al.* (2020). Briefly, GPMV formation was induced adding the GPMV formation reagent [freshly prepared 2 mM dithiothreitol, 25 mM paraformaldehyde in GPMV buffer (2 mM CaCl₂, 10 mM HEPES, 150 mM NaCl, pH 7.4)] to T25 flasks with cells at confluence. Cells were incubated for 1 h at 37°C. After incubation, the GPMV-containing fluid was collected from the flasks and centrifuged at 14,000 xg for 20 min. Supernatant was discarded and

several washing and centrifugation steps were conducted to remove traces of dithiothreitol and paraformaldehyde. Finally, the GPMV were resuspended in 500 μ l GMPV buffer (Manni *et al.*, 2015).

PM patches were isolated by a modification (Monasterio *et al.*, 2020) of the protocol described by Bezrukov *et al.* (2009). In summary, cells were seeded at approximately 50% confluence and incubated for 2 h so that they adhered to the support. After incubation, 2 washing steps were performed using cold TBS (Tris Buffer Saline: 150 mM NaCl, 25 mM Tris-HCl, 2 mM KCl) to discard non-attached cells. Then, cold distilled water was added for 2 min to induce cell swelling. Mechanical cell disruption was achieved using a pressure stream from a 20-ml syringe coupled to a 19X1-1/2(TW)A needle. In the process, intracellular contents were released, while PM stayed attached to the support. Several washing steps were performed to discard the released intracellular contents. Purification quality was checked using Di-4-ANEPPDHQ ($\lambda_{ex} = 465$ nm, $\lambda_{em} = 635$ nm) as a general fluorescent stain, together with organelle-specific fluorophores as described in Monasterio *et al.* (2020). Images were taken in a Leica TCS SP5 II microscope (Leica Microsystems GmbH, Wetzlar, Germany) at room temperature with ImageJ software. The fluorescence intensities of the various markers were comparatively measured in PM patches and intact cells, so that specific organelle contamination could be estimated.

7.2.3.2. Whole cell lipid extract

Lipid extraction was performed following the method used in Ahyayauch *et al.* (2018). Briefly, cell pellets were first dispersed in aqueous perchloric acid (60% v/v), then centrifuged at 14,000 \times g for 15 min, and the supernatant was discarded. Pellets were resuspended in 2.5 ml chloroform:methanol (2:1, v/v) and samples were mixed for 15 min. Then, 5 ml cold 0.1 mM HCl was added to the mixture. After homogenizing, samples were centrifuged at 1,700 \times g for 20 min. Supernatants were discarded while the lipid-containing organic phase remained in the bottom layer. Phospholipid concentration was assayed as inorganic phosphorus after acid digestion.

7.2.3.3. GUV formation

GUV were formed in a PRETGUV 4 chamber supplied by Industrias Técnicas ITC (Bilbao, Spain) using an electroformation method (Montes *et al.*, 2010), modified from Angelova and Dimitrov (1986).

7.2.3.3. SUV formation

The sample was kept under vacuum for 2 h to remove solvent traces and the lipids were swollen in PBS buffer. SUV were obtained by sonication of the swollen lipid suspensions with a probe-type Soniprep 150 sonicator (MSK, London, U.K.) for 10 min, in 10-s on, 10-s off intervals.

7.2.4. SM quantification with lysenin

7.2.4.1. Lysin-mCherry expression and purification

The non-toxic monomeric C-terminal domain of the SM-specific toxin, NT-lysenin, was expressed and purified as described by Carquin *et al.* (2014). Briefly, the expression plasmid pET28/lysenin encoded NT-lysenin as a fusion protein with an N-terminal 6xHis-tag followed by the monomeric red fluorescent protein mCherry. The plasmid was expanded in *Escherichia coli* BL21 (DE3) and the recombinant protein was expressed in lysogeny broth (LB) medium at 16°C for 72 h in the presence of 0.4 mM isopropyl β -D-thiogalactoside. Bacterial extracts were prepared as described (Maliyekal *et al.*, 2006) and the recombinant protein was purified using an Ni-NTA Superflow cartridge (Qiagen, Hilden, Germany) and eluted with imidazol (Veiga-da-cunha *et al.*, 2012). Fraction analysis by SDS-PAGE revealed recombinant NT-lysenin with the expected size (45 kDa). The most enriched fractions were pooled, concentrated, and desalted. The aliquots were stored in 20 mM NaCl and 25 mM Hepes pH 7.2 and 5% glycerol at -80°C. Protein concentration was calculated by measuring absorbance at 280 nm.

7.2.4.2. SM staining and quantification with lysenin-mCherry

Whole cells and PM patches containing SM were stained with lysenin-mCherry, and visualized using a confocal microscopy Nikon D-ECLIPSE C1 (Nikon, Melville, NY). In whole cells the mCherry signal was also quantified using a FL-3 FACS Calibur

flow cytometer (Becton-Dickinson, Franklin Lakes, NJ) with $\lambda_{\text{ex}} = 532$ nm and $\lambda_{\text{em}} = 561$ nm.

For sample visualization, cells were seeded in glass-bottom dishes and grown as above. PM patches were first stained with 100 μM NBD-PE as a control for all membrane staining. A washing step was performed with PBS, and lysenin-mCherry was added at 100 μM . For flow cytometry analysis, cells were stained in suspension at a final concentration of 100 μM lysenin-mCherry.

7.2.5. Mass spectroscopic analysis

Mass spectroscopic analysis was performed essentially as described in Monasterio *et al.* (2020). A methodological summary follows.

7.2.5.1. Sample treatment

Lipid extraction was performed using a modified methyl *tert*-butyl ether (MTBE) protocol (Guri *et al.*, 2017). Briefly, cells were washed with cold PBS and scraped off in 500 μl cold PBS on ice. The suspension was transferred to a 2-ml tube in which it was spun down at 3200 rpm for 5 min at 4°C. After removing the PBS, samples were stored at -20°C or directly used for further extraction. GPMV and PM patch samples were prepared as previously mentioned. Then, 360 μl methanol was added and vortexed. A mixture of lipid standards (Table 7.1) was added and samples were vortexed for 10 min at 4°C using a Cell Disruptor Genie (Scientific Industries, Inc., Bohemia, NY, US). MTBE (1.2 mL) was then added and the samples were incubated for 1 h at room temperature with shaking (750 rpm). Phase separation was induced by adding 200 μl H₂O. After 10 min incubation at room temperature, the sample was centrifuged at 1,000 $\times g$ for 10 min. The upper (organic) phase was transferred to a 13-mm screw-cap glass tube and the lower phase was extracted with 400 μl artificial upper phase [MTBE/methanol/water (10:3:1.5, v/v/v)]. The two upper phases were combined and the total lipid extract was divided into 3 equal aliquots (one for phospholipids (TL), one for sterols (S) in 2-mL amber vials, and one for sphingolipid (SL) detection in a 13-mm glass tube) and dried in a Centrivap at 50°C or under a nitrogen flow. The SL aliquot was deacylated by methylamine treatment (Clarke method) to remove glycerophospholipids. 0.5 mL monomethylamine reagent [MeOH/H₂O/*n*-butanol/methylamine solution (4:3:1:5 v/v)] was added to the dried lipid, followed by

sonication (5 min). Samples were then mixed and incubated for 1 h at 53°C and dried (as above). The monomethylamine-treated lipids were desalted by n-butanol extraction. 300 µl H₂O-saturated n-butanol was added to the dried lipids. The sample was vortexed, sonicated for 5 min and 150 µl MS-grade water was added. The mixture was vortexed thoroughly and centrifuged at 3200 xg for 10 min. The upper phase was transferred to a 2-mL amber vial. The lower phase was extracted twice more with 300 µl H₂O-saturated n-butanol and the upper phases were combined and dried (as above).

7.2.5.2. Glycerophospholipid and sphingolipid detection with a Triple Quadrupole Mass Spectrometer

TL and SL aliquots were resuspended in 250 µl chloroform/methanol (1:1 v/v) (LC-MS/HPLC grade) and sonicated for 5 min. The samples were pipetted in a 96-well plate (final volume = 100 µl). The TL were diluted 1:4 in negative-mode solvent (chloroform/methanol (1:2) + 5 mM ammonium acetate) and 1:10 in positive-mode solvent (chloroform/methanol/water (2:7:1 v/v) + 5 mM ammonium acetate). The SL were diluted 1:10 in positive-mode solvent and infused onto the mass spectrometer. Tandem mass spectrometry for the identification and quantification of sphingolipid molecular species was performed using Multiple Reaction Monitoring (MRM) with a TSQ Vantage Triple Stage Quadrupole Mass Spectrometer (ThermoFisher Scientific, Waltham, MA) equipped with a robotic nanoflow ion source, Nanomate HD (Advion Biosciences, Ithaca, NY). The collision energy was optimized for each lipid class. The detection conditions for each lipid class are listed below (Table 7.1). Cer species were also quantified with a loss of water in the first quadrupole. Each biological replica was read in 2 technical replicas (TR). Each TR comprised 3 measurements for each transition. Lipid concentrations were calculated relative to the relevant internal standards and then normalized to the total lipid content of each lipid extract (mol %).

7.2.6. Gas chromatography–mass spectrometry for cholesterol assay

Lipid extracts were analyzed by GC-MS as described previously (Guan *et al.*, 2010). Briefly, samples were injected into a VARIAN CP-3800 gas chromatograph equipped with a FactorFour Capillary Column VF-5ms 15 m × 0.32 mm i.d., DF = 0.10, and analyzed in a Varian 320 MS triple quadrupole with electron energy set to –70 eV at 250°C. Samples were applied to the column oven at 45°C, held for 4 min, then raised

to 195°C (20°C/min). Sterols were eluted with a linear gradient from 195°C to 230°C (4°C/min), followed by rising to 320°C (10°C/min). Cholesterol was identified by its retention time (compared with an ergosterol standard) and fragmentation patterns, which were compared with the NIST library.

7.2.7. Quantitation of lipids per cell

An estimate of the amounts of lipids per cell, or per weight protein, was obtained as follows. Szelióva *et al.* (2020) measured the average dry weight of CHO cells as 264 pg/cell. Alberts *et al.* (1994) indicated that the mammalian cell contained 10 dry wt% phospholipids and 7 dry wt% other lipids. Taking into account that HAP1 cells are 2.53 times smaller in volume than CHO cells, dry weight of HAP1 cells was estimated as 104 pg/cell. Moreover, the average amount of protein per cell was measured experimentally with the BCA protein assay. Cell numbers were counted with a hemocytometer. From the above data, and knowing from MS analysis the concentration of a given lipid in a sample, the amount of such lipid per cell and per wt protein could be estimated.

7.2.8. Laurdan General Polarization

Laurdan is a fluorescence polarity probe whose emission undergoes a spectral shift due to the reorientation of water molecules in the glycerol backbone region of the membrane, and this shift can be correlated to the lipid phase (Krasnowska *et al.*, 1998). In the gel phase, when little water is present, laurdan maximum emission is around 440 nm, whereas in the liquid crystalline phase the spectrum is red shifted to around 490 nm. Intact cells, PM preparations and model membranes formed from whole cell lipid extracts have been used to compare the laurdan fluorescence of HAP1 and HAP1-SPT cells grown in standard and deficient media. Fluorescence microscopy imaging and spectrofluorometric analysis have been performed for laurdan fluorescence characterization.

7.2.8.1. Confocal microscopy

For intact cells, cells grown in glass-bottom dishes were stained with 5 μ M laurdan (Molecular Probes, Eugene, OR) for 5 min. Several washes were performed with PBS before cells were visualized. PM patches were formed as previously explained

and stained with 5 μM laurdan. GPMV were stained with 5 μM laurdan and transferred to polylysine-coated glass-bottom dishes (MatTek, Ashland, OR). Vesicles were left to sediment for 3 h before visualization (Manni *et al.*, 2015). For GUV, 0.2 mM lipid extracts in chloroform:methanol (2:1, v/v) were mixed with 0.01 mM laurdan. 3 μl of the lipid stocks were added onto the surface of Pt electrodes and solvent traces were removed under high vacuum for at least 2 h. The Pt electrodes were then covered with 400 μl of 300 mM sucrose buffer and the Pt wires were connected to an electric wave generator (TG330 function generator, Thurlby Thandar Instruments, Huntington, UK) under alternating current field conditions (10 Hz, 2.5 VRMS for 2 h) at 37°C. After GUV formation, the chamber was placed on an inverted confocal fluorescence microscope for GUV visualization.

7.2.8.2. Image acquisition and analysis

A Leica TCS SP5 II microscope (Leica Microsystems GmbH, Wetzlar, Germany) was used for image acquisition. A 63x water-immersion objective (numerical aperture NA = 1.2) was used and samples were imaged at 512 x 512 pixel and 400 Hz per scanning line. Equatorial planes were imaged to avoid photoselection effects. A pulsed titanium-sapphire (Mai-Tai Deepsee, Spectra-Physics) laser tuned at 780 nm was used for two-photon imaging of laurdan-labeled samples. Fluorescence emission was collected by non-descanned (NDD) hybrid detectors, as they offer higher sensitivity compared to descanned photomultipliers. The blue edge of the emission spectrum was collected by NDD 1 at 435 ± 20 nm and the red edge by NDD 2 at 500 ± 10 nm. Irradiance at the sample plane was $\approx 500 \text{ GW}\cdot\text{cm}^{-2}$ for two-photon excitation (Parasassi & Gratton, 1997).

Generalized polarization (GP) value of samples was calculated using a MATLAB (MathWorks, Natick, MA, US) based software. Images were smooth in each channel with 2 pixel averaging, and the GP value was calculated using the following equation (Carravilla *et al.*, 2015):

$$\text{GP} = \frac{I_B - G \cdot I_R}{I_B + G \cdot I_R}$$

where I_B is the intensity collected by NDD 1, I_R is the intensity collected by NDD 2, and G is the correction factor. The G factor is calculated measuring the GP value of the

same fluorophore concentration used in sample staining, dissolved in this case in pure DMSO (Owen *et al.*, 2012). In whole cell images, the region of interest, i.e. the PM, was selected when required.

7.2.8.3. Fluorescence spectroscopic analysis

SUV formed with whole cell lipid extracts were measured in a spectrofluorometer. Samples (82.5 μM lipid concentration) were labeled with 0.75 μM laurdan. For this purpose lipid extracts in chloroform:methanol (2:1) were mixed with laurdan and the solvent was evaporated to dryness under a stream of N_2 . Then, the sample was kept under vacuum for 2 h to remove solvent traces and the lipids were swollen in buffer (NaCl 150 mM, Hepes 25 mM, pH 7.4). Sonicated SUV were obtained as described above and fluorescence measurements were performed using a QuantaMaster 40 spectrofluorometer (Photon Technology International, Lawrenceville, NJ, US) (Santis *et al.*, 2018).

7.2.9. AFM

Contact mode AFM imaging has been used to study bilayer topography, looking for possible lateral segregation effects through bilayer thickness analysis. A NanoWizard II AFM (JPK Instruments, Berlin, Germany) was used to perform topographic measurements under contact mode scanning (constant vertical deflection). For measurements, the AFM was coupled to a Leica microscope and mounted onto a Halcyonics Micro 40 antivibration table (Halcyonics, Inc., Menlo Park, CA) and inside an acoustic enclosure (JPK Instruments, Berlin, Germany) (Monasterio *et al.*, 2017). V-shaped MLCT Si_3N_4 cantilevers (Bruker, Billerica, MA, US) were used, with nominal spring constants of 0.1 or 0.5 N/m. Sample thickness was estimated by cross-section height analysis (García-Arribas *et al.*, 2015).

7.2.9.1. Force Spectroscopy

V-shaped MLCT Si_3N_4 cantilevers with nominal spring constants of 0.1 or 0.5 N/m were individually calibrated in a lipid-free mica substrate in assay buffer using the thermal noise method. After proper bilayer area localization by means of AFM topography and direct epifluorescence microscopy, force spectroscopy was performed at a speed of 1 $\mu\text{m/s}$. Force steps were determined for each of the indentation curves as

reproducible jumps within the extended traces. At least three independent sample preparations were scanned for each case and 50-100 curves were measured in each sample.

Topographic images and force spectroscopy analysis of PM patches and supported planar bilayers (SPB) formed from whole cell lipid extracts, and force spectroscopy analysis of GPMV were performed. GPMV topographic observations could not be performed for experimental reasons; these structures would not flatten on the mica for AFM examination.

SPB were prepared on high V-2 quality scratch-free mica substrates (Asheville-Schoonmaker Mica Co., Newport News, VA, US). 180 μL assay buffer containing 3 mM CaCl_2 was added onto a 1.2 cm^2 freshly cleaved mica substrate mounted onto a BioCell (JPK Instruments, Berlin, Germany). Then, 80 μL 0.4 mM SUV formed with HAP1 or HAP1-SPT sonicated lipid extract was added on top of the mica. BioCell temperature was gradually increased (5°C every 5 min) up to 80°C. Vesicles were let to adsorb and extend for 30 min keeping the sample temperature at 80°C. Samples were left to equilibrate for 30 min at room temperature before performing five washing steps with non- CaCl_2 buffer in order to discard non-adsorbed vesicles and remove the remaining Ca^{2+} cations (Monasterio *et al.*, 2017). Isolated PM patches for force spectroscopy were prepared as previously described (Bezrukov *et al.*, 2009; Monasterio *et al.*, 2020), this time using polylysine-coated mica slips instead of glass-bottom dishes. GPMV were first stained using Di-4-ANEPPQHD to allow detection on the mica slip. Then, samples were left for 3 h to sediment over the polylysine-coated mica slip before AFM measurements were performed.

7.3. Results

7.3.1. Cell growth

The only SL source for the HAP1-SPT (SPT-defective) cell line would be the FBS present in the growth medium. HAP1-SPT cells cannot *de novo* synthesize SL, although they can assimilate and metabolize them from the medium. Thus, SL depletion could be accomplished by decreasing FBS concentration in the growth medium, in order to characterize the biophysical effects of a SL deficit in cell membranes. Cell adaptation to a SL-depleted medium was conducted as in Monasterio *et al.* (2021a).

HAP1 (wild type) and HAP1-SPT cell integrity, when grown in SL-deficient medium, was assessed by measuring cell growth and viability. For this purpose, cells were grown in media containing different FBS concentrations for 24 h (Fig. 7.1A), 48 h (Fig. 7.1B), or 72 h (Fig. 7.1C), in order to establish the optimum conditions (FBS concentration and timing) for performing the desired membrane biophysical measurements.

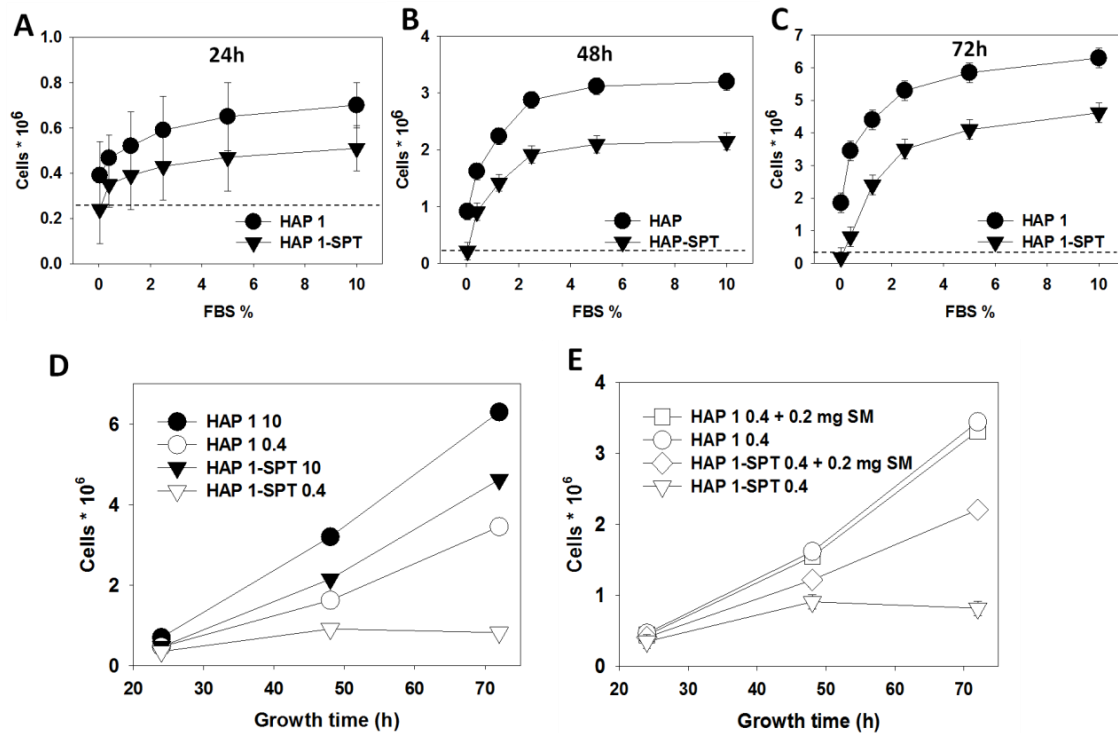


Figure 7.1. HAP1 and HAP1-SPT cell growth. (A-C) HAP1 and HAP1-SPT cell numbers as a function of FBS concentration in the culture medium. Growth time: (A) 24 h, (B) 48 h, (C) 72 h. (D, E) HAP1 and HAP1-SPT cell growth as a function of time in (D) standard or deficient medium, or (E) deficient medium with or without SM supplementation. (Seeded cells: 2.5×10^5). Average values \pm S.D. ($n = 3$). Symbols are often larger than the error bars.

Cell counts were performed using a BioRad TC20 hemocytometer. Figures 7.1A-C show that HAP1 and HAP1-SPT produced different numbers of cells even if standard medium (containing 10% FBS) was used. The number of wild-type HAP1 cells was highest at all measured times, indicating that they divided faster than the mutated HAP1-SPT. This differs from what occurred with CHO and LY-B cells, whose cell growth did not differ when they were grown in standard medium (Monasterio *et al.*, 2021a).

As seen in figures 7.1A-C, the different degrees of SL limitation influence growth; cell growth increased gradually from the lowest FBS-concentration containing medium (0.04% FBS), to the standard medium (10% FBS). To determine the lowest FBS concentration allowing cell growth, the experiments shown in figures 7.1A-C were performed. When 0.04% FBS, i.e. the minimum FBS concentration allowing growth of CHO cells, was used, the HAP1-SPT cell number was below the dashed line at all measured times: 24 h (Fig. 7.1A), 48 h (Fig. 7.1B) and 72 h (Fig. 7.1C), indicating that cells were dying under these conditions (dashed line in figures 7.1A-C corresponds to the seeded cells at t_0 : $2.5 \cdot 10^5$ cells). Thus, it was concluded that the previously used low-FBS medium for CHO and LY-B cell adaptation (0.04%) (Monasterio *et al.*, 2021a), was inadequate for HAP1 or HAP1-SPT growth.

When 0.4% FBS-containing medium was used, the HAP1-SPT cell number was above the dashed line after 24 h (Fig. 7.1A) and 48 h (Fig. 7.1B). Nevertheless, a clear decrease was observable between 48 h (Fig. 7.1B) and 72 h (Fig. 7.1C), indicating that HAP1-SPT cells were dying when grown beyond 48 h in the 0.4%-FBS medium. This phenomenon can be comparatively observed in figure 7.1D, where cell counts of HAP1 and HAP1-SPT as a function of time, in standard (10% FBS) and deficient (0.4% FBS) media, are shown. After analyzing all growth data, it was concluded that a maximum of 48 h in the 0.4%-FBS medium was the most suitable condition for the study of the putative changes in biophysical properties that the HAP1-SPT cell line could undergo as a consequence of SL depletion in their membranes.

To ascertain that the poor cell growth at low FBS concentrations was indeed due to a lack of SL, it was tested whether HAP1-SPT cells were able to reach the full cell growth when the SL-deficient medium was supplemented with SL. For this purpose, equimolar mixtures of egg PC and SM were sonicated in fresh growth medium and added to the culture flasks (0.2 mg/5 ml; $\approx 80 \mu\text{M}$ SM). Figure 7.1E, in which the time-course of cell growth in SL-deficient medium supplemented with SM can be seen, shows that statistically significant differences existed between HAP1-SPT cell growth using non-supplemented and SM-supplemented deficient media (Fig. 7.1E). The number of cells was higher when using SM-supplemented medium for 48 h, and cells continued dividing at least for the first 72 h (Fig. 7.1E). On the contrary, significant differences did not exist when adding SM supplementation to the wild type HAP1 cells (Fig. 7.1E).

In summary, growth of the SPT-defective HAP1-SPT cell line differed from the wild type HAP1, not only when grown in deficient medium [as occurred with the LY-B vs. CHO cell line (Monasterio *et al.*, 2021a)], but also in standard medium (Fig. 7.1D). In addition, HAP1-SPT cells were more sensitive than LY-B cells to the medium containing low FBS, as they required tenfold the FBS concentration needed by the LY-B cells [0.4% vs. 0.04% (Monasterio *et al.*, 2021a)] to continue dividing. Even under these conditions, HAP1-SPT only divided for the first 48 h, while LY-B continued dividing for at least 96 h (Monasterio *et al.*, 2021a).

7.3.2. Viability

The possible effect of growing cells in a SL-deficient medium on cell viability was tested using the Annexin-V-FITC/propidium iodide staining kit. Flow-cytometry measurements demonstrated that, despite the low cell growth (Fig. 7.1), 75% of HAP1-SPT cells grown in SL-deficient medium for 48 h (Fig. 7.S1F), and 81% of those grown for 24 h (Fig. 7.S1E), remained viable. Statistically significant differences did not exist when compared with the control, grown in standard medium (82%; Fig. 7.S1D). With the HAP1 cell line, 86% of the cells grown in standard medium (Fig. 7.S1A), 84% of those grown with 0.4% FBS medium for 24 h (Fig. 7.S1B) and 85% of the ones grown with 0.4% FBS medium for 48 h (Fig. 7.S1C) were viable. Taking into account that even HAP1-SPT cells grown in 0.4% FBS retained a fair viability, these cells were considered as a good tool to obtain reliable information on the putative effects of a defective SPT activity on their biophysical properties.

7.3.3. Lysenin-staining

Cells were stained with SM-specific NT-lysenin-mCherry and visualized with confocal microscopy. Most, but not all, HAP1 cells grown in standard medium appeared stained with lysenin-mCherry (Fig. 7.2A) and there was no significant difference when compared with the HAP1 cells grown in 0.4 % FBS medium for 24 h (Fig. 7.2B), or for 48 h (Fig. 7.2C). On the contrary, both, HAP1-SPT cells grown in SL-deficient medium for 24 h (Fig. 7.2E) and for 48 h (Fig. 7.2F) showed a considerable decrease of the mCherry signal as compared with the control (Fig. 7.2D), indicating that they had undergone a marked SM depletion.

For lysenin quantification, flow-cytometry-mediated mCherry-lysenin quantification was performed (Fig. 7.S2). When HAP1 and HAP1-SPT were grown in standard medium, mCherry-lysenin analysis revealed that mCherry intensity was lower in HAP1-SPT (Fig. 7.S2C) than in HAP1 (Fig. 7.S2A) cells: 87.1 ± 6.52 vs. 96.3 ± 6.24 respectively. Moreover, when HAP1 cells were grown in SL-deficient medium for 24 h (Fig. 7.S2A) and 48 h (Fig. 7.S2B), staining remained almost unchanged: 93.1 ± 4.16 vs. 92.2 ± 5.24 respectively, i.e. there was no significant difference with the control cells. However, when HAP1-SPT cells were grown in deficient medium, mCherry-lysenin fluorescence was largely decreased in the first 24 h of growth [32.5 ± 5.37 ; Fig. 7.S2C], and even further after 48 h (26.4 ± 7.19 ; Fig. 7.S2D).

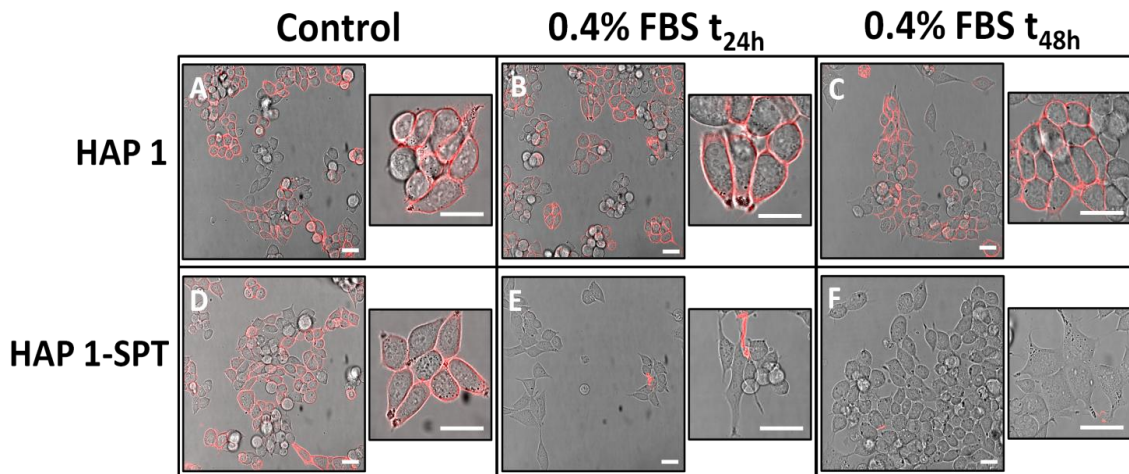


Figure 7.2. mCherry-lysenin staining of HAP1 and HAP1-SPT cells. (A-C) HAP1 grown in medium containing: (A) 10% FBS for 48 h, (B) 0.4% FBS for 24 h. (C) Medium containing 0.4% FBS for 48 h. (D-F) HAP1-SPT grown in medium containing: (D) 10% FBS for 48 h, (E) 0.4% FBS for 24 h. (F) Medium containing 0.4% FBS for 48 h. Bar = 10 μ m.

A parallel behavior was detected in the microscopy images of PM patches (Fig. 7.S3). PM patches derived from HAP1-SPT cells grown in deficient medium for 24 h (Fig. 7.S3E) and 48 h (Fig. 7.S3F) appeared almost exclusively stained with the non-specific fluorophore NBD-PE, i.e. they exhibited a very low lysenin-mCherry signal as compared with the patches from HAP1-SPT cells grown in standard medium (Fig. 7.S3D). In the latter, a clear colocalization between the NBD-PE and the mCherry-lysenin fluorophores can be observed throughout the PM patches. PM patches derived from HAP1 cells appeared stained with both fluorophores under all measured conditions (Fig. 7.S3A, 7.S3B and 7.S3C).

A relevant phenomenon is that not all of the HAP1 (Fig. 7.2A) or HAP1-SPT (Fig. 7.2D) cells appeared stained with the mCherry-Lysenin fluorophore when grown in the standard medium [unlike the CHO and LY-B cells, all homogeneously stained with mCherry-Lysenin (Monasterio *et al.*, 2021a)]. However all PM patches appeared equally stained (Fig. 7.S3). This may be linked to fluorophore accessibility depending on cell types, or with the individual differences in membrane SM contents. This point will be discussed below in combination with mass-spectrometric measurements (Figs. 7.3 and 7.4).

In summary, even if HAP1 and HAP1-SPT cells showed different growth rates when grown in standard medium (Fig. 7.1D), they did not exhibit differences in their mCherry-lysenin signals (Fig. 7.S2). However, mCherry-lysenin fluorescence was largely decreased in HAP1-SPT cells (Fig. 7.S2C), but not in HAP1 cells (Fig. 7.S2A), in the first 24 h of growth in deficient medium. This signal was further decreased for HAP1-SPT cells after 48 h (Fig. 7.S2D). Under the same conditions, HAP1 cells showed only a slight decrease in lysenin-reacting SM (Fig. 7.S2B).

7.3.4. Mass-spectrometric measurements

To understand the existing differences between HAP1 and HAP1-SPT membrane lipid composition in high- and low-SL media, and their homeostatic regulation capacity, the lipid redistribution undergone by cells when passing from standard to SL-deficient medium was analyzed. To this aim, a lipidomic study of whole cell samples and PM preparations (PM patches and GPMV) of HAP1 and HAP1-SPT cells grown in standard and deficient media was performed. Cells had been in contact with dithiothreitol and paraformaldehyde for GPMV formation, but not for PM patch isolation, thus different controls were used for each case, as in Monasterio *et al.* (2020). The ensemble of lipidomic data has been collected in table 7.S1. A summary of the most relevant results is shown in figure 7.3.

Figure 7.3A-C shows SL (SM, Cer and HexCer) concentrations in HAP1 and HAP1-SPT whole cells and PM preparations. These three specific SL were selected from the lipidomic data respectively because SM is usually the most abundant SL, Cer is particularly important in cell signaling, and HexCer is at the origin of the biosynthetic pathway leading to the complex glycoSL.

Remarkably, for cells grown in standard medium, the SM proportion in HAP1 or HAP1-SPT was one order of magnitude lower than the corresponding values for CHO and LY-B cells in Monasterio *et al.* (2021a) and also lower than in many mammalian cells and cell membranes (Table 7.S2). CHO cells contained 6.68% SM (mol % of total lipids) when grown in standard medium, while Fig. 7.3A shows that HAP1 cells contained only 0.54% SM, and the corresponding values for LY-B and HAP1-SPT were of 3.78% and 0.48% respectively. This is probably the main reason why microscopy images of HAP1 and HAP1-SPT grown in standard medium (Fig. 7.2A and Fig. 7.2D respectively) were heterogeneously and generally weakly stained with the SM specific lysenin-mCherry (Fig. 7.2). Some SL, that could be derived from SM, are known to bolster cell growth via calcium mobilization from intracellular stores and activation of the mitogen-activated protein kinase (MAP kinase) pathway and transcription factors (AP-1) (Spiegel & Merrill, 1996). The low SM percentage in HAP1 and HAP1-SPT is probably related to the stricter (as compared with CHO/LY-B) FBS requirement for growth in deficient medium (Fig. 7.1). In general, PM preparations contained higher proportions of SM than whole cell samples (Fig. 7.3A) as previously observed in other systems (van Meer *et al.*, 2008; Fahy *et al.*, 2009).

When HAP1 and HAP1-SPT cells grown in standard medium were compared, their membranes were seen to contain almost the same SM concentrations, in contrast with the differences that existed between CHO 10 and LY-B 10 (Monasterio *et al.*, 2021a). When FBS percentage in the medium was lowered to 0.4%, SM percentage in HAP1 remained constant in whole cells and PM fractions [unlike in CHO cells when grown in 0.04% FBS (Monasterio *et al.*, 2021a)]. SM was largely decreased, however, in HAP1-SPT -derived samples when FBS concentration in the medium was decreased (Fig. 7.3A). The decrease was of 76-77% for whole cells and 60-68% for PM patches when %FBS went from 10% to 0.4%. This is in good agreement with the lysenin-mCherry intensities measured by flow cytometry (Fig. 7.S2).

The main observation in relation to Cer is that concentrations in HAP1 were of the same order of magnitude as SM, irrespective of FBS concentration in the medium. This meant that Cer concentrations in HAP1 cells were very similar to those in CHO cells, despite the different SM concentrations. As expected, Cer concentration was higher in PM preparations than in whole cell samples (Fig. 7.3B), in agreement with parallel data in CHO and LY-B cells (Monasterio *et al.*, 2021a). Except in GPMV, Cer

concentrations were clearly lower in whole HAP1-SPT (and, to a lesser extent, in HAP1-SPT PM patches) than in the corresponding HAP1 samples. The decrease in whole cell samples was of 80-85%, and of 40-45% in PM patches. In addition, when cells were grown in 0.4% FBS-containing medium, neither HAP1 nor HAP1-SPT cells showed differences in comparison with the 10% FBS controls (Fig. 7.3B), again at variance with what occurred with LY-B, in which Cer percentage was greatly decreased when grown in low FBS (Monasterio *et al.*, 2021a). The constancy of Cer concentration irrespective of % FBS in the medium may be an indication that, already with 10% FBS, HAP1 cells contain the minimum Cer concentration required for their survival. The clear decrease in Cer contents observed in HAP1-SPT as compared with HAP1 is reporting on an overall metabolic change as a result of SPT annulment.

As with Cer, the HexCer percentage was larger in PM preparations than in whole cell samples, both in HAP1 and in HAP1-SPT lines (Fig. 7.3C). This phenomenon was also observed with CHO and LY-B cells (Monasterio *et al.*, 2021a). The HexCer percentages were again lower (by about 78%) in whole HAP1-SPT than in whole HAP1 cells grown in standard medium. HexCer percentage was not markedly decreased when HAP1 or HAP1-SPT were grown in 0.4% FBS medium (Fig. 7.3C), as observed with Cer (Fig. 7.3B), and unlike the case of LY-B cells (Monasterio *et al.*, 2021a).

Glycerophospholipid (GPL) acyl chain saturation and length play an important role in the membrane physical properties, specifically their rigidity/fluidity. Unsaturated and short-chain GPL increase membrane fluidity (van Meer *et al.*, 2008). For HAP1 and HAP1-SPT cells, mass spectrometric analysis showed only small differences in chain length, unsaturation or ether links between native and mutant cells, grown on either standard or SL-limiting conditions (Fig. 7.3D-I). Besides, PM preparations contained a somewhat higher proportion of short (30-32C combining both chains) GPL than whole cell samples (Fig. 7.5D), and also PM preparations, particularly GPMV, contained less polyunsaturated fatty acids than the whole cells on average. These differences were independent of SPT functionality or growth conditions (Figs. 7.1, 7.3).

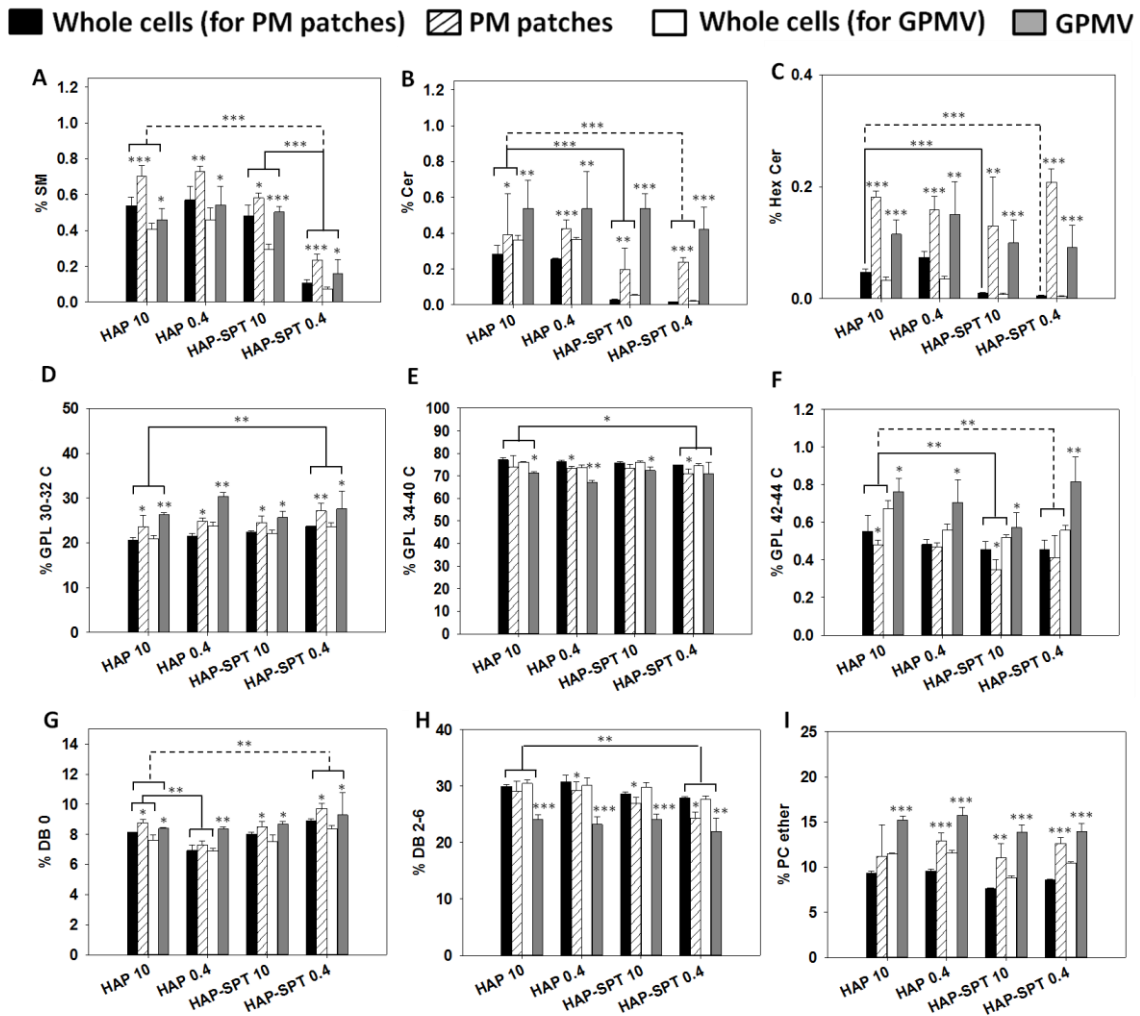


Figure 7.3. Lipidomic analysis of whole cells and plasma membrane preparations. (A) SM, (B) Cer, (C) Hex Cer, (D) Chol. E-G: GPL length distribution. (E) 30 - 32 C, (F) 34 - 40 C, (G) 42 - 44 C. (the figures correspond to the sum of the two acyl chains). H-I: GPL saturation distribution. (H) No double bonds (DB 0), (I) Two – six double bonds per molecule (DB 2-6). (J) PC ether. Mean values \pm S.D. (n = 3). Statistical significance was calculated with ANOVA and Student's t-test: (*) $p < 0.05$; (**) $p < 0.01$; (***) $p < 0.001$.

PM samples contained more ether-PC than whole cell controls (Fig. 7.3I). Nevertheless, statistically significant differences were not observed between HAP1 and HAP1-SPT cells, grown in standard or deficient medium. Related to this observation, LY-B measurements showed a small but significant increase of ether-PC in samples grown in SL-deficient medium (Monasterio *et al.*, 2021a).

A quantitative estimate of the amount of SM and Chol, two representative lipids in this context, was carried out as described under Methods. The results can be seen in figure 7.4. With respect to Chol, the concentration in HAP1 cells grown in SL deficient-

medium was the same of those grown in standard medium (data in pg Chol/cell). The corresponding figure for HAP1-SPT was 20% lower for cells grown in deficient medium (Fig. 7.4B). As for Chol data, HAP1 cells grown on medium with 0.4% FBS were not different from the SM found in cells grown on 10% FBS [data in pg SM/cell (Fig. 7.4B), or in pg SM/ng protein (Fig. 7.4A)]. For the SPT-defective HAP1-SPT cells, the corresponding figures are 78% (Fig. 7.4B), and 76% (Fig. 7.4A) lower. Thus, a 25-fold reduction in sphingolipid supply to HAP1-SPT cells leads to a 6-fold decrease in membrane sphingolipids.

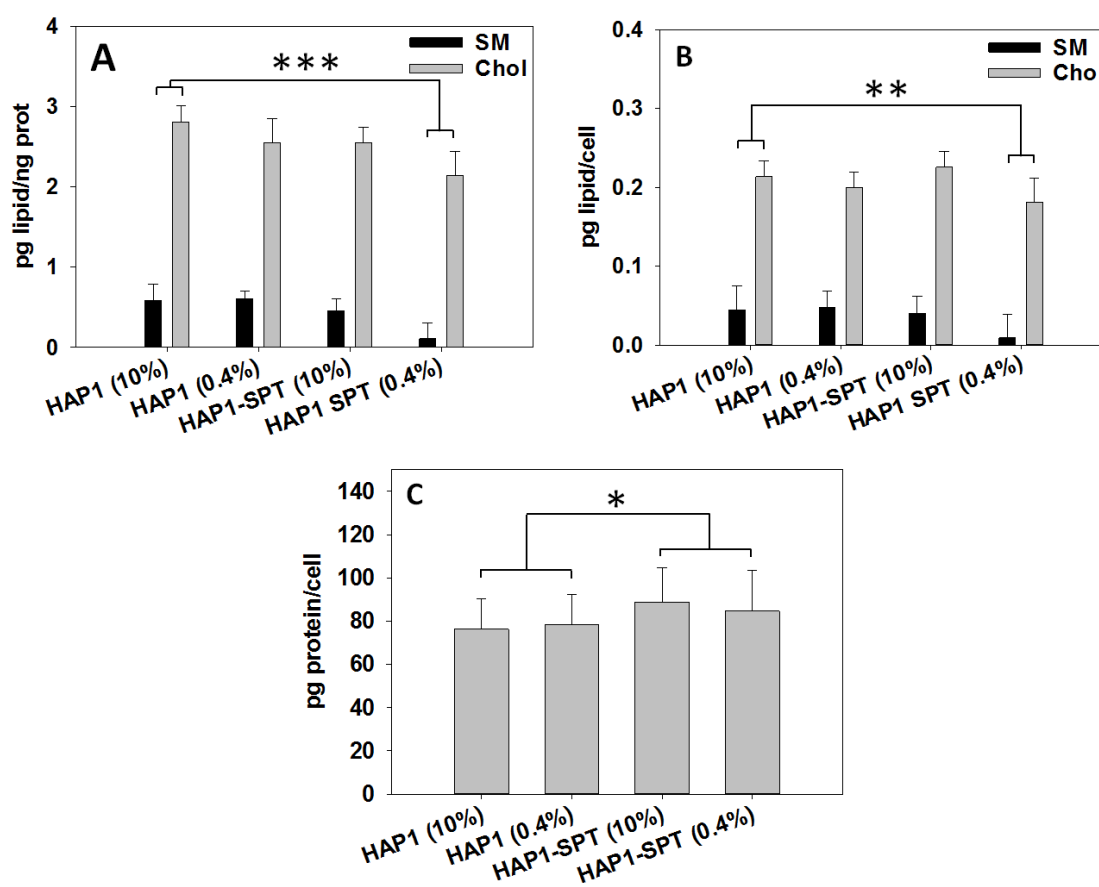


Figure 7.4. SM and Chol contents per cell and per ng protein in the various preparations. SM and Chol pg/ng protein (A). SM and Chol pg/cell (B). pg protein/cell (C). Average values \pm S.D. (n = 3). Statistical significance was calculated with ANOVA and Student's t-test: (*) $p < 0.05$; (**) $p < 0.01$; (***) $p < 0.001$.

7.3.5. Membrane lipid order measurements

Laurdan generalized polarization (GP) measurements were performed to evaluate how the SPT activity suppression affected the rigidity/fluidity changes of cell membranes. GP provides an estimation of membrane lipid molecular order. GP values

of: GUV formed with whole cell lipid extracts, PM selection of whole cell images, PM patches and GPMV, were measured using two-photon microscopy. Whole-cell lipid extract GP values were also measured in a spectrofluorometer (Fig. 7.S4) GP values of both HAP1 and HAP1-SPT cell lines were measured and compared (Table 7.1).

First, whole HAP1 and HAP1-SPT cells grown in standard and deficient medium for 24 or 48 h were stained with laurdan and images were taken in a two-photon microscope. Then, a selection of pixels corresponding to the PM was performed, discarding the intracellular GP signal, in images from HAP1 and HAP1-SPT cells grown in standard (Fig. 7.5A and 7.5D respectively) and SL-deficient medium for 24 h (Fig. 7.5B and 7.5E respectively) or 48 h (Fig. 7.5C and 7.5F respectively). PM exhibited a homogenous GP value around 0.42 - 0.44 in all measured samples, at variance with the previously observed CHO and LY-B PM GP values in Monasterio *et al.*, where measurements decreased from 0.52 (CHO and LY-B cells grown in standard medium) to 0.44 (LY-B grown in deficient medium) (Monasterio *et al.*, 2021a). As seen in table 7.1, GP of the selected PM region remained unchanged when FBS concentration in the medium was lowered from 10% to 0.4%. GP images of PM appeared to be slightly non-homogenous, but the presence of nanodomains could not be ascertained because of the spatial and temporal resolution limit of conventional two-photon microscopy (Frisz *et al.*, 2013b, 2013a; Nicovich *et al.*, 2018).

GP values of PM patches showed values around 0.34 – 0.36 (Fig. 7.5M-R, Table 7.1). As with the PM selection (Fig. 7.5A-F, Table 7.1), no significant differences were seen between HAP1 and HAP1-SPT PM patches under any measured conditions. GP values of GPMV were also of 0.35 – 0.36 (Table 7.1), again showing no statistically significant differences between any of the samples.

GP values of GUVs formed from whole-cell lipid extracts were also measured (Fig. 7.5G-5L and Table 7.1) as in Monasterio *et al.* (2020). GUVs formed from HAP1-SPT lipids of cells grown in SL-deficient medium for 48 h (Fig. 7.5L), were significantly more rigid than those formed with the corresponding HAP1 lipid extracts (Fig. 7.5I). This difference was not observable nor in control, neither after 24 h growth (Fig. 7.5G, H for HAP1 and Fig. 7.5J, K for HAP1-SPT).

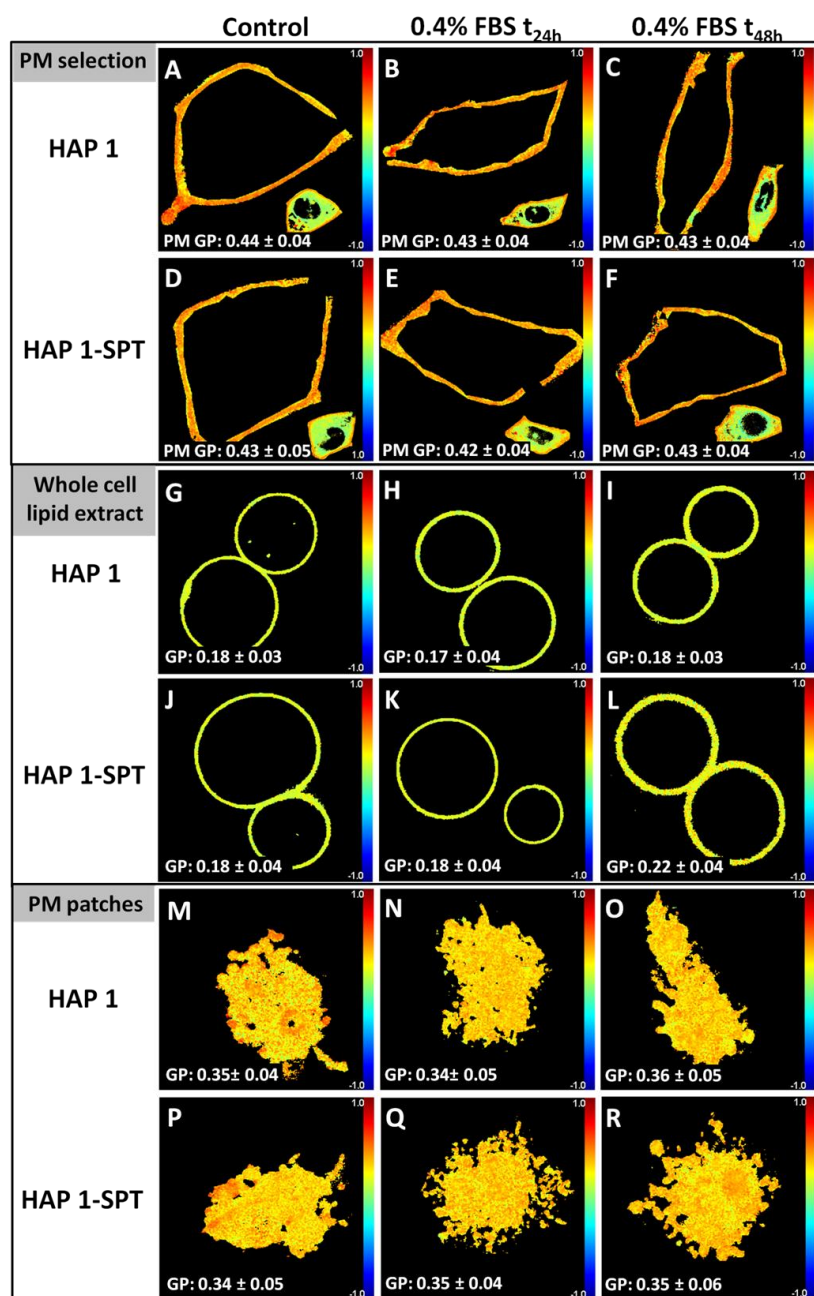


Figure 7.5. Two-photon microscopy images of samples stained with laurdan and the corresponding GP measurements. **(A-C)** Plasma membrane selection of HAP1 grown in **(A)** standard medium for 24 h, **(B)** deficient medium for 24 h, and **(C)** deficient medium for 48 h. **(D-F)** Plasma membrane selection of HAP1-SPT grown in **(D)** standard medium for 24 h, **(E)** deficient medium for 24 h, and **(F)** deficient medium for 48 h. **(G-I)** GUV formed from whole cell lipid extracts from HAP1 grown in **(G)** standard medium for 24 h, **(H)** deficient medium for 24 h, and **(I)** deficient medium for 48 h. **(J-L)** GUV formed from whole cell lipid extracts from HAP1-SPT grown in **(J)** standard medium for 24 h, **(K)** deficient medium for 24 h, and **(L)** deficient medium for 48 h. **(M-O)** PM patches from HAP1 cells grown in **(M)** standard medium for 24 h, **(N)** deficient medium for 24 h, and **(O)** deficient medium for 48 h. **(P-R)** PM patches from HAP1-SPT cells grown in **(P)** standard medium for 24 h, **(Q)** deficient medium for 24 h, and **(R)** deficient medium for 48 h. GP values are given as averages \pm S.D. ($n = 3$).

To confirm the above data, the emission spectra of aqueous suspensions of SUV formed from whole-cell lipid extracts and stained with laurdan were measured at 20°C, 30°C and 40°C (Fig. 7.S4) as in Monasterio *et al.* (2020). GP values derived from these emission spectra showed statistically significant differences between HAP1 (Fig. 7.S4C) and HAP1-SPT cells grown in 0.4% medium for 48 h (Fig. 7.S4F), the latter spectra being further shifted towards 440 nm at the three measured temperatures, indicating a more rigid behavior: GP = 0.25 vs. 0.28 at 20°C; 0.12 vs. 0.15 at 30°C and 0.01 vs. 0.08 at 40°C (HAP1 vs. HAP1-SPT in 0.4% medium for 48 h). This result is in good agreement with the GP values from two-photon microscopy images at room temperature (Table 7.1).

Table 7.1. Laurdan GP values obtained from two-photon microscopy images. Statistically significant differences were calculated with ANOVA and Student's t test with similar results. n=150. Significance: (**) p<0.01.

	GUV	GPMV	PM Patches	PM selection
HAP 10	0.18 ± 0.03	0.36 ± 0.05	0.35 ± 0.04	0.44 ± 0.04
HAP-SPT 10	0.18 ± 0.04	0.35 ± 0.04	0.34 ± 0.05	0.43 ± 0.05
HAP 0.4 24 h	0.17 ± 0.04	0.35 ± 0.05	0.34 ± 0.05	0.43 ± 0.04
HAP-SPT 0.4 24 h	0.18 ± 0.04	0.36 ± 0.05	0.35 ± 0.04	0.42 ± 0.04
HAP 0.4 48 h	0.18 ± 0.03	0.35 ± 0.06	0.36 ± 0.05	0.43 ± 0.04
HAP-SPT 0.4 48 h	0.22 ± 0.04	0.36 ± 0.04	0.35 ± 0.06	0.43 ± 0.04

Differences were not statistically significant, neither between HAP1 and HAP1-SPT control cells (Fig. 7.S4A and 7.S4D), nor between cells grown in deficient medium for 24 h, at 20°C or 30°C. But they were so at 40°C, the emission maximum of HAP1-SPT samples at 40°C exhibiting a spectral component further shifted to ≈440 nm than the one from HAP1, indicating a more rigid behavior when grown both in standard (0.06 vs. -0.02) and deficient medium for 24 h (0.05 vs. -0.02).

7.3.6. Breakthrough force measurements

SPB derived from hydrated whole cell lipid extracts, PM patches and GPMV were studied under the atomic force microscope (AFM), mainly in the force-spectroscopy mode, to detect putative differences in the breakthrough forces of the various samples. All measured breakthrough force values are summarized in table 7.2. The corresponding breakthrough force distribution plots are shown in figure 7.S5.

Figure 7.6 shows the topology of PM patches (Fig. 7.6A-F) and of SPB formed from whole cell lipid extracts (Fig. 7.6G-L) from HAP1 and HAP1-SPT cells grown in standard and SL-deficient medium for 24 h or 48 h. According to the topographic images, a minimum thickness of 4-5 nm was regularly observed in all samples, corresponding with the thickness of a lipid bilayer (Umagai *et al.*, 2006). Even if in PM patches other membrane components [perhaps (glyco)proteins or protein aggregates] gave rise to higher elements in the AFM pictures, no significant differences were seen between the thicknesses of the various samples, PM patches or SPB.

The breakthrough force distributions showed no significant differences in the PM patch samples, HAP1: 3.38 nN (Fig. 7.6A) and HAP1-SPT: 3.02 nN (Fig. 7.6D) for cells grown in standard medium; HAP1: 2.84 nN (Fig. 7.6B) and HAP1-SPT: 2.87 nN (Fig. 7.6E) when grown in 0.4% FBS for 24 h; HAP1: 3.14 nN (Fig. 7.6C) and HAP1-SPT: 2.94 nN (Fig. 7.6F) when grown in 0.4% FBS for 48 h.

Table 7.2. AFM mediated breakthrough force average values. Statistically significant differences were calculated with ANOVA and Student's t test with similar results. n=150. Significance: (**) p<0.01.

	Whole cell lipid extract	GPMV	PM patches
HAP 10	1.58 ± 0.35	5.21 ± 2.00	3.38 ± 1.22
HAP-SPT 10	1.36 ± 0.44	5.18 ± 2.16	3.02 ± 1.28
HAP 0.4 24 h	1.51 ± 0.41	4.65 ± 0.81	2.84 ± 1.35
HAP-SPT 0.4 24 h	1.61 ± 0.38	4.77 ± 1.87	2.87 ± 1.20
HAP 0.4 48 h	1.57 ± 0.17	5.72 ± 1.19	3.14 ± 1.29
HAP-SPT 0.4 48 h	1.98 ± 0.25	6.02 ± 1.61	2.94 ± 1.55

SPB formed from whole HAP1 and HAP1-SPT cell lipid extracts grown in standard or SL-deficient medium were also scanned (Fig. 7.6G-L). Depending on the cell type, the SPB breakthrough force showed a different response to the decrease of available SL. No significant differences were found between the breakthrough forces of SPB from lipid extracts of cells grown in standard (Fig. 7.6G) or deficient (Fig. 7.6H and 6I) medium, with values around 1.5 - 1.6 nN. However, the corresponding values for HAP1-SPT are significantly lower for cells grown in standard medium (1.36 nN; Fig. 7.6J), than for those grown in deficient medium for 48 h (1.98 nN; Fig. 7.6L). An

intermediate value of 1.61 nN was measured in the case of deficient medium for 24 h (Fig. 7.6K).

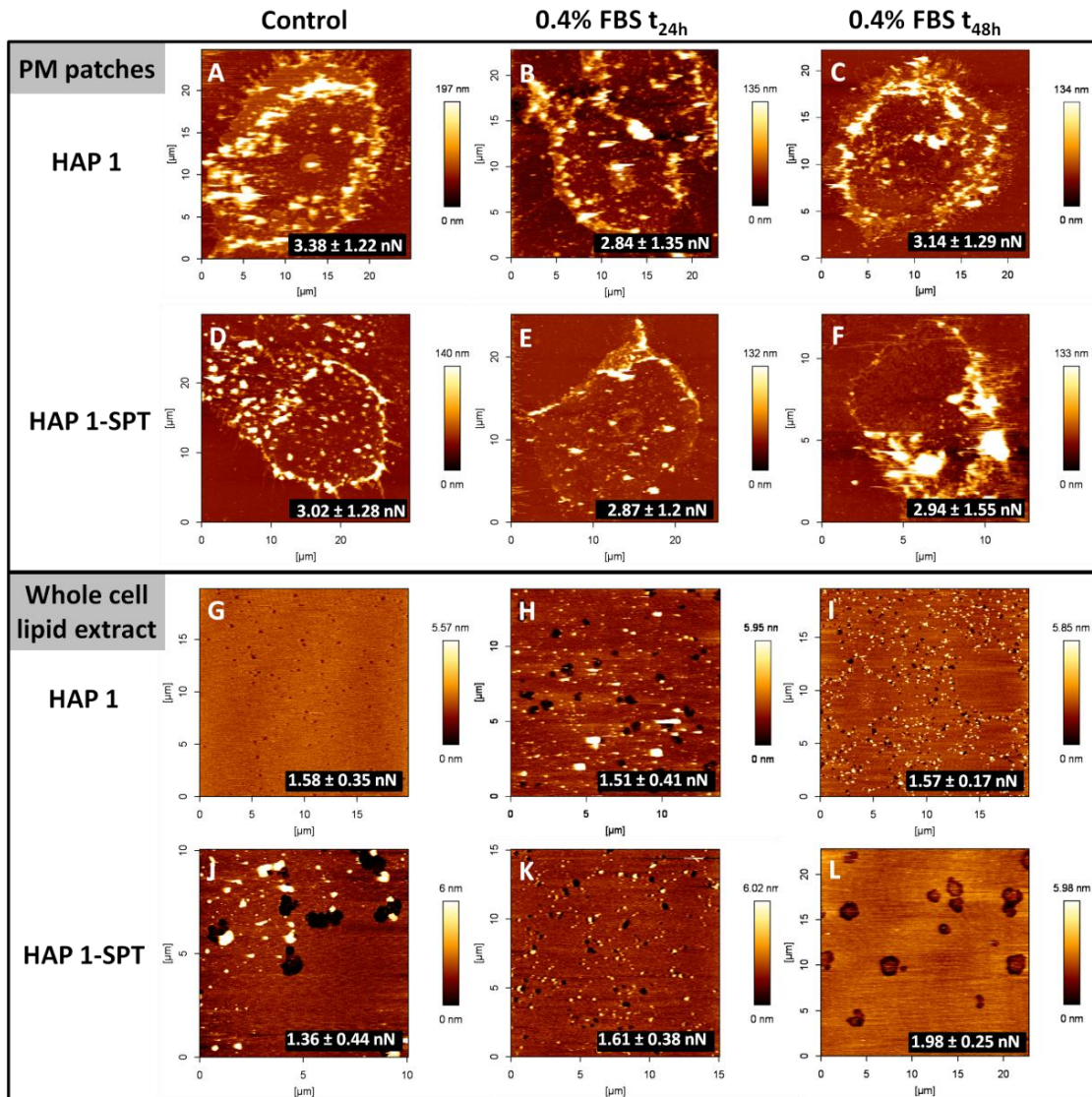


Figure 7.6. Topology images and the corresponding breakthrough force values. (A-C) *PM patches* from HAP1 cells grown in (A) standard medium for 24 h, (B) deficient medium for 24 h, and (C) deficient medium for 48 h. (D-F) *PM patches* from HAP1-SPT cells grown in (D) standard medium for 24 h, (E) deficient medium for 24 h, and (F) deficient medium for 48 h. (G-I) *SPB* formed from whole cell lipid extracts of HAP1 grown in (G) standard medium for 24 h, (H) deficient medium for 24 h, and (I) deficient medium for 48 h. (J-L) *SPB* formed from whole cell lipid extracts of HAP1-SPT grown in (J) standard medium for 24 h, (K) deficient medium for 24 h, and (L) deficient medium for 48 h. Breakthrough force values are given as averages ± S.D. (n = 150).

GPMV breakthrough forces were also measured (Fig. 7.S5 M-R). No significant differences were detected between samples from HAP1 and HAP1-SPT cells grown under the same conditions. AFM breakthrough forces are summarized in table 7.2.

In summary, breakthrough force measurements were in good agreement with laurdan GP values. Statistically significant differences were seen with either technique only between lipid extracts from HAP1 and HAP1-SPT grown in deficient medium for 48 h.

As most SL are lipids that confer rigidity to the membrane (Goñi & Alonso, 2009), the measured low SM percentages (Fig. 7.3A) are probably related to the observed differences in biophysical properties between both cell line groups (CHO/LY-B vs. HAP1/HAP1-SPT) (Figs. 7.5, 7.6; Tables 7.1, 7.2). The low SM value would be related to the fact that HAP1 and HAP1-SPT cells have both lower GP (Table 7.1) and lower breakthrough force (Table 7.2) values than the ones measured for CHO and LY-B samples (Monasterio *et al.*, 2021a). In addition, HAP1-SPT values were slightly but significantly increased in comparison to HAP1. This was against the expectation that samples derived from HAP1-SPT should had a lower GP and breakthrough force, as compared with the wild type HAP1, due to the presumed depletion of SM, a lipid that is characterized for conferring membrane rigidity (Goñi & Alonso, 2009; Goñi *et al.*, 2020)

7.4. Discussion

In a recent series of studies, our laboratories have intended to clarify the role of SL on some biophysical properties of cell membranes, mainly lipid fluidity/disorder and membrane penetrability (breakthrough forces). These studies have been performed on whole cells, vesicles derived from cell lipid extracts, and plasma membrane preparations, namely patches and blebs (GPMV) (Monasterio *et al.*, 2020). Cells have been grown under conditions of minimal SL concentrations in the growth medium, in which FBS was virtually the only source of exogenous SL (Monasterio *et al.*, 2021a). First, the well-known CHO cells were studied in parallel with the LY-B mutant, that lacks a functional SPT, the key enzyme in sphingolipid *de novo* synthesis. The combination of limiting SL concentrations in the growth medium with the absence of sphingosine synthesis led to a severe SL deprivation in LY-B cells (Monasterio *et al.*, 2021a). A clear correlation was found between decreased SL contents and changes in biophysical properties in membranes. A different strategy consisted of chemically inhibiting SPT, using the specific inhibitor myriocin, in CHO cells (2021b), with very similar results in what concerned SL composition, lipid molecular order, and

penetrability of membranes. SL composition of CHO and LY-B cell membranes was also modified using cyclodextrins loaded with phospholipids and cholesterol.

The present study, complementary to the above, uses a human SPT-defective cell line, the near-haploid HAP1 SPTLC1(-) strain (abbreviated as HAP1-SPT), obtained by CRISPR/Cas editing of HAP1.

Perhaps the main observation in this paper is that HAP1 cells, even when grown in full FBS-containing medium, contain a very low proportion of SM, one order of magnitude below that of CHO or LY-B cells grown under the same conditions (Figs. 7.3, 7.4, and reference Monasterio *et al.*, 2021a). In mammalian cells in general SM is the major sphingolipid, and its concentration is clearly above that of Cer or HexCer (Table 7.S2). This is not the case with HAP1 or HAP1-SPT, in which SM, Cer and HexCer exist at similar concentrations (Fig. 7.3). This unexpected property of HAP1 cells provides a new vantage point from which the membrane effects of SL deprivation can be examined, i. e. trying to lower SL in membranes that constitutively contain very low SL concentrations. In fact, this work has demonstrated that HAP1-SPT cells, lacking any SPT activity, but not the native HAP1 ones, when grown under SL-limiting conditions, exhibit a large decrease in SM concentration, not only in whole cell samples, but also in PM preparations.

Neither the Cer levels in HAP1, nor those in HAP1-SPT, varied with FBS concentration in the medium (Figs. 7.3 A-C). The corresponding values for HAP1 grown with 10% FBS were also similar to those of CHO 10 (Monasterio *et al.*, 2020). The constancy of Cer concentration irrespective of FBS concentration in the medium suggests that, even with 10% FBS, HAP1 cells contain the minimum Cer concentration required for their survival. In any case, Cer concentrations are usually below 0.5 mol% of the total lipids in mammalian membranes (Table 7.S2). This is understandable because of the very potent membrane disrupting activities of Cer, including trans-bilayer lipid scrambling and membrane permeabilization (Alonso & Goñi, 2018). There is probably a narrow range of Cer concentrations allowing the necessary metabolic functions but not causing the dangerous side effects. Having this in mind, an even further decrease in Cer contents as observed in HAP1-SPT (as compared with HAP1) is surprising (Fig. 7.3B). The data are probably reporting on an overall metabolic change as a result of SPT annulment. HexCer concentrations change in parallel with Cer,

although they are 3-fold lower. The observed parallelism may be due to the known fact that HexCer is mainly synthesized from Cer.

Not surprisingly, ablation or inhibition of SPT activity has little effect on membrane GPL, however some effects are worth mentioning. The main difference between GPL chain lengths of HAP1/HAP1-SPT vs. CHO/LY-B cells, resides in the percentage of short-chain GPL. CHO and LY-B cells contained around 10-15% short-chain GPL (Monasterio *et al.*, 2021a), while HAP1 and HAP1-SPT contained twice as much (Fig. 7.3E). Both the above-mentioned low SM (Fig. 7.3A) and the increased short-chain GPL will probably influence the membrane biophysical properties in the same sense, specifically the lower GP (Table 7.1) and the lower breakthrough forces (Table 7.2) of HAP1/HAP1-SPT as compared to CHO and LY-B cells (Monasterio *et al.*, 2021a). Note however that laurdan GP and breakthrough force values in HAP1-SPT PM preparations failed to show any statistically significant difference associated to the amount of SL in the growth medium; this reveals a homeostatic adaptation of the cell PM even to extreme SL deprivation conditions.

Comparing these results with the previous ones for CHO and LY-B cells (Monasterio *et al.*, 2021a), the most notorious differences are the following: First, when the SPT-defective LY-B cells were grown in deficient medium, GP values of their PM patches were decreased from 0.45 to 0.37. On the contrary, PM patches derived from HAP1-SPT cells did not suffer any GP change when grown in SL-deficient medium, it remained constant within the low range, around 0.34 – 0.36 (Table 7.1). Second, GP values of whole cell lipid extract from LY-B cells were lower than the corresponding CHO samples when cells were grown in either SL-deficient medium or in standard medium. On the contrary, the GP value of HAP1-SPT cell lipid extract significantly increased when cells were grown in SL-deficient medium. GP results are in agreement with the mass-spectrometric measurements discussed above (Tables 7.1, 7.2; Fig. 7.3).

Plasma membrane investigations in living cells under physiological conditions remain a challenging task (Meddens *et al.*, 2014). The complex nature of the plasma membrane and the variety of interactions with its local environment requires applying specific advanced research methods. The capacity shown by certain cells to grow under extremely demanding low concentrations of SL and to buffer the rigidity/fluidity differences by modulating its lipid composition opens the way to a variety of functional

studies on the role of SL in membranes. One of them is related to HAP1 cells as a model for chronic myeloid leukemia. It has been reported that the sensitivity of chronic myeloid leukemia cells to Bcr-Abl tyrosine kinase inhibitors is modulated by Cer levels (Wang *et al.*, 2016), thus it could be of interest to examine how reconstitution with different sphingoid base backbones affects the sensitivity of HAP1 and HAP1-SPT cells to Bcr-Abl tyrosine kinase inhibitors; this might shed some light on drug resistance (Camgoz *et al.*, 2013).

7.5. Supplementary Material

Table 7.S1. A summary of the various lipid compositions of HAP1 and HAP1-SPT cells

https://drive.google.com/file/d/16k_7P7URduxLXw92vA4h1XNzJKIBwtY8/view?usp=sharing

Table 7.S2. SM and Cer contents in different cells and cell membrane fractions.

Cell		SM	Cer
Human RBC	Ghost	12.1 ± 2.1 (Maté <i>et al.</i> , 2014)	<1 (Lorent <i>et al.</i> , 2020)
HeLa (Lorizate <i>et al.</i> , 2013)	Total	≈ 3.7	≈ 0.3
	PM	≈ 5.6	≈ 0.2
MT-4 (Lorizate <i>et al.</i> , 2013)	Total	≈ 9.3	≈ 0.2
	PM	≈ 13.5	≈ 0.1
MDCK/influenza (Gerl <i>et al.</i> , 2012)	Total	≈ 0.8	≈ 4.1
BHK (Kalvodova <i>et al.</i> , 2009)	Total	5.7 ± 1.1	0.3 ± 0.16
	PM	8.6 ± 1.1	0.09 ± 0.03
Rat CNS cell cultures (Fitzner <i>et al.</i> , 2020)	Total	5.61	0.54
Rat CNS brain regions (Fitzner <i>et al.</i> , 2020)	Total	1.48	0.32
PC-3 (Llorente <i>et al.</i> , 2013)	Total	6.9 ± 0.55	0.24 ± 0.02
	exosomes	16.3 ± 1.11	0.32 ± 0.02
Mouse lung (Karnati <i>et al.</i> , 2018)	Homogenates	≈ 15	≈ 7
CHO 10 (Monasterio <i>et al.</i> , 2021a)	Total	6.68 ± 1.04	0.41 ± 0.01
	PM patches	3.47 ± 0.48	0.45 ± 0.03
LY-B 10 (Monasterio <i>et al.</i> , 2021a)	Total	3.78 ± 0.30	0.12 ± 0.01
	PM patches	1.9 ± 0.22	0.15 ± 0.02
CHO 0.04 (Monasterio <i>et al.</i> , 2021a)	Total	4.67 ± 0.31	0.25 ± 0.05
	PM patches	4.18 ± 0.36	0.44 ± 0.02
LY-B 0.04 (Monasterio <i>et al.</i> , 2021a)	Total	0.48 ± 0.03	0.04 ± 0.01
	PM patches	0.50 ± 0.05	0.11 ± 0.02
HAP1 10	Total	0.54 ± 0.05	0.28 ± 0.05
	PM patches	0.70 ± 0.09	0.39 ± 0.21
HAP1-SPT 10	Total	0.48 ± 0.06	0.03 ± 0.00
	PM patches	0.58 ± 0.03	0.19 ± 0.12
HAP1 0.4	Total	0.57 ± 0.08	0.26 ± 0.01
	PM patches	0.73 ± 0.28	0.42 ± 0.05
HAP1-SPT 0.4	Total	0.11 ± 0.02	0.02 ± 0.00
	PM patches	0.23 ± 0.03	0.24 ± 0.02

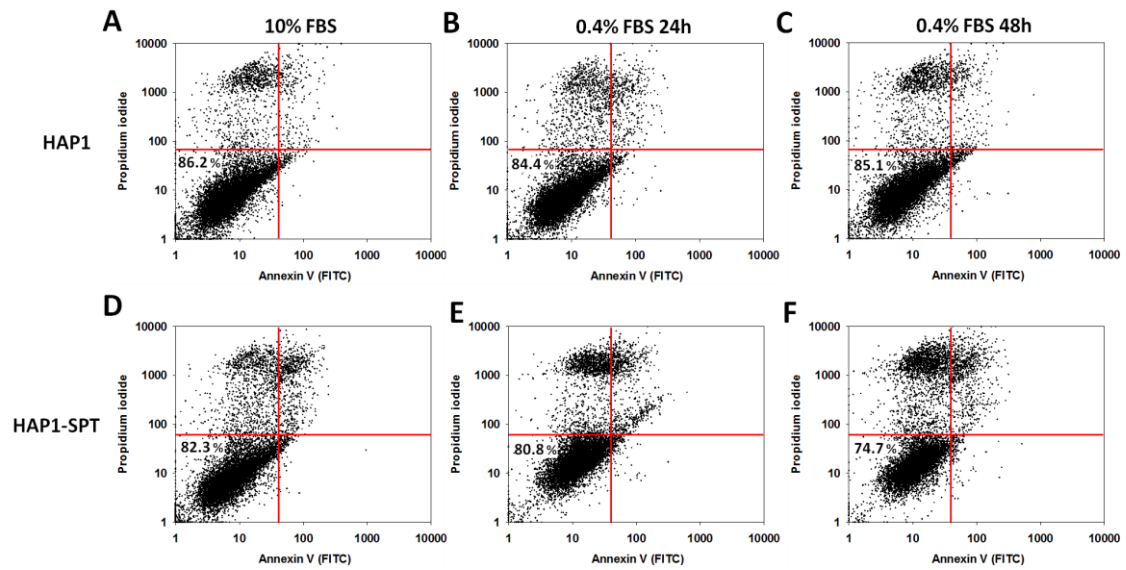


Figure 7.S1. HAP1 and HAP1-SPT cell viability in standard and SL-deficient media. (A-C) *HAP1* grown in medium containing (A) 10% FBS for 24 h, (B) 0.4% FBS for 24 h, and (C) 0.4% FBS for 48 h. (D-F) *HAP1-SPT* grown in medium containing (D) 10% FBS for 24 h, (E) 0.4% FBS for 24h, and (F) 0.4% FBS for 48 h.

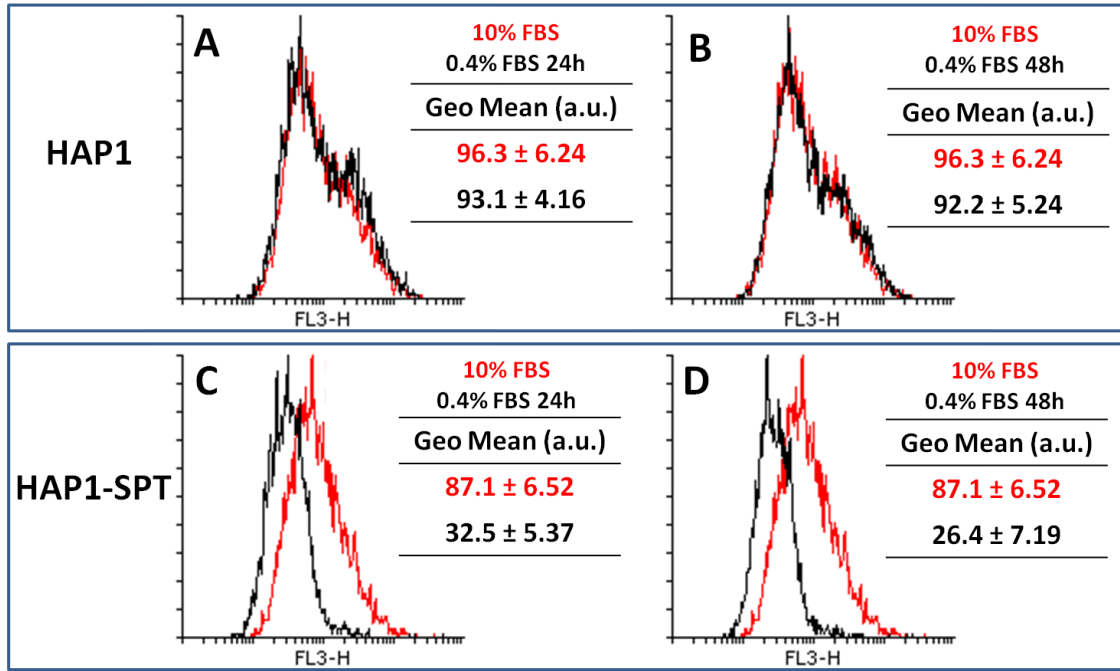


Figure 7.S2. Quantification of cells stained with mCherry-lysenin by flow cytometry. (A, B) *HAP1* cells grown in standard or deficient medium (A) for 24 h, and (B) for 48 h. (C, D) *HAP1-SPT* cells grown in standard or deficient medium (C) for 24 h, and (D) for 48 h. Histograms correspond to the mCherry-lysenin signals of cells grown in standard medium (red) or under SL-limited conditions (black). Geometric mean ± S.D. (n = 3).

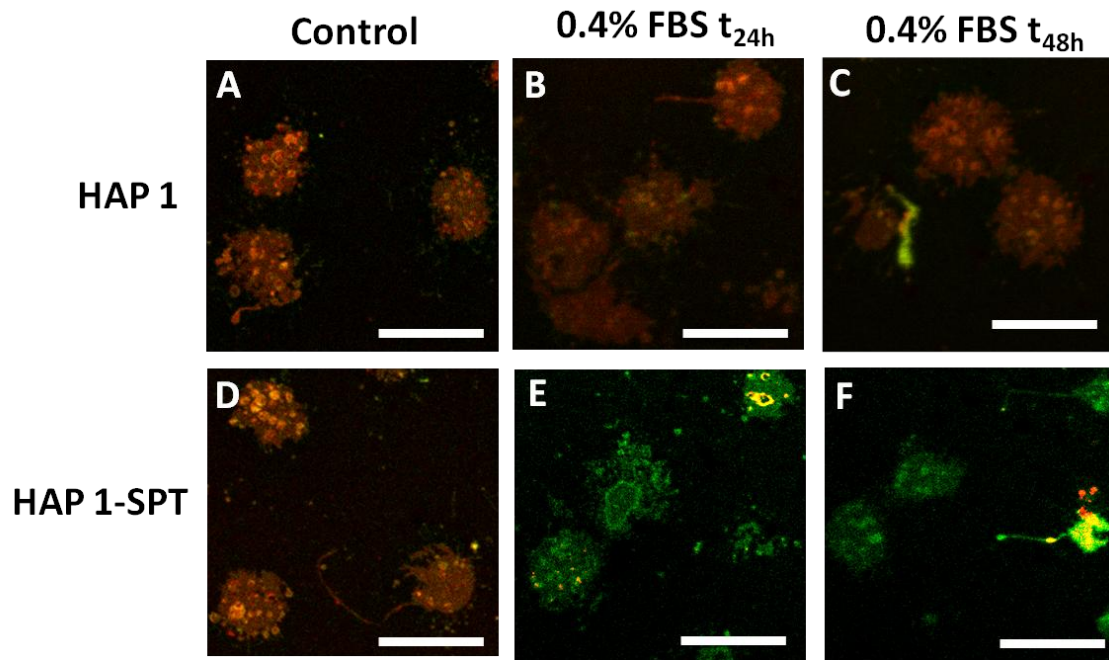


Figure 7.S3. Fluorescence microscopy images of PM patches stained with mCherry-lysenin (red). (A-C) *HAP1* grown in medium containing (A) 10% FBS for 24 h, (B) 0.4% FBS for 24 h, and (C) 0.4% FBS for 48 h. (D-F) *HAP1-SPT* grown in medium containing (D) 10% FBS for 24 h, (E) 0.4% FBS for 24h, and (F) 0.4% FBS for 48 h.. Bar = 10 μ m. NBD-PE (green) was used as a non-specific membrane staining control.

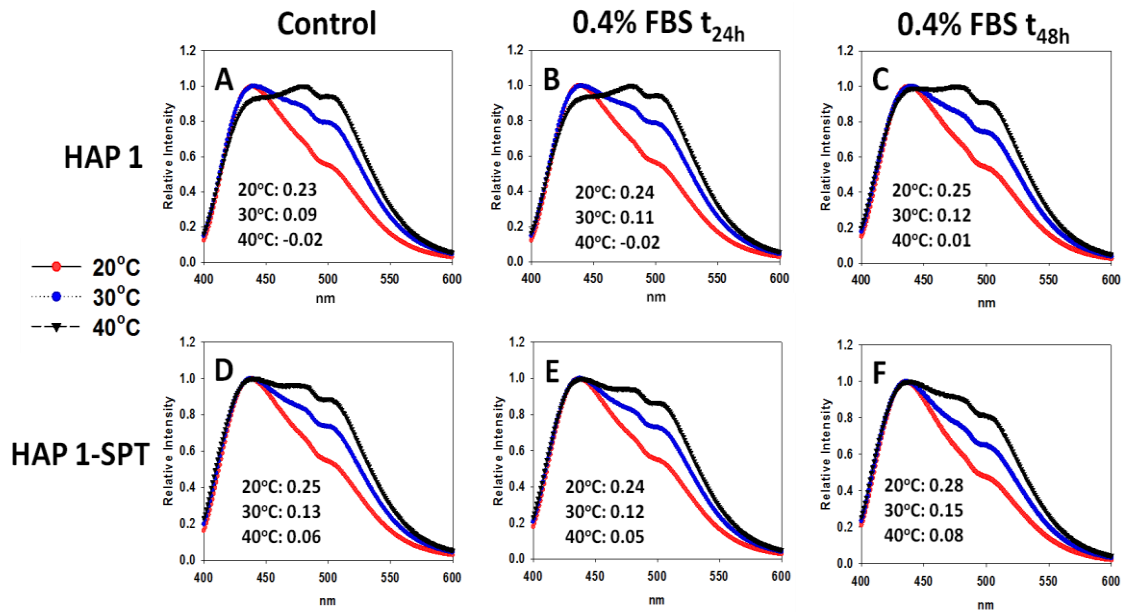


Figure 7.S4. Laurdan emission spectra (at 20°C, 30°C and 40°C) of SUV formed from whole cell lipid extracts, and their corresponding GP values. (A-C) HAP1 grown in medium containing (A) 10% FBS for 24 h, (B) 0.4% FBS for 24 h, and (C) 0.4% FBS for 48 h. (D-F) HAP1-SPT grown in medium containing (D) 10% FBS for 24 h, (E) 0.4% FBS for 24h, and (F) 0.4% FBS for 48 h. Red spectra: 20°C. Blue spectra: 30°C. Black spectra: 40°C.

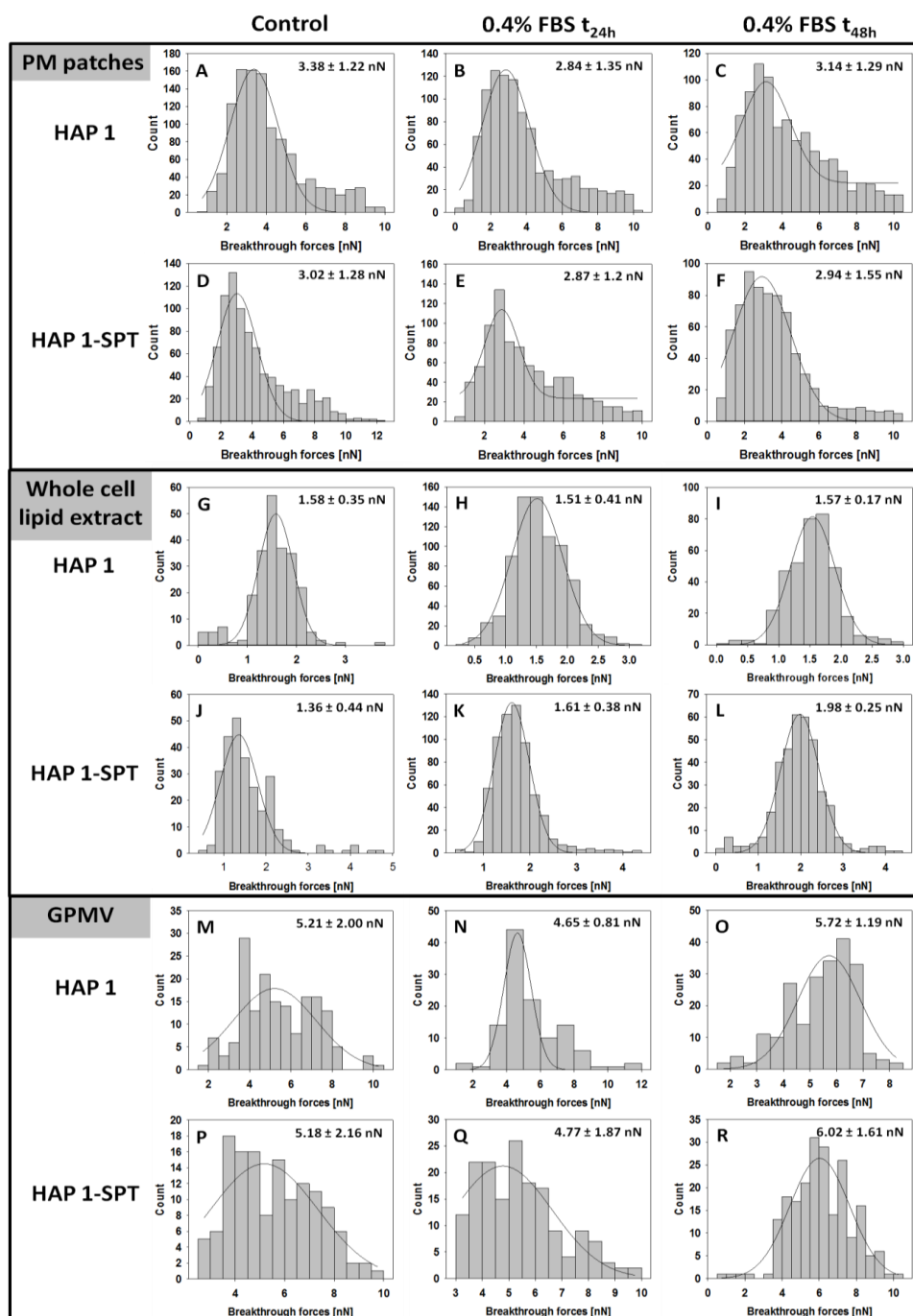


Figure 7.S5. Frequency distributions of breakthrough forces. (A-C) *PM patches* of (A) HAP1 cells grown in standard medium for 24 h, (B) in deficient medium for 24 h, and (C) in deficient medium for 48 h. (D-F) *PM patches* of HAP1-SPT cells grown in (D) standard medium for 24 h, (E) deficient medium for 24 h, and (F) deficient medium for 48h. (G-I) *SPB* formed from whole cell lipid extracts of HAP1 grown in (G) standard medium for 24 h, (H) deficient medium for 24 h, and (I) deficient medium for 48 h. (J-L) *SPB* formed from whole cell lipid extracts of HAP1-SPT grown in (J) standard medium for 24 h, (K) deficient medium for 24 h, and (L) deficient medium for 48 h. (M-O) *GPMV* from HAP1 cells grown in (M) standard medium for 24 h, (N) deficient medium for 24 h, and (O) deficient medium for 48 h. (P-R) *GPMV* from HAP1-SPT cells grown in (P) standard medium for 24 h, (Q) deficient medium for 24 h, and (R) deficient medium for 48 h. GP values are given as averages \pm S.D. ($n = 150$).

8. KAPITULUA:

**ESFINGOLIPIDOAK ETA
KOLESTEROLA, EGITURA
LIPIDOAK BAINO GEHIAGO**

8. KAPITULUA: ESFINGOLIPIDOAK ETA KOLESTEROLA, EGITURA LIPIDOAK BAINO GEHIAGO

8.1. Sarrera

Azken urteotan zenbait lipido familiaren eginkizunak (Castro *et al.*, 2014) eta horien eragin terapeutikoak (Sahu *et al.*, 2019) birplanteatu dira. Horien artean, esanguratsua da ikusi dela esfingolipidoen azpifamiliako zeramidak zerikusia izan dezaketela zelulen heriotza programatuan, nahiz eta heriotza horretarako mekanismoak ez diren oraindik guztiz ulertzen. Zenbait ikerketaren arabera, badirudi kate luzeko zeramidak —16 Ckoek (naturan ugariak) edo luzeagoek— lipido-fase oso paketatutako sortzeko joera daukatela eta gainera albo-desplazamendu/banaketak eragiten dituztela. Albo-banaketa horien bidez, zeramidan aberastutako domeinuak sortzen dira, eta horiek heriotza zelularra eragin dezaketen mekanismoekin lotuak egon daitezke (Goñi & Alonso, 2009).

Kolesterola animalien mintz plasmaticoetan dagoen eta egitura-funtzioa daukan lipidoa da. Gainera, jakina da mintzen jariakortasuna ere kontrolatzen duela. Kolesterola lipido-urraelaren (*lipid raft*) hipotesian garrantzi handia daukan lipidoa da (Simons & Ikonen, 1997). Urmael horiek kolesterolak eta esfingolipidoek momentu eta gune konkretuetan daukaten kontzentrazio-igoeren ondorioz sortutako mintz-heterogeneotasunak dira. Urmael edo domeinu horiek, beren molekula maila oso ordenatua dela medio, esfingolipidoak eta proteina espezifikoak mintz bidezko garraioa arautu dezakete. Dena den, daukaten iraupen labur eta tamaina txikiaren ondorioz, ez da oraindik mintz heterogeneotasun hauek *in vivo* ikustea lortu.

Ikuspuntu fisiko-kimiko batetik, bai kolesterola, baita zeramida ere, buru polarrean hidroxilo talde bakarra daukaten egitura oso hidrofobikoak dira. Bi horiek, behin geruza bikoitzetan txertatuta, antzeko era batean antolatzen dira. Gainera, hainbat egoeratan, bien arteko albo-desplazamenduak gerta daitezkeela suposatzen da (Megha & London, 2004).

8.2. Zeramida Testuinguruan: Esfingolipidoen Seinalizazioa

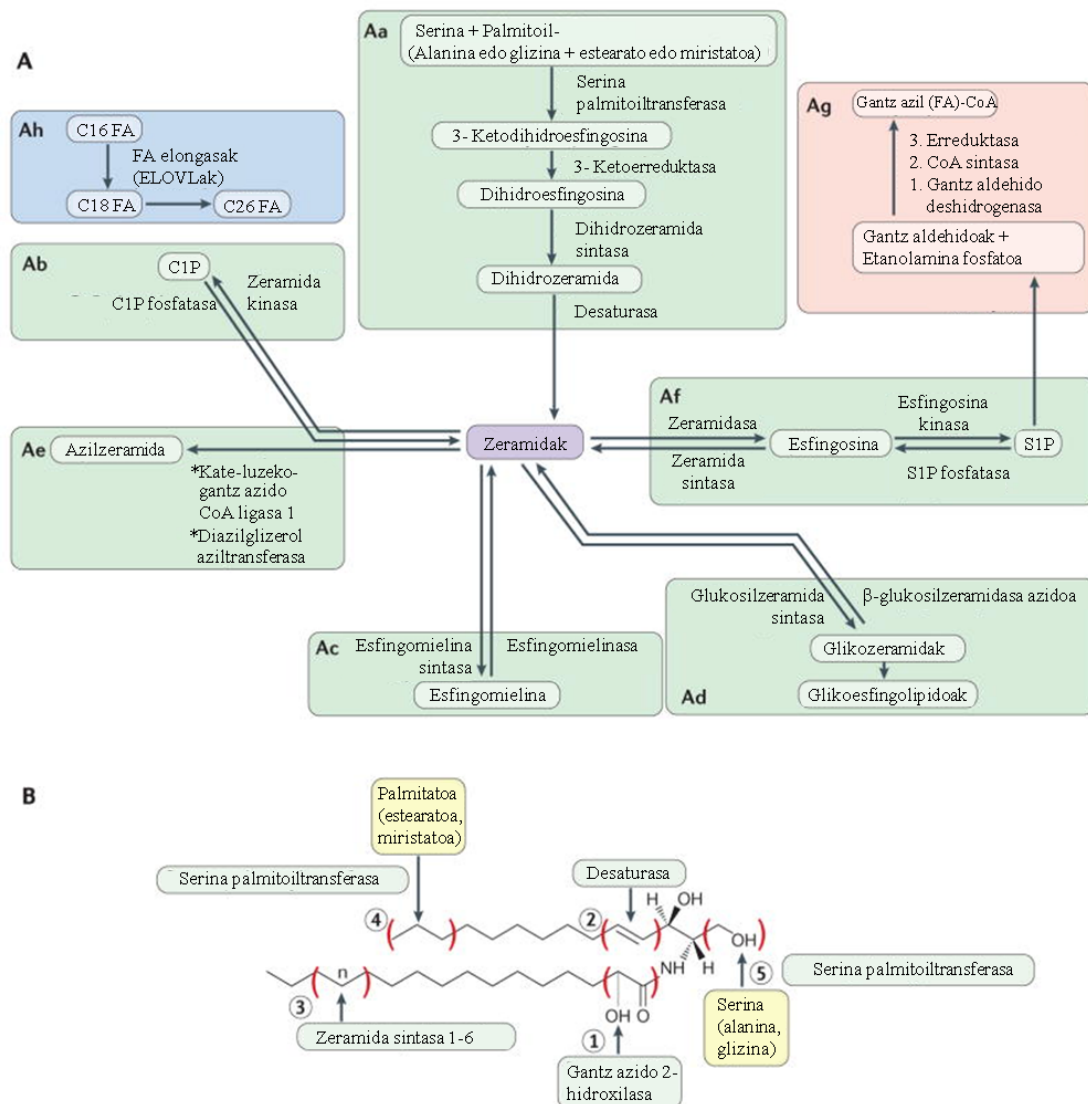
Zeramidek bitartekari-lana dute zelulak estres-egoeren aurrean eman ditzakeen hainbat erantzunetan. Erantzun horien artean, apoptosia eta zelula seneszentzia (Hannun & Obeid, 2018) aurkitzen dira hain zuzen ere. Gainera, aipatutako eginkizunez gain, gaur egun, maila konplexuko beste hainbat esfingolipido bidezko seinalizazio ere deskribatzen ari dira (Garcia-Barrros *et al.*, 2014; Garcia-Gonzalez *et al.*, 2018). Konplexutasun hori lipido bioaktiboen arteko lotze metabolikotik (8.1 irudia), lipido baten egitura-aldaketak dauzkan efektu metaboliko ezberdinetara doa. Lotze metaboliko horren adibide da, hain zuzen ere, zeramida zeramida kinasa bidez zeramida-1-fosfatora eraldatua izan daitekeela eta azken honek jatorriko zeramidak zeuzkanen guztiz aurkako efektu edota eginkizunak dauzkala. Besteak beste, zelula ugalketan, hanturan eta zelula-biziraupenean garrantzia izan dezakeela uste da (Gomez-Muñoz *et al.*, 2013). Dena den, beste hainbat ikerketak erakutsi dutenaren arabera, hantura aurkako eginkizuna ere izan dezake (Lamour *et al.*, 2011). Argi dago gaiaren inguruko desadostasun handiak existitzen direla eta horiei aurre egiteko ikerketa sakonagoak beharrezkoak direla.

Zeramida, zeramida-1-fosfatora eraldatzeaz gain, esfingosinara ere degrada daiteke. Esfingosina izan zen, hain zuzen ere, haren bioaktibitatea deskribatzea lortu zen lehen esfingolipidoa (Hannun *et al.*, 1986). Zenbait ikerketaren arabera, esfingosinarekin eta esfingosinarekin harremana daukaten esfingo baseek endozitosis, ziklo zelularra, aktinazko zitoskeletoaren kontrola eta apoptosia erregulatzeko eginkizunak dituzte (Adada *et al.*, 2014). Beste ikerketa batzuen arabera, arteriosklerosiarekin ere izan dezakete loturaren bat (Jiménez-Rojo *et al.*, 2014b).

Azkenaldiko hainbat artikulutan argitaratu denaren arabera, esfingolipidoen metabolismoaren aldaketak ikertuz eta aldaketa horiek oinarri gisa hartuz, minbizi-terapietan garrantzia izan dezaketen estrategiak sor litezke (Dai *et al.*, 2014; Morad & Cabot, 2012). Gehienetan, terapia horiek gauzatzeko, ur-medio batean disolbagarriagoak diren kate laburreko C6-zeramidak (Flowers *et al.*) edota C2-zeramidak (Zhu *et al.*, 2014) erabiltzen dira.

Zenbait ikertzailek diotenaren arabera, esfingolipidoek prozesu mitotikoetan (Atilla-Gokcumen *et al.*, 2014) eta glaukoma gaixotasunean (Aljohani *et al.*, 2013) ere izan dezakete garrantzia. Aipatutakoa kontuan edukita, eragin metaboliko konplexuak

sortzen dituzten eta esfingolipidoekin harremana daukaten konposatu natural berrien aurkikuntzan jar liteke arreta.



8.1 irudia. Esfingolipidoen metabolismoa (A) eta zeramidaren egitura (B). [Hannun & Obeid (2018)tik] moldatua.

8.3. Zeramida: Hilkortasun-Etengailua Ulertzeko Saiakera

Zeramida apoptosian, zelula hazkuntzaren gelditzean, seneszentzian, diferentziazioan, erantzun immunean eta ziklo zelularra etetearen molekula mailako seinalizazioan eragina izan lezakeen esfingolipidoa da (Kolesnick, 2002). Duela hainbat hamarkadatik, jakina da zeramidak esfingolipidoen metabolismoan bitartekari gisa jarduten duela. Dena den, laurogeiko hamarkadara arte ez zen frogatu zeramidak

seinalizazio metaboliko garrantzitsuekin daukan lotura garrantzitsua (Hannun *et al.*, 1986; Kolesnick, 1987; Merrill *et al.*, 1986).

Zeramida oso kantitate baxuan aurkitzen da ugaztunen artean. Gainera, daukan muturreko hidrofobizitateak ur-medioan ia disolbagaitz egiten duenez, gehienbat mintzetan txertatua aurkitzen da. Hori da, hain zuzen ere, *stratum corneumean*, azal bidezko lurrunketa ekiditen duen mintzean, daukan ugaritasunaren arrazoi nagusia (Wertz & Downing, 1983).

Egituren dagokionez, zeramidak luzera, asegabete, eta hidroxilazio aldakorrek gantz-azido kate batez osatuak daude. Gantz-azido hori amida lotura baten bidez esfingo base baten amino talde batera lotua aurkitzen da. Zeramidak daukan gantz-azidoaren luzera 2 Ctik 28 Cra bitartekoa izan daiteke; dena den, ugaztunen artean, 16 eta 24 Ckoak dira ugariak. Gantz azido horiek, gehienetan, aseak edo monoasegabeak izan ohi dira, eta, batzuetan, C2an (α -hidroxi gantz-azidoa) edota C amaieran (ω -hidroxi gantz-azidoa) hidroxilo talde bat eduki dezakete. Haien hidroxilozitate baxua dela eta, kate luzeko zeramida oso gutxitan aurkitzen da zitosolean; beste hitz batzuetan esanda, gehienetan zelula-mintzetan txertatua aurkitzen da.

Zeramidak zenbait bidezidorretatik sor daitezke: esfingomielinasa bidezko esfingomielinaren degradazio entzimatikoz edota, esfingosinatik abiatuz, zeramida sintasa edo zeramidasas eta tioesterasa neutralen konbinazio bidez (Novgorodov *et al.*, 2011). Bidezidor horien estimulazio ezberdinen ondorioz, zeramidaren sorrera bultzatzea eta horrela gune espezifiko kontzentrazioa ugartzea lortzen da. Zenbait ikerketatan ikusienez, bai esfingomielinasa azidoak, bai neutroak ezberdintasunak daukate beren ioi-dependenzian, pH optimoan eta zelula barneko kokapenean (Chatterjee, 1994). Gainera, esfingomielinasak beste lipido batzuen presentzia bidez erregula daitezke. Izan ere, kardiolipina edota bis(monoazilglizero)fosfato lipido anionikoak esfingomielinasen aktibitate entzimatikoa aktibatzeke gai direla ikusi da. Aipatutakoaz gain, lipido okerdurak ere eragina izan dezake erregulazioan (Goñi *et al.*, 2012).

Hainbat laborategi-ikerketak iradokitzen dutenaren arabera, zeramiden eragin biologikoetako batzuk haien ezaugarri biofisiko bakarren ondoriozkoak dira. Azken 15 urteotan, mintz-ereduetan egindako ikerketen bidez, zeramidek mintzetan daukaten

eginkizunaren inguruko informazio asko argitaratu da. Beste eragin batzuen artean, zeramidaren oso kontzentrazio baxuak (%2-3 mol), hainbat fosfolipidoz osatutako mintz batean, zeramidan aberastutako gel-fase bat albora banatzeko nahikoa dela ikusi da (Carrer & Maggio, 1999). Zeramidaren muturreko kontzentrazioek, berriz, %33tik gorako kontzentrazioek, besikulak ezegonkortzen dituzte (Busto *et al.*, 2009). Zeramida hidrofobikoek mintzaren interfasean urarekin izan lezaketen kontaktua ekiditeko, zeramida molekulek gantz-azidoen gunea betetzen dute, eta honen ondorioz sortzen diren domeinuetako lipidoek molekularreko paketatze handiagoa eta molekulen arteko mugimendu murriztua daukate.

Zeramidan aberastutako domeinu horien presentziak eta egonkortasunak mintzean aurkitzen diren beste lipido guztien ordena molekularrean ere eragina dute. Izan ere, domeinuek, zeramidan aberastuak badaude ere, mintz-ereduan aurkitzen diren beste lipidoen ratio ezberdinak ere bere baitan txertatuak daukate. Horrek geruza bikoitzaren iragazkortasuna handitzea dakar, eta, horrela, edukia edota solutuen fluxua areagotzea eragiten da (Montes *et al.*, 2002; Siskind *et al.*, 2002). Prozesu hori aurrera eramateko mekanismoak ez dira oraindik guztiz ulertzen: alde batetik, domeinuan zeharreko zeramidazko kanal/poroak iradoki dira (Siskind *et al.*, 2002). Dena den, zeramida molekulek, zeramidan aberastutako domeinuetan, bat-batean, poro toroide hipotetiko batean antolatzeke, energia-hesi (entropikoa) handi bati aurre egin beharko liekete. Beste alde batetik, hipotesi horren ordezkoko ideia bat proposatu da. Honen arabera, solutuaren fluxua geruza bikoitzaren egiturak daukan akatsen ondoriozkoa da. Akats horiek zeramidan aberastutako domeinuen eta domeinu horiek inguratzen dituen fasearen arteko faseartean gertatuko lirateke. Hau da, bi faseen arteko paketamendumaila ezberdinak eta geruza bikoitzaren barnean dauden lodiera-ezberdintasunak direla medio, fasearteko muga ez-eraginkor bat sortuko litzateke, zeinetatik solutuen fluxua gertatuko litzatekeen (Goñi *et al.*, 2014). Zeramidak, fase ez-lamelarrak sortzeko daukan joera geruza bikoitza ezegonkortzeko faktore gehigarri bat litzateke; horrela, besikula barneko edukia kanporatzea erraztuko litzateke (Veiga *et al.*, 1999).

Aipatutako mintzean zeharreko solutu-fluxua areagotzeaz gain, kate luzeko zeramidek 3 efektu gehigarri daukate: (i) geruza bikoitzek okerdura negatiboa hartzea (alderantzizko fase hexagonal baten gisa) (Veiga *et al.*, 1999), (ii) flip-flop mugimendua areagotzea (Contreras *et al.*, 2003) eta (iii) geruza bikoitzaren barneko bolumen libreko guneak areagotzea (Axpe *et al.*, 2015). Ezaugarri biofisiko berezi horiek, hain zuzen

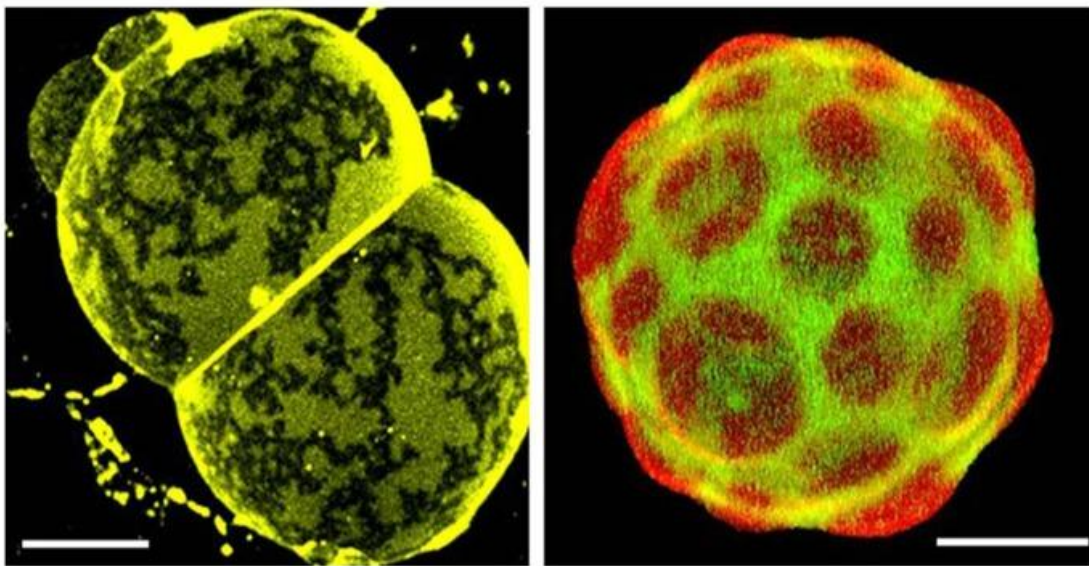
ere, zeramidak heriotza zelularra eragiteko daukan mekanismoarekin lotuak egon daitezke. Beraz, prozesua ondo ulertzeko informazio baliagarria eman lezakete (Cremesti *et al.*, 2002; Alonso & Goñi, 2018). Bestalde, kate laburreko zeramidak fosfolipidoekin hobeto nahasten dira, txertatuta dauden geruza bikoitzetan okerdura positiboa eragiten dute, eta geruza bikoitzaren iragazkortasuna edota mintzean zeharreko solutu-mugimendua areagotzeko ahalmen oso urria dute (Sot *et al.*, 2005).

8.4. Lipido-Domeinuak: Kolesterola eta Lipido-Urmaelaren Hipotesiaren Gaur Egungo Egoera

Azken 40 urteetan, mintz-ereduetan egin diren ikerketek albo-domeinuen sorreran zeresana daukaten oinarri garrantzitsuenak ulertzea erraztu dute. Mintzetako lipido-domeinuen sorrera oso lotua dago lipidoen ezaugarri fisikoen arabera den lipido-lipido elkarrekintzekin. Hirurogeita hamarreko hamarkadan, Chapman eta lankideek, ekortze-kalorimetria bereizgarria (DSC) erabiliz, ikusi zuten zenbait fosfatidilkolina ase ez direla nahaskorrak (Phillips *et al.*, 1970). Ordutik, beste hainbat teknikan oinarrituz, ikerketa askok zenbait lipidok albora banatzeko daukaten ahalmena erakutsi dute (Oldfield & Chapman, 1972). Gaur egun, ondo ulertzen da gantz-azido asedun lipidoek lipido-domeinuak sortzeko joera daukatela lipido asegabeekin nahasten direnean. Izan ere, gantz-azido aseak Van der Waals elkarrekintza sendoagoak gauzatzen dituzte; horien bidez, gel-fluido fase-trantsizioaren tenperatura altuak sortzen dira. Beraz, lipido aseak (16 C-koak edo luzeagoak), normalean, gel fasean aurkitu ohi dira 20-37 gradu zentigradu bitarteko tenperaturetan. Horrek azalduko luke, hain zuzen ere, lipido ase horiek lipido asegabeekin kontaktatzean gertatzen den albo-domeinuen sorrera. Lipido asean artean, esfingosinara gantz-azido ase bat itsatsia daukan esfingomielinak, beste hainbat lipidorekin nahastean, albora banatzeko joera handia dauka. Mintz-ereduetan, urte- tenperatura baxuko fosfolipidoekin nahastean sortutako esfingomielina eta kolesteroletan aberastutako likido antolatudun domeinuak albo-domeinuen adibide interesgarria lirateke.

Lipido-urmaelaren hipotesiak, 1997an Simons eta Ikonenek proposatuak, eragin nabarmena izan zuen gaiaren inguruan (Simons & Ikonen, 1997). Hipotesi horren arabera, zelula bizien mintzetan domeinu nanometrikoak egon daitezke. Domeinu horiek, *in vitro* egindako entsegetan mikroi batzuetako tamaina izan dezaketen arren (8.2 irudia), *in vivo* daukaten tamaina txikiaren eta existentzia-denbora laburraren

ondorioz, oraindik ez dira detektatu, ezta haiek kuantifikatzea lortu ere. Singer eta Nicolsonek ideia hori beren teoriaran plazaratu ez zutela kontuan izanda (Singer & Nicolson, 1972), Simons eta Ikononen albo-banaketen ideia kontzeptu oso berritzaile bat izan zen. Azken urteotan, mosaiko jariakorraren eredua eredu berritzaile batera moldatua izan da, zeinetan kontzeptu berriak kontuan hartzen diren, hala nola albo-banatuak fasek, lipido asimetria edota proteina-proteina elkarrekintzak (Engelman, 2005; Goñi, 2014; Bagatolli & Mouritsen, 2013).



8.2 irudia. Mikroji batzuetako tamainako domeinua duten mintzen irudiak, mikroskopio konfokalk bidez lortuak. Ezkerrean: gizakien azaleko *stratum corneum*eko lipidoz osatutako mintz naturala. Espezializatutako mintz honek 11 zeramida ezberdin, kolesterola eta kate luzeko (C24–C26) gantz-azidoak ~1:0,9:0,4 mol ratioan dauzka. Bertan, gel motako bi fase bereiz daitezke (Plasencia *et al.*, 2007). Mintza DiIC_{18z} markatua dago, T = 32°C (azaleko tenperatura fisiologikoa). Eskuinean: txerriaren birrika surfaktanteko mintzak. Mintz espezializatu hori batez ere fosfolipidoz eta era bereizgarrian lotutako proteinez (SP-B eta SP-C) osatua dago. Fosfolipidoen artean, animalia-mintz gehienetan ezohikoak diren dipalmitoilfosfatidilkolina eta fosfatidilglizerola dauzka. Fosfatidilkolina monoasegabeak, fosfatidilinositola eta lipido neutroak (horien artean kolesterola) proportzio ezberdinetan ageri dira (Bernardino de la Serna *et al.*, 2004). Mintz natural hau DiIC_{18z} (gorria) eta Bodipy-PCz (berdea) markatua dago. Bertan, batera existitzen diren fase jariakor eta antolatua dauzka, T = 37°C. Eskala-barrak= 10µm. [Bagatolli & Mouritsen (2013)tik] hartua.

Lipido-urmelaren hipotesiaren arabera, lameladun likido-antolatuaren fasea, esfingomielinaren eta kolesterolaren arteko elkarrekintzaren lehentasunean oinarritzen da (Patra *et al.*, 1992). Hipotesi horren planteamenduaren aurretik, ideia hori, tradizionalki, azaldu da gantz-azidoen eta talde polarren bitartean kolesterolak betetzen

dituen guneen bidez, eta geruza bikoitzetako geruza ezberdinen digitazio arteko gertakizunetan eragina izateko aukeraren arabera (McIntosh *et al.*, 1992). Dena den, existitzen den elkarrekintza garrantzitsuena bi molekularen arteko hidrogeno-lotura sendo baten bidez ere azal daiteke (Lönnfors *et al.*, 2011; Slotte *et al.*, 2017). Esfingomielinaren eta kolesterolaren kasuan, horien arteko elkarrekintza eragiten duen indar garrantzitsuena esfingomielina molekularen amida taldearen eta kolesterolaren 3-hidroxil taldearen arteko hidrogeno-lotura bat dela dirudi (Ramstedt & Slotte, 2002). Badirudi elkarrekintza hori ezinbestekoa dela, bai esfingomielinatan bai kolesteroletan aberastuak diren domeinu likido- antolatuak sortzeko.

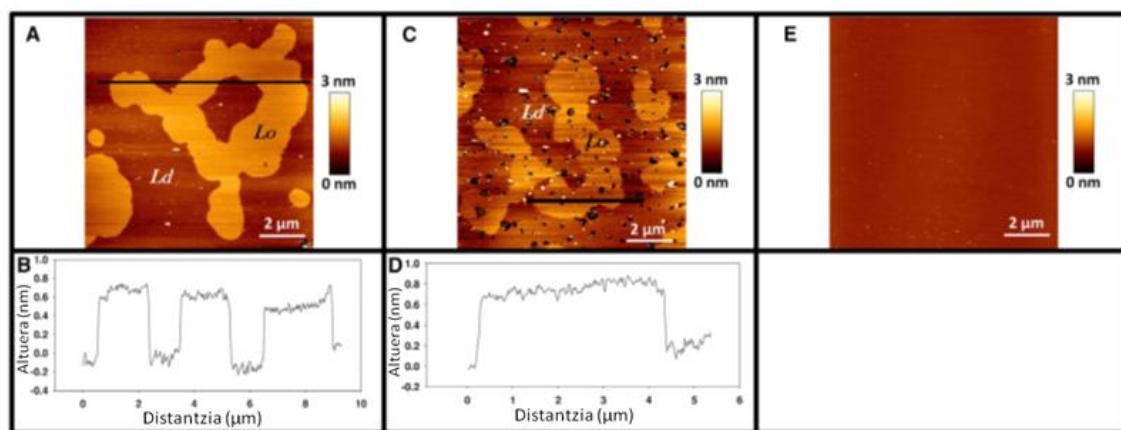
Esfingomielinak daukan elkarrekintza-ahalmen handiak molekula horrek zeramidak ere daukan elkarrekintza estua ere azal lezake. Izan ere, zeramidak esfingomielinaren amida taldeko hidrogenoarekin lotura sor dezakeen hidroxilo taldeak dauka. Badirudi esfingomielinak daukan zeramidakiko edo kolesterolakiko lehentasunak elkarren arteko alboratzeak gertatzea ahalbidetu lezakeela.

Lipido-urmaelaren hipotesiak arazoak ere badauzka barnean; izan ere, hipotesia *in vivo* egiaztatzeko eragozpen nabarmenak daude. Aurretik aipatu den bezala, arazo garrantzitsuenak domeinuen trantsizio-natura eta beraien tamaina nanometrikoak dira, mintz-ereduetan domeinu horiek mikroi batzuetako tamaina daukaten arren (8.2 irudia). Gainera, mintz ereduak ez bezala, zelula bizidunek zitoskeletoa edukitzeak ere zeresana izan lezake. Izan ere, zitoskeletoak domeinuen tamaina izugarri murriztuko luke, haien tamaina eskala nanometrikora eramanez (Honigmann *et al.*, 2013). Ideia hori azaltzeko, taktet-hesi edota *picket fence* izeneko ereduak proposatu da; horretan, aktina-sareak mintza konpartimentutan bananduko luke, eta, horrela, lipidoen alboratzea eragingo (Kusumi *et al.*, 2012).

Esfingomielinaren eta kolesterolaren arteko lipido-lipido elkarrekintza guztiak ez dira urmael-sortzaileak. Kontuan eduki behar da esfingolipidoen artean bai esfingomielinen eta bai zeramiden egitura-aldaketa txikiak erabakigarriak izan daitezkeela beraien ezaugarri biofisikoentzat (Pinto *et al.*, 2011; Slotte, 2013). Esfingolipidoak eraldatuta ager daitezke, deoxiesfingolipido (Jiménez-Rojo *et al.*, 2014a; Zuellig *et al.*, 2014; Lone *et al.*, 2019) edota dihidroesfingolipido (Vieira *et al.*, 2010) gisa, eta horien lipido-lipido elkarrekintza-ahalmenak ez dira oraindik ondo

ezagutzen. Dena den, dagoen informazioaren arabera, badirudi egitura-aldaketa txikiak jasateak molekularen ezaugarri fisiko-kimikoetan eraldaketa handiak sor ditzaketela.

Mintz-ereduen bitartez, C24:1 esfingomielinak likido antolatudun domeinuetan disolbagarritasuna areagotzeko eragina daukala egiaztatu da; izan ere, beste lipido batzuk fase bakarrean barneratzen ditu (Maté *et al.*, 2014) (8.3 irudia). Ikerketa horren arabera, animalia batzuen globulu gorrien erauzkintan ere gertatzen da hori. Izan ere, ikertu diren erauzkintetik batek ere ez du likido antolatuaren faserik sortzen, nahiz eta horietan C24:1 esfingomielina aurkitzen den. Beste lipido batzuek izan dezaketen disolbagarritasun-efektua neurtzeko, disolbagarritasun-ugaritzea eta domeinu-sortzea eragiten duten lipidoen arteko ratioei buruzko ikerketa gehiago beharrezko dira.



8.3 irudia. Geruza bikoitzeko lipidoen irudia topografikoak, indar atomikoko mikroskopia (AFM) bidez lortuak. (A) DOPC / 16:0 SM / kolesterola (2:1:1 ratio molarra). (B) A irudian agertzen den lerro beltzaren altuera-profila. (C) DOPC / 24:0 SM / kolesterola (2:1:1 ratio molarrean). (D) C irudian agertzen den lerro beltzaren altuera-profila. (E) DOPC / 24:1 SM / kolesterola (2:1:1 ratio molarra). E irudiak erakusten du ea 24:1 esfingomielinaren presentziak likido antolatuaren fasea alboratzea eragozten duen. [Maté *et al.* (2014)etik] hartua.

8.5. Zeramidetan Aberastutako Domeinuak: Ikuspuntu Zelularrak eta Garrantzia Terapeutikoa

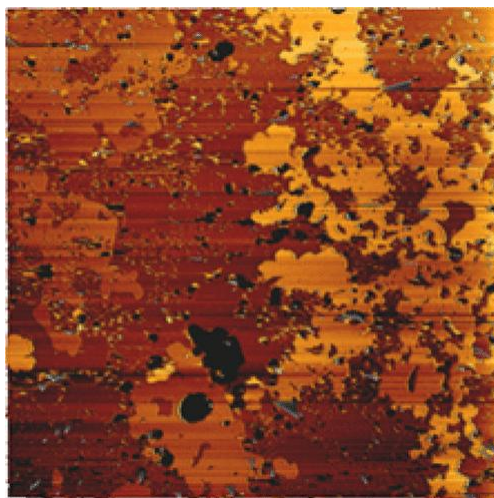
Fosfolipidoz, zeramidaz eta kolesterolez sortutako geruza bikoitzetan zeramidatan aberastutako domeinuak agertzea geruza bikoitz horiek daukaten kolesterol kantitatearen menpekoa da. Agerpen hori, batez ere, bietako bat edota biak kantitate handian dudenean nabarmentzen da. Horrela bada, seinalizazio apoptosikoak bideratzen dituen prozesuetan, kolesterolaren eta zeramidaren arteko balantze kritiko batek

modulatzaile gisa jardun lezake (Sot *et al.*, 2008; Busto *et al.*, 2010, 2014). Gainera, jakina da zeramidak apoptosia erregulatzen duela, eta badirudi mitokondrien lipido-konposizioa guztiz aldatu ostean haien mintzean zeharreko zitokromo C oxidasaren fluxua gertatzen dela (Cosentino & García-Sáez, 2014; Zhang *et al.*, 2014). Dena den, poro apoptosikoa sortzeko mekanismoak (bai lipido-lipido eta baita proteina-lipido modulazioak ere) oraindik argitu gabe daude (Basañez *et al.*, 2012).

Zelula-mintzetan ere, mintz-ereduetan gertatzen den antzera, zeramidak daukan alboratze-gaitasun handiak garrantzia izan dezake. Asetasun-egoeretan, zeramidaren eta kolesterolaren arteko elkarrekintza positibo bat existi daiteke (García-Arribas *et al.*, 2015, 2016b; Garcia-Arribas *et al.*, 2016). Kontuan eduki behar da, hortaz, sasoi batean globulu gorrien bero-hotz bidezko hemolisian zeramidatan aberastutako gisa deskribatu ziren domeinu haiek (Montes *et al.*, 2008) kolesteroletan aberastuak diren gel-domeinuak ere izan litezkeela. Izan ere, giza globulu gorrien mintz plasmaticoak kolesterol kantitate handiak (%40 molarretik gora) dauzka (Owen *et al.*, 1982). Kolesterol-kontzentrazio altuko egoera horietan, guneko zeramida-kontzentrazio altuen ondorioz, bai zeramidatan eta bai kolesteroletan aberastuak egon daitezkeen gel-faseak sor litezke (Montes *et al.*, 2008). Egoera hori dagoeneko azaldua da globulu gorrien lipido-erazkintetan (García-Arribas *et al.*, 2016a).

Garrantzitsua da aipatzea mitokondrietan ere egon litezkeela kolesteroletan eta zeramidatan aberastutako gel-domeinu konplexu halakoak. Mitokondrien kanpo-mintza kolesteroletan urria dela uste bada ere, azken hamarkadetako ikerketek erakutsi dutenez, kolesterolaren presentzia altuagoa izan daiteke zenbait gaixotasunen adierazgarri (Garcia-Ruiz *et al.*, 2009). Berriki egin diren beste ikerketa batzuen arabera, kolesterola DNA mitokondrialaren bitartekaria izan daiteke (Gerhold *et al.*, 2015; Desai *et al.*, 2017). Ikerketa batek dioenaren arabera, mitokondrien kanpo-mintzeko kolesterol-kontzentrazioaren ugartzea kimioterapia bidezko heriotzaren erresistentziarekin lotua dago (Montero *et al.*, 2008). Hori kontuan izanda, kolesterol-zeramida orekaren hipotesiak garrantzia izan dezake honako bi ideietatik: zeramida heriotza zelularraren prozesuekin lotua dago, eta estres-egoeran dauden mitokondrien mintzetan zeramidatan aberastutako domeinuak ageri dira (Lee *et al.*, 2011). Kolesterol kantitate handiako batek elkarrekintzak izango lituzke zeramidatan aberastutako domeinuekin, edo bai zeramidatan eta bai kolesteroletan aberastua dagoen beste era bateko fase bat sor lezake, zeinak, segur aski, zelularen seinalizazio-segidan efektu ezberdinak izango lituzke.

Tumore aurkako gaur egungo terapietarako dagokienez, hainbat esfingolipido lotu dira kimiorresistentzia-mekanismoarekin. Esfingomielinak eta glikoesfingolipidoak hainbat drogarekiko erresistenteak den ABCB1 proteinarekin lotu dira. Lee eta Kolesnickek mintzean aurkitzen den esfingomielina, zeramida edota kolesterol eta drogak lotzeko eta garraiatzeko garrantzitsuak direla diruditen ABCB1en mintzean zeharreko domeinuaren hainbat elkarrekintza-gune postulatu zituzten (Lee & Kolesnick, 2017). Esfingolipidoek DNA kaltetuaren erantzun-mekanismoan ere parte hartzen dute (gutxienez legamietan) (Ferrari *et al.*, 2017). Gainera, gibelean, drogen glutazio- eta detoxifikazio-prozesuetan ere zerikusia daukatela ikusi da (Park *et al.*). Kimioterapia osteko zelula-ugaltzearen edota heriotza zelular murriztuaren inhibizio eskasaz arduratzen diren mekanismo molekularrak tumore identitatearen, pilatutako gene mutazioaren edota epigenetika bidezko gene-eraldaketen menpekoak dira. Kimioterapia osteko heriotza zelularrekin lotutako bidezidor garrantzitsuenak mekanismo apoptosikoa eta autofagikoa dira. Bi mekanismo horiek kinasaren, fosfatasaren, p53-aren eta beste batzuen eraginpean egon daitezke, eta esfingolipidoak, hain zuzen ere, aipatutako proteina horien erregulatzaile garrantzitsuak dira (Flowers *et al.*).



8.4 irudia. 16:0 zeramida eta 24:1 zeramida kontzentrazio molekular bereberetan dituen DOPC / 24:1 esfingomielina / kolesterol bidez sortutako mintz baten AFM bidezko irudia. Bi lipido-domeinu identifika daitezke, bietako bakoitza zeramida batean aberastua dago. Esfingolipido (eta batez ere zeramida) ezberdinek dauzkaten betebeharrak biofisikoen ebidentzia argia da hau. [García-Arribas *et al.* (2017)tik hartua].

Hainbat argitalpenek maiz erakutsi dute esfingolipidoek zelulan dauzkaten efektuak esfingolipido mota ezberdinen menpekoak direla. Berriki argitaratu diren bi

berrikuspenetan ongi laburbiltzen da esfingolipido ezberdin horiek minbizian izan dezaketen zelulen seinalizazioan nola eragiten duten (Hannun & Obeid, 2018; Ogretmen, 2018). Luzera eta asegabetze ezberdinetako zeramidek izan ditzaketen efektu biofisiko ezberdinak eta existi daitezkeen hainbat lipido-domeinuren aldi bereko existentzia kontuan edukiz (8.4 irudia), esfingolipidoen konplexutasuna eta haien efektuak era esponentzian hazten ari dira. Gainera, azpifamiliak (deoxiesfingolipidoak, dihidroesfingolipidoak etab.) kontuan hartzen baditugu, atea irekitzen zaie horiek terapietan erabili ahal izateko aukera berriei

8.6. Ondorioak

Laburbilduz, esparruko azken aurrerapenek erakusten dute zelulen mintzetan gero eta garrantzitsuagoak diruditelako zeramidaren eta kolesterolaren arteko lipido-lipido elkarrekintzek, eta antzekoek. Dena den, azken hamarkadan, lipido-lipido elkarrekintza eta esfingolipido bidezko seinalizazio-ebidentzia gehienak mintz-ereduetan karakterizatu dira. Arrazoi horregatik, gaiaren inguruko ikerketa aurreratuenak eredu konplexuago batera eraman beharko liriateke, hau da, zelula-mintzetara edota *in vivo* eginiko esperimentuetara. Horrek egituraren (lipido faseen existentzia) eta funtzioaren (mintz-trafikoa eta seinalizazio zelularra) arteko erlazioa guztiz argituko luketen ereduak garatzen lagunduko luke. Gainera, espero da eredu horiek garrantzia izango dutela minbiziaren aurkako terapien inguruko jakinduria hobetzean eta tumoreen aurkako tratamenduen eragina handitzean.

CHAPTER 9:
OVERVIEW AND
CONCLUSIONS

CHAPTER 9: OVERVIEW AND CONCLUSIONS

The present thesis intends to explore the role of SL on cell growth and cell membrane composition and physical properties, using genetically modified or chemically treated cells with impaired SL synthesis. Different biophysical techniques, mainly fluorescence spectroscopy and microscopy, AFM, and mass spectrometry have been used with the following aims:

- To define the fluidity changes undergone by the PM and intracellular membranes when CHO and HAP1 cell lines are depleted in SL.
- To characterize by AFM the changes in PM and intracellular membrane breakthrough forces after SL-depletion in CHO and HAP1 cell lines.
- To apply lipidomic techniques to provide information on the lipid homeostatic response undergone by PM and intracellular membranes when CHO and HAP1 cell lines are depleted in SL.
- To integrate the cellular and molecular data in a unified description of our advances in defining the role of SL in cell function.

9.1. Patches and Blebs: Two Plasma Membrane Preparations From CHO Cells

Model membranes have been widely used in membrane biophysical studies making possible the observation of heterogeneities in synthetic lipid membranes. However, they do not maintain the compositional complexity and they lack the variety of protein-lipid interactions found in nature. Taking this into account, subcellular membrane preparations, in particular those derived from the PM, are now more than ever required for biochemical and biophysical studies.

In chapter 3, two different PM preparation methods have been used to describe the composition and physical properties of PM from CHO cells. One was based on adhering cells to a polylysine-coated surface, followed by a hypotonic lysis and the removal of intracellular components, so that PM patches remained adhered to the support. A second one consisted of inducing bleb formation in cells, followed by a

separation of the “free blebs”, or GPMV. Both methods gave rise to PM in sufficient amounts to allow their structural, biophysical and biochemical study.

Molecular lipid order (measured with laurdan GP) and nanomechanical resistance (measured with AFM in the force spectroscopy mode) were rather similar in GPMV and PM patches, and higher than in the average cell membranes. Lipid analysis revealed that PM also exhibit peculiarities in their lipid composition, e.g. being rich in Chol and relatively poor in polyunsaturated fatty acids. These differences between PM preparations and whole cell membranes should not obscure the fact that other (minor, but significant) variations exist between blebs and patches, arising probably from the peculiar methods used in each preparation. The current work opens the way to more detailed structural and functional studies of CHO cell PM.

9.2. LY-B: A CHO Cell Line with Genetically Induced SL-Restricted Cell Membranes

In vivo studies of the SL roles are hampered, among other reasons, by the fact that they can be either synthesized *de novo* or taken up from the diet. A plausible approach would be to investigate mutant cells containing the smallest possible amounts of SL. This is the case of LY-B, a SPT-defective mutant CHO cell line with a suppressed *de novo* SL synthesis, while maintaining its capacity of taking up and metabolizing exogenous sphingoid bases from the culture medium. To avoid the external uptake of lipids, LY-B cells were adapted to grow with a very low external source of SL, i.e. a medium containing 0.04 FBS%, 250-fold less than the standard (10%) concentration used in this kind of cell cultures.

In chapter 4, PM preparations and lipid vesicles derived from the LY-B cell line were compared to those from the wild type CHO strain. a) Laurdan fluorescence of LY-B recorded a significant decrease in their membrane rigidity, b) AFM-mediated force measurements demonstrated that lower breakthrough forces were required to penetrate samples obtained from SL-poor LY-B cells, and c) mass-spectroscopic measurements indicated that SM was decreased by about 85% as a result of SL limitation in the medium. Smaller, though significant, changes were also detected in GPL under SL-restriction conditions. PM compositions exhibited similar changes, at least qualitatively, as the whole cells with SL restriction.

A 250-fold reduction in SL supply to LY-B cells led only to a 6-fold decrease in membrane SL, underlining the resistance to changes in composition of these cells. A linear correlation was observed between the SM concentration in the membranes, the degree of lipid order and the membrane breakthrough forces.

9.3. SL Synthesis Inhibition by Myriocin in CHO Cells: A Biophysical and Lipidomic Study

Two main strategies for establishing the cellular effects of a given enzyme activity suppression are (a) the use of a stably mutated cell line that lacks a functional gene, or (b) treating the wild type with an inhibitory compound that affects the same gene-product protein. Thus, one strategy to detect the effects of an overall SL decrease would be the specific inhibition of the SPT enzyme.

SPT can be inhibited with non-natural and also natural products, among the latter the antifungal antibiotic myriocin. In chapter 5, we explore the effects of myr-induced SPT inactivation of CHO cells on, a) cell growth, b) lipid composition and c) membrane physical properties, compared to a SPT-defective mutant CHO cell line (LY-B).

Similar effects were observed with both approaches: SM values were markedly decreased in myr-treated CHO cells and, in consequence, their membrane molecular order (measured as laurdan GP) and mechanical resistance (AFM-measured breakthrough forces) happened to be lower than in the native, non-treated cells. Cells treated with myr reacted homeostatically to maintain membrane order, synthesizing more fully saturated and less polyunsaturated GPL than the non-treated ones. However, only partial homeostatic reorganization was achieved, as their PM remained somewhat more fluid and penetrable than those from the control cells.

9.4. SM Depletion in Plasma Membrane by CD: Physical and Compositional Consequences

CDs possess a hydrophilic surface that makes them soluble in water, while their non-polar cavity provides them with the ability to entrap specific lipids when interacting with membranes.

In chapter 6, a comparative analysis of M α CD and M β CD effects on the PM of wild type CHO and SPT-deficient LY-B cell lines was carried out. Both CDs can accommodate phospholipids in their inner cavity, while only the larger M β CD can also accommodate sterols. CD can be used in the unidirectional extraction of lipids from the PM, or, when pre-loaded with the desired lipids, they can cause an exchange of lipids.

Treatment with M β CD was more deleterious than with M α CD. A loss of SM of 36-93% was measured, depending on the experimental conditions. M α CD led to a larger SM depletion than M β CD, and CD loading increased the loss of the mCherry-lysenin signal, a specific SM probe. Both, laurdan GP and AFM- mediated breakthrough forces were lowered after treating cells with CD, indicating more fluid, less stiff membranes. This decrease was larger for cells treated with PC-loaded M α CD than for those treated with PC:Chol-loaded M β CD. LY-B cells were invariably more sensitive to CD than CHO. CD-mediated lipid exchange was more easily performed than unidirectional lipid extraction.

It was concluded that M α CD and M β CD are interesting and efficient tools for modulating PM lipid composition, in particular for SM depletion. Apart from this, the exchange method would also make possible the introduction of particular SM species of interest in the PM, in order to study their biophysical properties. CDs constitute a significant alternative to more complex methods, such as engineering of lipid metabolic pathways(Dowhan, 2009)(Dowhan, 2009)(Dowhan, 2009)(Dowhan, 2009)(Dowhan, 2009)(Dowhan, 2009)(Dowhan, 2009)(Dowhan, 2009)(Dowhan, 2009), or to slower and less specific procedures such as the use of biochemical inhibitors. In addition, these dextrins can be used in the study of membrane asymmetry because they only extract lipids from the outer leaflet.

9.5. SL Restriction in HAP1 Cells that Constitutively Contain Low Amounts of SL

The analysis of membrane properties of real cells containing minimal amounts of SL would help in understanding the biophysical properties of “simple” SL and “more complex” glycoSL.

In chapter 7, the biophysical properties of human origin, SPT-defective, near-haploid HAP1 SPTLC1(-) strain membranes were measured and compared to the wild type HAP1 and to previously studied CHO and LY-B cell lines.

In most mammalian cells, SM is by far the major SL, its concentration being one order of magnitude above that of Cer or of HexCer. This is not the case with HAP1/HAP1-SPT, in which SM concentration is one order of magnitude below that in CHO/LY-B cells grown in full FBS-containing medium, thus at a concentration similar to that of Cer or HexCer. In addition, HAP1-SPT, but not HAP1 cells, exhibit a further large decrease in SM, both in whole cell and PM preparations, when grown under SL-limiting conditions. Studying membranes with lowered SL, in membranes that constitutively contain very low SL concentration, provides a new vantage point from which the membrane effects of SL deprivation can be examined.

In addition, CHO and LY-B cells contained around 10-15% short-chain GPL, while HAP1 and HAP1-SPT contained twice as much. Both, the above-mentioned low SM and the increased short-chain GPL will probably influence the membrane biophysical properties in the same sense, specifically lowering GP and breakthrough forces of HAP1/HAP1-SPT as compared to CHO and LY-B cells. When HAP1-SPT were grown in SL-deficient medium, laurdan GP and breakthrough force values of their PM preparations failed to show any statistically significant change with respect to the control samples, revealing an homeostatic adaptation of the cell to extreme SL deprivation conditions.

The capacity shown by certain cells, either genetically modified or treated with specific inhibitors, to buffer the rigidity/fluidity differences by modulating their lipid composition opens the way to a variety of functional studies on the role of SL in membranes.

9.6. Sphingolipids and Cholesterol “sociability”

In recent years the specific interaction of SM with Chol has been examined, largely in the context of the “lipid raft” hypothesis. Nevertheless, the existence of rafts has been questioned and it is currently a matter of controversy; the use of the expression “transient nanodomains” instead of “rafts” has been proposed.

Raft-like nanodomains are membrane heterogeneities caused by transient, localized, high concentrations of Chol and SL that would govern membrane trafficking for both SL and specific proteins, perhaps due to their high degree of molecular order. In chapter 9, the existing knowledge on SL and Chol in the transient nanodomains has been reviewed.

Studies indicate that long-chain Cer have a tendency to form highly packed lipid phases that tend to segregate laterally, giving rise to Cer-enriched domains that could be related to the cell death-inducing mechanisms. Besides, Chol is a component of animal cell membranes known to regulate their fluidity or molecular order.

From a physicochemical point of view, both Chol and Cer are highly hydrophobic components with a single hydroxyl group in their polar head. They tend to be oriented similarly in the bilayer, and mutual displacement or exchange between them could be expected under certain circumstances. In addition, Cer can be generated enzymatically from those SL (such as SM) that interact with Chol for lipid nanodomain formation. This event connects nanodomain disassembly with Cer synthesis through SM hydrolysis and it is the key point of interest as to the “sociability” of Cer and cholesterol.

The short lifetime and small size of these domains would be one of the main drawbacks that hamper their direct observation *in vivo*. Domains have been characterized in model systems over the last decade in the context of lipid-lipid interactions and SL-driven signaling. More complex models closer to cell membranes or even *in vivo* experiments, will contribute to clarify the relationship between structure (lipid phase coexistence) and function (membrane trafficking and cell signaling) in these domains.

9.7. Advances Related to the Role of SL in Cell Function

One of the aims of this thesis was “to integrate the cellular and molecular data in a unified description of our advances in defining the role of SL in cell function”. Not unexpectedly, this aim has not been fully achieved, mainly due to the complexity of the cellular events in which SL are involved. We were able to study in certain detail only three SL classes, namely SM, Cer and HexCer, and only one aspect of cell function, i.e. membrane fluidity, apart from the global function of cell division.

To begin with, the question has been posed in the literature on the possibility of mammalian cells totally dispensing with SL. However, in view of our results, and particularly considering the virtual impossibility of decreasing the amount of SL in membranes below a certain level, even under conditions of suppressed *de novo* synthesis and extremely low SL concentrations in the growth medium, it can be stated that, in the light of our experimentation, a minimum SL concentration in membranes is essential for mammalian cell division.

SM, the most abundant SL in the cell, plays at least two roles, one in the regulation of membrane fluidity, actually tending to decrease it, then an equally important one in providing a metabolic depot and/or source of other SL, of which Cer and HexCer are representative examples, Cer as a metabolic signal, HexCer as a primer molecule in the synthesis of the complex glycoSL, e.g. globosides or gangliosides. The data presented in this thesis demonstrate that the amount of SM in membranes can decrease markedly, membrane fluidity (molecular order) being homeostatically compensated by changes in glycerophospholipid chain length and unsaturation. However, Cer and HexCer concentrations are much more conserved, undoubtedly because of their specific roles for which no other molecule may substitute.

If our attempts to define the SL role in cell function have not gone very far, we could be moderately satisfied with the integration of cellular and molecular data, also a part of this aim. In fact, the combination of (i) the various genetic and chemical techniques to decrease *de novo* synthesis of SL in mammalian cells, (ii) the fluorescence and atomic force spectroscopic studies on the basic property of membrane fluidity, and (iii) the lipidomic data of the cells and cell membranes under study, provides a sound technological framework to pursue this kind of studies in the future.

9.8 Conclusions

The main conclusions of this work include:

- A clear correlation exists between decreased SL contents and changes in biophysical properties in membranes.
 - Cell PM and intracellular membranes are more fluid, or less ordered, according to laurdan general polarization, when cell lines are depleted in SL.
 - Cell PM and intracellular membranes become more penetrable according to AFM-mediated force spectroscopy measurements, when cell lines are depleted in SL.
- CHO and HAP1 try to maintain membrane order undergoing a lipid homeostatic response when they are depleted in SL synthesizing more fully saturated GPL and less polyunsaturated ones.
 - LY-B cells maintain membrane order only partially as their PM are more penetrable when compared to CHO grown in SL-deficient medium.
 - HAP1-SPT cells maintain membrane order as their PM are not more penetrable as compared to HAP1 even under extreme SL deprivation conditions.

9. KAPITULUA:
LABURPENA ETA ONDORIOAK

9. KAPITULUA: LABURPENA ETA ONDORIOAK

Tesi honetan, SLen sintesi ez-egokia duten genetikoki eraldatutako zelulak erabiliz, SLeK hazkuntza zelularrean eta mintzen konposizio eta ezaugarri fisikoetan duten zeregina ikertu nahi izan da. Teknika biofisiko ezberdinak erabiliz; batez ere espektroskopia eta mikroskopia fluoreszentea, AFMa eta masa-espektrometria, jarraian aipatuko diren helburuak bete nahi izan dira:

- CHO eta HAP1 zeluletan SLak murrizten direnean, PMek eta zelula barneko mintzek jasaten dituzten jariakortasun aldaketak definitzea.
- CHO eta HAP1 zeluletan SLak murrizten direnean, AFM bidez, PMen eta zelula barneko mintzen apurtze indarrek jasaten dituzten aldaketak atzematea.
- CHO eta HAP1 zeluletan SLak murrizten direnean, teknika lipidomikoak erabiliz, zelula barneko mintzek ematen duten erantzun homeostasikoaren inguruko informazioa lortzea.
- Entseguen bidez lortutako aurrerapenak, SLeK zelulen funtzioan duten eginkizunaren gaineko deskribapen batean bateratzea.

9.1. Partxeak eta Babak: CHO Zelulen Mintz Plasmaticoaren Prestakinak Lortzeko Bi Aukera Ezberdin

Azken urteotan mintz ereduak era zabal batean erabili izan dira mintzen ikerketa biofisikoak gauzatzeko. Ikerketa hauen bidez mintz sintetikoetan lipido heterogeneotasunak ikustea posible izan da. Dena den, kontutan izan behar da, mintz ereduak ez dituztela zelulek dauzkaten konposizio konplexuak, ezta naturan aurkitzen diren proteina-lipido elkarrekintza sarerik ere. Hau kontuan hartuta, zenbait mintz prestakin azpizelular ezberdin, batez ere PMA, ikerketa biokimiko eta biofisikoak gauzatzeko inoiz baino erakarriago bilakatu dira.

3. kapituluuan, CHO zelulen PMaren konposizioa eta ezaugarri fisikoak deskribatzeko baliagarriak diren PM prestakinak lortzeko bi metodo ezberdin azaltzen dira. Bata, zelulak polilisinaz gaineztatutako gainazal batera itsatsi, eta lisi hipotoniko baten bidez zelulak lehertzean oinarritu zen. Kanporatutako zelula barneko osagaiak mediotik kendu ostean, emaitza gisa, gainazalera itsatsitako PM partxeak lortu ziren.

Bestean, zelulen baba formazioa eragin eta gero, “baba aske” edo GPMVak eskuratzen ziren. Bi metodoen bidez, PMaren egitura, biokimika eta biofisika ikertzea ahalbidetzen duten prestakinak kantitate egokian lortu ziren.

GPMV eta PM partxeak beraien artean alderatuz, bi kasuetan, lipidoen ordena molekularren (laurdan GP gisa neurtua) eta erresistentzia nanomekanikoaren (AFMaren indar espektroskopia eran neurtua) balioak nahikoa antzekoak izan ziren. Gainera, zelula osoko mintz guztien erauzkinez eginiko laginen batez bestekoa baino altuagoak izan ziren. Lipidoen analisi kuantitatiboak erakutsi zuenez, PMak propioak dituen lipido konposizio berezitasunak dauzka; Cholean aberatsa eta gantz azido poliasegabeetan erlatiboki pobrea da. PMaren eta zelularen gainerako mintzen artean existitzen diren ezberdintasunez gain, baba eta PM partxeen artean ere beste aldaera batzuk (txikiagoak baina esanguratsuak) existitzen direla kontuan izan behar da. Ezberdintasun hauek, ziur aski, prestakin mota bakoitza lortzeko erabilitako metodoaren berezitasun zehatzak direla medio existitzen dira. Lan honen bidez, CHO zelulen PMaren inguruko egitura eta funtzio ikerketak zehaztasunez egitea ahalbidetzen duten oinarriak garatu dira.

9.2. LY-Ba: SPT Funtzioa Ez Duen Genetikoki Eraldatutako CHO Zelula Lerroa

Zelulek, SLak *de novo* sintetizatzeaz gain, hauek dietatik ere har ditzakete. Hau da hain zuzen ere, SLen *in vivo* ikerketak burutzeko gaintitu beharreko oztopo nagusienetarikoa. Oztopo honi aurre egiteko aukera posible bat, ahalik eta SL kantitate gutxien duten zelula mutanteak ikertzea izango litzateke. SPT ez funtzionala duen CHO zelula lerro mutanteak esaterako: LY-B zelula lerroak, ezin ditu SLak *de novo* sintetizatu. Dena den, *de novo* sintetizatu ezin baditu ere, hazten ari den hazkuntza mediotik esfingo baseak hartu eta metabolizatzeko gaitasuna mantentzen du. Horregatik, lipidoak ingurutik hartzea ekiditeko, LY-B zelulak %0.04 FBSdun medioan haztera egokitu ziren. Hau da, normalean erabiltzen den %10 FBS kontzentrazioa baino 250 aldiz gutxiagodun medioan.

4. kapituluaren, PM prestakin eta LY-B zeluletatik eratorritako lipido besikulak CHO *wild type*arekin alderatu ziren. A) LY-B laginen laurdan fluoreszentzia neurriek jaitziera esanguratsua jasan zuten; mintzaren zurruntasunaren galera bat adieraziz, b) AFM bidezko apurtze indar neurketek SL gutxidun LY-B zelulen laginak zeharkatzeko

aplikatu beharreko apurtze indarrak baxuagoak zirela erakutsi zuten, c) masa-espektrometria neurketek, medioan SL iturria mugatzearen ondorioz, SMA %85ean murriztu zela erakutsi zuten. SL mugatudun baldintzetan, GPLek ere aldaketa txiki (baina esanguratsu) batzuk jasan zituzten. PM eta zelula osoetatik eratorritako laginek antzeko aldaketak (behintzat kualitatiboak) izan zituen.

LY-B zelulen SL iturria 250 aldiz murriztu arren, mintzen SL kopurua soilik 6 aldiz jaitsi zen. Ezberdintasun honek, zelula hauek beraien konposizioan aldaketak jasateko erakusten duten erresistentzia azpimarratzen du. Mintzen SM kontzentrazioaren eta ordena molekular eta apurtze indarren arteko korrelazio zuzen bat zegoela ikusi zen.

9.3. Miriozina Bidezko CHO Zelulen SL Sintesiaren Inhibizioa: Ikerketa Biofisiko eta Lipidomikoa

Entzima jakin bat ezabatzeak eragiten dituen efektu zelularrak zehazteko existitzen diren bi estrategia (a) gene funtzional bat era egonkor batean mutatu duen zelula lerro bat erabiltzea, edo (b) *wild type* zelula lerroaren gene berak sortzen duen proteina konposatu baten bidez inhibitzea izan daitezke. Hau kontuan izanda, SL orokorren murrizteak izango lukeen efektua ikertzeko estrategia posible bat, SPT entzima espezifikoki inhibitzea izango litzateke.

SPTa, hainbat produktu ez-natural edo naturalen bidez inhibi daiteke, azken honen adibide da onddoen aurkako miriozina antibiotikoa hain zuzen ere. 5. kapituluan, miriozinak induzitutako CHO zelulen SPTaren desaktibazioak a) zelula hazkuntzan, b) konposizio lipidikoan eta c) mintzaren ezaugarri fisikoetan, duen eragina ikertu zen. Ondoren, SPT defektibodun CHO zelula lerro mutante batekin (LY-B zelula lerroarekin) alderatu zen.

Bi kasuetan antzeko efektuak ikusi ziren: SM balioak nabarmen jaitsi ziren miriozinaz tratatutako zeluletan. Ondorioz, beraien ordena molekularra (laurdan GP gisa neurtua) eta erresistentzia mekanikoa (AFM bidezko apurtze indar gisa neurtua) zelula natibo ez tratatuena baino baxuagoa izan zen. Miriozinaz tratatutako zelulek, mintzaren ordena mantentzearen, erantzun homeostasiko bat eman zuten: tratatu gabeak baino GPL guztiz ase gehiago eta poliasegabe gutxiago sintetizatuz. Dena den, ordena

mantentzearen helburua soilik partzialki lortu zuten, izan ere, beraien PMak zelula kontrolena baino jariakorrago eta sarkorrago izaten jarraitzen zuen.

9.4. CD Bidez Mintz Plasmatikoko SMA Murriztea: Eraginak Konposizio eta Ezaugarri Fisikoetan

CDeK, uretan disolbagarri izatea egiten dieten gainazal hidrofiliako bat dute. Gainera, mintzekin elkarreragiten dutenean, beraien barrunbe ez polarren bidez mintzetako lipido espezifikoak harrapatzeko ahalmena izan ohi dute.

6. kapituluan, M α CD eta M β CDak, *wild type* CHO, eta SPT ez funtzionaldun LY-B zelula lerroen PMan duten efektuaren analisi konparatibo bat burutu zen. Bi CD motek beraien barrunbean fosfolipidoak aloka ditzaketan arren, soilik handiagoa den M β CDak dauka esterolak bere baitan harrapatzeko gaitasuna. CDeK noranzko bakarreko PMan lipido erauzketa, edo mintzekin lipido elkartruke bat gauzatu dezakete. Azken honetarako, aurretik CDak intereseko lipidoz kargatu behar dira.

Zelulen biziraupena kontuan hartuz, zelulak M β CDz tratatzea M α CDz egitean baino kaltegarriagoa zela ikusi zen. Baldintza esperimentalen arabera, %36-93ko SMaren murrizketa neurtu zen. Gainera, M α CDak, M β CDak baino SM jaitsiera handiagoa eragin zuen, eta CDak aurrez lipidoz kargatzeak, SMarekiko espezifikoak den *mCherry*-lisenina seinalearen galera areagotzea ekarri zuen. Zelulak CDarekin tratatu ostean, bai laurdan bidez neurtutako GPa, baita AFM bidez neurtutako mintzen apurtze indarrak, baxuagoak izan ziren. Mintzak jariakorragoak eta zurruntasun baxuagokoak bilakatzen zirela adieraziz. Jaitsiera hau handiagoa izan zen zelulak PCz kargatutako M α CDz tratatzean, PC:Cholez kargatutako M β CDz tratatzean baino. CHO zelulekin alderatuz gero, LY-Bak CDarekiko sentikorragoak ziren. Gainera, aipatzekoa da, CD bidezko lipido elkartrukea, noranzko bakarreko lipido erauzketa baino errazago gauzatu zela.

M α CD eta M β CD bidezko tratamenduak, PMan konposizio lipidikoa (batez ere SM jaitsiera) aldatzeko erreminta interesgarriak direla ondorioztatu zen. Erabilera honetaz gain, elkartruke metodoaren bidez, interesgarriak diren SM espezie jakinak PMan txertatzeko erabil litezke. Honela espezie hauen ezaugarri biofisiko zehatzak ikertzea ahalbidetuz. CD tratamendua, mintzak modulatzeko existitzen diren beste metodo konplexuago batzuen ordez erabil liteke. Adibidez, lipidoen bidezidor

metabolikoaren ingeniaria, edota geldoagoak diren, eta maiz hain espezifikoak ez diren inhibitzaile biokimikoen orde. Gainera, dextrina hauek mintzen asimetria ikertzeko ere erabil litezke. Izan ere, lipidoak kanpo monogeruzatik soilik erauz ditzakete.

9.5. Jatorriz SL Kantitate Txikia Duten HAP1 Zelulen SL Errestrikzioa

SL kantitate minimoak dauzkaten benetako zelulen mintzen ezaugarriak ikertzeak, SL “simple”, eta “konplexuagoak” diren glysoSLen, ezaugarri biofisikoak ulertzen lagunduko luke.

7. kapitulan, giza jatorriko SPT defektibodun HAP1 SPTLC1(-) zelula lerro ia-haploidearen mintzen ezaugarri biofisikoak neurtu, eta *wild type* den HAP1 zelula lerroarekin eta aurretik aztertutako CHO eta LY-B zelulekin konparatu ziren.

Ugaztun zeluletan, SMa SL ugariena da, eta bere kontzentrazioa Cer eta HexCerenaren gainetik egon ohi da. Dena den, hau ez da HAP1/HAP1-SPT zelula lerroen kasua. Hauetan, SM kontzentrazioa %10 FBSdun medioan hazitako CHO/LY-B zelulen kontzentrazioa baino magnitude orden bat beherago dago. Hau da, Cer eta HexCeren antzeko kontzentrazioan. Gainera, SL-murrizteko baldintzetan haztean, HAP1-SPTak, baina ez HAP1 zelula lerroak, SMaren jaitsiera handi bat jasan zuen, bai zelula oso, baita PM prestakinetan ere. Jatorriz oso SL kontzentrazio baxuak dauzkaten zelulak SL-murriztailedun baldintzetan hazteak, SL eliminazioak mintzetan izan dezakeen efektua ikertzeko ikuspuntu berri bat eskaintzen du.

Aipatzekoa da, CHO eta LY-B zelulek %10-15 kate-laburreko GPL zeuzkaten bitartean, HAP1 eta HAP1-SPT zelulen portzentaia bikoitza zela. Aurretik aipatu den SM kopuru baxuak eta ugaritutako kate-laburreko GPLek, ziur aski mintzen ezaugarri biofisikoak zentzu berean eragin zituzten. Hau da, CHO eta LY-B zelulekin alderatuz, HAP1/HAP1-SPT zelula lerroek GP eta apurtze indar baxuagoak zeuzkaten. HAP1-SPT zelulak SL-gabeziadun medioan hazi zirenean, beraien PM prestakinen laurdan GParen eta apurtze indarren balioek ez zuten estatistikoki ezberdintasun adierazgarri aldaketarik izan. Hau da, SLak kentzean zelulek adaptazio homeostasiko bat jasaten zuten.

Bai genetikoki eraldatutako, zein inhibitzaile espezifikoekin tratatutako zenbait zelulen lipido konposizioa eraldatzean, zelulek beraien mintzen zurruntasunean/jariakortasunean jasandako aldaketak konpentsatzeko ahalmena erakusten dutela esan daiteke. Gertaera honek SLEk mintzetan duten eginkizunaren inguruko hainbat ikerketa funtzional egitea ahalbidetzen du.

9.6. Esfingolipido eta Kolesterolaren “soziabilitatea”

Azken urteotan, SM eta Cholaren elkarrekintza espezifikoa asko ikertu da, batez ere “lipido urmael” hipotesiaren testuinguruan. Dena den, gaur egun urmaelen existentzia oso eztabaidatua eta zalantza handiko gaia da. Arrazoi honengatik, “urmael” hitza erabili ordez, “nanodomeinu iragankor” terminoa erabiltzea proposatu izan da.

Urmael-motako nanodomeinuak, iragankorrak, gunekoak, eta Chol eta SL kontzentrazio altukoak diren mintz heterogeneotasun gisa ulertzen dira. Egindako ikerketen arabera, beraien ordena molekular altua dela medio, mintzen trafikoa (bai SLEntzako baita proteina espezifikoetarako) gobernatu lezaketela uste da. 8. kapituluaren SL eta Cholen nanodomeinu iragankorren inguruan dagoen jakinduria biltzen da.

Ikerketek iradokitzen dutenaren arabera, kate-luzeko Cerek paketatze maila altua duten lipido faseak sortzeko eta alboz barreiatzeko joera dute. Modu honetan, zelula heriotza gobernatzen duten mekanismoekin lotuak egon daitezkeen Ceran aberastutako domeinuak sortuz. Aipatzekoa da, animalien zelula mintzetan aurkitzen den Chola, domeinu hauen ordena molekularra edo jariakortasuna arautzen duen berebiziko garrantziadun osagaia dela.

Ikuspuntu fisiko-kimiko batetik, bai Chola, baita Cera ere, beraien buru polarrean hidroxilo talde bakarra duten osagai oso hidrofobikoak dira. Geruza bikoitzean antzeko eran orientatzen dira eta zenbait baldintzetan elkarrekiko desplazamendua edo elkartrukea gauzatzen dute. Gainera, Cera, lipido nanodomeinuak sortzeko Cholarekin elkarreagiten duten SLEtatik (adibidez SMtik), era entzimatik batean ere sor daiteke. Gertaera hauek, nanodomeinuen desmuntatzea, SMaren hidrolisitik sortutako Ceraren sintesiarekin lotzen dute, zeina Cer eta kolesterolaren “soziabilitatearen” funtsezko gakoa den.

Domeinu hauen *in vivo* ikuskapena zailtzen duen oztopo nagusienak, beraien biziraupen labur eta tamaina txikia dira. Azken hamarkadan zehar lipido domeinuak

mintz ereduetan karakterizatu izan dira. Batez ere lipido-lipido elkarrekintzetan eta SL bidezko seinalizazioan. Dena den, mintz zelularrekiko antzekoagoak diren eredu konplexuagoek, edota *in vivo* entseguek, domeinu hauetan dagoen egitura (lipido faseen arteko koexistentzia) eta funtzioaren (mintz trafikoa eta zelula seinalizazioa) erlazioa argitzen lagun lezakete.

9.7. SLek Zelulen Funtzioan Duten Eginkizunarekin Erlazionatutako Aurrerapenak

Tesi honen helburuetako bat “gure aurrerapenak SLek zelulen funtzioan duten eginkizunaren inguruko deskribapen batean batzea” izan da. Espero zen bezala, helburu hau ez da osotasunean bete. Batez ere, SLek parte hartzen duten gertaera zelular anitzek duten konplexutasun arrazoiak direla eta. Era zehatz batean soilik hiru SL mota; SMA, Cera eta HexCera, eta zelula funtzioaren aspektu bakarra; mintzaren jariakortasuna (zelulen zatiketa funtzio globalaz gain) ikertzeko gai izan gara.

Hasteko, SLak ugaztun zeluletatik guztiz kendu nahi izan ziren. Dena den, hau ezin izan da lortu; ezta *de novo* sintesi gabedun zelulak SL kontzentrazio oso baxuko hazkuntza medioan izanda ere. Gure emaitzak ikusita, mintzetako SL kantitatea ehuneko jakin batetik jaistean dagoen ezintasun birtuala kontuan hartuta, ugaztun jatorriko zelulen zatiketa burutzeko beraien mintzek SL kontzentrazio minimo bat behar- beharrezkoa dutela uler daiteke.

Zeluletan ugariena den SLak; SMak, zeluletan gutxienez bi eginkizun betetzen ditu. Lehena, mintzen jariakortasuna jaistea. Bigarrena, beste SL batzuentzat gordailu edo/eta iturri metaboliko bat izatea. Zeintzuen artean Cera eta HexCera adibide diren: Cera seinale metaboliko gisa eta HexCera glikoSL konplexuen (adibidez globosidoak edo gangliosidoak) sintesirako lehen molekula gisa. Tesi honetan erakusten denaren arabera, mintzek duten SM kantitatea asko murriztu daiteke. Gainera, gertaera honen aurrean, zelulek lipido sintesian izandako glizerofosfolipido kate luzera eta asegabete aldaketan bidez, beraien mintzen jariakortasuna (ordena molekularra) lipido sintesiaren erantzun homeostasiko egoki baten bidez konpentsa dezakete. Kontuan izan behar da, Cer eta HexCer kontzentrazioak, SM kontzentrazioak baino askoz kontserbatuagoak daudela. Inongo zalantzarik gabe, beste molekulek ordezkari ezin dezaketen eginkizun espezifikoak betetzen baitituzte.

SLek zelularen funtzioan duten eginkizuna definitzerako orduan, gure ahaleginak oso urrun joan ez badira ere, nahiko pozik egon gaitzke lortutako informazio zelular eta molekularren integrazioarekin, zeina helburu honen parte diren. Izan ere, (i) ugaztun zeluletan SLaren *de novo* sintesia murrizteko teknika genetiko eta kimikotik, (ii) mintzaren jariakortasunaren oinarriko propietateen espektroskopia fluoreszente eta indar atomikozko espektroskopia ikerketetatik, eta (iii) ikertuak izan diren zelula eta mintz zelularren analisi lipidikotik eskuratutako informazioa bateratuz, etorkizunean, mota honetako ikerketekin jarraitu ahal izateko azpiegitura teknologikoaren funtsak definitu dira.

9.8. Ondorioak

Lan honen ondorio nagusiak ondorengoak dira:

- SL kopuruaren murriztearen eta mintzen aldaketa biofisikoen artean korrelazio bat existitzen da.
 - Zelulen SL kantitatea murrizten denean, laurdan bidezko polarizazio orokorraren neurketen arabera, beraien PMA eta zelula barneko mintzak jariakorragoak, edo ordena molekular baxuagokoak, dira.
 - Zelulen SL kantitatea murrizten denean, AFM bidezko indar espektroskopia bidezko neurketen arabera, beraien PMA eta zelula barneko mintzak sarkorrago bilakatzen dira.
- Zelulen SL kantitatea murrizten denean, CHO eta HAP1 zelulek mintzen ordena molekularra mantentzeko ahalegina egiten dute. Horretarako bidezidor lipidikoa eraldatzen duen erantzun homeostasiko bat ematen dutelarik: GPL guztiz ase gehiago eta poliasegabe gutxiago sintetizatuz.
 - CHO zelulekin alderatuz, LY-B zelulek mintzen ordena soilik partzialki mantentzen dute. Zelulak SL gabedun medioan haztean beraien PMA sarkorragoa bilakatzen baita.
 - HAP1 zelulekin alderatuz, HAP1-SPT zelulek mintzen ordena guztiz mantentzen dute. Nahiz eta SL gabeziadun medioan hazi, beraien PMA ez baita sarkorragoa bilakatzen.

BIBLIOGRAFIA

BIBLIOGRAFIA

- Adachi-Yamada T, Gotoh T, Sugimura I, Tateno M, Nishida Y, Onuki T & Date H (2015) De novo synthesis of sphingolipids is required for cell survival by down-regulating c-Jun N-terminal kinase in Drosophila imaginal discs. *Mol Cell Biol* 19: 7276–7286
- Adada M, Canals D, Hannun Y & Obeid L (2014) Sphingolipid regulation of ezrin, radixin, and moesin proteins family: implications for cell dynamics. *Biochim Biophys Acta* 1841: 727–737
- Adada M, Luberto C & Canals D (2016) Inhibitors of the sphingomyelin cycle : Sphingomyelin synthases and sphingomyelinases. *Chem Phys Lipids* 197: 45–59
- Agrawal H, Zelisko M, Liu L & Sharma P (2016) Rigid proteins and softening of biological membranes-with application to HIV-induced cell membrane softening. *Sci Rep* 6: 1–12
- Ahyayauch H, García-Arribas AB, Sot J, Go EJ, Busto J V, Monasterio BG, Jiménez-rojo N & Contreras FX (2018) Pb (II) induces scramblase activation and ceramide-domain generation in red blood cells. *Sci Rep* 8: 1–17
- Alberts B, Bray D, Lewis J, Raff M, Roberts K & Watson J (1994) *Molecular Biology of the Cell* 3rd ed. New York: Garland Sc
- Albi E & Magni MV (2008) Sphingolipid metabolism inhibitors and cell function. *Open Enz Inhibi J* 1: 72–79
- Alessandrini A & Facci P (2005) AFM: A versatile tool in biophysics. *Meas Sci Technol* 16: 65–92
- Alessandrini A, Seeger H, Caramaschi T & Facci P (2012) Dynamic force spectroscopy on supported lipid bilayers: effect of temperature and sample preparation. *Biophys J* 103: 38–47
- Aljohani A, Munguba G, Guerra Y, Lee R & Bhattacharya S (2013) Sphingolipids and ceramides in human aqueous humor. *Mol Vis* 19: 1966–1984
- Almeida PFF (2009) Thermodynamics of lipid interactions in complex bilayers. *Biochim Biophys Acta* 1788: 72–85
- Alonso A & Goñi FM (2018) The physical properties of ceramides in membranes. *Annu Rev Biophys* 47: 633–654

- Andersson B, Collins V, Kurzrock R, Larkin D, Childs C, Ost A, Cork A, Trujillo J, Freireich E & Siciliano M (1995) KBM-7, a human myeloid leukemia cell line with double Philadelphia chromosomes lacking normal c-ABL and BCR transcripts. *Leukemia* 9: 2100–2108
- Angelova D & Dimitrov M (1986) Liposome electro formation. *Faraday Discuss Chem SOC* 81: 303–311
- Angelova M, Soléau S, Méléard P, Faucon F & Bothorel P (1992) Preparation of giant vesicles by external AC electric fields. Kinetics and applications. *Trends Colloid Interface Sci* 131: 127–131
- Antonny B (2011) Mechanisms of membrane curvature sensing. *Annu Rev Biochem* 80: 101–123
- Antwerpen P Van & Govaerts C (2016) Phosphatidylethanolamine is a key regulator of membrane fluidity in eukaryotic cells. *J Biol Chem* 291: 3658–3667
- Aron M, Browning R, Carugo D, Sezgin E, Bernardino de la Serna J, Eggeling C & Stride E (2017) Spectral imaging toolbox: Segmentation, hyperstack reconstruction, and batch processing of spectral images for the determination of cell and model membrane lipid order. *BMC Bioinform* 18: 1–8
- Artetxe I, Sergelius C, Kurita M, Yamaguchi S, Katsumura S, Slotte J & Maula T (2013) Effects of sphingomyelin headgroup size on interactions with ceramide. *Biophys J* 104: 604–612
- Atila-Gokcumen G, Muro E, Relat-Goberna J, Sasse S, Bedigian A, Coughlin M, Garcia-Manyes S & Eggert U (2014) Dividing cells regulate their lipid composition and localization. *Cell* 156: 428–439
- Attwood S, Choi Y & Leonenko Z (2013) Preparation of DOPC and DPPC supported planar lipid bilayers for atomic force microscopy and atomic force spectroscopy. *Int J Mol Sci* 14: 3514–3539
- Axpe E, Garcia-Arribas A., Mujika JI, Merida D, Alonso A, X L, Garcia JA, Ugalde JM, Goñi F & Plazaola F (2015) Ceramide increases free volume voids in DPPC membranes. *RSC Adv* 5: 44282–44290
- Bagatolli LA (2006) To see or not to see: Lateral organization of biological membranes and fluorescence microscopy. *Biochim Biophys Acta - Biomembr* 1758: 1541–1556
- Bagatolli L & Mouritsen O (2013) Is the fluid mosaic (and the accompanying raft hypothesis) a suitable model to describe fundamental features of biological membranes? What may be missing? *Front Plant Sci* 4: 457

- Bangham A & Horne R (1964) Negative staining of phospholipids and their structural modification by surface-active agents as observed in the electron microscope. *J Mol Biol* 8: 660–IN610
- Bangham AD, Standish MM & Watkins JC (1964) Diffusion of univalent ions across the lamellae of swollen phospholipids. *J Mol Biol* 13: 238–252
- Barth B, Cabot M & Kester M (2011) Ceramide-based therapeutics for the treatment of cancer. *Anti-cancer Agent ME* 11: 911–919
- Bartke N & Hannun Y (2009) Bioactive sphingolipids: metabolism and function. *J Lipid Res* 50: S91–S96
- Bartlett G (1958) Phosphorous assay in column chromatography. *J Biol Chem* 234: 466–468
- Basañez G (2002) Membrane fusion: the process and its energy suppliers. *Cell Mol life Sci* 59: 1478–1490
- Basañez G, Soane L & Hardwick J (2012) A new view of the lethal apoptotic pore. *PLoS Biol* 10: e1001399
- Baumgart T, Hammond AT, Sengupta P, Hess ST, Holowka DA, Baird BA & Webb WW (2007a) Large-scale fluid/fluid phase separation of proteins and lipids in giant plasma membrane vesicles. *PNAS* 107: 3165–3170
- Baumgart T, Hunt G, Farkas E, Webb W & Feigenson G (2007b) Fluorescence probe partitioning between Lo/Ld phases in lipid membranes. *Biochim Biophys Acta* 1768: 2182–2194
- Beattie A, Gupta S, Frankova L, Kazlauskaitė A, Harmon J, Dunn T & Campopiano D (2013) The pyridoxal 5'-phosphate (PLP)-dependent enzyme serine palmitoyltransferase (SPT): effects of the small subunits and insights from bacterial mimics of human hLCB2a HSN1 mutations. *Biomed Res Int* 2013: 194371
- Bejaoui K, Uchida Y, Yasuda S, Ho M, Nishijima M, Brown RH, Holleran WM & Hanada K (2002) Hereditary sensory neuropathy type 1 mutations confer dominant-negative effects on serine palmitoyltransferase, critical for sphingolipid synthesis. *J Clin Invest* 110: 1301–1308
- Bernardino de la Serna J, Perez-Gil J, Simonsen A & Bagatolli L (2004) Cholesterol rules: direct observation of the coexistence of two fluid phases in native pulmonary surfactant membranes at physiological temperatures. *J Biol Chem* 279: 40715–40722

- Bezrukov L, Blank PS, Polozov I V. & Zimmerberg J (2009) An adhesion-based method for plasma membrane isolation: Evaluating cholesterol extraction from cells and their membranes. *Anal Biochem* 394: 171–176
- Bhattacharyyas L, Ceccarinit C, Lorenzonit P & Brewerst F (1987) Concanavalin A interactions with asparagine-linked glycopeptides. *J Biol Chem* 262: 1288–1293
- Bieberich E (2018) Sphingolipids and lipid rafts: Novel concepts and methods of analysis. *Chem Phys Lipids* 216: 114–131
- Binnig G, Quate C & Gerber C (1986) Atomic Force Microscope. *Phys Rev Lett* 56: 930–933
- Boggs JM (1987) Lipid intermolecular hydrogen bonding: influence on structural organization and membrane function. *BBA - Rev Biomembr* 906: 353–404
- Boone CW, Ford LE, Bond HE, Stuart DC & Lorenz D (1969) Isolation of plasma membrane fragments from HeLa cells. *J Cell Biol* 41: 378–392
- Böttcher C & Pries C (1961) A rapid and sensitive sub-micro phosphorus determination. *Anal Chim Acta* 24: 203–204
- Bourquin F, Capitani G & Grutter M (2011) PLP-dependent enzymes as entry and exit gates of sphingolipid metabolism. *Protein Sci* 20: 1492–1508
- Bouvrais H, Méléard P, Pott T, Jensen KJ, Brask J & Ipsen JH (2008) Softening of POPC membranes by magainin. *Biophys Chem* 137: 7–12
- Bovée JVMG, Cleton-Jansen AM, Kuipers-Dijkshoorn NJ, Van Den Broek LJCM, Taminiau AHM, Cornelisse CJ & Hogendoorn PCW (1999) Loss of heterozygosity and DNA ploidy point to a diverging genetic mechanism in the origin of peripheral and central chondrosarcoma. *Genes Chromosom Cancer* 26: 237–246
- Breslow D, Collins S, Bodenmiller B, Aebersold R, Simons K, Shevchenko A, Ejsing C & Weissman J (2010) Orm family proteins mediate sphingolipid homeostasis. *Nature* 463: 1048–1053
- Burger K (2000) Greasing membrane fusion and fission machineries. *Traffic* 1: 605–613
- Burns M, Wisser K, Wu J, Levental I & Veatch SL (2017) Miscibility transition temperature scales with growth temperature in a zebrafish cell line. *Biophys J* 113: 1212–1222
- Buschmann H-J & Schollmeyer E (2002) Applications of cyclodextrins in cosmetic products : A review. *J Cosmet Sci* 53: 185–191
- Busto JV, Fanani ML, De Tullio L, Sot J, Maggio B, Goni FM & Alonso A (2009)

- Coexistence of immiscible mixtures of palmitoylsphingomyelin and palmitoylceramide in monolayers and bilayers. *Biophys J* 97: 2717–2726
- Busto JV, Garcia-Arribas AB, Sot J, Torrecillas A, Gomez-Fernandez JC, Goni FM & Alonso A (2014) Lamellar gel (lbeta) phases of ternary lipid composition containing ceramide and cholesterol. *Biophys J* 106: 621–630
- Busto JV, Sot J, Requejo-Isidro J, Goni FM & Alonso A (2010) Cholesterol displaces palmitoylceramide from its tight packing with palmitoylsphingomyelin in the absence of a liquid-disordered phase. *Biophys J* 99: 1119–1128
- Camgoz A, Gencer E, Ural A & Baran Y (2013) Mechanisms responsible for nilotinib resistance in human chronic myeloid leukemia cells and reversal of resistance. *Leuk Lymphoma* 54: 1279–1287.
- Capasso S, Sticco L, Rizzo R, Pirozzi M, Russo D, Dathan NA, Campelo F, van Galen J, Hölttä-Vuori M, Turacchio G, *et al* (2017) Sphingolipid metabolic flow controls phosphoinositide turnover at the trans Golgi network. *EMBO J* 36: 1736–1754
- Carette J, Raaben M, Wong A, Herbert A, Obernosterer G, Mulherkar N, Kuehne A, Kranzusch P, Griffin A & Ruthel G (2011) Ebola virus entry requires the cholesterol transporter Niemann-Pick C1. *Nature* 477: 340–343
- Carette JE, Pruszk J, Varadarajan M, Blomen VA, Gokhale S, Camargo FD, Wernig M, Jaenisch R & Brummelkamp TR (2010) Generation of iPSCs from cultured human malignant cells. *Blood* 115: 4039–4042
- Carquin M, Pollet H, Veiga-da-Cunha M, Cominelli A, Van Der Smissen P, N’kuli F, Emonard H, Henriët P, Mizuno H, Courtoy PJ, *et al* (2014) Endogenous sphingomyelin segregates into submicrometric domains in the living erythrocyte membrane. *J Lipid Res* 55: 1331–1342
- Carravilla P, Nieva JL, Goñi FM, Requejo-isidro J & Huarte N (2015) Two-photon laurdan studies of the ternary lipid mixture DOPC:SM:Cholesterol reveal a single liquid phase at Sphingomyelin:Cholesterol ratios lower than 1. *Langmuir* 31: 2808–2817
- Carreira A, Ventura A, Varela A & Silva L (2015) Tackling the biophysical properties of sphingolipids to decipher their biological roles. *Biol Chem* 396: 597–609
- Carrer D & Maggio B (1999) Phase behavior and molecular interactions in mixtures of ceramide with dipalmitoylphosphatidylcholine. *J Lipid Res* 40: 1978–1989
- Cartier A & Hla T (2019) Sphingosine 1-phosphate: Lipid signaling in pathology and therapy. *Science* 366: eaar5551

- Castro B, Prieto M & Silva L (2014) Ceramide: a simple sphingolipid with unique biophysical properties. *Prog Lipid Res* 54C: 53–67
- Catapano E, Arriaga L, Espinosa G, Monroy F, Langevin D & Lopez-Montero I (2011) Solid character of membrane ceramides: a surface rheology study of their mixtures with sphingomyelin. *Biophys J* 101: 2721–2730
- Chakraborty M & Jiang X (2013) Sphingomyelin and its role in cellular signaling. *Adv Exp Med Biol* 991: 1–14
- Chalfant CE, Ogretmen B, Galadari S, Kroesen BJ, Pettus BJ & Hannun YA (2001) FAS activation induces dephosphorylation of SR proteins: Dependence on the de novo generation of ceramide and activation of protein phosphatase 1. *J Biol Chem* 276: 44848–44855
- Chapman D (1975) Phase transitions and fluidity characteristics of lipids and cell membranes. *Q Rev Biophys* 8: 185–235
- Chatterjee S (1994) Neutral sphingomyelinase action stimulates signal transduction of tumor necrosis factor- α in the synthesis of cholesteryl esters in human fibroblasts. *J Biol Chem* 269: 879–882
- Chen L, Yu Z, Lee Y, Wang X, Zhao B & Jung YM (2012) Quantitative evaluation of proteins with bicinchoninic acid (BCA): Resonance Raman and surface-enhanced resonance Raman scattering-based methods. *Analyst* 137: 5834–5838
- Cheng H-T, Megha & London E (2009) Preparation and properties of asymmetric vesicles that mimic cell membranes: Effect upon lipid raft formation and transmembrane helix orientation. *J Biol Chem* 284: 6079–6092
- Cheng K, Lepock J, Hui S & Yeagle P (1986) The role of cholesterol in the activity of reconstituted Ca-ATPase vesicles containing unsaturated phosphatidylethanolamine. *J Biol Chem* 261: 5081–5087
- Chernomordik L (1996) Non-bilayer lipids and biological fusion intermediates. *Chem Phys Lipids* 81: 203–213
- Chianese R, Coccurello R, Viggiano A, Scafuro M, Fiore M, Coppola G, Operto FF, Fasano S, Laye S, Pierantoni R, *et al* (2017) Impact of dietary fats on brain functions. *Curr Neuropharmacol* 16: 1059–1085
- Chiantia S, Kahya N, Ries J & Schwille P (2006) Effects of ceramide on liquid-ordered domains investigated by simultaneous AFM and FCS. *Biophys J* 90: 4500–4508
- Chiantia S & London E (2013) Sphingolipids and membrane domains: recent advances. *Handb Exp Pharmacol* 215: 33–55

- Chiantia S, Schwille P, Klymchenko AS & London E (2011) Asymmetric GUVs prepared by M b CD-mediated lipid xchange : An FCS study. *Biophys J* 100: L1–L3
- Cohen CM, Kalish DI, Jacobson BS & Branton D (1977) Membrane isolation on polysysine-coated beads. *J Cell Biol* 75: 119–134
- Contreras FX, Ernst AM, Haberkant P, Björkholm P, Lindahl E, Gönen B, Tischer C, Elofsson A, Von Heijne G, Thiele C, *et al* (2012) Molecular recognition of a single sphingolipid species by a protein's transmembrane domain. *Nature* 481: 525–529
- Contreras FX, Sánchez-Magraner L, Alonso A & Goñi FM (2010) Transbilayer (flip-flop) lipid motion and lipid scrambling in membranes. *FEBS Lett* 584: 1779–1786
- Contreras FX, Villar AV, Alonso A, Kolesnick RN & Goñi FM (2003) Sphingomyelinase activity causes transbilayer lipid translocation in model and cell membranes. *J Biol Chem* 278: 37169–37174
- Contreras X, Sot J, Alonso A & Goñi FM (2006) La esfingosina aumenta la permeabilidad del modelo y las membranas celulares. *Biophys J* 90: 4085–4092
- Cortajarena AL, Goñi FM & Ostolaza H (2001) Glycophorin as a receptor for Escherichia coli alpha-hemolysin in erythrocytes. *J Biol Chem* 276: 12513–12519
- Cosentino K & García-Sáez A (2014) Mitochondrial alterations in apoptosis. *Chem Phys Lipids* 181: 62–75
- Cramer F (1954) *Einschlussverbindungen* 1st ed. Berlin: Springer-Verlag OHG
- Cremesti AE, Goni FM & Kolesnick R (2002) Role of sphingomyelinase and ceramide in modulating rafts: do biophysical properties determine biologic outcome? *FEBS Lett* 531: 47–53
- Cullis PR, de Kruijff B, Hope M, Verkleij AJ, Nayar R, Farren SB, Tildock C, Madden TD & Bally MB (1983) Structural properties of lipids and their functional role in biological membranes. *Membrane fluidity in Biology* 1st ed. Aloia RC (ed) New York: Academic Press
- Dai L, Xia P & Di W (2014) Sphingosine 1-phosphate: a potential molecular target for ovarian cancer therapy? *Cancer Invest* 32: 71–80
- Danielli J & Davson H (1935) A contribution to the theory of permeability of thin films. *J Cell Comp Physiol* 5: 495–508
- Das A, Goldstein JL, Anderson DD, Brown MS & Radhakrishnan A (2013) Use of mutant 125 I-Perfringolysin O to probe transport and organization of cholesterol in membranes of animal cells. 110: 10580–10585

- Dass CR & Jessup W (2000) Apolipoprotein A-I, Cyclodextrins and liposomes as potential drugs for the reversal of atherosclerosis. A Review. *J Pharm Pharmacol* 52: 731–761
- Delgado A, Casas J, Llebaria A, Luís J & Fabrias G (2006) Inhibitors of sphingolipid metabolism enzymes. *Biochim Biophys Acta* 1758: 1957–1977
- Depince-Berger AE, Aanei C, Iobagiu C, Jeraiby M & Lambert C (2016) New tools in cytometry. *Morphologie* 100: 199–209
- Desai R, Frazier A, Durigon R, Patel H, Jones A, Dalla Rosa I, Lake N, Compton A, Mountford H, Tucker E, *et al* (2017) ATAD3 gene cluster deletions cause cerebellar dysfunction associated with altered mitochondrial DNA and cholesterol metabolism. *Brain* 140: 1595–1610
- Désert C, Duclos M, Blavy P, Lecerf F, Moreews F, Klopp C, Aubry M, Herault F, Le Roy P, Berri C, *et al* (2008) Transcriptome profiling of the feeding-to-fasting transition in chicken liver. *BMC Genomics* 9: 611
- Devaux PF (1991) Static and dynamic lipid asymmetry in cell membranes. *Biochemistry* 30: 1163–1173
- Diaspro A, Bianchini P, Vicidomini G, Faretta M, Ramoino P & Usai C (2006) Multi-photon excitation microscopy. *Biomed Eng Onl* 5: 1–14
- Dickson R (1998) Sphingolipid functions in *Saccharomyces cerevisiae*: comparison to mammals. *Ann Rev Biochem* 67: 27–48
- Dietrich C, Han G, Chen M, Berg R, Dunn T & Cahoon E (2008) Loss-of-function mutations and inducible RNAi suppression of Arabidopsis LCB2 genes reveal the critical role of sphingolipids in gametophytic and sporophytic cell viability. *Plant J* 54: 284–298
- Dimitrov DS & Angelova MI (1988) Lipid swelling and liposome formation mediated by electric. *Bioelectrochemistry Bioenerg* 253: 323–336
- Dougherty A, McDonald F & Liotta D (2006) Synthesis of 1- deoxysphingosine derivatives with conformationally restricted pyrrolidinediol head groups. *Org Lett* 8: 649–652
- Dowhan W (2009) Molecular genetic approaches to defining lipid function. *J Lipid Res* 50: S305–S310
- Duzgunes N ed. (2009) Liposomes, part F 1st ed. San Francisco: Elsevier
- Dyck P (1993) Neuronal atrophy and degeneration predominantly affecting peripheral sensory and autonomic neuron B Saunders. Dyck P Thomas P Lambert E & Bunge

- R (eds) Philadelphia: WB Saunders
- Eastburn SD & Tao BY (1994) Applications of modified cyclodextrins. *Biotech Adv* 12: 325–339
- Edidin M (2003a) Lipids on the frontier: a century of cell-membrane bilayers. *Nat Rev Mol Cell Biol* 4: 414–418
- Edidin M (2003b) The state of lipid rafts: from model membranes to cells. *Annu Rev Biophys Biomol Struct* 32: 257–283
- Edidin M (2006) Switching sides: The actin/membrane lipid connection. *Biophys J* 91: 3963
- Engelman D (2005) Membranes are more mosaic than fluid. *Nature* 438: 578–580
- Eoin F (2005) A comprehensive classification system for lipids. *J Lipid Res* 5: 839–862
- Epand R (1998) Lipid polymorphism and protein-lipid interactions. *Biochim Biophys Acta* 1376: 353–368
- Epstein S, Kirkpatrick CL, Castillon GA, Muñoz M, Riezman I, David FPA, Wollheim CB & Riezman H (2012) Activation of the unfolded protein response pathway causes ceramide accumulation in yeast and INS-1E insulinoma cells. *J Lipid Res* 53: 412–420
- Estep T, Mountcastle D, Barenholz Y, Biltonen R & Thompson T (1979) Thermal behavior of synthetic sphingomyelin-cholesterol dispersions. *Biochemistry* 18: 2112–2117
- Fabrias G, Munoz-Olaya J, Cingolani F, Signorelli P, Casas J, Gagliostro V & Ghidoni R (2012) Dihydroceramide desaturase and dihydrosphingolipids: debutant players in the sphingolipid arena. *Prog Lipid Res* 51: 82–94
- Fahy E, Subramaniam S, Murphy R, Nishijima M, Raetz C, Shimizu T, Spener F, van Meer G, Wakelam M & Dennis E (2009) Update of the LIPID MAPS comprehensive classification system for lipids. *J Lipid Res* 50: S9–S14
- Feigenson G (2007) Phase boundaries and biological membranes. *Annu Rev Biophys Biomol Struct* 36: 63–77
- Feingold K (1991) The regulation of epidermal lipid synthesis by permeability barrier requirements. *Crit Rev Ther Drug Carr Syst* 8: 193–210
- Fenske D & Cullis P (2008) Liposomal nanomedicines. *Expert Opin Drug Deliv* 5: 25–44
- Ferrari E, Bruhn C, Peretti M, Cassani C, Carotenuto W, Elgendy M, Shubassi G, Lucca C, Bermejo R, Varasi M, *et al* (2017) PP2A controls genome integrity by

- integrating nutrient-sensing and metabolic pathways with the DNA damage response. *Mol Cell* 67: 266–281
- Fiske CH & Subbarow Y (1925) The colorimetric determination of phosphorous. *J Bio* 66: 375–400
- Fitzner D, Bader J, Penkert H, Bergner C, Su M, Weil M, Surma M, Mann M, Klose C & Simons M (2020) Cell-type- and brain-region-resolved mouse brain lipidome. *Cell Rep*. 2020. *Cell Rep* 32: 108132
- Flowers M, Fabriás G, Delgado A, Casas, Abad J & Cabot M C6-ceramide and targeted inhibition of acid ceramidase induce synergistic decreases in breast cancer cell growth. *Breast Cancer Res Treat* 133: 447–445
- French D & Rundle RE (1942) The molecular weights of Schardinger alpha and beta dextrans. *J Am Chem Soc* 64: 1651–1653
- Freudenberg K & Meyer-Delius M (1938) Über die Schardinger-dextrine aus starke. *Ber Chem* 71: 1596–1600
- Frisz JF, Klitzing HA, Lous K, Hutcheon ID, Weber PK, Zimmerberg J & Kraft ML (2013a) Sphingolipid domains in the plasma membranes of fibroblasts are not enriched with cholesterol. *J Biol Chem* 288: 16855–16861
- Frisz JF, Lou K, Klitzing HA, Hanafin WP, Lizunov V, Wilson RL, Carpenter KJ, Kim R, Hutcheon ID, Zimmerberg J, *et al* (2013b) Direct chemical evidence for sphingolipid domains in the plasma membranes of fibroblasts. *Proc Natl Acad Sci* 110: E613–E622
- Fujita T, Inoue K & Yamamoto S (1994) A potent immunosuppressive activity found in *Isaria sinclairii* metabolite. *J Antibiot* 47: 208–215
- Fulwyler M (1965) Electronic separation of biological cells by volume. *Science* 150: 910–911
- Futerman A & Hannun Y (2004) The complex life of simple sphingolipids. *EMBO rep* 5: 777–782
- Futerman AH, Stieger B, Hubbard AL & Pagano RE (1990) Sphingomyelin synthesis in rat liver occurs predominantly at the cis and medial cisternae of the Golgi apparatus. *J Biol Chem* 265: 8650–8657
- Gable K, Han G, Monaghan E, Bacikova D, Natarajan M, Williams R & Dunn T (2002) Mutations in the yeast LCB1 and LCB2 genes, including those corresponding to the hereditary sensory neuropathy type I mutations, dominantly inactivate serine palmitoyltransferase. *J Biol Chem* 277: 10194–10200

- Gable K, Slife H, Bacikova D, Monaghan E & Dunn TM (2000) Tsc3p is an 80-amino acid protein associated with serine palmitoyltransferase and required for optimal enzyme activity. *J Biol Chem* 275: 7597–7603
- Galisteo-González F, Monasterio BG, Gil D, Valle M & Goñi FM (2020) Photoacoustic effect applied on model membranes and living cells: direct observation with multiphoton excitation microscopy and long-term viability analysis. *Sci Rep* 10: 299
- García-Arribas AB, Ahyayauch H, Sot J, López-González PL, Alonso A & Goñi FM (2016a) Ceramide-induced lamellar gel phases in fluid cell lipid extracts. *Langmuir* 32: 9053–9063
- García-Arribas AB, Alonso A & Goñi FM (2016) Cholesterol interactions with ceramide and sphingomyelin. *Chem Phys Lipids* 199: 26–34
- García-Arribas AB, Axpe E, Mujika JI, Mérida D, Busto JV, Sot J, Alonso A, Lopez X, García JÁ, Ugalde JM, *et al* (2016b) Cholesterol-ceramide interactions in phospholipid and sphingolipid bilayers as observed by positron annihilation lifetime spectroscopy and molecular dynamics simulations. *Langmuir* 32: 5434–5444.
- García-Arribas AB, Busto J V, Alonso A & Goñi FM (2015) Atomic force microscopy characterization of palmitoylceramide and cholesterol effects on phospholipid bilayers: A topographic and nanomechanical Study. *Langmuir* 31: 3135–3145
- García-Arribas AB, González-Ramírez EJ, J S, Areso I, Alonso A & Goñi FM (2017) Complex effects of 24:1 sphingolipids in membranes containing dioleoylphosphatidylcholine and cholesterol. *Langmuir* 33: 5545–5554.
- García-Barrros M, Coant N, Truman JP, A.J. S & Hannun YA (2014) Sphingolipids in colon cancer. *Biochim Biophys Acta* 1841: 773–782
- García-Gonzalez V, Diaz-Villanueva J, Galindo-Hernandez O, Martinez-Navarro I, Hurtado-Ureta G & Perez-Arias A (2018) Ceramide metabolism balance, a multifaceted factor in critical steps of breast cancer development. *Int J Mol Sci* 19: 2527.
- García-Manyes S & Sanz F (2010) Nanomechanics of lipid bilayers by force spectroscopy with AFM: a perspective. *Biochim Biophys Acta* 1798: 741–749
- García-Ruiz C, Mari M, Colell A, Morales A, Caballero F, Montero J, Terrones O, Basañez G & Fernández-Checa J (2009) Mitochondrial cholesterol in health and disease. *Histol Histopathol* 24: 117–132

- Gault C, Obeid L & Hannun Y (2010) An overview of sphingolipid metabolism: from synthesis to breakdown introduction to sphingolipid metabolism. *Adv Exp Med Biol* 688: 1–23
- Gerhold J, Cansiz-Arda Ş, Löhmus M, Engberg O, Reyes A, van Rennes H, Sanz A, Holt I, Cooper H & Spelbrink J (2015) Human mitochondrial DNA-protein complexes attach to a cholesterol-rich membrane structure. *Sci Rep* 5: 15292
- Gerl MJ, Sampaio JL, Urban S, Kalvodova L, Verbavatz JM, Binnington B, Lindemann D, Lingwood CA, Shevchenko A, Schroeder C, *et al* (2012) Quantitative analysis of the lipidomes of the influenza virus envelope and MDCK cell apical membrane. *J Cell Biochem* 196: 213–221
- Gerstle, R., Desai, R. & Veatch S (2017) Dithiothreitol raises transition temperatures in giant plasma membrane vesicles. *Biophys J* 112: 519a
- Gilbert R (2016) Protein-lipid interactions and non-lamellar lipidic structures in membrane pore formation and membrane fusion. *Biochim Biophys Acta* 1858: 487–499
- Gillard BK, Clement RG & Marcus DM (1998) Variations among cell lines in the synthesis of sphingolipids in de novo and recycling pathways. *Glycobiol* 8: 885–890
- Giussani P, Tringali C, Riboni L, Viani P & Venerando B (2014) Sphingolipids: key regulators of apoptosis and pivotal players in cancer drug resistance. *Int J Mol Sci* 15: 4356–4392
- Gómez-Fernández JC, Goñi FM, Bach D, Restall C & Chapman D (1979) Protein-lipid interactions. A study of (Ca²⁺-Mg²⁺) ATPase reconstituted with synthetic phospholipids. *Febs Lett* 98: 211–223
- Gomez-Muñoz A, Gangoiti P, Arana L, Ouro A, Rivera I, Ordoñez M & Trueba M (2013) New insights on the role of ceramide 1-phosphate in inflammation. *Biochim Biophys Acta* 1831: 1060–1066
- Gomez-Munoz A, Presa N, Gomez-Larrauri A, Rivera I, Trueba M & Ordonez M (2016) Control of inflammatory responses by ceramide, sphingosine 1-phosphate and ceramide 1-phosphate. *Prog Lipid Res* 61: 51–62
- Goñi FM (2002) Non-permanent proteins in membranes: when proteins come as visitors. *Mol Membr Biol* 19: 237–245
- Goñi FM (2014) The basic structure and dynamics of cell membranes: An update of the Singer-Nicolson model. *Biochim Biophys Acta Biomembr* 1838: 1467–1476

- Goñi FM (2019) 'Rafts': A nickname for putative transient nanodomains. *Chem Phys Lipids* 218: 34–39
- Goñi FM & Alonso A (2006) Biophysics of sphingolipids I. Membrane properties of sphingosine, ceramides and other simple sphingolipids. *Biochim Biophys Acta* 1758: 1902–1921
- Goñi FM & Alonso A (2009) Effects of ceramide and other simple sphingolipids on membrane lateral structure. *Biochim Biophys Acta* 1788: 169–177
- Goñi FM, Alonso A, Bagatolli LA, Brown RE, Marsh D, Prieto M & Thewalt JL (2008) Phase diagrams of lipid mixtures relevant to the study of membrane rafts. *Biochim Biophys Acta - Mol Cell Biol Lipids* 1781: 665–684
- Goñi FM, Alonso A & Contreras FX (2020) Membrane nanodomains. In *eLs* Chichester: John Wiley & Sons
- Goñi FM, Montes LR & Alonso A (2012) Phospholipases C and sphingomyelinases: Lipids as substrates and modulators of enzyme activity. *Prog Lipid Res* 51: 238–266
- Goñi FM, Sot J & Alonso A (2014) Biophysical properties of sphingosine, ceramides and other simple sphingolipids. *Biochem Soc Trans* 42: 1401–1408
- González-Ramírez EJ, Goñi FM, Alonso A & 1 (2019) Mixing brain cerebroside with brain ceramides, cholesterol and phospholipids. *Sci Rep* 9: 13326
- Göppert-Mayer M (1931) Über elementarakte mit zwei Quantensprüngen. *Ann Phys* 9: 273–295
- Gorter F & Grendel E (1925) On bimolecular layers of lipoids on the chromocytes of the blood. *J Exp Med* 41: 9–443
- Gounaris K & Barber J (1983) Monogalactosyldiacylglycerol: The most abundant polar lipid in nature. *Trends Biochem Sci* 8: 378–381
- Grassme H, Jekle A, Riehle A, Schwarz H, Berger J, Sandhoff K, Kolesnick R & Gulbins E (2001) CD95 signaling via ceramide-rich membrane rafts. *J Biol Chem* 276: 20589–20596
- Griswold M (1998) The central role of Sertoli cells in spermatogenesis. *Semin Cell Dev Biol* 9: 411–416
- Guan XL, Riezman I, Wenk MR & Riezman H (2010) Yeast lipid analysis and quantification by mass spectrometry. *Methods Enzym* 470: 369–391
- Gulshan K, Brubaker G, Wang S, Hazen SL & Smith JD (2013) Sphingomyelin depletion impairs anionic phospholipid inward translocation and induces

- cholesterol efflux. *J Biol Chem* 288: 37166–37179
- Gupta B & Tiwary AK (2002) Role of sphingosine synthesis inhibition in transcutaneous delivery of levodopa. *Int J Pharm* 238: 43–50
- Gupta M, Mahajan A, Babita, Gupta S & Tiwary A (2004) Inhibition of skin sphingosine synthesis: enhanced percutaneous permeation of 5-fluorouracil. *Pharmazie* 59: 212–216
- Guri Y, Colombi M, Dazert E, Hindupur SK, Roszik J, Moes S, Jenoe P, Heim MH, Riezman I, Riezman H, *et al* (2017) mTORC2 Promotes tumorigenesis via lipid synthesis. *Cancer cell* 32: 807–823
- Gurr MI, Harwood JL, Frayn KN, Murphy DJ & Michell RH (2016) Lipids: Biochemistry, Biotechnology and Health, 6th Edition Wiley Blac. Oxford
- Hafez I & Cullis P (2001) Roles of lipid polymorphism in intracellular delivery. *Adv Drug Deliv Rev* 47: 139–148
- Hallett PJ, Engelender S & Isacson O (2019) Lipid and immune abnormalities causing age-dependent neurodegeneration and Parkinson's disease. *J Neuroinflammation* 16: 1–15
- Han G, Gupta SD, Gable K, Niranjanakumari S, Moitra P & Eichler F (2009) Identification of small subunits of mammalian serine palmitoyltransferase that confer distinct acyl-CoA substrate specificities. *Proc Natl Acad Sci* 106: 8186–8191
- Han S, Lone M, Schneiter R & Chang A (2010) Orm1 and Orm2 are conserved endoplasmic reticulum membrane proteins regulating lipid homeostasis and protein quality control. *Proc Natl Acad Sci USA* 107: 5851–5856
- Hanada K, Hara T, Fukasawa M, Yamaji A, Umeda M & Nishijima M (1998) Mammalian cell mutants resistant to a sphingomyelin-directed cytolysin. *J Biol Chem* 273: 33787–33794
- Hanada K, Hara T & Nishijima M (2000a) Purification of the serine palmitoyltransferase complex responsible for sphingoid base synthesis by using affinity peptide chromatography techniques. *J Biol Chem* 275: 8409–8415
- Hanada K, Hara T, Nishijima M, Kuge O, Dickson R & Nagiec M (1997) A mammalian homolog of the yeast LCB1 encodes a component of serine palmitoyltransferase, the enzyme catalyzing the first step in sphingolipid synthesis. *J Biol Chem* 272: 32108–32114
- Hanada K, Nishijima M & Akamatsu Y (1990) A temperature-sensitive mammalian cell

- mutant with thermolabile serine palmitoyltransferase for the sphingolipid biosynthesis. *J Biol Chem* 265: 22137–22142
- Hanada K, Nishijima M, Fujita T & Kobayashi S (2000b) Specificity of inhibitors of serine palmitoyltransferase (SPT), a key enzyme in sphingolipid biosynthesis, in intact cells. A novel evaluation system using an SPT-defective mammalian cell mutant. *Biochem Pharmacol* 59: 1211–1216
- Hannun C & Linares Y (1993) Sphingolipid breakdown products: Anti-proliferative and tumor-suppressor lipids. *Biochim Biophys Acta* 1154: 223–236
- Hannun YA, Loomis CR, Merrill AHJ & Bell RM (1986) Sphingosine inhibition of protein kinase C activity and of phorbol dibutyrate binding in vitro and in human platelets. *J Biol Chem* 261: 12604–12609
- Hannun YA & Obeid LM (2008) Principles of bioactive lipid signalling: lessons from sphingolipids. *Nat Rev Mol Cell Biol* 9: 139–150
- Hannun YA & Obeid LM (2018) Sphingolipids and their metabolism in physiology and disease. *Nat Rev Mol Cell Biol* 19: 175–191
- Harayama T & Riezman H (2018) Understanding the diversity of membrane lipid composition. *Nat Rev Mol Cell Biol* 19: 281–296
- Van Helvoort A, Van't Hof W, Ritsema T, Sandra A & Van Meer G (1994) Conversion of diacylglycerol to phosphatidylcholine on the basolateral surface of epithelial (Madin-Darby canine kidney) cells. Evidence for the reverse action of a sphingomyelin synthase. *J Biol Chem* 269: 1763–1769
- Henry B, Ziobro R, Becker K, Kolesnick R & Gulbins E (2013) Sphingolipids: basic science and drug development 1st ed. Gulbins E & Petrache I (eds) New York: Springer Heidelberg
- Heung L, Luberto C & Del Poeta M (2006) Role of sphingolipids in microbial pathogenesis. *Infect Immun* 74: 28–39
- Hinkovska-Galcheva V, Boxer L, Mansfield PJ, Schreiber AD & Shayman JA (2003) Enhanced phagocytosis through inhibition of de novo ceramide synthesis. *J Biol Chem* 278: 974–982
- Hogue M (1919) The effect of hypotonic and hypertonic solutions on fibroblasts of the embryonic chick heart in vitro. *J Exp Med* 30: 617–648
- Hojjati M, Li Z, Zhou H, Tang S, Huan C, Ooi E, Lu S & Jiang X (2005) Effect of myriocin on plasma sphingolipid metabolism and atherosclerosis in apoE-deficient mice. *J Biol Chem* 280: 10284–10289

- Holland W, Brozinick J, Wang L, Hawkins E, Sargent K, Liu Y, Narra K, Hoehn K, Knotts T, Siesky A, *et al* (2007) Inhibition of ceramide synthesis ameliorates glucocorticoid-, saturated-fat-, and obesity-induced insulin resistance. *Cell Metab* 5: 167–179
- Holleran W, Feingold K, Man M, Gao W, Lee J & Elias P (1991) Regulation of epidermal sphingolipid synthesis by permeability barrier function. *J Lipid Res* 32: 1151–1158
- Hong K, Baldwin PA & Allen, Theresa M. Papahadjopoulos D (1988) Fluorometric detection of the bilayer-to-hexagonal phase transition in liposomes. *Biochemistry* 11: 3947–3955
- Honigsmann A, Mueller V, Hell S & Eggeling C (2013) STED microscopy detects and quantifies liquid phase separation in lipid membranes using a new far-red emitting fluorescent phosphoglycerolipid analogue. *Faraday Discuss* 161: 77–89
- Hori T & Sugita M (1993) Sphingolipids in lower animals. *Prog Lipid Res* 32: 25–45
- Hornemann T, Richard S, Rutti M, Wei Y & von Eckardstein A (2006) Cloning and initial characterization of a new subunit for mammalian serine-palmitoyltransferase. *J Biol Chem* 281: 37275–37281
- Huang S, Liu K, Jiang D & Fang D (2019) Codetermination of sphingomyelin and cholesterol in cellular plasma membrane in sphingomyelin-depletion-induced cholesterol efflux. *Anal Chem* 91: 1501–1506
- Hurley J (2006) Membrane binding domains. *Biochim Biophys Acta* 1761: 805–811
- Huwiler A, Kolter T, Pfeilschifter J & Sandhoff K (2000) Physiology and pathophysiology of sphingolipid metabolism and signaling. *Biochim Biophys Acta* 1485: 63–99
- Ibarguren M, Bomans PHH, Frederik PM, Stonehouse M, Vasil AI, Vasil ML, Alonso A & Goñi FM (2010) End-products diacylglycerol and ceramide modulate membrane fusion induced by a phospholipase C/sphingomyelinase from *Pseudomonas aeruginosa*. *Biochim Biophys Acta Biomembr* 1798: 59–64
- Iessi E, Marconi M, Manganelli V, Sorice M, Malorni W, Garofalo T & Matarrese P (2020) On the role of sphingolipids in cell survival and death. *Int Rev Cell Mol Biol* 351: 149–195
- Ikushiro H, Hayashi H & Kagamiyama H (2001) A water-soluble homodimeric serine palmitoyltransferase from *Sphingomonas paucimobilis* EY2395T strain: purification, characterization, cloning, and overproduction. *J Biol Chem* 276:

18249–18256

- Israelachvili J, Marcelja S & Horn R (1980) Physical principles of membrane organization. *Q Rev Biophys* 13: 121–200
- Jacobson K, Mouritsen O & Anderson R (2007) Lipid rafts: at a crossroad between cell biology and physics. *Nat Cell Biol* 9: 7–14
- Jass J, Tjarnhage T & Puu G (2000) From liposomes to supported, planar bilayer structures on hydrophilic and hydrophobic surfaces: an atomic force microscopy study. *Biophys J* 79: 3153–3163
- Jiménez-Rojo N, Leonetti MD, Zoni V, Colom A, Feng S, Iyengar NR, Matile S, Roux A, Vanni S, Weissman J., *et al* (2020) Conserved functions of ether lipids and sphingolipids in the early secretory pathway. *Curr Biol* 30: 3775–3787
- Jiménez-Rojo N, Sot J, Busto JV, Shaw WA, Duan J, Merrill AJ, Alonso A & Goñi FM (2014a) Biophysical properties of novel 1-deoxy-(dihydro)ceramides occurring in mammalian cells. *Biophys J* 107: 2850–2859
- Jiménez-Rojo N, Viguera AR, Collado MI, Sims KH, Constance C, Hill K, Shaw WA, Goñi FM & Alonso A (2014b) Sphingosine induces the aggregation of imine-containing peroxidized vesicles. *Biochim Biophys Acta* 1838: 2071–2077
- Juhász J, Davis J & Sharom F (2010) Fluorescent probe partitioning in giant unilamellar vesicles of ‘lipid raft’ mixtures. *Biochem J* 430: 415–423
- Kainu V, Hermansson M & Somerharju P (2010) Introduction of phospholipids to cultured cells with cyclodextrin. *J Lipid Res* 51: 3533–3541
- Kalvodova L, Sampaio JL, Cordo S, Ejsing CS, Shevchenko A & Simons K (2009) The lipidomes of vesicular stomatitis virus, semliki forest virus, and the host plasma membrane analyzed by quantitative shotgun mass spectrometry. *J Virol* 83: 7996–8003
- Kamil B, Anna F, Anna S, Sławomir P & Halina C (2016) Regulation of sphingomyelin metabolism. *Pharmacol Rep* 68: 570–581
- Karlsson K-A (1970) Sphingolipid long chain bases. *Lipids* 5: 878–891
- Karnati S, Garikapati V, Liebisch G, Van Veldhoven, PP Spengler B, Schmitz G & Baumgart-Vogt E (2018) Quantitative lipidomic analysis of mouse lung during postnatal development by electrospray ionization tandem mass spectrometry. *PLoS One* 13: e0203464
- Kates M & Kuksis A (1980) Membrane Fluidity Totowa, Nueva Jersey: Humana Press
- Keller H, Lorizate M & Schwille P (2009) PI(4,5)P2 degradation promotes the

- formation of cytoskeleton-free model membrane systems. *Chem Phys Chem* 10: 2805–2812
- Keyvanloo A, Shaghghi M, Zuckermann M & Thewalt J (2018) The phase behavior and organization of sphingomyelin/cholesterol membranes: A deuterium NMR study. *Biophys J* 114: 1344–1356
- Kiessling V, Wan C & Tamm LK (2009) Domain coupling in asymmetric lipid bilayers. *Biochim Biophys Acta* 1788: 64–71
- Klein U, Gimpl G & Fahrenholz F (1995) Alteration of the myometrial plasma membrane cholesterol content with β -cyclodextrin modulates the binding affinity of the oxytocin receptor? *Biochemistry* 34: 13784–13793
- Kluepfel D, Charest M, Sehgal SN, Vezina C, Bagli J & Baker H (1972) Myriocin, a new antifungal antibiotic from *Myriococcum arbutomyces*. *J Antibiot (Tokyo)* 22: 109–115
- Klymchenko AS & Kreder R (2014) Fluorescent probes for lipid rafts: From model membranes to living cells. *Chem Biol* 21: 97–113
- Kolesnick R (1987) 1,2-Diacylglycerols but not phorbol esters stimulate sphingomyelin hydrolysis in GH3 pituitary cells. *J Biol Chem* 262: 16759–16762
- Kolesnick R (2002) The therapeutic potential of modulating the ceramide/sphingomyelin pathway. *J Clin Invest* 1: 3–8
- Kolesnick RN, Goñi FM & Alonso A (2000) Compartmentalization of ceramide signaling: Physical foundations and biological effects. *J Cell Physiol* 184: 285–300
- Kotecki M, Reddy PS & Cochran BH (1999) Isolation and characterization of a near-haploid human cell line. *Exp Cell Res* 252: 273–280
- Kovanen P, Nikkilä E & Miettinen T (1975) Regulation of cholesterol synthesis and storage in fat cells. *J Lipid Res* 16: 211–223
- Krasnowska EK, Gratton E & Parasassi T (1998) Prodan as a membrane surface fluorescence probe: Partitioning between water and phospholipid phases. *Biophys J* 74: 1984–1993
- Kroesen BJ, Jacobs S, Pettus BJ, Sietsma H, Kok JW, Hannun YA & De Leij LFMH (2003) BcR-induced apoptosis involves differential regulation of C16 and C24-ceramide formation and sphingolipid-dependent activation of the proteasome. *J Biol Chem* 278: 14723–14731
- Kurek K, Piotrowska D, Wiesiołek-Kurek P, Łukaszuk B, Chabowski A, Górski J & Zendzian-Piotrowska M (2013) Inhibition of ceramide de novo synthesis reduces

- liver lipid accumulation in rats with nonalcoholic fatty liver disease. *Liver Int* 34: 1074–1083
- Kusumi A, Fujiwara T, Morone N, Yoshida K, Chadda R, Xie M, Kasai R & KG S (2012) Membrane mechanisms for signal transduction: the coupling of the meso-scale raft domains to membrane-skeleton-induced compartments and dynamic protein complexes. *Semin Cell Dev Biol* 2: 126–144
- Kusumi A, Fujiwara TK, Tsunoyama TA, Kasai RS, Liu AA, Hirosawa KM, Kinoshita M, Matsumori N, Komura N, Ando H, *et al* (2020) Defining raft domains in the plasma membrane. *Traffic* 21: 106–137
- Lakshini M (2016) Distribution of lipids in the human brain and their differential expression in Alzheimer's disease: a matrix-assisted laser desorption/ionisation-imaging mass spectrometry (MALDI-IMS) study. Doctoral Thesis University College London
- Lamour N, Wijesinghe D, Mietla J, Ward K, Stahelin R & Chalfant C (2011) Ceramide kinase regulates the production of tumor necrosis factor α (TNF α) via inhibition of TNF α -converting enzyme. *J Biol Chem* 286: 42808–42817
- Langmuir I (1917) The constitution and fundamental properties of solids and liquids. II. Liquids. *Liq J Am Chem Soc* 39: 1848–1906
- Larsson K (1989) Cubic lipid-water phases: structures and biomembrane aspects. *J Phys Chem* 93: 7304–7314
- Lawson EL, Clifton JG, Huang F, Li X, Hixson DC & Josic D (2006) Use of magnetic beads with immobilized monoclonal antibodies for isolation of highly pure plasma membranes. *Electrophoresis* 27: 2747–2758
- Lee H, Rotolo J, Mesicek J, Penate-Medina T, Rimner A, Liao W, Yin X, Ragupathi G, Ehleiter D, Gulbins E, *et al* (2011) Mitochondrial ceramide-rich macrodomains functionalize Bax upon irradiation. *PLoS One* 6: e19783
- Lee W & Kolesnick R (2017) Sphingolipid abnormalities in cancer multidrug resistance: Chicken or egg? *Cell Signal* 38: 134–145
- Lee Y, Block G, Chen H, Folch-puy E, Foronjy R, Jendresen CB, Kimura M, Kraft E, Lindemose S, Lu J, *et al* (2009) One-step isolation of plasma membrane proteins using magnetic beads with immobilized concanavalin A1. *Protein Expr Purif* 62: 223–229
- Lemmon M (2008) Membrane recognition by phospholipid-binding domains. *Nat Rev Mol Cell Biol* 9: 99–111

- Lenard J & Singer S (1966) Protein conformation in cell membrane preparations as studied by optical rotatory dispersion and circular dichroism. *Proc Natl Acad Sci USA* 56: 1828–1835
- Levental I, Levental KR & Heberle FA (2020) Lipid rafts: Controversies resolved, mysteries remain. *Trends Cell Biol* 30: 341–353
- Li G, Kakuda S, Suresh P, Canals D, Salamone S & London E (2019) Replacing plasma membrane outer leaflet lipids with exogenous lipid without damaging membrane integrity. *PLoS ONE* 14: 1–22
- Li G, Kim J, Huang Z, St JR, Brown DA & London E (2016a) Efficient replacement of plasma membrane outer leaflet phospholipids and sphingolipids in cells with exogenous lipids. *PNAS* 113: 14025–14030
- Li H, Yun HY, Baek KJ, Kwon NS, Park KC & Kim DS (2014) Myriocin, a serine palmitoyltransferase inhibitor, increases melanin synthesis in Mel-Ab cells and a skin equivalent model. *Pharmazie* 69: 187–191
- Li J, Yin J, Rong C, Li K, Wu J, Huang L, Zeng H & Kumar S (2016b) Orosomucoid proteins interact with the small subunit of serine palmitoyltransferase and contribute to sphingolipid homeostasis and stress responses in Arabidopsis thaliana and Nan Yao2. *Plant Cell* 28: 3038–3051
- Li Z, Kabir I, Tietelman G, Huan C, Fan J, Worgall T & Jiang XC (2018) Sphingolipid de novo biosynthesis is essential for intestine cell survival and barrier function. *Cell Death Dis* 9: 1–13
- Lidgerwood G, Pitson S, Bonder C & Pébay A (2018) Roles of lysophosphatidic acid and sphingosine-1-phosphate in stem cell biology. *Prog Lipid Res* 72: 42–54
- Lin G, Lee P, Chen K, Mao D, Tan K, Zuo Z, Lin W, Wang L & Bellen H (2018) Phospholipase PLA2G6, a parkinsonism-associated gene, affects Vps26 and Vps35, retromer function, and Ceramide levels, similar to α -synuclein gain. *Cell Metab* 28: 605–618
- Llorente A, Skotland T, Sylvänne T, Kauhanen D, Róg T, Orłowski A, Vattulainen I, Ekroos K & Sandvig K (2013) Molecular lipidomics of exosomes released by PC-3 prostate cancer cells. *Biochim Biophys Acta* 1831: 1302–1309
- Lone MA, Hülsmeier AJ, Saied EM, Karsai G, Arenz C, von Eckardstein A & Hornemann T (2020) Subunit composition of the mammalian serine-palmitoyltransferase defines the spectrum of straight and methyl-branched long-chain bases. *PNAS* 117: 15591–15598

- Lone M, Santos T, Alecu I, Silva L & Hornemann T (2019) 1-Deoxysphingolipids. *Biochim Biophys Acta Mol Cell Biol Lipids* 1864: 512–521
- Lönnfors M, Doux J, Killian J, Nyholm T & Slotte J (2011) Sterols have higher affinity for sphingomyelin than for phosphatidylcholine bilayers even at equal acylchain order. *Biophys J* 100: 2633–2641
- Lorent J, Levental K, Ganesan L, Rivera-Longworth G, Sezgin E, Doktorova M, Lyman E & Levental I (2020) Plasma membranes are asymmetric in lipid unsaturation, packing and protein shape. *Nat Chem Biol* 16: 644–652
- Lorizate M, Sachsenheimer T, Glass B, Habermann A, Gerl MJ, Kräusslich HG & Brügger B (2013) Comparative lipidomics analysis of HIV-1 particles and their producer cell membrane in different cell lines. *Cell Microbiol* 15: 292–304
- Los D & Murata N (2004) Membrane fluidity and its roles in the perception of environmental. *Biochim Biophys Acta* 1666: 142–157
- Luberto C, Kravetska J & Hannun Y (2002a) Ceramide regulation of apoptosis versus differentiation: A walk on a fine line. *Neurochem Res* 27: 609–617
- Luberto C, Kravetska JM & Hannun YA (2002b) Ceramide regulation of apoptosis versus differentiation: A walk on a fine line. Lessons from neurobiology. *Neurochem Res* 27: 609–617
- Luckey M (2008) *Membrane Structural Biology* Cambridge: Cambridge University Press
- Luzzati V (1968) X-ray diffraction studies of lipid-water systems. *Biophys J* 1: 71–123
- Maddy A & Malcolm B (1965) Protein conformations in the plasma membrane. *Science* 150: 1616–1618
- Maggio B, Fanani ML, Rosetti CM & Wilke N (2006) Biophysics of sphingolipids II. Glycosphingolipids: An assortment of multiple structural information transducers at the membrane surface. *Biochim Biophys Acta Biomembr* 1758: 1922–1944
- Maliekal P, Vertommen D, Delpierre G & Schaftingen E Van (2006) Identification of the sequence encoding N -acetylneuraminase-9-phosphate phosphatase. *Glycobiol* 16: 165–172
- Malinsky J & Opekarová M (2016) *New insight into the roles of membrane microdomains in physiological activities of fungal cells* Elsevier Inc.
- Mandon E, Ehses I, Rother J, van Echten G & Sandhoff K (1992) Subcellular localization and membrane topology of serine palmitoyltransferase, 3-dehydrosphinganine reductase, and sphinganine N-acyltransferase in mouse liver. *J*

- Biol Chem* 267: 11144–11148
- Manni MM, Sot J & Goñi FM (2015) Interaction of *Clostridium perfringens* epsilon-toxin with biological and model membranes: A putative protein receptor in cells. *Biochim Biophys Acta Biomembr* 1848: 797–804
- Martin Del Valle EM (2004) Cyclodextrins and their uses : a review. *Process Biochem* 39: 1033–1046
- Matanes F, Twal WO & Hammad SM (2019) Sphingolipids as biomarkers of disease. *Exp Med Biol* 1159: 109–138
- Maté S, Busto JV, García-Arribas AB, Sot J, Vazquez R, Herlax V, Wolf C, Bakás L & Goñi F (2014) N-nervonoylsphingomyelin (C24:1) prevents lateral heterogeneity in cholesterol-containing membranes. *Biophys J* 106: 2606–2616.
- McIntosh T, Simon S, Needham D & Huang C (1992) Structure and cohesive properties of sphingomyelin/cholesterol bilayers. *Biochemistry* 31: 2012–2020
- Meddens MBM, de Keijzer S & Cambi A (2014) Chapter 4: High spatiotemporal bioimaging techniques to study the plasma membrane nanoscale organization Cornea A & Conn PM (eds) Elsevier Inc.
- van Meer G, R. Voelker D & W. Feigenson G (2008) Membrane lipids: where they are and how they behave. *Nat Rev Mol Cell Biol* 9: 112–124
- Van Meer G, Wolthoorn J & Degroote S (2003) The fate and function of glycosphingolipid glucosylceramide. *Philos T R Soc B* 358: 869–873
- Megha & London E (2004) Ceramide selectively displaces cholesterol from ordered lipid domains (rafts): implications for lipid raft structure and function. *J Biol Chem* 279: 9997–10004
- Merrill AH, Schmelz EM, Dillehay DL, Spiegel S, Shayman JA, Schroeder JJ, Riley RT, Voss KA & Wang E (1997) Sphingolipids--the enigmatic lipid class: biochemistry, physiology, and pathophysiology. *Toxicol Appl Pharmacol* 142: 208–222
- Merrill AH, Wang MD, Park M & Sullards MC (2007) (Glyco)sphingolipidology: an amazing challenge and opportunity for systems biology. *Trends Biochem Sci* 32: 457–468
- Merrill AJ, Sereni A, Stevens V, Hannun Y, Bell R & Kinkade JJ (1986) Inhibition of phorbol ester-dependent differentiation of human promyelocytic leukemic (HL-60) cells by sphinganine and other long-chain bases. *J Biol Chem* 261: 12610–12615
- Mikłosz A, Łukaszuk B, Baranowski M, Górski J & Chabowski A (2013) Effects of

- inhibition of serine palmitoyltransferase (SPT) and sphingosine kinase 1 (SphK1) on palmitate induced insulin resistance in L6 myotubes. *PLoS ONE* 8: 1–9
- Mise K, Akifusa S, Watarai S, Ansai T, Nishihara T & Takehara T (2005) Involvement of ganglioside GM3 in G2/M cell cycle arrest of human monocytic cells induced by *Actinobacillus actinomycetemcomitans* cytolethal distending toxin. *Infect Immun* 73: 4846–4852
- Miyake Y, Kozutsumi Y, Nakamura S, Fujita T & Kawasaki T (1995) Serine palmitoyltransferase is the primary target of a sphingosine-like immunosuppressant, ISP-1/myriocin. *Biochem Biophys Res Commun* 211: 396–403
- Mizuno H, Abe M, Dedecker P, Makino A, Rocha S, Ohno-Iwashita Y, Hofkens J, Kobayashi T & Miyawaki A (2011) Fluorescent probes for superresolution imaging of lipid domains on the plasma membrane. *Chem Sci* 2: 1548–1553
- Monasterio BG, Alonso B, Sot J, García-Arribas AB, Gil-Cartón D, Valle M, Zurutuza A & Goñi FM (2017) Coating graphene oxide with lipid bilayers greatly decreases its hemolytic properties. *Langmuir* 33: 8181–8191
- Monasterio BG, Jiménez-Rojo N, B. García-Arribas A, Riezman H, Goñi FM & Alonso A (2020) Patches and blebs: A comparative study of the composition and biophysical properties of two plasma membrane preparations from CHO cells. *Int J Mol Sci* 21: 2643
- Monasterio BG, Jiménez-Rojo N, García-Arribas AB, Riezman H, Goñi FM & Alonso A (2021a) CHO/LY-B cell growth under limiting sphingolipid supply: correlation between lipid composition and biophysical properties of sphingolipid-restricted cell membranes. *FASEB J* 35: e21657
- Monasterio BG, Jiménez-Rojo N, García-Arribas AB, Riezman H, Goñi FM & Alonso A (2021b) Plasma membrane effects of sphingolipid-synthesis inhibition by myriocin in CHO cells: a biophysical and lipidomic study. *Res Sq*
- Montero J, Morales A, Llacuna L, Lluís J, Terrones O, Basañez G, Antonsson B, Prieto J, García-Ruiz C, Colell A, *et al* (2008) Mitochondrial cholesterol contributes to chemotherapy resistance in hepatocellular carcinoma. *Cancer Res* 68: 5246–5256
- Montes LR, Ahyayauch H, Ibarguren M, Sot J, Alonso A, Bagatolli LA & Goñi FM (2010) Electroformation of giant unilamellar vesicles from native membranes and organic lipid mixtures for the study of lipid domains under physiological ionic-strength conditions. *Methods Mol Biol* 606: 105–114

- Montes LR, Alonso A, Goñi FM & Bagatolli LA (2007) Giant unilamellar vesicles electroformed from native membranes and organic lipid mixtures under physiological conditions. *93*: 3548–3554
- Montes LR, López DJ, Sot J, Bagatolli LA, Stonehouse MJ, Vasil ML, Wu BX, Hannun YA, Goñi FM & Alonso A (2008) Ceramide-enriched membrane domains in red blood cells and the mechanism of sphingomyelinase-induced hot-cold hemolysis. *Biochemistry* 47: 11222–11230
- Montes LR, Ruiz-Argüello MB, Goñi FM & Alonso A (2002) Membrane restructuring via ceramide results in enhanced solute efflux. *J Biol Chem* 277: 11788–11794
- Morad S & Cabot M (2012) Ceramide-orchestrated signalling in cancer cells. *Nat Rev Canc* 13: 51–65
- Moravcevic K, Mendrola J, Schmitz K, Wang Y, Slochower D, Janmey P & Lemmon M (2010) Kinase associated-1 domains drive MARK/PAR1 kinases to membrane targets by binding acidic phospholipids. *Cell* 143: 966–977
- Morigaki K & Tanimoto Y (2018) Evolution and development of model membranes for physicochemical and functional studies of the membrane lateral heterogeneity. *Biochim Biophys Acta - Biomembr* 1860: 2012–2017
- Mouritsen OG (2005) Life as a matter of fat 1st ed. Berlin: Springer-Verlag Berlin Heidelberg
- Mueller P, Rudin D, Tien H & Wescott W (1962) Reconstitution of cell membrane structure in vitro and its transformation into an excitable system. *Nature* 194: 979–980
- Mullen T & Obeid L (2012) Ceramide and apoptosis: exploring the enigmatic connections between sphingolipid metabolism and programmed cell death. *Anti-cancer Agent ME* 12: 340–363
- Munro S (2003) Lipid rafts: elusive or illusive? *Cell* 115: 377–388
- Nakamura H, Wakita S, Yasufuku K, Makiyama T, Waraya M, Hashimoto N & Murayama T (2015) Sphingomyelin regulates the activity of secretory phospholipase A2 in the plasma membrane. *J Cell Biochem* 116: 1898–1907
- Nelson DL & Cox MM eds. (2008) Lehninger principles of biochemistry 5th ed. New York: W. H. Freeman and Company
- Nicovich PR, Kwiatek JM, Ma Y, Benda A & Gaus K (2018) FSCS reveals the complexity of lipid domain dynamics in the plasma membrane of live cells. *Biophys J* 114: 2855–2864

- Nieto FL, Pescio LG, Favale NO, Adamo AM & Sterin-Speziale NB (2008) Sphingolipid metabolism is a crucial determinant of cellular fate in nonstimulated proliferating Madin-Darby Canine Kidney (MDCK) cells. *J Biol Chem* 283: 25682–25691
- Nieva JL, Alonso A, Basáñez G, Goñi FM, Gulik A, Vargas R & Luzzati V (1995) Topological properties of two cubic phases of a phospholipid:cholesterol:diacylglycerol aqueous system and their possible implications in the phospholipase C-induced liposome fusion. *FEBS Lett* 368: 143–147
- Nieva JL, Goñi FM & Alonso A (1989) Liposome fusion catalytically induced by phospholipase C. *Biochemistry* 28: 7364–7367
- Novgorodov S, Wu B, Gudz T, Bielawski J, Ovchinnikova T, YA H & Obeid L (2011) Novel pathway of ceramide production in mitochondria: thioesterase and neutral ceramidase produce ceramide from sphingosine and acyl-CoA. *J Biol Chem* 286: 25352–25362
- Nyholm T, Grandell P, Westerlund B & Slotte J (2010) Sterol affinity for bilayer membranes is affected by their ceramide content and the ceramide chain length. *Biochim Biophys Acta* 1798: 1008–1013
- Ogretmen B (2018) Sphingolipid metabolism in cancer signalling and therapy. *Nat Rev Cancer* 18: 33–50
- Ohtani Y, Irie T, Uekama K, Fukunaga K & Pitha J (1989) Differential effects of α -, β - and γ -cyclodextrins on human erythrocytes. *Eur J Biochem* 186: 17–22
- Oldfield E & Chapman D (1972) Dynamics of lipids in membranes: Heterogeneity and the role of cholesterol. *FEBS Lett* 23: 285–297
- Oshimura M, Freeman A & Sanberg AA (1977) Chromosomes and causation of human cancer and leukemia. *Cancer* 40: 1143–1148
- Overton E (1895) Über die osmotischen Eigenschaften der lebenden Pflanzen und Thierzelle. *Vierteljahrschr d Naturf* 40: 159–201
- Owen DM, Rentero C, Magenau A, Abu-Siniyeh A & Gaus K (2012) Quantitative imaging of membrane lipid order in cells and organisms. *Nat Prot* 7: 24–35
- Owen J, Bruckdorfer K, Day R & McIntyre N (1982) Decreased erythrocyte membrane fluidity and altered lipid composition in human liver disease. *J Lipid Res* 23: 124–132
- Parasassi T & Gratton E (1997) Two-photon fluorescence microscopy of laurdan

- generalized polarization domains in model and natural membranes. *Biophys J* 72: 2413–2429
- Parasassi T, De Stasio G, D'Ubaldo A & Gratton E (1990) Phase fluctuation in phospholipid membranes revealed by LAURDAN fluorescence. *Biophys J*, 57: 1179–1186
- Park T, Rosebury W, Kindt E, Kowala M & Panek R (2008) Serine palmitoyltransferase inhibitor myriocin induces the regression of atherosclerotic plaques in hyperlipidemic ApoE-deficient mice. *Pharmacol Res* 58: 45–51
- Park W, Park J, Erez-Roman R, Kogot-Levin A, Bame J, Tirosh B, Saada A, Merrill AJ, Pewzner-Jung Y & Futerman A (2013) Protection of a ceramide synthase 2 null mouse from drug-induced liver injury: role of gap junction dysfunction and connexin 32 mislocalization. *J Biol Chem* 288: 30904–30916
- Pascher I (1976) Molecular arrangements in sphingolipids. Conformation and hydrogen bonding of ceramide and their implication on membrane stability and permeability. *Biochim Biophys Acta* 455: 433–451
- Patra SK, Alonso A, Arrondo JL & Goñi FM (1992) Liposomes containing sphingomyelin and cholesterol: detergent solubilisation and infrared spectroscopic studies. *J Liposome Res* 9: 247–260.
- Perlmutter J & Sachs J (2011) Interleaflet interaction and asymmetry in phase separated lipid bilayers: molecular dynamics simulations. *J Am Chem Soc* 14: 6563–6577
- Phillips MC, Ladbroke BD & Chapman D (1970) Molecular interactions in mixed lecithin systems. *BBA - Biomembr* 196: 35–44
- Piccolo N Del, Placone J, He L, Agudelo SC & Hristova K (2012) Production of plasma membrane vesicles with chloride salts and their utility as a cell membrane mimetic for biophysical characterization of membrane protein interactions. *Anal Chem* 84: 8650–8655
- Pike LJ (2006) Rafts defined: a report on the keystone symposium on lipid rafts and cell function. *J Lipid Res* 47: 1597–8
- Pinto S, Silva L, Futerman A & Prieto M (2011) Effect of ceramide structure on membrane biophysical properties: the role of acyl chain length and unsaturation. *Biochim Biophys Acta* 1808: 2753–60
- Pinto W, Srinivasan B, Shepherd S, Schmidt A, Dickson R & Lester R (1992) Sphingolipid long-chain-base auxotrophs of *Saccharomyces cerevisiae*: genetics, physiology, and a method for their selection. *J Bacteriol* 174: 2565–2574

- Plasencia I, Norlén L & Bagatolli L (2007) Direct visualization of lipid domains in human skin stratum corneum's lipid membranes: effect of pH and temperature. *Biophys J* 93: 3142–3155
- Pletikapić G & DeNardis N (2017) Application of surface analytical methods for hazardous situation in the Adriatic sea: monitoring of organic matter dynamics and oil pollution. *Nat Hazards Earth Syst Sci* 17: 31–44
- Ramstedt B & Slotte J (2002) Membrane properties of sphingomyelins. *FEBS Lett* 531: 33–37
- Rayermann S, Rayermann G, Cornell C, Merz A & Keller S (2017) Hallmarks of reversible separation of living, unperturbed cell membranes into two liquid phases. *Biophys J* 113: 2425–2432
- Reeves J & Dowben R (1969) Formation and properties of thin-walled phospholipid vesicles. *J Cell Physiol* 73: 49–60
- Ridgway N & McLeod R (2016) *Biochemistry of Lipids, Lipoproteins and Membranes* 6th ed. Amsterdam: Elsevier
- Rief M, Gautel M, Oesterhelt F, Fernandez J & Gaub H (1997) Reversible unfolding of individual titin immunoglobulin domains by AFM. *Science* 276: 1109–1112
- Robertson J (1959) The molecular structure and contact relationships of cell membranes. *Prog Biophys Mol Biol* 10: 343–418
- Robinson B, Johnson D & Poulos A (1992) Novel molecular species of sphingomyelin containing 2-hydroxylated polyenoic very-long-chain fatty acids in mammalian testes and spermatozoa. *J Biol Chem* 267: 1746–1751
- Rosetti CM, Mangiarotti A & Wilke N (2017) Sizes of lipid domains: What do we know from artificial lipid membranes? What are the possible shared features with membrane rafts in cells? *Biochim Biophys Acta - Biomembr* 1859: 789–802
- Sadeghlar F, Sandhoff K & van Echten-Deckert G (2000) Cell type specific localization of sphingomyelin biosynthesis. *FEBS Lett* 478: 9–12
- Sahoo H & Schwille P (2013) Influence of glycosaminoglycans on lipid dynamics in supported phospholipid bilayers. *Soft Matter* 9: 3859–3865
- Sahu S, Hannun Y & Yao N (2019) Emergence of membrane sphingolipids as a potential therapeutic target. *Biochimie* 158: 257–264
- Sampaio JL, Gerl MJ, Klose C, Ejsing CS, Beug H, Simons K & Shevchenko A (2011) Membrane lipidome of an epithelial cell line. *Proc Natl Acad Sci* 108: 1903–1907
- Sanchez S, Tricerri M, Ossato G & Gratton E (2010) Lipid packing determines protein-

- membrane interactions: challenges for apolipoprotein A-I and high density lipoproteins. *Biochim Biophys Acta* 1798: 1399–408
- Santis A De, Varela Y, Sot J, Errico GD, Goñi FM & Alonso A (2018) Omega-3 polyunsaturated fatty acids do not fluidify bilayers in the liquid-crystalline state. *Sci Rep* 8: 1–13
- Schardinger F (1903) Über thermophile bakterien aus verschiedenen speisen und milch. *Starke Z Untersuch Nahr u Genussm* 6: 865–880
- Schmid G (1989) Cyclodextrin glycosyltransferase production : yield enhancement by overexpression of cloned genes. *TIBTECH* 7: 244–248
- Schmidt CF, Barenholz Y & Thompson TE (1977) A nuclear magnetic resonance study of sphingomyelin in bilayer systems. *J Phys Soc Jpn* 42: 719–720
- Scolaro B, de Andrade L & Castro I (2020) Cardiovascular disease prevention: the earlier the better? A review of plant sterol metabolism and implications of childhood supplementation. *Int J Mol Sci* 1: 21
- Scott R (1976) Plasma membrane vesiculation : A new technique for isolation of plasma membranes. *Science* 194: 743–745
- Semrau S & Schmidt T (2009) Membrane heterogeneity – from lipid domains to curvature effects. *Soft Matter* 5: 3129–3364
- Sezgin E, Gutmann T, Buhl T, Grzybek M, Coskun Ü, Solimena M, Simons K, Levental I & Schwille P (2015a) Adaptive lipid packing and bioactivity in membrane domains. *PLoS One* 4: 1–14
- Sezgin E, Kaiser H, Baumgart T, Schwille P, Simons K & Levental I (2012) Elucidating membrane structure and protein behavior using giant plasma membrane vesicles. *Nat Protoc* 7: 1042–1051
- Sezgin E, Levental I, Mayor S & Eggeling C (2017a) The mystery of membrane organization: composition, regulation and physiological relevance of lipid rafts. *Nat Rev Mol Cell Biol* 18: 361–374
- Sezgin E, Schneider F, Zilles V, Urban I, Garcia E, Waithe D, Klymchenko AS & Eggeling C (2017b) Polarity-sensitive probes for superresolution stimulated emission depletion microscopy. *Biophys J* 113: 1321–1330
- Sezgin E & Schwille P (2012) Model membrane platforms to study protein-membrane interactions. *Mol Membr Biol* 29: 144–154
- Sezgin E, Waithe D, Bernardino J, Serna D & Eggeling C (2015b) Spectral imaging to measure heterogeneity in membrane lipid packing. *Chemphys* 16: 1387–1394

- Shamim A, Mahmood T, Ahsan F, Kumar A & Bagga P (2018) Lipids: an insight into the neurodegenerative disorders. *Clini Nutr Exp* 20: 1–19
- Sharma N, He Q & Sharma RP (2004) Sphingosine kinase activity confers resistance to apoptosis by fumonisin B1 in human embryonic kidney (HEK-293) cells. *Chem Biol Interact* 151: 33–42
- Shchelokovskyy P, Tristram-Nagle S & Dimova R (2011) Effect of the HIV-1 fusion peptide on the mechanical properties and leaflet coupling of lipid bilayers. *New J Phys* 13: 1–17
- Siddique M, Li Y, Chaurasia B, Kaddai V & Summers S (2015) Dihydroceramides: From Bit Players to Lead Actors. *J Biol Chem* 290: 15371–15379
- Simons K & Ikonen E (1997) Functional rafts in cell membranes. *Nat* 387: 569–572
- Simons K & Sampaio JL (2011) Membrane organization and lipid rafts. *Cold Spring Harb Perspect Biol* 3: a004697
- Singer G & Nicolson J (1972) The fluid mosaic model of the structure of cell membranes. *Science* 175: 720–731
- Singh S & Keller D (1991) Atomic force microscopy of supported planar membrane bilayers. *Biophys J* 60: 1401–1410
- Siskind L, Kolesnick R & Colombini M (2002) Ceramide channels increase the permeability of the mitochondrial outer membrane to small proteins. *J Biol Chem* 277: 26796–26803
- Skinkle A, Levental K & Levental I (2020) Cell-derived plasma membrane vesicles are permeable to hydrophilic macromolecules. *Biophys J* 2020 118: 1292–1300
- Slotte J (2013) Molecular properties of various structurally defined sphingomyelins-- correlation of structure with function. *Prog Lipid Res* 52: 206–219
- Slotte J (2016) The importance of hydrogen bonding in sphingomyelin's membrane interactions with co-lipids. *Biochim Biophys Acta* 1858: 304–310
- Slotte J, Yasuda T, Engberg O, Al Sazzad M, Hautala V, Nyholm T & Murata M (2017) Bilayer interactions among unsaturated phospholipids, sterols, and ceramide. *Biophys J* 112: 1673–1681
- Smith WS, Baker EJ, Holmes SE, Koster G, Hunt AN, Johnston DA, Flavell SU & Flavell DJ (2017) Membrane cholesterol is essential for triterpenoid saponin augmentation of a saporin-based immunotoxin directed against CD19 on human lymphoma cells. *Biochim Biophys Acta Biomembr* 1859: 993–1007
- Solomon JC, Sharma K, Wei LX, Fujita T & Shi YF (2003) A novel role for

- sphingolipid intermediates in activation-induced cell death in T cells. *Cell Death Differ* 10: 193–202
- Sot J, Aranda FJ, Collado MI, Goñi FM & Alonso A (2005) Different effects of long- and short-chain ceramides on the gel-fluid and lamellar-hexagonal transitions of phospholipids: a calorimetric, NMR, and x-ray diffraction study. *Biophys J* 88: 3368–3380
- Sot J, Bagatolli LA, Goni FM & Alonso A (2006) Detergent-resistant, ceramide-enriched domains in sphingomyelin/ceramide bilayers. *Biophys J* 90: 903–914
- Sot J, Ibarguren M, Busto J, Montes L, Goni FM & Alonso A (2008) Cholesterol displacement by ceramide in sphingomyelin-containing liquid-ordered domains, and generation of gel regions in giant lipidic vesicles. *FEBS Lett* 582: 3230–3236
- Spiegel S, Cuvillier O, Edsall L, Kohama T, Menzeleev R, Olah Z, Olivera A, Pirianov G, Thomas D, Tu Z, *et al* (1998) Sphingosine-1-phosphate in cell growth and cell death. *Ann N Y Acad Sci* 19: 11–28
- Spiegel S & Merrill A (1996) Sphingolipid metabolism and cell growth regulation. *FASEB J* 10: 1388–1397
- Spiegel S & Milstien S (2003) Exogenous and intracellularly generated sphingosine 1-phosphate can regulate cellular processes by divergent pathways. *Biochem Soc Trans* 31: 1216–1219
- Stancevic B & Kolesnick R (2010) Ceramide-rich platforms in transmembrane signaling. *FEBS Lett* 584: 1728–1740
- Staneva G, Momchilova A, Wolf C, Quinn P & Koumanov K (2009) Membrane microdomains: role of ceramides in the maintenance of their structure and functions. *Biochim Biophys Acta* 1788: 666–675
- Stella VJ & Rajewski RA (1997) Cyclodextrins: Their future in drug formulation and delivery. *Pharm Res* 14: 556–567
- Stillwell W (2016) An introduction to biological membranes: composition, structure and function 2nd ed. New York: Elsevier Science
- Stockman-Juvala, H. Savolainen K (2008) A review of the toxic effects and mechanism of action of fumonisin B1. *Hum Exp Toxicol* 27: 799–809
- Stoffel W (1971) Sphingolipids. *Annu Rev Biochem* 40: 57–82
- Straková K, López-Andarias J, Jiménez-Rojo N, Chambers JE, Marciniak SJ, Riezman H, Sakai N & Matile S (2020) HaloFlippers: A general tool for the fluorescence imaging of precisely localized membrane tension changes in living cells. *ACS Cent*

- Sci* 6: 1376–1385
- Szejtli J (1989) Downstream processing using cyclodextrins. *TIBTECH* 7: 170–174
- Szejtli J (2004) Past , present , and future of cyclodextrin research. *Pure Appl Chem* 76: 1825–1845
- Széliová D, Ruckerbauer, David E. Galleguillos SN, Petersen LB, Natter K, Hanscho M, Troyer C, Causon T, Schoeny H, Christensen HB, Lee D-Y, *et al* (2020) What CHO is made of: Variations in the biomass composition of Chinese hamster ovary cell lines, *Metabolic Engineering. Metab Eng* 61: 288–300
- Szoka F & Papahadjopoulos D (1980) Comparative properties and methods of preparation of lipid vesicles liposomes. *Annu Rev Biophys Bioeng* 9: 467–508
- Takahashi K & Yamanaka S (2006) Induction of pluripotent stem cells from mouse embryonic and adult fibroblast cultures by defined factors. *Cell* 126: 663–676
- Tamm L & McConnell H (1985) Supported phospholipid bilayers. *Biophys J* 47: 105–113
- Tan M, Choong P & Dass C (2010) Recent developments in liposomes, microparticles and nanoparticles for protein and peptide drug delivery. *Peptides* 31: 184–193
- Tanford C (1974) The hydrophobic effect. Formation of micelles and biological membranes. *Science* 184: 559–560
- Tharkeshwar AK, Trekker J, Vermeire W, Pauwels J, Sannerud R, Priestman DA, Vruchte D, Vints K, Baatsen P, Decuypere J, *et al* (2017) A novel approach to analyze lysosomal dysfunctions through subcellular proteomics and lipidomics: the case of NPC1 deficiency. *Nat Publ Group* 7: 1–20
- Thomson J (1913) Rays of positive electricity, discovery of neon isotopes. *Proc R Soc A* 89: 1–20
- Thudichum J (1884) A treatise on the chemical constitution of the brain: based throughout upon original researches London: Baillière, Tindall, and Cox
- Tidhar R & Futerman A (2013) The complexity of sphingolipid biosynthesis in the endoplasmic reticulum. *BBA-Mol Cell Res* 1833: 2511–2518
- Tomassini B & Testi R (2002) Mitochondria as sensors of sphingolipids. *Biochimie* 84: 123–129
- Tomishige M, Sako Y & Kusumi A (1998) Regulation mechanism of the lateral diffusion of band 3 in erythrocyte membranes by the membrane skeleton. *J Cell Biol* 142: 989–1000
- Tristram-nagle S, Chan R, Kooijman E, Uppamoochikkal P, Qiang W, Weliky DP &

- Nagle JF (2010) HIV Fusion peptide penetrates, disorders, and softens T-Cell membrane mimics. *J Mol Biol* 402: 139–153
- Umagai IZK, Keda KAI, Obayashi TOK & Ada HIW (2006) Imaging by atomic force microscopy of the plasma membrane of prestin-transfected Chinese Hamster Ovary cells. *J Assoc Res Oto* 278: 267–278
- Valdez-Taubas J & Pelham H (2003) Slow diffusion of proteins in the yeast plasma membrane allows polarity to be maintained by endocytic cycling. *Curr Biol* 18: 1636–1640
- Varela A, Ventura A, Carreira A, Fedorov A, Futerman A, Prieto M & Silva L (2017) Pathological levels of glucosylceramide change the biophysical properties of artificial and cell membranes. *Phys Chem Chem Phys* 19: 340–346
- Veatch SL & Keller SL (2005) Phase diagrams of lipid mixtures relevant to the study of membrane rafts. *Biochim Biophys Acta* 1746: 172–185
- Veiga-da-cunha M, Hadi F, Balligand T, Stroobant V & Schaftingen E Van (2012) Molecular identification of hydroxylysine kinase and of ammoniophospholyases acting on 5-Phosphohydroxy- L -lysine and phosphoethanolamine. *J Biol Chem* 287: 7246–7255
- Veiga MP, Arrondo JL, Goñi FM & Alonso A (1999) Ceramides in phospholipid membranes: effects on bilayer stability and transition to nonlamellar phases. *Biophys J* 76: 342–350.
- Verkleij A, Zwaal R, Roelofsen B, Comfurius P, Kastelijn D & van Deenen L (1973) The asymmetric distribution of phospholipids in the human red cell membrane. A combined study using phospholipases and freeze-etch electron microscopy. *Biochim Biophys Acta* 323: 178–193
- Vieira C, Munoz-Olaya J, Sot J, Jiménez-Baranda S, Izquierdo-Useros N, Abad J, Apellániz B, Delgado R, Martínez-Picado J, Alonso A, *et al* (2010) Dihydrospingomyelin impairs HIV-1 infection by rigidifying liquid-ordered membrane domains. *Chem Biol* 17: 766–775
- Villiers A (1891) Sur la fermentation de la fécule par l'action du ferment butyrique. *Compt Rend Acad Sci* 112: 536–538
- Voet D, Voet J & Pratt C (2013) Fundamentals of Biochemistry: Life at the Molecular Level 4th ed. Cambridge: John Wiley & Sons, Inc.
- Wang J, Hu J, Jin Z & Wan H (2016) The sensitivity of chronic myeloid leukemia CD34 cells to Bcr- Abl tyrosine kinase inhibitors is modulated by ceramide levels.

- Leuk Res* 47: 32–40
- Weber G & Farris F (1979) Synthesis and spectral properties of a hydrophobic fluorescent probe: 6-propionyl-2-(dimethylamino)naphthalene. *Biochemistry* 18: 3075–3078
- Weiss B & Stoffel W (1997) Human and murine serine-palmitoyl-CoA transferase—cloning, expression and characterization of the key enzyme in sphingolipid synthesis. *Eur J Biochem* 249: 239–247
- Wertz P & Downing D (1983) Ceramides of pig epidermis: structure determination. *J Lipid Res* 24: 759–765
- Wien W (1898) Ueber die Fragen, welche die translatorische Bewegung des Lichtäthers betreffen. *Ann der Phys* 301: 1–18
- Yasuda S, Nishijima M & Hanada K (2003) Localization, topology, and function of the LCB1 subunit of serine palmitoyltransferase in mammalian cells. *J Biol Chem* 278: 4176–4183
- Yasuda T, Al Sazzad M, Jääntti N, Pentikäinen O & Slotte J (2016) The influence of hydrogen bonding on sphingomyelin/colipid interactions in bilayer membranes. *Biophys J* 110: 431–440
- Yatomi Y, Ruan F, Megidish T, Toyokuni T, Hakomori S & Y I (1996) Dimethylsphingosine inhibition of sphingosine kinase and sphingosine-1-phosphate activity in human platelets. *Biochemistry* 35: 626–633
- Yeagle P (2012) *The Structure of Biological Membranes* 3rd ed. Portland: CRC Pres, Boca Raton
- Yeagle PL (2016) *The Membranes of Cells* 3rd ed. London: Academic Press
- Yingchoncharoen P, Kalinowski D & Richardson D (2016) Lipid-based drug delivery systems in cancer therapy: what is available and what is yet to come. *Pharmacol Rev* 68: 701–787
- Yoshino O, Yamada-Nomoto K, Kano K, Ono Y, Kobayashi M, Ito M, Yoneda S, Nakashima A, Shima T, Onda T, *et al* (2019) Sphingosine 1 phosphate (S1P) increased IL-6 expression and cell growth in endometriotic cells. *Reprod Sci* 26: 1460–1467
- Zahler P, Donald B & Wallach F (1966) Protein conformations in cellular membranes. *Biochemistry* 56: 1552–1559
- Zarrouk A, Debbabi M, Bezine M, Karym E, Badreddine, Rouaud, Moreau T, Cherkaoui-Malki M, El Ayeb M, Nasser B, *et al* (2018) Lipid Biomarkers in

- Alzheimer's Disease. *Curr Alzheimer Res* 15: 303–312
- Zhang Q, Tamura Y, Roy M, Adachi Y, Iijima M & Sesaki H (2014) Biosynthesis and roles of phospholipids in mitochondrial fusion, division and mitophagy. *Cell Mol Life Sci* 71: 3767–3767
- Zhu W, Wang X, Zhou Y & Wang H (2014) C2-ceramide induces cell death and protective autophagy in head and neck squamous cell carcinoma cells. *Int J Mol Sci* 15: 3336–3355
- Ziesemer S, Möller N, Nitsch A, Müller C, Beule AG & Hildebrandt JP (2019) Sphingomyelin depletion from plasma membranes of human airway epithelial cells completely abrogates the deleterious actions of *S. aureus* alpha-toxin. *Toxins* 11: 126
- Ziulkoski AL, Zimmer AR & Guma FCR (2001) De novo synthesis and recycling pathways of sphingomyelin in rat sertoli cells. *Biochem Bioph Res CO* 281: 971–975
- Zuellig R, Hornemann T, Othman A, Hehl A, Bode H, Güntert T, Ogunshola O, Saponara E, Grabliauskaite K, Jang J, *et al* (2014) Deoxysphingolipids, novel biomarkers for type 2 diabetes, are cytotoxic for insulin-producing cells. *Diabetes* 63: 1326–1339
- Zweerink MM, Edison AM, Wells GB, Pinto W & Lester RL (1992) Characterization of a novel, potent, and specific inhibitor of serine palmitoyltransferase. *J Biol Chem* 267: 25032–25038

ARGITARATZEAK

ARGITARATZEAK

Tesi Honekin Lotura Dutenak

- Monasterio BG, García-Arribas AB, Alonso A, Goñi FM. 2019. Esfingolipidoak eta kolesterola, egitura lipidoak baino gehiago. *Ekaia*. 36, 109-126. DOI: 10.1387/ekaia.20791
- Monasterio BG, Jiménez-Rojo N, García-Arribas AB, Riezman H, Goñi FM, Alonso A. 2020. Patches and blebs: A comparative study of the composition and biophysical properties of two plasma membrane preparations from CHO cells. *Int J Mol Sci*. 21, 2643. DOI: 10.3390/ijms21072643
- Monasterio BG, Jiménez-Rojo N, García-Arribas AB, Riezman H, Goñi FM, Alonso A. 2021. CHO/LY-B cell growth under limiting sphingolipid supply: Correlation between lipid composition and biophysical properties of sphingolipid-restricted cell membranes. *FASEB J*. 35, e21657. DOI: 10.1096/fj.202001879RR
- Monasterio BG, Jiménez-Rojo N, García-Arribas AB, Riezman H, Goñi FM, Alonso A. 2021. Plasma membrane effects of sphingolipid-synthesis inhibition by myriocin in CHO cells: a biophysical and lipidomic study. *In second revision*
- Monasterio BG, Jiménez-Rojo N, García-Arribas AB, Riezman H, Goñi FM, Alonso A. 2021. Plasma membrane sphingomyelin depletion by cyclodextrins: physical and compositional consequences. *In preparation*
- Monasterio BG, Jiménez-Rojo N, García-Arribas AB, Riezman H, Goñi FM, Alonso A. 2021. Sphingolipid restriction in HAP1 cells that constitutively contain low amounts of sphingolipids. *In preparation*

Beste Argitaratze Batzuk

- Acosta-Andrade C, Artetxe I, G. Lete M, Monasterio BG, Ruiz-Mirazo K, Goñi FM, Sánchez-Jiménez F. 2017. Polyamine-RNA-membrane interactions: from the past to the future of biology. *Colloids and Surfaces B*. 155, 173-181. DOI: 10.1016/j.colsurfb.2017.04.005

- Monasterio BG, Alonso B, Sot J, García-Arribas AB, Gil-Cartón D, Valle M, Zurutuza A, Goñi FM. 2017. Coating graphene oxide with lipid bilayers greatly decreases its hemolytic properties. *Langmuir*. 33, 8181-8191. DOI: 10.1021/acs.langmuir.7b01552
- Ahyayauch H, García-Arribas AB, Sot J, González-Ramírez EJ, Busto JV, Monasterio BG, Jiménez-Rojo N, Contreras FX, Rendón-Ramírez A, Martín C, Alonso A, Goñi FM. 2018. Pb(II) induces scramblase activation and ceramide-domain generation in red blood cells. *Sci. Reports*. 8, 1-17 DOI: 10.1038/s41598-018-25905-8
- Lete MG, Monasterio BG, Collado MI, Medina M, Sot J, Alonso A, Goñi FM. 2019. Fast and slow biomembrane solubilizing detergents: Insights into their mechanism of action. *Colloids surf b biointerfaces*. 183, 110430. DOI: 10.1016/j.colsurfb.2019.110430
- Galisteo-González F, Monasterio BG, Gil D, Valle M, Goñi FM. 2020. Photoacoustic effect applied on model membranes and living cells: Direct observation with multiphoton excitation microscopy and long-term viability analysis. *Sci. Rep.* 10, 299 DOI: 10.1038/s41598-019-56799-9
- Monasterio BG, Goñi FM. 2020. Izozte-urtze ziklo bidezko mintz-ereduen fusioa Ekaia. 37, 175-188. DOI: 10.1387/ekaia.21109
- Sot J, Esnal I, Monasterio BG, León-Irra R, Niko Y, Goñi FM, Klymchenko A, Alonso A. 2021. Phase-selective staining of model and cell membranes, lipid droplets and lipoproteins with fluorescent solvatochromic pyrene probes. *Biochim. Biophys. Acta Biomembr.* 1863, 183470. DOI: 10.1016/j.bbamem.2020.183470.

ESKER ONAK

ESKER ONAK

Tesi hau Biofisika Institutuan (UPV/EHU, CSIC) eta Felix M. Goñi eta Xabier Contreras doktoreen zuzendaritzapean gauzatu da. Burututako ikerketa, Eusko Jaurlaritzak (IT264-19, IT270-19) eta Espainiar Gobernuak (FEDER/MINECO GC2018-099857-B-I00) babestua izan da. Egileak, Euskal Herriko Unibertsitatearen ikerketa beka bat jaso zuen (2017ko martxoa - 2021eko martxoa).

Eskerrik asko Alicia Alonso eta Jesús Sot doktoreei tesi guztian beraiengandik jasotako laguntza handiagatik. Gainera, Alonso-Goñi laborategiko beste kideak, eta Howard Riezman eta Noemi Jimenez-Rojo (Genevako unibertsitatea, Suitza) doktoreak ere eskertu nahi ditut. Azken bi hauek, masa espektrometria ikerketan eskeinitako laguntza eta lankidetasun apartagatik.